Saint Petersburg State University

ISRS-18

International Symposium on the Reactivity of Solids

Book of Abstracts

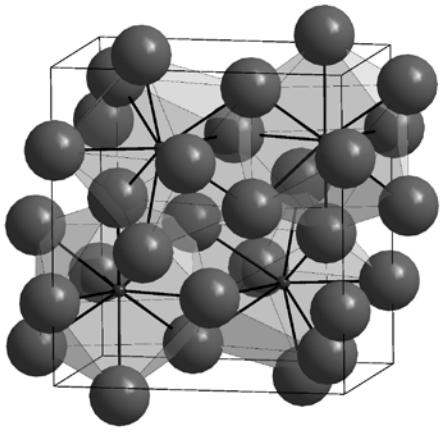

9—13 June 2014
Saint Petersburg, Russia
www.isrs2014.spbu.ru

ISRS-18. International Symposium on the Reactivity of Solids. 9—13 June 2014. Saint Petersburg, Russia. Book of Abstracts. WM Publishing. 306 pp.

ISBN 978-5-9651-0838-1

Book Credits

This book was edited by Nikita A. Kuznetsov, SPbSU, Saint Petersburg, and designed by Stanislav V. Roningrad, Yekaterinburg

Elena G. Panchenko and Yana K. Saidova prepared the Authors Index

Photographs by E.Alekseeva, A.Savin, V.Fedorovski

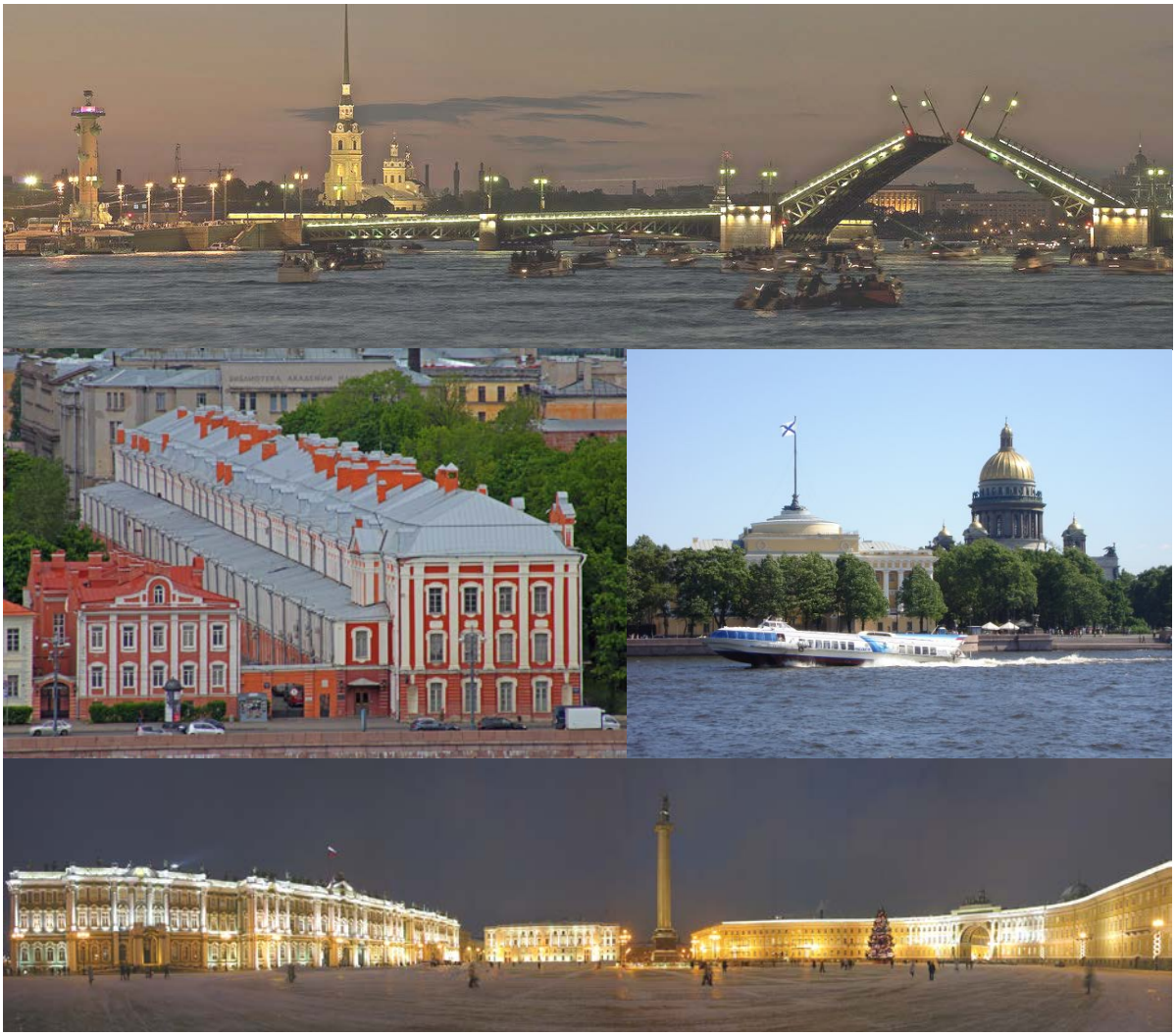

Welcome to Saint Petersburg!

Organizing Committee

- **Prof. Sergey Tunik**, **Chairman** (SPbSU, Russia)
- **Prof. Evgeny Antipov, Chairman of the Program Committee** (MSU, Russia)
- **Prof. Irina Balova** (SPbSU, Russia)
- **Prof. Elena Boldyreva** (NSU, Russia)
- **Prof. Viktor Gusarov** (SPbSTU, Russia)
- **Dr. Vladislav Gurzhij** (SPbSU, Russia)
- **Dr. Sergey Kazakov** (MSU, Russia)
- **Prof. Veniamin Kondratiev** (SPbSU, Russia)
- **Prof. Sergey Krivovichev** (SPbSU, Russia)
- **Prof. Valery Malev** (SPbSU, Russia)
- **Prof. Andrei Shevelkov** (MSU, Russia)
- **Prof. Irina Zvereva** (SPbSU, Russia)
- ***Dr. Oleg Levin, secretary*** (SPbSU, Russia)

Scientific Committee

- **M.A. Alario-Franco** (Spain)
- **E. V. Antipov** (Russia), Chairman of the Scientific Committee 2014
- **P. Attfield** (UK)
- **J. Le Bideau** (France)
- **M.A. Blesa** (Argentina)
- **E.V. Boldyreva** (Russia)
- **V.V. Boldyrev** (Russia)
- **C.B. Carter** (USA)
- **C.R.A. Catlow** (UK)
- **P.K. Davies** (USA)
- **C. Delmas** (France)
- **G.R. Desiraju** (India)
- **P.P. Edwards** (UK)
- **A. Fuertes** (Spain)
- **J. Grin** (Germany)
- **D. Jiang** (P. R. China)
- **M. Jansen** (Germany)
- **H. Kageyama** (Japan)
- **V.V. Kondratiev** (Russia)
- **S.V. Krivovichev** (Russia)
- **A. Maignan** (France)
- **V.V. Malev** (Russia)
- **M. Martin** (Germany)
- **A. Negro** (Italy)
- **T. Norby** (Norway)
- **K. Poeppelmeier** (USA)
- **A. Reller** (Germany)
- **M. Rosseinsky** (UK)
- **T. Sasaki** (Japan)
- **M. Senna** (Japan)
- **A.V. Shevelkov** (Russia)
- **S. Shimada** (Japan)
- **F. Solymosi** (Hungary)
- **J. Thomas** (Sweden)
- **M. Takano** (Japan)
- **H. Verweij** (The Netherlands)
- **A. Weidenkaff** (Switzerland)
- **S. Whittingham** (USA)
- **A. Yamada** (Japan)
- **H-Ill Yoo** (S. Korea)
- **M. Yoshimura** (Japan)

Preface

Welcome to Saint-Petersburg, to ISRS-18, the 18th International Symposium on the Reactivity of Solids!

The International Symposium on the Reactivity of Solids is a platform for discussing various aspects of chemistry and physics of solid compounds and materials, both from the basic and applied points of view. The ISRS series is not intended for a closed society of devoted members, it spreads to a broad community of active researches, combining the efforts in the field of solid state, inorganic, organic, polymer and physical chemistry, electrochemistry, physics of condensed matter, crystallography, nanoscience and nanotechnology and other subdisciplines. In recent years the ISRS focuses more and more on the demands of materials science.

Following the trends in modern science, the ISRS-18 will cover basic and applied aspects of new materials design, advanced methods of preparation and characterization, mechanisms of reactions involving solids, structure-property relations, and new horizons of the materials application. It brings together scientists from academic, industrial and governmental research institutions all over the world to extend current knowledge, discuss future trends and developments, encourage new contacts, stimulate scientific insights, and help promoting young scientists into independent researches in academia or industry.

The scientific program of ISRS-18 consists of 6 plenary lectures, 18 invited lectures, 37 oral presentations, and 93 poster presentations on various topics concerning synthesis, structure, properties, and reactivity of solid compounds and materials. The program is not limited to the official time table of the symposium. Expression of different opinions and points of view and informal discussions are particularly welcome.

Saint-Petersburg University will host ISRS-18. Established in 1724 by the Russian tsar Peter the Great, the University is one of the largest and renowned academic establishments in Russia. It combines a great history glorified by works of Lomonosov and Mendeleev, to name just a few, with rapid development and achievements in sciences. Its historical Twelve Collegia building will be a venue of ISRS-18.

Organizing and Program Committees

Contents

Opening Ceremony

Plenary Lectures

Monday, 9th June 2014

Tuesday, 10th June 2014

Wednesday, 11th June 2014

Thurstday, 12th June 2014

Friday, 13th June 2014

Invited Lectures

Speaker is underlined

Monday, 9th June 2014

Tuesday, 10th June 2014

Wednesday, 11th June 2014

Thursday, 12th June 2014

Friday, 13th June 2014

Oral Presentations

Speaker is underlined

Monday, 9th June 2014

Tuesday, 10th June 2014

Wednesday, 11th June 2014

Thursday, 12th June 2014

Friday, 13th June 2014

Poster Presentations

Presenting author is underlined

Opening Ceremony

Reactivity of Solids. Retrospect and Prospects.

V.V. Boldyrev[a,b]

[a] Institute of Solid State Chemistry and Mechanochemistry SB RAS, Novosibirsk, Russia;
[b] Novosibirsk State University, Novosibirsk, Russia.

The International Symposium on the Reactivity of Solids in S-Petersbourg continues a long series of the international meetings which started in 1948 in Paris. Since that time, ISRS take place every four years, alternating location between Europe (dominates), USA (twice) and Asia (once, in Japan). Although Russia was always one of the leading centers of the research in the field of reactivity of solids, and the author of this contribution even served a term as an elected President of the ISRS Advisory Committee (1992 – 1996), an ISRS never took place in Russia untill 2014. In this respect, this is a notable event, and I am very happy that I can evidence it at least remotely.

I entered the field of reactivity of solids in the late 1940s, and I could see how this field developed with time. I would like to use this occasion to share my memories, thoughts and concerns with the younger generation who enters the field now.

The initiative of uniting the researchers involved in studying the reactivity of solids belonged to J. Bénard. The idea was to have a discussion on various topics related to the reactivity of solids, focusing on those aspects of the reactions which make reactions in the solid state different from the reactions of gases or liquids. The main focus areas at the first symposia were i) the mechanisms and kinetics of reactions in the solid state, the main factors influencing reactions of solids (introducing impurities and different types of defects, preliminary treatment by various types of radiation, crystal structure), ii) various practical applications, in particular – in the fileds of preventing corrosion of metals, processing inorganic minerals, preparing inorganic materials and catalysts, fast ionic conductors, solid-state inorganic synthesis (ceramic methos, sol-gel synthesis, precursor technique). Thermal decomposition (in particular – dehydration of crystal hydrates), reactions between solids and gases, reactions in the solid mixtures were considered. There was evidence that a solid “has a memory”, *i.e.* its reactivity depends on its prehistory – method of synthesis, conditions of storage, preliminary treatment. Different types of defects were shown to have different, often – opposite effect on reactivity. This was used to study the elementary stages of the transformations and to control reactivity of solids. The reactions in solids were shown to be heterogeneous, and studying their kinetics (“topokinetics”) was complicated enormously by the necessity to take into account the size and shape of the interface between the initial reactant(s) and the product(s). It was shown that reactivity of a solid can increase during phase transitions (Hedvall effect). The molecular structures of the products of the photochemical reactions in organic solids were shown to be predetermined by the juxtaposition of the neighbouring molecules in the parent crystal structure (“Schmidt-Cohen topochemical principle”). The concepts of “topotactic reactions” and “precursor selection method” were introduced and developed. For quite a long time the dominating topics were the role of defects in inorganic solid state reactions and the role of crystal structure in the reactions of organic and coordination compounds.

Comparing the scope of the ISRS in different years one can notice interesting trends. In the first decades, the main emphasis was on understanding the phenomena, in order to achieve a better control over reactivity, to be able to vary on purpose the reaction rate, spatial propagation, as well as the chemical composition, the molecular and crystal structures of the product, the texture of the product samples, the size and shape of the particles in powder products. This was the period of hot scientific discussions, questions, comments and answers being documented in the ISRS Proceedings. There was no large gap between inorganic and organic solid state chemitry: different research groups could understand each other quite well and were often using similar methods and applying similar general concepts to reactions in the solids of different chemical nature.

The fundamental knowledge of the reactivity of solids achieved by 1980s was widely exploited in materials sciences and chemical engineering. And, as it often happens, reactivity of solids became "a victim of its own success". The situation was very well characterized by B. Delmon in his plenary lecture presented at the ISRS-9 in Cracow in 1980. He noted that "chemistry of solids and, more precisely, research on the reactivity of solids, is far from having a place it deserves. There is some sort of a pause after the development experienced between 1930s and 1960s. Indeed, the discovery of new structures and of materials with new exciting properties continues at a rapid pace. But relatively little is done on reactivity. The words "chemistry of solids" and "reactivity of solids" tend, nowadays, to describe rather research on structures or physical properties than on kinetics, on the mechanism by which solids react or on possibilities one has to control the way they react... Nevertheless, those still working in the field think that chemistry of solids, namely the science of chemical transformations of solids, must develop. The requirements of energy saving already spurs research on processes occurring at lower temperatures. More selective reactions are necessary for saving natural resources or for exploiting lower grade ores. New materials, when they have proved useful, must be mass produced, and, correspondingly, the emphasis must be displaced from materials to processes." This advise was not followed for almost three decades, and the situation became only worse with time, as can be clearly seen from the materials presented at the ISRS after Cracow, especially – after Dijon. Reactivity of solids with a wide scope and deep insight into the control over properties and processes was practically substituted for inorganic materials sciences (with dominating focus on the synthesis), while organic solid state chemistry practically disappeared from the scope of the ISRS. This was reflected also by the fact that Proceedings of the ISRS were no longer published as separate volumes, but as special issues of Solid State Ionics. At the same time, research in the field of organic solid state chemistry continued very successfully, but was discussed at another series of conferences – ICCOSS (International Conferences on the Chemistry of Organic Solid State). The number of participants of the ISRS started decreasing, and the interest to these – formely highly prestigious – meetings declined.

However, in the last few years we can see some new trends which can be considered with a "cautious optimism" as a slow revival of the reactivity of solids. In particular, interesting papers discussing the mechanisms of mechanochemical and photochemical reactions in solids, the origin of photo- and thermo-mechanical effects, the methods of controling selectively the reaction products and the propagation of solid state reactions in time and space are being published not only in the "traditional solid-state chemistry journals", but also in such "main-stream editions" as ACIE, JACS, Nature, Science, Green Chemistry. Molecular materials, including pharmaceuticals, MOFs, high-energy materials, supramolecular machines; new inorganic and hybrid materials for energy storage and generation, *etc*. are now not only described as such, but the reactions resulting in their reliable and reproduceable synthesis and exploitation are studied in details. The program of the ISRS here in S-Petersbourg also reflects this positive trend. New experimental techniques open

prospects that could not be even imagined when reactivity of solids emerged. They give high space and time resolution and allow one not only to follow various static characteristics of reactants and products before and after the reaction, but also to monitor the dynamic processes, even very fast ones, *in situ* and at various locations in a solid. What is important now is that these really exciting experimental facilities are complemented by a careful design of experiments. Decades ago, when an optical microscope, a rather primitive X-ray powder diffractometer, DTA and TGM instruments were the main tools of research, the ideas of experiments were often so clear and elegant, that their results can still serve as a source of inspiration and fundamental knowledge. One more quotation, also dating back to the 1980s, but no less actual today, belongs to J.D. Dunitz: "Time to ponder the significance of the results is a luxury that few present-day researchers can afford. One might have hoped that the increased ease and rapidity of getting experimental data would have left more time for thinking, but the contrary seems to be true. The facts may be trying to tell us something, but we have no time to listen. Another long-overdue paper is waiting to be written" [J.D. Dunitz, X-ray analysis and the structure of organic molecules, Cornell University Press, Ithaca and London, 1979, 302-303]. I must confess that this comment is applicable to many papers published nowadays. At the same time, a new positive trend is that a profound interest in the mechanisms of the processes seems to recover.

As one of the eldest, though "virtual" participants of the ISRS in S-Petersbourg, I wish the Symposium a success not only in presenting new facts and describing new materials. I do hope that discussions will emerge which can improve our understanding of the basics of the reactivity of solids. I was very pleased to see that ISRS-2014 again has a balanced program in terms of considering inorganic and organic systems. I wish the participants coming from different research "sub-fields" of reactivity of solids to see similarities in the concepts and results known and used in these sub-fields, find "growth sites" for future development and points of cross-interests for potential collaboration. There is a demand in the "Renaissance of reactivity of solids" from industry, and this Renaissance is not possible without developing fundamental research with well-planned, original, inventive experiments and applying a complex of various instrumental and computational techniques. We live in a very pragmatic time now, but investing money into basic research is the only way to optimize usage of funds when developing new materials and technologies of their mass production.

ISRS-10, Dijon, 1984
Left (chairman) – J. Bénard, right (speaker moderator) – V. Boldyrev

ISRS-7, Bristol, 1972
From left to right: ?, J.M. Thomas, J .G. Sheppard, E.G. Prout, V.V. Boldyrev, P.A. Jackobs, S.R. Morrison; sitting M.D. Cohen

ISRS Symposia (retrospect)

Year	Location	Scope (main topics)
1948	Paris (France)	General problems of the reactivity of solids; oxidation of metals; experimental mineralogy
1952	Göteborg (Sweden)	General problems of the reactivity of solids; phase transformations; factors influencing reactivity of solids; Hedvall effect
1956	Madrid (Spain)	General problems of the reactivity of solids; defects and diffusion in solids; correlation effects; materials for reactors and fuel cycles
1960	Amsterdam (Netherlands)	Mechanism and kinetics; diffusion and sintering; reactions of solids with solids, gases and liquids; allotropic transitions; phase transformations; thermal decomposition; factors influencing reactivity; defects and impurities; reactivity induced by irradiation; influence of pressure on reactivity; influence of gas atmosphere, crystal size on reactivity; influence of crystal structure on reactivity; reactivity studies with technical implication; methods of investigation

1964	Munich (Germany)	Influence of structure on solid-state reactions; influence of radiation on reactivity and catalytic activity of solids; kinetics and mechanisms of solid-state reactions; material transport in solid-state reactions; effect of particle size on the mechanism of solid-state reactions
1968	Schenectady (USA)	Crystal structures, surfaces, defects and diffusion processes in chemical reactions involving solids; nucleation and growth of new phases in the solid state; thermal decomposition of inorganic solids; reactions of elements, alloys and chemical compounds with gases and solutions; production of crystalline solids from reactants in the gaseous phase; chemical reactions between crystalline solids; chemical reactions in vitreous systems; chemical processes in high pressure systems;
1972	Bristol (UK)	Defect chemistry; topology of reacting crystals; vitreous state; diffusion and diffusion controlled reactions; amorphous materials and phase transformations; dislocations and nucleation; reactions of the organic solid state; surface structure and processes; reaction processes – structural and mechanistic
1976	Göteborg (Sweden)	New crystallographic developments applicable in studies of reactions in solids; reactions at surfaces and interfaces; influence of structural defects on the reactivity of solids; defects; diffusion, non-stoichiometry; kinetics; reactions in vitreous solids; surface reactions; diffusion controlled solid-state sintering, hot pressing and creep; size effects; sol-gel technique; coupled reactions
1980	Crakow (Poland)	Defects and transport; chemical vapour deposition; surface phenomena; non-crystalline solids; phase transitions; hybrid crystals; non-diffusional transformations; superstructure ordering; novel technologies
1984	Dijon (France)	Accumulation of solid reaction products and reactivity of solids; the role of surfaces in reactivity of solids; ordering induced by chemical, thermal and mechanical constraints at solid interfaces; corrosion of materials by gaseous reactants; reactivity of non-crystalline solids; defects and transport in solids; soft chemistry – intercalation compounds; solid-liquid reactions; solid-solid reactions; thermal decomposition; reactivity in the organic solid state; mechanical activation of reactions in the solid state; reactions in ceramics and materials for electronics and electrochemistry; structural relationships in solid state reactions; surface phenomena; kinetics and kinetic models; reactivity of solids connected with the catalyst preparation; industrial applications of the reactivity of solids
1988	Princeton (USA)	Materials chemistry; minerals and reactivity; synthesis and reactivity; polymers and the organic solid state; oxides and ceramics; sol-gel process; tailored solids; films, glasses and catalytic materials; high temperature oxide superconductors

1992	Madrid (Spain)	Mechanochemistry; synthesis and characterization; heterogeneous kinetics; thermal decomposition; intercalation and soft chemistry; structure, defects and properties; surface and catalysis; superconducting materials and related solids
1996	Hamburg (Germany)	Novel synthesis pathways to tailor-made materials; formation and reactivity of nanoscale and mesoscale systems; defects and transport phenomena in solids; metastable systems and phase transformations; processes at interfaces and surfaces; formation and reactivity of organic and polymer materials; applied processes and energy technology; materials exhibiting novel specific properties;
2000	Budapest (Hungary)	Surface materials; in situ spectroscopy in solid state chemistry; topotactic oxidation; plasma assisted techniques; melting and phase transformation of hardmetal powders; defects; diffusion; solid oxide ionics; microstructural modifications resulting from the dehydration
2003	Kyoto (Japan)	Battery and energy conversion; catalysts and functional devices; theoretical aspects and computation; mechanochemistry; plasma and other nonconventional processes; process in nanoscopic dimension; reactions under electromagnetic field; solid state atomic processes; sustainable and soft chemistry
2007	Minneapolis (USA)	Complex solid ionics; solid oxide fuel cells; oxide superconductors; electrochromic oxide solid films
2011	Bordeaux- Arcachon (France)	Transport phenomena in solids: point defects and reactivity of solids; reactivity and nanomaterials; reactivity and catalysis; reactivity of materials for energy and environment; reactivity and composite materials; functional materials for sustainable energy systems (batteries, thermoelectrics, solar cells); reactivity of solids in the geologic and planetary environment; novel materials and new synthesis routes; chemistry in unconventional media (ionic liquids, supercritical fluids); advances in characterization of reacting solids; theory and modelling. Only inorganic solids.
2014	Saint Petersburg (Russia)	Basic and applied aspects of new materials design; advanced methods of preparation and characterization; mechanisms of reactions involving solids; structure property relations; new horizons of the materials application; inorganic and organic solids

Plenary Lectures

Advanced materials science for energy storage & conversion

Doron Aurbach
Department of Chemistry
Bar-Ilan university
Ramat-Gan, 5290000, Israel

It is impossible to imagine modern society without electrochemical power sources. The electronic revolution, which relies on the extensive use of highly sophisticated portable devices such as cellular phones with amazing applications, laptops, video cameras and more, depends on the availability of high-energy density, safe and cheap power sources. The challenge in delineating rechargeable power sources has increased markedly in recent years, spurred by the demand for electro-mobility to replace propulsion by fossil fuels that power internal combustion engines.

Challenges such as electrochemical propulsion by electric vehicles (EV), and the need for large-scale storage of sustainable energy (i.e. load-levelling applications) motivate and stimulate the development of novel rechargeable batteries and super-capacitors. While batteries deliver high energy density but have limited cycle life and power density, supercapacitors provide high power density and very prolonged cycling. Lithium-ion batteries are the focus of intensive R&D efforts because they promise very high energy density that may be suitable for electrical propulsion. In this presentation we review research on batteries with an emphasis on Li-ion battery technology, examining its suitability for EV applications. We also briefly examine other battery systems that may be of importance for load-levelling applications. Batteries (especially when dealing with high energy density systems such as Li batteries) are highly complicated devices: 3 active bulks and 2 active interfaces have to work simultaneously with no side reactions & detrimental reflections. In Li ion batteries there is no thermodynamic stability at both electrodes. Their operation depends on complicated passivation phenomena, which are developed via electrodes-solution reactions.

Consequently, R&D of novel battery system requires to invest great efforts in basic science, in order to understand the correlation among structure, morphology, surface chemistry and electrochemical performance of all the components in the power sources and storage devices. Our approach at BIU: it is important to study all the components alone & together . Use as many tools as possible, electrochemistry, spectroscopy, diffractometry, high resolution microscopy and calorimetry in each single study.

In this presentation we review first the frontier of advanced Li ion batteries: replacement of graphite by Si at the anode side, the possible use of high voltage ($LiCoPO_4$ and $Li[MnNi]_2O_4$ spinel) or high capacity ([Li rich, layered Li_2MnO_3-$Li[MnNiCo]O_2$) cathode materials and

development of new electrolyte solutions with higher anodic stability. Then, we will review the chance to develop long life, high energy density Li-Sulfur batteries. Main questions: how to stabilize sulfur electrodes and which anodes are really relevant? Then, we will review the chance to develop rechargeable Li-oxygen batteries. The key question here is: what are the limiting factors? Do we really have relevant electrolyte solutions, suitable for rechargeable Li-oxygen battery systems?

Finally, we will discuss load leveling applications. We will review in brief how where Li ion battery technology can be relevant of storage of sustainable energy. We will demonstrate how the use of advanced nano-materials such as carbon nano-tubes (CNT) can improve lead acid batteries and super (EDL) capacitors and we will briefly review the chance to develop practical rechargeable Mg batteries.

Today we are experiencing a nano revolution that seems to stimulate the introduction and use of nano-materials in all possible areas of technology and medicine. The field of energy research is also influenced by these trends, and intensive attempts are underway to synthesize and introduce nano-materials in devices for energy storage and conversion. There are obvious advantages to the use of nano-materials in photo-voltaic solar cells, and as catalysts in fuel cells. There are serious questions regarding the use of nanomaterials for energy storage in batteries. The use of nano-particles may mean indeed a faster kinetics of the electrodes' reactions, but also, highly reactive surface of the active mass for side (parasitic) reactions, low density, bad inter-particle electrical contact, and complicated syntheses (compared to micronic-size particles). This presentation will discuss also the relevance of nano-materials to the field of high energy density batteries. We will describe the use of electrochemical techniques in conjunction with XRD, HRTEM, HRSEM, FTIR, XPS, Raman spectroscopy, DSC and ARC for thermal analysis, ICP and ESR. We will demonstrate several critical basic studies on the way of R&D of new materials for Li ion batteries and will outline directions for future R&D efforts in this field.

References:

[1]. Si anodes: E. Markevich, G. Salitra, D. Aurbach et Al, *J. Electrochem. Soc.* , **160**, A1824 (2013).
[2]. Li air systems: D. Sharon, V. Etacheri, D. Aurbach et Al , *J. Phys. Chem. Lett*. **4**, 127(2013).
[3]. High voltage cathodes: R. Sharabi, E. Markevich et Al , *Electrochem. Comm*. **28**, 20, **(2013)**.
[4]. Li(Si)-Sulfur systems: R. Elazari, G. Salitra, D. Aurbach et Al, *Electrochem. Comm.*, **14**, 21 **(2012)**.
[5]. Mg batteries: H.D. Yoo, N. Pour, Y. Gofer and D. Aurbach et Al, *Ener. & Environ. **Sci.,*** 6**, 2265** (2013).

Reactivity between fluorine and various carbonaceous materials: mechanisms, structural changes and applications

Alain Tressaud[a*], Henri Groult[b] and Etienne Durand[a]
[a)] ICMCB-CNRS, University Bordeaux 1, 33608-Pessac, France ;
[b)] Laboratoire PECSA, Université Pierre & Marie Curie, 75005-Paris, France
* e-mail : tressaud@icmcb-bordeaux.cnrs.fr

The physics and chemistry of carbonaceous materials can be drastically modified through reaction with fluorine and fluorinated reagents. This behavior is due to the extreme reactivity of these gases that allow important changes in the electronic configuration of carbon, even at low temperatures. In many carbon-fluorine systems, the modification of either surface or bulk properties depends on the physical-chemical characteristics of the pristine material and/or the experimental parameters of the fluorination. The different types of C-F bonding present in the final material have been correlated using several physical investigations, including XPS and electron microscopies. Several reaction mechanisms have been proposed depending on the nature and morphology of the pristine carbon material. The importance of such systems in electrochemistry will be pointed out, such as the reactivity of carbon materials in molten KH.2HF, during the electrochemical synthesis of fluorine (F_2), or the production of graphene during the electrochemical decomposition of molten carbonates.

The physical properties that are intensely modified may concern:

- Electrical conductivity in graphitised carbons and high-temperature treated carbon fibres, that may vary from metallic to insulating behavior, depending on the amount of intercalated fluorine;
- Electrical permittivity in fluorinated carbon blacks;
- Hydrophobic/hydrophilic balance in materials treated with fluorinated rf plasmas;
- Reversible capacities of lithium-ion secondary batteries using F-treated carbon anodes;
- New kinds of carbon-fluorine compounds allowing to provide higher potential and energy density values, thus improving the electrochemical performances of primary Li-battery.

The effect of nanosized carbon materials, as in carbon nanotubes, nanoparticles or graphene will be demonstrated.

Organic solid state chemistry and the delivery of new pharmaceutical materials

Bill Jones
Chemistry Department
University of Cambridge
CB2 1EW UK

There has been a long interest at ISRS meetings in organic solids and especially in the early days with regard to solid state reactivity and what is known as the topochemical postulate - that because of limited movement reactivity in an organic solid is controlled by the local crystal structure. This led naturally to the idea of crystal engineering whereby reactivity (or stability) might be controlled by deliberate design of the crystal structure.

In the area of the delivery of new drugs an understanding of the role of crystal packing on reactivity or stability of a solid form of a drug is crucial. Approximately 80% of drugs are delivered in solid form. Stringent regulatory requirements are made concerning stability – both chemical and physical. Phase transformations (e.g. from one polymorph to another, hydration/dehydration) are not allowed since significant variations in, for example, stability, solubility and bioavailabilty will subsequently result.

In my lecture I will review various aspects of pharmaceutically-related organic solids. In particular I will describe the recently applied use of multicomponent crystals as a way of taking to market active molecules which otherwise would be extremely problematic in terms of development and manufacture. I will outline how mechanochemistry is an important process in screening for new polymorphic forms and also new systems with tuneable properties.

Equally important is the continued recognition – made numerous times at previous Symposia – that the crystal surface itself and defects within the solid will also be important. This aspect of organic solid state chemistry will also be reviewed, utilising recent results from atomic force microscopy and transmission electron microscopy.

Low temperature synthesis of (noncentrosymmetric) oxide-fluorides

Kenneth R. Poeppelmeier[a]

[a] Department of Chemistry, Northwestern University
Evanston, IL, USA

The design and discovery of novel noncentrosymmetric materials – materials that lack an inversion center – with large second-order dielectric responses, $\chi(2)$, that efficiently achieve frequency conversion has been a long-standing and difficult goal of inorganic chemistry. Recently, nanolithography has sought UV lasers to create increasingly small lithographic features. To pursue UV lasers, scientists have sought new SHG active crystals to double the frequency of laser light to higher energies. One such material is the oxide-fluoride $KBe_2BO_3F_2$. Professor Chen's Anionic Group Theory has established that efficient SHG-active crystals often have anions with aligned polar moments in the solid state.

Therefore, to synthesize highly-efficient SHG crystals, a promising strategy is to utilize anions that inherently contain polar moments. For this reason, our group has examined oxide-fluoride early transition materials; the d^0 early transition metal cations undergo out-of-center distortions owing to electronic effects (specifically Second-Order Jahn-Teller distortions). These polar distortions are observed in oxide-fluoride anions of the cations vanadium (V^{5+}), niobium (Nb^{5+}), tantalum (Ta^{5+}), molybdenum (Mo^{6+}) and tungsten (W^{6+}).

In oxide phases of these metals, the Second-Order Jahn-Teller distortion is directed towards oxide ligand(s) of corner, edge, or face(s) of the anionic octahedra. The use of oxide-fluoride compounds enhances the distortion of the anion as the metal-fluoride bonds contain less valence than would exist for metal-oxide bond. The additional valence thus creates stronger M=O bonds within the anions of the solid state compound and thus a stronger distortion. Our syntheses of numerous inorganic and organic-inorganic hybrid oxide-fluoride phases have allowed the analysis of the electronic environments of the early transition metal polyhedra; the distortions of the anions and non-spherical electronic environments have allowed us to synthesize non-centrosymmetric materials and establish principles and guidelines to target syntheses of SHG-active materials.

Structure of materials: advanced TEM meets advanced crystallography

Artem M. Abakumov

EMAT, University of Antwerp, Groenenborgerlaan 171, B-2020, Antwerp, Belgium
Department of Chemistry, Moscow State University, 119991, Moscow, Russia

Advanced transmission electron microscopy techniques transform a modern electron microscope from a simple "imaging" tool to a sophisticated material science laboratory. The 3D reciprocal electron tomography methods enable reconstructing the reciprocal space of submicrometer crystals and the quasi-kinematical diffracted intensities measured with precession electron diffraction allow structure solution and refinement. Aberration-corrected scanning transmission electron microscopy provides mapping of projected scattering density in the unit cell, visualization of the light atoms, displacive and occupational ordering. Being combined with electron energy loss spectroscopy and atomic resolution energy-dipersive X-ray analysis, wealth of chemical information can be simultaneously retrieved, including mapping the chemical composition and coordination number of elements. Transmission electron microscopy methods are particularly useful being combined with high quality powder diffraction data and modern crystallographic approaches, especially to reveal the nature of incommensurate modulations causing extreme structure complexity.

The benefit of employing the reciprocal and real space information obtained using advanced transmission electron microscopy will be illustrated on the examples of various materials, including complex oxides, oxychlorides, hydrides and polyanionic compounds:

- Li_2CoPO_4F and $LiBH_4$ and incommensurately modulated scheelites $CaGd_{2(1-x)}Eu_{2x}(MoO_4)_{4(1-y)}(WO_4)_{4y}$ exemplifying the structure solution with the precession electron diffraction data [1–3];
- $Li_{3x}Nd_{2/3-x}TiO_3$ perovskites with frustrated incommensurately modulated octahedral tilting pattern [4];
- perovskite-based ferrites with the lone pair A-cations [5] and perovskite Mn_2O_3 [6];

References:

[1] J. Hadermann, A.M. Abakumov, S. Turner, Z. Hafideddine, N.R. Khasanova, E.V. Antipov, G. Van Tendeloo, *Chem. Mater.*, **23** (2011) 3540.
[2] J. Hadermann, A. Abakumov, S. Van Rompaey, T. Perkisas, Y. Filinchuk, G. Van Tendeloo, *Chem. Mater*., **24** (2012) 3401.
[3] V.A. Morozov, A. Bertha, K.W. Meert, S. Van Rompaey, D. Batuk, G. T. Martinez, S. Van Aert, P.F. Smet, M.V. Raskina, D. Poelman, A.M. Abakumov, J. Hadermann, *Chem. Mater.*, **25** (2013) 4387.
[4] A.M. Abakumov, R. Erni, A.A. Tsirlin, M.D. Rossell, D. Batuk, G. Nenert, G. Van Tendeloo, *Chem. Mater.*, **25** (2013) 2670.
[5] D. Batuk, M. Batuk, A. M. Abakumov, A.A. Tsirlin, C. McCammon, L. Dubrovinsky, J. Hadermann, *Inorg. Chem*., **52** (2013) 10009.
[6] S. V. Ovsyannikov, A.M. Abakumov, A. A. Tsirlin, W. Schnelle, R. Egoavil, J. Verbeeck, G. Van Tendeloo, K. Glazyrin, M. Hanfland, L. Dubrovinsky, *Angew. Chem.,* **52** (2013) 1494.

Structural complexity of crystalline solids: quantitative measures and application

Sergey V. Krivovichev[a]

[a] St. Petersburg State University

Evolution of matter toward states of higher complexity in the course of the evolution of the Universe is one of the most interesting topics in modern science and in modern chemistry in particular [1]. A number of different approaches exist that allow to quantitatively evaluate complexity of chemical, biological, technological and even social systems. Most of these approaches are based upon the extensive use of concepts and techniques borrowed from the information theory developed in the second half of the XXth century as a theory of communication and transmission of information. It is interesting, however, that complexity theorists have always regarded crystals as 'intuitively simple objects' [2], in contrast to much more complex and dynamic biological systems. On the other hand, it was largely appreciated that crystal structures may possess different degrees of complexity, which has been reflected in the titles of scientific papers with the use of expressions such as 'complicated structure', 'the most complex structure', 'complexity', 'complex superstructures', 'a masterpiece of structural complexity', etc. However, until recently complexity of crystal structures was destined to be 'largely a qualitative, frequently intuitive, notion' [3], which escaped a quantitative definition.

In a series of recent papers [4–6], we have used Shannon information theory to evaluate complexity of crystal structures. This theory allows to quantitatively evaluate both size- and symmetry-dependent properties of complex structures, thus combining their symbolic and combinatorial complexities [7] in the same measure.

Quantification of crystal-structure complexity using information theory allows to identify basic mechanisms responsible for the appearance of complex structures in inorganic systems. The first and the most obvious one is a combination of chemically different components taken in complex proportions. This usually leads to the association in the same structure of different building blocks that can be considered as extracted from parent solids of higher structural simplicity. This feature of inorganic structures is known as modularity and has been widely applied to the description of complex materials. Another complexity-generating mechanism is of genetic origin and depends upon the presence in crystallization media (solution, melt, gas, etc.) of clusters of high nuclearity that self-assemble to form highly ordered three-dimensional crystalline arrays. This group of complex structures includes different kinds of polyoxometallates, cluster compounds, fullerene-containing inorganic solids, etc. It is very probable that the same mechanism is at work in the crystallization of porous frameworks containing various types of large building blocks (e.g., zeolites and microporous sulphide frameworks). Finally, complexity may be generated by local rather than global bonding requirements in compounds with simple chemical compositions. In this case, topologically simple frameworks acquire high structural complexity due to the local atomic ordering and formation of superstructures and superlattices on cooling.

Identification of structural complexity with information encoded in the atomic arrangement and its density allows to quantitavely examine relations between information and kinetics and

thermodynamic parameters in crystalline materials. For instance, quantitative verification can be made for the principle of simplexity [8], which states that, in the course of fast processes such as spontaneous crystallization at non-equlibrium conditions, structurally simpler metastable phases form more easily that their more complex but stable counterparts. Another interesting problem is the behaviour of information along the path of phase transitions induced by changing pressure and temperature. Probably, the most fundamental question of interest is the relation between information and energy [9] in the processes that involve transformations of crystalline phases.

References:

[1] J.-M. Lehn, *Angew. Chem. Int. Ed*. **52** (2013) 2836-2850.
[2] C. H. Bennet, in *Complexity, Entropy, and the Physics of Information. Santa Fe Institute Studies in the Sciences of Complexity* (Ed: W. H. Zurek), Vol. VIII, Addison-Wesley, 1990, pp. 137-148.
[3] J. K. Burdett, C. Marians, J. F. Mitchell, *Inorg. Chem.* **33** (1994) 1848.
[4] S.V. Krivovichev, *Acta Crystallogr*. **A68** (2012) 393.
[5] S.V. Krivovichev, *Miner. Mag*. **25** (2013) 275.
[6] S.V. Krivovichev, *Angew. Chem. Int. Ed*. **53** (2014) 654.
[7] W. Steurer, *Acta Crystallogr.* **A67** (2011) C184.
[8] J.R. Goldsmith, *J. Geol.* **61** (1953) 439.
[9] A. Bérut, A. Arakelyan, A. Petrosyan, S. Ciliberto, R. Dillenschneider, E. Lutz, *Nature* **483** (2012) 187.

Invited Lectures

Digging holes and refilling : Reversible Fe-extrusion in layered compounds

Olivier Mentré[a], Rénald David[a], Ignacio Blazquez[a], Marielle Huvé[a], Pascal Roussel[a], Sylvie Daviero-Minaud[a], Alain Pautrat[b].

[a] Université Lille Nord de France, UMR 8181 CNRS, Unité de Catalyse et de Chimie du Solide (UCCS USTL), F-59655 Villeneuve d'Ascq, France

[b] Laboratoire CRISMAT, UMR 6508 CNRS, ENSICAEN et Université de Caen, 6 Bd Maréchal Juin, F-14050 Caen 4, France

Topotactic modifications of solid oxides at moderate temperature ideally enable the tuning of structural and physical properties in a remarkable manner. It most often involves changes of the anionic sublattice, while the charge of the rigid cationic framework eventually self-adapts via metal redox centers.[1] At the other side, the topotactic modification of the cationic sublattice mainly concerns the (des)intercalation of mobile ions, at the basis of the strategical research for mobile energy. Most rarely, it happens that the metal framework itself participates to extrusion phenomena, while metal is displaced outside crystalline domains. Increasingly intriguing can we find a handful of compounds that exhibit a spontaneous extrusion of lattice cations only driven by temperature, *e.g.* nano-sized particles of the olivine $LiFe^{2+}PO_4$ transforms into $LiFe^{2/3+}_{2-x}PO_4$ as soon as 140°C in air with co-formation of Fe_2O_3 clusters.[2,3] This scarce behavior seems restricted to ferrous Fe^{2+} ions[4], reminiscent of the exsolution of Fe-rich inclusions in minerals or meteorite rocks.[5,6]

In searching for potential candidates for such reactions, we have intuitively focused on $BaFe^{2+}(PO_4)_2$ recently prepared in our group.[7] It was identified as the first 2D-Ising ferromagnetic oxide with an original reentrant structural transition at low temperature.[8] This phenomenon is driven by the specificities of high-spin Fe^{2+} ions arranged in disconnected *honeycomb* layers. Indeed, it possesses all prerequisites for cationic lattice instability since ferrous ions form bidimensional (2D) layers separated by large interleave of ~7.8 Å. Such features could mediate cationic diffusion outward out exaggeratedly depleted Fe-sublattices. Also, all oxygen atoms are tightly hold to the structure by strongly covalent P-O bonds, which could reinforce the preferred modification of the cationic array. In this lecture we will show how above 375°C in air, $BaFe^{2+}_2(PO_4)_2$ topotactically oxidizes into an iron-depleted compound with mixed Fe^{2+}/Fe^{3+} valence. This process is characterized by :

a) An efficient Fe-extrusion even from single crystal with preservation of the initial crystallinity and segregation of Fe into external nanosized Fe_2O_3 domains.
b) The structure of the deficient $BaFe_{2-x}(PO_4)_2$ ($x<\sim0.66$) are fully ordered for particular x values x= 0.29, x=1/3 with creation of novel types of depleted triangular lattices. In

addition we have recently shown that the Fe-extrusion into fully ordered mesoscopic domains can occur even at room temperature, promoted by particular media such as grease.

c) Under flowing H_2/Ar, Fe is reincorporated in the original structure on heating, as reproduced under the electron beam in a transmission microscope.

d) After Fe extrusion the insulating ferromagnetic compound turns into an antiferromagnetic semiconductor, which offers promising perspective for further 2D-lattices created by Fe-extrusion using Fe/M mixed isomorphs (to be presented here as well).

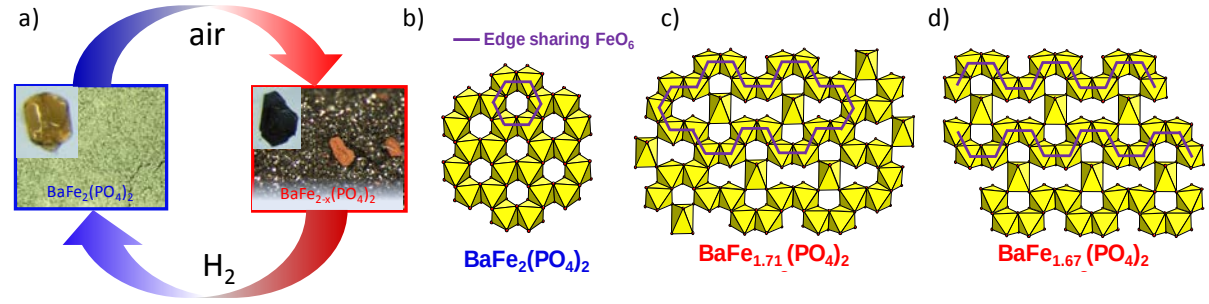

Figure 1: a) physical changes accompanying the Fe-extrusion and modification of the FeO_6 based honeycomb lattice : from the pristine honeycomb lattice (a) to fully ordered Fe-depleted-lattices in x=0.29 (b) and x =0.33.

It follows that this reversibility of this phenomenon opens broad possibilities for the prospect of new inorganic materials, but also for the controlled modification of oxides, e.g. the transformation of insulators into semiconductors, the changes of magnetic couplings …etc. Besides, the general interest of low-D electronic materials and their possible connection to magneto-dependent transport and spintronic specificities, it is worth proposing that the controlled tuning of cationic vacancies rather than the standard modification of the anionic vacancies appears as an innovating alternative to tune *redox* of oxides.

References:

(1) Schöllhorn, R. *et al.*, *Angew. Chem. Int. Ed. Engl.* 19, 983–1003 (1980).
(2) Hamelet, S. *et al.*, *Chem. Mater.* 23, 32–38 (2011).
(3) Hamelet, S. *et al.*, *J. Mater. Chem.* 19, 3979–3991 (2009).
(4) Kondoh, S. *et al.*, *Am. Mineral.* 70, 737–746 (1985).
(5) Lattard, D. *et al. Am., Mineral.* 80, 968–981
(6) Takashi Mikoushi, H. T.*et al.*, *Am. Mineral.* 80, 585–592
(7) Kabbour, H. *et al.*, *Angew. Chem. Int. Ed.* 51, 11745–11749 (2012).
(8) David, R. *et al.*, *J. Am. Chem. Soc.*, 135, 13023–13029 (2013).

Controlling Reactions at Solid-Solid Interfaces: Access to New Materials with Designed Nanoarchitecture

David C. Johnson

Materials Science Institute and Department of Chemistry, University of Oregon, Eugene, Oregon, USA

We have developed a synthetic approach to new materials that uses composition control on an Angstrom length scale to control solid-state reaction pathways (Figure1), leading to the self-assembly of new nanostructured compounds consisting of two or more compounds with different crystal structures that are precisely interleaved on the nanoscale.[1] By avoiding compounds on equilibrium phase diagrams, we have prepared hundreds of new metastable compounds with designed nanostructure, including structural isomers. Many of these materials have unprecedented physical properties, including the lowest thermal conductivities ever reported for a fully dense solid,[2] systematic structural changes dependent on nanostructure,[3,4] and unusual electrical behavior.[5] The designed precursors also enable diffusion to be followed and quantified over distances of less than a nanometer, providing insights to the mechanism that gives control of the nanoarchitecture of the final product. We believe the ability to prepare entire families of new nanostructured compounds and equilibrating them to control carrier concentrations permits a new "thin film metallurgy" or “nanochemistry” in which nanostructure and composition can both be used to tailor physical properties, interfacial structures can be determined for precisely defined constituent thicknesses, and interfacial phenomena and modulation doping can be systematically exploited.

Figure:

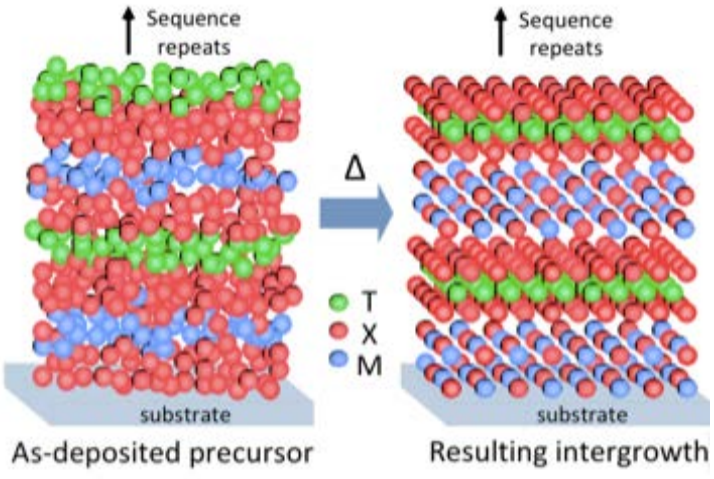

Fig. 1

References:

[1] Colby L. Heideman, Sara Tepfer, Qiyin Lin, Raimar Rostek, Paul Zschack, Michael D. Anderson, Ian M. Anderson, David C. Johnson, “Designed Synthesis, Structure and Properties of a Family of Ferecrystalline Compounds [(PbSe)1.00]m(MoSe2)n“ , *J. Am. Chem. Soc.*, **135** (2013) 11055–11062.

[2] Catalin Chiritescu, David G. Cahill, Ngoc Nguyen, David Johnson, Arun Bodapati, Pawel Keblinski, Paul Zschack, “Ultra-low thermal conductivity in disordered, layered crystals” *Science*, **315** (2007) 351-353.
[3] Michael D. Anderson, Colby L. Heideman, Mary Smeller, Robert Kykyneshi, Andrew A. Herzing, Ian M. Anderson, Douglas A. Keszler, Paul Zschack, David C. Johnson, “Size-Dependent Structural Distortions in One Dimensional Nanostructures“, *Angew, Chemie Int. Ed.*, **52** (2013) 1-5.
[4] Matt Beekman, Sabrina Disch, Sergei Rouvimov, Deepa Kasinathan, Klaus Koepernik, Helge Rosner, Paul Zschack, Wolfgang S. Neumann, David C. Johnson, "Controlling size induced phase transformations using chemically designed nanolaminates," *Angew. Chem. Int. Ed.*, **52** (2013) 13211 –13214.
[5] Daniel B Moore, Matt Beekman, Sabrina Disch, David C. Johnson, "Synthesis and Structural Characterization of the First Telluride Misfit Layer Compounds: $[(PbTe)_{1.17}]_m(TiTe_2)_{n"}$, *Angew. Chem. Int. Ed.*, **52** (2014) accepted.

Mechanical Effects in Dynamic Crystals – A Revival

Panče Naumov

New York Univesrsity Abu Dhabi, Abu Dhabi, United Arab Emirates

The classical perception of single crystals of molecular materials as rigid and brittle entities has downsized the research interest in mechanical effects that had been initiated and was active back in the 1980s. More recently, the modern analytical techniques for mechanical, electron-microscopic, structural, spectroscopic and kinematic characterization have contributed to accumulate compelling evidence that under certain circumstances, even some seemingly rigid single crystals can deform, bend, twist, hop, wiggle or perform other 'acrobatics' that are atypical for non-soft matter. These examples contribute to a paradigm shift in our understanding of the elasticity of molecular crystals and also provide direct mechanistic insight into the structural perturbations at the limits of the susceptibility of ordered matter to internal and external mechanical force. As the relevance of motility and reshaping of molecular crystals is being recognized by the crystal research community as a demonstration of a very basic concept—conversion of thermal or light energy into work—a new and exciting crystal chemistry around mechanically responsive single crystals rapidly unfolds.

References:

[1] Naba K. Nath, Manas K. Panda, Subash C. Sahoo, Pance Naumov, *CrystEngComm* **16** (2014) 1850 (review).

Figure:

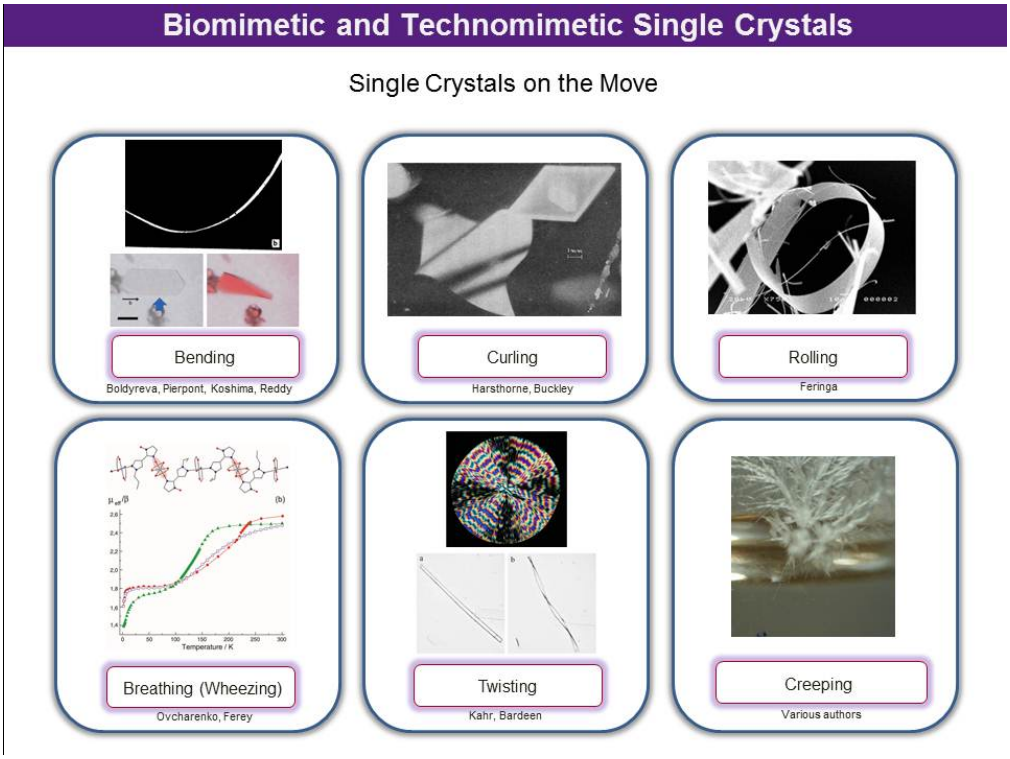

Development of novel borides, silicides, sulfides, and oxides, as effective thermoelectric materials through particular features of crystal structure

Takao Mori,[a,b]

[a] National Institute for Materials Science (NIMS), Tsukuba 305-0044, Japan;
[b] University of Tsukuba, Tsukuba 305-8671, Japan.

Approximately two thirds of all primary energy (fossil fuels, etc.) being consumed in the world, sadly turns out to be unutilized, with much of it being waste heat. The direct conversion of waste heat to electricity is a large incentive to find viable thermoelectric (TE) materials and efforts worldwide are intensifying [1]. One need exists to develop TE materials which can utilize high temperature unutilized/waste heat in thermal power plants, steelworks, factories, and incinerators, etc. We have been focused on developing novel mid to high temperature thermoelectric materials through focusing on particular features of the crystal structure. I will give an overview on this strategy, which has yielded promising systems in the medium to high temperature range on materials based on novel borides, silicides, oxides, and sulfides.

Particular network structures engender intrinsic low thermal conductivity, an inherent advantage for TE application. Rattling is well known in cage compounds [2], but several novel mechanisms [3,4] have become clear like boron dumbbells (Fig. 1) and "building defects" in layered borides (Fig. 2) [5].

Doping into the voids and framework of boron cluster compounds are powerful routes to control the thermoelectric properties. For example, through transition metal doping into the voids, α of $YB_{22}C_2N$, the potential n-type counterpart to boron carbide, could be increased by 220% while electrical resistivity was simultaneously reduced by more than 100 times [6]. Carbon substitution into the framework was also shown to be effective. Recently, excellent ($|\alpha|>200$ μV/K) p-type or n-type characteristics could be controlled in $Y_{\sim 0.6}Al_yB_{14}$ by varying occupancy of the Al site (Fig. 3) [7]. This is p, n control with same crystal structure (i.e. good matching) and no necessity for doping of foreign elements (i.e. no migration problems). The discovery is surprising, since in metal borides, the metal site occupancies are typically with small homogeneity region. Theoretical investigations reveal the stable configuration of the atomic sites and density of states variation behind the thermoelectric properties.

The borosilicide $RB_{18}Si_5$ which has notable silicon and boron bonding, was also synthesized in large amounts for the first time with a one-shot sintering utilizing SPS. The thermoelectric properties reveal that this is a p-type boride with large Seebeck coefficients at high temperatures. Boron sulfide B_6S_{1-x} also exhibits large Seebeck coefficients with indications that this can be a much lower processing temperature replacement to boron carbide, one of the few TE materials previously commercialized [8]. Hole-doped $CuFeS_2$ has shown enhanced thermoelectric properties proposed to be due to magnetic interactions [9]. A homologous Ga-Zn-O with novel structure is a new n-type oxide which has low thermal conductivity and good thermoelectric performance at least as good as the well studied IZO [10]. I will present further results on SPS processed samples.

References:

[1] *Thermoelectric Nanomaterials,* ed. K. Koumoto and T. Mori, Springer Series in Materials Science (Springer, Heidelberg, 2013) pp. 1-373.
[2] I. Ishii, Y. Suetomi, T. K. Fujita, K. Suekuni, T. Tanaka, T. Takabatake, T. Suzuki, M. A. Avila, Phys. Rev. B, 85, 085101 (2012).
[3] T. Mori, J. Martin, and G. Nolas, J. Appl. Phys., 102, 073510 (2007).
[4] T. Mori, in *Modules, Systems, and Applications in Thermoelectrics*, ed. D. M. Rowe, (CRC Press, London, 2012) 14.
[5] X. J. Wang *et al.*, "Thermal Conductivity of Layered Borides: the Effect of Building Defects on the Thermal Conductivity of $TmAlB_4$ and the Anisotropic Thermal Conductivity of AlB_2" submitted to APL Materials.
[6] A. Prytuliak, S.Maruyama, and T. Mori, Mat. Res. Bull., 48, 1972 (2013).
[7] T. Mori *et al.*, Patent application (2012), S. Maruyama *et al.*, Appl. Phys. Lett. 101, 152101 (2012).
[8] O. Sologub, Y. Matsushita, and T. Mori, Scripta Mater. 68, 288 (2013).
[9] N. Tsujii and T. Mori, Appl. Phys. Express, 6, 043001 (2013). Selected as a SPOTLIGHT
[10] Y. Michiue, T. Mori, A. Prytuliak, Y. Matsushita, M. Tanaka, and N. Kimizuka, RSC Advances, 1, 1788 (2011).

Figures:

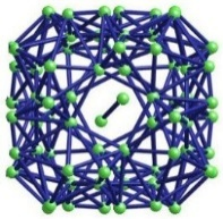

Fig. 1: B dumbbell in B_{80} cluster of RB_{66}

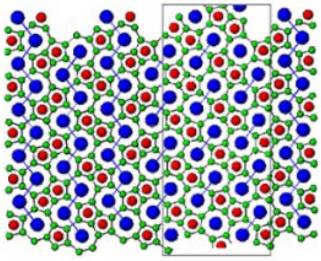

Fig. 2: β-type building defect in α-$TmAlB_4$

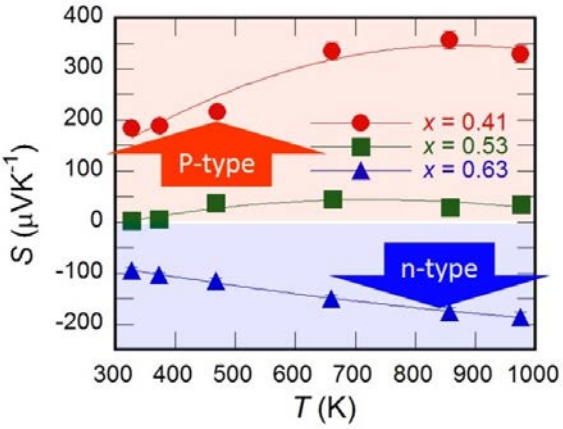

Fig. 3: Seebeck coefficient of $Y_{0.56}Al_xB_{14}$

Solid state electrochemistry: a tool for synthesis and characterization of solids

C. Delmas, M. Guignard, D. Carlier and J. Darriet
ICMCB-CNRS, Université de Bordeaux,
87, av. Dr. Schweitzer, 33608 Pessac, France

Researches on battery materials has considerably increased during the last 30 years due to the huge development of lithium-ion batteries for portable devices (laptops, cellular phones, …) and more recently with the need to store energy in order optimize its consumption. The next goal is the development of batteries for electric vehicles and their use into the grid. Nevertheless, the aqueous batteries (Ni-Cd, Ni-MH and Lead Acid) are always used in numerous applications thanks to their low price. In most of the batteries, the intercalation (deintercalation) of monovalent cations (H^+, Li^+, Na^+) and electrons is the basic electrochemical reaction. The cell voltage is equal to the difference in Fermi level between the two electrodes. If one electrode exhibits a constant voltage it can acts as reference and therefore, the cell voltage reflects all structure modifications which occurs on the material upon intercalation. Fig. 1 gives the change in the cell voltage when the process occurs through a solid solution. The change is cell voltage depends on: (i) the electronic band filling, (ii) the change in the band structure due to change in composition, (iii) the modification of the Magdelung energy. In the schematic example reported in Fig. 1 the monotonous decreases of the voltage during the intercalation reaction indicates that the reaction occurs through a monophasic domain. In numerous cases, the reaction mechanism is more complicated and involves biphasic domains and/or formation of materials with a specific composition. The voltage vs composition curve is much more complicated and gives directly the phase diagram on the studied system. Fig. 2 gives the cycling curve obtained from the P2-$Na_{0.73}VO_2$ phase.

For the solid state chemist the studies of the electrochemical reaction using a battery open new possibility to determine phase diagram at RT, but also to synthesize new metastable phases from a precursor made by classical solid state chemistry.

In this presentation we report here about the Na_xVO_2, systems with a special focus on the phase diagram. Depending on the composition and the experimental conditions O3 or P2 structures are obtained for the layered starting phases. The structures of all starting materials were determined by Rietveld refinement of their X-Ray diffraction patterns. As the transformation between O3 and P2 structural types would require M-O bond breaking, the O3 and P2 systems present different behaviors although they have the same chemical formulae.

The electrochemical study was carried out in sodium batteries with a solution of $NaClO_4$ or $NaPF_6$ in propylene carbonate as electrolyte. For all materials, a very good reversibility of the electrochemical process was observed. In all systems at least 0.5 Na can be cycled that corresponds to a capacity higher than 130 mAh/g of active material.

Three different phases were obtained for the $Na_{1/2}VO_2$ composition depending of the packing of the starting material. These phases exhibit very similar sodium ordering in the interslab space but very different vanadium ordering in the VO_2 slab. Depending on the oxygen packing the vanadium ions can be isolated or can form pairs or trimers within the VO_2 slab.
A general overview of the properties of these materials will be presented with a special focus on the structures and the properties.

References:
[1] Marie Guignard, Christophe Didier, Jacques Darriet, Pierre Bordet, Erik Elkaïm and Claude Delmas, Nature Mat ; **12**,74 (2013)

Figures:

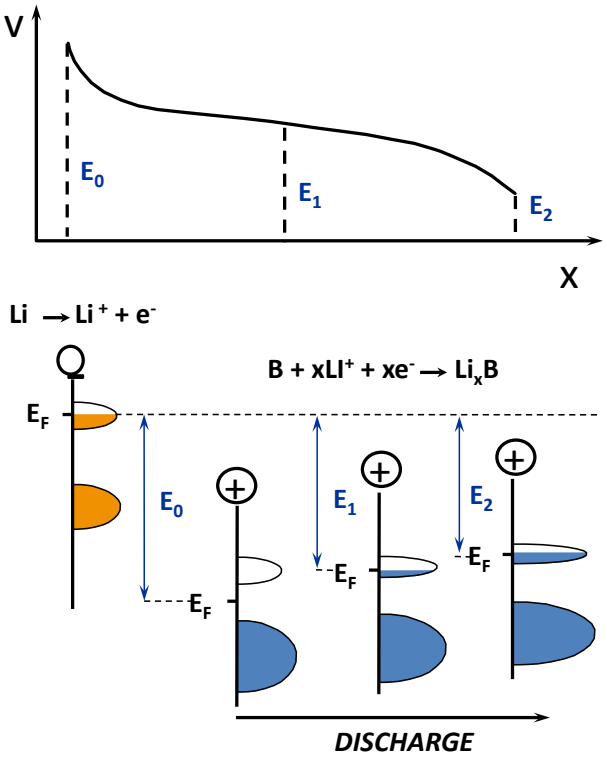

Fig. 1. Changes in the Fermi level during Li intercalation via a solid solution

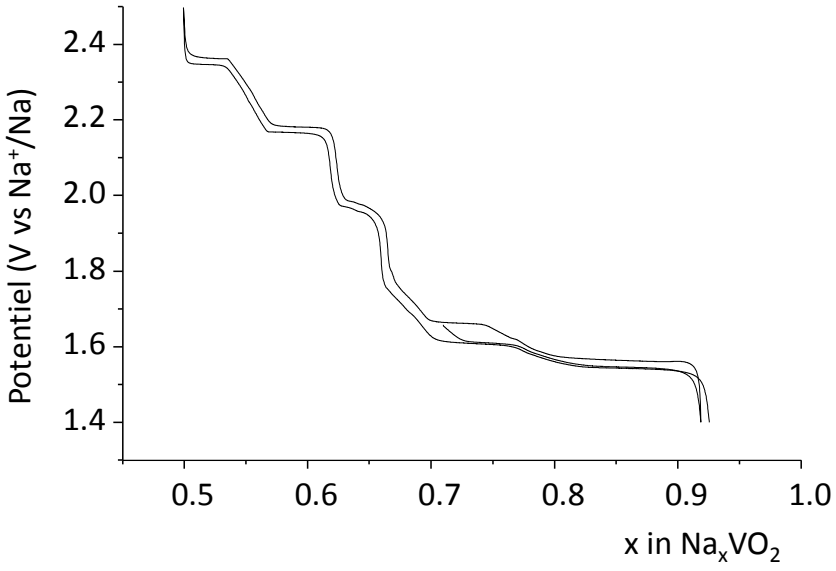

Fig. 2. Cycling curve of the P2-Na_xVO_2 phase

Is there a general reaction pathway for Li insertion into cubic spinel materials?

Wolfgang Bensch,[a] Stefan Permien,[a] Sylvio Indris[b]

[a]Institute of Inorganic Chemistry, University of Kiel, Max-Eyth-Straße 2, 24118 Kiel, Germany
[b 2]Institute for Applied Materials – Energy Storage Systems, Karlsruhe Institute of Technology, P.O. box 3640, 76021 Karlsruhe, Germany

The classical chemical reactions in Li-based batteries are intercalation and deintercalation of Li into a host material during the discharge and charge processes. The crystal structure of the host is only slightly affected during the reactions and remains almost intact during cycling [1, 2]. An attractive alternative is the so-called conversion reaction in which an electrode material with general formula TMQ_y (TM = metal; Q = anion) is consumed by Li and reduced to the metal TM and a corresponding Li compound according to the equation
$TM_xQ_y + 2y\ e^- + 2y\ Li^+ \leftrightarrow x[TM]^0 + yLi_2Q$

For such conversion reactions specific capacities larger than 500 $mAhg^{-1}$ can be achieved because 2y/x Li ions can be converted per TM ion [3]. In addition, the capacity can be tuned by selecting compounds with TM ions in high oxidation states and the strength of the metal-oxygen bond determines the potential of a battery cell. Cubic spinel materials with general formula AB_2Q_4 (A = Mg, Co, Cu, Mg, Ni, Zn, Mn etc.; B = Cr, Mn, Fe, Co etc.; Q = O, S, Se) are attractive candidates for conversion reactions due to the pronounced compositional flexibility. Many spinels contain earth abundant and cheap elements and some are also environmentally more benign than e.g. Co. In the first study of Li insertion into a spinel (Fe_3O_4) it was proposed that at a critical Li concentration the Fe^{3+} ions on the tetrahedral 8a site are cooperatively displaced to empty octahedral 16 c sites and the end composition corresponds to the partially ordered rocksalt phase $Li_1Fe_3O_4$ with all Fe and Li ions located on octahedral sites [4]. In a recent study on the Li insertion into nanosized partial inverse $MnFe_2O_4$ applying a variety of analytical techniques like in-situ Quick EXAFS, X-ray diffraction, Mössbauer spectroscopy, HRTEM, ^{7}Li-MAS NMR, and electrochemical measurements we were able to formulate a detailed reaction mechanism [5]. At the beginning of Li insertion Fe^{3+} on 8a site is reduced and is displaced to the empty 16 c site. All results suggest that only a very small amount of Li is intercalated. For 0.7 Li per $MnFe_2O_4$ further Fe^{3+} is reduced and Mn^{2+} being located on the 8a site moves to empty octahedral sites thus forming a defect NaCl-type structure. The X-ray powder pattern for 2 Li per $MnFe_2O_4$ demonstrate the disappearance of the spinel and only reflections of a monoxide with rocksalt structure are observed. For larger Li contents a conversion into nanosized metal particles dispersed in a Li_2O matrix occurs. In a further study the reaction mechanism between Li and $MgFe_2O_4$ was investigated. Figure 1 shows a sequence of X-ray powder patterns recorded at different Li concentrations. With increasing Li content per formula unit the intensity of the reflections decrease while new reflections start to appear and become more intense during Li insertion. The pattern for 2 Li per $MgFe_2O_4$ can be refined assuming a monoxide with the NaCl-type structure. Increasing the amount of Li leads to a successive disappearance of the reflections of the monoxide.

In the talk results of our investigations on the reaction mechanisms of Li insertion into different cubic spinel materials are presented and discussed.

References:

[1] John B. Goodenough, *J. Solid State Electrochem*., **16** (2012) 2019.
[2] John B. Goodenough, Youngsik Kim, *Chem. Mater*., **22** (2010) 587.
[3] P. Poizot, S. Laruelle, S. Grugeon, J.-M. Tarascon, *J. Electrochem. Soc.*, **149** (2002) A1212.
[4] M.M. Thackeray, W.I.F. David, John B. Goodenough, *Mat. Res. Bull*., **17** (1982) 785.
[5] Stefan Permien, Holger Hain, Marco Scheuermann, Stefan Mangold, Valeriu Mereacre, Annie K. Powell, Sylvio Indris, Ulrich Schürmann, Lorenz Kienle, Viola Duppel, Svenja Harm, Wolfgang Bensch, *RSC Adv*., **3** (2013) 23001.

Figure:

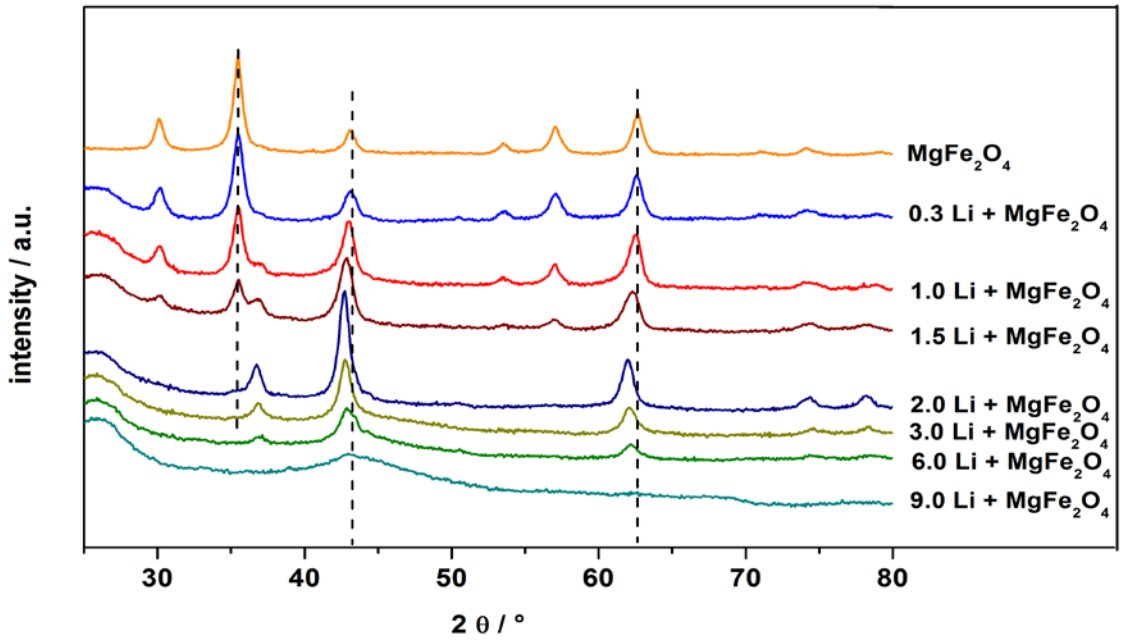

Fig.1. X-ray powder patterns recorded for different Li concentrations during reaction of Li with $MgFe_2O_4$.

Design and Optimization of Crystalline Hybrid Materials for Use in Rare-Earth Free WLEDs

Jing Li, Xiao Zhang, Wei Liu, Qihan Gong, Zhichao Hu, Debasis Banerjee, George Z. Wei, Yang Fang

Department of Chemistry and Chemical Biology
Rutgers University, Piscataway, NJ 08854, USA

Solid state lighting (SSL) technologies, primarily light emitting diodes (LEDs) and organic light emitting diodes (OLEDs), are rapidly developing in recent years. The main advantages of SSL, compared to conventional lighting sources, are lower energy consumption, higher efficiency, and longer lifetime.[1] White light emitting diodes (WLEDs) are of particular interest because of the great need in general lighting and illumination applications. Common approaches to fabricate WLEDs include blending of three primary colored LED chips, namely red (R), green (G), and blue (B) or RGB diodes, or combination of a blue (or UV) LED with a yellow or white phosphor or multi phosphors. At the present time, commercially available WLEDs are predominantly phosphor based (e.g. a yellow emitting phosphor YAG:Ce^{3+} coupled with a blue emitting InGaN/GaN diode). However, supply shortage for rare earth metals, specially europium, terbium, and yttrium may seriously impede the future growth of SSL technologies.[2-4] To resolve this problem, it is vital to develop new types of phosphor materials that are free of REEs. A number of REE-free white-light phosphors have been reported, including organic molecules and inorganic nanomaterials.[5-9] But all of them suffer from either low luminous efficiency or high cost, or both.

Since our first discovery of II-VI based $Cd_2S_2(L)$ (L = organic monoamines) white phosphors,[10] we have made significant progress to improve their quantum yields (QYs), from the initial 3-4% to the current >40%, an increase of more than 10 times.[11] Very recently, we have also expanded our research to explore several other hybrid material classes. By systematically controlling dimensionality of the crystal structures and changing chemical composition of the compounds, we have successfully developed a number of yellow and white phosphors by simple and cost effective solution synthesis. The high quantum yield and optimum color quality, coupled with solution processability, make them highly promising for use as REE free phosphors in WLEDs.

References:

1. a) *Worldwide Trends in Energy Use and Efficiency;* International Energy Agency: Paris, France 2008; b) *Solid-State Lighting* http://ssls.sandia.gov/; c) U.S. department of energy http://www1.eere.energy.gov/buildings/ssl/; d) A. Bergh, G. Craford, A. Duggal, R. Haitz, *Phys. Today* **2001**, *54*, 42-47.
2. http://energy.gov/sites/prod/files/DOE_CMS2011_FINAL_Full.pdf (CRITICAL MATERIALS STRATEGY, U.S. DEPARTMENT OF ENERGY, DECEMBER 2011).
3. The Principal Rare Earth Elements Deposits of the United States - A Summary of Domestic Deposits and a Global Perspective, Scientific Investigations Report 2010-5220, U.S. Department of the Interior, U.S. Geological Survey.
4. N. D. Hensel "Economic Challenges in the Clean Energy Supply Chain: The Market for Rare Earth Minerals and Other Critical Inputs", *Business Economics*, **2011**, *46*(3), 171-184.

5. Abbel, R.; Grenier, C.; Pouderoijen, M. J.; Stouwdam, J. W.; Leclere, P. E. L. G.; Sijbesma, R. P.; Meijer, E. W.; Schenning, A. P. H. J. *J. Am. Chem. Soc.* **2009**, 131, 833.
6. Adhikari, R. M.; Duan, L.; Hou, L. D.; Qiu, Y.; Neckers, D. C.; Shah, B. K. *Chem. Mater.* **2009**, 21, 4638.
7. Ner, Y.; Grote, J. G.; Stuart, J. A.; Sotzing, G. A. *Angew. Chem. Intern. Ed.* **2009**, 48, 5134.
8. Park, S.; Kwon, J. E.; Kim, S. H.; Seo, J.; Chung, K.; Park, S. Y.; Jang, D. J.; Medina, B. M.; Gierschner, J.; Park, S. Y. *J. Am. Chem. Soc.* **2009**, 131, 14043.
9. Vanithakumari, S. C.; Nanda, K. K. *Adv. Mater.* **2009**, 21, 3581.
10. Ki, W.; Li, J. *J. Am. Chem. Soc.*, **2008**, *130*, 8114-8115.
11. Roushan, M.; Zhang, X.; Li, J., *Angew. Chem. Int. Ed.*, **2012**, *51*, 436-439.

Oxide nanosheets as water splitting catalysts: a structural perspective

Scott T. Misture

Kazuo Inamori School of Engineering, Alfred University, Alfred, New York, USA

$Bi_2NaCaNb_3O_{12}$ (BCNN) is an Aurivillius phase with $[Bi_2O_2]^{2+}$ sheets interleaved between perovskite-like layers (Fig. 1). Topochemical conversion to the protonated form may be achieved using simple acid treatment that removes the $[Bi_2O_2]^{2+}$ sheets, protonates the perovskite sheet surfaces, and introduces interlayer water. Subsequent exfoliation of the ion-exchanged phase then yields suspensions of nanosheets that can be used as photocatalysts, or re-assembled with themselves or with particles to make composite photocatalysts. The process is generally applicable and we demonstrate the ability to make nanosheet catalysts with 2, 3, 4 or even 5 octahedral layers. Furthermore, we have developed a new process to exfoliate the protonated forms using a chemomechanical approach, without the aid of organic exfoliating agents. Therefore, our niobate nanosheets are pristine, without adsorbed organics. The nanosheet suspensions demonstrate remarkably high photocatalytic activity for water splitting to produce H_2, ranging from 20,000-44,000 μmol/h/g with no added cocatalyst. In contrast, the photoactivity of the proton-exchanged form is some 50 times lower. The structural and electronic origins of the remarkable photoactivity of the pristine nanosheets remain poorly understood.

Powder XRD data for protonated BCNN suggest stacking disorder that differs from turbostratic disorder in the proton-exchanged form. Multiple models were used to fit the XRD data. Of these, only models which allow incommensurate shifts along the a-b plane of the perovskite sheets, along with varied interlayer spacings, can successfully describe the data. Optimized models show that the interlayer shifts between successive perovskite blocks are centered on the expected commensurate value (0.25 along *a*- and *b*-axes) but with a broad distribution. Likewise, the absolute interlayer spacings show a broad distribution, ranging from 1.80 to 4.13Å, with an average value of 2.37(53)Å, yielding physically-reasonable oxygen-oxygen distances. On average, one H_2O per formula unit can be accommodated in the interlayer galleries in the superstructure model, but again with a wide distribution from layer to layer.

Additional structure characterization using neutron total scattering provides the first direct evidence that ferroelectric structure distortions in the parent phase are maintained in the exfoliated nanosheets. Optically, nanosheets in aqueous suspension and wet ion-exchanged BCNN show strong near band edge emissions at 350 nm, which is quenched after air drying to remove the labile water. Dry proton ion-exchanged BCNN fluoresces red light with an exceedingly sharp and intense emission at 692 nm. Detailed modeling of inelastic neutron scattering (INS) data indicates that water reversibly physisorbs to surface Nb-OH sites to functionalize the nanosheets, suggesting that adsorbed water functionalizes the nanosheets. Furthermore, the INS study provides a picture of the surface structure, with protons terminating most surface oxygens, and dynamically exchanging with Zundel cations, ($H_5O_2^+$ ions), with the remaining surface sites coordinated by free water constrained by adsorption to act as a surface ligand. In combination, the data indicates that the off-centered Nb ions within the nanosheets provide internal electric fields to promote charge separation and increase the photoreaction rate. It is interesting to note that the high photoreaction rates are not typical for

oxides without a cocatalyst, suggesting that the nanosheets have very different surface properties than bulk materials that facilitate long-lifetime excited states.

The nanosheets may also be re-assembled to form 2-D and 3-D structures, where the porous 3-D assemblies likewise show very high photoreaction rates. Figure 1 shows an overview of the various catalyst forms.

Figures:

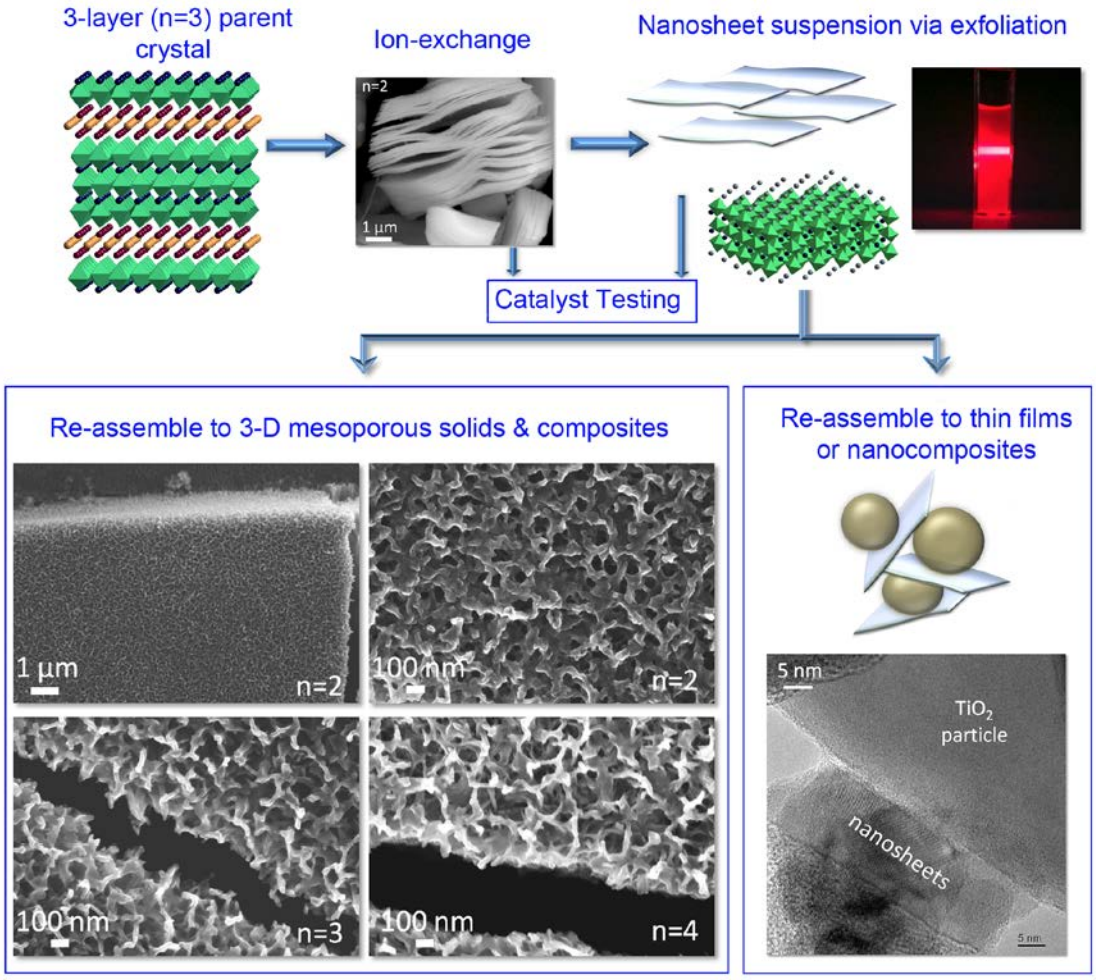

Fig. 1. Overview of the ion-exchange, exfoliation, and re-assembly processes to produce nanosheet suspensions, nanosheet-particulate composites, and 3-D mesostructures from the parent Aurivillius phase $Bi_2A_{n-1}B_nO_{3n+3}$.

Redox reactions for preparation of intermetallic compounds

Yuri Grin

Max-Planck-Institut für Chemische Physik fester Stoffe, Dresden, Germany

Traditionally, intermetallic compounds are prepared by direct interaction of the elements, which can be realized in form of the homophase reaction (in melt or in solid state) or of the heterophase reaction (solid-liquid, in particular for the single crystal preparation). Full understanding of the composition, structural features and – as a consequence - creation of the new preparation routes to the intermetallic compounds requires re-consideration of the traditional chemical tools like oxidation numbers and their application to this group of inorganic materials. The concept of the electron localizability is employed to understand chemical bonding in intermetallic compounds and get new access to their chemistry. Utilizing the oxidation of chemically active intermetallic phases, a new way to prepare intermetallic clathrates was developed. Applying heterophase liquid-solid or gas-solid processing and depending on the process condition it may lead to an 'empty' clathrate – a new modification of elements of the group 14, e.g. germanium [1], or to metastable clathrate-I or clathrate-II phases [2,3]. Ionic liquids used as the reaction medium are also participating in the reaction with complex mechanisms including several organic intermediates [4]. Redox reactions leading to new intermetallic compounds can be performed as solid-solid process under high pressure as this was shown for Cs_8Ge_{44-x} [5]. Another route to obtain new clathrate phases is application of electrical field, e.g. using the spark-plasma technique and separation different subreactions within the reactor space [6,7].

The so-obtained intermediate phases are often metastable and decompose at elevated temperatures passing several non-obvious stages. So the clathrate-I $Ba_{6.2}Si_{46}$ - synthesized by oxidation of $Ba_4Li_2Si_6$ with gaseous HCl [2] – undergoes complex structural rearrangement by increasing temperature including Ba redistribution between different cages along with the formation of vacancies within the silicon framework [8].

References:

[1] A. M. Guloy et al. *Nature* **443** (2006) 320.
[2] Y. Liang et al. *Inorg. Chem.* **50** (2011) 452.
[3] P. Simon et al. *J. Am. Chem Soc.* **133** (2011) 7596.
[4] B. Böhme et al. *Z. Naturforsch. B* **66** (2011) 230.
[5] I. Veremchuk et al. *Z. Anorg. Allg. Chem.* **637** (2011) 1281.
[6] M. Beekman et al. *J. Am. Chem. Soc.***131** (2009) 9642.
[7] I. Veremchuk et al. *Inorg. Chem.* **52** (2013) 4458.
[8] Y. Liang et al. *J. Phys. Chem. Solids* **74** (2013) 225.

Thermoelectric oxides and sulfides: understanding the structure property relationships

A. Maignan,[a] E. Guilmeau,[a] D. Berthebaud,[a] R. Daou,[a] and S. Hébert [a].

[a] Laboratoire CRISMAT UMR 6508 ENSICAEN/CNRS, ENSICAEN, UCBN
6 boulevard du Maréchal Juin, 14050 Caen cedex 4 – France
antoine.maignan@ensicaen.fr

Strongly correlated systems have attracted much interest for thermoelectricity. In particular, the different physics of transition metal oxides, as compared to that of degenerate semiconductors as the Bi_2Te_3 prototypical thermoelectric material, leads to an unusual T dependence for the Seebeck coefficient (S) as illustrated for ruthenates and layered cobaltites [1]. Magnetic ordering can also play a role on S as demonstrated in several ruthenates derived from the $SrRuO_3$ perovskite (quadruple perovskites and $La_{3.5}Ru_4O_{13}$ [2]). Despite that magnetism plays a role, the power factor (PF) of all these magnetic oxides ($PF=S^2/\rho$, where ρ is the electrical resistivity) remains too limited, with $PF_{300K}\sim10^{-4}W.K^{-2}.m^{-1}$. This motivated the study of more covalent materials such as sulfides (and selenides).

Higher PF value, $PF_{300K}\approx10^{-3}W.K^{-2}.m^{-1}$, is reached in the CoS_2 itinerant ferromagnet, a ceramic sample densified by SPS [3]. However, its 3D pyrite structure leads to a too high thermal conductivity ($\kappa_{300K}\sim10W.K^{-1}.m^{-1}$). In that respect, the 2D structures, offer the possibility to tailor the thermal conductivity. For that purpose, chemical intercalations and substitutions in TiS_2 have been performed for both dense ceramics and crystals [4-7]. Intercalations between two successive TiS_2 slices, by Cu or Co ions [4, 7], lead to a strong reduction of the lattice part of κ. Similar effects are reached by substitutions at the Ti or S sites [5, 6].

In the crystals case, different growth routes have allowed us to compare the effect of Co intercalation ($Co_{0.04}TiS_2$) with the composite effect of CoS_2 dots deposited on the TiS_2 crystal surface [$(CoS_2)_{0.04}TiS_2$] and also with the effect of self-doping according to the $Ti_{1+x}S_2$ formula [7]. It is expected that the phonon glass limit could be reached in these layered materials as found in the $AgCrSe_2$ layered selenide [8], a zT=1 at 800K thermoelectric material.

References:

[1] For a review, S. Hébert, W. Kobayashi, H. Muguerra, Y. Bréard, N. Ragavendra, F. Gascoin, E. Guilmeau and A. Maignan, *Phys. Status Solidi A*, **210**, (2013) 69.
[2] S. Hébert, D. Pelloquin and A. Maignan, *submitted*.
[3] S. Hébert, E. Guilmeau, D. Berthebaud, O.I. Lebedev, V. Roddatis and A. Maignan, *J. of Appl. Phys.* **114** (2013) 103703.
[4] E. Guilmeau, Y. Bréard and A. Maignan, *Appl. Phys. Lett*. **99** (2011) 052107.
[5] F. Gascoin, N. Raghavendra, E. Guilmeau and Y. Bréard, *J. Alloys. Compd*. **521**, (2012) 21.
[6] M. Beaumale, T. Barbier, Y. Bréard, S. Hébert, Y. Kinemuchi and E. Guilmeau, *J. of Appl. Phys*., **115** (2014) 043704.
[7] R. Daou, H. Takahashi, S. Hébert, M. Beaumale, E. Guilmeau and A. Maignan *(submitted)*.
[8] F. Gascoin and A. Maignan, *Chem. Mater.* **23** (2011) 2510.

Soft Chemistry Approach to Materials Synthesis

Evgeny V. Dikarev[a]

[a]Department of Chemistry, University at Albany, SUNY, Albany, NY, USA

Conventional routes to mixed-metal materials are based on direct solid state reactions of simple metal compounds and often require high temperature/high pressure processes. In the recent years, a broad variety of synthetic procedures to obtain the desired products under mild conditions have been developed. Those received the common name of *Soft Chemistry (Chimie Douce)* approach, and can be divided into three general categories: (1) chemical vapor deposition (CVD) and atomic layer deposition (ALD); (2) solution deposition, such as sol-gel technology and metal-organic decomposition (MOD); (3) physical vapor deposition, including radio-frequency and magnetron sputtering, ion beam sputtering, molecular beam epitaxy, and laser ablation. The majority of these techniques involve the application of metal complexes with organic ligands, which are easily hydrolytically or thermally decomposable substances usually referred to as *Molecular Precursors*.

The interest in materials that incorporate more than one type of metal atoms has brought a great need for *Single Source Precursors* (SSP) – molecules containing all the necessary elements in the proper ratio and decomposable in a controllable manner under mild conditions. Single-source precursors are known to have significant advantages over the mixtures of homometallic complexes (*Multi-Source Precursors*): (i) homogeneity at the molecular level as a consequence of the intimate mixing of the elements in a single molecule that diminishes diffusion problems in the following reaction steps; (ii) easier control of the stoichiometry, at least for simple compositions; (iii) limiting the chances of pre-reactions in the gas phase and overcoming the problem of differences in thermal behavior or chemical incompatibility of the different precursors; (iv) formation of crystalline materials at significantly lower temperatures, which opens broad opportunities for synthesizing new multimetallic phases that do not exist at higher temperatures; (v) more flexibility in preparation of functional materials, since the single source precursors can be used with both spin-casting techniques to grow thin films and with thermolytic/hydrolytic procedures to form discrete crystallites.

Our group has developed a new class of *heterometallic main group/transition metal β-diketonates* [1-4] that can be used as effective single-source precursors in preparation of functional materials. In the course of this work we focus on *volatile precursors* that are suitable for MOCVD preparation of thin films and nanocrystals. We design heterometallic complexes that are stable, resistant to hydrolysis and exhibit clean, low-temperature decomposition pattern as well as *proper metal:metal ratio* for the desired material. Heterometallic diketonates were shown to be universal precursors that can be employed in the preparation of a wide variety of materials: oxides, silicates, fluorides, and phosphates. Heterometallic molecules are also explored for the synthesis of new prospective materials that cannot be obtained by conventional solid-state synthesis. The potential of the single-source precursor approach and its advantages over conventional synthetic methods as well as over multi-source precursor technique will be presented.

References:

[1] Anantharamulu Navulla, Alexander A. Tsirlin, Artem M. Abakumov, Roman V. Shpanchenko, Haitao Zhang, Evgeny V. Dikarev *J. Am. Chem. Soc.*, **133** (2011) 602.
[2] Anantharamulu Navulla, Lan Huynh, Zheng Wei, Alexander S. Filatov, Evgeny V. Dikarev *J. Am. Chem. Soc.*, **134** (2012) 5762.
[3] Zheng Wei, Alexander S. Filatov, Evgeny V. Dikarev *J. Am. Chem. Soc.*, **135** (2013) 12216.
[4] Zheng Wei, Haixiang Han, Alexander S. Filatov, Evgeny V. Dikarev *Chem. Sci.*, **5** (2014) 813.

Coordination-Selective Transition Metal Intercalation in a Layered Telluride

Hiroshi Kageyama,[a]

[a]Graduate School of Engineering, Kyoto University

Layered oxides, chalcogenides and halides embrace rich intercalation reactions to accommodate high concentrations of foreign species within their structures, and find a variety of applications spanning from energy storage, ion exchange to secondary batteries. Light alkali metals are generally most easily intercalated or ion-exchanged due to their light mass, high charge/volume ratio, and in many cases strong reducing properties. An evolving area of materials chemistry, however, is to capture metals selectively which is of technological and environmental significance but rather unexplored [1, 2]. Here we show that some layered telluride displays exclusive insertion of transition metals (Zn, Cd, Cu, Fe, Me) [3] as opposed to alkali cations, with tetrahedral coordination preference to tellurium. Interestingly, the intercalation reactions proceed in solid state and at surprisingly low temperatures (e.g. 80 °C for elemental cadmium). The new method of controlling selectivity provides opportunities in the search for new materials for various applications.

References:

[1] M. J. Manos et al., *Proc. Natl. Acad. Sci. USA* **105**, 3696 (2008).
[2] N. Ding and M. G. Kanatzidis, *Nat. Chem.* **2**, 187 (2010).
[3] T. Yajima *et al*., submitted.

Topochemical reactions for the Construction of Metal-Nonmetal Arrays within Perovskite Hosts

Lea Gustin, Dariush Montasserasadi, Elisha Josepha, and John B. Wiley

Department of Chemistry and Advanced Materials Research Institute
2000 Lakeshore Dr., University of New Orleans, New Orleans, LA USA 70148

Ion exchangeable layered perovskites of the Dion-Jacobson (DJ) and Ruddlesden-Popper (RP) structure types have been effectively explored by many researchers as platforms for the creation of new compounds under mild conditions. Topochemical reaction strategies based on these starting materials have led to a series of new compounds with varied structural and cooperative properties. Our efforts in this area have sought to build metal-nonmetal arrays within the various hosts. Multistep reactions involving sequential intercalation of DJ perovskites have resulted in new metal-halide and metal-chalcogen-hydride arrays while in the RP systems, reactions based on ion exchange have been exploited to make a series of new transition metal compounds. Details on the synthesis and characterization of these compounds will be presented and the future of topochemical reaction strategies discussed.

Significance of Defect Chemistry for Reactivity of Solids

Joachim Maier

Max Planck Institute for Solid State Research, Stuttgart, Germany, s.weiglein@fkf.mpg.de

As the point defects in solids are the most reactive and most mobile species in a given solid, it is their “chemistry” that needs to be understood as far as reactivity of solids is concerned.

The contribution essentially deals with two complementary examples: oxygen reduction involving oxides and peroxides at high temperatures, and lithium storage in oxides and sulfides at room temperature.

While in both cases the overall kinetics is determined by local chemical kinetics as well as by transport steps, the charge carrier chemistry is different because of the different temperature regimes. Unlike the high temperature situation, the room temperature situation is rather characterized by interactions, frozen-in situations and ordering effects.

The contribution sets out the various parameters with the help of which the charge carrier chemistry can be influenced. Two of these parameters that deserve special attention, are size and phase complexity. Recent examples from the contexts of fuel cells and Li/Na-based batteries show the power of these morphological tools.

High-pressure research in relation to reactivity of solids

E.V. Boldyreva[a,b]

[a] Novosibirsk State University, Novosibirsk, Russia;
[b] Institute of Solid State Chemistry and Mechanochemistry SB RAS, Novosibirsk, Russia.

Temperature and pressure are equally important for reactivity of solids. However, if one compares the number of publications describing solid-state reactions induced by heating at ambient pressure as compared with those dedicated to the processes at high pressures, one can see that the variable-temperature research obviously dominates. As some exception, one can consider numerous publications discussing mechanochemical reactions, which result from a mechanical action on solid samples (usually, milling). However, many of the mechanochemical reactions are in fact of thermal origin, or take place in the fluid phases at the inter-particle contacts [1 and refs. therein].

The aim of the present contribution is to attract attention to the role of high-pressure research in relation to reactivity of solids. It can be considered in several aspects: 1) using high pressure as a tool to synthesize new phases (quenchable on decompression, or used in devices at high pressure *in situ*), 2) using high pressure to understand the mechanisms of reactions induced by various types of mechanical action on solids, 3) using high pressure to understand the role of internal stress and strain in reactivity of solids and feed-back phenomena, 4) using high pressure to study the characteristics of intermolecular and interatomic interactions in solids and their role in crystallization and in solid-state reactivity.

The following types of processes at high pressure will be considered: 1) pressure-induced phase transitions in solids at ambient and variable temperatures, 2) crystallization of fluids at high pressure, 3) crystallization of solids dissolved in liquids with increasing pressure or on reverse decompression, 4) reactions in individual solids induced by pressure, also compared with shear-induced transformations, 5) reactions between different phases at high pressures, also in relation to the experiments in the diamond anvil cells and to mechanochemical reactions in solid mixtures.

The importance of the high-pressure experiments in relation to all the Topical Areas of the ISRS will be illustrated, in particular to the fundamental problems of the solid-state synthesis, properties and reactivity, as well as to applications in geochemistry, planetary sciences, physics, pharmaceutical and chemical technologies.

The research was supported in parts by Russian Academy of Sciences (including Integration project 108 of the SB RAS, and Project 24.38 of the Praesidium of RAS), grants 13-03-00795, 13-03-92704, and 14-03-00902 from RFBR, Russian Ministry of Science and Education.

"Synthetic Clay Minerals: Materials Chemistry in Two Dimensions"

Prof. Dr. Josef Breu

Universität Bayreuth, Lehrstuhl für Anorganische Chemie I,
Universitätsstr. 30, 95440 Bayreuth, e-mail: josef.breu@uni-bayreuth.de

The intrinsically anisotropic bonding in layered materials may enable a vivid intracrystalline reactivity that allows for post synthetic functionalization via ion exchange or intercalation. Melt synthesis of layered silicates not only allows for a subtle balancing of layer charge and intracrystalline reactivity, it also delivers large and better ordered crystals of superb charge homogeneity [1-3].

By pillaring such synthetic clay minerals by molecules, a largely unknown class of microporous hybrid materials is obtained that may be used for gas separation and enantiodiscrimination [4-6].
Moreover, clay minerals represent anionic platelets that may be spontaneously delaminated into singular layers by osmotic swelling [7, 8] that differ from the bulk materials in mechanical characteristics [9-11] offering flexibility and high tensile strength at the same time (Fig. 1). Incorporation of such large aspect ratio fillers into polymeric matrices introduces huge interface areas in such nanocomposites responsible for pronounced reinforcement [12], excellent gas barrier [13, 14] and improved flame retardancy [15, 16].

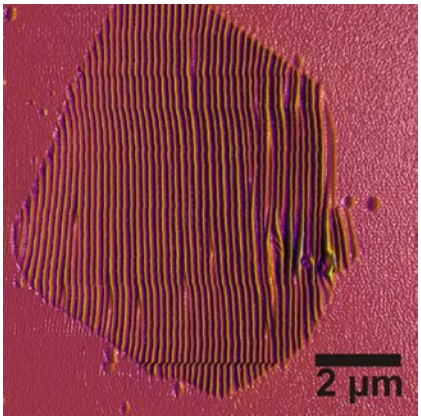

Figure 1: AFM topographical image of a wrinkled Na-hec nanoplatelet.

Finetuning of intracrystalline reactivity, moreover, allows the synthesis of regular heterostructures with two alternating types of interlayers (staging, interstratifications, Fig. 2) [17]. Such interstratified materials may in turn be delaminated into double-stacks. With the help of such heterostacks emitters may be oriented in a quasi-epitaxial way allowing for polarized emission. Alternatively, they may be turned into Janus-type nanoplatelets [18] representing efficient Pickering emulgators.

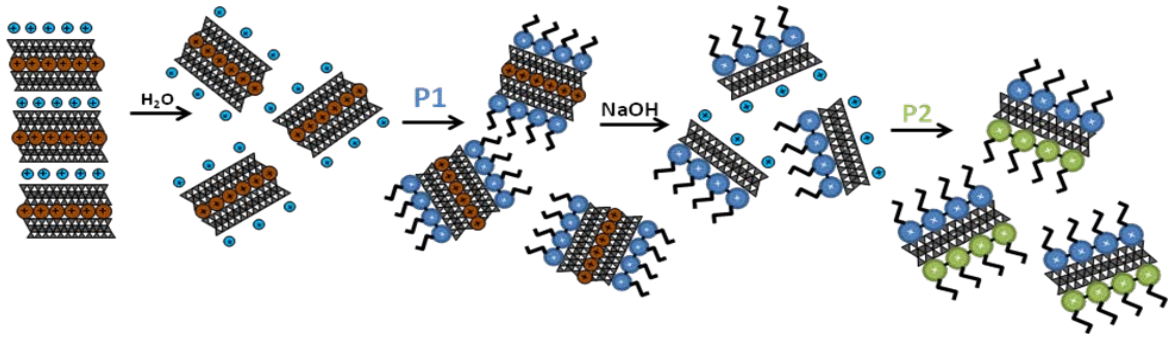

Figure 2: From regularly interstratified materials to Janus-type Pickering emulgators.

References:

[1] H. Kalo, W. Milius, M. Bräu, J. Breu, J. Solid State Chem. **198** (2013) 57-64.
[2] H. Kalo, W. Milius, J. Breu, Rsc Advances **2** (2012) 8452-8459.
[3] H. Kalo, M. Möller, M. Ziadeh, D. Dolejs, J. Breu, Appl. Clay Sci. **48** (2010) 39-45.
[4] M.M. Herling, H. Kalo, S. Seibt, R. Schobert, J. Breu, Langmuir **28** (2012) 14713-14719.
[5] A. Baumgartner, K. Sattler, J. Thun, J. Breu, Angew. Chem. Int. Ed. **47** (2008) 1640-1644.
[6] M. Stöcker, W. Seidl, L. Seyfarth, J. Senker, J. Breu, Chem. Commun. (2008) 629-631.
[7] M. Stöter, D.A. Kunz, M. Schmidt, D. Hirsemann, H. Kalo, B. Putz, J. Senker, J. Breu, Langmuir **29** (2013) 1280-1285.
[8] H. Kalo, M.W. Möller, D.A. Kunz, J. Breu, Nanoscale **4** (2012) 5633-5639.
[9] D.A. Kunz, P. Feicht, S. Godrich, H. Thurn, G. Papastavrou, A. Fery, J. Breu, Adv. Mater. **25** (2013) 1337-1341.
[10] D.A. Kunz, J. Erath, D. Kluge, H. Thurn, B. Putz, A. Fery, J. Breu, Acs Applied Materials & Interfaces **5** (2013) 5851-5855.
[11] D.A. Kunz, E. Max, R. Weinkamer, T. Lunkenbein, J. Breu, A. Fery, Small **5** (2009) 1816-1820.
[12] B. Fischer, M. Ziadeh, A. Pfaff, J. Breu, V. Altstadt, Polymer **53** (2012) 3230-3237.
[13] M.W. Möller, D.A. Kunz, T. Lunkenbein, S. Sommer, A. Nennemann, J. Breu, Adv. Mater. **24** (2012) 2142-2147.
[14] M. Möller, T. Lunkenbein, H. Kalo, M. Schieder, D.A. Kunz, J. Breu, Adv. Mater. **22** (2010) 5245-5249.
[15] M.R. Schütz, H. Kalo, T. Lunkenbein, A.H. Groschel, A.H.E. Müller, C.A. Wilkie, J. Breu, J. Mater. Chem. **21** (2011) 12110-12116.
[16] M.R. Schutz, H. Kalo, T. Lunkenbein, J. Breu, C.A. Wilkie, Polymer **52** (2011) 3288-3294.
[17] M.W. Möller, D. Hirsemann, F. Haarmann, J. Senker, J. Breu, Chem. Mater. **22** (2010) 186-196.
[18] D. Hirsemann, S. Shylesh, R.A. De Souza, B. Diar-Bakerly, B. Biersack, D.N. Mueller, M. Martin, R. Schobert, J. Breu, Angew. Chem. Int. Ed. **51** (2012) 1348-1352.

Quantum Chemistry of V_2O_5 Nanostructures

Robert A. Evarestov,[a*] Vitaly V. Porsev,[a] and Andrei V. Bandura[a]

[a]Chemistry, Quantum Chemistry Division, St. Petersburg State University
St. Petersburg, Russia.

*Corresponding Author, E-mail: re1973@re1973.spb.edu

Crystalline divanadium pentoxide, V_2O_5, is a key technological material widely used in applications such as optical switches, chemical sensors, catalysts, and solid-state batteries. The layered structure of this oxide is favorable for production of numerous nanostructures and nanocomposites such as nanotubes or nanoscrolls, nanorods, fullerene analogues, nanocables or nanourchins and various nanorings. Most of them exhibit properties, which are very attractive for future applications in various areas of industry. For example, the high specific surface area of the nanotubes (NT) renders them even more attractive as positive electrodes in Li-ion batteries. The synthetic route employed in the preparation of the NTs involves a sol-gel reaction and uses organic molecules as structure directing agents. The tubes produced are up to 15 mm long and have inner diameters between 5 and 15 nm while the outer diameters range from 15 to 100 nm. Their walls consist of several vanadium oxide layers with the organic molecules intercalated in between them. The experimental works on synthesis of the V_2O_5 NTs and the experimental studies of their properties are numerous. However the theoretical investigations of V_2O_5 nanotubes and nanoscrolls are restricted to a few publications of Enyashin et al., 2004, where the density functional based tight binding method has been used.

At present time the preparation techniques and structure of three layered phases of the divanadium pentoxide V_2O_5 are known. The most stable phase is orthorhombic *Pmmn* α-V_2O_5. The orthorhombic *Pnma* γ-V_2O_5 phase has been prepared by chemical and electrochemical deintercalation of lithium from γ-LiV_2O_5. At 6 GPa and 1073 K the monoclinic $P2_1/m$ β-V_2O_5 has been obtained. All the three layered V_2O_5 polymorphs provide the free layers which potentially can be rolled up into the nanotubes.

In this work we present the results of hybrid DFT-HF calculations with PBE0 exchange-correlation functional of the structure and energy of V_2O_5 bulk, single layers and single-wall nanotubes. The basis of atomic orbitals implemented in CRYSTAL09 computer code (R. Dovesi, at al., 2005) has been used in all simulations. All the lattice parameters and the atomic positions have been totally optimized.

In agreement with the experimental data we have found that α-V_2O_5 is the most stable bulk polymorph. We have estimated the formation energy of the considered systems according to the equation: $\Delta E_{form}(\text{phase}) = E(\text{phase})/N(\text{phase}) - E_\alpha/N_\alpha$, where E(phase), N(phase) and E_α, N_α are the total energy and the number of formula units per translational unit cell in a given phase and in the α-V_2O_5 phase, respectively. The obtained stability of the three layered phases decreases in order: $\alpha > \gamma > \beta$. The relative stability of corresponding free layers of V_2O_5 differs from that of the bulk phases and decreases in order: $\beta > \alpha \geq \gamma$ (see Figure 1a).
We have calculated the energy, atomic and electronic structure of nanotubes rolled up from both the layers of α-phase (α-NT) and layers of γ-phase (γ-NT) with (n, 0) chirality. The simulations have been performed in ranges from (6, 0) to (16, 0) which correspond to the NT

diameters *D* from 20 Å to 56 Å. The largest considered *D* value is comparable to the minimal inner diameters of the experimentally observed V_2O_5 nanotubes.

The two factors may favor the nanotubes (NTs) formation. The first one is the low layer formation energy, and the second – the layer flexibility defining the NT strain energy. All the considered layers have the small values of the formation energy and thus satisfy the first condition. Because of close values of their formation energy it is difficult to define a priori which structure is more favorable for the supposed NTs. So, the second condition becomes more important. The large rigidity of layer increases the NT bending strain energy and may lead to break of the chemical bonds and loss of the layered structure.

We have calculated the strain energy E_{str} which is the NT formation energy with respect to the 2D-periodic precursor layer: $E_{str} = E_{NT}/N_{NT} - E_{layer}/N_{layer}$, where E_{layer}, N_{layer} and E_{NT}, N_{NT} are the total energy and the number of formula units per translational unit cell in a layer and in NT, respectively. The obtained data show that the strain energy of NTs just after folding is considerable but becomes much smaller upon the NT relaxation (see Figure 1b). Due to their unique flexibility, the relaxed γ-NTs show almost zero strain energy for all investigated *n*. The E_{str} values of the relaxed α-NTs are larger than those of γ-NTs ones, but quickly decrease with *n* increasing. When the difference between E_{str} values for α- and γ-NTs becomes less than the energy difference between α- and γ-layers (0.8 kJ/mol) the formation energy of α-NTs becomes more favorable than that of γ-NTs. This alteration occurs at $n = 12$. Hence, γ-NTs or α-NTs are more stable at $n < 12$ or $n \geq 12$, respectively.

At the relaxation process the change of bond distances is insignificant, and NTs mainly relax through the modification of V–O–V and O–V–O bond angles. The angle changes can be so considerable as to provoke a conversion of concave angles to convex angles, especially for small *n*. The relaxed NT structures are illustrated in Figure 1c for the both types of layers.

References:

[1] A. N. Enyashin, et al., *Phys. Lett.*, **A326** (2004) 152.
[2] R.Dovesi et al., CRYSTAL09 User's Manual (Torino: University of Torino,2010)

Figure 1a:

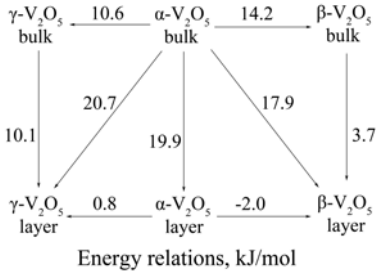

Figure 1b:

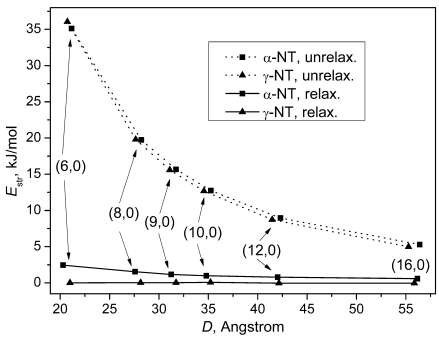

Figure 1c:

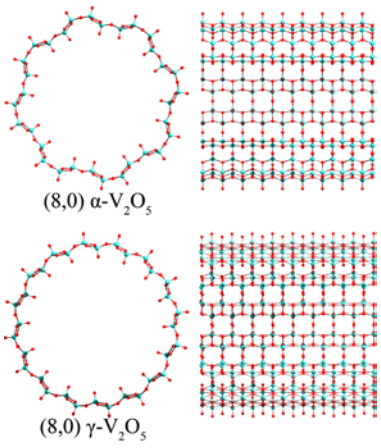

Multiferroic Properties of Organic-Hybrid Compounds

Thomas T.M. Palstra[a], A.O. Polyakov[a] and Graeme R. Blake[a]

[a]Zernike Institute for Advanced Materials
University of Groningen, The Netherlands.

We have investigated organic-inorganic hybrids that combine properties of the perovskite structures and metal-organic framework compounds. The inorganic and organic components of the hybrids introduce different functional properties. The chemistry of inorganic materials is characterized by covalent and ionic interactions, offering the potential for a wide range of band gaps or band widths with high carrier density and mobility, magnetic interactions, ferroelectric transitions and thermal stability. On the other hand, organic solids typically have their macroscopic effects dominated by weaker interactions like hydrogen bonds and Van der Waals interactions. They provide nearly unlimited flexibility in structural diversity, good polarizability and they can also be made conductive. The aim of investigating hybrid materials is to combine properties from both the inorganic and the organic moiety in one material and produce useful combinations or even completely new phenomena. Robust magnetic properties, originating from transition metal ions forming the inorganic building block, are combined with the easy processing and structural flexibility provided by the organic block. The recent discovery of coexisting ferromagnetic and ferroelectic properties of $CuCl_4$-based organic-inorganic hybrids is an example of such combined functionality.

We show that ferroelectricity and (anti-)ferromagnetism coexist in Cu- and Mn-based hybrids and explore possibilities to optimize these phenomena by changing building blocks of the compound. The magnetic properties of the hybrids are determined by the inorganic block, while the ferroelectric properties arise from the bonding of the organic block. Importantly, the magnetic response also changes with the introduction of different organic moieties. We performed a systematic study of structure and magnetic properties of Cu-based hybrids with general formula $CuCl4(YNH_3)_2$. Our findings show that the magnetic response surprisingly depends on the organic ligand. Also the magnetic anisotropy is different for different compounds, despite the fact that the inorganic structural parameters are quite similar. We also report that the magnetic properties, such as preferential orientation of the magnetization, can change. Therefore, by varying the metal ions and organic ligands we can tailor the magnetic properties such as Tc and the degree of anisotropy.

We report the coexistence of ferromagnetism and ferroelectricity in $CuCl_4(C_6H_5C_2H_4NH_3)_2$. In this compound the organic moiety induces a ferroelectric state above room temperature. We show that the organic-inorganic interface plays a crucial role for the ferroelectric properties of the compounds. In particular, the ferroelectric transition at 340K is caused by the buckling of the inorganic $CuCl_6$ octahedra, inducing NH_3 group hydrogen bonds reordering and a site-shift of the organic moiety.

Another interesting family is the $NiCl_3$-based organic-inorganic hybrids. Ni-hybrids with general formula $NiCl_3(YNH_3)_2$, represent 1D magnetic S=1 chains, where magnetism originates from chains of $NiCl_3$ face-sharing octahedra, separated by the organic molecules. We show that the magnetic properties of the inorganic block can be subtly tuned by using

different organic moieties. Different organic moieties cause structural modifications, resulting in changes of the intra-chain magnetic interactions. Remarkably, the in-chain nearest neighbor exchange constants *J* can be substantially modified for different compounds, even though the Ni-Ni distances and Ni-Cl-Ni angles in the chain are very similar.
We performed systematic structural and magnetic studies of Ni-based hybrids with different organic ligands. It was found that variation the organic moiety introduce subtle changes in the relevant structural parameters of the inorganic chain responsible for the magnetism, such as the intra-chain and inter-chain Ni-Ni distance. Thus, by introducing different organic ligands we can tune the magnetic properties of the spin chains and induce 3D magnetic order at low temperatures, even though the inorganic chains are well separated.

References:

[1] A.O. Polyakov, A.H. Arkenbout, J. Baas, G.R. Blake, A.M. Meetsma, A. Caretta, P.H.M. van Loosdrecht, T.T.M. Palstra, *Chemistry of Materials* **2012**, *24*, 133–139.

Figures:

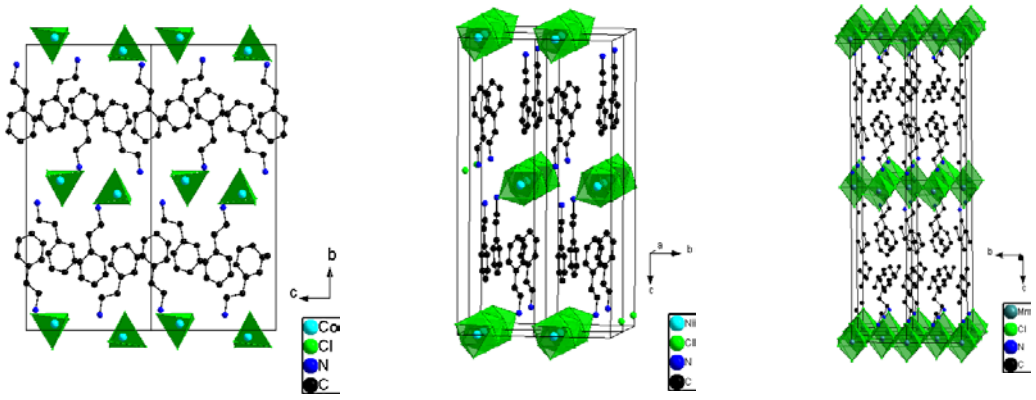

Figure 1: Crystal structure of an isolated $CoCl_4$-based hybrid, a 1-dimensional $NiCl_3$-based chain hybrid and a 2-dimensional $CuCl_4$-based hybrid, that is ferromagnetic and ferroelectric.

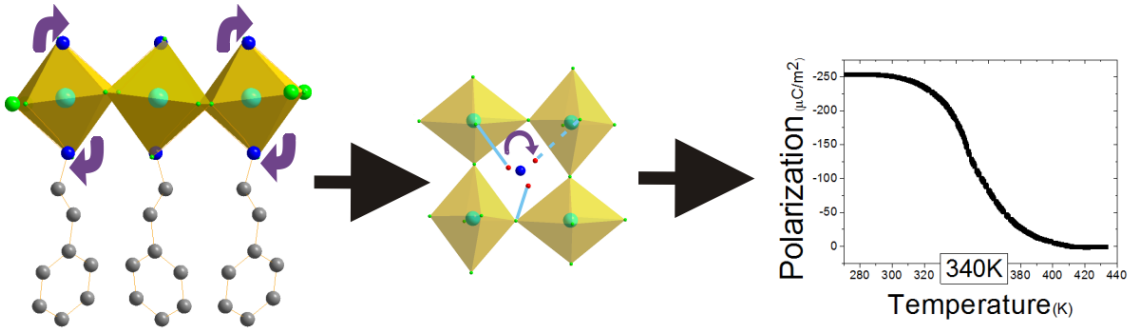

Figure 2. Cartoon of the buckling of the $CuCl_6$ octahedra resulting below 340K in a ferroelectric polarization by hydrogen bonding and an organic moiety site-shift.

Oral Presentations

Superconductivity and Mo/Cu Charge Equilibrium in $(Mo_{0.3}Cu_{0.7})Sr_2ErCu_2O_y$

M. A. Alario-Franco[a], Sourav Marik[a,b], A. J. Dos santos-Garcia[a], Christine Labrugere[b], Emilio Morán[a], O. Toulemonde[b]

[a]Dpto. Química Inorgánica, Facultad de CC.Químicas, Universidad Complutense de Madrid, 28040-Madrid (Spain)
[b]CNRS, Université de Bordeaux, ICMCB, 87 avenue du Dr. A. Schweitzer, Pessac, F-33608, (France)

Most of the work devoted to the search of high temperature superconductors (HTSC) has relied upon the cationic substitution in orthorhombic $CuYBa_2Cu_2O_{7-\delta}$ ($YBa_2Cu_3O_{7-\delta}$, YBCO or Y-123). Since its discovery, several cation substitutions were made for the small ion copper and for the large barium and yttrium ions. In all cases, substitutions for copper were found to decrease superconducting transition temperature (T_C) and, concomitantly to this, it has been observed a progressive decrease of the orthorhombic distortion with increasing the substitution degree, ending in a more symmetric tetragonal structure. From the structural point of view, the superconducting $CuYBa_2Cu_2O_{7-\delta}$ and related phases contain two crystallographically distinct Cu sites: the chain site (Cu1), forming the so-called CuO chain and the square-pyramidal (Cu2), which base forms the CuO_2 planes. The connecting layer (CuO chain) can act as a *charge reservoir* by supplying the carriers necessary for superconductivity to take place in the CuO_2 planes [1-3]. When Ba is fully replaced by the smaller Sr cation, the strontium analogue of the "123"-YBCO superconductor, that is $CuYSr_2Cu_2O_{7-\delta}$ (YSCO, $T_{C,onset}$ = 60K), can only be prepared at high pressure [4]. However, these phases can be stabilized at ambient pressure by substituting Pb, Li, Al, Ti, V, Cr, Fe, Co, Ga, Ge, Mo, W, Re, Rh and Ir partially or completely for the Cu in the chains [5-8].

As molybdenum can exists in several-oxidation states (commonly IV, V, VI in oxides), it is of interest to investigate the effect of Mo substitution for copper in the crystal structure, magnetic properties and superconductivity in "123" superconductors. Also, it is important to examine the effect of Mo-substitution on the oxidation state of copper to understand the superconductivity in these types of materials. Previous work on Mo-stabilized $CuRESr_2Cu_2O_{7-\delta}$ (RE = Rare earth,) [9] phases clearly stated that these compounds display a superconducting transition centering around 30 K, with the exception for the bigger RE = La, Pr and Nd lanthanide-compounds, which are not superconducting [9]. Recently, our work on $Mo_xCu_{1-x}Sr_2YCu_2O_y$ has revealed that full replacement of Mo for Cu in the chain site is not possible at ambient pressure [10]. Superconductivity (T_C = 30 K) and magnetic ordering (T_N = 5.4 K) has been found in $Mo_{0.3}Cu_{0.7}Sr_2TbCu_2O_y$ material [11-13]. On the other hand,

$Mo_{0.3}Cu_{0.7}Sr_2TmCu_2O_y$ shows an interesting spin glass to superconducting phase transformation following an oxidation reaction [14].

In this paper, we report the detailed crystal structure determination both at room temperature and at 1.5 K, as determined by the joint X-ray/neutron powder diffraction (NPD) refinement and Transmission Electron Microscopy as well as the magnetic and superconducting properties for the as prepared (AP) and oxygenated $Mo_{0.3}Cu_{0.7}Sr_2ErCu_2O_y$ samples. The influence of oxygenation in the electronic states for the $Mo_{0.3}Cu_{0.7}Sr_2ErCu_2O_y$ system associated with an oxidation reaction leading to a superconducting state has also been studied by means of X-ray photoelectron spectroscopy.

References:

[1] R. Gagnon, C. Lupien, and L. Teillefer, Phys. Rev. B 50, 3458 (1994).
[2] Gang Xiao, M. Z. Cieplak, A. Gavrin, F. H. Streitz, A. Bakhshai, and C. L. Chien, Phys. Rev. Lett. 60, 1446 (1988).
[3] S. F. Hu, R. S. Liu, S. C. Su, D. S. Shy and D. A. Jefferson, J. Solid State Chem. 112 (1994) 203.
[4] B. Okai, Jpn. J. Appl. Phys., 29 (1990), p. L2180.
[5] A. J. Dos santos-Garcia, M. H. Aguirre, R. Saez Puche and M. A. Alario-Franco, J. Solid State Chem. **179,** 1296 (2006).
[6] J. M.S. Skakle, Materials Science and Engineering, **R23**, 1-40, (1998).
[7] D. G. Joshi, M. V. Subbrarao, A. N. Shah, D. G. Kuberkar, and R.G. Kulkarni, Applied superconductivity 6, 7-9, pp. 471-481 (1998).
[8] L. Bauernfeind, W. Widder and H. F. Braun, Physica C **254**, 151-158, (1995).
[9] Q. Xiong, Y.Y. Xue, J.W. Chu, Y.Y. Sun, Y.Q. Wang, P.H. Hor and C.W. Chu, Phys. Rev. B 47, 11337 (1993).
[10] S.Marik, E.Moran, Christine Labrugère, O. Toulemonde and M. A. Alario-Franco, JSSC **191,** 40-45 **(**2012).
[11] H. L.Tsay, C. R. Shih, Y. C. Chen, W. H. Lee, T. H. Meen and H. D. Yang, Physica C **252**, 79-86 (1995).
[12] H. L. Tsay, Y. C. Chen, S. S. Weng, C. F. Chang and H. D. Yang, Phys. Rev. B **59**, 636-640 (1999- I).
[13] Q. Xiong, Y.Q. Wang, J.W. Chu, Y.Y. Sun, K. Matsuishi, H.H. Feng, P.H. Hor and C.W. Chu, Physica C, **198**, 70-74 (1992).
[14] S.Marik, A. J. Dos santos-Garcia, E.Moran, O. Toulemonde and M. A. Alario-Franco, JPCM **25,** 165704 **(**2013).

Acknowledgements:

We thank EU (SOPRANO project FP7/2007-2013 under Grant Agreement n°214040) for a grant to S. Marik. The Spanish “Ministerio de Ciencia e Innovación” and the “Comunidad de Madrid” are also acknowledged for financial support given through projects MAT2010- 9460 and S2009/PPQ-1626, respectively. Institut Laue-Langevin (ILL), Grenoble, France is acknowledged for providing neutron facilities. Authors also wish to thank Dr. Clemen Ritter (ILL) for his help in collecting the neutron powder pattern.

Cathode materials for IT-SOFC based on perovskites with 3d-metal cations.

S.Ya. Istomin

Department of Chemistry, Moscow State University, Leninskie Gory, Moscow, 119991, Russia

A major target in the development of solid-oxide fuel cells (SOFC) is the decrease of their operating temperature down to 550-750^{o}C (intermediate temperature SOFC or IT-SOFC). For this purpose standard cathode material based on Sr doped $LaMnO_3$ (LSM) should be replaced by oxygen-deficient perovskites with 3d-elements like Fe, Co, Ni or Cu. Requirements for cathode materials for IT-SOFC include high electronic and oxide-ion conductivities, high catalytic activity for oxygen reduction, thermal expansion coefficient (TEC) match with that one for electrolyte and absence of chemical interaction with neighbouring components of fuel cell. In the present study influence of the crystal structure and chemical composition on the properties of perovskite-related cobalt and copper oxides important for their use as cathode materials for IT-SOFC are discussed.

Complex perovskite-related cobaltates with Co^{3+} fit perfectly to the majority of the requirements for cathode materials for IT-SOFC listed above. However, they posses high TEC due to thermally activated transition between low (LS) and high-spin (HS) state of Co^{3+}. One of the ways to decrease their TEC is to reveal cobaltates with HS Co^{3+} in ground state. Such compounds can be found among cobaltates with brownmillerite-type structure.

Cuprates R_2CuO_4, R – rare-earth cation with layered crystal structures contain perovskite slab alternating with rock-salt slab (R=La, so called T-phase) and fluorite slab (R=Nd-Gd, so called T'-phase) are considered as prospective cathode materials for IT-SOFC due to their low TEC (~12 ppm K^{-1}) and moderate high-temperature conductivity (>100 S/cm for Pr_2CuO_4). Correlation between the presence of the particular structural slab in the crystal structure of layered cuprates and their high-temperature oxide-ion conductivity is discussed.

This work was partially supported by RFBR (grant no. 14-03-01083) and MSU-development Program up to 2020.

Reactivity of *zwitterionic* mesostructured bioceramics

Montserrat Colilla,[a,b,c,d] Marina Martínez-Carmona,[a,b,c,d] Sandra Sánchez-Salcedo,[a,b,c,d] María Vallet-Regí[a,b,c,d*]

[a] Departamento de Química Inorgánica y Bioinorgánica, Facultad de Farmacia, Universidad Complutense de Madrid (UCM), Spain;
[b] Instituto de Investigación Sanitaria Hospital 12 de Octubre i+12, Madrid, Spain;
[c] Center on Bioengineering, Biomaterials and Nanomedicine (CIBER-BBN), Spain;
[d] CEI Campus Moncloa, UCM-UPM, Madrid, Spain.
vallet@ucm.es

Introduction

The biomedical scientific community is dedicating a growing effort to design implantable bioceramics that fulfill particular clinical needs. To achieve this goal it is essential that material surface exhibit suitable reactivity once in contact with physiological fluids and living tissues.[1] Silica-based mesoporous materials exhibit unique structural and textural features that make them promising bioceramics with drug delivery and bone regeneration capabilities. [1-3] Nonetheless, the reactivity of bone implants is a major concern, since they can be ideal substrates for bacterial adhesion and growth, leading to postoperative implant infections. [4] Thus, the current challenge relies in tailoring the surface reactivity of mesoporous materials to inhibit bacterial adhesion and permit loading and releasing antibiotics in a sustained way.
Herein, *zwitterionic* SBA-15 type mesoporous material was synthesized by a one-step method using [N-(2-aminoethyl)-3-aminopropyl] trimethoxysilane (DAMO) as functionalizing agent. DAMO holds basic primary and secondary amine groups capable of interacting with silanol groups of the silica matrix, providing it of *zwitterionic* nature (**Figure**). The low bacterial adhesion capability of this *zwitterionic* SBA-15 was *in vitro* evaluated using *S. aureus*. Moreover, this matrix was tested as cephalexin (CPX) delivery system, an antibiotic used to treat some pathologies caused by bacteria including dental infections and otitis media.

Materials and Methods

Zwitterionic SBA-15 type mesoporous material was synthesized by solving the non-ionic surfactant Pluronic P123® into acidified water. Then, appropriate amounts of tetraethyl orthosilicate (TEOS) and DAMO were added (90/10 TEOS/DAMO molar ratio). After hydrothermal treatment, surfactant was removed by solvent extraction, affording SBA-ZWIT material. For comparative purposes, pure silica SBA-15 was synthetized. Materials were characterized by chemical analysis, TGA, FTIR, XRD, HR-TEM-EDX, N_2 adsorption porosimetry, ^{13}C and ^{29}Si solid state NMR and ζ-potential measurements. For bacterial adhesion assays powdered samples were compacted into discs (6×1 mm) using uniaxial pressure. Discs were incubated into a $1.5{\cdot}10^6$ CFU/mL of *S. aureus* suspension in PBS during 90 min at 37 ºC under orbital stirring. The number of adhered bacteria was determined as previously reported.[5] CPX loading was performed by soaking powdered materials in an aqueous solution of CPX at 37ºC during 24 h under stirring. *In vitro* delivery assays were performed by soaking disc-shaped pieces of loaded materials into PBS at 37°C under continuous stirring. The amount of CPX released was monitored by UV-Vis spectroscopy.

Results and Discussion

The effective functionalization process and the *zwitterionic* nature of SBA-ZWIT were confirmed by FTIR spectroscopy, where the characteristic vibration bands of protonated amine groups are detected in the spectrum. These results were also confirmed by ^{13}C NMR.

The structural and textural characterization of materials indicates a highly ordered arrangement of cavities distributed in 2D-hexagonal structure. TEM images and their corresponding FT confirm these results. Moreover, N_2 adsorption analysis evidences good textural properties of SBA-ZWIT to host drug molecules, being 553 m^2/g, 0.8 cm^3/g and 9.2 nm the surface area, pore volume and pore diameter values, respectively. The isoelectric point of SBA-ZWIT, determined by ζ-potential measurements, was *ca.* 7.4, pointing to the preservation of the *zwitterionic* character at the physiological pH. *In vitro* bacterial adhesion assays with *S. aureus* demonstrated that SBA-ZWIT reduces the bacterial adhesion by 99.9% compared to SBA-15 (**Figure**). Loading CPX tests indicate that SBA-ZWIT is able to entrap the antibiotic molecules into the mesoporous channels, being *ca.* 13 mg/g the amount of drug loaded. *In vitro* release assays in PBS proved that the diamine functional groups present in SBA-ZWIT significantly decrease the release rate of CPX. Thus, after 400 h of assay SBA-ZWIT released 40% of the loaded CPX, whereas SBA-15 released 100% of CPX.

Conclusion

Tailoring the surface reactivity of SBA-15 by providing it of *zwitterionic* nature permits reducing bacterial adhesion and allows the sustained release of antibiotics.

References

[1] *Bioceramics with Clinical Applications*, Ed. M. Vallet-Regí, John Wiley & Sons Ltd, Chichester, UK (2014)
[2] M. Vallet-Regí, F. Balas, D. Arcos. *Angew. Chem., Int. Ed.*, **46** (2007) 7548.
[3] M. Vallet-Regí, M. Manzano García, M. Colilla, *Biomedical Applications of Mesoporous Ceramics: Drug Delivery, Smart Materials and Bone Tissue Engineering*, CRC Press, Taylor and Francis, New York, 2013.
[4] P. Stoodley, L Hall-Stoodley, B. Costerton, P. DeMeo, M. Shirtliff, E. Gawalt, S. Kathju, *Biofilms, biomaterials and device-related infections*, in Biomaterials Science: An Introduction to Materials in Medicine, 3rd edition. Eds. B. D. Ratner, A. S. Hoffman, F. J. Schoen, J. E. Lemons, New York, (2013).
[5] I. Izquierdo-Barba, S. Sánchez-Salcedo, M. Colilla, M.J. Feito, C. Ramírez-Santillán, M.T. Portolés, M. Vallet-Regí, Acta Biomaterialia, **7** (2011) 2977.

Figures:

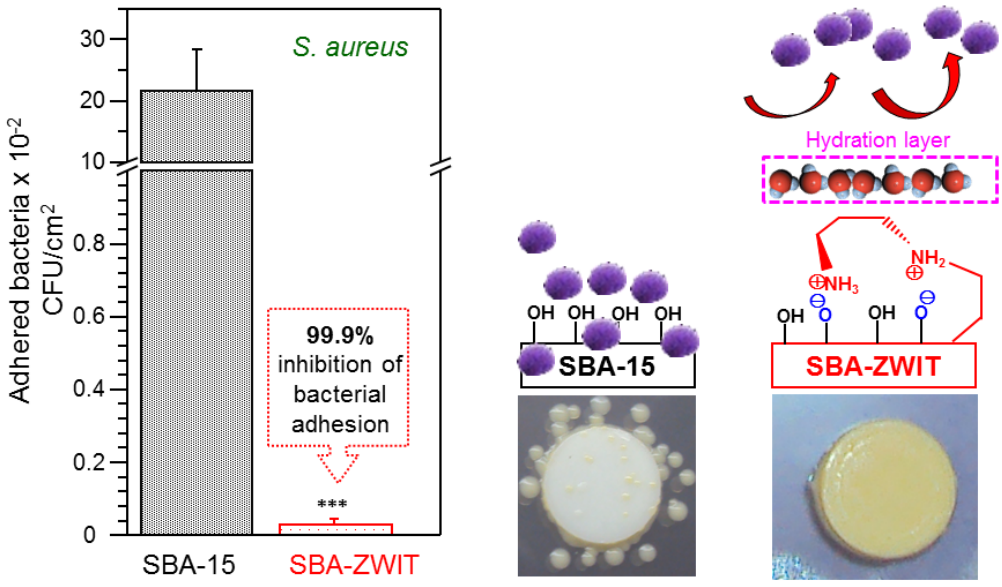

Left: S. aureus attachment to SBA-15 and SBA-ZWIT surfaces. Three different measurements were performed for each specimen [$p < 0.001$ (***)]. *Right*: schematic depiction of the performance of both materials during the *in vitro* bacterial adhesion assays.

Influence of low temperatures and high pressures on crystals containing amino acids

Boris A. Zakharov,[a, b] Evgeniy A. Losev,[a, b] Boris A. Kolesov,[b, c] Elena V. Boldyreva[a, b]

[a]Institute of Solid State Chemistry and Mechanochemistry SB RAS, Novosibirsk, Russia;
[b]REC-008, Novosibirsk State University, Novosibirsk, Russia;
[c]Institute of Inorganic Chemistry SB RAS, Novosibirsk, Russia.

Multicomponent crystals with components present in a well-defined stoichiometric ratio (salts and co-crystals) attract much attention. Multicomponent crystals containing amino-acids are of special interest for studies at non-ambient conditions. They are interesting for improving our understanding of factors determining the formation of a crystal structure and its variations vs. temperature and pressure. They are also promising as new materials. A remarkable feature of most of these compounds is that very short O–H...O hydrogen bonds are present in the crystal structures. The structure-forming units in these crystals are similar to those in the biopolymers and can be used as biomimetics.

The main aim of this study was to follow the effects of cooling and increasing pressure on crystal structures of bis(DL-serinium) oxalate dihydrate, DL-alaninium semi-oxalate monohydrate and glycine-glutaric acid co-crystal by combination of single-crystal X-ray diffraction and polarized Raman spectroscopy selected as main experimental techniques.

The properties of several types of O–H...O hydrogen bonds in bis(DL-serinium) oxalate dihydrate and DL-alaninium semi-oxalate monohydrate have been studied by a combination of variable-temperature single-crystal X-ray diffraction and polarized Raman spectroscopy. The changes in the hydrogen bonds geometry could be compared with the changes of the corresponding spectral modes. The correlation suggested by Novak [1] is roughly followed, better for medium and weak, than for short hydrogen bonds (Figure *a*). Fine details of spectral changes are different for individual bonds. The way how H bonds are affected by cooling depends on their environment in the crystal structure. Short O–H...O hydrogen bonds in bis(DL-serinium) oxalate dihydrate expand or remain almost unchanged on cooling, whereas in DL-alaninium semi oxalate monohydrate all strong H-bonds are compressed under these conditions. The distortion of individual hydrogen bonds on temperature variations is correlated with the anisotropy of lattice strain [2]. Originally, we supposed that a co-crystal - salt transition may be possible for co-crystal of glycine with glutaric acid, similarly to what has been observed for some other compounds, but real behavior of the system turned out to be quite unexpected and more complex. The molecules of glutaric acid remained non-ionized in all the temperature range from ambient down to 100 K, but conformational polymorphic transformation with a change in the space symmetry group and doubling of Z' has been observed at 220-230 K [3].

In contrast to what was observed on cooling, bis(DL-serinium) oxalate dihydrate and DL-alaninium semi-oxalate monohydrate were shown to undergo a phase transitions at high pressures (~4 and ~2 GPa respectively) with domains formation. Pressure-induced phase transitions in bis(DL-serinium) oxalate dihydrate related to lowering symmetry. A crystal structure disordering was shown by Raman spectroscopy on increasing pressure for this system and confirmed by appearance of diffuse scattering on diffraction patterns (Figure *b*)

[4]. A single-crystal to single-crystal transition in DL-alaninium semi-oxalate monohydrate without changing a space group ($P2_1/c$) was detected at a pressure between 1.5 and 2.4 GPa. During the phase transition selected hydrogen bonds switch-over and become bifurcated, whereas the others are compressed continuously (Figure *c*). The transition is accompanied by pronounced discontinuities in the changes of cell parameters and volume vs. pressure, although no radical changes in the molecular packing are induced and no crystal breaking was detected [5]. Glycine-glutaric acid co-crystal was shown to undergo high-pressure phase transition already at 0.1 GPa to give the same phase as low-temperature phase transition.

Using this results we can conclude that polarized Raman spectroscopy complemented by single crystal X-ray diffraction provide an excellent instrument for detailed studies not only fine effects in hydrogen bonds on cooling but also for studying phase transitions and hydrogen bonds on increasing pressure. High-pressure phase transitions were detected for all systems studied. Crystal structure disordering was shown to occur in bis(DL-serinium) oxalate dihydrate. A correlation between donor-acceptor distances and frequencies of OH-stretching vibrations was studied for selected individual hydrogen bonds on cooling.

This work was supported by a grant from RFBR (12-03-31541 mol_a), by the Ministry of Education and Science of Russia (project 14.B37.21.1093), and by a grant of President of Russia for State support of Russian leading Scientific Schools (project NSh-279.2014.3).

References:

[1] A. Novak, *Structure and Bonding*, **18** (1974) 177.
[2] B.A. Zakharov, B.A. Kolesov, E.V. Boldyreva, *PCCP*, **13** (2011) 13106.
[3] B.A. Zakharov, E.A. Losev, B.A. Kolesov, V.A. Drebushchak, E.V. Boldyreva, *Acta Cryst. B.*, **68** (2012) 287.
[4] B.A. Zakharov & E.V. Boldyreva, *J. Mol. Str.*, (2014), *in press*.
[5] B.A. Zakharov & E.V. Boldyreva, *Acta Cryst. B,* **69** (2013) 271.
[6] B.A. Zakharov, E.A. Losev, E.V. Boldyreva, *CrystEngComm*, **15** (2013) 1693.

Figure:

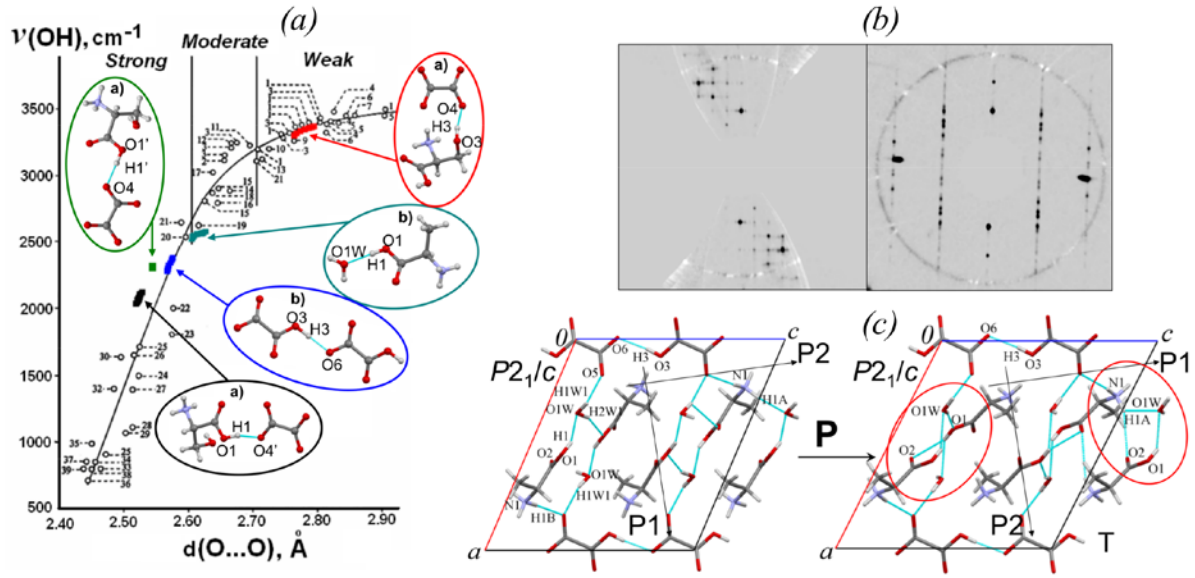

Architecture of Bismuth Oxysalts: Handling Oxocentered Bricks Into Walls and 3D Architectures.

Marie Colmont,[a] Almaz Aliev[a], Minfeng Lü[a,b], Marielle Huvé[a], Pascal Roussel[a] and Olivier Mentré[a]

[a] Université Lille Nord de France, UMR 8181 CNRS, Unité de Catalyse et de Chimie du Solide (UCCS USTL), F-59655 Villeneuve d'Ascq, France
[b] State Key Laboratory of Rare Earth Resource Utilization, Changchun Institute of Applied Chemistry, Chinese Academy of Sciences, Changchun 130022, P.R. of China.

The search for new materials with targeted properties has always been a hot research field in solid state chemistry due to promising properties in many fields. For example, new inorganic compounds, at the basis of novel properties are studies for their application in energy, electronics, nuclear etc…

In this context, an original predictive approach, to elaborate novel inorganic compounds is going on[1]. Concretely, the design of new compounds with 1D, 2D and 3D structures using original building units, consisting in oxo-centered OM_4 polyhedrons assembled into a structuring framework, the empty spaces being filled by groups of various natures, can be fully rationalized. In that sense, our approach is innovative and placed in the frame of the renewal of inorganic chemistry since the majority of structures predicted up to now were obtained through variable stacking of 2D building blocks.

The meticulous study of numerous new compounds in the Bi_2O_3-X_2O_5-M_xO_y (M= P, V, As…, X= Li, Na, Cu, Co, Ni, Mg, Cd…)[2–5] chemical system already enriched our experience in this field and opens great perspectives. From a structural point of view, these phases are deduced from one another by the reorganization of secondary building units based on $O(Bi,M)_4$ tetrahedrons. We evidenced a particular dependence between the nature of the units and the inter-layers space, leading to empirical rules at the basis of the real prediction of new complex structures. Nevertheless, we present here the extension of this predictive approach to various chemical systems and the "Design" of structures with various dimensionalities (1D to 3D), leading to different expected properties (dielectric, magnetic, optical…)[5,4]. The work consists in the diversification of the building units' sizes and topologies, in order to enlarge the self-assembly possibilities. The structure v.s. reactivity of each independent sub unit is tested, depending on its size and nature. This work involves a systematic rationalization of the preexisting phases to evidence the structural analogies and the chemical parameters controlling the final structure.

The richness of the crystal chemistry of the cationic blocks is governed is the same time by the asymmetric coordination of Bi^{3+} cations due to their stereoactive $6s^2$ lone pair but and by their ability to form oxo-centered OBi_n polyhedra stacked into zero-dimensional (0D), 1D, 2D and 3D frameworks. The typical Bi^{3+}-O bond valence often results in distorted OBi_4 tetrahedra that can admit the co-presence of other M^{n+} cations into $O(Bi,M)_4$ units, for relaxing the oxygen bonding scheme. The great diversity of aliovalent M^{n+} cations that can be incorporated into the $O(Bi,M)_4$ tetrahedral bricks make this class of inorganic compounds a gold mine of inspiration for the findings of novel structural motifs and physical properties.

Indeed, the reactivity of Bi-substituting elements was recently reviewed[1]. The nature of cations is of great importance, changing drastically the dimensionality and backbone of the rigid part of the crystal structure. Thus, the potentiality to combine in the same compound 2D-layers and 1-D channels of halides was firstly explored, yielding unique structural types (figure 1).

A succesfull substitution of Bi/La will also be presented, solved by precession electron crystallography[6]. It is a new 2D-layered compound built on OLa_4 oxocentered units and surrounded by isolated VO_4 tetrahedra and K+ cations with potential interesting catalytic properties.

Figures:

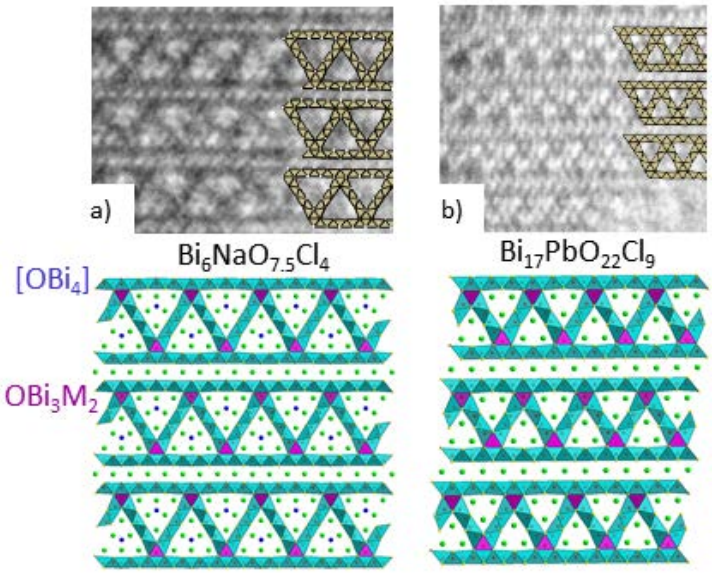

Fig.1. HREM image and crystal structure of a) $Bi_6NaO_{7.5}Cl_4$ and b) $Bi_{17}PbO_{22}Cl_9$: two innovative multi-dimensional compounds.

References:

(1) Krivovichev, S. V.; Mentré, O.; Siidra, O. I.; Colmont, M.; Filatov, S. K. *Chem. Rev.* **2013**.
(2) Kozin, M. S.; Colmont, M.; Endara, D.; Aliev, A.; Huvé, M.; Siidra, O. I.; Krivovichev, S. V.; Mentré, O. *J. Solid State Chem.* **2013**, *199*, 123–128.
(3) Colmont, M.; Huvé, M.; Abraham, F.; Mentré, O. *J. Solid State Chem.* **2004**, *177*, 4149–4162.
(4) Huvé, M.; Colmont, M.; Lejay, J.; Aschehoug, P.; Mentré, O. *Chem. Mater*. **2009**, *21*, 4019–4029.
(5) Endara, D.; Colmont, M.; Huvé, M.; Capet, F.; Lejay, J.; Aschehoug, P.; Mentré, O. *Inorg. Chem.* **2012**, *51*, 9557–9562.
(6) Colmont, M., Huvé, M., Palatinus, L., Djelal, N., Mentré, O. and Roussel, P. *Inorg. Chem.*, submitted.

$Cr_{1-x}V_xO_2$: HP/HT synthesis, structure and magnetic properties

Emilio Morán,[a] Ivan Pirrotta,[a] Miguel Angel Alario-Franco[a]

[a]Departmento de Química Inorgánica. Fac. C. Químicas. Universidad Complutense. 28040 Madrid. Spain. EU-

Introduction

Chromium dioxide is the only stoichiometric binary oxide that is both ferromagnetic and metallic. It is the simplest and best studied half-metal. First suggested to be half-metallic by Schwarz, CrO_2 has been studied extensively both theoretically and experimentally [1]. Its half-metallic behavior gives rise to relatively low electrical resistivity for an oxide, ~300 $\mu\Omega cm^{-1}$, and is commonly referred to as a "bad metal". CrO_2 is also ferromagnetic at room temperature with a high Curie temperature of Tc = 390 K. Concerning the synthesis, all methodologies include high pressure, i.e. the thermal decomposition of CrO_3 under conditions, there is a narrow stability range near 300 °C which extends to high oxygen pressure [2]. There is evidence, using angle-resolved synchrotron x-ray diffraction and high sensitivity confocal Raman spectroscopy under pressure for a structural phase transition from the α-CrO_2, phase I, tetragonal, rutile-type structure (S.G. P42 /mnm) to an orthorhombic β-CrO_2, phase II, ($CaCl_2$ -like, Pnnm) [3]. On the other hand, another rutile oxide, vanadium dioxide VO_2 experiences one of the more studied metal to insulator (MIT) phase transition: above 340 K crystallizes in the rutile tetragonal structure and at this temperature undergoes a first order transition, accompanied by structural distortions to the M1 phase with a monoclinic symmetry S. G. C2/m (C52h). In 1973, Chamberland conducted a series of experiments under high pressures and temperatures on the (M1) V_2O_4 monoclinic form: by applying a pressure of 65 Kbar and temperature from 500°C up to 1200°C on the (M1) form of vanadium dioxide he obtained in powder two new polymorphs named (M2) and (M3) as well as some crystals of the (M2) form [4]. The (M2) VO_2 exhibited a structural transition and an abrupt, reversible change in resistivity (approx. 4 orders of magnitude) at 66° C similar to that observed in (M1) VO_2. This behavior has been explained in terms of the V-V interatomic distances, clearly showing the presence of homopolar V^{4+} pairs. Finally, a room pressure phase diagram for the system $V_{0.9}Cr_{0.1}O_2$ (but containing Cr^{3+}) which is based on magnetic susceptibility, electrical resistivity, and powder x-ray diffraction measurements has been reported [5]. Thus, taking all this complexity into acccount, it seems interesting to prepare –under high pressure conditions to preserve Cr^{4+}- several members of the solid solution between these two rutile-type oxides and to study their structure and properties, which is the aim of this contribution.

Results and discussion

In this work, by applying a pressure of 40 Kbar and 900°C in a "Belt"-type press, and using the binary oxides as reactants, several members of the solid solution $Cr_{1-x}V_x O_2$ ($0{,}1 \leq x \leq 0{,}9$ have been prepared. A structural change as a function of composition has been observed when $0.500(6) \leq x \leq 0.580(1)$. We can propose two different rutile-like models corresponding to the two different regions of the solid solution: powder X-Ray Rietveld data refinements show a rutile-like structure that varies, as a function of V content, from $CaCl_2$ rutile-like ($x < 0.50$) to the (M3) VO_2 structure ($x > 0.58$) (see figure below). Moreover, it

has been observed that the presence of V in CrO_2 "induces a pressure effect" allowing the structural transition from rutile to the $CaCl_2$ structure taking place at 40 Kbar. Electron diffraction experiments revealed a diffuse polarized streaks that suggest a short range order V/Cr for the composition $Cr_{0.499(4)}V_{0.500(6)}O_2$. The magnetic properties showed a transition from paramagnetic (PM) to antiferromagnetic (AFM) in lowering the temperature. Also, independently of the type of structure ($CaCl_2$ or (M3) – VO_2) all samples showed AFM order in decreasing the temperature. The transition temperature T_N is linearly dependent of the V content in the structure; this trend has been explained by the presence of mixed Cr and V oxidation states in the structure.

Figures:

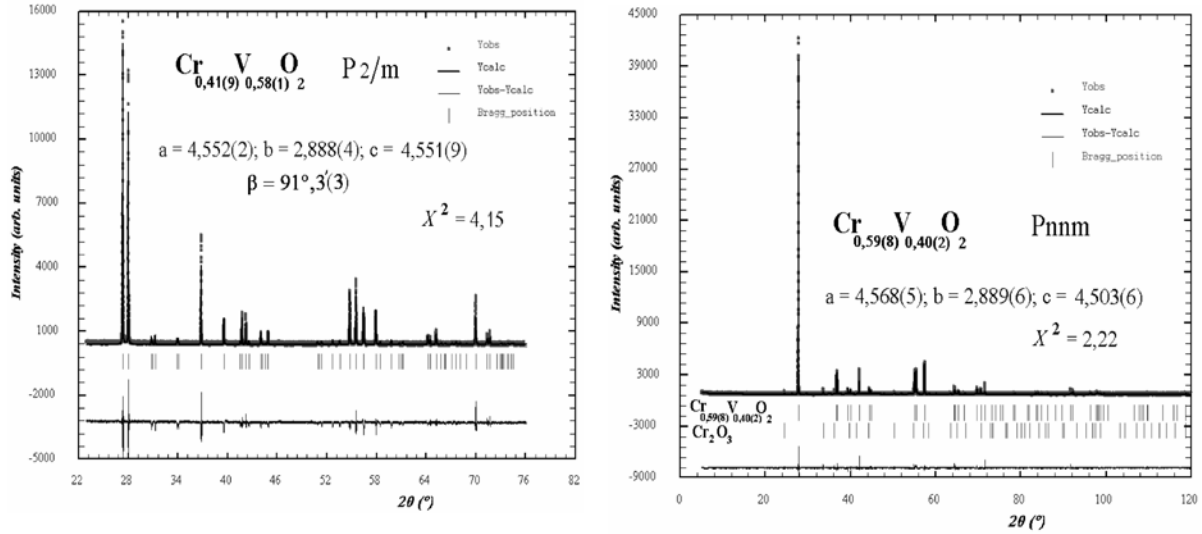

Figure 1. Rietveld refinements for $Cr_{0.42}V_{0.58}O_2$ (left) and $Cr_{0.59}V_{0.41}O_2$ (right)

Acknowledgements
The authors acknowledge financial support from the European Union through the FP7-PEOPLE-2007-1-1-ITN SOPRANO network and from the Comunidad de Madrid through the MATERYENER project S2009-PPQ-1626. The authors wish to express their gratitude to Dr. J.M. Gallardo Amores the high pressure / high temperature synthesis.

References:

[1] Y. Ji, G. J. Strijkers, F. Y. Yang, C. L. Chien, J. M. Byers, A. Anguelouch, Gang Xiao, and A. Gupta, *Phys. Rev. Lett*. (2001), 5585.
[2]. P. G. Ivanov, S. M. Watts, and D. M. Lind, *J. Appl. Phys*. **89** (2001), 1035.
[3] B. R. Maddox, C. S. Yoo, D.Kasinathan, W. E. Pickett, and R. T. Scalettar, *Physical Review B* **73** (2006), 144111.
[4] B. L. Chamberland, *J. Solid State Chem*. **7** (1973), 377-
[5] P. Porta, M. Marezio, J. P. Remeika, P. D. Dernier, *Mat. Res. Bull*. **7 (**1972), 157.

3D Fluorophosphates as Cathode Materials for Rechargeable Batteries

Khasanova N.R.,[a] Fedotov S.S.,[a] Drozhzhin O.A.,[a] Abakumov A.M.,[b] Antipov E.V.[a]

[a] Department of Chemistry, Moscow State University, Moscow 119991, Russia;
[b] University of Antwerp, Groenenborgerlaan 171, B-2020, Antwerp, Belgium.

Li-containing transition metal compounds containing two types of anions (fluoride and polyatomic oxyanions) show perspectives as high-voltage cathode materials by taking advantage of the electronegativity of fluorine in combination with the inductive effect of the polyanion group. Furthermore, appearance of the monovalent fluoride anion might expand the free unit cell volume available for lithium ion migration thus promoting its faster mobility. Fluorophosphates of the general formula A_2MPO_4F have captured much attention because of their potential for two-electron activity per transition metal, which would result in higher specific capacity and energy density.

In the search for high-energy cathode materials for Li-ion batteries we have explored the Li_2MPO_4F (M=Co, Mn, Fe) fluorophosphates with 3D structure comprised of one-dimensional chains of metal octahedra interconnected by phosphate groups and intersecting channels capable of alkali-ion diffusion [1]. The flurophosphate phases and their substituted analogs were prepared through different synthetic routes (solid-state reactions, cryochemistry, ion-exchange) depending on the nature and chemistry of transition metal. Combination of synchrotron X-ray/neutron diffraction and electron microscopy were applied to present a thorough structural characterization of this fluorophosphate family. The electrochemical investigation revealed that lithium de/intercalation in this system proceed by a single-phase mechanism with average discharge voltages ranging from 3.4 V (vs. Li/Li^+) for Li_2MPO_4F to 4.8 V for the Co-counterpart; and the redox potential might be tuned by appropriate substitution on the transition metal site [2,3]. Electrochemical properties of this fluorophosphate family will be compared with electrochemical performance of other fluorophosphate and phosphate cathode materials.

The work was supported in part by Russian Foundation for Basic Research (RFBR grant 13-03-00495a).

References:

[1] M. Dutreilh, C. Chevalier, M. El-Ghozzi, D. Avignant, *J. Solid State Chem.*, **142** (1999) 1.
[2] Nellie R. Khasanova, Oleg A. Drozhzhin, Darya A. Storozhilova, Claude Delmas, Evgeny V. Antipov, *Chem. Mat.* **24** (2012) 4271.
[3] Nellie R. Khasanova, Oleg A. Drozhzhin, Stanislav S. Fedotov, Darya A. Storozhilova, Rodion V. Panin, Evgeny V. Antipov, *Beilstein J. Nanotechnol*. **4** (2013) 860.

Fischer-Tropsch Synthesis with Bimetallic Nanoparticles: *In Situ* Surface Monitoring by Synchrotron X-Ray Spectroscopy

Sophie Carenco,[a] Selim Alayoglu,[a] Cheng Hao Wu,[a] Hendrik Bluhm,[b] Miquel Salmeron[a]

[a]Materials Sciences Division, Lawrence Berkeley National Lab, 1 Cyclotron Road, Berkeley, Californie, USA;
[b]Chemical Sciences Division, Lawrence Berkeley National Lab, 1 Cyclotron Road, Berkeley, Californie, USA.

Fischer Tropsch synthesis is a major process for forming alkanes and alkenes, synthetic fuels, etc. Catalysts of choice are generally cobalt and iron. However, there is a growing interest for shifting the selectivity of the reaction to oxygenates products (alcohols, aldehydes, ketones, etc.) because these compounds have a higher added value both as precursors and as next-generation fuels.

A typical solution to improve the catalyst's selectivity is to use bimetallic (alloy, core-shell, etc.) catalysts, such as manganese-doped cobalt nanoparticles or copper-cobalt nanoparticles. Unfortunately, little is known about the behavior of these complex structures under reaction condition. Amongst the possible changes, metal inter-diffusion and segregation can happen, depending on the nature of the two metal and their propensity to form alloys as well as their respective interaction with the gaseous reactants.

Here, nickel-cobalt core-shell nanoparticles will be compared to copper-cobalt core-shell nanoparticles. Both systems show a very interesting selectivity for oxygenates vs. alkanes and alkenes but their fate under reaction conditions was found to be completely opposite. Indeed, in the copper-cobalt case is was recently demonstrated that the nanoparticles undergo degradation through dealloying of cobalt, due to the strong interaction of cobalt with carbon dioxide in reducing conditions, as well as the limited stability of cobalt-copper alloy.[1,2]

By contrast with this, nickel-cobalt nanoparticles were shown to be much more robust, under reaction conditions, in particular when using CO_2 as a carbon source instead of CO. This was demonstrated using 25 nm core-shell nickel-cobalt nanoparticles that were prepared through a new synthetic route, allowing an excellent control of the nanoparticles size and composition.[3]

Using synchrotron-based Ambient-Pressure X-Ray Photo-electron Spectroscopy (APXPS), a technique that allows collecting XPS spectra under pressure atmosphere up to a few mbar, it was demonstrated that the core-shell nanoparticles undergo alloying as early as during the pretreatment steps of the catalysis process (cycles of oxidation and reduction). This finding was confirmed by STEM-EDS mapping using more traditional *ex situ* TEM, which also revealed a profund structural rearrangement with the formation of voids into the nanoparticles. The resulting surface alloy was found to be stable under model reaction conditions.

As a main finding, we proposed that the surface alloy could be responsible for the selectivity of the nanocatalyst for oxygenates (alcohols and formaldehyde). This works proposes a

general methodology for monitoring of bimetallic nanocatalysts, using APXPS on a model core-shell system. Moreover, it suggests that nanoscale alloys may have unexpected selectivity in industrially-relevant processes, opening an avenue for further exploration of these original structures.

References:

[1] S. Carenco, A. Tuxen, M. Chintapalli, E. Pach, C. Escudero, T.D. Ewers, P. Jiang, F. Borondics, G. Thornton, A.P. Alivisatos, H. Bluhm, J. Guo, M. Salmeron, *J. Phys. Chem. C* **117** (2013) 6259.
[2] S.K. Beaumont, S. Alayoglu, V. V. Pushkarev, Z. Liu, N. Kruse, G. A. Somorjai, *Faraday Discuss.* **162** (2013) 31.
[3] S. Carenco, S. Alayoglu, C.-H. Wu, A. Shavorskiy, H. Bluhm, G. A. Somorjai, M. Salmeron, *manuscrit in preparation*.

Figures:

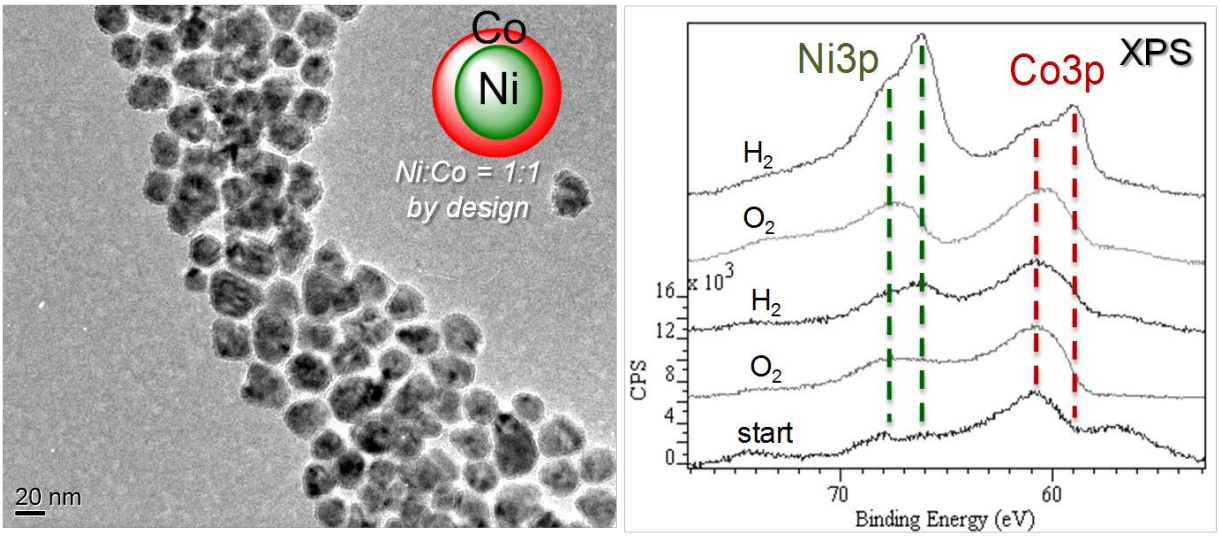

Fig.1. Left: TEM observation of core-shell Nickel-Cobalt Nanoparticles. Right: Ambient-pressure XP spectra collected in the Ni3p and Co3p region at several steps of the nanocatalyst pretreatment.

Synthesis and Electrochemical Study of Nanostructured PEDOT/MnO_2 Composites for Supercapacitor Applications

V.V. Kondratiev, A.O. Nizhegorodova, S.N. Eliseeva, E.G. Tolstopjatova

Institute of Chemistry, St. Petersburg State University
Russian Federation, 198504, St.Petersburg, Petrodvoretz, Universitetsky pr.26
e-mail: vkondratiev@mail.ru

Supercapacitor materials have been intensively investigated last decades due to exponential growth of the demand in energy devices for portable electronics and transport. One of the perspective ways for development of pseudocapacitive materials, based on faradaic surface reactions, is the combination of dispersed transition metal oxides and conducting polymer matrices. In particular, the manganese oxide in combination with poly-3,4-ethylenedioxythiophene (PEDOT) has attracted interest as low-cost materials with high specific capacitance and reversible charge-discharge processes.

In the present work a simple and cost-effective methods of synthesis of composite PEDOT/MnO_2 with layered or uniformly dispersed manganese oxide particles have been employed. The morphology of highly dispersed manganese oxide on PEDOT surface was characterized by STM. XPS spectroscopy was used for identification of valence states of manganese at different oxidation states of composites. Electrochemical properties of composites, obtained with variation of synthesis conditions, were investigated using cyclic voltammetry , constant current charging-discharging method and electrochemical impedance spectroscopy.

The obtained results indicates that the combination of PEDOT and MnO_2 could reduce the internal resistance and enhance electrochemical capacitive performance of electrode.
The specific capacitance values related to total mass of composite materials and mass of separate active components (PEDOT and MnO_2) were calculated from CV and other methods. The specific capacitances of PEDOT were in the range of 60-80 F/g, that is in accord with typical literature data for PEDOT in aqueous solution. The values of specific capacitances of MnO_2 layers were much higher and varied within the range 270 – 330 F/g. The enhanced capacitive properties of composites can be mainly attributed to 3-D distribution of disperse MnO_2 in the mesoporous/microporous structure of PEDOT with high surface area. The presence of conducting porous matrix facilitates ion diffusion and electron transfer, leads to the lowering the internal resistance of composite material and improves the electrochemical utilization of manganese oxide. The high stability of composite materials was shown by means of long-term cycling, where the low decrease in capacitance values were observed. The capacitive parameters of composites with different ratio between PEDOT and MnO_2 layers were systematically investigated and analyzed.

Acknowledgements: The authors are thankful to the colleagues from Interdisciplinary Resource center for Nanotechnology and Resource center “Physical methods of surface investigation” of St.Petersburg State University. Financial support from Russian Foundation for Basic Research (grant №13-03-00894) is gratefully acknowledged.

Photochemical syntheses in anhydrous hydrogen fluoride – a pathway to high oxidation state fluorides

Zoran Mazej,[a]

[a]Department of Inorganic Chemistry and Technology, Jožef Stefan Institute, Jamova 39, SI-1000 Ljubljana, Slovenia, zoran.mazej@ijs.si.

Preparation of fluorides in the highest oxidation states usually requires high temperature and high pressure of fluorine. At ambient temperature they can be synthesized by the use of strong oxidizers as KrF_2. Another way for the preparation of thermally less stable fluorides is the use of photochemical reactions with elemental fluorine. For example, the preparation of very reactive and thermally unstable fluorides of noble gases (XeF_2, XeF_4 and KrF_2) is well established. Later it was found that reactions with UV-irradiated elemental fluorine at ambient temperature can be used for the preparation of some ternary fluorides with transition metal in the highest oxidation state using anhydrous hydrogen fluoride (aHF) as a solvent.[1]. In this contribution some examples of photochemical syntheses done in our department would be presented including Mn(IV), Cr(V), Au(V) and Xe(VI) compounds (Figure 1).

In the case of Mn(IV) we succeed in the preparation of large quantities of pure A_2MnF_6 (A = Li-Cs) compounds and MnF_4.[2] They were further used for high-temperature mass spectrometry studies of their thermal decomposition [3] and they were also used in the studies of the high-temperature reactions with C_{60}.[4]

Since only $CsCrF_6$ was known before we were interested in the preparation of $[CrF_6]^-$ salts with other alkali metal cations. The new $[CrF_6]^-$ salts of Li, Na, K, and Rb and previously known $CsCrF_6$ were prepared. All of them were structurally characterized for the first time.[5]

The AuF_6 salts with divalent metals are also poorly structurally characterized. Our attempts to grow single crystals and determine their crystal structures were successful in the case of $M(AuF_6)_2$ (M = Cd, Hg, Ag). Additionally, $AgFAuF_6$ and, $Mg(HF)AuF_4AuF_6$ were structurally characterized.[6,7]

In spite of a large number of existing compounds in the XeF_6/MF_4 (M = transition element) system, reports about the crystal structures of the corresponding $[XeF_5]^+$ salts are limited to M = Pd, Ni and Cr. Instead of XeF_6, we used XeF_2 as a starting material and as precursor for the *in situ* preparation of XeF_6. The XeF_2/MF_4 mixtures could be prepared in the requested molar ratios and loaded into reaction vessels in a dry box; meanwhile, XeF_6 could be added onto TiF_4 only by condensation in a vacuum system. XeF_2 is converted into XeF_6 by photochemical reaction with UV-irradiated elemental fluorine in anhydrous hydrogen fluoride as a solvent. Crystal structures of $[XeF_5]_3[Ti_4F_{19}]$ and $[Xe_2F_{11}][PbF_6]$ were determined.[8]

The described photochemical syntheses of some ternary fluorides at room temperature offer milder approach for the formation of these compounds. All reactions were carried out in reaction vessels made of fluorinated polymers, which are very resistant and inert materials and therefore there is no danger of final product contamination by by-products formed between reagents and reaction vessel material. This possibility should be taken into account when metal reaction vessels and very high temperatures are involved. The advantages of reactions in solution are easier control of fluorination and homogeneous products with uniform particle

sizes. Therefore, the described approach deserves more frequent use in the preparation of various very pure fluorides, not only for ones described here. However, this approach can be used only in laboratories properly equipped for the work with anhydrous HF.

References:

[1] K. Lutar, H. Borrmann, M. Leblanc, *Recent developments in the Synthesis of Inorganic Fluorides,* in: T. Nakajima, B. Žemva, A. Tressaud (Eds.), *Advanced Inorganic Fluorides: Synthesis, Characterization and Applications*, Elsevier, Oxford, 2000.
[2] Z. Mazej, *J. Fluorine Chem.* **114** (2002) 75-80.
[3] M. S. Leskiv, S. V. Abramov, L. I. Oleinik, A. V. Kepman, V. F. Sukhoverkhov, Z. Mazej, D. V. Rau, N. S. Chilingarov, L. N. Sidorov, *Inorganic Materials*, **41** (2005) 1327–1333.
[4] A.A. Goryunkov, I.E. Kareev, I.N. Ioffe, A.A. Popov, I.V. Kuvychko, V.Y. Markov, I.V. Goldt, A.S. Pimenova, M.G. Serov, S.M. Avdoshenko, P.A. Khavrel, L.N. Sidorov, S.F. Lebedkin, Z. Mazej, B. Žemva, S.H. Strauss, O.V. Boltalina, *J. Fluorine Chem.* **127** (2006) 123-1435.
[5] Z. Mazej, E. Goreshnik, *Eur. J. Inorg. Chem.* (2008) 1795–1812.
[6] Z. Mazej, E. Goreshnik, *Solid State Sciences* **8** (2006) 671–677.
[7] Z. Mazej, E. Goreshnik, G. Tavčar, *J. Fluorine Chem.* **132** (2011) 686–689.
[8] Z. Mazej, E. Goreshnik, *Eur. J. Inorg. Chem.* (2009) 4503–4506.

Figure:

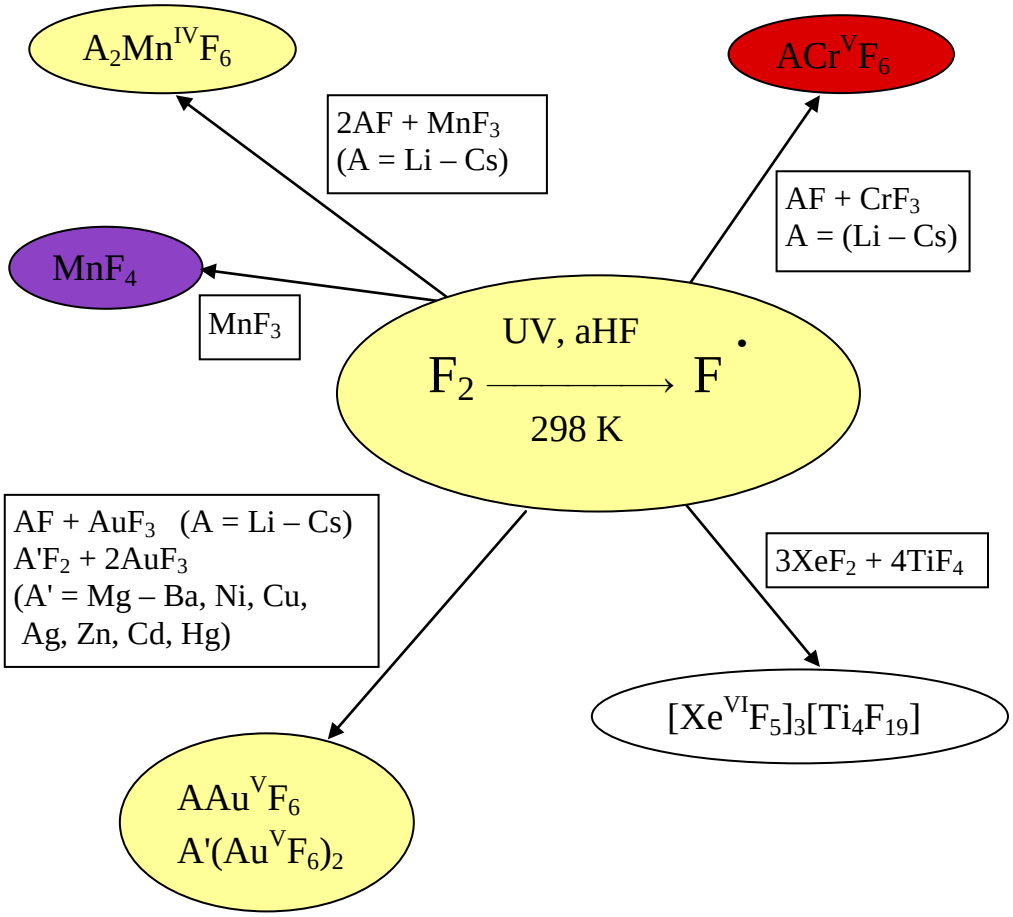

Figure 1. Some examples of high oxidation state fluorides prepared by photochemical reactions in anhydrous hydrogen fluoride (aHF = anhydrous hydrogen fluoride)

Functionalized ionic liquids based on piperidinium cations with ester group as electrolytes for lithium battery

Peixia Yang, Jun Hou, Jing Li, Jinqiu Zhang, Maozhong An,

School of Chemical Engineering and Technology, Harbin Institute of Technology, Harbin 150001, China

In 21st century, energy resources are dwindling day by day, the problem cannot be ignored. So, there is necessary for us to replace the traditional energy resources. Lithium battery has a lot of advantages like the high working voltage, high specific energy, long cycle life and so on. It has been the future of chemical power sources. But the safety performance is always the limit to lithium battery, especially in the condition that of abusing. To solve the problem, it is urgency to find safe lithium battery electrolytes.

Ionic liquids (ILs) are formed by organic cations and various anions, which have melting points at or below ambient temperature. ILs has many superior properties including nonvolatility, nonflammability, good thermal stability, great electrochemical stability and high ionic conductivity[1]. Basing on these properties, ILs has showed potential as safe electrolytes for lithium battery system. But, there exist some questions. ILs are easy to absorb the moisture in the air, so that the adhibition of them is limited in lithium battery. And most of the ILs have the high viscosity, it will reduce the ionic conductivity. Due to these disadvantages, there is necessary to synthesize the new functionalized ionic liquids. Functionalized ionic liquids are ionic liquids which have specific functions through the introduction of functional groups on the cation or anion of ionic liquids[2]. The introducing functional groups can be endowed with special performance of ionic liquids. For example, we can introduce special groups on ionic liquid to reduce its viscosity, which can improve the electrical conductivity. Because of these qualities, introducing one or more functional groups on the cation or anion of ionic liquids has become new focus. Ester-functionalized ionic liquids have been reported in using of lubrication, Suzuki cross linking reaction, organic synthesis and so on[3]. In this essay, a new functional ionic liquid based on piperidinium cations with ester group was synthetized. The ionic liquid was investigated in terms of physical-chemical properties electrochemical characteristics and it was used as lithium battery electrolytes without additives [4].

Take as mole ratio of N-methyl-methyl acetate base piperidine bromide (PPO2Br) with two, three fluorinated methyl sulfonyl imide lithium (Li-TFSI) dissolved in deionized water, stir at room temperature after 12 h, use dichloromethane extraction below oily liquid, ion and wash with silver nitrate to detect the upper aqueous solution without turbidity is generated. Collect belower solution, rotary evaporation out methylene chloride, finally will product vacuum drying 24 h, get ionic liquids (three fluorinated methyl sulfonyl) imine N-methyl-methyl acetate base piperidine (PPO2TFSI). Measure this kind of ionic liquid conductivity and electrochemical window and the determination of lithium ion transference number. Results show that the ionic liquid at room temperature (25 ℃) conductivity is 0.77 $mS \cdot cm^{-1}$, electrochemical window is 4.5V, lithium ion transference number is 0.56. Assemble the “Li/PPO2TFSI LiTFSI/LiFePO4” half cell and test the performance of the battery.

References:

[1] P. Davide Cozzoli, Teresa Pellegrino, Liberato Manna, *Chem. Soc. Rev.*, **35** (2006) 1195.
[2] Hyungrak Kim, Marc Achermann, Laurent P. Balet, Jennifer A. Hollingsworth, Victor I. Klimov, *J. Am. Chem. Soc.*, **127** (2005) 544.
[3] Marianna Casavola, Vicenzo Grillo, Elvio Carlino, Cinzia Giannini, Fabia Gozzo, Enrique Fernandez Pinel, Miguel Angel Garcia, Liberato Manna, Roberto Cingolani, P. Davide Cozzoli, *Nano Lett.*, **7** (2007) 1386.
[4] Hao Zeng, Jing Li, Z. L. Wang, J. P. Liu, Shouheng Sun, *Nano Lett.*, **4** (2004) 187.

.

Figures:

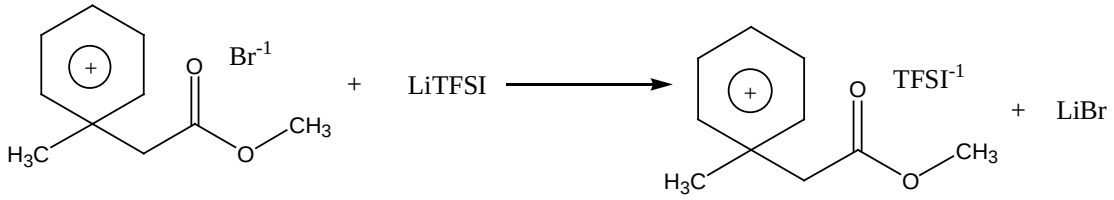

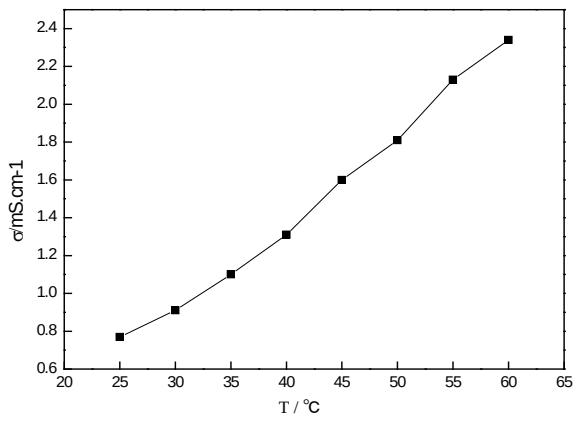

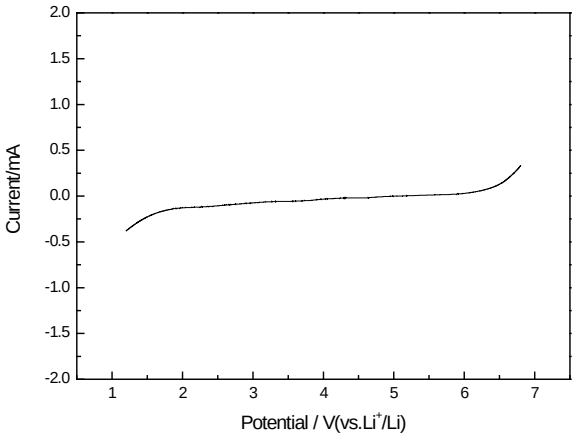

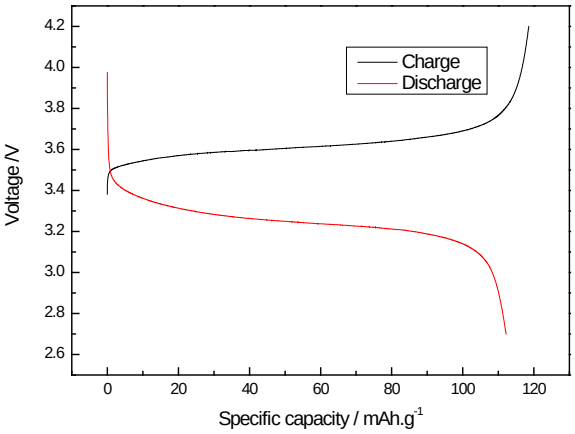

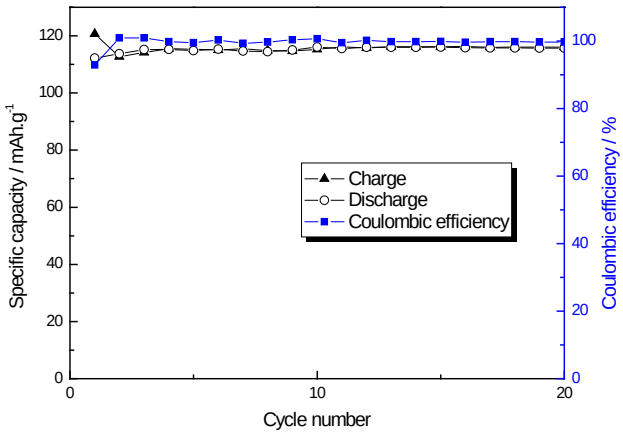

Studies on rate performance of spherical natural graphite used as anode material of lithium ion battery

Guohui Yuan,[a] Min Yue,[b] Dongliang Kong, [b] Lixia Fu, [a] Lei Du [a]

[a]School of Chemical engineering and Technology, Harbin Institute of Technology, China;
[b] Shenzhen BTR New Energy Materials Inc., China.

As anode material of lithium ion battery, graphite has the advantages of high Specific capacity, low potential, and low cost. Graphite occupies an irreplaceable position in commercial lithium ion battery [1-2]. However, the poorer rate performance and cycle performance of graphite seriously restricts its further application in EVs.

In this work, the spherical natural flake graphite, produced by Shenzhen BTR New Energy Materials Inc. China, was modified by oxidation and carbon-coating to improve its rate performance and cycle performance. The oxidation was carried in the mixture of concentrated sulfuric acid and hydrogen peroxide at 0ºC and the carbon coating was performed by mixing of the oxidized graphite powder with phenolic resin precursor.

Fig.1. shows the XRD patterns of natural graphite and oxidized natural graphite. The typical peak (002) of oxidized graphite moves to the left. So the layer spacing of carbon-coated graphite is larger than natural graphite according to Brag equation.

The SEM images of the spherical natural graphite and carbon-coated one are shown in Fig.2. All the graphite powder are potato-shape. The natural graphite has a rough surface and the flake structure can be observed on the surface. In contrast to the graphite, the surface of carbon-coated one is smoother. The smooth layer on the graphite is the carbon coating. So the core-shell structure of anode material was formed.

Fig.3. shows the first-cycle of CV curves for the spherical natural graphite and carbon-coated one. The reduction peak of carbon-coated graphite at 0.2-0.8V (vs. Li^+/Li), related to the SEI, was less than that of natural graphite. The result indicates the less irreversible capacity of carbon-coated graphite.

Fig. 4 shows the first-cycle of galvanostatic charge/discharge curves for the spherical natural graphite and carbon-coated one. The initial irreversible capacity of carbon-coated graphite was 362.3 mAh/g, large than the 317.1 mAh/g of natural graphite. The first-cycle coulombic efficiency was enlarged from 85% of natural graphite to 92% of carbon-coated one.

Fig.5 shows the relationship between specific capacities and cycle numbers at 1C galvanostatic charge/discharge. The capacity of natural graphite was decreased from 137.2 mAh/g to 99.5 mAh/g after 150 cycles and the capacity retention was 72.5%. The capacity of carbon-coated graphite was decreased from 281.3mAh/g to 231.9mAh/g after 150 cycles and the capacity retention was 82.4%.

The specific capacities of the spherical natural graphite and carbon-coated one at different constant currents are compared in Fig.6. The data show that the difference of capacity between the spherical natural graphite and carbon-coated one was enlarged with the increasing discharge current in the range of 0.1C-2C. The carbon-coated graphite possesses much better rate property than the natural graphite. This indicates that the rate ability of spherical natural graphite was improved by oxidation and carbon-coating.

The results above indicate that the oxidation in the mixture of concentrated sulfuric acid and hydrogen peroxide at 0ºC and the carbon coating was the effective way to improve the rate and cycle performance of spherical natural graphite for lithium ion battery.

The authors gratefully acknowledge financial support from the Natural Science Foundation of China (21076050) and National Science and Technology Support Program of China (2013BAE04B04).

References:

[1] M Winter, J O Besenhard, M E Spahr, *Advanced Materials*, **10**(1998) 725.
[2] Hassoun J, Lee K S, Sun Y K, *J. Am. Chem. Soc.*, **133(**2011) 3139.

Figures:

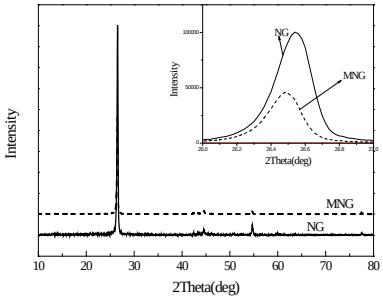

Fig.1. the XRD patterns of natural graphite and oxidized natural graphite

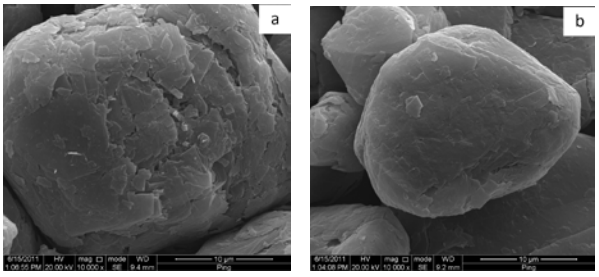

Fig.2. SEM images of spherical natural graphite (a) and oxidized natural graphite (b)

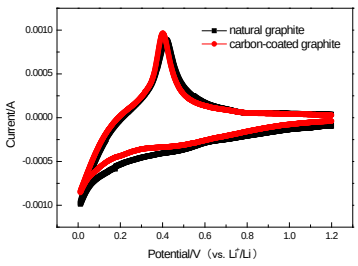

Fig.3. The first-cycle of CV curves

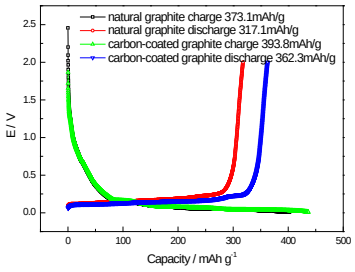

Fig.4. The first-cycle of galvanostatic charge/discharge curves

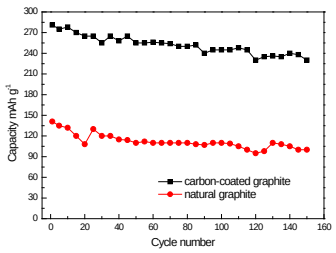

Fig.5. The cycle performance curves at 1C

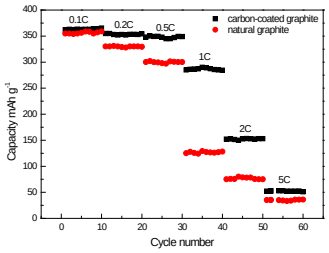

Fig.6. The rate performance curves

Charge transfer processes on electrodes modified by polymer films of metal complexes with the Schiff bases.

O. V. Levin[a], E. V. Alekseeva[a], V.V. Sizov[a], A. M. Timonov[b], M. V. Novozhilova[a], V. V. Malev[a]

[a] St. Petersburg State University,
[b] State Pedagogical University "A. I. Herzen", St. Petersburg;
Universitetsky pr. 26, Petergof 198504, Russia
levin@chem.spbu.ru

Polymer transition metal complexes with tetradentate N_2O_2 Schiff base ligands derived from salicylaldehydes and aliphatic diamines, often denoted as poly-[M(Schiff)] can be formed easily on inert electrode surfaces via oxidative electrochemical polymerization of corresponding Schiff base monomers in moderately/weak donor solvents. The interest to such materials is caused by a variety of potential applications, including their use in chemical and biological sensors, electrocatalytic systems, molecular electronic devices, advanced batteries, and ultracapacitors [1, 2]. Schiff base metal polymer-modified electrodes have been studied by several groups.

Despite intensive studies, many features of poly-[M(Schiff)] films have still remained unclear. In particular, there is some inconsistency between the observed voltammetric response of the polymer in the potential range from 0 to 1.3 V and one-electron character of the polymer redox-switching. To clarify this feature, a series of Salen-type complexes with different substituents in imino bridges and phenyl rings was selected. Their charge transfer properties were studied in acetonitrile solutions by means of impedance spectroscopy, cyclic voltammetry, quartz crystal microbalance and UV-visible spectroscopy methods. It was observed that introduction of substitutes into phenyl rings leads to a noticeable splitting of cycling voltammetric curves into at least two ox/red transitions, while substituents in imino bridges slightly affect the shape of voltammograms. The obtained impedance results as a whole were satisfactorily treated in scope of the so-called model of homogeneous films with two kinds of charge carriers. However, it was established that in the ranges of overlapping ox/red transitions the Warburg and the pseudo-capacity types of the impedance frequency dependencies were simultaneously observed. This, most likely, resulted from the presence of three kinds of charge carriers in the film interior. In other words, two charge/discharge processes exists in the studied polymers. In fact, spectroscopic and microbalance data demonstrated that even in non-substituted poly-[Ni(Salen)] films two charge transfer processes do exist, and introducing of substituents into ligand structure changes the nature of only one of them. According to literature data and DFT calculations preformed by our group the first process was attributed to ligand oxidation, and the second one – to the oxidation of the metal atom, stabilized by solvent coordination in the axial positions.

Acknowledgements:
Financial support of the Russian Foundation for Basic Research (grants # 12-03-00560-a, # 12-03-00843-a) and the St. Petersburg State University (grant # 12.38.77.2012) is gratefully acknowledged.

References:

[1.] C.E. Dahm, D.G. Peters, Catalytic reduction of α, ω-dihaloalkanes with nickel(I) salen as a homogeneous-phase and polymer-bound mediator, J. Electroanal. Chem. 406 (1996) 119.
[2.] A. Timonov, S. Logvinov, N. Shkolnik, S. Kogan, Polymer-modified electrode for energy storage devices and electrochemical supercapacitor based on said polymer-modified electrode, US Patent No 6,795,293 (2004)

3D Ordered Macroporous Germanium Electrodeposited from Ionic Liquid and Its Electrochemical Properties

Jiupeng Zhao, Xin Liu

School of Chemicl Engineering and Technology, Harbin Institute of Technology, 150001

Germanium is a promising candidate for negative electrodes in lithium ion batteries due to its large theoretical capacity[1-3]. However, its use is frustrated by comparatively poor capacity retention due to mechanical stresses caused by the volume changes during charge/discharge cycles. It was reported that order-aligned nano-structured materials have significant advantages in their kinetics and electronic conduction during the lithium insertion /extraction process. Here we use the strategy to improve the electrochemical performance of Ge electrodes by constructioin of 3D ordered macroporous (3DOM) germanium. Three dimensionally macroporous materials provide a high accessible surface areas, continuous networks, short diffusion lengths and fast transport of reagents inside the porous structure and therefore, it will minimize the mechanical stress induced by the volume change of Ge, shorten the lithium solid-state diffusion distances and lead to enhanced capacity and cycling stability.

Here we present a method of preparing 3D ordered macroporous germanium negative electrode materials. The preparation is based on filling the interstices of self-assembled polystyrene (PS) colloidal crystal templates by eletrodeposition directly on copper foil from ionic liquids, containing $GeCl_4$ as precursor. 3D ordered macroporous germanium electrodes are then obtained by the etching of PS templates and used as the electrode for Li ions batteries. The ordered macroporous germanium was characterized by SEM, EDX, Raman spectroscopy and charge-discharge measurement. The electrochemical characteristics of anodes were studied in a cell with a lithium counterelectrode. The deposited germanium has a well-ordered macroporous nanoarchitecture consisting of uniform close-packed spherical pores. The holes into the layer below are clearly visible, indicating the three-dimensional ordering of the structure.

In ordered to compare, the electrochemical performance of dense gemanium film has also been tested. 3DOM Ge exhibits a reversible capacity of 1024 mAh/g and retains a capacity of 844mAh/g after 50 cycles at the rate of 0.2C, while dense Ge film only has 611mAh/g after 50 cycles. The results suggest that 3DOM Ge film shows significantly improved cycleability and rate performance compared with the dense Ge film. The high capacity and good cycle life of such 3DOM structured Ge could be attributed to the ordered and very open macroporous structure, which offers highly efficient and fast pathways for electron transport to enhance the battery performance. 3DOM Ge electrode with high irreversible specific capacity is a very promising material for next-generation lithium ion battery.

References:

[1] M. H. Park, Y. Cho, K. Kim, J. Kim, M. L. Liu, J. Cho, *Angew. Chem., Int. Ed.*, 50 (2011), 9647.
[2] S. Yoon, C. M. Park, H. J. Sohn, *Electrochem. Solid-State Lett.*, 11(2008) A42.
[3] M. H. Park, K. Kim, J. Kim, J. Cho, *Adv. Mater.*, 22(2010)415.
[4] O. D. Velev, T. A. Jede, R. F. Lobo, A. M. Lenhoff, *Nature*,389(1997)44.

Figure:

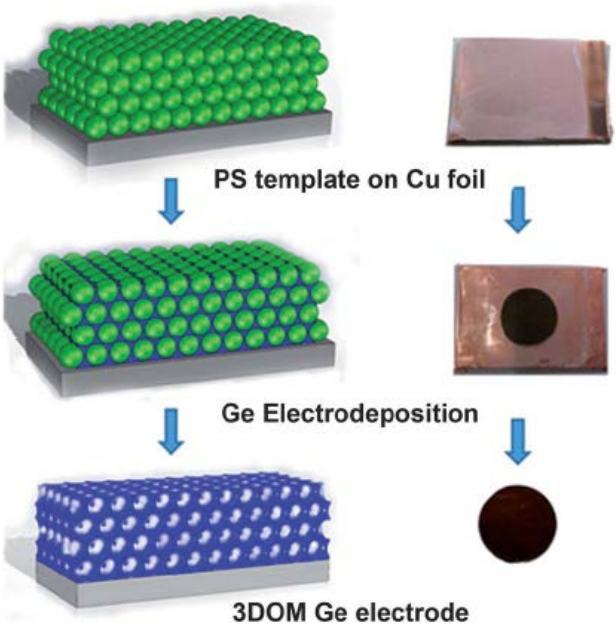

Fig.1. Schematic of the synthesis of the 3DOM Ge electrode.

Soft Chemical Synthesis and Electrochemical Lithium Insertion Properties of a Novel Hydrogen Titanium Oxide $H_2Ti_{12}O_{25}$

Junji Akimoto,[a] Kunimitsu Kataoka,[a] Hideaki Nagai,[a] Tomoyuki Sotokawa,[b] Yoshimasa Kumashiro[b]

[a] National Institute of Advanced Industrial Science and Technology (AIST), Tsukuba, Japan
[b] Ishihara Sangyo Kaisha Ltd., Yokkaichi, Mie, Japan

The spinel-type lithium titanium oxide, $Li_4Ti_5O_{12}$ is attractive as one of the oxide negative electrode materials for advanced lithium ion batteries, since this compound exhibits the reversible Li insertion and extraction properties around 1.55 V (versus Li/Li^+). Because of the structural restriction of the spinel structure, unfortunately, the theoretical capacity of $Li_4Ti_5O_{12}$ was limited to be 175 mAh g^{-1}. Among the titanium oxide compounds, TiO_2(B) has been investigated as a promising candidate having a high theoretical capacity of 335 mAh g^{-1}.

TiO_2(B) can be prepared by using soft chemical synthetic technique from layered potassium titanium oxide $K_2Ti_4O_9$ precursor via K^+/H^+ ion exchange, followed by dehydration, as originally reported by Marchand et al. A similar synthetic technique gave an access to additional titanium dioxide compounds, i.e., TiO_2(H) and TiO_2(R). We recently re-examined the crystal structure and electrochemical properties of some lithium titanium oxides, $Li_2Ti_3O_7$ [1] and $Li_2Ti_6O_{13}$ [2], and some hydrogen titanium oxides $H_2Ti_3O_7$ [3] and $H_2Ti_6O_{13}$ [4]; all of these compounds have successfully synthesized by soft chemical synthetic methods. In the present study, we report the synthesis, chemical characterization and electrochemical Li insertion and extraction properties of a novel hydrogen titanium oxide $H_2Ti_{12}O_{25}$.

The $H_2Ti_{12}O_{25}$ samples were prepared using two synthetic routes in the present study as summarized in Fig. 1. In the first synthetic route [5], the precursor $Na_2Ti_3O_7$ was first prepared by a conventional solid state reaction. A mixture of Na_2CO_3 (99.9% pure) and TiO_2 (99.99% pure) in a molar ratio of 1:3 was heated at 800°C for 20 h in air. The resultant specimens were reground and the same temperature program sequence was repeated once again [6]. Then, the $H_2Ti_3O_7$ sample was prepared from $Na_2Ti_3O_7$ via Na^+/H^+ ion exchange reaction using a 0.5 M HCl solution for 5 days at 60°C. After the acidic treatment, the produced $H_2Ti_3O_7$ sample was washed with water and ethanol, and then dried at 60°C for 1 day in air. Finally, the $H_2Ti_{12}O_{25}$ samples were prepared upon heating the $H_2Ti_3O_7$ sample at 260°C for 5 h in air. On the other hand, in the second synthetic route [6], the precursor $Na_2Ti_6O_{13}$ was first prepared by a conventional solid state reaction using a method similar to that reported previously [2,4]. A mixture of Na_2CO_3 and TiO_2 in a molar ratio of 1:6 was heated at 800°C for 20 h in air. The resultant specimens were reground and the same temperature program sequence was repeated once again. Then, the $Li_2Ti_6O_{13}$ sample was prepared from $Na_2Ti_6O_{13}$ via Na^+/Li^+ ion exchange reaction using $LiNO_3$ molten salt at 380°C for 10 h in air, as recently reported [2]. After heat-treatment, the reaction mixture was washed with water and ethanol, and then dried at 60°C for 1 day in air. Next, the $H_2Ti_6O_{13}$ sample was prepared from $Li_2Ti_6O_{13}$ via Li^+/H^+ ion exchange reaction using a 0.5 M HCl solution for 5 days at 60°C [4]. After the acidic treatment, the produced $H_2Ti_6O_{13}$ sample was washed with water and

ethanol, and then dried at 60°C for 1 day in air. Finally, the $H_2Ti_{12}O_{25}$ samples were prepared upon heating the $H_2Ti_6O_{13}$ sample at 260°C for 100 h in air.

From the results of powder XRD and TG-DTA measurements, it was clearly revealed the $H_2Ti_{12}O_{25}$ sample can be successfully synthesized by two synthetic routes from $Na_2Ti_3O_7$ and $Na_2Ti_6O_{13}$ as starting compounds in the present study [5,6]. The electrochemical Li insertion and extraction experiments showed a reversible capacity of 250 mAh g^{-1} for the present $H_2Ti_{12}O_{25}$ sample, as shown in Fig. 2. Although $H_2Ti_{12}O_{25}$ contains hydrogen atoms as a main component element, the FT-IR and ^{1}H-MAS NMR measurements indicated that this compound did not contain water species such as H_2O and H_3O^+ in the structure. Accordingly, $H_2Ti_{12}O_{25}$ is suggested to be one of the promising high-voltage oxide negative electrodes in advanced lithium ion batteries.

References:

[1] K. Chiba, N. Kijima, Y. Takahashi, Y. Idemoto, J. Akimoto, *Solid State Ionics*, **178** (2008) 1725.
[2] K. Kataoka, J. Awaka, N. Kijima, H. Hayakawa, K. Ohshima, J. Akimoto, *Chem. Mater*., **23** (2011) 2344.
[3] K. Kataoka, N. Kijima, J. Akimoto, *Inorg. Chem*., **52** (2013) 13861.
[4] K. Kataoka, N. Kijima, J. Akimoto, *Solid State Ionics*, **252** (2013) 109.
[5] J. Akimoto, K. Chiba, N. Kijima, H. Hayakawa, S. Hayashi, Y. Gotoh, Y. Idemoto, *J. Electrochem. Soc*., **158** (2011) A546.
[6] J. Akimoto, K. Kataoka, N. Kojima, S. Hayashi, Y. Gotoh, T. Sotokawa, Y. Kumashiro, *J. Power Sources*, **244** (2013) 679.

Figures:

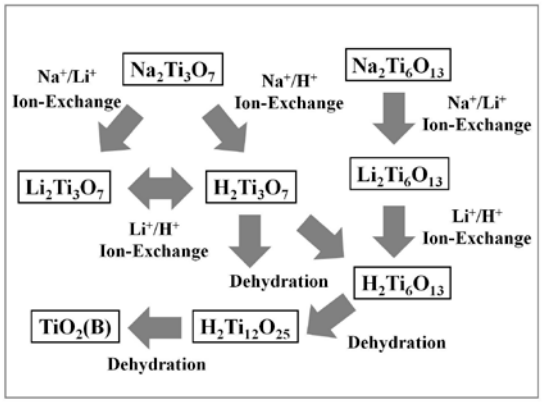

Fig. 1. Soft chemical synthetic routes of $H_2Ti_{12}O_{25}$ and related compounds using two starting compounds, $Na_2Ti_3O_7$ and $Na_2Ti_6O_{13}$.

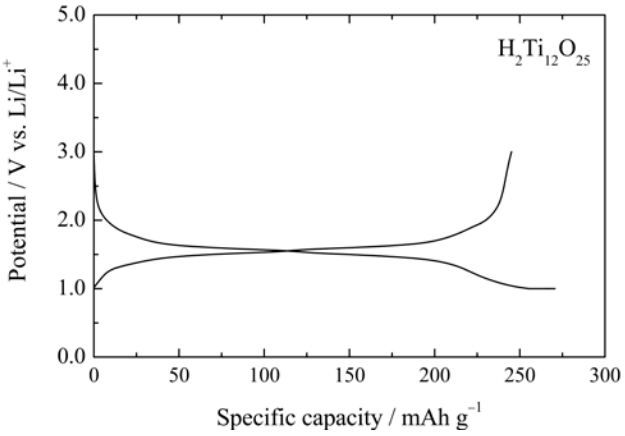

Fig. 2. Galvanostatic charge (Li insertion) and discharge (Li extraction) profiles of the present $H_2Ti_{12}O_{25}$ sample.

Peculiarities of perovskite related oxides formation in the Ln – M – T – O systems (Ln = Lanthanoid, Y; M = Ca, Sr, Ba; T = Mn, Fe, Co, Ni). Phase equilibria and oxygen nonstoichiometry.

V.A. Cherepanov, L.Ya. Gavrilova, T.V. Aksenova, N.E. Volkova, A.S. Urusova, E.A. Kiselev, A.R. Gilev

[a]Department of Chemistry, Institute of Natural Sciences, Ural Federal University.

Perovskite related materials based on the rare earth, alkali earth and 3d-transition metals draw considerable attention in recent decades due to their potential application in the intermediate temperature solid oxide fuel cells (IT-SOFC) as cathode materials. Their target functional properties such as mixed electronic and ionic conductivity, oxygen diffusivity thermal and chemical expansion, compatibility with the electrolyte materials depends on their chemical composition, crystal and defect structure. The latter is strongly related with the oxygen content (nonstoichiometry), i.e. the conditions that have been used during the preparation and treatment procedures. In some cases existing impurities can determine significant changes in the materials' properties. In this respect knowledge of phase equilibria and and defect structure of the complex oxides with the particular chemical composition defining the nature and concentration of charge carriers are the items of vital importance for that class of materials.

Since a variety of complex oxides within the mentioned above class of the perovskite related materials suggested as promising for IT-SOFCs and other electrochemical applications is wide it is important to analyze the changes of phase formation with the chemical composition variations, for example, within the row of rare earth elements from La to Nd, Sm, Ho, and even Y (when the radius of RE ions is decreasing), or changing Ca/Sr for Ba, and finally using different 3d-transition metals Mn – Fe – Co – Ni – Cu. The phase diagrams of corresponding systems are assigned to show a number of important features: (i) the types of phases that can be formed in the different compositional areas of the system, (ii) the homogeneity ranges of possible solid solutions formed in the system, (iii) thermodynamic stability ranges and particular thermodynamic conditions for stability boundaries. These can be illustrated by the transformations of phase diagrams with different chemical constituents variations, for example La – *M* – Co – O systems, where *M* = Ca, Sr, Ba [1-4], or *Ln* – Ba – Co – O systems, where *Ln* = La, Nd, Sm, Y [3-6], or La – Sr – T – O [7-9] and La – T – T' – O systems [10-15], where T, T' = Mn, Fe, Co, Ni, Cu. The homogeneity ranges and distortion type of solid solutions with perovskite type structure can be changed by simultaneous introduction of different dopants in A- and B-sublattice [16-20].

Special attention has been paid to the formation of perovskite related complex oxides belonging to the Ruddlesden-Popper series, preparation conditions, homogeneity ranges while doping in A- and B-sublattices.

Although in general most of the phases under consideration reveal relatively high values of conductivity and oxygen diffusivity a noticeable difference in the values and temperature behavior can be explained by their chemical composition which include both the nature fractions of cations and oxygen content. The dependencies of oxygen nonstoichiometry as a

function of temperature and oxygen partial pressure allow discussing possible defect structures and calculate the concentrations of charge carriers [21-24].

References:

[1] V.A. Cherepanov, L.Yu. Barkhatova, A.N. Petrov, V.I. Voronin, *Solid Oxide Fuel Cells IV, Ed. by M.Dokiya, O.Yamamoto, H.Tagawa and S.C.Singhal*, **PV 95-1** (1995) 434.
[2] L.Ya. Gavrilova, V.A. Cherepanov, T.V. Surova, V.A. Baimistruk, V.I. Voronin, *Russ. J. Phys. Chem.*, **76** (2002) 150.
[3] V.A. Cherepanov, L.Ya. Gavrilova, L.Yu. Barkhatova, V.I. Voronin, M.V.Trifonova, O.A. Bukhner, *Ionics*, **4** (1998) 309.
[4] V.A. Cherepanov, L.Ya. Gavrilova, E.A. Filonova, M.V. Trifonova, V.I. Voronin, *Mat. Res. Bull.*, **34** (1999) 983.
[5] L.Ya. Gavrilova, T.V. Aksenova, N.E. Volkova, A.S. Podzorova and V.A. Cherepanov, *J. Solid State Chem.*, **184** (2011) 2083.
[6] A.S. Urusova, V.A. Cherepanov, T.V. Aksenova, L.Ya. Gavrilova, E.A. Kiselev, *J. Solid State Chem.*, **202** (2013) 207.
[7] M.A. Bobina, N.A. Yakovleva, L.Ya. Gavrilova, V.A. Cherepanov, *Russ. J. Phys. Chem.*, **78** (2004) 1340.
[8] L.Ya. Gavrilova, T.V. Aksenova, V.A. Cherepanov, *Russ. J. Inorg. Chem.*, **53** (2008) 953.
[9] V.A. Cherepanov, L.Yu. Barkhatova, V.I. Voronin, J. Solid State Chem., **134** (1997) 38.
[10] A.N. Demina, V.A. Cherepanov, A.N. Petrov, M.V. Klokova, *Inorg. Mater.*, **41** (2005) 736.
[11] N.V.Proskurnina, V.A.Cherepanov, O.S.Golynets, and V.I.Voronin, *Inorg. Mater.*, **40** (2004) 955.
[12] E.A. Kiselev, N.V. Proskurnina, V.I. Voronin, V.A. Cherepanov, *Inorg. Mater.*, **43** (2007) 167.
[13] N.V. Proskurnina, V.I. Voronin, V.A. Cherepanov, E.A. Kiselev, *Progr. .Solid State Chem.*, **35** (2007) 233.
[14] I.L. Tikhonova, A.V. Bakhtin, A.Yu. Zuev, A.N. Petrov, *Russ. J. Phys. Chem.*, **73** (1999) 365.
[15] I.L. Tikhonova, A.Yu. Zuev, A.N. Petrov, *Russ. J. Phys. Chem.*, **72** (1998) 1794.
[16] V.A. Cherepanov, E.A. Filonova, V.I. Voronin, I.F. Berger, L.Yu. Barkhatova, *Mat. Res. Bull.*, **34** (1999) 1481.
[17] V.A. Cherepanov, E.A. Filonova, V.I. Voronin, I.F. Berger, *J. Solid State Chem.*, **153** (2000) 205.
[18] L.Ya. Gavrilova, T.V. Aksenova, L.A Bannykh, Ya.V. Teslenko, V.A. Cherepanov, *J. Struct. Chem.*, **44** (2003) 248.
[19] T.V. Aksenova, L.Ya. Gavrilova, V.A. Cherepanov, *Inorg. Mater.*, **40** (2004) 1336.
[20] T.V. Aksenova, M.V. Anan'ev, L.Ya. Gavrilova, V.A. Cherepanov, *Inorg. Mater.*, **43** (2007) 296.
[21] A.N. Petrov, V.A. Cherepanov, T.V. Aksenova, and L.Ya. Gavrilova, *Russ. J. Phys. Chem.*, **80** (2006) S134.
[22] V. Cherepanov, T. Aksenova, E. Kiselev, L. Gavrilova, *Solid State Scien.*, 10 (2008) 438.
[23] T.V. Aksenova, L.Yu. Gavrilova, A.A. Yaremchenko, V.A. Cherepanov and V.V Kharton, *Mat. Res. Bull.*, **45** (2010) 1288.
[24] A.N. Petrov, V.A. Cherepanov, A.Yu. Zuev, *J. Solid State Electrochem.*, **10** (2006) 517.

Novel one-stage electrochemical method for synthesis of electroactive composite materials. Its application for Prussian Blue/polypyrrole film coated electrodes for electrocatalytic applications

M.A. Vorotyntsev[a,b,c], E.V. Zolotukhina[a], I.S. Bezverkhyy[d]

[a] Institute for Problems of Chemical Physics, Russian Academy of Sciences, Chernogolovka, Russia, mivo2010@yandex.ru
[b] ICMUB, UMR 6302 CNRS-Universite de Bourgogne, Dijon, France, mv@u-bourgogne.fr
[c] M.V.Lomonosov Moscow State University, Moscow, Russia
[d] ICB, UMR 6303 CNRS-Universite de Bourgogne, Dijon, France

Novel electrochemical method of one-stage deposition of composite films on electrode surface has been proposed [1]. The procedure includes a periodical series of potentiostatic or galvanostatic pulses of alternative polarities imposed at electrode in contact with a mixture of two solute precursors. During the anodic pulse one of these precursors is able to generate irreversibly a solid phase via its electrooxidation. During the cathodic pulse another precursor is transformed into another solid phase via its electroreduction.

Parameters of anodic and cathodic pulses (values of their potentials or currents, pulse durations) may be chosen independently from one another, their relation allowing one to vary the relative contents of components in the deposited composite. The values of the anodic and cathodic charges passed during each cycle determine the amounts of the deposited solid-phase components so that they may be used to control their dispersibilities. In particular, this factor might be used to produce a component in the nanodispersed form. Overall thickness of the composite film may be regulated by the number of pulses.

The crucial condition for application of this procedure is an irreversible type of the precursor-to-product transformation of both components of the composite. Another necessary condition is in the stability of both solid-state components to both the anodic and cathodic potentials imposed in the course of the procedure. The latter condition may be achieved by the proper choice of parameters of the procedure. The third condition is a sufficient stability of the mixed solution containing both precursors, with respect to their direct redox reaction in the bulk solution, i.e. the stability period should be long enough to carry out the electrochemical deposition of the composite film.

To reduce the effect of the depletion-layer formation for precursors near the electrode surface due to these anodic and cathodic processes one may carry out the deposition procedure as a set of series of such periodical double pulses separated by "relaxation periods" (Fig. 1) which allow the precursor concentrations to return to their unperturbed profiles. Such breaks in the deposition process may also be used to characterize the redox state of the already deposited film by performing a cyclic voltammogram during each relaxation period.

The above composite deposition procedure may be supplemented by a preceding or/and concluding interval(s) where a single-component layer is generated electrochemically. The former allows one to coat the bare electrode surface by the film of the corresponding component, e.g. to improve the subsequent composite-film adhesion to the surface. The latter

represents a means to generate an external homogeneous layer, e.g. to protect the underlying composite film or to control its exchange with solution.

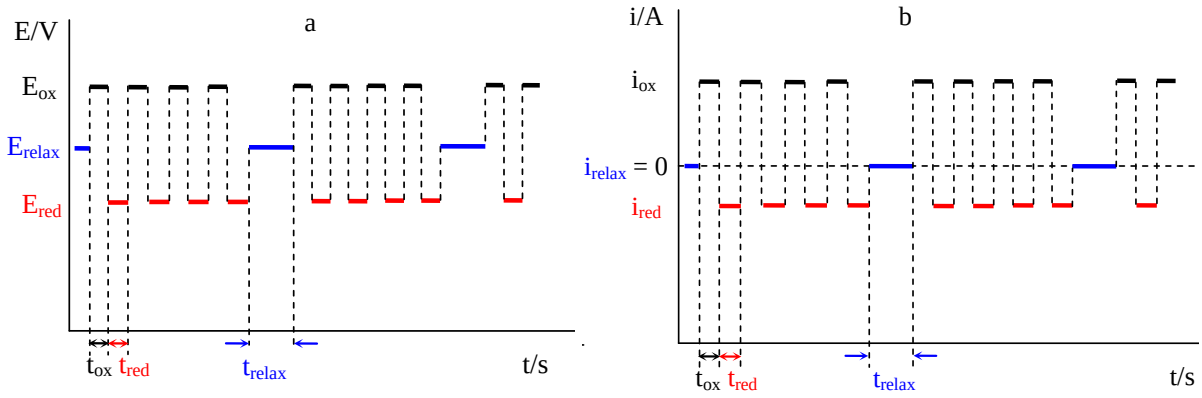

Fig. 1. Periodical double potential (a) or current (b) pulse regime patterns consisting of several series of cycles separated by relaxation periods.

For illustration this method has been applied for growing films where particles of Prussian Blue (**PB**) are distributed inside polypyrrole (**PPy**) matrix. The aqueous solution used for the composite (**PB/PPy**) deposition contained pyrrole (**Py**) as well as a mixture of two ions, Fe(III) and $[Fe(III)(CN)_6]$. The anodic and cathodic processes taking place in the course of the composite deposition procedure may be presented by brutto reactions:

$n\ Py - 2\ e^- = PPy_n + 2n\ H^+$; $4\ Fe^{3+} + 3\ [Fe(III)(CN)_6]^{3-} + 3\ e^- = Fe(III)_4[Fe(II)(CN)_6]_3 + e^-$

CV responses in the course of the composite-film deposition are shown in Fig. 2a. Such modified electrode demonstrates a high catalytic activity and a good stability in the reaction of hydrogen peroxide electroreduction (Fig. 2b).

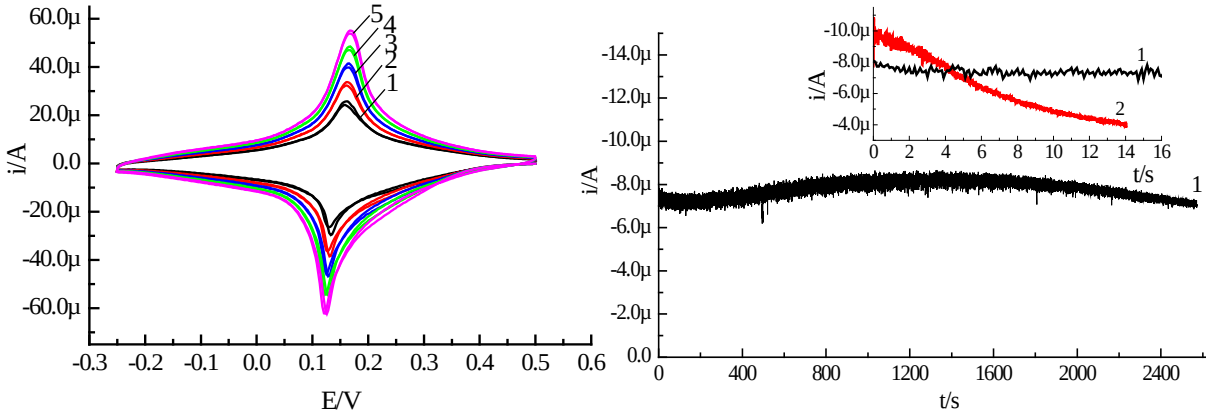

Fig. 2 Electrochemical properties of Pt disk electrode coated with PB/PPy composite film deposited via double potential-pulse procedure: (a) CV responses during relaxation periods in the course of the film deposition; (b) chronoamperometric response for this electrode (*1*) in contact with 1 mM H_2O_2 + phosphate buffer solution; E_{red} = 0 V. Insert: Comparison of this response (1) with that of pure PB coated Pt electrode in the same conditions (2)

References:

[1] E. V. Zolotukhina, I. S. Bezverkhyy, M. A. Vorotyntsev, *Electrochim. Acta*, doi.org/10.1016/j.electacta.2013.10.182 (2014).

NMR studies in an amorphous solid ion conductor $(Li_2S)_7(P_2S_5)_3$
Lithium ion diffusion studied by ^{7}Li PGSE NMR

Kikuko Hayamizu,[a] Yuichi Aihara[b]

[a] National Institute of Advanced Industrial Science and Technology, AIST Tsukuba Center 2, Ibaraki 305-8568, Japan; E-mail: hayamizu.k3@gmail.com.
[b] Samsung R&D Institute Japan, 2-1-11 Senba-nishi, Minoshi, Osaka 562-0036, Japan.

The sulfide based solid electrolytes are known to have large ionic conductivity, and thus its application in solid-state lithium rechargeable batteries as electrolytes has been developed [1]. We have reported the ^{7}Li and ^{31}P nuclear magnetic resonance (NMR) spectra of crystalline $(Li_2S)_7(P_2S_5)_3$ [2]. In this study, NMR studies are performed for amorphous $(Li_2S)_7(P_2S_5)_3$and found that narrow and broad components coexist in wide temperature range of the ^{7}Li resonance. The measurements of ^{7}Li ion diffusion were performed for the narrow component between 303 and 353 K by the pulsed-gradient spin-echo (PGSE) NMR method. Lithium ion diffusion scattered in a polydispersive manner and the apparent diffusion constants of the Li^+ (D_{Li}) varied depending on measurement conditions at a certain temperature. The translational movement of Li^+ observed by the PGSE NMR is extremely complex. Within a short distance and a short period, Li^+ ions move quickly and slow down with time and distance. This is the important trial to measure the lithium diffusion directly for continuous space in the solid electrolyte.

Sample Preparation: Solid electrolyte $(Li_2S)_7(P_2S_5)_3$ was prepared by the high-energy ball milling of Li_2S (Alfa, 99.9%) and P_2S_5 (Aldrich, 99.9%) (mole ratio 7: 3) using a grinding bowl fasteners, P-5 (Fritsch, Germany). The amorphous phase $(Li_2S)_7(P_2S_5)_3$ powder was first prepared at 300 rpm for 40 h in an Ar-gas filled Al_2O_3 pot and hereafter the amorphous sample was denoted by 7030A. The sample pellet was prepared using a 13-mm-die in a diameter and a hydraulic press (4 tons). To measure ionic conductivity, a couple of indium-foil blocking electrodes were used. The sample pellet was sandwiched by indium foils of the same diameter (13 mm) and placed in a Teflon cell with two stainless-steel electrodes. The whole procedures were performed under an Ar-box. The ionic conductivity was 3.4 x 10^{-4} Scm^{-1} at 303 K. For the NMR measurement, the sample was broken into small pieces (larger than 1 mm^3 block) and put into a symmetrical micro-NMR glass tube (5-mm diameter) in height of 10 mm within the linear pulsed field gradient (PFG) region The NMR tube was flame-sealed.

NMR measurement: All NMR spectra were measured on a Tecmag Apollo spectrometer (Houston, USA) equipped with a 6.35 T wide bore magnet using a JEOL PFG probe and controlled by a JEOL console (Tokyo, Japan). The maximum strength of the PFG was 22 Tm^{-1}. The ^{7}Li and ^{31}P NMR spectra were measured at 105.0 and 109.4 MHz, respectively. ^{7}Li diffusion

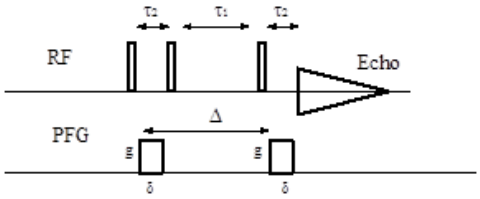

Fig. 1. STE-mode PGSE pulse sequence, where g and δ are the strength and duration time of the PFG, respectively. Δ is the observation time of diffusion. The echo attenuation E is related to Eq. 1 as $E = \exp\left(-\gamma^2 g^2 \delta^2 D(\Delta - \delta/3)\right)$,where δ, g and Δ are measuring parameters.

phenomena were observed in the temperature range between 303 and 353 K using the stimulated-echo (STE)-mode PGSE NMR pulse sequence as shown in Fig. 1..

^{7}Li and ^{31}P spectra: Since the target of the present study is the observation of mobile portion, the measurements were performed by so-called solution mode without sample spinning. The rigid portion was buried in baseline. ^{7}Li spectra in lower temperatures were composed two components and the narrow component afforded the echo attenuation in the diffusion measurements. The ^{31}P spectra were composed of $P_2S_7^{4-}$ and PS_4^{3-} and the ratio of the latter increased as the temperature increased.

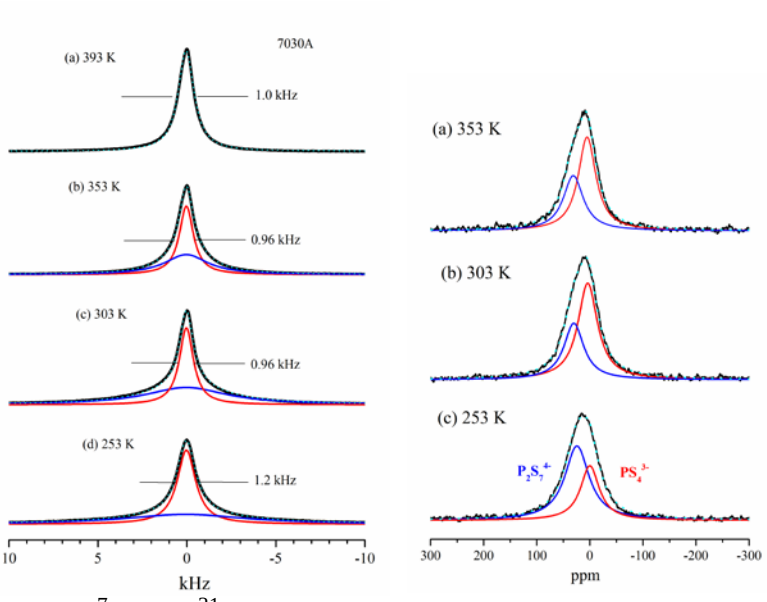

Fig. 2. ^{7}Li and ^{31}P NMR spectra for 7030A observed by solution-mode conditions.

Lithium ion diffusion: In our previous studies for crystalline 7030C[2], we found Li diffusion in the solid conductor is very complicated and depends on observation time Δ as well as PFG strength *g*. As an example, the diffusion plots following to Eq. 1 observed at 353 K are shown in Fig. 3. The collision phenomena of ions in solid conductors are often observed for various conductors under certain measuring conditions and further studies will be necessary.

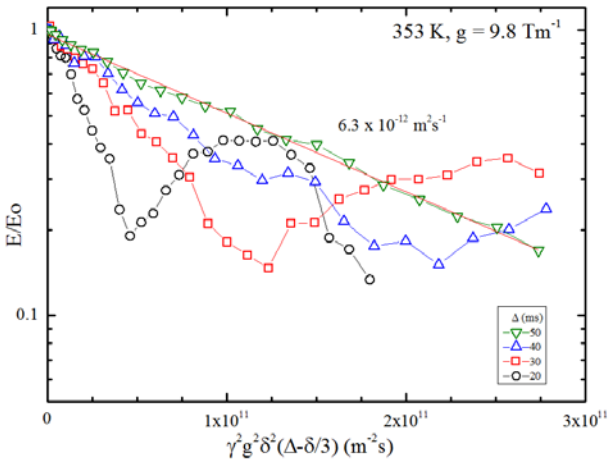

Fig. 3. The diffusion plots following to Eq. (1) measured at 353 K with *g* = 9.8 Tm^{-1} for various Δ of 20, 30, 40 and 50 ms.

References:

[1] A. Hayashi and M. Tatsumisago, *Electron. Matter. Lett*. **8** (2012) 199.
[2] K. Hayamizu, Y. Aihara, *Solid State Ioncs*, **238** (2013) 7.

Strategy for improving the functional properties of MIEC oxides, new methods and approaches for their research

Alexandr.P. Nemudry,

Institute of Solid State Chemistry and Mechanochemistry,
Siberian Branch of Russian Academy of Science, Novosibirsk
nemudry@solid.nsc.ru

Nonstoichiometric oxides with mixed ion/oxygen electron conductivity (MIEC) attract the attention by the possibility of their use as oxygen permeable membranes, selective sorbents, electrode materials for SOFC, etc. Reasonable oxygen transport in MIEC oxides for practical purposes can be achieved only at high temperatures above ca. 600 °C, however, in some cases, a lack of it turns into a virtue: for example, the separation of oxygen from air using ion transport membranes can easily be embedded in high-temperature processes of partial oxidation of hydrocarbons, coupling of methane and oxy-fuel combustion [1].

To improve functional properties of MIEC oxides we have suggested new strategy of doping: partial isomorphic substitution of B-cations (Co/Fe) by highly charged Nb/Ta (V) and Mo/W(VI) ions [2, and refs. 15-26 in 2].

It allows:

(i) to increase the chemical stability of the materials at low pO_2 due to the stable oxidation state (V, VI) of dopants;

(ii) to reduce the degradation of membrane materials in the atmosphere of CO_2 due to the acidic properties of highly charged cations;

(iii) to obscure phase transition "perovskite-brownmillerite" because the oxygen index of doped materials $AB_{1-x}M_xO_{2.5+\delta}$ (δ = x and 3/2x for M = Nb/Ta and Mo/W, respectively) at low pO_2 is outside the stability range of brownmillerite structure (2.5 ± 0.02);

(iv) to stabilize the cubic structure of cobalt-containing perovskites (SCF, BSCF, etc.) due to the formation of randomly distributed double perovskite-like clusters A_2BMO_6 (where A = Sr, Ba; B = Co, Fe; M = Nb, Ta, Mo, W) which pillar the cubic lattice of pristine materials;

(v) to obtain nanostructured materials as result of phase separation with the formation of nanosized coherently jointed domains having the composition $ABO_{3-1/n}$ and $ABO_{3-1/n+2}$ when, for doped perovskites $AB_{1-x}M_xO_{3-\delta}$, the oxygen content corresponds to the two phase region $1/n>\delta>1/(n+2)$ (n=2, 4);

(vi) to maintain high values of oxygen fluxes due to nanostructuring and elimination of trapping effect which is characteristic of doped materials (dopant ions (M = Nb, Ta, Mo, W) and defects (Vo, Oi), providing oxygen transport screened by oxide ions of octahedra MO_6);

(vii) to increase the electron conductivity of MIEC oxides at low pO_2 by stabilization of oxidation state (II) of B-cations (B=Co, Fe).

As a result, we have obtained nanostructured materials for catalytic conversion of methane in membrane reactor, which possess enhanced thermochemical stability at low pO_2 and in CO_2 containing atmosphere, phase stability and a high oxygen and electron conductivity.

The mechanism of oxygen release from MIEC oxides is of wide interest because oxygen exchange of the oxide with gas phase is a key factor and determines the functional properties of the high-temperature superconductors, giant magnetoresistive materials, the

oxygen permeable ceramic membranes, electrode materials for SOFC, sensors etc [3 and refs. 1-7 in 3].

To study both equilibrium and nonequilibrium processes of oxygen release from MIEC oxides the installation has been made, on the basis of which we have developed:

- new original method of obtaining of the detailed equilibrium "3-δ - lgpO_2 - T" diagrams for MIEC oxides(Fig. 1a) based on the determination of the oxygen nonstoichiometry as a *continuous* function of oxygen partial pressure in the course of oxygen release in quasi-equilibrium regime [4].

- new original *oxygen partial pressure relaxation* technique in which the measured parameter is the pO_2.

To obtain reliable data on the mechanism and kinetics of oxygen exchange in MIEC oxide it has been proposed and successfully applied *isostoichiometric* approach. The approach takes into account a broad region of homogeneity MIEC oxides which leads to the influence of oxygen stoichiometry both on structural and thermodynamic and transport properties of the oxides. The use of isostoichiometric conditions allowed us to demonstrate that the activation energy of the oxygen release from MIEC perovskites is a function of the oxide stoichiometry. E.g., the decrease of the oxygen content 3-δ in $SrCo_{0.8}Fe_{0.2}O_{3-\delta}$ samples from 2.53 to 2.47 results in an increase of the apparent activation energy from 100 to 230 kJ/mol. This growth correlates with variation of the oxygen partial enthalpy in the $SrCo_{0.8}Fe_{0.2}O_{3-\delta}$ oxide (Fig. 1b).

Thus, the kinetic data obtained in the isostoichiometric mode can give more reliable understanding of the oxygen exchange in nonstoichiometric oxides with wide homogeneity range because this approach excludes simultaneous effects of temperature and stoichiometry on the oxygen exchange.

References:

[1]. Sunarso J, Baumann S, Serra JM, Meulenberg WA, Liu S, Lin YS, da Costa JC Diniz (2008) J Membrane Sci 320:13–41

[2]. O.A. Savinskaya, A.P. Nemudry. (2014) http://dx.doi.org/10.1016/j.memsci.2014.01.074

[3]. I.A. Starkov, S. F. Bychkov, S. A. Chizhik, A. P. Nemudry. (2014) Chem. Mat. in press.

[4]. I.A. Starkov, S. F. Bychkov, S. A. Matvienko, A. P. Nemudry.(2013) PCCP, DOI: 10.1039/C3CP52143E

Figures:

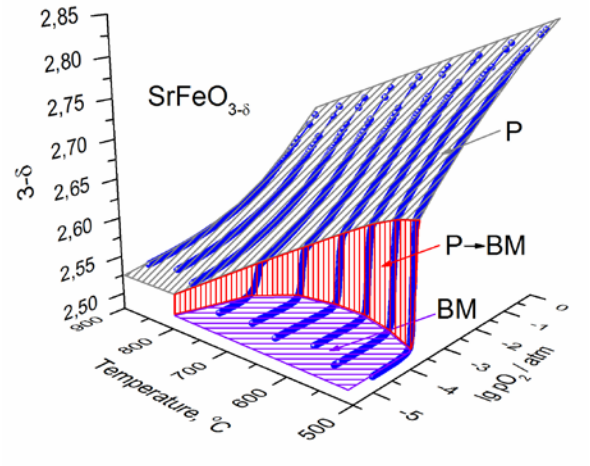

Fig. 1 a. *"3-δ - pO_2 – T"* diagrams for $SrFeO_{3-\delta}$ oxide obtained by new oxygen release technique.

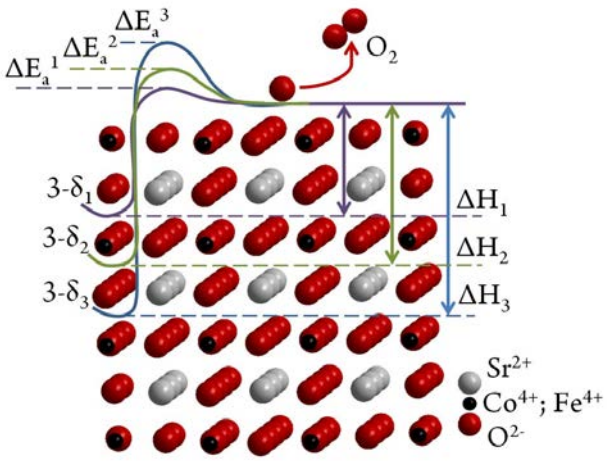

Fig. 1 b. The activation energy of the oxygen release from $SrCo_{0.8}Fe_{0.2}O_{3-\delta}$ perovskite is a function of the oxide stoichiometry.

Ab initio MODELLING OF OXYGEN REDUCTION REACTION IN MIXED CONDUCTING PEROVSKITES FOR SOLID OXIDE FUEL CELLS

E. A. Kotomin[1,2], *R. Merkle*[1], *Yu. A. Mastrikov*[2,3], *M.M. Kuklja*[3], *J. Maier*[1]

[1]Max Planck Institute for Solid State Research, Heisenbergstr.1, Stuttgart, Germany
[2]Institute for Solid State Physics, University of Latvia, Kengaraga str. 8, Riga, Latvia
[3] Materials Science and Engineering Dept., University of Maryland, College Park, USA

Complex ABO_3-type perovskite solid solutions with oxygen deficiency exhibit a perceptible ionic and electronic conductivity, leading to their promising use as electrolytes ($(La,Sr)(Ga,Mg)O_{3-x}$), oxygen permeation membranes, and solid oxide fuel cell (SOFC) cathodes ($(La,Sr,Ba)(Mn,Fe,Co)O_{3-\delta}$). Oxygen stoichiometry strongly affects transport properties of these materials, which, in turn, determine the suitability of the material for targeted applications [1-3]. As it is well established now, there are two key factors, which control the oxygen reduction reaction (ORR), are high oxygen vacancy (V_O) concentration at the cathode surface and high vacancy mobility.

In this talk, based on first principles DFT calculations combined with large supercells, we discuss the atomic and electronic structure of oxygen vacancies, their formation and migration energies in the bulk and in the surface layer, the defect-induced electron density redistribution, and the dependence of the defect chemistry on the composition of $(Ba,Sr)(Co,Fe)O_3$ (BSCF) (Fe/Co ratio) [4]. Our calculations confirm that the O-vacancy formation and, in particular, migration energies in BSCF are considerably smaller than in similar $(La,Sr)MnO_3$ (LSM) [5] and $(La,Sr)(Co,Fe)O_3$ (LSCF) perovskites [6] which explains its good performance. The gradual increase of the formation energies with increasing iron content is explained by analysis of the calculated density of the states. We discuss also briefly the problem of the phase stability of these complex perovskites with respect to the decomposition into a mixture of cubic and hexagonal phases or parent perovskites and binary oxides [7].

Based on the calculated formation and migration energies of oxygen vacancies and adsorbed oxygen species at the LSM surface as well as dissociation barriers, we calculated *the rates of elementary steps* in the ORR and suggested different scenarios of this process in LSM, BSCF, LSCF as a function surface concentration of adsorbed oxygen species and oxygen vacancies [1,4]. We predict that in both LSCF and BSCF perovskites, the dissociation of surface peroxide or superoxide ions occurs with assistance of V_O, their encounter being the *rate-determining step*. The estimated reaction rate for this mechanism is significantly higher than that in LSM perovskites, in good agreement with experimental observations.

This work was partly supported by the COST Action CM1104 and National Science Foundation.

References

[1] L. Wang, R. Merkle, E. Kotomin et al, J. Mater. Res. **27**, 2000 (2012) (a review).

[2] M. Kuklja, E. Kotomin, R. Merkle et al, Phys. Chem. Chem. Phys. **15**, 5443 (2013) (a review).
[3] E. Kotomin, R. Merkle, Yu.A. Mastrikov et al. Chapter 6 in book: *Computational Approaches to Energy Materials* (eds. A. Walsch, A. Sokol, C.R.A. Catlow, Wiley), 2013, p. 149-186
[4] R.Merkle, E. Kotomin, Yu. Mastrikov et al, J Electrochem. Soc. **159**, B 219 (2012).
[5] Yu. Mastrikov, R. Merkle, E. Heifets et al, J. Phys. Chem. C **114**, 3017 (2010).
[6] Yu. Mastrikov, R. Merkle, E. Kotomin et al, Phys. Chem. Chem. Phys. **15**, 911 (2013).
[7] M. Kuklja, Yu. Mastrikov, E. Kotomin et al, J Phys Chem C **116**, 18605 (2012).

Figures:

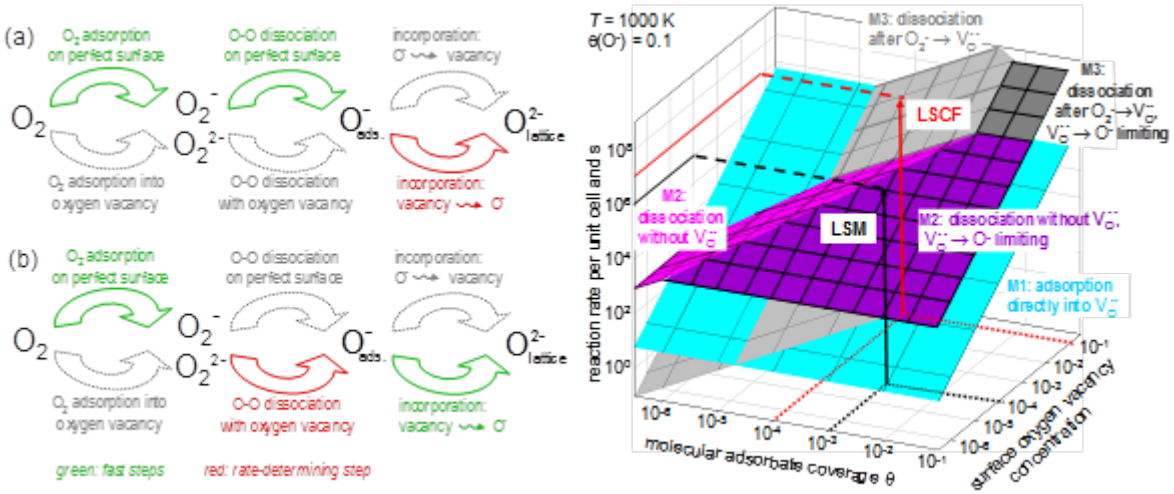

Fig. 1. Left panel--Schematic network of possible reaction steps for the oxygen incorporation into mixed-conducting perovskites. (a) perovskites with very low O vacancy concentration such as LSM (b) perovskites with high vacancy concentration such as LSCF, BSCF.
Right panel - Reaction rates for three alternative reaction pathways of oxygen incorporation on the MnO_2(001) surface of LSM (black lines) and LSCF (red lines) estimated based on DFT results (from ref.[1]).

Large magnetocaloric effect and magnetic properties of polymorphic $RCrO_4$ (R=rare earth) oxides

R. Sáez Puche[a], A. J. Dos santos-García[a, c], J. M. Gallardo[a], J. Romero[a], E. Palacios[b], M. Castro[b] and R. Burriel[b]
[a] Departamento Química Inorgánica, Facultad Químicas, Universidad Complutense Madrid, 28040, Spain
[b]Instituto de Ciencia de Materiales de Aragón, CSIC, Universidad de Zaragoza, 50009, Spain.
[c] Departamento de Química Industrial y Polímeros, ETSIDI, Universidad Politécnica de Madrid, 28012, Spain.
rsp92@quim.ucm.es

$RCrO_4$ oxides, where R=rare earth, crystallize at ambient conditions with the tetragonal zircon-type structure, *S.G.* $I4_1/amd$. [1] Recently, we have succeeded to synthesize the scheelite polymorphs (*S.G.* $I4_1/a$) for most of the R elements, by treating the zircon phases at 40 kbar and 813 K. [2, 3] These scheelite high pressure forms are quencheable after releasing the pressure, and TGA and X-ray diffraction data reveal a reversible transition from scheelite polymorph to zircon at 700 K. The coexistence of two paramagnetic ions in these phases, namely Cr^{5+} and R^{3+}, constitutes a very interesting scenario to study 3d-4f magnetic interactions. In this sense, most of the zircon-type $RCrO_4$ oxides behave as ferromagnetic, while the scheelite polymorphs are antiferromagnetic. The change in the sign of the magnetic interaction can be explained by considering the changes in both distances and bond angles of Cr-O-R pathway through which the superexchange interactions take place. [4]
Neutron diffraction studies have been used to determine the nuclear and magnetic structures for these zircon and scheelite $RCrO_4$ polymorphs. The analysis of the data reveals the onset of new reflections below the estimated Néel temperature from the previous magnetic susceptiblity data corresponding to the scheelite phases. The magnetic structure for these scheelite $RCrO_4$ oxides can be described with a propagation vector κ = [0 0 0], where the moments of R^{3+} and Cr^{5+} are aligned along the *c*-axis or confined in the *ab*-plane of the tetragonal structure depending on the nature of the R element, Figure 1. [4, 5] This behavior has been confirmed from heat capacity measurements where the onsets of λ-anomalies at the ordering temperatures are almost coincident with those determined from magnetic susceptibility and neutron diffraction analysis, see Figure 2. A detailed analysis of the zircon and scheelite structural types is included in this work to explain the different magnetic behavior showed by these two polymorphic phases allowing establishing relationships structure-magnetic properties.
Very recently it has been reported that the zircon $RCrO_4$ (R= Ho and Dy) phases show large values of the magnetocaloric parameters that make of these oxides potential refrigerant materials to be used for the liquefaction of hydrogen. [6] It is noting that the field induced magnetization in the case of the scheelite polymorphs yields magnetic moments larger than in the case of the homologous zircon phases and hence the magnetocaloric effect is expected to be larger for the scheelite polymorphs in comparison with the zircon ones. In this work a preliminary study has been done in order to determine the magnetocaloric parameters of the two polymorphic phases of $TbCrO_4$ and $HoCrO_4$. In this sense the isothermal entropy change, ΔS_T, as a function of temperature has been calculated for magnetic field variations from the measurements of magnetization versus field at different temperatures. Both

magnetocaloric parameters, ΔS_T and the adiabatic temperature change, ΔT_{ad}, have also been evaluated from the entropy functions at different fields obtained from the heat capacity data.

Figures:

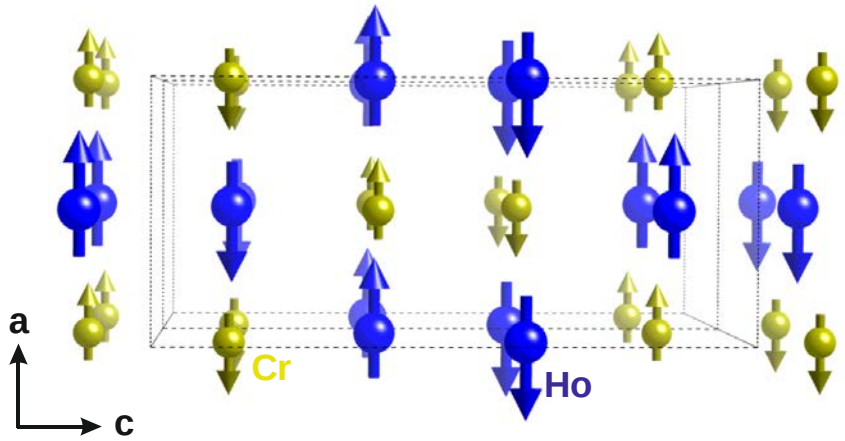

Figure 1. Magnetic structure of $HoCrO_4$-scheelite

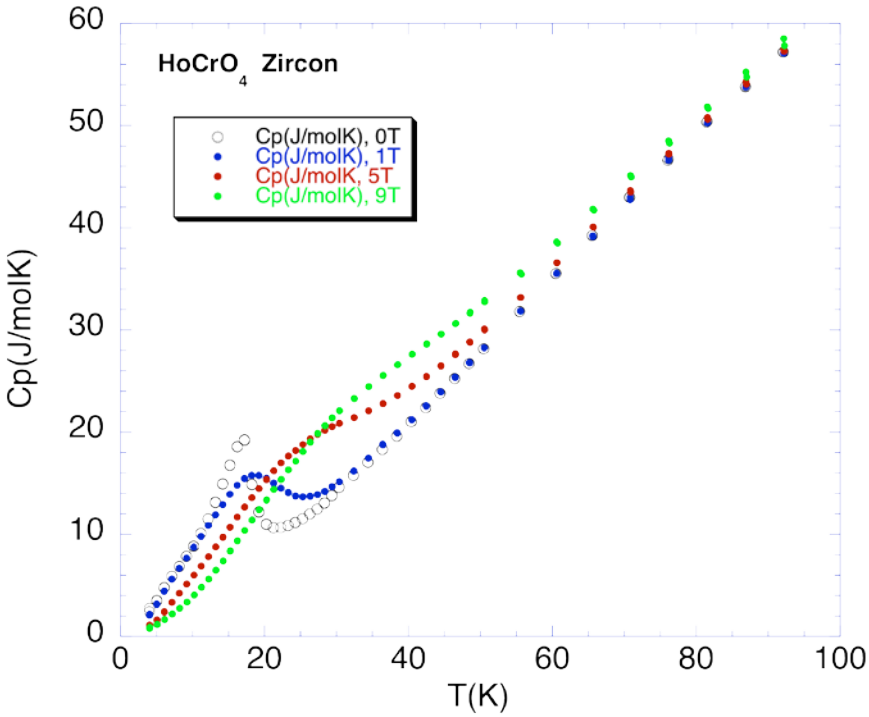

Figure 2. Heat capacity of $HoCrO_4$-zircon under different magnetic fields

References

[1.] R. Sáez Puche, E. Jimenez, J. Isasi, M.T. Fernández Diaz and J.L. Garcia Muñoz (2003) J. Solid State Chem. 172 , 161-170.
[2.] E. Climent Pascual, J. Romero, J.M. Gallardo, R. Sáez Puche (2007) Solid State Sci. 9, 574-579.
[3.] M. Rabie (2013) PhD. Thesis, Universidad Complutense Madrid.
[4.] E. Climent Pascual, J.M. Gallardo, R. Sáez Puche, M. Castro, N. Taira, J. Romero L.C. Chapon (2010) Phys. Rev. B 81, 174419-174425.
[5.] A.J. Dos santos-García, E. Climent-Pascual, J.M. Gallardo-Amores, M.G. Rabie, Y. Doi, J. Romero de Paz, B. Beuneu, R. Sáez-Puche (2012) J. Solid State Chem. 194 , 119-126.
[6.] A. Midya, N. Khan, D. Boi, P. Mandal (2013) Appl. Phys. Lett. 103, 092402-092407.

Solid state synthesis of phase pure cubic $Li_7La_3Zr_2O_{12}$ nanoparticles from a highly reactive precursor

M. Senna[1, 2], K. Nishimura[1], H. Sakamoto[3], N. Wakiya[3], H. Suzuki[3]

[1]Graduate School of Engineering, Shizuoka University, Japan; 432-8561, Hamamatsu, Japan
[2]Faculty of Science and Technology, Keio University, 223-8522, Yokohama, Japan
[3]Research Institute of Electronics, Shizuoka University, Japan; 432-8561, Hamamatsu, Japan

.

Introduction

Garnet type cubic $Li_7La_3Zr_2O_{12}$ (LLZO) is a promising candidate as an electrolyte for an all-solid Li-ion battery, due to its high ionic conductivity [1]. One of the bottlenecks of its practical application is a preparative technique to obtain in its pure phase. Examples of successful LLZO synthesis are mostly via a sol-gel route [1,2]. Products of sol-gel technique are suitable for thin films. However, it is desirable to obtain LLZO fine powders for an affordable battery production technology. The objectives of the present study is to establish a preparative technique to prepare LLZO fine powders via a solid-state route. Efforts are paid to start from a precursor with its highest possible reactivity, and keep the homoneneity of the reactants throughout the solid state processes.

Experimental section

A precursor was prepared in two-steps. Precursor *A* comprises ZrO_2 (Tosoh, av. particle diameter, d_{av}, 270 nm) and $La(OH)_3$ (Aldrich, d_{av} 190 nm) in a molar ratio 2:3, with 1 mass% AlOOH (Wako, d_{av} 150 nm). They were mixed intimately in a planetary mill (Fritsch, Pulverisette 6) for 3h. The precursor *A* was put into a 15 mass% ethanol solution of lithium acetate (Wako) to set an exact molar ratio of LLZO, and milled under the same condition for Procursor *A*, dried at 200 ºC and homogenized by milling in acetone, under otherwise the same condition as previous milling treatment, to obtain precursor *B*.
Precursor *B* was calcined in two steps, i.e. at 450 ºC in air for 3 h, and subsequently at 625 - 1000 ºC for 1–3 h. This was done after an intermediate homogenization by milling in acetone. under the same condition as before, with varying milling time up to 6 h. All the calcination procedures were carried out in an ambient atmosphere.
The calcined products were characterized mainly by X-ray diffractometer (XRD, Bruker) for crystallographic phase analysis, and dynamic light scattering photo spetrometer (DLS, Otsuka Electronics) for particle size analyusis.

Results and discussion

As we carried out the second calcination after homogenizing the calcined sample for 4 h and calcined at different temperature for 3 h, we observed always the second phase, $La_2Zr_2O_7$ (LZO), as shown in Fig. 1. Note that the amount of LZO increased with increasing temprature of the second calcination. Therefore, we attibute the coexistence of LZO as a consequence Li thermal loss, presumably even after the formation of the LLZO phase. However, at the temperature as low as 625 ºC, no LLZO was formed. From these results, it is obvious, that a precursor with higher reactivity is needed, in order to form LLZO at lowest possible temperature, in order to avoid Li loss. We therefore extended the milling time for homogenization of the pre-calcined maerial to 6 h and the second calcination was performed at 800 ºC, by varying the calcination time.

In Fig. 2, we compared the XRD profiles for the samples obtained from the precursor *B* after milling for 6h, calcined at 800 ºC for varying period. We notice that LZO persisted for the calcination time up to 2 h. After calcining for 3 h, LZO peaks were vanished and we obtained pure LLZO. This might suggest that the coexistence of LZO is attributable to two difference pathways, i.e. i) for insufficient reaction time for the completion of Li^+ ion diffusion into the rest of the ingredient included in the precursor *A*, and ii) Li loss after the formation of LLZO due to inappropriately high temperature. Therefore, the success of phase pure LLZO depends on the optimization of these mutually trading-off conditions.
As shown in Fig. 3, the average and median particle size values are, 89.5 nm and 75.1 nm, respectively. We also note that the synthesis was not successful without Al addition, since Al ions on the 24*d* site is known to be indispensable to stabilize the cubic garnet [3].

Conclusion

Phase pure garnet type cubic $Li_7La_3Zr_2O_{12}$ nano particles were obtained via a two-step solid-state synthesis at 450 ºC and 800 ºC for 3 h in air. The success of the phase pure synthesis is attributed to start from a homogeneous, highly reactive precursor, obtained by an intimate mixing of the starting materials, addition of 1 mass% Al, and a through intermediate homogenization between two calcination steps, to avoid negative effects of reaction induced inhomogenization.

References

[1] J. Tan, A. Tiwari, Electrochem. *Solid-State Lett*. **15** (2012) A37.
[2] I. Kokal, M. Somer, P.H.L. Notten, H.T. Hintzen, *Solid State Ionics*, **185** (2011) 42;
[3] H. Buschmann, J. Dölle, S. Berendts et al, *Phys. Chem. Chem. Phys*. **13** (2011) 19378.

Figures:

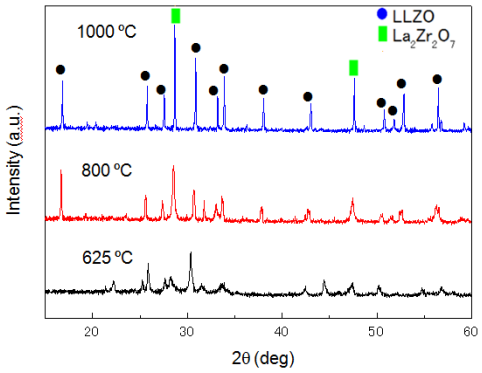

Fig. 1 X-ray diffractograms of LLZO, obtained from the precursor B after homogenizing after first calcination for 4 h with the second step calcination at varying temperature.

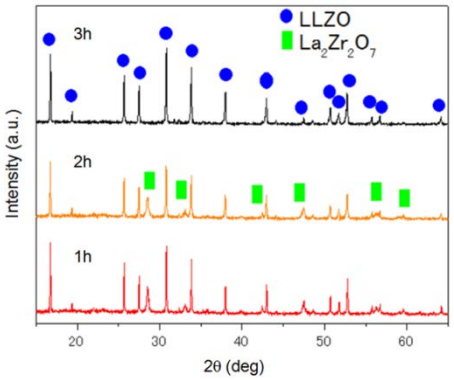

Fig. 2 X-ray diffractograms of LLZO, obtained from the precursor B after homogenizing after first calcination for 6 h with the second step calcination at 800 ºC for varying period

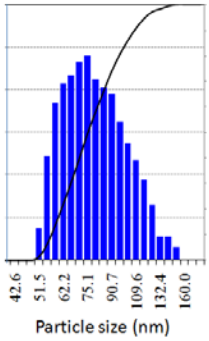

Fig. 3 Particle size distribution profile of LLZO, obtained from the precursor B after homogenizing after first calcination for 6 h with the second step calcination at 800 C for 3 h. Average and median particle size values are, 89.5 nm and 75.1 nm, respectively.

Titanium matrix composites reinforced with TiC particles: Kinetics towards thermodynamic equilibrium.

Jérôme Andrieux,[a,*] Jérôme Roger,[a,b] Bruno Gardiola,[a] Nathalie Peillon,[c] Sebastien Saunier,[c] Christophe Desrayaud,[c] Olivier Martin,[d] Nikhil Karnatak,[d] Sophie Gourdet,[e] Jean-Claude Viala,[a] Olivier Dezellus [a]

[a] Université Claude Bernard Lyon 1, Laboratoire des Multimatériaux et Interfaces (LMI) UMR CNRS n°5615, 43 Bd du 11 Novembre 1918, 69622 Villeurbanne Cedex, France.
[b] Université de Bordeaux, CNRS, Laboratoire des Composites ThermoStructuraux UMR 5801, 33600 Pessac, France.
[c] Laboratoire Claude Goux, UMR CNRS 5146, Ecole des Mines, 158 Cours Fauriel, 42023 Saint-Etienne Cedex, France.
[d] Mecachrome, rue de l'Artisanat, 72320 Vibraye France
[e] EADS France, EADS Innovation Works, 12 rue Pasteur - BP 76 92152 Suresnes Cedex France
* jerome.andrieux@univ-lyon1.fr

Introduction

Thanks to their high specific modulus (E/ρ) and yield stress (σ_e/ ρ), metal matrix composites (MMCs) have attracted research and industrial attentions as unique materials for high technological applications such as in the aerospace and automotive sectors. Al-based matrix composites are already widely used in applications with moderate mechanical loading at low temperature. The main issue is now to extend the use of MMCs to new applications concerned by higher temperature and stress. Ti-based matrix composites are potential candidates for such applications not only because of their low density and high corrosion resistance, but also because of their improved behavior under fretting loading compared to Ti alloys. Among the fibers or particulate materials used as reinforcement for Ti-based composites, TiC has been recognized as paramount reinforcing phase due to its excellent compatibility with the matrix. In order to achieve a Ti/TiC metal matrix composite, the classical powder metallurgy route is usually used, starting from pure titanium and stoichiometric TiC [1]. During the high temperature stage of elaboration process, the carbide evolves toward the equilibrium sub-stoichiometric composition following reaction 1.

reaction 1: $$(1-y)Ti + yTiC \rightarrow TiC_y$$

The aim of this work was to study the kinetics of solid state reaction between TiC and Ti metal.

Experimental Methods

The reactivity kinetics was investigated by two experimental approaches.

In the first one, short time isothermal heat treatments were performed on Ti-TiC powder compacts at 920°C. A graphite crucible containing the compact and a getter powder was immersed in a molten aluminium bath, held during the desired time (from 1.5 to 20 min) at 920 °C and then quenched in water. The particles evolution and the advancement of the reaction were monitored by removing the Ti-matrix by selective etching to focus on the TiC reinforcement. The characterization of the remaining TiC particles was done by chemical analyses, Scanning Electron Microscopy (SEM) and X-Ray Diffraction (XRD).
In the second approach, the reaction kinetics was studied by in-situ X-Ray Diffraction at the European Synchrotron Radiation Facility (ESRF – ID15B). A graphite crucible containing

the compact and a getter powder was heated by induction in a high vacuum chamber and XRD patterns were collected in transmission mode using a MAR345 detector. Sample-detector distance was chosen to optimize the angular resolution. A first set of experiments was carried out at 10 °C.min^{-1} from RT to 920 °C. Then, other experiments were conducted under isothermal conditions for reaction temperature of 700 and 800 °C.
The evolutions of the TiC cell parameter and its stoichiometry during heat treatment, i.e. during the course of reaction 1, were followed by sequential rietveld refinement using the FullProf Suite software.

Results
First, short time heat treatments revealed a very fast kinetics rate for reaction 1. 50% advancement of the reaction was reached after only 1.5 min and 75% after 5 min at 920°C. Rietveld refinement lead to a final cell parameter of 4.316 nm which is in good agreement with the refined stoichiometry of the particles ($TiC_{0.66}$) and previous works [2]. Second, in-situ XRD under anisothermal conditions (from RT to 920°C at 10°C.min^{-1}) revealed an onset temperature for reactivity at about 400 °C. In addition, a continuous evolution of stoichiometry from TiC to TiC_y was evidenced (Figure 1). The final TiC_y stoichiometry was in accordance with short time isothermal heat treatment experiments ($TiC_{0.67}$).

Discussion
Discussion of experimental data is associated with some thermokinetics calculation performed by using the ThermoCalc and DICTRA packages. Both experimental and calculation results indicated that the kinetics of solid state reaction of TiC with Ti metal is quite fast. From the point of view of Ti/TiC MMCs synthesis, the consequence of the fast reaction is an evolution of the particle size distribution associated with an increase of the reinforcement volume fraction.

Figure:

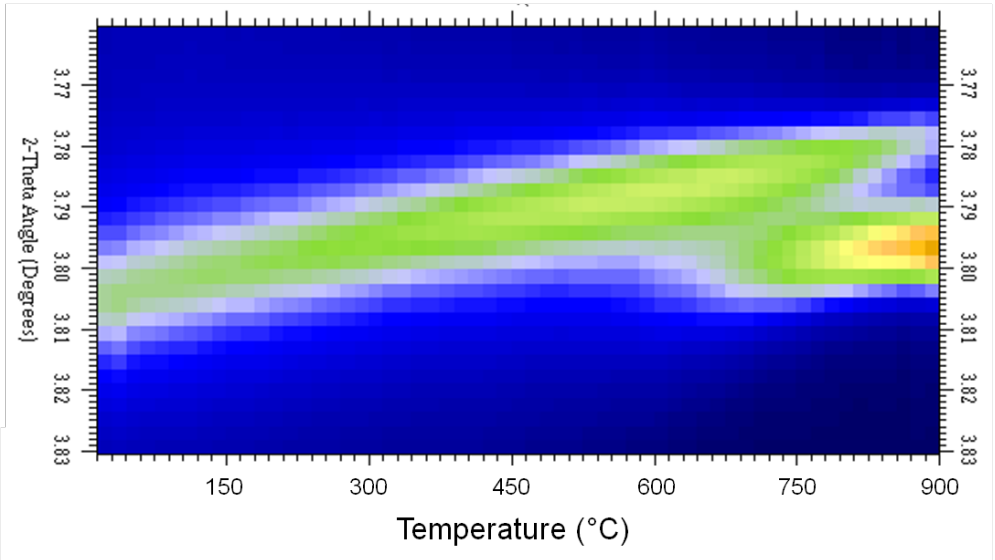

Figure 1. Evolution of (200) TiC peak as a function of the temperature.

References:
[1] G. Liu, D. Zhu and J.K. Shang, *Scr. Metall. Mater.*, **28** (1993) 729.
[2] S. S. Kiparisov, V. K. Narva, and S. Y. Kolupaeva, *Soviet Powder Metallurgy and Metal Ceramics*, **14** (1975) 549.

Concentration pressure in solid solutions of ionic salts

N.F. Uvarov [a,b,c], A.A. Iskakova [a], A.V. Anikeenko [d], N.N. Medvedev [b,d]

[a]*Institute of Solid State Chemistry and Mechanochemistry, SB RAS, Kutateladze, 18, Novosibirsk, 630128, Russia*
[b]*Novosibirsk State University, Pirogova, 2, Novosibirsk, 630090, Russia*
[c]*Novosibirsk State Technical University, Prospekt Karla Marksa, 20, 630073, Novosibirsk, Russia*
[d]*Institute of Chemical Kinetics and Combustion SB RAS, Institutskaya, 2, Novosibirsk, 630090, Russia*

In the report we discuss reasons of a similarity between a PT - diagram of pure substance and the phase diagram of solid solutions obtained by doping this compound with some additives. Examples of such similarity are PT-diagrams of iron or titanium and phase diagrams of iron- or titanium-based binary metallic systems in the solid solutions regions [1, 2] (Fig.1). Another example is zirconia at high pressure in comparison with solid solutions containing different oxides, known as metal-stabilized zirconia. From such a similarity one could propose that dopants may produce effective positive or negative concentration pressure in the crystal lattice of the host matrix. Really this effect may be explained by positive or negative strains in the crystal lattice generated by introduction of large- or small-sized atoms or ions into the host matrix. The change in the Gibbs energy of the crystal internally deformed by inclusion of the dopant atoms (or ions) may be expressed as [3]

$$dG \approx -SdT - e_{ij}dt_{ij} + \mu dN$$

where e_{ij} and t_{ij} are strain and deformation contributions which may be expressed as tensor components. The values of both e_{ij} and t_{ij} depend on the volume misfit between the host and guest atoms (or ions) and the total concentration of the guest. In general, the concentration pressure can be expressed as a derivative dG/de and may be calculated in the low-concentration limit.

The clear effect of the concentration pressure was found in nitrite systems based on $RbNO_3$. Phase transition temperatures in rubidium nitrate change as a result of ionic substitutions. Introduction of large-sized Cs^+ cations leads to effects similar to ones occurring at application of high pressure to rubidium nitrate [4]. In contrast, the substitution of nitrate ions with smaller nitrite ones leads to an decrease in the temperature of phase transitions IV↔III and III↔II, so that highly conducting phase III becomes stable at low temperatures. Comparison with the PT diagram of $RbNO_3$ [4] shows that such doping induces negative concentration pressure within the lattice of $RbNO_3$ (Fig. 2). On the other hand, the introduction of smaller NO_2^- anions results in the increase in the conductivity of $RbNO_3$-III phase, the activation energy and a pre-exponential factor of conductivity decrease with the doping and III-IV transition becomes diffusive [5]. These results were confirmed using a Molecular Dynamics (MD) computer modeling. Possible reason of these effects is a strong influence of nitrite ions to the orientational disorder of the anionic sublattice of $RbNO_3$ due to negative strains which nitrite ions generate in the crystal lattice of the $RbNO_3$ matrix. Results of MD simulations also indicate the appearance of small negative effective pressure within the crystal lattice of $RbNO_2$ on its doping with rubidium nitrite.

Acknowledgement: The work was supported by the Ministry of Education and Science of the Russian Federation and by the Programme of Presidium RAS #27.59.

References:
[1] E.Yu. Tonkov, *Phase diagrams of elements at high pressure.* Phys. Math. Lit. Pbls., Moscow, 1979.
[2] *ASM Handbook, Vol. 3: Alloy Phase Diagrams*, ASM International, 1992
[3] A.I. Rusanov, *Thermodynamic Bases of Mechnochemistry*, Nauka Pbls., Saint Petersburg, 2006.
[4] E.Yu. Tonkov, *Phase diagrams of compounds at high pressure (Compounds of Li, Na, K, Pb, Cs, Be, Mg, Ca, Sr, Ba),* Nauka Pbls., Moscow, 1983..
[5] A.A. Iskakova, N.F. Uvarov, *Solid State Ionics* **188** (2011) 83-85.

Figures:

Fig.1. PT-diagram of iron (a) in comparison with typical phase diagrams of binary iron alloys in the case of positive (austenite stabilized steels, b) and negative (ferrite stabilized steels, c) concentration pressure.

Fig.2. Experimental phase diagram of binary system $RbNO_3$ - $RbNO_2$ obtained from the data of calorimetric study and electrical measurements (left plot) compared with the PT diagram of rubidium nitrate (right plot).

Molecular strategies toward original nanomaterials: sub-oxides and boron-based compounds

David Portehault,*[a,b,c] V. Maneeratana,[a,b,c] Julie Besnardière,[a,b,c] Guillaume Gouget,[a,b,c] Sophie Cassaignon,[a,b,c] Clément Sanchez[a,b,c]

[a] Sorbonne Universités, UPMC Univ Paris 06, UMR 7574, Chimie de la Matière Condensée de Paris, F-75005, Paris, France;
[b] CNRS, UMR 7574, Chimie de la Matière Condensée de Paris, F-75005, Paris, France;
[c] Collège de France, Chimie de la Matière Condensée de Paris, 11 place Marcelin Berthelot, 75231 Paris Cedex 05, France.

Corresponding and presenting author: david.portehault@upmc.fr

Reactions between molecule-scale species are often the most suitable for the cost effective fabrication of materials with controlled crystal structure, nano-, meso- and micro-structures. While such chemical pathways are intensively studied since three decades for nanostructured metals, chalcogenides and oxides of metals with high oxidation state, many other compounds families were only scarcely, if ever, reported at the nanoscale. These systems show at the bulk scale mechanical, catalytic, optical and electronic properties without equivalent among common compounds. The design of corresponding nanostructures could therefore lead to important changes or enhancement of existing properties, emergence of new behaviours and novel processing possibilities. The difficulty to isolate nanostructures of such compounds lies mainly in the high energy input, often through high temperatures (>1000 °C), required for crystallization. As a consequence, metastable states, including nanostructures with high surface energy, are destroyed. Strong research efforts are therefore necessary to unveil new synthetic routes at lower temperatures which could lead to genuinely new nanomaterials. This is the motivation of the research performed in our group at the *Laboratory of Chimie de la Matière Condensée de Paris*: we are aiming at the design of functional nanomaterials with innovative compositions. In this presentation, we will discuss some innovative molecular-based syntheses in the light of some specific cases (**Figure 1**), including reduced titanium oxides, so-called Magnéli phases, metal-boron alloys and boron-carbon-nitrogen covalent frameworks.

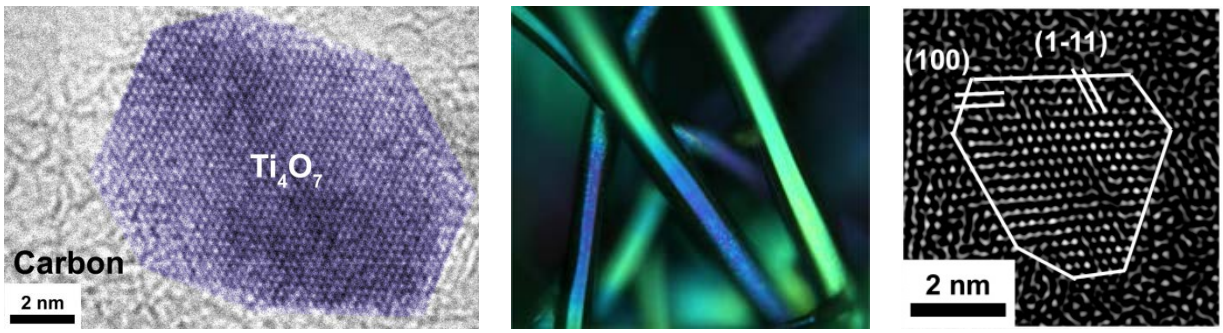

Figure 1. Left: HRTEM picture of a Magnéli phase Ti_4O_7 nanocrystal; **Middle**: True color optical microscope image of nanostructured and electrospun Magnéli phase Ti_8O_{15} microfibers; **Right**: FFT filtered HRTEM pciture of a NbB_2 nanocrystal.

Mixed valence titanium oxides, especially Magnéli phases Ti_nO_{2n-1} ($4 < n < 10$) provide versatile tuning of the electrical properties, from wide band gap semiconductor TiO_2 to low band gap Ti_8O_{15} and metallic Ti_4O_7. The first occurrences of nanostructuration of these compounds were obtained by a one-pot combination of the sol-gel process and carbothermal reduction.[1,2] Tuning the molecular reactants, the temperature and the atmosphere leads to precise adjustment of the stoechiometry and the particle size.[1,2] Shaping processes were then especially adressed toward specific properties. For instance, spark plasma sintering yielded nanostructured bodies with enhanced thermoelectric figures of merit compared to bulk materials,[1] while electrospinning of the initial solution led to microfibers with unprecedented electrical memory effects.[2]

Metal borides are metal-boron alloys where the high covalency of the boron-boron bonds results in superhardness (eg. ReB_2), superconductivity (eg. MgB_2), high temperature metallic conductivity (HfB_2) without equivalent in other compounds families. Covalency however requires high temperature processes to trigger crystallization, so that nanostructures cannot be retrieved.[3,4] The first general route toward metal boride nanocrystals [5] was discovered by using inorganic solvents stable at high temperature (900°C). These liquids were used for performing colloidal syntheses from metallic salts and borohydrides as metal and boron sources, respectively. The use of alkali halide eutectic mixtures as solvents where reaction kinetics were enhanced enabled to fasten crystallization and to maintain the nanoparticle size, so that the metal to boron ratio and the particle diameter can be tuned for a wide range of compounds, including HfB_2, YB_4, CaB_6, NiB, Ni_2B, MoB_2, CoB.

Layered boron carbon nitrides, similar to graphite, provide a very versatile lever to tune the electronic properties of graphene-like nanomaterials by the adjustment of the B-C-N composition. As for metal borides, synthesis in molten salts provides an interesting plateform to design B-C-N compounds by using organic C and N sources.[5] The reactant ratio and synthesis temperature can be adjusted to tune the materials composition and the nanoparticle shape from 5 nm diameter spheres to 5 nm-thick nanosheets. Composition, particle size and materials porosity can then be used to control the photoluminescence,[5] the hydrogen storage,[6] Li storage [7] and environmental remediation [8] properties.

References:

[1] D. Portehault, V. Maneeratana, C. Candolfi, N. Oeschler, I. Veremchuk, Y. Grin, S. Sanchez, M. Antonietti, *ACS Nano* **5** (2011) 9052.
[2] V. Maneeratana, D. Portehault, J. Chaste, D. Mailly, M. Antonietti, C. Sanchez, *Adv. Mater.* **In press** (2014).
[3] S. Carenco, D. Portehault, C. Boissière, N. Mézailles, C. Sanchez, *Chem. Rev.* **113** (2013) 7981.
[4] S. Carenco, D. Portehault, C. Boissière, N. Mézailles, C. Sanchez, *Adv. Mater.* **26** (2014) 371.
[5] D. Portehault, S. Devi, P. Beaunier, C. Gervais, C. Giordano, C. Sanchez, M. Antonietti, *Angew. Chem. Int. Ed.* **50** (2011) 3262.
[5] W. Lei, D. Portehault, R. Dimova, M. Antonietti, *J. Am. Chem. Soc.* **133** (2011) 7121.
[6] D. Portehault, C. Giordano, C. Gervais, I. Senkovska, S. Kaskel, C. Sanchez, M. Antonietti, *Adv. Funct. Mater.* **20** (2010) 1827.
[7] W. Lei, S. Qin, D. Liu, D. Portehault, Z. Liu, Y. Chen, *Chem. Commun.* **49** (2013) 352.
[8] W. Lei, D. Portehault, D. Liu, S. Qin, Y. Chen, *Nat. Commun.* **4** (2013) 1777.

Structural diversity and complexity of uranyl selenates and sulfates

Vladislav V. Gurzhiy,[a] Sergey V. Krivovichev,[a] Ivan G. Tananaev[b]

[a] Department of Crystallography, St. Petersburg State University, University Emb. 7/9, 199034 St. Petersburg, Russia, vladgeo17@mail.ru;
[b] Frumkin Institute of Physical Chemistry and Electrochemistry RAS, Leninsky Av. 31-4, 119071, Moscow, Russia.

Uranium compounds containing tetrahedral oxoanions are of special importance from the environmental and mineralogical points of view. In this work, we examine structural relations and systematics for uranyl selenates and sulfates, i.e. uranyl compounds with tetrahedrally coordinated Se^{6+} and S^{6+} cations.

The U^{6+} atoms is almost always present as approximately linear uranyl-ions $[O=U=O]^{2+}$, that are coordinated by four, five or six additional anions in the equatorial plane. Apical oxygen atoms in the bipyramids formed by such way are almost completely valence saturated, whereas it is necessary to form additional chemical bonds for the valence saturation of equatorial anions. Hence the uranyl polyhedra are usually polymerize with each other only through the equatorial vertices and edges, that results in prevalence of layered structures among the minerals and synthetic uranyl compounds.
Analysis of uranyl selenate structures known at present demonstrates predominance of structural connectivities based upon corner-sharing coordination polyhedra. The most convenient method for the description of such structures is representation of their topologies in terms of bicolored graphs. Within this description, vertices correspond to coordination polyhedra, and the presence of an edge between the neighboring vertices complies with the presence of bridging O atom between the respective coordination polyhedra. Crystal structures of uranyl sulfates often based on edge-sharing heteropolyhedral units. These condensed structural complexes could be more clearly described by the means of anionic topologies. In this approach, the connectivity of the sheet of polyhedra is analyzed and only those anions that are bonded to two or more cations within the sheet are considered.

In the crystal structures of inorganic uranyl compounds, uranyl selenate and uranyl sulfate complexes are linked via monovalent cations (K^+, Na^+, Rb^+, etc.) or octahedrally coordinated divalent cations ($[Ni(H_2O)_6]^{2+}$, $[Zn(H_2O)_6]^{2+}$, $[Mg(H_2O)_6]^{2+}$, etc.). In the crystal structures of amine-templated uranyl compounds, structure formation is regulated by hydrogen bonding systems and by arrangement of hydrophobic and hydrophilic parts of molecules with voids and dense fragments of inorganic complexes. The basic structural principle of organic-inorganic uranyl composites templated by electroneutral molecules (such as crown ethers), is the translation of interactions between organic and inorganic components by means of protonated water molecule complexes (e.g., $H_5O_2^+$ and H_3O^+).

This work was supported by St. Petersburg State University and President of Russian Federation grant for young scientists (no. MK-1737.2014.5). XRD studies have been performed at the X-ray Diffraction Centre of St. Petersburg State University.

Electrochemical activity of Li_2MnO_3 induced by coexisting with CuO

Yoshinori Arachi, Yu Taura, Shinya Akiyama

Kansai University
Suita, Osaka 564-8680, Japan
arachi@kansai-u.ac.jp

For many years, challenges to develop lithium ion secondary batteries with high energy density have been examined. Li_2MnO_3-based positive electrodes such as $LiNi_{1/3}Mn_{1/3}Co_{1/3}O_2$ have attractive cell performances which are suitable for the electrical vehicles using lithium ion batteries. A material including a large amount of Li is preferable to show large capacity as a positive electrode. These electrodes have been expected to be alternative materials to conventional $LiCoO_2$. However, Li_2MnO_3 itself without Co or Ni has a poor electrochemical activity except for those of prepared at lower temperature such as 773 K. Recently, we have found out the way to activate Li_2MnO_3 electrochemically by coexisting CuO, not by substitution [1]. The objective is to clarify the reason why the existence of CuO induces the electrochemical activity of Li_2MnO_3 by our using SR-XRD, XAFS and *ab-initio* calculation. In addition, the electrochemical performance of "Li_2MnO_3-CuO composite" will be discussed.

The samples were prepared by combining coprecipitation and solid state reaction. After dissolving $CuSO_4$ and $Mn(CH_3COO)_2$ into the distilled water, the co-precipitates were obtained by changing pH from 10 to 12. Dry precipitates and $LiOH{\cdot}H_2O$ were mixed and after calcination at 743 K, sintered at 973 K for 12hr under O_2 flow. Electrochemical testing was carried out using coin-type cells with Li/1M $LiPF_6$ in EC:DMC(3:7)/samples. X-ray diffraction (XRD) measurements using both Cu*K*α radiation and a synchrotron radiation source were performed and for the latter on BL02B2 and BL19B2 at SPring-8. Structural refinements were carried out by Rietveld analysis using the RIETAN-FP program[2]. X-ray absorption measurements of above samples at the Mn and Cu *K*-edges by transmission method were performed on BL14B2 at SPring8. The first principle calculations were carried out using the WIEN2k program package, which is based on the full potential augmented plane wave and local orbitals (APW+lo) method within the generalized gradient approximation (GGA).

XRD patterns showed that all the samples for x=1/5, 1/4, 3/8, 1/2 in $(1\text{-}x)Li_2MnO_3$-xCuO composed of two-phases of Li_2MnO_3 and CuO phases. By TEM observations the particle sizes of Li_2MnO_3 for both x =1/5 and 1/2 were about 65 nm, whereas those of CuO were 0.5 to 1.0 μm for x =1/5, and 0.2 to 0.3 μm for 1/2 which are much larger than those of Li_2MnO_3. The particle size of Li_2MnO_3 did not differ by the amount of CuO. However, in proportion to x the electrochemical activities of the samples were enhanced, as shown in Figure 1. In addition, the rate performance of the samples was improved by CuO addition. The 240 $mAhg^{-1}$ of discharge capacity was kept after 20 cycles at the rate of 1/20 C.

To clarify the reason why coexisitng with CuO enhances the electrochemical activity of Li_2MnO_3, at first we fouced on the crystal structure of Li_2MnO_3 and carried out Rietveld analysis using SR-XRD for all the samples, based on the structural model of monoclinic

Li_2MnO_3, S.G. *C*2/*m*. It was found that Li and Mn locate on both 2*b* and 4*g* sites of Wyckoff positions. A disordering of Li and Mn in the structure of Li_2MnO_3 increased by CuO contents. The results of neutron diffraction patterns supports those of XRD. These disordering behaviour probably may correlate closely with the electrochemical activity of Li_2MnO_3. In addition, a significnat difference of electron diffraction patterns was observed between x = 1/5 which showed discharge capacity of 160 $mAhg^{-1}$ and x = 1/2 that of 355 $mAhg^{-1}$. A distinguished streaks along c^* axis appeared for x = 1/2 suggesting a stacking fault, wheares some diffraction spots did for x = 1/5. A similar results for Li(Ni, Mn, Co)O_2 are rescribed in ref. [3]. The coexsisting with CuO intoroduce a stacking fault into Li_2MnO_3. Next, we considered an effect of partial substiontion of Cu. The *ab-initio* electronic structure calculation allows us to know more about the electrical property. Density of States (DOS) of our assumed supercell, $Li_{16}(Mn_7Cu_1)O_{24}$ indicated a new sharp band which expect to show higher electrical conductivity than that of Li_2MnO_3 itself. Hence, the partial replacing Mn by Cu suggests an improvement of the electrochemical property. Next, we focused on CuO coexisting with Li_2MnO_3. Whereas a pure CuO is an insulator, Li-doped CuO could be a semiconductor in the literature [4]. Therefore, it is reasonable that the kinetic barrier of the electrode reaction for Li_2MnO_3 was depressed by coexisting with CuO.
We will present a new way to activate Li_2MnO_3 electrochemically by coexisting CuO, not by substitution and discuss the mechanism why coexisitng with CuO enhances the electrochemical activity of Li_2MnO_3 based on both experimental and calculation results.

Acknowledgement:
This research was supported by Japan Society for the Promotion of Science (25410255).

References:
[1] Y. Arachi, K. Hinoshita and Y. Nakata, *ECS Transactions*, **41**(29) (2012) 1.
[2] F. Izumi and K. Momma, *Solid State Phenom.*, **130** (2007) 15.
[3] A. Boulineau, L. Croguennec, C. Delmas, F. Weill, *Solid State Ionics*., **29** (2010) 1652.
[4] R. R. Heikes, W. D. Johnston, *J. Chem. Phys*., **26** (1957)582.

Figures:

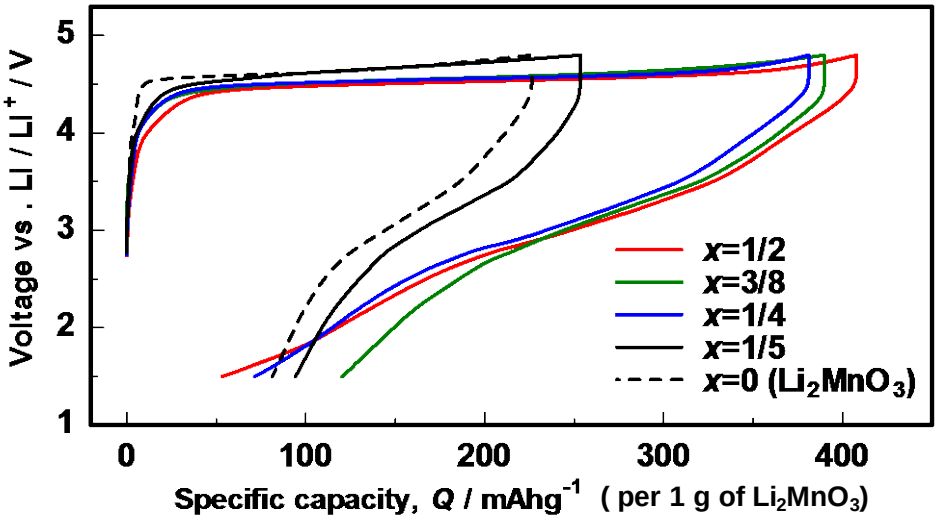

Figure 1. Charging and discharge curves for (1-x) Li_2MnO_3-x CuO cell.

New functional materials for energy applications

M. Karushev[a], A. Timonov[b]

[a]Powermers Inc.;
[b] State Pedagogical University of Russia "A.I.Herzen", Dpt. of Chemistry.

Polymer transition metal complexes with tetradentate N_2O_2 Schiff base ligands derived from salicylaldehydes and aliphatic diamines, often referred to as poly[M(Schiff)], belong to a class of conductive polymers. They can be easily formed on inert electrode surfaces (e.g. carbon, platinum, ITO, etc.) via oxidative electrochemical polymerization of corresponding Schiff base monomers (Figure 1) in moderately/weak donor solvents.

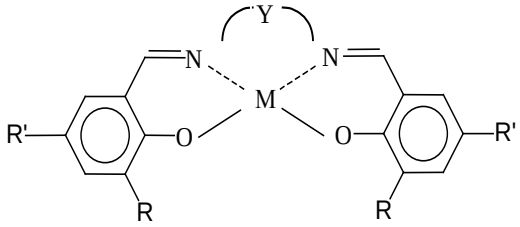

Figure 1. Structure of some monomers M(Schiff)] M(II) = Mn, Co, Ni, Cu, Pd, Pt; R, R' = H; Y = -CH_2-CH_2- – [M(SalEn)]; R, R' = H; Y = -$C(CH_3)_2$-$C(CH_3)_2$- – [M(SaltmEn)]; R = OCH_3, R' = H, Y = -CH_2-CH_2- – [M(CH_3O-SalEn)]; R = OCH_3, R' = H, Y = -$C(CH_3)_2$-$C(CH_3)_2$- – [M(CH_3O-SaltmEn)]

Due to their unique characteristics, such as broad potential range of electrochemical activity (> 3 V), high specific energy stored in the polymer (> 300 J/g), unique thermal stability (up to 350 ^oC), high chemical and electrochemical reversibility of redox processes, electrochromic properties, easy synthesis and low cost polymer Schiff base transition metal complexes are promising materials for energy storage/conversion applications. We report herein on the results of our attempts of poly[M(Schiff)] applications in ultracapacitors (**I**), metal-air batteries (**II**) and photoelectrochemical energy converters (**III**).

I. High reversibility and fast kinetics of red/ox processes in poly[M(Schiff)]'s allows to use them as pseudocapacitive materials for electrochemical supercapacitors. Adsorption-electrochemical modification procedure, developed in our lab, utilizes an unused space in high-porous carbon material by filling it with poly[M(Schiff)] polymer. As a result, double-

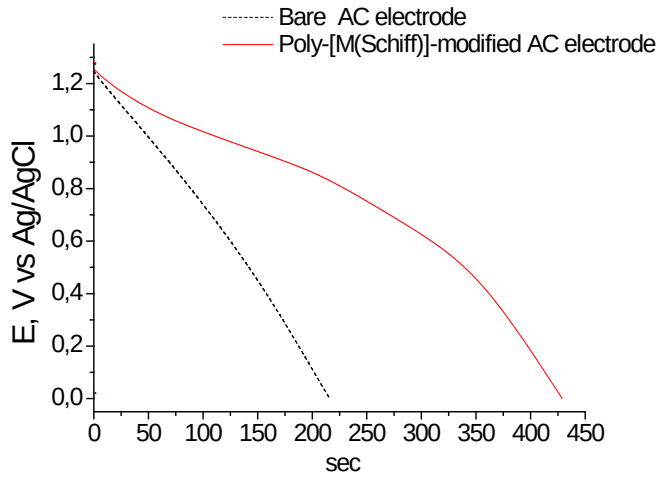

Figure 2. Galvanostatic discharge of positive electrodes for double-layer capacitors, 2mA/cm^2, 1M Et_4NBF_4/AN electrolyte.

layer capacitance of positive activated carbon (AC) electrode enhanced by redox capacitance of poly[M(Schiff)]. Achievable improvement depends on carbon pore structure and now reaches doubling of volumetric capacity for meso-porous carbon (Fig. 2).

II. Affinity of planar cobalt macrocycles to dioxygen and ability of such complexes to catalyze oxygen reduction reactions (ORR) are well known. Conductive and electroactive poly[Co(Shiff)]'s are promising materials for electrocatalysis of ORR, as they can be easily polymerized, have tunable structure and high affinity to dioxygen. Poly[Co(Schiff)]'s – modified electrodes in Li^+ and O_2 - containing solutions demonstrate sufficient electrocatalytic effect in ORR associated with Co(III)/Co(II) red/ox pare.

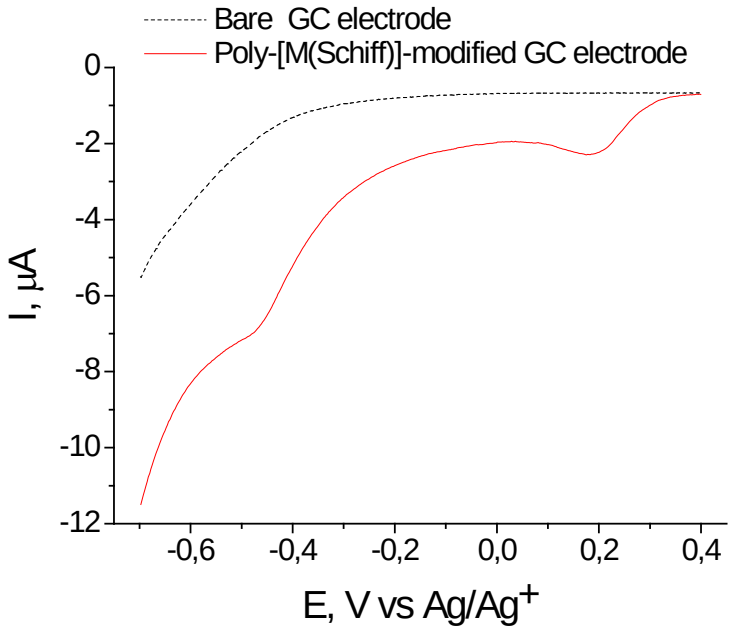

Figure 3. 50mV/sec polarization curves of GC electrodes in O_2 -saturated 0.1M $LiBF_4$/AN electrolyte

III. When the optically transparent electrode, modified with a poly[M(Schiff)] film, irradiated with visible light, the electrode potential is increased by 100 - 500 mV, depending on the nature of the metal center and ligand environment. Upon light excitation one electron from the M degenerate d orbitals is promoted to the π anti-bonding orbital of the Schiff ligand giving the metal-to-ligand electron transfer excited state which could undergo intersystem crossing to the corresponding triplet charge-separated state. Emission of this state is effectively quenched by molecular oxygen dissolved in the solution. This quenching completes the charge separation process and leads to the increase of degree of oxidation of polymer metal centers. In turn, the increased concentration of oxidized polymer metal centers leads to a shift of the electrode potential in the positive region. The report will be presented results of the study of described above photogalvanic effect for various poly[M(Schiff)] polymers, as well as test results of model photoelectrochemical converters based on these polymers.

Highly reactive nanooxides prepared by mechanochemical routes

Vladimir Šepelák,[a,b] Andre Düvel,[c] Martin Wilkening,[d] Horst Hahn,[a] Klaus Dieter Becker,[e] Paul Heitjans[c]

[a]Institute of Nanotechnology, Karlsruhe Institute of Technology, Hermann-von-Helmholtz-Platz 1, D-76344 Eggenstein-Leopoldshafen, Germany;
[b]Institute of Geotechnics, Slovak Academy of Sciences, Watsonova 45, SK-04001 Košice, Slovakia;
[c]Institute of Physical Chemistry and Electrochemistry, Leibniz University Hannover, Callinstr. 3-3a, D-30167 Hannover, Germany;
[d]Institute for Chemistry and Technology of Materials, Graz University of Technology, Stremayrgasse 9, A-8010 Graz, Austria;
[e]Institute of Physical and Theoretical Chemistry, Braunschweig University of Technology, Hans-Sommer-Str. 10, D-38106 Braunschweig, Germany.

It is widely appreciated that the performance of oxides and of materials, in general, is closely related to the ways in which they are processed. One goal of modern solid state chemistry research and materials development has been to identify simpler processing schemes that do not rely upon high-temperature treatments for inducing solid state reactions. Among the many types of preparation techniques, the non-conventional mechanochemical synthesis (the so-called mechanosynthesis) has been recognized as an efficient route providing a single-step and facile access to nanomaterials [1].

In the present work, selected examples are presented of mechanochemical formation reactions leading to complex oxide nanoparticles with a nonequilibrium structure and unique functional properties. One of the most important aspects of studies on mechanically induced reactions in oxides is the exploration of simple routes to compounds with a large amount of defective cation centers with an unsaturated oxygen coordination which can easily be adjusted by the milling time (t_m) as well as time and temperature of a subsequent annealing step. This is exemplarily demonstrated in Fig. 1, where mechanical action on the mullite-type $Bi_2(Ga_2Al_2)O_9$ material gives birth to three- and fivefold coordinated Al centers [1,2]. The concentration of these defective AlO_3 and AlO_5 configurations increases with increasing t_m, reaching the value of about 21% in nanomaterials with crystallite sizes below 10 nm. The so prepared nanostructured oxides might be of large interest for the preparation of catalysts since the unsaturated Al centers act as anchoring sites for catalytically active materials [3]. Thus, the mechanical preparation route found might establish a basis for the design of catalysts whose activity can be thoroughly tailored. It is demonstrated that mechanochemical methods provide highly effective tools to create (metastable) compounds which are not available by conventional synthesis routes.

The present work is supported by the DFG within the framework of the Priority Program "*Crystalline Nonequilibrium Phases*" (SPP 1415). Partial support from the APVV (project 0528-11) and the VEGA (2/0097/14) is gratefully acknowledged.

References:

[1] V. Šepelák, A. Düvel, M. Wilkening, K. D. Becker, P. Heitjans, *Chem. Soc. Rev.*, **42** (2013) 7507.
[2] V. Šepelák, S. Bégin-Colin, G. Le Caër, *Dalton Trans.*, **41** (2012) 11927.
[3] J. H. Kwak, J. Hu, D. Mei, C.-W. Yi, D. H. Kim, C. H. F. Peden, L. F. Allard, J. Szanyi, *Science*, **325** (2009) 1670.

Figures:

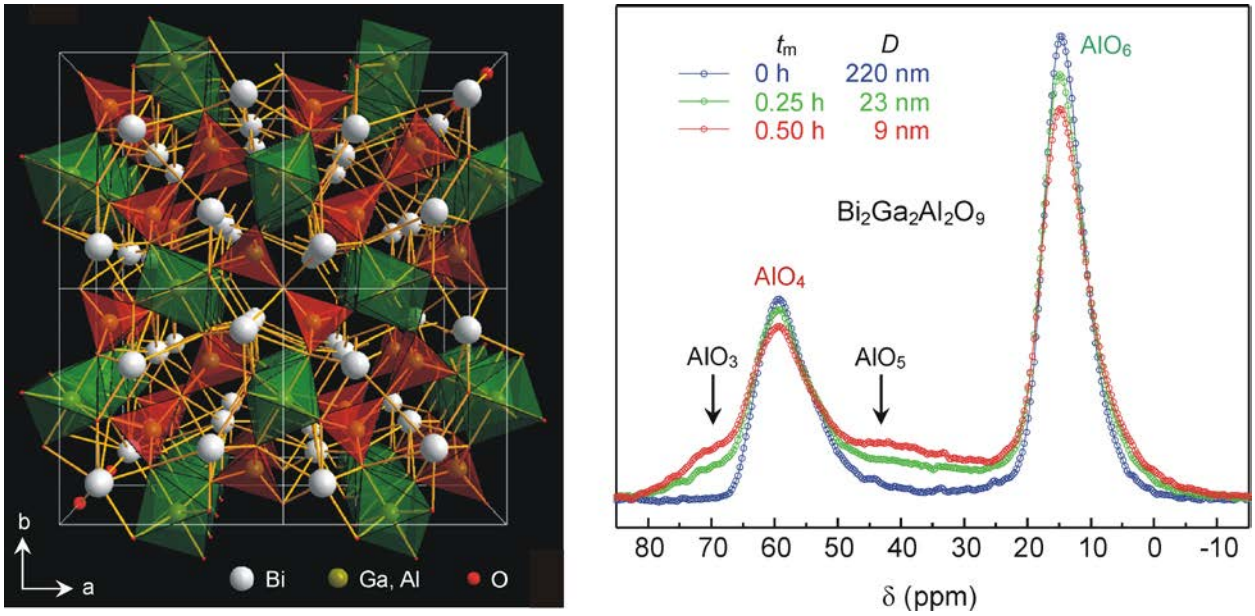

Fig. 1. (left) The orthorhombic mullite-type crystal structure of $Bi_2Ga_2Al_2O_9$ is characterized by chains of edge-connected MeO_6 octahedra along the *c*-axis which are interconnected by Me_2O_7 double tetrahedra (Me = Ga^{3+}, Al^{3+}).

(right) ^{27}Al MAS NMR spectra of $Bi_2Ga_2Al_2O_9$ milled for various times in a Pulverisette 7 planetary ball mill (Fritsch, Germany). The milling times (t_m) and the corresponding crystallite sizes (D) are shown in the figure. Arrows denote the spectral components corresponding to the anomalous AlO_3 and AlO_5 nearest-neighbor atomic configurations. ^{27}Al MAS NMR spectra were recorded at a spinning rate of 20 kHz. The ^{27}Al chemical shifts are referenced to 1 M $Al(NO_3)_3$ aqueous solution.

The study of kinetics, structural and morphological changes during thermal decomposition of $M_2(C_2O_4)_3 \cdot 10H_2O$ (M=Ce, Sm).

Matvienko Alexander,[a,b] Maslennikov Daniel,[b],Chizhik Stanislav,[a,b] Sidelnikov Anatoly,[a] Zakharov Boris [a,b].

[a] Institute of Solid State Chemistry and Mechanochemistry, Kutateladze, 18, 630128, Novosibirsk, Russia
[b] Novosibirsk State University, Pirogova, 2, 630090, Novosibirsk, Russia.

Thermal decomposition of salts precursors (e.g., hydrates, nitrates, carbonates and oxalate) were commonly used to yields metal oxide powders both in laboratories and in industries. Despite the numerous publications on thermal decomposition reactions, there is still an open question about the possibility to control the size, shape and phase composition of the particles of the product. In [1,2] we proposed the approach based on feedback between reaction and fracture. Fracture is result of large shrinkage during reaction and low plasticity of initial salts. This approach allows predicting of stationary front velocity (the reaction rate) and morphology of product (shape and size of particles, porosity). The validity of the approach had been proved experimentally for dehydration of some inorganic and organic hydrates and calcite decomposition. The approach was elaborated in this work. Cerium and samarium oxides were obtained during decomposition of oxalate precursors. The influence of a reaction staging, crystal habitus and reaction condition (temperature and water or oxygen pressure) on kinetics, structural and morphological changes were studied. X-ray diffraction, TG-DTA methods, optical microscopy, TEM, SEM, small-angle X-ray scattering, Raman spectroscopy and N_2 sorption isotherm techniques were employed for morphology and structure characterizations.

Two types of topotactic structural transformations were observed during dehydration of cerium oxalate decahydrate. The metastable structure was obtained in vacuum. Detailed analysis of atomic displacements was carried out and strain ellipsoids were obtained for each case. The reaction-related deformation determines the character of the fracture. It was shown that reactions with different mode of structural transformation had different morphology of fracture. Observed deformation of crystals and suggested structural modification are presented on Figure. The structure of $Ce_2(C_2O_4)_3 \cdot 10H_2O$ is composed of infinite cerium oxalate layers, perpendicular to b-axis. The layers are held together by hydrogen bonds via water molecules situated between the layers. The evolution of (100) habitus crystals in vacuum is presented on Figure (a). 30% compression along b axis is observed. Other cell parameters are not changed. We suggest that the removal of water molecules causes a decrease of interlayer distance. The structure of layer is not changed in this case. The evolution of (010) habitus crystals during reaction at high water vapor pressure is presented on Figure (b). Changing the crystal form is observed in this case. It is suggested that the shear deformation of layer occurs during dehydration. Samarium and cerium oxalate decahydrates are isostructural. Only one phase was formed during dehydration of samarium oxalate decahydrate. Its structure is similar to the structure of the stable modification of dehydrated cerium oxalate (Fig (b)).

Porous crystalline CeO_2 and Sm_2O_3 were obtained from dehydrated oxalates during heating in air. It was shown that solid product of thermal decomposition was formed as pseudomorph with porosity 35-40%, which consists of metal oxide nanoparticles. Specific surface area of

cerium oxide measured by the BET method was 140 m^2/g. The values of particle size obtained from TEM data were about 5 nm. It should be noted that reaction rates of cerium oxalate obtained under different conditions were varied significantly. Thus, it is possible to control the kinetics and morphology of the final product by varying the conditions of dehydration. Possible mechanisms of pore formation were discussed. The analysis of the methods to control the size, shape and phase composition of the product was carried out.

References:

[1] S.A. Chizhik, A.A. Sidelnikov, *Solid State Ionics*, **178** (2007) 1487.
[2] A.A. Matvienko, S. A. Chizhik, A. A. Sidel'nikov, *Doklady Phisical Chemistry*, **451**(2013) 184.

Figures:

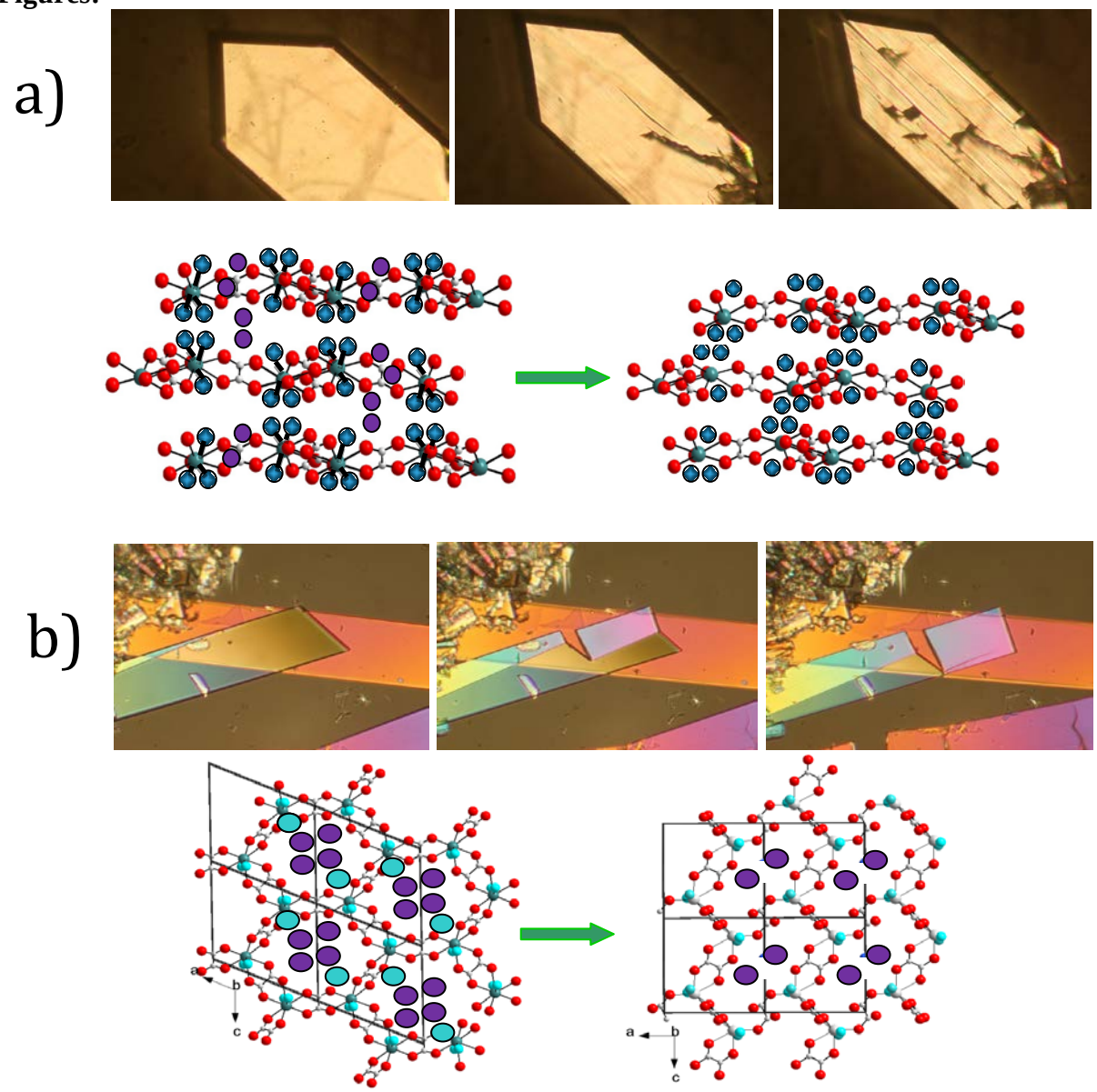

Figure 1. Observed deformation of $Ce_2(C_2O_4)_3 \cdot 10H_2O$ crystals and suggested structural modification during dehydration in vacuum (a) and at high water pressure (b). x100.

Imaging of Charge Ordering and Oxygen Vacancies of the Multifunctional Oxide $TbBaMn_2O_{5.75}$

Susana García-Martín,[a] David Ávila-Brande,[a] Esteban Urones-Garrote,[b] Graham King[c]

[a] Departamento de Química Inorgánica, Facultad de C.C. Químicas, Universidad Complutense de Madrid, 28040-Madrid, Spain.
[b] Centro Nacional de Microscopía Electrónica, Universidad Complutense de Madrid, 28040-Madrid, Spain.
[c] Lujan Neutron Scattering Center, Los Alamos National Laboratory, Los Alamos, NM 87545, USA.
sgmartin@quim.ucm.es

$TbBaMn_2O_{6-\delta}$ has a perovskite-related structure with layered-type ordering of the Tb and Ba atoms. We have carried out Selected Area Electron Diffraction (SAED) and High Resolution Transmission Electron Microscopy (HRTEM) studies on this compound. The results reveal a modulation of the crystal structure. Besides, our Electron Energy-Loss Spectroscopy (EELS) indicates that the average oxidation state of Mn is 3.24 and therefore non-stoichiometry in the anion sublattice giving a $TbBaMn_2O_{5.75}$ general formula. A combination of techniques has allowed us to solve the crystal structure of $TbBaMn_2O_{5.75}$ [1].

Taking into account that charge ordering (CO) at room temperature is predicted in $REBaMn_2O_6$ oxides with RE ions of smaller size than Nd [2, 3], we ascribe the modulation of the perovskite-type crystal structure in $TbBaMn_2O_{5.75}$ to a combination of charge ordering, Ba/Tb ordering and anion vacancies ordering.

Different models for the CO structure of $MBaMn_2O_6$ (M = Tb, Sm, Y) have been proposed so far [4, 5]. However, all these models are based on Mn^{3+} and Mn^{4+} ordering in stoichiometric oxides (equal amount of Mn^{3+} and Mn^{4+}), which is not the case of our compound. We have proposed a model according to our SAED, HRTEM and EELS results. We deduce a $\sqrt{2}a_p \times 2\sqrt{2}a_p \times 4a_p$ unit cell (a_p refers to the lattice parameter of the cubic perovskite structure) and $P2_12_12$ space group from the reciprocal lattice constructed from different SAED patterns. The HRTEM images along the $[001]_p$ zone axis show contrast differences in agreement with the $\sqrt{2}a_p \times 2\sqrt{2}a_p$ periodicity. Our CO model consist of $\{001\}_p$ layers of one Mn^{4+} stripe alternating with three Mn^{3+} stripes along the $[110]_p$ direction. Packing of CO bi-layers along the *c*-direction, shifted by $2a_p$ along the $[100]_p$ direction every other bi-layer, leads to $4a_p$ periodicity along $[001]_p$.

We have also carried out Powder Neutron Diffraction experiments for solving the crystal structure and PDF analysis, which gives us complementary information on the oxidation states of the Mn cations and the positions of the oxygen vacancies. The results suggest that the anion vacancies are located mainly within the TbO layers and that there is at least some degree of oxygen vacancy ordering within the TbO layers.
In addition to this, we have carried out Exit Wave Reconstruction (EWR) processing of the HRTEM images, which clearly shows imaging of the oxygen sublattice at the unit cell level, to locate the anion vacancies. Analysis of the intensity of the averaged phase image along the $[010]_p$ zone axis has revealed columns with lower occupation of oxygen atoms (i.e. with

anion vacancies) in the Tb planes of the structure. Layered-type ordering of the Ba and RE cations may drive this complex association between CO and the location of the anion vacancies within the Tb planes.

Our current studies on magnetic properties and neutron powder diffraction measurements collected over broad temperature ranges of $TbBaMn_2O_{5.75}$ reveal that the nature of the charge ordering is different than originally proposed and consists of ferromagnetically coupled $(Mn^{3.33+})_3$ trimer polarons and Mn^{3+} in a 1:1 ratio. This CO model also agrees with our studies on SAED, HRTEM, EELS and EWR.

$TbBaMn_2O_{5.75}$ might has interesting properties such as oxygen conduction [6, 7] or multiferroic behavior that could be explained taking into account their crystal structure and particularly the combination of the ordering effects in the structure.

References:

[1] D. Ávila-Brande, G. King, E. Urones-Garrote, A. Llobet, S. García-Martín, *Adv. Funct. Mater.* Article first published online: 27 Dec 2013 | DOI: 10.1002/adfm.201303564.
[2] Y. Ueda, T.Nakajima, *J. Phys. Condens.Matter.* **16** (2004) S573.
[3] T. Nakajima, H.Yoshizawa, Y.Ueda, *J. Phys. Soc. Japan.* **73** (2004) 2283.
[4] T.Arima, D.Akahoshi, K.Oikawa, T.Kamirama, M. Uchida, Y.Matsui, T. Tokura, *Phys. Rev. B.* **66 (**2002) 140408.
[5] A. J.Williams, J.P. Attfield, *Phys. Rev. B* **72** (2005) 024436.
[6] A. A. Taskin, A. N. Lavrov, A.Yoichi, *Appl. Phys. Letters.*, **86** (2005) 091910.
[7] A. A.Taskin, A. N.Lavrov, A.Yoichi, *Progress in Solid State Chemistry.*, 35 **(**2007) 481.

Ion transport in defect structures of tysonite-like $La_{1-y}Sr_yF_{3-y}$ crystals

N.B. Bolotina,[a] T.S. Chernaya,[a] A.I. Kalukanov,[a,b] I.A. Verin,[a] N.I. Sorokin,[a] B.P. Sobolev[a]

[a] Shubnikov Institute of Crystallography, Moscow, Russia,
[b] Karpov institute of Physical Chemistry, Branch in Obninsk, Russia
bolotina@ns.crys.ras.ru

Tysonite-like crystals of RF_3 and $R_{1-y}M_yF_{3-y}$ (R – 16 rare-earth elements; M = Ca, Sr, Ba) are of interest as fluorine-conductive compounds [1]. There is almost no information, however, about an impact of cationic admixtures in general and heterovalent (as most active) ones in particular on structural transformations of RF_3. It is often difficult to compare properties of the tysonite-like phases using literature data, since few of them report a fine content of admixtures both in the reagents used and the crystals obtained. Only few tysonite-like crystal structures have been published with the determinate content of alkaline-earth elements (AEE). This is not enough to settle the issue of an influence of AEE on the crystal chemistry of the 43 tysonite-like phases formed in the 48 systems $MF_2 - RF_3$.

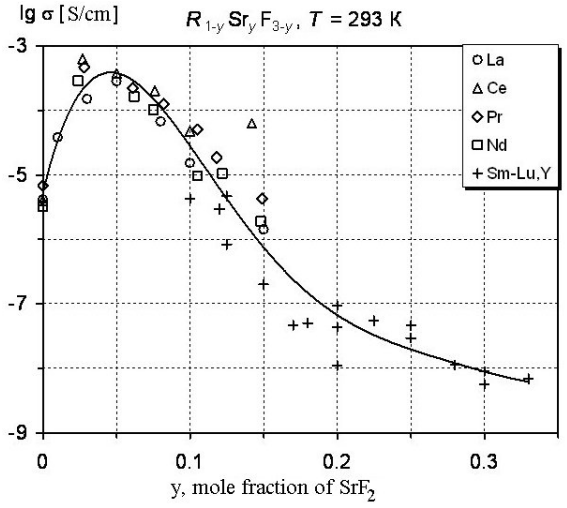

Fluorine-ionic conductivity σ strongly depends (up to 10^6 times at some temperatures) on the quantitative (y) and qualitative (R,M) composition of the crystal. At the fixed values of R and M, the conductivity non-linearly depends on y reaching its highest value near y = 0.05 - 0.07 for many well-conducting phases (Fig. 1). Possible structural reasons for such dependences were never analyzed. Recent work is performed with the view of addressing this issue.

Figure 1. Fluorine-ionic conductivity at room temperature as a non-linear function of a mole fraction (y) of SrF_2 [2].

Single crystals of $La_{1-y}Sr_yF_{3-y}$ (y = 0, 0.05, 0.07 and 0.15) were obtained from the melt by Bridgman technique. This phase is selected for the structure analysis since the crystals of $La_{0.95}Sr_{0.05}F_{2.95}$ have the high conductivity $\sigma = 3\times10^{-4}$ S/cm at room temperature with the low activation energy ~ 0.34 eV of the ion transport what enables them to be used in solid-state electrochemical units.

Defect structures of the 'as grown' crystals $La_{1-y}Sr_yF_{3-y}$ have been studied using X-ray and neutron diffraction techniques. The concentration-induced symmetry changes have been revealed first for this phase. The merohedral twins of LaF_3 и $La_{0.95}Sr_{0.05}F_{2.95}$ belong to the trigonal system (sp. gr. $P\ \bar{3}c1$; Z = 6) whereas the single-domain crystals of $La_{0.85}Sr_{0.15}F_{2.85}$ change the symmetry group for $P6_3/mmc$; Z = 2 (Fig. 2). One should note that it happens near those mole fractions of SrF_2 (y = 0.05 – 0.10), which correspond to the best conductivity. The crystals of $La_{0.93}Sr_{0.07}F_{2.93}$ show different symmetries being studied using X-rays or neutrons.

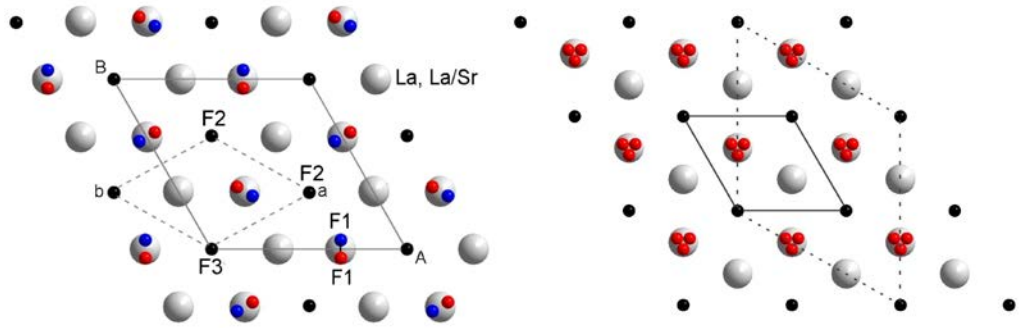

Fig. 2. Type structures of $La_{1-y}Sr_yF_{3-y}$ projected on (001). Large unit cell (left, Z=6) and small unit cell (right, Z=2) are accompanied with 'complementary' cells shown by dotted lines. The sites F1 at $z \sim 0.58$ and $z \sim 0.92$ are given in blue and red, respectively. The F1 sites (red) of the right hexagonal structure are split.

Fluorine atoms are distributed among three independent sites F1, F2, F3 of the large unit cell. The last two, F2 and F3, are equivalent in the small cell of the hexagonal structure. Each site determines the anionic subsystem of the same name. NMR techniques [3] denote in LaF_3 the mobile F1 subsystem and the less active F2+F3 subsystem at room temperature, but authors [4] come to the conclusion that the ionic transport in LaF_3 is most probable through F3 (along the *c*-axis). At the same time, the effect of crystallographic orientation on the conductivity and anionic mobility was studied by a number of authors. Below 400 K, a weak anisotropy in conductivity ($\sigma_{\|c}$ / $\sigma_{\perp c}$ = 3-4 at 320 K) for RF_3 and $R_{1-y}M_yF_{3-y}$ with $y < 0.02$ and full isotropy for those with $y > 0.08$ were found. These contradictions must be settled.

In this work, we considered structure-dependent possibilities for the charge transfer in different directions through the F1, F2 and F3 subsystems of the crystals studied. It was assumed that fine changes of the F3 subsystem at *y* near 0.05 can simplify the F1-F1 as well as F3-F3 ion transport giving rise to better conductivity. Different trajectories are presented and discussed. Also, a possible contribution of the twin phenomenon to the conducting properties of the tysonite-like crystals is analyzed. It has been assumed that charge carriers can move along the twin boundaries through the sites of the F1 subsystem of LaF_3 using metrically adequate interstitials at the boundaries. Besides, an attention is given to the matter why the conductivity decreases at the further increase of the AEE content.

This study was partly supported by Russian Fund of Basic Research, grant No 13-02-00105, and by Council on Grants from the President of the Russian Federation for Support of Leading Scientific Schools (grant No. NSh-1130.2014.5).

References:

[1] Anji Reddy M., Fichtner M., *J. Materials Chem.*, **21** (2011) 17059.
[2] Sorokin N.I.. Sobolev B.P., *Crystallography Reports*, **39** (1994) 810.
[3] Privalov A.F., Murin I.V., *Physics of the Solid State*, **41** (1999) 1482.
[4] Brach I., Schulz H., *Solid State Ionics*, **15** (1985) 135.

Reactivity of Transparent Conducting ITO Film on Exposing to NO Gas

Hao Gong[*,1], Jianqiao Hu[2] and Furong Zhu[3]

[1] Department of Materials Science & Engineering, National University of Singapore
[2] Department of Physics, Faculty of Science, Yunnan University, China
[3] Department of Physics, Hong Kong Baptist University, Hong Kong
[*]Presenter

Transparent conducting oxide films are electrically conducting and visible light transparent. Such films have a wide range of applications in display panels, solar cell, touch screens etc.[1] Among various transparent conducting films, indium zinc oxide (ITO) is probably the most widely used. In this presentation, we will demonstrate that some ITO films can react with nitric oxide gas even at room temperature.

The sheet resistance of fresh ITO film on insulating glass was measured using a four-point probe placed in the glove box. The four-point probe measurements showed that NO adsorption induced an increase in ITO sheet resistance at room temperature as seen in Table 1. It was proposed that a low conductivity layer was formed near the ITO surface region, and this was NO induced. The increase in the sheet resistance can be associated with adsorbed NO species on the ITO surface. Figure 1 shows that the frequency changes for a ITO coated quartz crystal microbalance after exposing to NO gas at room temperature, and the frequency change rate Δf increases with NO gas concentration.

In order to explore the interaction between the ITO surface and NO, various characterizations were carried out and the results are discussed.

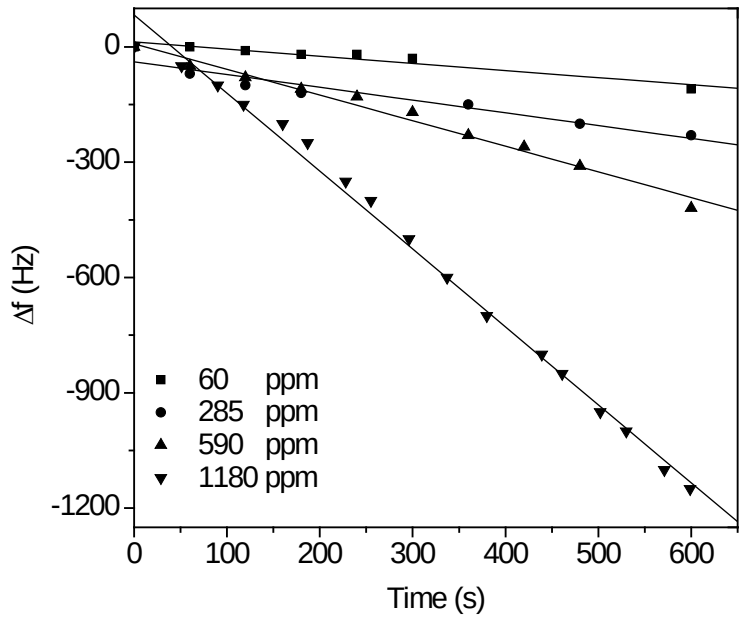

Figure 1. Time-dependent frequency change of ITO coated on QCM, after exposing to difference concentrations of NO gas.

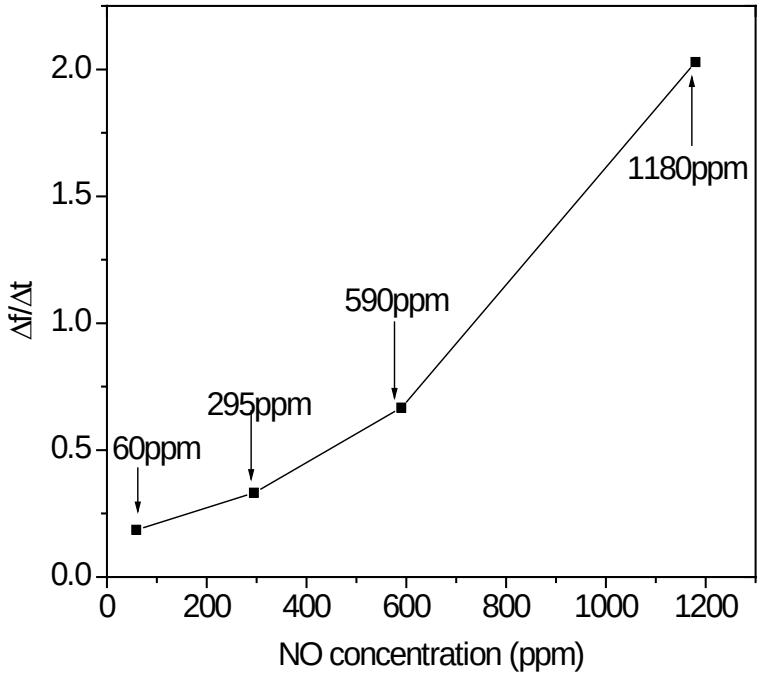

Figure 2. Frequency change rate Δf/Δt as a function of NO concentration

Table 1. NO-induced resistance increase Δ*R* of the ITO films exposed at different NO partial pressures.

Sample	NO partial pressure (Pa)	Δ*R* (Ω/sq)
1	0	0
2	0.42	42
3	0.79	44

References:

1. Chen, Z.X.; Li, W.; Li, R.; Zhang, Y.; Xu, G.; Cheng, H.S. Langmuir **2013**, 29 (45), 13836.

Non-classical mechanism of crystal growth by agglomeration of the nanoparticles

P.P. Fedorov,[a] V.V. Osiko,[a] S.V. Kuznetsov,[a] V.K. Ivanov,[b] A.E. Baranchikov[b]

[a] Prokhorov General Physics Institute of Russian Academy of Sciences, Moscwo, Russia;
[b] Kurnakov Institute of General and inorganic chemistry of Russian Academy of Sciences, Moscwo, Russia.
ppfedorov@yandex.ru

Classic theory of crystal growth states that all crystals grow by adding new building units (i.e., atoms, ions, molecules or their complexes) to their surfaces from solution, melt, vapor or another solid phase [1]. However, there is another theory of the alternative mechanism of the crystal growth – micro-block mechanism – that suggests that the crystal growth occurs by the intergrowth of the independently grown smaller crystals that made a contact in the course of their size increase. The latter approach, initially developed by P. Goubert as early as in the 19-th century, was actively pursued and developed by E.S. Fedorov, A. Traube, M.P. Shaskolskaya, A.V. Schubnikov, N.N. Sheftal, D. Balarev, N. Uyeda [2], N.P. Yushkin [3], R.A. Buyanov, O.P. Krivoruchko [4], A.M. Askhabov, I.V. Melikhov and other. Recently, the aforementioned micro-block mechanism has been rebranded and reappeared in the literature under the name of "oriented attachment growth", especially in the publications of scanning (SEM) and transmission (TEM) electron microscopy studies as well as other advanced experimental methods (e.g., [5-7]).

In our presentation, we would like to report our novel results related to the formation of nanopowders in the course of their co-precipitation from aqueous solutions. Our data confirm the aforementioned micro-block mechanism of crystal growth for the obtained fluoride nanopowders [8-11].

Specifically, we would like to emphasize the following highlights of the observed processes:

1. The formed primary particles are not X-ray amorphous, they are nanocrystals.
2. The primary nanoparticles participating in the oriented attachment growth possess smooth morphology instead of clearly shaped facets.
3. Nanoparticles can mutually orient each other in colloid solutions as well as in solid-state phases.
4. Describing the dynamics of the nanoparticle formation, one may name the above force as "orientation ordering force" for convenience.
5. Crystallization has a step-wise hierarchical nature with the periods of rapid nanoparticle growth changing to the relaxation periods; the latter periods include processes of imperfection decrease and stress elimination**.**
6. The above transformations occur at temperatures much lower than the melting temperatures (i. e., the so-called Tammann temperatures $T < 0.6*T_{melt}$).
7. In aqueous media, the aforementioned processes are typical for the crystal growth of low solubility phases, precipitated by the chemical reactions.
8. Primary merging of nanoparticles in the course of oriented attachment crystallization allows the formed crystalline particles to exceed the critical nucleation seed size and, therefore, can be one of several possible nucleation mechanisms. Crystallographically imprecise merging of the nanoparticles introduces a dislocation in the formed single crystal, which, in turn, opens the way for the classical Burton-Cabrera-Frank crystal

growth mechanism. The latter means that the crystal growth occurs via spiral dislocations. These dislocations generate growth steps, which, in turn, spread because of the diffusion of atoms.

References:

[1] L.N. Rashkovich, J.J. De Yoreo, C.A. Orme, and A.A.Chernov. *Crystallography Reports*, **51** (6) (2006) 1063.
[2] N. Uyeda, M. Nishino, E. Suito. *J. Coll. Int. Sci*., **43** (1973) 264.
[3] N.P. Yushkin. Theory of micro-block crystal growth in natural heterogeneous solutions. *Syktyvkar*, 1971 (in Russian).
[4] R.A. Buyanov, O.P.Krivoruchko, *React. Kinet. Catal. Lett*., **35** (1987) 293.
[5] [8] R.L. Penn, J.F. Banfield, *Science,* **281** (1998) 969.
[6] H. Colfen, M. Antonietti. Mesocrystals and nonclassical crystallization. John Wiley & Sons Ltd. 2008. 276 p.
[7] V.K. Ivanov, P.P. Fedorov, A.E. Baranchikov, V.V. Osiko. *Russian Chemical Review* (2014 in press).
[8] P.P. Fedorov, A.A. Luginina, S.V. Kuznetsov, and V.V. Osiko. *J. Fluorine Chemistry.* **132** (2011) 1012.
[9] P.P. Fedorov, M.N. Mayakova, S.V. Kuznetsov, V.V. Voronov, V.V. Osiko, R.P. Ermakov, I.V. Gontar, A.A. Timofeev, and L.D. Iskhakova. *Nanotechnologies in Russia*. **6** (2011) 203.
[10] P.P. Fedorov, V.K. Ivanov. *Doklady Physics*. **56** (2011) 205.
[11] P.P. Fedorov, V.V. Osiko, S.V. Kuznetsov, et. al. *J.Crystal Growth* (2014 in press), DOI: 10.1016/j.jcrysgro.2013.12.069

Figure:

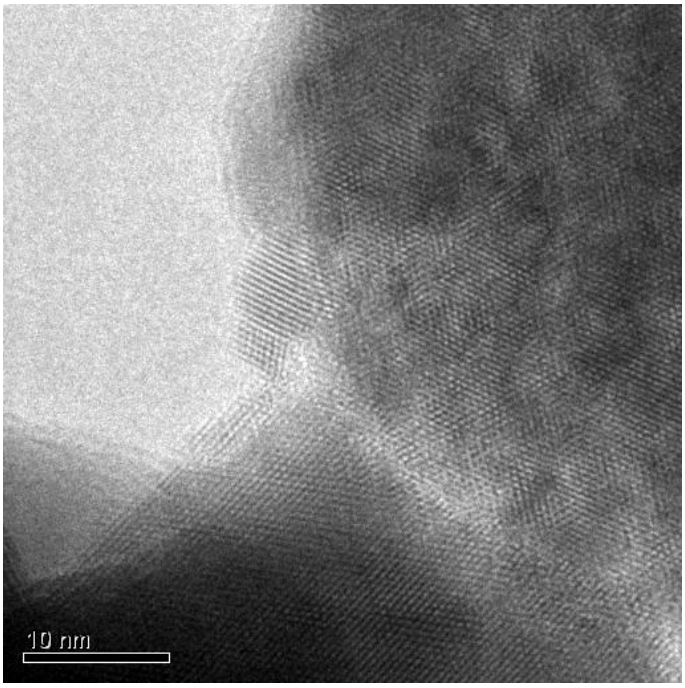

Fig. 1. TEM image of $Ba_4Bi_3F_{17}$ powder [11].

Cathode materials for H-SOFC: proton uptake, bulk transport and oxygen surface exchange kinetics

D. Poetzsch, R. Merkle, J. Maier

MPI for Solid State Research, Stuttgart, Germany

The use of proton conducting oxides (e.g. Y-doped $BaZrO_3$) with high ionic conductivity in the range of 300-600 °C as electrolytes offers a chance to lower the operating temperature of solid oxide fuel cells (H-SOFC). The change from oxide ion conductors to proton conducting electrolytes requires an optimization of the catalytically active material at the cathode. In H-SOFC oxygen is reduced to water at the cathode, which, in contrast to oxide ion electrolytes, does not necessarily require incorporation of the oxygen into the catalyst material (or finally at least into the electrolyte). On the other hand, a mixed proton / electron hole conductivity of the cathode would be very beneficial in order to allow for oxygen reduction to extend beyond the triple phase boundary and to occur on the whole surface ("bulk path").

This motivated us to investigate the thermodynamics and kinetics of proton incorporation into redox-active perovskites. In presence of three carriers (protons, oxygen vacancies, holes) proton uptake can occur by hydration of oxygen vacancies (acid-base reaction) as well as including a valence change of transition metal ions (redox reaction). This can lead to complex diffusion kinetics (two-fold relaxation [1]), which is analyzed in detail by numerical simulations [2].

For $Ba_{0.5}Sr_{0.5}Fe_{0.8}Zn_{0.2}O_{3-d}$ (BSFZ) ceramics lower bounds for proton concentration and mobility are extracted from thermogravimetry transients [3]. Comparing this lower bound for the proton conductivity with the ionic conductivity of $(La,Sr)MnO_3$ films on YSZ indicates that the bulk path for oxygen reduction is possible on BSFZ cathodes. Impedance spectroscopy on dense thin-film microelectrodes on $Ba(Zr,Y)O_{3-d}$ electrolytes shows that the resistance related to the oxygen reduction scales inversely proportional to the electrode area, supporting that the reduction proceeds by the "bulk path" on the whole BSFZ/gas surface. For these measurements, one has to properly account for the non-negligible hole conductivity of $Ba(Zr,Ce,Y)O_{3-d}$ in high pO_2 [4].

[1] J.H. Yu, J.S. Lee, J. Maier, Angew. Chem. Int .Ed. 46 (2007) 8992
[2] R. Merkle, D. Poetzsch, J. Maier, in preparation
[3] D. Poetzsch, R. Merkle, J. Maier, in revision
[4] D. Poetzsch, R. Merkle, J. Maier, J. Power Sources 242 (2013) 784

Carbon dioxide (CO_2) reactivity on lithium and sodium ceramics. A high temperature CO_2 capture option

Heriberto Pfeiffer[a]

[a]Instituto de Investigaciones en Materiales, Universidad Nacional Autónoma de México, Circuito exterior s/n, Cd. Universitaria, Del. Coyoacán, México DF, CP 04510, MEXICO.
E-mail: pfeiffer@iim.unam.mx

The anthropogenic amounts of carbon dioxide (CO_2) in the atmosphere have been raised dramatically, mainly due to the combustion of different carbonaceous materials used in energy production, transport and other important industries such as cement production, iron and steelmaking. To solve or mitigate, at least, this environmental problem, several alternatives have been proposed. A promising alternative for reducing the CO_2 emissions is to capture and concentrate the gas and its subsequent chemical transformation.

Different materials have been proposed as potential CO_2 captors. Among these materials, different lithium and sodium ceramics have been proposed as possible high temperature CO_2 captors. Some of the alkaline ceramics most studied are the lithium and sodium silicates (Li_4SiO_4, Li_8SiO_6, Li_2SiO_3 and Na_2SiO_3), lithium aluminate (Li_5AlO_4) lithium and sodium zirconates (Li_2ZrO_3 and Na_2ZrO_3) and lithium cuprate (Li_2CuO_2), among others. All these ceramics have been tested, producing interesting results at different temperature ranges between 30 and 700 °C.

In this kind of ceramics CO_2 capture is produced throughout a chemisorption process. Initially, the alkaline ceramic particles react with CO_2 at the surface. The superficial reaction implies the formation of an external shell of Li_2CO_3 or Na_2ZrO_3 and secondary phases. Once the external shell is produced, the reaction mechanism is controlled by different diffusion processes. Therefore, the correct understanding of all these phenomena is a very important step during the selection of the ideal CO_2 capture conditions. In other words, the selection of materials, temperature range, gas and/or vapor concentrations, flows, etc. Then, the aim of this work is to present different experiments related to the CO_2 reactivity, chemisorption, on lithium and sodium ceramics and to propose how different factors control this process. The work will be focused on diffusion controlled CO_2 chemisorption, which has been shown to be the limiting step of the CO_2 chemisorption process. Diffusion controlled CO_2 chemisorption appears to be mainly influenced by the chemical composition of a product's external shell.

References:

[1] J. Ortiz-Landeros, T. Ávalos-Rendón, C. Gómez-Yáñez, H. Pfeiffer, *J. Therm. Anal. Calorim.*, **108** (2012) 647.
[2] S. Choi, J. H. Drese, C. W. Jones, *ChemSusChem*, **2** (2009) 796.
[3] H. Pfeiffer, Advances in CO_2 Conversion and Utilization, Chapter 15, ACS ed., 1056 (2010) 233.
[4] H. A. Mosqueda-Altamirano, C. Vazquez, P. Bosch, H. Pfeiffer, *Chem. Mater.*, **18** (2006) 2307.
[5] K. Nakagawa, T. Ohashi, *J. Electrochem. Soc.*, **145** (1998) 1344.
[6] B. N. Nair, R. P. Burwood, V. J. Goh, K. Nakagawa, T. Yamaguchi, *Prog. Mater. Sci.*, **54** (2009) 511.

Reformulation of Charge Carriers Fluxes and Material Balance Equations for Polaron-Conducting Polymer Films

V.V. Malev [a, b]

[a] Department of Chemistry, St. Petersburg State University, St. Petersburg, Russian Federation
[b] Institute of Cytology, Russian Academy of Sciences, St. Petersburg, Russian Federation
e-mail address: valerymalev@gmail.com

Electroactive polymer films formed by compounds of different nature are materials of a great interest owing to a wide spectrum of their applications. A sufficient understanding of charge transfer mechanisms that take place in such objects is obviously desirable to design concrete devices. Meanwhile, a use of the representations elaborated earlier for redox-polymers, as a rule, leads only to a qualitative agreement between theoretical and experimental results in case of polaron-conducting films. The accepted treatment of the polaron conductance is in essence the same, as that used for redox polymers with the only premise that a polaron quasi-particle includes three-five monomer units in contrast to one unit assumed for any charged or neutral fragment of redox polymers. As pointed out in [1, 2], the similar treatment creates some problems especially in the case of non-stationary conditions of charging/discharge of polaron conducting films.

The main feature of the proposed approach is a polaron flux reformulation, which assumes a polaron translocation length to be of a one monomer size independently of the number of monomer fragments included into polaron quasi-particles. As a result, material balance equations of polaron-conducting films take a more complicated form than that accepted in the existing theory of redox-conducting polymers. It is shown that, at equilibrium conditions, the obtained equations, as it must be, lead to the relationships being in accordance with thermodynamic ones. At the same time, a proper analysis reveals some difference between quantitative results that follow from the proposed and traditional approaches. Although the derived equations are valid for a special system modeling a polaron-conducting film, the possibility of their generalization does not provoke any doubt.

Financial support of the Russian Foundation for Basic Research (grant # 12-03-00560) and the St. Petersburg State University (grant # 12.38.77.2012) is gratefully acknowledged. The work was also supported with program “Molecular Biology” of the Russian Academy of Sciences.

References

[1] V.V. Malev, O.A. Levin, A.M. Timonov, *Electrochimica Acta*, 108 (2013) 313
[2] V.V. Malev, O.A. Levin, V.V. Kondratiev, *Electrochimica Acta*, In Press, doi.org/10.1016/j.electacta.2013.09.158 (2014)

Electrodeposition of CIGS thin films from an ionic liquid BMIM-OTF

Maozhong An, Jie Zhang, Shanshan Ji, Ye Lian, Peixia Yang, and Jinqiu Zhang

State Key Laboratory of Urban Water Resource and Environment, School of Chemical Engineering and Technology, Harbin Institute of Technology, Harbin 150001, China

An ionic liquid 1-butyl-3-methylimidazolium trifluoromethanesulfonate (BMIM-OTF) was employed to electrodeposit copper indium gallium diselenide (CIGS) thin films, which are among the most promising materials for thin film solar cell[1]. Compact, dense and relatively smooth CIGS films, whose composition could be controlled, were obtained by one-pot electrodeposition.

Potentiostatic method was used to electrodeposit CIGS films on a nickel substrate from ionic liquid electrolytes with $CuCl_2$, $InCl_3$, $GaCl_3$, and $SeCl_4$ as main salts and BMIM-OTF as the solvent. Inductively coupled plasma-optical emission spectroscopy (ICP-OES) and scanning electron microscopy (SEM) were used to analyze atomic composition and observe the morphology of the films, respectively. The influences of the potential, time and temperature on composition and morphology of films were investigated. The growth mechanism and the photovoltaic features of the films are being studied.

The atomic composition of CIGS films as a function of deposition potential is given in Fig. 1. With the decrement of deposition potential from -1.4 to -2.0 V, the content of selenium decreased and that of indium increased drastically. And the amount of copper in the film had a little decrement. The deposition potential had no significantly effect on the level of gallium. These results can be explained from their electrodeposition potentials in aqueous electrolyte: +0.75 V vs NHE for selenium, +0.34 V for copper, -0.34 V for indium, and -0.53 V for gallium[2]. As selenium and copper can be electrodeposited at very positive potential, the films obtained at -1.4 V was selenium-rich. More indium could be deposited at relative negative potential, and at the same time the content of selenium was reduced. Gallium is very difficult to be deposited even at -2.2 V. So its content was very low and rarely changed with potential changes. Therefore, the composition of the films electrodeposited from this ionic liquid electrolyte could be controlled by electrodeposition potential. In addition, the deposition time and temperature also had a big effect on the film composition.

The SEM images of CIGS obtained at various deposition potential is shown in Fig. 2. Porous thin films with clusters were obtained at the investigated range of potential from -1.4 to -2.2 V. The cracks diminished and clusters became jointed together when the potential decreased to -2.0 V. With further decreasing the deposition potential, the thin film became compact and uniform. A lot of flake-like deposits, which was accordance with the copper selenides phase[3], could be observed on the films obtained at -2.0 V. The ionic liquid would decomposes when the deposition potential was more negative than -2.2 V. Therefore, the deposition potential for constant potential deposition should not exceed -2.2 V.

The authors are grateful for financial support from the National Science Foundation of Heilongjiang Province in China (No. ZD201107).

References:
[1] V.S. Saji, I.H. Choi, C.W. Lee, Sol Energy 85/11 (2011) 2666.
[2] D. Lincot, J.F. Guillemoles, S. Taunier, D. Guimard, J. Sicx-Kurdi, A. Chaumont, O. Roussel, O. Ramdani, C. Hubert, J.P. Fauvarque, N. Bodereau, L. Parissi, P. Panheleux, P. Fanouillere, N. Naghavi, P.P. Grand, M. Benfarah, P. Mogensen, O. Kerrec, Sol Energy 77/6 (2004) 725.
[3] J. Kois, S. Bereznev, E. Mellikov, A. Öpik, Thin Solid Films 511–512/0 (2006) 420.

Figures:

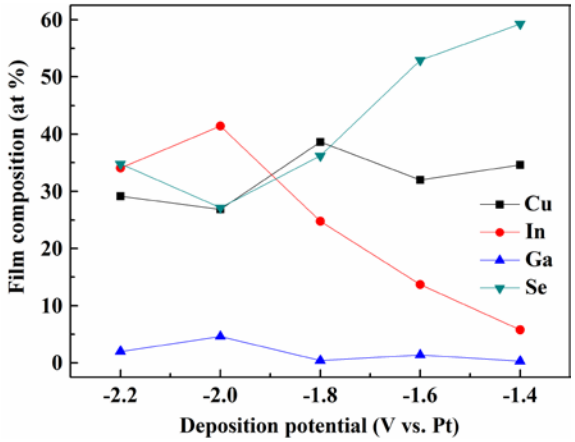

Fig. 1. Film composition of CIGS thin films deposited as a function of deposition potential

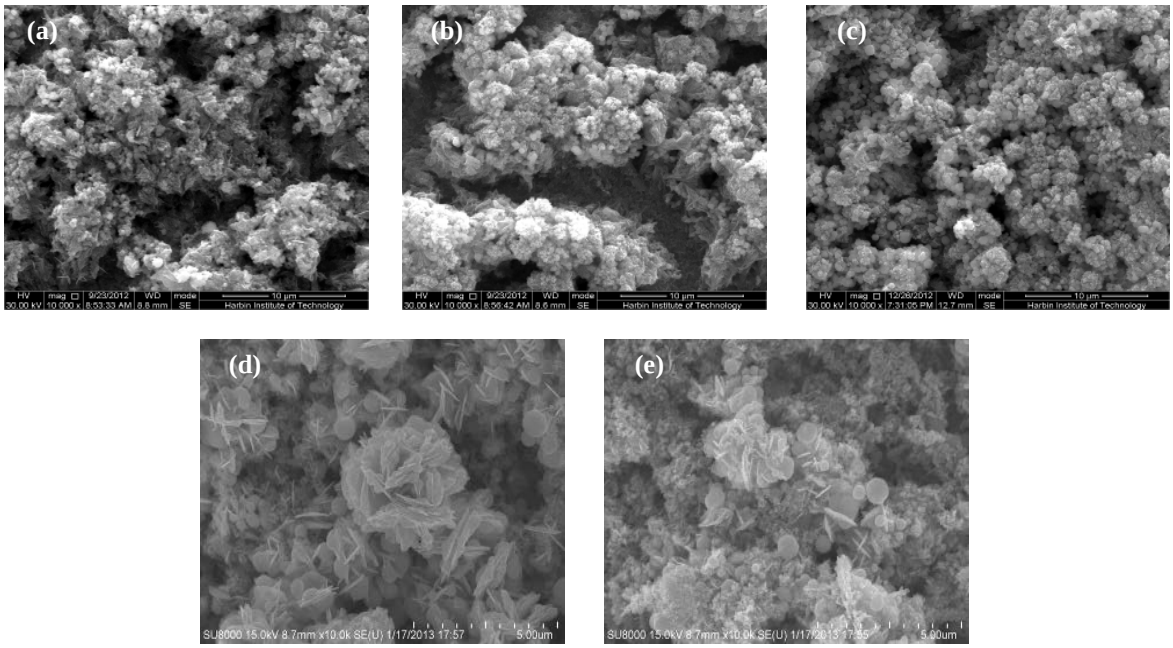

Fig. 2. Morphology of CIGS films deposited at various deposition potentials: (a) -1.4 V, (b) -1.6 V, (c) -1.8 V, (d) -2.0 V, and (e) -2.2 V.

Poster Presentations

Long-Range Chemical Interactions in Solid-State Reactions: Effect of an Inert Ag Interlayer on the Formation of $L1_0$-FePd in Epitaxial Pd(001)/Ag(001)/Fe(001) and Fe(001)/Ag(001)/Pd(001) Trilayers

V. G Myagkov [a], L. E. Bykova [a], V. S Zhigalov [a], G. N. Bondarenko [b]

[a] Kirensky Institute of Physics, Russian Academy of Sciences, Siberian Branch, Krasnoyarsk, 660036 Russia
[b] Institute of Chemistry and Chemical Technology, Russian Academy of Sciences, Siberian Branch, Krasnoyarsk, 660049 Russia

Diffusion is one of the unique phenomena that control major natural processes. It is a basic contributor to chemical reactions and structural transformations in solids.[1,2] Solid-state reactions, including those occurring in thin films and multilayers, comprise three successive stages: (1) breakage of reagent chemical bonds, (2) diffusion transfer of reagent atoms via a reaction product, and (3) rearrangement and formation of new bonds. The reaction rate is determined by step 2, which is the primary stage. Traditionally, solid-state diffusion of reacting atoms via a layer of a reaction product is considered to occur through an atomic exchange with nearest neighbors that leads to their random walk over a crystal lattice. The mean distance d that an atom moves over time t equals the mean-square atomic displacement $\langle \Delta x^2 \rangle$ and satisfies the Einstein equation $d = \langle \Delta x^2 \rangle = 2Dt$. In numerous studies on solid-state reactions in thin films and multilayers, the parabolic growth of the reaction layer thickness d which satisfies the Einstein equation is presented as experimental proof of the diffusive nature of the reaction.

However, the nature of atomic migration during the low-temperature solid-state reactions in bilayers and multilayers is as yet unclear. To a large extent, this effect is inconsistent with the diffusion mechanism. The major inconsistencies are the following:

1) The threshold character of a thin-film solid-state reaction. According to calorimetric and resistance measurements, intense mixing on the interface begins after the initiation temperature T_0 is exceeded. Meanwhile, the diffusion scenario suggests that the solid-state reactions on the interface between reagents should occur at any temperature, and that the reaction layer thickness depends only on the temperature and annealing time.
2) In the diffusion reaction mechanism, the break of a chemical bond in the film reagents comprising the bilayers at $T > T_0$ (stage 1) is not related to the further interdiffusion of atoms via a reaction layer (stage 2). However, the layers of the same film reagents separated by a certain distance do not exhibit a break in the atoms' chemical bond or their diffusion from the surface. In other words, the breakage of chemical bonds and mutual atomic migration only occur when reacting layers are included in the bilayers and multilayers and the temperature exceeds the initiation temperature ($T > T_0$).
3) Ultrafast atomic transport occurs at the initiation of solid-state reactions in Co/Si [3] and Mo/Si [4] multilayer thin films by femtosecond laser irradiation. In Co/Si and

Mo/Si samples, mixing of the layers with thicknesses of ~10 nm occurs for an irradiation time of 150 fs. This corresponds to diffusivity D ~ (10^{-10}–10^{-8}) m^2/s, which is unrealistic for solid state diffusion.

We investigated the effect of a chemically inert Ag buffer layer on the solid–state reaction between epitaxial Pd(001) and Fe(001) films. To suppress the reaction, we chose two thicknesses of the chemically inert Ag film: 0.5 and 1 μm. For comparison, we used samples without a buffer layer in the experiments. At an annealing temperature of 400°C, in all samples the ordered L10–FePd(001) phase was the first to form. Regardless of the buffer layer thickness, above 500°C the disordered FexPd1–x(001) phase begins to form and becomes the only phase at annealing temperatures above 600°C. The absence of mixing on the Ag/Pd and Ag/Fe interfaces and the fast migration of Pd atoms via a thick inert Ag buffer in the Fe film in the Pd/Ag/Fe trilayers prove the occurrence of long-range chemical interactions (LRCIs) between Pd and Fe during the solid-state reaction. Our study takes an unprecedented look at the common nature of the long-range chemical interactions and chemical bonds.

The literature review shows that long-range atomic transfer via inert buffer layers has also been observed for the mass transport of Au and Pb atoms through an Ag(300nm) interlayer [5], outdiffusion of Au through Pt(1μm) [6], outdiffusion of Si through Au(230nm) [7], and diffusion of Fe, Ni, and Co through an Au(300nm) film [8].

It is well known that all fundamental interactions in solids are described by short-range potentials. However, the nature of the chemical bonds which underlie these interactions remains a subject for discussion [9–13]. We believe that the chemical interaction between reacting atoms is not limited by a chemical bond length. The long-range chemical interaction between reacting atoms is a fundamental characteristic of the initial stage of chemical reactions that precede the formation of a stable chemical bond.

Although the long-range chemical interactions (LRCIs) originate from the study of solid–state reactions, they undoubtedly underlie any chemical reaction. We believe that the LRCIs broaden one's outlook regarding the nature of the chemical bonds and demonstrate that the notion of the chemical bond is many–sided and more completed than what is typically presented in science. The discovered feature of a chemical bond-the long-range character of chemical interactions-should underlie the formation of supramolecular structures, self-assembly mechanisms, self-organization phenomena, and the construction of a great number of biological objects.

References:

[1] A. Van der Ven, H. -C. Yu, G. Ceder, and K. Thornton, Prog. Mater. Sci. 55 (2010) 61.
[2] P. Heitjans and J. Kärger, Diffusion in Condensed Matter:Methods, Materials, Models (Springer, Berlin, Heidelberg, 2005).
[3] Y. N. Picard and S. M. Yalisove, Appl. Phys. Lett. 92 (2008) 014102.
[4] T. Höche, D. Ruthe and T. Petsch, Appl. Phys. A: Mater. Sci. Process. 79 (2004) 961.
[5] K. N. Tu, J. Appl. Phys. 43 (1972)1303.
[6] C. C. Chang, and G. Quintana, Appl. Phys. Lett. 29 (1976) 453.
[7] C. -A. Chang, and G. Ottaviani, Appl. Phys. Lett. 44 (1984) 901.
[8] W. E. Swartz, Jr., J. H. Linn, J. M. Ammons, and M.G. Kovac, Thin solid films 114 (1984) 349.
[9] F. J. DiSalvo, Science 247 (1990) 649.
[10] L. Pauling, J. Chem. Educ., 69 (1992) 519.
[11] 90 Years of Chemical Bonding (Special Issue), J. Comput. Chem. 28 (1) (2007).
[12] F. Weinhold, and C. R. Landis, Science 316 (2007) 61.
[13] H. S. Rzepa, Nature Chem. 1 (2009) 510.

Influence of the pressure and temperature on the LDH structural evolution and its effect onto the CO_2 sorption capacity

M. J. Ramírez-Moreno [a,b], I. C. Romero-Ibarra [a], M. A. Hernández-Pérez [b], H. Pfeiffer [a]

[a] Instituto de Investigaciones en Materiales, Universidad Nacional Autónoma de México, Circuito exterior s/n, Ciudad Universitaria, CP 04510, Del. Coyoacán, México D.F., Mexico.
[b] Departamento de Ingeniería en Metalurgia y Materiales, ESIQIE, Instituto Politécnico Nacional, UPALM, Av. Instituto Politécnico Nacional s/n, CP 07738, México D.F., Mexico.
E-mail address: ramm321@hotmail.com

The 90% of the world energy necessity has been supplied by the use of fossil fuels. The use of these fuels has contributed to increase the atmospheric CO_2 concentration up to 380 ppm, causing an increase of 0.7 °C in the temperature at the earth's surface [1]. Unfortunately, if the CO_2 emissions rate remains constant, it is expected that by 2050 the concentration of this gas in the atmosphere reaches 550 ppm [2] producing an increase up to 5 °C in the temperature at surface [1]. In order to reduce the amount of anthropogenic CO_2 and its effects, several materials have been used as CO_2 captors [3-6].

In this work, a layered double hydroxide (LDH) with Mg/Al ratio equal to 3 was prepared by the coprecipitation method. The sorption capacity of the materials was studied at high pressures, up to 4.35 MPa. LDH sample was tested as a layered structure, but as well as a mixed oxide (calcined-LDH) and as a K-impregnated mixed oxide. All materials were characterized before and after their CO_2 capture evaluation at higher pressure by XRD, FTIR, SEM and N_2 adsorption, to determine the structural and microstructural changes due to the CO_2 atmosphere, temperature and pressure.

The materials were evaluated in CO_2 atmosphere at temperatures in the range of 30 to 350 °C, with a pressure from ~ 6 to 4350 kPa. At atmospheric pressure, the CO_2 capture was similar to reported in other studies (< 1 mmol/g), independently of the temperature [3,7, 8]. Nevertheless, the final CO_2 trapped at high pressures were considerably higher than those typically obtained at atmospheric pressure, reaching up to 5.7, 10 and 5 mmol/g to LDH, calcined-LDH and K-impregnated calcined-LDH samples, respectively. The results showed that the increase in the surface area positively affects the sorption capacity of the materials and there is an optimal sorption temperature witch depends of the material. Finally, it was observed that the pressure and CO_2 atmosphere diminish the temperature in witch commonly occurs the LDH structure evolution to its mixed oxide and $MgAl_2O_4$ spinel. The next figure summarizes the LDH TG structural evolution [9, 10], the maximum CO_2 adsorption observed at high pressure and how the crystalline structure evolved as a function of pressure and temperature.

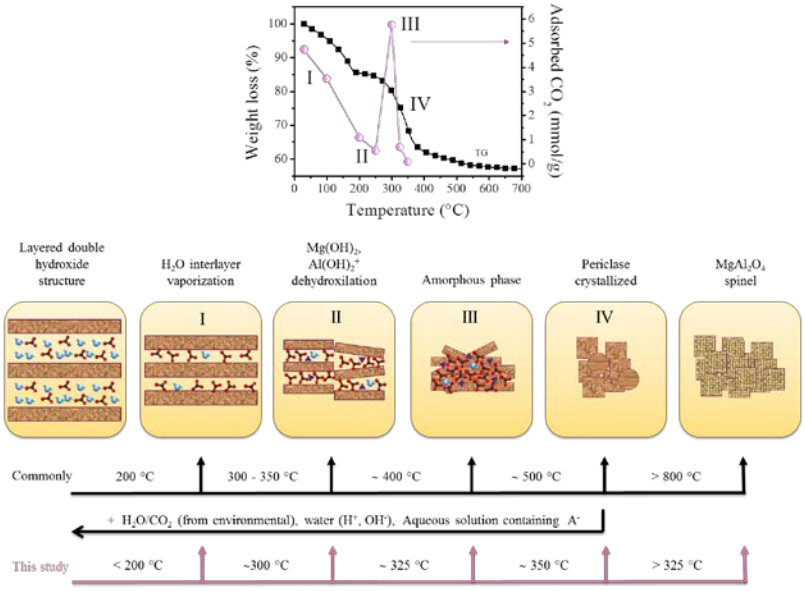

References:

[1] J. Srinivasan, *Resonance*, (2008), 1146.
[2] Q. Wang, et al, *Energy Environ. Sci.*, **4** (2011), 42.
[3] S. Choi, et al, *ChemSusChem*, **2** (2009), 796.
[4] M. Wang, et al, *Chem. Eng. Res. Des.*, **89** (2011), 1609.
[5] S. Loganathan, et al, *Langmuir*, **29** (2013), 3491-3499.
[6] S. Garcia, et al, *Langmuir*, **29** (2013), 6042.
[7] Y.Ding and E.Alpay, *Chem. Eng. Sci.*, **55** (2000), 3461.
[8] E. Oliveira, et al, *Sep. Purif. Technol.*, **62** (2008), 137.
[9] M. Bellotto, et al, *J. Phys. Chem.*, **100** (1996), 8535.
[10] W. Yang, et al, *Chemical Engineering Science*, **27** (2002), 2945.

Production of biodiesel and value-added products from glycerol using sodium zirconate

Issis C. Romero-Ibarra, Nicolás Santiago-Torres, Heriberto Pfeiffer.

Instituto de Investigaciones en Materiales, Universidad Nacional Autónoma de México.
Ciudad Universitaria s/n Coyoacán 04510, México D. F., México.
e-mail:issis@unam.mx

The alarming trends in energy demand and the finite nature of fossil fuel reserves have motivated the search for energy sources more sustainable. In this regard, biodiesel can provide a significant contribution in the energy independence. Biodiesel is a sustainable, renewable, non-toxic, biodegradable diesel fuel substitute that can be employed in current diesel infrastructure without major modification to the engines, offering an interesting alternative to petroleum-based diesel [1-3]. The combustion of biodiesel can decrease carbon monoxide (CO) emissions by 46.7%, particulate matter emissions by 66.7% and unburned hydrocarbons by 45.2%. The most common method for producing biodiesel is via triglyceride (TG) transesterification from vegetable oils and animal fats in the presence of short-chain alcohols and homogeneous acid or base catalysts; these yield fatty acid methyl esters (FAME) or fatty acid ethyl esters (FAEE) and glycerol (also called glycerin) as products [1-3]. Figure 1 shows the general well-known transesterification reaction with alcohols. Every triglyceride molecule reacts with 3 equivalents of alcohol to produce glycerol and three fatty acid (methyl) ester molecules. In Figure 1, R- means long-chain hydrocarbons. The alcohols (R-OH) used in the transesterification are normally methanol or ethanol, where methanol is the most common because of its low cost, low reaction temperatures, fast reaction times and higher quality methyl ester products. The reaction is facilitated with a suitable catalyst. Heterogeneous catalysts are most efficient in transesterification reaction due to many advantages such as easy catalyst separation and reusability, improved selectivity, reducing process stages, no water formation or saponification reaction, included under green technology and cost effective [2-5].

In addition, the production of biodiesel generates millions of tons of crude glycerol waste per year (generally, 10 to 20% of the total volume of biodiesel produced is made up of glycerol) and this amount is growing rapidly along with the dramatic growth of biodiesel industry. Thus, new markets or new applications of glycerol such as converting it into value-added products would have to be explored [6, 7].

In this work, sodium zirconate (Na_2ZrO_3) was synthesized via a solid-state reaction and evaluated as a potential catalytic material. The structure and microstructure of the catalyst were characterized using X-ray diffraction, scanning electron microscopy and N_2 adsorption. Then, Na_2ZrO_3 was tested as a basic catalyst for the production of biodiesel from transesterification reaction. The influence of some parameters was investigated, such as the reactant concentrations (molar ratios), catalyst percentage, reaction time, temperature and re-use of the catalyst. The maximum FAME conversion efficiency was 98.3% after 3 h of reaction time and 3wt% of catalyst [8]. The cyclic behavior revealed that the catalyst had a relatively stability. Besides, the same Na_2ZrO_3 was tested as catalyst of the by-glycerol transformation into different valued-added products. The products were characterized using

infrared spectroscopy, gas chromatography coupled to mass spectrometry and proton nuclear magnetic resonance. The use of this kind of alkaline ceramics may become a good option for the catalytic transesterification reaction with high yields. A combination of biodiesel production with subsequent glycerol conversion to value-added products by directly using the heterogeneous catalyst is a good option to reduce cost and pollution.

References:

[1] I. M. Atadashi, M. K. Aroua, A. Aziz, *Renew Energ.*, **36** (2011) 437.
[2] K. G. Georgogianni, A. K. Katsoulidis, P. J. Pomonis, G. Manos, M. G. Kontominas, *Fuel Process Technol.*, **90** (2009) 1016.
[3] L. Luque, J. C. Lovett, B. Datta, J. Clancy, J. M. Campeloa, A. Romero, *Energy Environ Sci.*, **7** (2010) 1706.
[4] J. X. Wang, K. T. Chen J. S. Wu, P. H. Wang, S. T. Huang, C. C. Chen, *Fuel Process Technol.*, **104** (2012) 167.
[5] P. Guo, C. Zheng, M. Zheng, F. Huang, W. Li, Q. Huang, *Renew Energ.*, **53** (2013) 377.
[6] Y. D. Long and Z. Fang, *Biofuels, Bioprod Bioref.*, **6** (2012) 686.
[7] Y. D. Long, F. Guo, Z. Fang, X. F. Tian, L. Q. Jiang, F. Zhang, *Bioresour. Technol.* **102** (2011) 6884.
[8] N. Santiago-Torres, I. C. Romero-Ibarra, H. Pfeiffer, *Fuel Process Technol.*, **120** (2014) 34.

Figure:

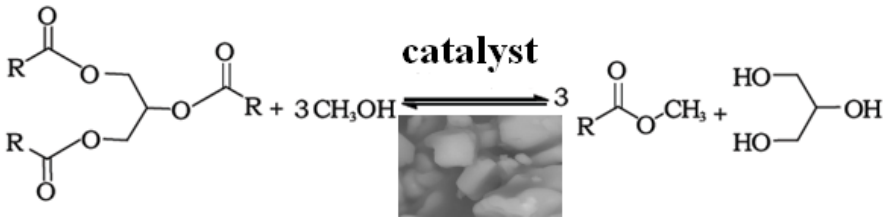

Fig. 1. General scheme of the transesterification reaction

Structural features and electron transport in $Ca_{1-x-y}Sr_xLa_yMnO_{3-\delta}$

E.I. Goldyreva,[a] V.L. Kozhevnikov,[a] I.A. Leonidov,[a] M.V. Patrakeev,[a]
V.I. Voronin,[b] I.F. Berger,[b] K.N. Mikhalev [b]

[a]Institute of Solid State Chemistry, UB RAS, Ekaterinburg, Russian Federation;
[b]Institute of Metal Physics, UB RAS, Ekaterinburg, Russian Federation.

Rare-earth and alkaline earth perovskite-like manganites exhibit properties combination favorable for applications as cathodes in SOFCs, thermoelectrics, magnetoresistive materials, etc. In this work we studied structural parameters and electron transport in the doped derivatives $Ca_{0.6-y}Sr_{0.4}La_yMnO_{3-\delta}$ of the parent manganite $CaMnO_{3-\delta}$. The specimens were obtained by high-temperature firing of glycin-nitrate precursors. The powder neutron and X-ray diffraction both show orthorhombic (s.g. *Pnma*) and tetragonal (*I4/mcm*) crystal structure for the samples $y = 0 – 0.1$ and $y \geq 0.13$, respectively. The elementary unit volume increases with lanthanum content, which is consistent with electronic charge compensation due to replacement of Mn^{4+} for larger Mn^{3+} cations. The deformations of MnO_6 octahedra are minimal in the orthorhombic structure according to neutron diffraction at 380 K. Sharp increase in the length of Mn-O1 bonds is observed in the tetragonal structure ($y = 0.15$), which results in elongation of MnO_6 octahedra along *c*-axis. The deformations of the structural octahedra tend to decrease with the increase of temperature so that a phase transition to cubic structure occurs at 770 K. The electrical conductivity in $Ca_{0.6-y}Sr_{0.4}La_yMnO_{3-\delta}$ is thermally activated. The negative sign of thermopower is indicative of n-type predominant charge carriers. The smallest apparent activation energy 0.03 eV for conductivity is observed in the cubic phase with regular MnO_6 octahedra, and it slightly increases to about 0.05 eV when small deformations of the octahedra occur at transitions to orthorhombic and tetragonal structures at $T \sim 300$ and 500 K, respectively. The impact of the geometry of MnO_6 octahedra upon electron transport is clearly seen in the tetragonal phase $y \geq 0.13$ below 400 K, where deformations of the structural octahedra result in a sharp increase of the activation energy to about 0.16 eV and large negative thermopower. The magnetic susceptibility measurements suggest that the large distortions of the manganese-oxygen octahedra favor formation of the local antiferromagnetic clusters, which serve as traps for mobile electrons.

$Pt/Ga_2O_3–SiO_2$ nanoparticles for efficient visible-light photocatalysis

E.S. Baeissa[a], R.M. Mohamed[a,b]

[a] Chemistry Department, Faculty of Science, King Abdulaziz University, P.O. Box 80203, Jeddah 21589, Saudi Arabia
[b] Advanced Materials Department, Central Metallurgical R&D Institute, CMRDI, P.O. Box 87, Helwan, Cairo, Egypt

$Ga_2O_3–SiO_2$ nanoparticles were prepared via a sol–gel method, and Pt was immobilized on the surface of $Ga_2O_3–SiO_2$ via a photo-assisted deposition (PAD) method. The catalytic performance of the samples was evaluated for the photocatalytic oxidation of cyanide using visible light. XRD and EDX results show that Pt is well dispersed within $Ga_2O_3–SiO_2$. The BET results reveal that the surface area of $Ga_2O_3–SiO_2$ is higher than that of the $Pt/Ga_2O_3–SiO_2$ samples. 0.3 wt % $Pt/Ga_2O_3–SiO_2$ has the highest photocatalytic activity for the degradation of cyanide. The catalyst can be reused with no loss in activity during the first 10cycles.

Phase equilibria in the Y – Ba – Fe – O system and physicochemical properties of $BaFe_{0.9-x}Y_{0.1}Co_xO_{3-\delta}$

A.S. Urusova, A.V. Bruzgina, T.V. Aksenova, V.A. Cherepanov

Department of Chemistry, Institute of Natural Sciences, Ural Federal University, Yekaterinburg, Russia

The phase equilibria in the Y – Ba – Fe – O system were systematically studied at 1373 K in air. The intermediate phases formed in the Y – Ba – Fe – O system at 1373 K in air were: $YBa_3Fe_2O_{8-\delta}$ and $BaFe_{1-y}Y_yO_{3-\delta}$ [1]. It was shown that $YBa_3Fe_2O_{8-\delta}$ possesses orthorhombic unit cell (sp.gr. Pmmm). Homogeneity range for the $BaFe_{1-y}Y_yO_{3-\delta}$ solid solution at studied conditions appears within $0.75<y<0.125$. Intensity of impurity phases in boundary regions is at most 3 %. The projection of isothermal-isobaric phase diagram for the Y – Ba – Fe – O system to the compositional triangle of metallic components was presented.

According to the results of XRD the intermediate phases formed in studied system at 1373 K in air were: $YBa_3Fe_2O_{8-\delta}$ and $BaFe_{1-y}Y_yO_{3-\delta}$ ($0.75<y<0.125$) solid solution. $YBa_3Fe_2O_{8-\delta}$ possesses orthorhombic unit cell (sp.gr. Pmmm). According to the results of X-ray diffraction the homogeneity range for the $BaFe_{1-y}Y_yO_{3-\delta\delta}$ solid solution at studied conditions appears within $0.75<y<0.125$. Intensity of impurity phases in boundary regions is at most 3 %. High-temperature X-ray diffraction analyses of the $BaFeO_{3-\delta}$ in the temperature range from 298 K up to 1273 K under Po2 = 0.21 atm was founded to demonstrate at temperature below 673 K exist single phase $BaFeO_{3-\delta}$ with orthorhombic structure (sp. gr. P21 21 2), at temperature above 1273 K – cubic structure (sp. gr. Pm3m), mixture among two phases was obtained in the temperature range 673–1273 K, which correlate with data obtained by TGA and dilatometry methods. The substitution of yttrium for iron in $BaFe_{1-y}Y_yO_{3-\delta}$ ($0.75<y<0.125$) oxides leads to form cubic structure stable in air at all studied temperatures.

Polycrystalline $BaFe_{0.9-x}Y_{0.1}Me_xO_{3-\delta}$ (Me=Co, Ni, Cu) with $0.0\leq x\leq 0.2$ samples were synthesized by a conventional route and glycerol–nitrate technique. According XRD patterns of single phase solid solutions $BaFe_{0.9-x}Y_{0.1}Co_xO_{3-\delta}$ ($0.0\leq x\leq 0.15$) were indexed using Pm3m space group (Figure). The unit cell parameters were refined using Rietveld full-profile analysis. The substitution of cobalt for iron leads to the monotonous decrease of the unit cell parameters and the unit cell volume result in decrease bond length B-O, since the ionic radii of cobalt ($r_{Co^{3+}/Co^{4+}}$ = 0.75/0.67 Å, CN=6) are less than ionic radii of iron ($r_{Fe^{3+}/Fe^{4+}}$ = 0.785/0.725 Å, CN=6) [2]. As can be seen, oxygen content decreases with decrease temperature and mass saturation occurs at $T<630$ K upon cooling. The substitution of cobalt for iron sites results in a decrease of oxygen content. Such behavior can be explained by the fact that cobalt is more electronegative element in comparison to iron (χ_{Co} = 1.88; χ_{Fe} = 1.83 in the Pauling scale [3]).All thermal expansion curves curves of the $BaFe_{0.9-x}Y_{0.1}Co_xO_{3-\delta}$ have nonlinear shape. Two extremum points are observed on thermal expansion curve of $BaFe_{0.9-x}Y_{0.1}Co_xO_{3-\delta}$ (x=0, 0.05, 0.1, 0.15) sample.

References:

[1]. Liu X., Zhao H., Yang J., Li Y., Chen T., Lu X., Ding W., Li F., *J. Membrane Science*. **383**. (2011) 235.
[2] Shannon R.D., *Acta Cryst. A.* **32**. (1976) 751.
[3] Huheey J.E., *Inorganic Chemistry*. Harper & Row. New York. (1983).

Figure:

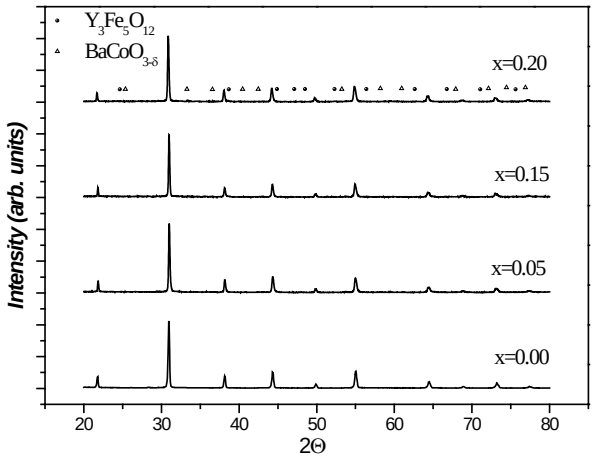

Fig.1. XRD patterns of the $BaFe_{0.9-x}Y_{0.1}Co_xO_{3-\delta}$ $0.0 \leq x \leq 0.2$.

X-Ray Diffraction Study of Oxygen-Conducting Compounds $Ln_2Mo_2O_9$ (Ln = La, Pr)

A. M. Antipin[a], O. A. Alekseeva,[a] N.I. Sorokina,[a] A.N. Kuskova[a], M.Yu. Presniakov,[a] E.P. Kharitonova,[b] V. I. Voronkova.[b]

[a]*Shubnikov Institute of Crystallography, Russian Academy of Science, Moscow (Russia);*
[b]*Moscow State University, Moscow (Russia).*

Lanthanum molybdate $La_2Mo_2O_9$ (LM) was synthesized in the La_2O_3—MoO_3 oxide system [1-3]. It was found that near 580°C, LM undergoes a phase transition from the low-temperature monoclinic α-phase to the high-temperature cubic β-phase [3]. LM and the doped compounds on its basis (LAMOX) attract much attention since the high oxygen conductivity ($6\cdot10^{-2}$ Sm/cm) in LM was found by Lacorre group in 2000 year [4] and the structure of its high-temperature β-phase was determined by the Rietveld method [5]. The high-temperature β-phase has the cubic structure (at 617°C the unit cell parameter a = 7.20114(5) Å; space group $P2_13$). The lanthanum and molybdenum atoms, as well as one of the three independent oxygen atoms (O1), are located on threefold axes. The positions of O2 and O3 oxygen atoms are occupied incompletely, by 78% and 38%, respectively. It was also shown that the unique angle of the monoclinic cell of the low-temperature α-phase is close to 90°. The X-ray diffraction patterns of the α-and β-phases coincide so closely that only a high-resolution X-ray study revealed the splitting of some peaks associated with the monoclinic distortion. In 2005 the structure of the low-temperature phase was determined from a single-crystal X-ray diffraction experiment [6]. The parameters of the monoclinic unit cell are as follows: a = 14.325 Å, b = 21.482 Å, c = 28.585 Å, and β = 90.40°; space group $P2_1$. Three types of coordination environments of molybdenum (tetrahedron, trigonal–bipyramid, and octahedron) are distinguished in the structure. Later it was concluded [7] that although the distortion of crystal lattice in the course of transition from the cubic β-phase to the monoclinic α-phase is insignificant, the oxygen sublattice undergoes an essential rearrangement: the state of oxygen atoms changes from dynamic order to static disorder. Kinetic features of the phase transitions were studied in [8,9]. In [10] it was found that depending on the rate of cooling after the synthesis, LM specimens exist at room temperature in the form of stable monoclinic α-phase ($P2_1$), metastable cubic β_{ms} phase, or their mixture. In [11,12] synthesis and properties of $Pr_2Mo_2O_9$ (PM)compound were studied.
The purpose of this work was to determine the crystal structure of PM and LM, two samples each, at room temperature using X-ray diffraction and high-resolution transmission microscopy. The PM single crystals were studied for the first time. The redetermination of the LM single crystals was caused by new experimental potentialities and the opportunity to perform a correct comparison between the structures of PM and LM compounds.

Single crystals $La_2Mo_2O_9$ were obtained by spontaneous flux crystallization in the La_2O_3—MoO_3 oxide system by the procedure [9]. Single crystals of the compound $Pr_2Mo_2O_9$ were prepared by an analogous procedure in the Pr_2O_3—MoO_3 oxide system [12]. Note that crystals of LM were quenched in air from 1030°C to bring them into the metastable state with cubic symmetry. Crystals of PM were not quenched and, according to optical properties, were monoclinic at room temperature. Interplanar spacings obtained from the electron diffraction patterns are a = 7.15(2) Å for LM and a = 7.09(1) Å for PM. These values agree within the experimental error with the X-ray diffraction data: a = 7.155(1) Å for LM_I, a = 7.155(1) Å for LM_II, a = 7.087(1) Å for PM_I, and a = 7.090(1) Å for PM_II. More than 90% (LM_I) and 60% (LM_II) of the reflections measured were indexed in this

cubic cell and more than 90% of the reflections measured were indexed for both PM crystals. Analysis of the diffraction data sets for the LM_I, PM_I, and PM_II single crystals, which was performed with the CrysAlis program package, did not reveal superstructural reflections that would correspond to the monoclinic cell. It was found that the LM_II crystal consists of two cubic components grown together; $a \approx 7.155$ Å for both components. No regularities in the mutual arrangement of the bases of these components that would transform the cell into the monoclinic phase were found. The crystal structures for two LM and two PM samples are determined in space group $P2_13$. It is found that La and Pr atoms, as well as Mo1 and O1 atoms, are located in the vicinity of 3-fold axes rather than on the axes like in the high-temperature cubic phase. In the structures of LM and PM, Mo atoms are surrounded by oxygen atoms of the O1, O2, and O3 sorts, three atoms each, with average occupancy of 1.00, 0.72, and 0.36, respectively. The structure of a single crystal obtained in an X-ray experiment is always the time and space average of different local structures. In the $Ln_2Mo_2O_9$ structure, the oxygen environment of molybdenum atoms must be the average of three different configurations [13]. The coexistence of these configurations facilitates the oxygen ion migration in the crystal. X-ray diffraction data were used in the calculations of probability density functions, which provided the basis for the calculation of the activation energies of oxygen atoms in the four structures studied using the JANA program package. All possible variants of migration of oxygen atoms were analyzed. It was found that the activation energy of the O1 atom is significantly higher than the energies of the O2 and O3 atoms (on the average, 960, 570, and 145 meV, respectively). It follows that oxygen atoms O2 and O3 make the main contribution to ion conductivity in these compounds. This conclusion agrees with the X-ray data on the incomplete population of the atomic positions of these atoms. Identical (within the experimental error) activation energies of oxygen ions in $La_2Mo_2O_9$ and $Pr_2Mo_2O_9$ account for close values of their conductivity [12].

This study was supported in part by Russian Foundation for Basic Research (project no. 14-02-00531a), the Department of Physical Sciences of the Russian Academy of Science, and the Council of Grants from the President of the Russian Federation for Support of Leading Scientific Schools (grant no. NSh-1130.2014.5).

References:

[1] F.M. Alekseev, E.I. Getman, G.G. Kosheev, M.V. Mohosoev, *J. Inorganic Chemistry*, **14** (1969) 2954.
[2] E.I. Rode, G.V. Lisanova, L.Z. Gohman, *Inorganic materials,* **7** (1971) 2101.
[3] J.P. Fournier, J. Fournier, R. Kohlmuller. Bull. Soc. Chim. Fr., (1970) 4277
[4] P. Lacorre, F. Goutenoire, O. Bohnke, R. Retoux, Y. Laligant, *Nature*, **404** (2000) 856.
[5] F. Goutenoire, O. Isnard, R. Retoux, P. Lacorre, *Chem. Mater.*, **12** (2000) 2575.
[6] I.R. Evans, J.A.K. Howard, J.S.O. Evans, *Chem. Mater.*, **17** (2005) 4074.
[7] L. Malavasi, H. Kim, S.J.L. Billingy et al., *J. Am. Chem. Soc.*, **129** (2007) 6903.
[8] A. Selmi, G. Corbel, S. Kojikian et al., *Eur.J. Inorganic Chem.*, **11** (2008) 1813.
[9] V.I. Voronkova, E.P. Kharitonova, A.E. Krasilnikova, N.N. Kononkova, *J. Phys.: Condensed. Matter.*, **20** (2008) 195.
[10] V.I. Voronkova, V.K. Yanovskiy, E.P. Kharitonova, *Crystallography reports,* **50** (2005) 874.
[11] T. Yamazaki, T. Shimazaki, T. Hashizume, K. Terayama, *J. Mater. Sci. Lett.,* **21** (2002) 29.
[12] V.I. Voronkova, E.P. Kharitonova, E.I. Orlova, D.S. Kolesnikova, *Crystallography reports,* **56** (2011) 1066.
[13] C.J. Hou, Y.D. Li, P.J. Wang et al., *Physical Review,* **76** (2007) 014104.

Reactivity of layered perovskite-like photocatalysts $A_2Ln_2Ti_3O_{10}$ (A = Li, Na, K, Rb; Ln = La, Nd)

T.D. Utkina [a], I.A. Rodionov [a], E.V. Mechtaeva [a], Yu.P. Sokolova [a]

[a] Institute of Chemistry, St. Petersburg State University, 26 Universitetskiy pr., Petrodvorets, St. Petersburg, 198504, Russia

Layered perovskite-like oxides $A_2Ln_2Ti_3O_{10}$ (A - an alkali metal) are crystalline compounds in which two-dimensional perovskite slabs are interleaved with layers of other structure. Complex oxides $A_2Ln_2Ti_3O_{10}$ belong to three-layer Ruddlesden-Popper phases. Such materials are interesting because of their high ionic conductivity and photocatalytic activity, particularly in the reaction of water splitting with hydrogen production. Layered perovskite-type oxides are considered as promising photocatalysts for several reasons. Some members of the series are capable of reversible intercalation of water molecules into the interlayer space. Ion-exchange properties caused by high mobility of interlayer cations make it possible to vary composition of such compounds within a wide range, modifying their photocatalytic properties.

Alkaline forms of layered perovskite oxides are able to undergo protonation (substitution of cations to protons) and hydratation (introduction of water molecules into the interlayer space) when exposed to aqueous solution or humid atmosphere [1]. These processes can significantly influence the physico-chemical properties and should not be neglected while investigating them.

This report presents the results of a study of $A_2Ln_2Ti_3O_{10}$ layered oxides reactivity in an aqueous solution.

Complex oxides $A_2Ln_2Ti_3O_{10}$ (A= Li, Na, K, Rb; Ln = La, Nd) were prepared by solid state synthesis in the temperature range of 1100 – 1200^0C in air at atmospheric pressure:

$$A_2CO_3 + Ln_2O_3 + 3TiO_2 = A_2Ln_2Ti_3O_{10} + CO_2$$

Suspensions of obtained compounds were prepared by adding the powdered sample (1 mmol) to distilled water (100 ml). These suspensions were kept under constantly stirring for a different time (1-14 days), then the samples were centrifuged and dried. The summary protonation/hydration process occuring under contact with aqueous medium can be described as:

$$A_2Ln_2Ti_3O_{10} + (x+y)H_2O = H_xA_{2-x}Ln_2Ti_3O_{10}\cdot yH_2O + xAOH$$

The phase composition and structural parameters of the raw materials and the obtained samples were monitored by XRD analysis. To determine the degree of protonation and the number of intercalated water thermogravimetric analysis (Netzsch TG 209 F1 Iris) was used [2]. The thermal effects of dehydratation processes were determined by the STA 449 F1 Jupiter, combined with mass spectrometry (QMS 403 C Aëolos).

As a result, the interaction characteristics of layered oxides $A_2Ln_2Ti_3O_{10}$ (A = Li, Na, K; Ln = Nd, La) with water were determined. The composition and structure of the hydrated and

protonated forms were calculated. The only relatively stable oxide under these conditions was found to be $Li_2Ln_2Ti_3O_{10}$. Sodium, potassium and rubidium-containing forms undergo partially substitution of interlayer alkali metal cations for protons. This process is accompanied by the introduction of water molecules in the interlayer space. Thus, these materials exist in aqueous solution in the form of compounds with general formula $H_xA_{2-x}Ln_2Ti_3O_{10}*yH_2O$. Deviation of the photocatalytic activity caused by the process of protonation has been demonstrated.

The results were obtained with the support of SPSU resource centers "Research Centre for X-ray Diffraction Studies " and " Research Center of Thermal Analysis and Calorimetry".
This work was supported by the Russian Foundation for Basic Research (grants № 12-03-00761 and 14-03-31968).

References:

[1] I. A. Rodionov, O. I. Silyukov, T. D. Utkina, M. V. Chislov, Yu. P. Sokolova, I. A. Zvereva, *Russian Journal of General Chemistry*, 82 (2012) 1191-1196.

[2] Silyukov O., Chislov M., Burovikhina A., Utkina T., Zvereva I., *Journal of Thermal Analysis and Calorimetry*, **110** (2012) 187-192.

Cathode materials (100-*y*)$PrBaCo_{2-x}Fe_xO_{6-\delta}$ – *y*$Ce_{0.8}Sm_{0.2}O_2$ (*x*=0-0.6; *y*=0÷30) for intermediate temperature SOFCs

N.S. Tsvetkova, I.L. Ivanov, D.S. Tsvetkov, A.Yu. Zuev

Institute of Natural Sciences, Ural Federal University, Ekaterinburg, Russia

The application of Solid Oxide Fuel Cells (SOFCs) is one of the possible ways for reducing energy and ecological problems due to high-energy conversion efficiency and environmental safety of these devices. The lowering operating temperature is a principal way for the large-scale SOFCs introduction because it increases the number of suitable functional materials, life-time of the devices and therefore reduces cost of generating energy.

The double perovskites with general formula $RBaCo_2O_{6-\delta}$ (where R is a rare-earth element) are considered as promising cathode materials for intermediate temperature SOFCs (IT-SOFCs) due to their high mixed ionic-electronic conductivity and rapid oxygen transport [1, 2]. Nevertheless, these layered compounds suffer from very high thermal expansion coefficient (about $20 \cdot 10^{-6}$ K^{-}) [3] as compared to solid electrolyte one (e.g. $12.3 \cdot 10^{-6}$ K^{-1} for $Ce_{0.8}Sm_{0.2}O_2$ [4]). Mechanical mismatch between cathode and solid electrolyte materials leads to cracks during SOFC operation and, as a consequence, reduces its durability. The trade-off between electrochemical and mechanical properties is possible to achieve by using composite cathode materials [4, 5]. Therefore, the main aim of the current work was to study cathode materials based on $PrBaCo_{2-x}Fe_xO_{6-\delta}$ (x = 0-0.6) and composite cathodes (100-y) $PrBaCo_2O_{6-\delta}$ – y $Ce_{0.8}Sm_{0.2}O_2$ (y = 10÷30 wt. %) in contact with $Ce_{0.8}Sm_{0.2}O_2$ solid electrolyte.

Powder samples of double perovskites $PrBaCo_{2-x}Fe_xO_{6-\delta}$ (x = 0-0.6) and solid electrolyte $Ce_{0.8}Sm_{0.2}O_2$ (SDC) were prepared by glycerol – nitrate method. Pr_6O_{11}, $BaCO_3$, Co, $FeC_2O_4 \cdot 2H_2O$, Sm_2O_3 and $Ce(NO_3)_4 \cdot 6H_2O$ (99.99 % purity) were used as starting materials. The powders obtained were finally calcined at 1100 °C for 12 h in air. The phase composition of as-prepared samples was studied by means of X-ray diffraction (XRD) with Equinox 3000 diffractometer (Inel, France). XRD showed no indication for the presence of a second phases.

The chemical compatibility of cathode materials $PrBaCo_{2-x}Fe_xO_{6-\delta}$ (x = 0-0.6) and solid electrolyte SDC was studied by calcination of 50:50 wt. % mixtures at different temperatures in the range 900 – 1200 °C for 12 h in air followed by XRD analysis. Composite cathodes (100-y) $PrBaCo_2O_{6-\delta}$ – y SDC were prepared by mechanical mixing of the $PrBaCo_2O_{6-\delta}$ and SDC powders in different weight ratio (y = 10 – 30 wt. %). The rectangular bars of cathode materials and solid electrolyte used for thermal expansion and electrical conductivity measurements were dry pressed and sintered at 1200 °C and 1300 °C for 12 h in air, accordingly. Thermal expansion coefficients (TECs) of composite cathodes, double perovskites $PrBaCo_{2-x}Fe_xO_{6-\delta}$ (x = 0-0.6) and solid electrolyte SDC were measured using NETZSCH DIL 402 C dilatometer (Netzsch GmhH, Germany) in the temperature range from 30 to 1100 °C in air. Electrical conductivity was studied with a 4-probe dc method in the temperature range 30 – 1100 °C in air. Polarization measurements of cathodes investigated were carried out by electrochemical impedance spectroscopy using Elins Z500-PX impedance analyzer (Elins, Russia). The area specific resistance of cathodes studied was

measured in symmetrical cells *cathode material*|*electrolyte*|*cathode material* in the frequency range 1 Hz – 0.5 MHz and temperature range 600 – 750 °C with 25 °C steps. Impedance spectra were analyzed with ZView 2.0 software (Scribner Associates Inc., USA).

The chemical reactivity test showed no reaction between double perovskites $PrBaCo_{2-x}Fe_xO_{6-\delta}$ (x = 0-0.6) and solid electrolyte SDC in the temperature range investigated. It was shown that TECs and overall electrical conductivity of composite cathode materials (100-y) $PrBaCo_2O_{6-\delta}$ – y SDC (y = 10÷30 wt. %) decrease with concentration of SDC. At the same time electrical conductivity of composites maintains high enough for their application in IT-SOFCs. On the other hand, the influence of solid electrolyte on the ASR of composite cathodes is ambiguous as shown in Figure.
The general trend as seen in Figure is a slight increase of ASR for (100-y) $PrBaCo_2O_{6-\delta}$ – y SDC (y = 10÷30 wt. %) with concentration of SDC in composite contrary to what was found for (100-y) $GdBaCo_{2-x}Fe_xO_{6-\delta}$ – y SDC (x=0, 0.2; y=0÷50) [6]. In the latter case there was found an optimal concentration of SDC for minimum ASR value of the composite.

References:

[1] D.S. Tsvetkov, V.V. Sereda, A.Yu. Zuev, *Solid State Ionics*,**192** (2010) 215.
[2] M.-B. Choi, S.-Y. Jeon, J.-S. Lee, H.-J. Hwang, S.-J. Song, *J. Power Sources*, **195** (2010) 1059.
[3] Q. Zhou, F. Wang, Y . Shen, T. He, *J. Power Sources*, **195** (2010) 2174.
[4] E.Yu. Pikalova, V.I. Maragou, A.N. Demina, A.K. Demin, P.E. Tsiakaras, *J. Power Sources*, **180** (2008) 199.
[5] N. Li, B. Wei, Z. Lü, X. Huang, W. Su, *J. Alloys Compd.*, **509** (2011) 3651.
[6] N.S. Tsvetkova, A.Yu. Zuev, D.S. Tsvetkov, *J. Power Sources*, **243** (2013) 403.

Figure:

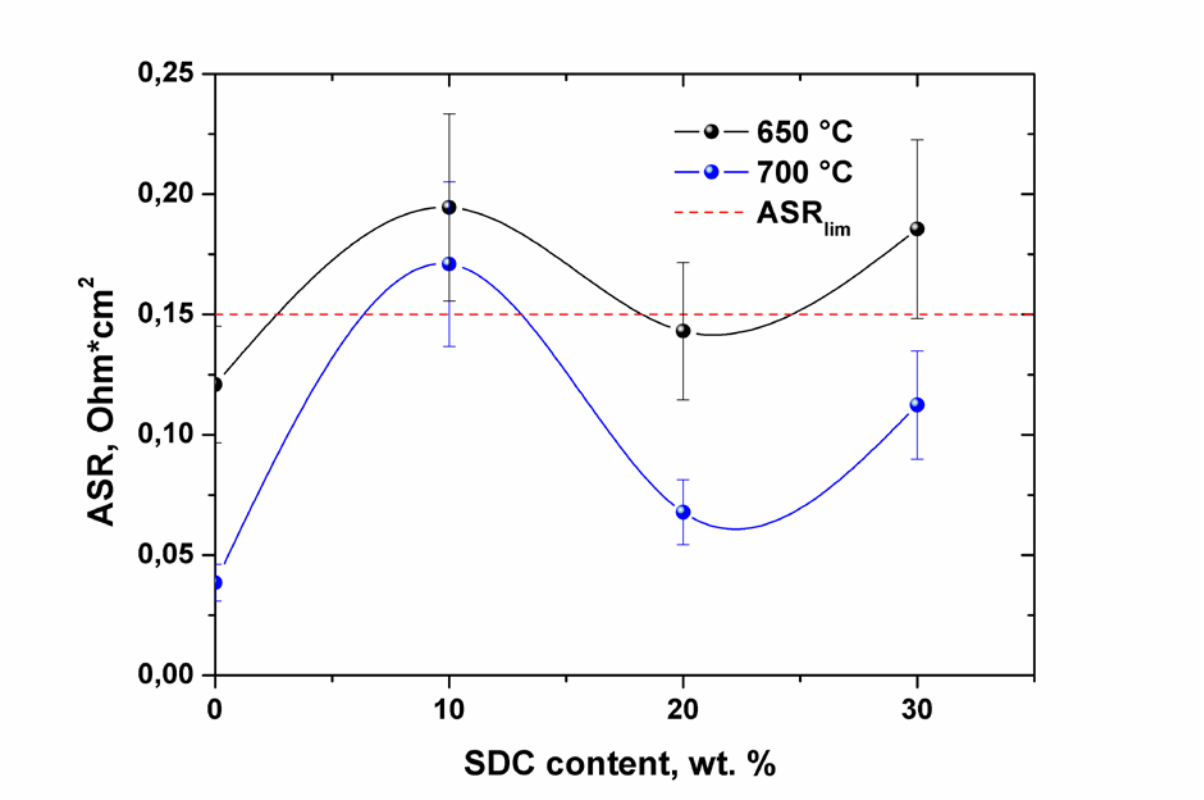

A_2MPO_4F (A = Na, Li; M = Mn, Fe, Co, Ni) materials for Li-ion batteries

V.R. Podugolnikov, E.T. Devyatkina, N.V. Kosova

Institute of Solid State Chemistry and Mechanochemistry SB RAS, Novosibirsk, Russia

The A_2MPO_4F (A = Na, Li) cathode materials have received considerable interest due to two-dimensional structure and the possibility of utilizing two alkali metal ions per transition metal ion during the battery operation, which would ultimately yield higher specific capacities and energy densities. Ellis *et al.* have reported that Na_2FePO_4F functions smoothly as a cathode in either Li-ion or Na-ion cells [1]. Na_2FePO_4F crystallizes in the *Pbcn* orthorhombic space group and has two crystallographically unique sodium sites. In a lithium-ion cell, one mobile Na in Na_2FePO_4F is rapidly exchanged for Li with the formation of $NaLiFePO_4F$. The compound exhibits 3.5 V potential for the Fe^{2+}/Fe^{3+} redox pair *vs.* Li/Li^+ and a theoretical capacity of 135 $mA{\cdot}h{\cdot}g^{-1}$; its electrochemical profile displays a quasi-solid solution behavior. The structure and electrochemistry of another sodium-metal fluorophosphates, Na_2MPO_4F (M = Mn, Co, Ni), are under study [2-4]. Kim *et al.* [3] have shown that Na_2MnPO_4F crystallizers in the monoclinic structure with the $P2_1/n$ space group and has a specific capacity of 120 $mA{\cdot}h{\cdot}g^{-1}$ and an average potential of 2.5 V upon cycling in Na cell. Na_2CoPO_4F is isostructural to Na_2FePO_4F, while the structure of Na_2NiPO_4F is debatable till now [4]. Na_2CoPO_4F exhibits a Co^{2+}/Co^{3+} potential at 4.8 V. On contrary, Na_2NiPO_4F shows no electrochemical activity below 5 V [2]. The aim of the present study was a comparable study on the structure and electrochemistry of Na_2MPO_4F (M = Mn, Fe, Co, Ni).

The samples were prepared by mechanochemically assisted solid state synthesis. The process consists of two steps including a covalent precursor formation ($NaMPO_4$) and incorporation of the ionic NaF salt into its framework. $NaMPO_4$ were prepared by carbothermal reduction relied on the use of the correspondent metal oxide with high oxidation state of *d*-metal (MnO_2, Fe_2O_3, Co_3O_4 and NiO) and a carbon as a selective reducing agent. Both steps included a preliminary mechanical activation using AGO-2 planetary mill and a subsequent heat treatment in Ar flow. The crystal structure was studied by X-ray powder diffraction (XRD) using D8 Advance Bruker diffractometer. The structural refinement of the XRD data was carried out by the Rietveld method using GSAS software package. Particle size and morphology were investigated by scanning electron microscopy (SEM) with Hitachi S-3400N scanning electron microscope. The samples were cycled in Swagelok-type half-cells with Li anode and 1M solution of $LiPF_6$ in a mixture of ethylene carbonate and dimethyl carbonate as an electrolyte. Galvanostatic intermittent titration technique (GITT) was applied for the evaluation of lithium diffusion coefficient D_{Li}.

According to SEM, the synthesized samples are comprised of large agglomerates that are composed of smaller particles about 100-200 nm in size. XRD analysis shows that they are phase homogeneous, except for Na_2NiPO_4F (Fig. 1). Na_2MPO_4F (M = Fe, Co, Ni) crystallize in the orthorhombic structure with the *Pbcn* space group, while Na_2MnPO_4F – in monoclinic structure with the $P2_1/n$ space group. The refined cell parameters are presented in Table 1. After termination of the Na^+/Li^+ ion electrochemical exchange in Na_2FePO_4F and the formation of $NaLiFePO_4F$, its discharge capacity comprises 115 $mA{\cdot}h{\cdot}g^{-1}$ within the 2.0-

4.2 V range. The average Li^+ diffusion coefficient D_{Li} in $NaLiFePO_4F$, determined from the GITT measurements, is 10^{-15} $cm^2 \cdot s^{-1}$. About 50 % of the theoretical capacity was obtained for Na_2MPO_4F (M = Mn, Co, Ni) at the 1st charge to 4.8 V. However, the discharge capacity was noticeably lower and quickly decreased upon the following cycling probably to the decomposition of the electrolyte at high voltage. Na^+/Li^+ ion exchange was also observed when the cells based on Na_2MPO_4F *vs*. Li were equilibrated at open circuit voltage in the $LiPF_6$-based electrolyte. The composition and the structure of as-obtained products were studied.

References:

[1] B. L. Ellis, W. R. M. Makahnouk, Y. Makamura, K. Toghill, L. F. Nazar, *Nat. Mater.*, **6** (2007) 749.
[2] B. L. Ellis, W. R. M. Makahnouk, W. N. Rowan-Weetaluktuk, D. H. Ryan, L.F. Nazar, *Chem. Mater*., **22** (2010) 1059.
[3] S.-W. Kim, D.-H. Seo, H. Kim, K.-Y. Park, K. Kang, *Phys. Chem. Chem. Phys.*, **14** (2012) 3299.
[4] H.B. Yahia, M. Shikano, S. Koike, K. Tatsumi, H. Kobayashi, *Dalton Trans*., **41** (2012) 5838.

Figure:

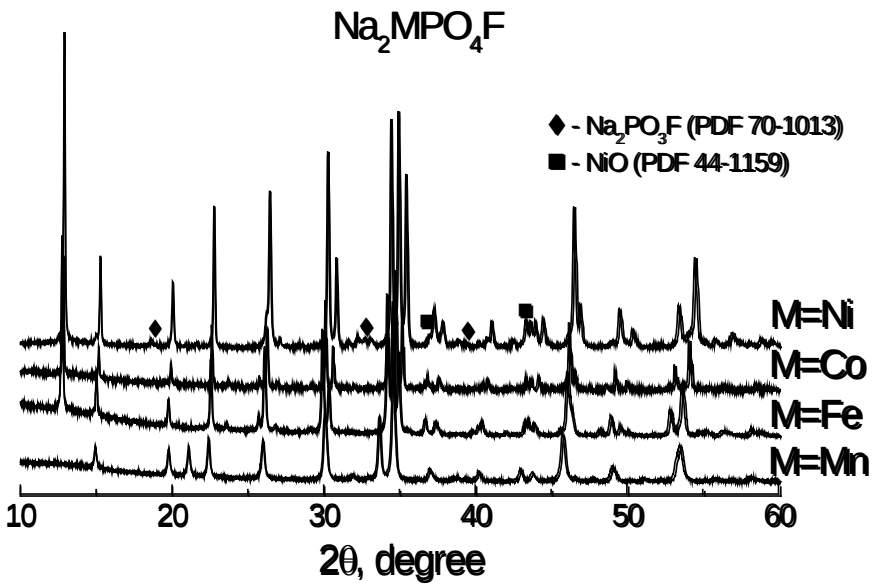

Figure 1. XRD patterns of as-prepared Na_2MPO_4F (M = Mn, Fe, Co, Ni).

Table 1. Refined cell parameters.

Sample	S.G.	*a*, Å	*b*, Å	*c*, Å	*β*, °	*V*, Å^3
Na_2MnPO_4F	$P2_1/n$	13.665(2)	5.3135(3)	13.676(2)	119.721(4)	862.4(1)
Na_2FePO_4F	*Pbcn*	5.2311(2)	13.8238(5)	11.7551(4)	90.000	850.06(6)
Na_2CoPO_4F	*Pbcn*	5.2333(1)	13.7509(4)	11.6538(2)	90.000	838.65(4)
Na_2NiPO_4F	*Pbcn*	5.1956(2)	13.6888(7)	11.5725(5)	90.000	823.05(9)

Reactivity and topochemical conversions of layered perovskite-like titanates for synthesis of nanostructured materials

Liliia D. Abdulaeva,[a] Irina A. Zvereva[a]

[a]Institute of Chemistry, Saint Petersburg State University, 26 Universitetskiy pr., Petrodvorets, Saint Petersburg, 198504, Russia

Layered perovskite-like oxides from the time of their discovery attract great attention due to their unique physicochemical properties, such as magnetic and electric properties, catalytic and photocatalytic activity. By reason of the growing role of these compounds in technology and industry there is increasing demand of development methods for obtaining such compounds with specified composition and structure. Using the methods of "soft chemistry" we can create materials with different particle morphology by a sequence of low-temperature topochemical syntheses.

In this work, layered perovskite-like oxides $ALnTiO_4$ and $A_2Ln_2Ti_3O_{10}$ (A = H, Na, K; Ln = La, Nd) were used as precursors for series of the "soft chemistry" syntheses, such as the ion exchange, the intercalation reactions and the topochemical condensation. Characterization by SEM, powder XRD, high temperature powder XRD, thermal analysis (TGA and DSC) have been performed for determination of structure, content and stability of synthesized oxides.

The thermal stability range of the protonic compounds $HLnTiO_4$ (Ln = La, Nd) (Fig. 1, a), which were obtained by treating initial alkali metal containing layered compounds in acid medium, the thermal effects accompanying the decomposition processes were determined and all stages of mass loss on the TGA curves were characterized. It was found that due to the loss of stability of the protonic forms $HLnTiO_4$ can be obtained following perovskite-like compounds:

- Cation-deficient perovskites $Ln_{2/3}TiO_3$ (Ln = La, Nd) (Fig. 1, b) have been obtained for the first time by leaching of Ln^{3+} ions in acid solution. The obtained samples did not save the morphology of the initial layered oxides $HLnTiO_4$ and consist of irregularly shaped particles of intergrown crystals with sizes less than 100 nm.
- Hydrated metastable compounds $Ln_2\square Ti_2O_7{*}yH_2O$ and defective layered compounds $Ln_2\square Ti_2O_7$ (Fig. 1, c) have been obtained by the topochemical dehydration without change of morphology.

Exfoliated nanostructured $(VO)_xH_{1-2x}LnTiO_4{*}yH_2O$ (Fig. 1, d) and $(VO)_xH_{2-2x}Ln_2Ti_3O_{10}{*}yH_2O$ have been synthesized by the exfoliation process of the protonic form $HLnTiO_4$ and $H_2Ln_2Ti_3O_{10}$ (Ln = La, Nd) by treatment in $VOSO_4$ solution. The morphology of exfoliated nanostructured oxides significantly changes compared with the morphology of the initial compounds. Along the exfoliation and reassembling of the initial protonic oxides exfoliated particles are formed up in interconnected flat crystallites with thickness less than 10 nm. If $NaLnTiO_4$ and $K_2Ln_2Ti_3O_{10}$ were treated by vanadyl sulfate under the same conditions, it was obtained partially exfoliated samples where some of the particles with layered structure while other part of particles undergoes exfoliation and self-assembly.

Figures:

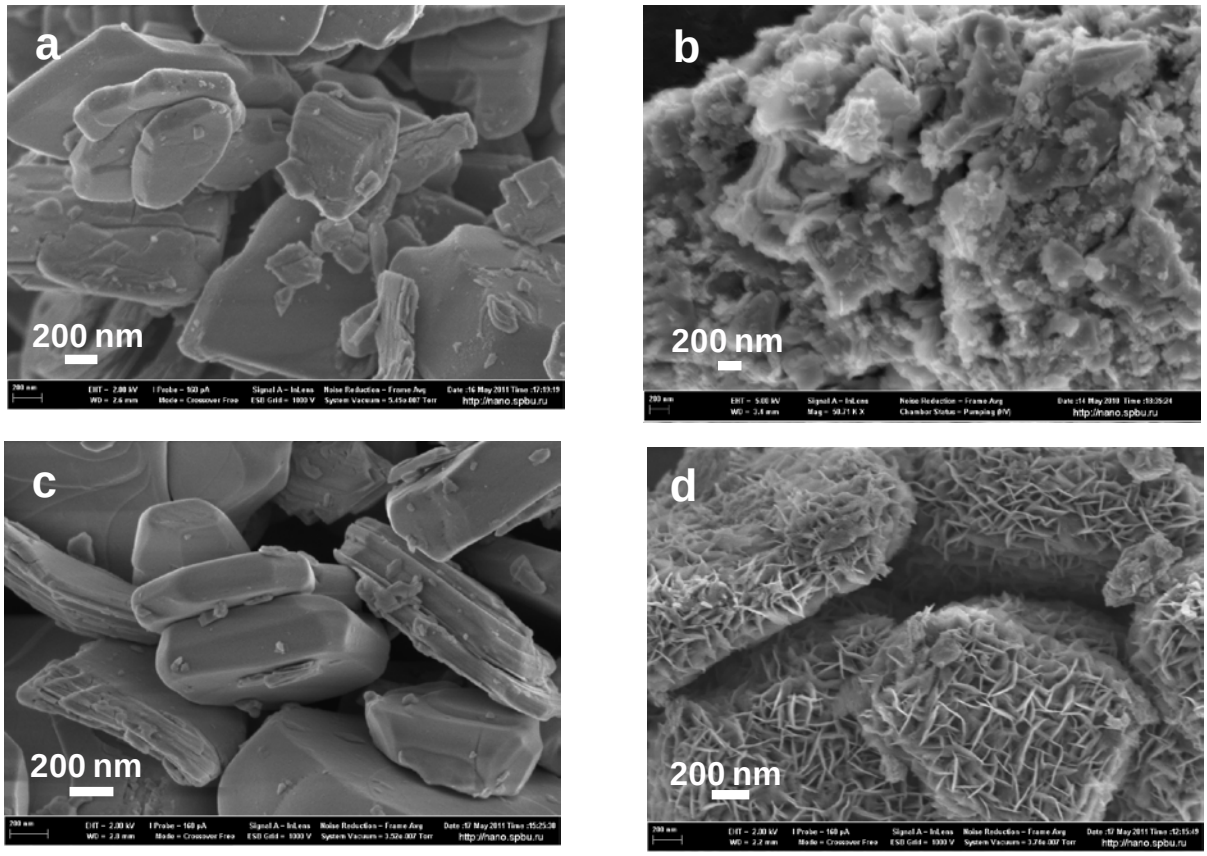

Figure 1: SEM images: a. $HNdTiO_4$, b. $Nd_{2/3}TiO_3$, c. $Nd_2\square Ti_2O_7$, d. $(VO)_xH_{1-2x}NdTiO_4*yH_2O$

Opportunity of using topochemical reactions of the layered perovskite-like titanates for “soft chemistry” syntheses is discussed in comparison with results of the sol-gel and the hydrothermal method.

This work was supported by RFBR (grant № 12-03-00761).

The effect of water on the outcome of mechanical treatment in "L-serine-oxalic acid" system

E. A. Losev[a,b]*, E.V. Boldyreva[a,b]
[a]Institute of Solid State Chemistry and Mechanochemistry, Kutateladze, 18, Novosibirsk, 630128, Russia,
[b]REC-008, Novosibirsk State University, Pirogova, 2, Novosibirsk, 630090, Russia.
*E-mail: losev.88@mail.ru, eboldyreva@yahoo.com

Mechanochemical synthesis of molecular functional materials is a hot topic. Mechanical treatment of molecular solids allows one to avoid the use of bulk solvent and to obtain new forms of compounds, which are difficult (or impossible) to synthesise by "classical solution chemistry". Investigation of the mechanisms of mechanochemical transformations could help to determine the optimal conditions of processes under consideration and to control the synthesis of desired product.

The aim of the present work was to study the effect of water in the "L-serine-oxalic acid" system under mechanical treatment. Both L-serine and oxalic acid can form the hydrates, and it was possible to study the effect of water in various forms (crystal water in either of hydrates or in both of them; liquid water added to solid anhydrous forms) on the outcome of mechanochemical reactions.

Co-grinding of dry anhydrous reagents gave only trace amounts of the product phase (anhydrous 1:1 L-serinium oxalate), apparently due to the interaction with the trace amounts of water in the air. In the presence of crystal water or water added as a liquid phase the polymorphs of $[L\text{-serH}]_2[ox]\bullet 2H_2O$ (as pure forms or in a mixture) were formed [1]. Neat co-grinding of anhydrous oxalic acid with L-serine monohydrate or of anhydrous L-serine with oxalic acid dihydrate gave polymorph II (kinetic form). Co-grinding of L-serine monohydrate with oxalic acid dihydrate as well as liquid-assisted grinding with sufficient amount of liquid water added gave polymorph I (thermodynamic form) and polymorph 2 (with a very low transformation degree) if too little water was added [1,2]. Based on the obtained results we proposed the outcome of the mechanochemical transformation mostly depends on the total amount of water but not on crystal structure of initial hydrates [3].

Further investigation of the system reveals ability of reaction between L—serine monohydrate and oxalic acid dihydrate without mechanical stress. The storage of the components in sealed vial resulted in formation of I polymorph of $[L\text{-serH}]_2[Ox]\bullet 2H_2O$. Moreover an intermediate in the reaction was form II of $[L\text{-serH}]_2[Ox]\bullet 2H_2O$. The analysis of crystal structures of the two polymorphs showed that the form II consists of blocks interacting with each other by weak van der Waals interactions whereas the form I comprise 3D-network of hydrogen bonds. After all one can conclude that the role of mechanical treatment in inducing the synthesis is merely bringing the reacting species into contact, improving their mixing, and facilitating the dehydration of crystal hydrates [3].

Srpay drying and antisolvent crystallisation techniques were also used in order to investigate an influence of conditions on crystallisation process in the system. Spray drying led to formation of kinetically controlled product of the reaction ($[L\text{-serH}]_2[Ox]\bullet 2H_2O$ II polymorph) whereas antisolvent crystallisation using acetone and ethanol resulted in

formation thermodynamically controlled polymorph I [1,2]. The obtained results correlates with ones of mechanochemical and storage experiments.

The results are analysed on the basis of X-ray powder diffraction, IR-spectroscopy, optical and polarising microscopy data.

The work was supported by the Russian Foundation for Basic Research (RFBR) (Grants No. 12-03-31663 mol-a,14-03-31866 mol-a, 11-03-00684-a, 10-03-00252-a), by grants from the Russian Ministry of Education and Science No. 14.B37.21.1093, NSH 4357.2010.3, NSH 221.2012.3., programs from RAS 54.38 and 24.38 and Ludo Frevel Crystallography Scholarship Award (2013).

References:

[1] Braga, D., Chelazzi, L., Ciabatti, I. and Grepioni, F. (2013) New J. Chem. 37, 97-104.
[2] Kulik, M., Pazio, A. and Wozniak, K. (2013) Acta. Cryst. E69, o1667-o1668.
[3] Losev, E.A., Boldyreva, E.V. (2014) CrystEngComm. DOI: 10.1039/C3CE42321B.

Heat treatment effects on thermoelectric properties of Co-Sb thin-films

Seungwoo Han,[a*] Minyoung Jeong[a]

[a] Korea Institute of Machinery and Materials, Department of Nanomechanics
Daejon, 305-343, South Korea
*E-mail: swhan@kimm.re.kr, TEL: +82-42-868-7188, FAX: +82-42-868-773

Thermoelectric materials have been attracting much attention due to their abilities to generate electricity from temperature-gradients. Materials that have high electrical transport properties and low thermal transport properties are desired for good thermoelectric materials. Skutterudite compounds are among the most promising thermoelectric materials because of their hign carrier mobilities and high Seebeck coefficients[1]. Cobalt Tri-antimonide (CoSb3) is a good exemplary skutterudite material.

In this work, we synthesized nano-sized thermoelectric Co-Sb thin-films using a novel sol-gel technique. The Co-Sb sol was prepared by mixing pre-determined amounts of reagent including CoCl26H2O, SbCl3 and citric acid. Ethanol was used as a solvent. The sol was deposited on silicon substrates by spin-coating. It turned out that spinning speed and time are very important in obtaining pure Co-Sb thin films. The films were then kept at 573K for 0.5 hour under pure hydrogen flow for reduction process. The temperatures were varied to observe how properties and phase-purity would change with varying process-temperatures. The X-ray diffraction (XRD) and Energy-dispersive X-ray spectroscopy (EDS) were conducted to check whether our samples have correct phase and stoichiometry required for CoSb3. The films' thermoelectric transport properties were measured. Heat treatment effects on thermoelectric properties of CoSb3 thin films from room temperature to 500 °C were investigated. The spin-coating's easiness in fabrication and sol-gel technique's ability to produce large quantities are certainly beneficial.

References:

[1] Y. Chu, X. Tang, W. Zhao, Q. Zhang, *Crystal Growth & Design*, **8** (2008) 208.

Figure:

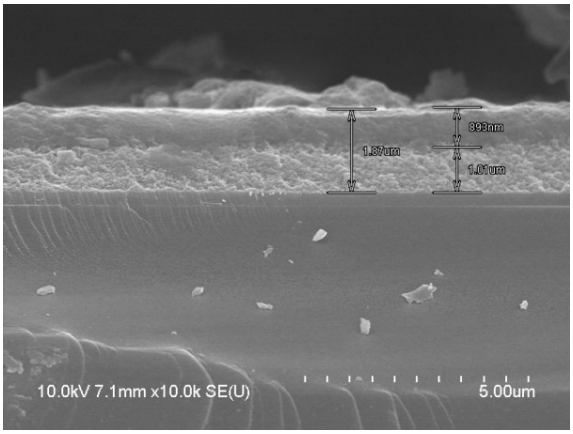

Fig.1. SEM image of cross section of Co-Sb thin film

Atomic and Molecular Oxygen Migration in the $SrCoO_{2.5}$ Brownmillerite Structure: DFT Study

V.M. Tapilin,[a] A.R. Cholach [a] A.P. Nemudry [b]
[a] Boreskov Institute of Catalysis, Novosibirsk, Russian Federation.;
[b] Institute of Solid State Chemistry and Mechanochemistry, Novosibirsk, Russian Federation

A unique property of high mixed oxygen-electron conductivity opens wide possibilities to use the perovskites oxides as membrane materials for oxygen separation from oxygen-containing gas mixtures, in catalysis, etc [1, 2]. The oxygen ion hopping between the occupied and empty sites determines the oxygen mobility in the $ABO_{3-\delta}$ compounds. The brownmillerite structure $Sr_2M_2O_5$ is of particular interest among $SrMO_{3-\delta}$ compounds (M=Fe, Co) due to reversible oxygen intercalation already at room temperature [3, 4]. The most of band structure calculations concern unique magnetic properties of oxides [5] and applications of this theory for the mixed ionic-electronic conductivity have been used infrequently [5].
The present paper deals with band structure calculations of strontium cobaltite $SrCoO_{2.5}$ in brownmillerite structure in order to reveal the sites of intercalation, chemical bonding and migration mechanism of intercalated oxygen. An LDA+U approximation with QUANTUM ESPRESS code [5] has been developed for optimized atom positions. Initial calculations were performed with the (1x3x1) Brillouin zone, the further calculations for ground, transition and intermediate states were performed with (2x6x2) and (4x8x4) mashes. Oxygen molecule electron structure was calculated at Γ point of the Brillouin zone for tetragonal unit cell with lattice parameters a=15 Å, a/c=1.5.
Fig. 1 shows notations related to fourfold Co_t and six fold coordinated Co_o, O_t and O_o for oxygen ions in Co_t and Co_o planes, and O_i for atoms connecting Co_t and Co_o planes. An elementary step of oxygen ion diffusion consists of rotation in *bc*-plane around lower Co ion in Fig. 2a in equivalent site between lower and left upper Co ions. The crossing occur throw transition state shown in Fig. 3b which energy is 0.6 eV above the initial one. Optimization of ion positions leads to the structures of CoO_6 octahedron and CoO_4 tetrahedron in Fig. 1. The brownmillerite valence band DOS is formed by the comparable contribution of cobalt *d* and oxygen *p* states. It means the covalent *O-Co* bonding and a very few of *O-Sr* bond. Therefore, just oxygen interaction with cobalt determines the oxygen ion migration mechanism.
The calculations show that oxygen can be intercalated in $SrCoO_{2.5}$ brownmillerite structure in molecular forms also, and to put an oxygen molecule into brownmillerite without dissociation requires 1.71 eV less energy than dissociative form. The oxygen molecule as well as oxygen atom takes the bridge position shown in Fig. 3a. The transition of the molecule from this position into equivalent position between Co upper and left lower ion occurs throw rotation in *bc*-plane around Co ion. On this path, there is an intermediate state shown in Fig.3c separated from the initial ones by transition state shown in Fig. 3b. The energies of the transition and intermediate states above the initial one are 0.72 eV and 0.38 eV, respectively. The oxygen molecule forms peroxide with Co ion in the intermediate state and superoxide in the transition state. The conversion of oxygen molecule into two separated ions requires 3.34 eV.

References:

[1] Fontaineb, M.-L., et al. (2008) Membrane Science and Technology; Ed.Wessling, M. S. K., Elsevier Sci. B.V., Amsterdam, pp. 401-458.
[2] A. Kleinert, et al., (2006) *Catal. Today* **118** 44.
[3] A. Nemudry, et al. (1996) Chem. Mat. 8, 2232;
[4] A. Nemudry et al. (1998) Chem. Mat. 10, 2403.
[4] V. Pardo, et al. *Phys. Rev. B* **76** (2007) 165120.
[5] P. Giannozzi et al. *J. Phys. – Cond. Matter* **21** (2009) 395502.

Figures:

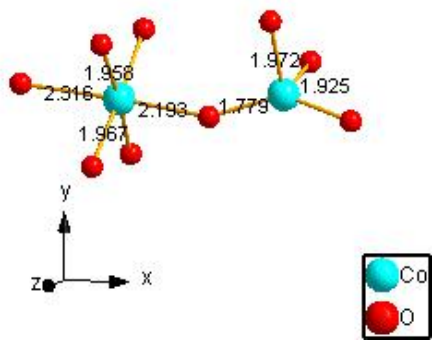

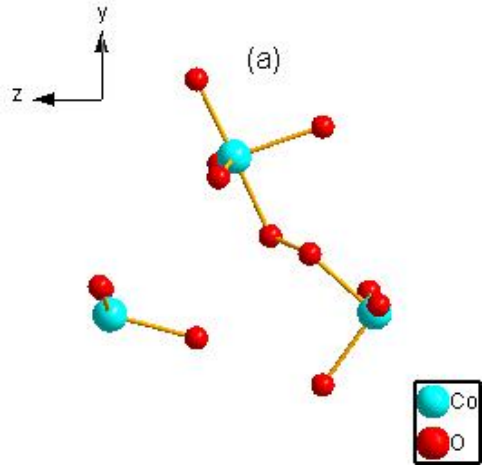

Figure 1. Co_t (right) and Co_o (left) oxygen environment, numbers show bond lengths.

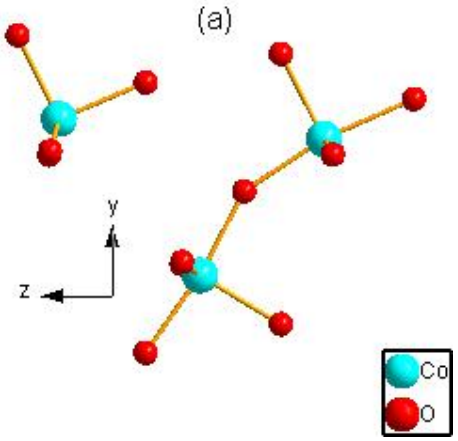

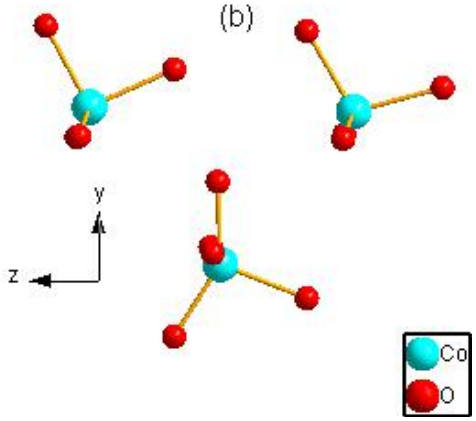

Figure 2. Fragments of Co_t plane with intercalated O ion in (a) ground and (b) transition state position.

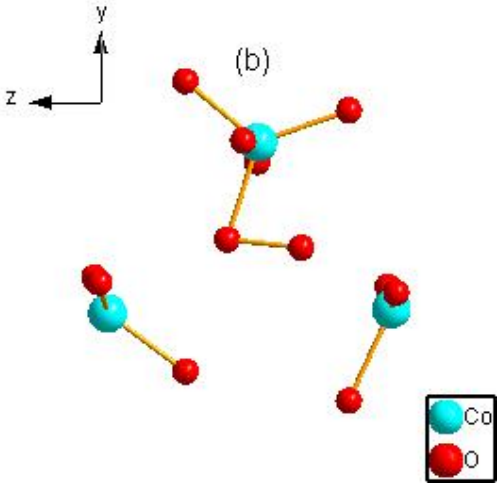

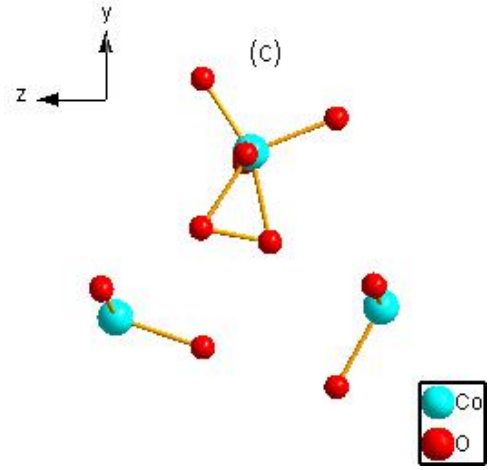

Figure 3. Fragments of Co_t plane with intercalated oxygen molecule in (a) ground, (b) transition, and (c) intermediate states.

Defect equilibrium in double perovskite-like cobaltites at elevated temperatures

A.Yu. Suntsov, I.A. Leonidov, M.V. Patrakeev, V.L. Kozhevnikov

Institute of Solid State Chemistry UB RAS, Yekaterinburg, Russian Federation

The main prospects of double perovskite cobaltites are associated with the design of materials for IT-SOFC cathodes and oxygen semi-permeable membranes for oxygen separation technologies. [1]. This is primarily due to the high ion and electron components of conductivity at quite moderate temperatures [2]. The specific structural feature in these compounds is presence of ordered oxygen vacancies which can falicitate fast oxygen ion transport and set up a wide range of oxygen non-stioichiometry [3]. In addition, the tendency of cobalt cations to charge disproportionation results in electron and hole defects in the crystal lattice. Hence, the description of defect equilibria is necessary in order to be able to correctly determine concentrations of defect species and their changes with temperature and oxygen pressure in the ambient.

The equilibration of cobaltites with gas phase oxygen occurs as a result of the oxygen exchange reaction:

$$2Co^{2+} + V_{\delta} + \frac{1}{2}O_2 = 2Co^{3+} + O_{\delta}^{2-} \quad (1)$$

The respective equilibrium constant makes it possible interrelation of the equilibrium pressure of oxygen p_{O_2} over the oxide with the concentration of movable oxygen species in the solid as:

$$p_{O_2}^{1/2} = \frac{[Co^{3+}]^2 \cdot [O_{\delta}]}{[Co^{2+}]^2 \cdot [V_{\delta}] \cdot K_{Ox}} \quad (2)$$

Here K_{Ox} is the equilibrium constant for reaction (1). Then, the structure conservation demand, the charge neutrality requirement and the intrinsic reaction of charge redistribution over cobalt cations (charge disproportionation):

$$2Co^{3+} = Co^{2+} + Co^{4+} \quad (3)$$

are to be taken into account in order to calculate concentrations of cobalt species. The thorough comparison with the experimental data has shown that one more intrinsic reaction may be possible that changes distribution of oxygen ions in the structure. It is suggested that this reaction involves positional exchange of oxygen ions O_{Eq}^{2-} in structural CoO_2 planes and oxygen vacancies V_{δ} in PrO_{δ} planes:

$$O_{Eq\delta}^{2-} + V_{\delta} = O_{Eq}^{2-} + V \quad (4)$$

The incorporation of this reaction into the model results in a perfect match of the calculated and measured data for equilibrium pressure of oxygen in the entire studied range of the experimental parameters. The expressions for concentrations of anion and electron defects $[O_{Eq}^{2-}]$, $[V_{\delta}]$, $[O_{\delta}^{2-}]$, $[V_{Eq}]$, $[Co^{2+}]$, $[Co^{3+}]$ and $[Co^{4+}]$ can also be obtained from the model. The fitting parameters, i.e. the equilibrium constants K_{Ox}, K_D and K_{OD} for reactions (1), (3) and (4), respectively, can be utilized for evaluation of the associated changes in enthalpy

and entropy [4]. It is shown that intrinsic reaction (4) in pristine cobaltites takes place at heating above 700 °C while copper doping promotes its further facilitation at even lower temperatures. Therefore, partial substitution of cobalt for copper may be a valuable means for development of advanced mid-temperature SOFCs cathodes and oxygen membranes.

References:

[1] Kun Zhang, Lei Ge, Ran Ran, Zongping Shao, Shaomin Liu, *Acta Materialia*, **56** (2008) 4876.
[2] Jung-Hyun Kim, Arumugam Manthiram, *J. Electrochem. Soc.*, **155** (2008) B385.
[3] Andrey A. Taskin, Alexander N. Lavrov, Yoichi Ando, *Appl. Phys. Lett.*, **86** (2005) 09191.
[4] Alexey Yu. Suntsov, Ilia A. Leonidov, Mikhail V. Patrakeev, Victor L. Kozhevnikov, *J. Solid State Chem.*, DOI: 10.1016/j.jssc.2014.02.004.

Improved Persistent Luminescence of $CaTiO_3:Pr^{3+}$ by Fluorine Substitution and Thermochemical Treatment

Songhak Yoon,[a,*] Eugenio H. Otal,[a] Alexandra E. Maegli,[a] Lassi Karvonen,[a] Santhosh K. Matam,[a] Stefan G. Ebbinghaus,[b] Bernhard Walfort,[c] Hans Hagemann,[d] Simone Pokrant,[a] Anke Weidenkaff [a,e]

[a] Laboratory for Solid State Chemistry and Catalysis, Empa - Swiss Federal Laboratories for Materials Science and Technology, Überlandstrasse 129, CH-8600, Dübendorf, Switzerland
[b] Institute of Chemistry, Martin-Luther University Halle-Wittenberg, Kurt-Mothes-Straße 2, 06120 Halle/Saale, Germany
[c] LumiNova AG, Speicherstrasse 60A, CH-9053, Teufen, Switzerland
[d] Department of Physical Chemistry, University of Geneva, Quai E. Ansermet 30, CH-1211 Geneva 4, Switzerland
[e] Institute for Materials Science, University of Stuttgart, Heisenbergstrasse 3, DE-70569 Stuttgart, Germany
*E-mail: songhak.yoon@empa.ch

Strong red phosphorescence of $CaTiO_3:Pr^{3+}$ has been extensively studied during the last decades because of the potential application for phosphor lamps, soft illumination, warning signs or field emission displays [1-2]. The persistent luminescence was attributed to detrapping of electrons stored in trapping centers like oxygen vacancies by thermal activation, which is followed by red emission due to the $^1D_2 \rightarrow {}^3H_4$ transition of Pr^{3+} [1-3]. Many attempts have been devoted to the improvement of the emission intensity and to the enhancement of the phosphorescence efficiency, and factors affecting the phosphorescence have been widely discussed. It is well accepted that the concentration of oxygen vacancies is a decisive factor to explain the phosphorescence behavior of $CaTiO_3:Pr^{3+}$ [4,5]. With respect to these findings different methodologies, for example, the synthesis methods, the co-dopants and the host modifications have been pursued [6,7]. In most cases, the influence of cation substitution in $CaTiO_3:Pr^{3+}$ has been investigated. However, comparatively few studies have been carried out concerning the anionic substitution and the influence of annealing atmosphere on persistent luminescence.

In the present study, $CaTi(O,F)_3:Pr^{3+}$ powders were synthesized by a solid-state reaction. For the substitution of O^{2-} by F^-, CaF_2 was used. Because of the different formal charges and ionic radii of O^{2-} and F^-, the distribution and concentration of the defects (including oxygen vacancies) can be varied depending on the degree of fluorine-substitution in $CaTiO_3:Pr^{3+}$. Expectedly, this can alter the afterglow properties of the oxyfluorides in comparison with the oxide phosphors. Furthermore, the influence of annealing atmosphere with optimized fluorine content was investigated and the resulting afterglow decay behaviors were studied by fluorescence spectrophotometry.

Powder X-ray diffraction and Rietveld refinements revealed that increasing fluorine-substitution led to the gradual shrinkage of the unit-cell. The $CaTi(O,F)_3:Pr^{3+}$ sample synthesized with 0.075 mol of CaF_2, 0.025 mol of $CaCO_3$ and 0.1 mol of TiO_2 along with 2 mmol of Pr_2O_3 (denoted as CTOF1.5) exhibited the smallest lattice strain and at the same time the highest afterglow intensities. The effect of annealing atmosphere was investigated by

thermochemical treatment of the CTOF1.5 in different atmospheres (Ar, air and NH_3). UV-Vis diffuse reflectance spectra and photoluminescence excitation spectra revealed that Pr^{4+} in the pristine CTOF1.5 was partially reduced to Pr^{3+} under NH_3 flow. As a result, the highest persistent luminescence intensity was obtained for CTOF1.5 annealed in NH_3 leading to an intensity improvement of ca. 450% compared to $CaTiO_3$:Pr^3. The substantial improvement of afterglow intensity by fluorine substitution and annealing in NH_3 is considered to be the result of the generation of oxygen vacancies and the partial reduction of Pr^{4+} to Pr^{3+}.

References:

[1] P. T. Diallo, P. Boutinaud, R. Mahiou, J. C. Cousseins, Phys. *Status Solidi A*, **160** (1997) 255-263.
[2] X. M. Zhang, J. H. Zhang, M. Y. Wang, X. Zhang, H. Zhao, X. J. Wang, *J. Lumin.*, **128** (2008) 818-820.
[3] E. Pinel, P. Boutinaud, R. Mahiou, *J. Alloy Compd.*, **380** (2004) 225-229.
[4] X. M. Zhang, J. H. Zhang, Z. G. Nie, M. Y. Wang, X. G. Ren, X. J. Wang, *Appl. Phys. Lett.*, **90** (2007) 151911.
[5] W. Y. Jia, W. L. Xu, I. Rivera, A. Perez, F. Fernandez, *Solid State Commun.*, **126** (2003) 153-157.
[6] S. Y. Yin, D. H. Chen, W. J. Tang, Y. H. Yuan, *J. Mater. Sci.*, **42** (2007) 2886-2890.
[7] D. Haranath, A. F. Khan, H. Chander, *J. Phys. D Appl. Phys.*, **39** (2006) 4956-4960.

Figures:

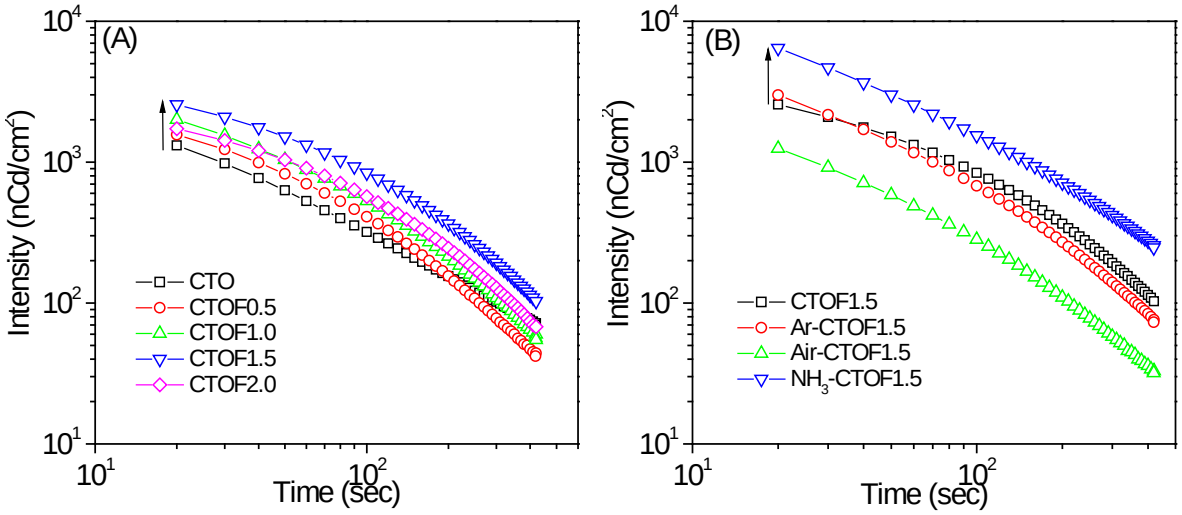

Figure shows the enhanced persistent luminescence of $CaTiO_3$:Pr^{3+} by fluorine substitution and annealing in NH_3 leading to an intensity improvement compared to $CaTiO_3$:Pr^3.

Improvement of $Ba_{0.5}Sr_{0.5}Co_{0.8}Fe_{0.2}O_{3-\delta}$ functional properties by tungsten doping

M.P. Popov, I.A. Starkov, S.F. Bychkov, A.P. Nemudry

Institute of Solid State Chemistry and Mechanochemistry, SB RAS
630128, Novosibirsk, Kutateladze str., 18;

Materials based on oxides with mixed ion-electron conductivity (MIEC) attract attention due to the possibility of their application in chemical, gas and energy industries. During the recent years, innovative technologies of oxygen separation from air are developing intensively. These technologies are based on selective oxygen permeability of MIEC oxides. In comparison with the basic methods of oxygen production, namely cryogenic and Swing Adsorption, the use of ceramic membranes theoretically allows one to obtain 100% pure oxygen [1]. In addition, the membrane technology can be easily built into high-temperature processes, such as partial oxidation of hydrocarbons, oxyfuel combustion etc.

As a rule, the materials for oxygen permeable membranes are perovskite related oxides based on strontium cobaltites and ferrites. At present the material having the composition $Ba_{0.5}Sr_{0.5}Co_{0.8}Fe_{0.2}O_{3-\delta}$ (BSCF) possesses the highest oxygen permeability [2]. A disadvantage of this compound is the occurrence of the phase transition from cubic to hexagonal perovskite at temperatures below 900^{o}C [3], which results in a substantial degradation of oxygen fluxes. Besides, BSCF is unstable in the atmosphere containing carbon dioxide.

In order to improve the functional properties of BSCF the method of isomorphous substitution of A and/or B cations is widely used [4]. We demonstrated previously that the isomorphous substitution of Co in $SrCo_{0.8}Fe_{0.2}O_{3-\delta}$ by highly charged cations M(V)=Nb, Ta with stable oxidation state allows one to enhance the chemical stability of membrane materials with the conservation of the high oxygen permeability. The substitution of Fe by cations M(VI)=Mo, W in $SrFeO_{3-\delta}$ is accompanied by an increase in the oxygen and electron conductivities [5]. Recently, this approach is used for modifying the properties BSCF and obtaining electrode $SrFe_{0.75}Mo_{0.25}O_{3-\delta}$ materials with high electronic conductivity.

In the present work we synthesized the samples having the composition $Ba_{0.5}Sr_{0.5}Co_{0.8-x}W_xFe_{0.2}O_{3-\delta}$ (x=0–0.1) and studied their functional properties. It is shown that the introduction of highly charged cation W^{6+} in the B–site, up to 2% inclusive, improves the functional properties of membrane materials: suppresses the phase transition from cubic to hexagonal perovskite at temperatures below 900^{o}C (Fig. 1), enhances the chemical stability of membranes in the atmosphere of carbon dioxide, and increases the long-term stability of oxygen fluxes (Fig. 2).

The continuous equilibrium «3-δ – lg pO_2 – T» diagrams obtained for the compositions $Ba_{0.5}Sr_{0.5}Co_{0.8}Fe_{0.2}O_{3-\delta}$ and $Ba_{0.5}Sr_{0.5}Co_{0.78}W_{0.02}Fe_{0.2}O_{3-\delta}$ allowed us to discover the phase transition P_1 (cubic perovskite phase, Pm3m) - P_2 (high-temperature perovskite phase, Fm3c) and to determine the dependence of the partial molar enthalpy of oxygen on the oxygen stoichiometry.

The data on selective oxygen permeability for gas-tight membranes $Ba_{0.5}Sr_{0.5}Co_{0.8}Fe_{0.2}O_{3-\delta}$ and $Ba_{0.5}Sr_{0.5}Co_{0.78}W_{0.02}Fe_{0.2}O_{3-\delta}$ of different thickness are presented; on this basis, it is concluded that the limiting stage of oxygen transport is the oxygen bulk diffusion.

The results obtained provide the evidence that membrane material doping with highly charged cations is a promising approach to improve the functional properties of membrane materials.

References:

[1] Tan X., Wang Z., Meng B., Meng X., Li K. (2010) J. Membr. Sci. 352:189-196.
[2] Shao Z.P., Yang W.S., Cong Y., Xiong G.X. (2000) J. Membr. Sci. 172:177-188.
[3] Švarcová S., Wiik K., Tolchard J., Bouwmeester H.J.M., Grande T. (2008) SSI. 178:1787–1791.
[4] Leo A., Liu S., Diniz da Costa J.C. (2009) J. Membr. Sci. 340:148–153.
[5] Markov A. A., Savinskaya O. A., Patrakeev M. V., Nemudry A. P., Leonidov I. A., Pavlyukhin Yu. T., Ishchenko A. V., Kozhevnikov V. L. (2009) J. Solid State Chem. 182:799–806.

Figures:

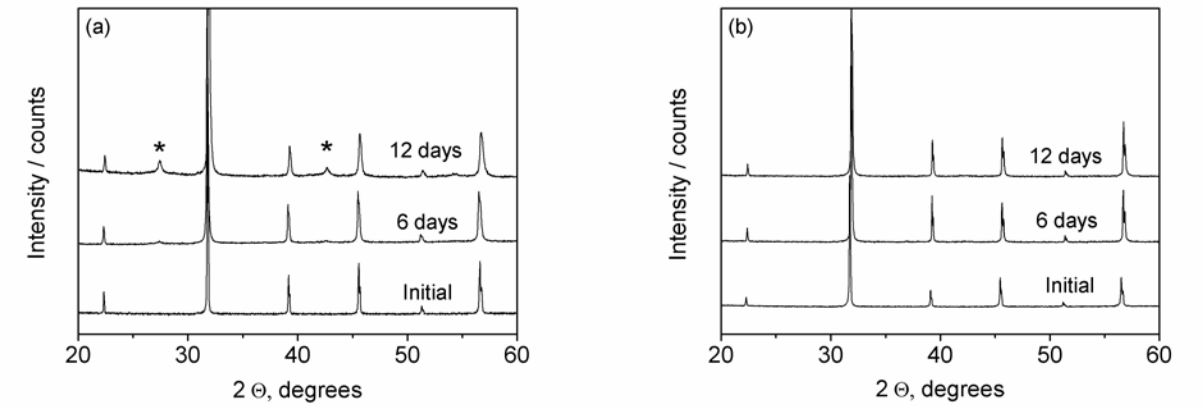

Fig. 1. *Ex situ* X-ray diffraction data for BSCF (a) and BSCFW2 (b) materials obtained after different exposure at 700°C in pure oxygen. The observed reflexes of the evolving 2H - phase are marked with an asterisk.

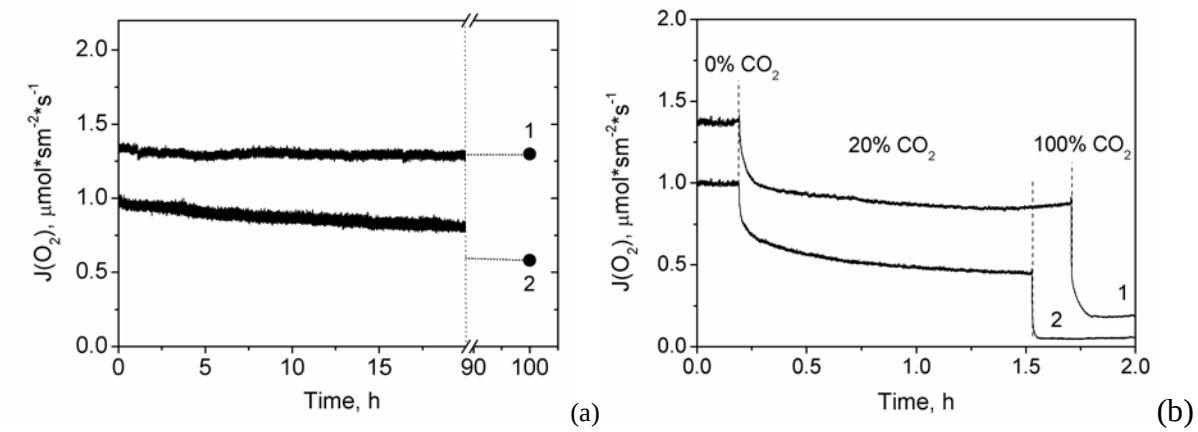

Fig. 2. Long-term stability test of BSCFW2 (1) and BSCF (2) membranes (L=1.6 mm, T=800°C) in pO_2=0.6 atm (a) and CO_2 –containing atmosphere (b).

Ceramic-Carbonate Dual Phase Membranes on Supports of Different Pore Structure for CO_2 Separation at High Temperatures

J. Ortiz-Landeros,[a] Y.S. Lin[b]

[a]Departamento de Ingeniería en Metalurgia y Materiales,
Escuela Superior de Ingeniería Química e Industrias Extractivas, IPN,
UPALM, México DF CP 07738, Mexico;

[b]School for Engineering of Matter, Transport and Energy
Arizona State University
Tempe, AZ 85260, USA.

Among the potential technologies considered for CO_2 mitigation, membrane-based separation processes are a promising alternative from the point of view of the selective separation of CO_2 from stationary sources. For instance, in the case of electricity power plants, the application of a high temperature carbon dioxide perm-selective membrane could offer potential for pre- and post-combustion CO_2 separation [1-3], wherein concentrated CO_2 can be subsequently use as a carbon feedstock for the synthesis of different chemicals [4]. Dual-phase membranes made of an oxygen ion conductive ceramic phase and a molten carbonate phase are perm-selective to carbon dioxide at high temperatures. Research conducted was focused on the fabrication and CO_2 permeation-separation studies of tubular dual-phase membranes composed of samarium doped ceria (SDC) and eutectic Li_2CO_3-Na_2CO_3 phases. Highly porous SDC supports with formula $Ce_{0.8}Sm_{0.2}O_{2-\delta}\square$ and different pore microstructures were prepared by pressing powder mixtures of SDC-graphite followed by sintering. Graphite powder acts as pore forming agent and supports with interconnected open porosity and adequate pore volume are obtained by sintering high temperature. The porosity to tortuosity ratios and pore volume for the SDC supports were characterized. The direct infiltration method allows complete filling of the ceramic support pores by the molten carbonate. CO_2 permeance of the obtained dual-phase membranes increases by using the supports prepared with additions of graphite.

The permeation results are explained based on the estimated total conductance which in turn, relates both, the effective carbonate and oxygen ionic conductivities of the membrane. Therefore, results suggest that the CO_2 permeance of the dual-phase membrane is controlled not only by the intrinsic oxygen and carbonate ionic conductivities of the ceramic and carbonate phases, but also by the membrane microstructure features such as porosity and solid microstructure of ceramic support. Tubular membranes are stable in CO_2 and H_2 containig environments and exhibit carbon dioxide perm-selectivity when are exposed to a CO_2/H_2 and CO_2/N_2 gradients. This investigation demonstrates the feasibility of the dul-phase membrane concept to the potential design of perm-selective membranes and membrane reactors for hydogen purification and dry reforming of methane.

References:

[1] P. Luis, T. Van Gerven, B. Van der Bruggen, Recent developments in Membrane-based technologies for CO_2, *Progress in Energy and Combustion Sci.* **38** (2012), 419.

[2] Anderson M.; Wang H.; Lin Y.S. Inorganic membranes for carbon dioxide and nitrogen separation. *Rev. Chem. Eng.*, **28** (2012) 101.

[3] X. Dong, J. Ortiz-Landeros, Y. S. Lin, An asymmetric tubular ceramic-carbonate dual phase membrane for high temperature CO_2 separation, *Chem. Comm.*, **49** (2013) 9654.

[4] Kai Man Kerry Yu, Igor Curcic, Joseph Gabriel, and Shik Chi Edman Tsang, Recent advances in CO_2 capture and utilization, *ChemSusChem.*, **1** (2008) 893.

Figure:

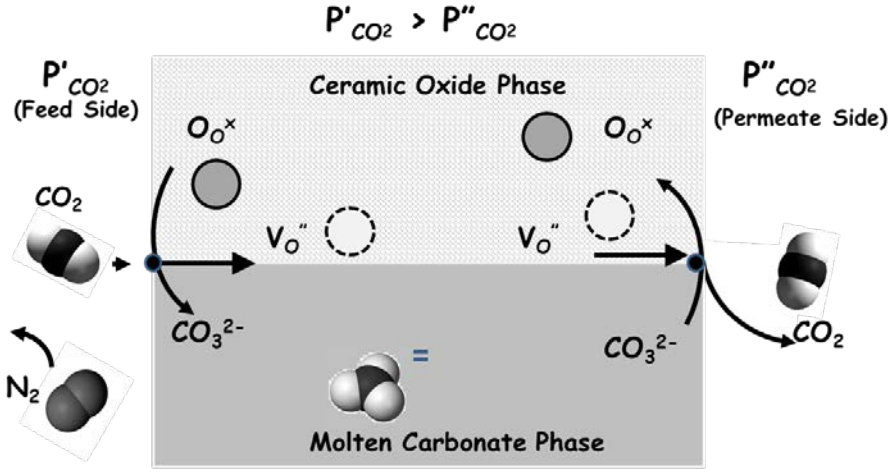

Pictorial representation of the concept of the ceramic-carbonate dual-phase membrane for CO_2 separation at high temperature

Oxidation Kinetics of Thin Metal Films

Yeliz Unutulmazsoy, Rotraut Merkle, Joachim Maier and Jochen Mannhart
Max Planck Institute Solid State Research, Stuttgart, Germany

The growth of oxide layers on metals is determined by formation and migration of point defects in the forming oxide layer and thus is an issue of fundamental importance. So far, mainly oxidation kinetics of thick metal films, crystals and bulk samples were investigated in the literature. The oxidation of thin metal films on insulating substrates can easily be monitored by measuring the conductivity of the remaining metal. The main interest is to understand the processes that limit the oxide growth (e.g. surface reaction or chemical diffusion), and also to increase or decrease the reaction rate for applications.

In this work, during the oxidation of metal films on Al_2O_3 substrates in a tube furnace, the resistance changes were measured by electrical impedance spectroscopy and fitted with an equivalent circuit model. The oxide thickness is calculated from the resistance values. Oxide growth follows the parabolic rate law of oxidation for Cr, Al, Ti, V. Zn, Ni and Co film samples with a thickness typically ranging from 10-150 nm. Thus the rate determining process of the oxidation of these metal films is chemical diffusion through the oxide layer according to the Wagner theory [1]. Ni and Co have a higher oxide growth rate than Cr, Al, Ti, V and Zn. The oxidation rate constant of Ni is not changed by applying different conditions such as different pO_2, UV illumination, ozone exposure and varying metal film thickness. This confirms the validity of parabolic rate law of oxidation for the samples with 10-150 nm thickness in the temperature range of 250-500 °C.

Comparison of diffusion coefficients for single crystalline NiO and polycrystalline NiO (grain size is 0.16-1 µm) from previous studies [2] and the present results with polycrystalline films having small grains (10-20 nm) shows that when the grain size is decreased, the effective diffusion coefficient is increased from $\approx 10^{-18}$ to 10^{-14} cm^2/s because of fast Ni diffusion along the grain boundaries.

Ni diffusion in NiO is mainly controlled by singly and doubly ionized Ni vacancies (V_{Ni} ‘,V_{Ni}‘‘) [3]. Thus, donor doping of NiO (e.g. doping with Al, Cr, etc.) is expected to increase the reaction rate by increasing the defect concentration in the oxide [4]. Therefore, oxidation of Cr doped Ni samples with low doping concentrations (< 1% wt.) are also investigated.

References:

[1] C. Wagner, Zeitschrift für Physikalische Chemie, Vol. B21, 1933, pp. 25-41
[2] A. Atkinson, R. I. Taylor, Journal of Material Science, Vol. 13, 1978, pp. 427-432
[3] Z. M. Jarzebski, S. Mrowec, Oxidation of Metals, Vol. 1, No 2, 1969, pp. 267-277
[4] H.V. Atkinson, Oxidation of Metals, Vol. 24, Issue 3-4, 1985, pp.177-197

Electrochemical characterization of Pr_2CuO_4-$Ce_{0.9}Gd_{0.1}O_{1.95}$ composite cathodes for IT-SOFCs

L.M. Kolchina,[a] N.V. Lyskov,[b] M.Z. Galin,[b] A.O. Demidovich, [a] L.S. Leonova,[b] G.N. Mazo[a]

[a]Moscow State University, Leninskie Gory, Moscow, 119991, Russia;
[b]Institute of Problems of Chemical Physics RAS, Acad. Semenov av. 1, Chernogolovka, 142432, Russia.

Recently, intermediate temperature solid oxide fuel cells (IT-SOFCs) operating at 500-700°C attract much attention as alternative power sources due to a high efficiency and much lower production of pollutants [1-3]. Pr_2CuO_4 (PCO) is regarded as a promising cathode material due to its high electronic conductivity ($\sigma_{900\ ^oC}$ ~ 100 S/cm), thermal and chemical stability, good thermal compatibility (TEC = 11.8×10^{-6} K^{-1}[4]) with gadolinium-doped ceria oxide (TEC = 12.4×10^{-6} K^{-1} for $Ce_{0.9}Gd_{0.1}O_{1.95}$ [5]) and relatively low area specific resistance (ASR = 1.7 Ω•cm^2 at 700°C) [6]. Addition of ionic-conducting phase such as Gd_2O_3-doped CeO_2 (GDC) into the electronic-conducting electrode material could enhance the cathode performance due to increasing of the TPB length. In present work, the influence of PCO-GDC cathode composition and its microstructure on the electrochemical behavior of composite electrodes was determined.

PCO-GDC*x* composites were prepared by ball-milling for 1 h under heptane of PCO powder with an appropriate amount of GDC (*x* showed GDC content which varied from 20 to 50 wt. %). The PCO powder was synthesized by a freeze-drying technique at 700°C for 4 h under open air conditions. Phase purity of the sample was checked by X-ray powder diffraction (XRD). Electrochemical characterization of electrode materials for the oxygen reduction was carried out using GDC electrolyte in a symmetrical cell configuration (electrode/CGO/electrode). Measurements were performed by AC impedance spectroscopy at the OCV conditions in the temperature range of 500-900°C at the oxygen partial pressures (pO_2) of 10^{-2}-0.21 atm.

The PCO/GDC/PCO electrochemical cells with different electrode thickness were prepared for minimization of area specific resistance (*ASR*). The lowest *ASR* value (0.57 Ω•cm^2 at 700°C) was achieved at the electrode thickness of 20 μm. Such electrode thickness was used for comparison of electrochemical characteristics of pure PCO electrodes with PCO-GDC composite electrodes.

To understand the electrochemical processes at the electrode/electrolyte interface and to define the rate-determining steps of oxygen reduction reaction (ORR), temperature and pressure dependences of *ASR* were examined. Isotherm log-log plots of *ASR* values vs. oxygen partial pressure for PCO-GDC20 (composition PCO with 20 wt. % GDC) are shown in Fig. 1. Dependences are linear, and the ASR varies with oxygen partial pressure according to the equation:

$$R \propto p_{O_2}^{-n}, \quad (1)$$

where *n*-value contains information about the type of species involved in ORR [7]. The rate-determining step of ORR in case of PCO-GDC20 composite electrode could involve both the

charge transfer at the electrode/electrolyte interface (n = ¼) and the dissociation of adsorbed molecular oxygen into the atomic oxygen species (n = ½) in the temperature range of 670-730°C.

The influence of GDC addition on microstructure and electrochemical behavior of composite electrodes was determined. It was shown that GDC addition decreased ASR value due to TPB extending and enhancing of the catalytic activity for oxygen reduction. The ASR for the optimum composition (33 wt. % GDC) is 0.41 Ω•cm^2 at 700°C that is 1.4 times lower than that for pure PCO. The obtained results allow to consider the PCO-GDC33 composite as a promising cathode material for IT-SOFCs.

This work was partially supported by Russian Foundation for Basic Research (Grant No. 14-08-01260) and MSU-development Program up to 2020.

References:

[1] B.C.H. Steele, A. Heinzel, *Nature*, **414** (2001) 345.
[2] A. Aguadero, L. Fawcett, S. Taub, R. Woolley, K.T. Wu, N. Xu, J.A. Kilner, S.J. Skinner, *J. Mater. Sci.*, **47** (2012) 3925.
[3] A. Tarancon, M. Burriel, J. Santiso, S.J. Skinner, J.A. Kilner, *J. Mater. Chem.*, **20 (**2010) 3799.
[4] M.S. Kaluzhskikh, S.M. Kazakov, G.N. Mazo, S.Ya. Istomin, E.V. Antipov, A.A. Gippius, Yu. Fedotov, S.I. Bredikhin, Y. Liu, G. Svensson, Z. Shen, *J. Solid State Chem.*, **184** (2011) 698.
[5] H. Hayashi, M. Kanoh, C.J. Quan, H. Inaba, S. Wang, M. Dokiya, H. Tagawa, *Solid State Ionics*, **132** (2000) 227.
[6] N.V. Lyskov, M.S. Kaluzhskikh, L.S. Leonova, G.N. Mazo, S.Ya. Istomin, E.V. Antipov, *Int. J. Hydrogen Energy*, **37** (2012) 18357.
[7] Y. Takeda, R. Kanno, M. Noda, Y. Tomida, O. Yamamoto, *J. Electrochem. Soc.*, **134** (1987) 2556.

Figure:

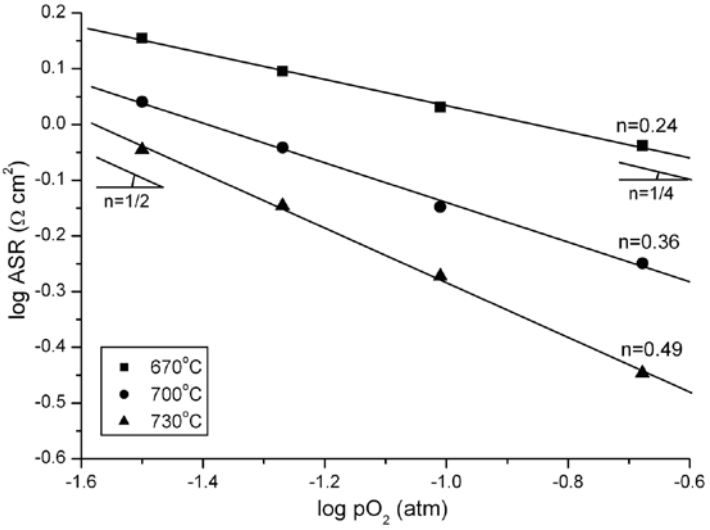

Fig.1. Log-log plots of the *ASR* values for PCO-GDC20 composite electrode vs. oxygen partial pressure at various temperatures (value over the lines corresponds to the slope of resistance curve).

Nanostructuring of MIEC oxides $SrCo_{0.8-x}Fe_{0.2}M_xO_{3-\delta}$ (M = Ta, Nb; $0 \le x \le 0.1$) with high oxygen transport properties

I.V. Belenkaya, A.A. Matvienko, A.P. Nemudry

Institute of Solis State Chemistry and Mechanochemistry, Siberian Branch of Russian Academy of Sceince, Novosibirsk.

Nonstoichiometric oxides with perovskite structure based on $SrCo_{0.8}Fe_{0.2}O_{3-\delta}$ are promising materials for such applications as oxygen separation from air, oxygen storage and transport, gas purification of oxygen impurities [1]. The reasonable oxygen exchange in MIEC oxides for practical purposes can be reached only at temperatures above 600°C. However the reasons of high oxygen mobility are not completely clear. One believes that high transport properties in nonstoichiometric perovskite compounds are related to high concentration of disordered oxygen vacancies of high temperature phase. From the other hand, perovskite type oxides are known to have a tendency to form a microdomain structure, which provides a high concentration of extended defects (domain, antiphase and twin boundaries) [2, 3]. Interactions of oxygen vacancies with the extended defects can result in formation of channels with enhanced oxygen diffusion along the domain boundaries, that can explain unique properties of such materials [4, 5]. In this work we investigate the microstructure of materials $SrCo_{0.8-x}Fe_{0.2}M_xO_{2.5+y}$ (M=Nb, Ta; $0 \le x \le 0.2$) at low and high temperatures to determine the real structure of high temperature phase.

Synthesis of samples $SrCo_{0.8-x}Fe_{0.2}M_xO_{3-\delta}$ (M = Ta, Nb; $0 \le x \le 0.1$) was carried out with ceramic method. To decrease oxygen stoichiometry as prepared samples were annealed at 950° in a quartz ampoule in dynamic vacuum ($P \sim 10^{-5}$ атм) for 2 h followed by quenching to liquid N_2. The oxygen content in the samples was determined by iodometric titration method. Phase analysis of the samples was carried out by X-ray diffraction at diffractometer Bruker D8 Advance (Cu-Kα radiation). Microstructural studies were performed using high-resolution transmission electron microscopy. The quenched samples $SrCo_{0.8-x}Fe_{0.2}M_xO_{3-\delta}$ (M = Ta, Nb; $0 \le x \le 0.1$) were shown to consist of coherently jointed domains with brownmillerite structure oriented by 90° to each other. Increase in dopant concentration results in decrease in domain sizes. The observed domain orientations are in good agreement with possible domain orientations predicted by theoretical-group analysis, which is typically used for ferroics.

To study high temperature structure of $SrCo_{0.8-x}Fe_{0.2}M_xO_{3-\delta}$ (M = Ta, Nb; $0 \le x \le 0.1$) different *in-situ* high-temperature techniques were used. X-ray diffraction experiments were carried out at high temperatures and oxygen partial pressure $P_{O2} \sim 10^{-4}$ atm. It was shown, that in doped compounds phase transition from brownmillerite phase to high temperature perovskite phase occurs at lower temperatures and acquires diffuse behaviour with increase of dopant concentration in comparison with pure $SrCo_{0.8}Fe_{0.2}O_{3-\delta}$. At dopant concentration $x \ge 0.1$ there is no brownmillerite structure in all temperature range. The decrease in phase transition temperature of doped materials allows us to carry out *in-situ* high temperature Mössbauer spectroscopy measurements of high temperature perovskite phase of investigating materials. Mössbauer spectra reveal that at high temperatures ...OTOT...ordering, which is typical for brownmillerite structure, is observed. The theoretical

calculations of electronic structure made by DFT show that state with ...OTOT...ordering is more favorable than disordered state at high temperatures and low oxygen partial pressure.

Thus, obtained results let us propose that structure of high temperature perovskite phase of nonstoichiometric oxide $SrCo_{0.8}Fe_{0.2}O_{3-\delta}$ has a complex microstructure, based on brownmillerite type domains with a very small sizes, that can explain anomaly high oxygen transport properties in this material.

Acknowledgement:
The work was supported by RFBR project (N 14-03-31240), Integration project of SB RAS (N 104), by grants of the President of the Russian Federation for support of leading scientific schools (project NS-2938.2014.3).

References:

[1] J. Sunarso, S. Baumann, J. M. Serra, W.A.Meulenberg, S. Liu, Y.S. Lin, *J. Membrane Sci.*, **320** (2008) 13.
[2] M. A. Alario-Franco, M.J.R. Henche, M. Vallet, J. M. Gonzalez-Calbet, J.C. Grinier, A. Wattiaux, P. Hagenmuller, *J. Solid State Chem.*, **46** (1983) 23.
[3] Y. Ito, R.F. Klie, N. D. Browning, *J. Am. Ceram. Soc*., **85** (2002) 969.
[4] A. Aird and E.K.H. Salje, *J. Phys. Condens. Matter* **10** (1998) 377.
[5] A. Aird and E.K.H. Salje, *Eur. Phys. J.* **B15** (2000) 205.

Figure:

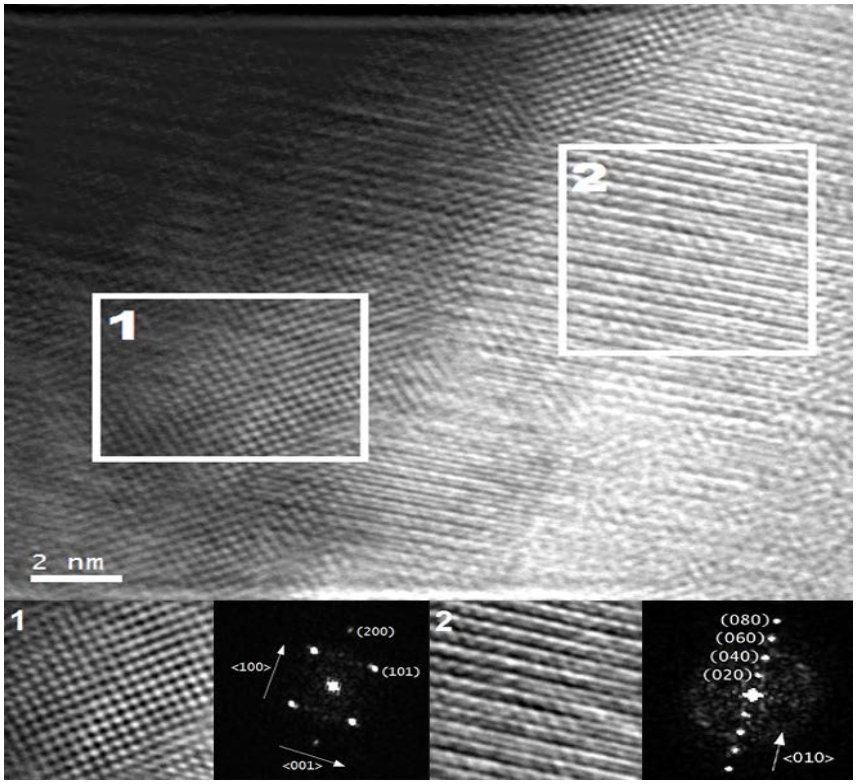

Fig.1. Nanodomain structure of material $SrCo_{0.7}Fe_{0.2}Nb_{0.01}O_{2.58}$.

The influence of oxygen nonstoichiometry on the oxygen permeability of MIEC membranes

Ilya A. Starkov, Sergey F. Bychkov, Alexandr P. Nemudry

Institute of Solid State Chemistry and Mechanochemistry,
Siberian Branch of Russian Academy of Science, Novosibirsk, Russia.

Oxides with mixed ion-electron conductivity (MIEC) are attracted the attention due to their prospective of using as membrane materials for producing pure oxygen [1], catalytic conversion of methane to synthesis gas [2], as a sorbents for oxy-fuel combustion [3], oxygen sensors [4] and electrodes for solid oxides fuel cells [4].

At the moment, perovskite $SrCo_{0.8}Fe_{0.2}O_{3-\delta}$ (SCF) is one of the record-breakers in oxygen permeability [6]. However, the reasons for high oxygen permeability of SCF still are not clear. There is a large scatter in the literature experimental data which prevents the development of a reliable conception of the oxygen permeability mechanism in the MIEC membranes and advance in technological aspects. Thus, understanding the factors that can ensure high oxygen permeability of SCF continues to be a challenging and actual problem.

Earlier, we have developed a new oxygen release technique and a mathematical model to obtain a detailed equilibrium "T – pO_2 – δ" diagrams [7]. Due to kinetic studies of the oxygen release from SCF perovskite in isostoichiometric mode we have shown that the activation energy of the oxygen release from SCF is a function of the oxide stoichiometry [8].

The aim of the work was study the oxygen permeability of MIEC membranes as a function of oxygen nonstoichiometry.

In the present work we have shown that the dependence of oxygen fluxes which traditionally presented as a function of the oxygen partial pressure (Fig. 1) are dependent on on the oxygen nonstoichiometry. We have shown that the non-Arrhenius dependence of oxygen fluxes through the membranes (Fig. 2, left), which usually interpreted as the "order-disorder" transition or change in rate-determining step of oxygen permeability, is associated with the dependence of the effective activation energy on oxide nonstoichiometry which varies with temperature (Fig. 2, right). Experimental data obtained by the oxygen permeability is consistent with experimental relaxation data on oxygen release obtained earlier [8].

The work was supported by RFBR project (N 13-03-00737), Integration project of SB RAS (N 104), by grants of the President of the Russian Federation for support of leading scientific schools (project NS-2938.2014.3).

References:

[1] Tan X., Wang Z., Meng B., Meng X., Li K., *J. Membrane Sci.*, **352 (**2010) 189.
[2] Wang H.H., Tablet C., Schiestel T., Werth S., Caro J., *Catal. Commun.*, 7 (2006) 907.
[3] Rui Z., Ding J., Li Y., Lin Y.S., *Fuel*, **89** (2010) 1429.
[4] Mori M., Itagaki Y., Sadaoka Y., *Sensors and Actuat. B: Chem.*, **163** (2012) 44.

[5] Meng X., Meng B., Tan X., Yang N., Ma Z.-F., *Mater. Res. Bull.*, **44** (2009) 1293.
[6] Teraoka Y., Zhang H.-M., Yamazoe N, *Chemistry Letters*, **14** (1985) 1367.
[7] I. Starkov, S. Bychkov, A. Matvienko, A. Nemudry, *Phys. Chem. Chem. Phys.*, (2013) DOI: 10.1039/C3CP52143E.
[8] I. Starkov, S. Bychkov, A. Matvienko, A. Nemudry, *Chem. Mat.*, (2014) in press.

Figures:

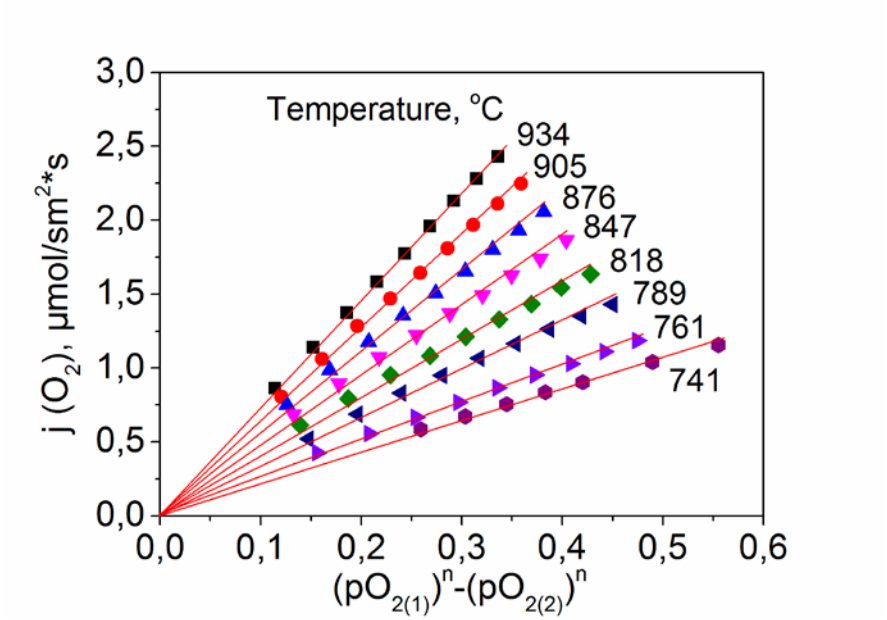

Fig. 1. Linearization of the oxygen permeability with the variation of n from 0.4 to 0.6. SCF dense membrane (h=1.89 mm).

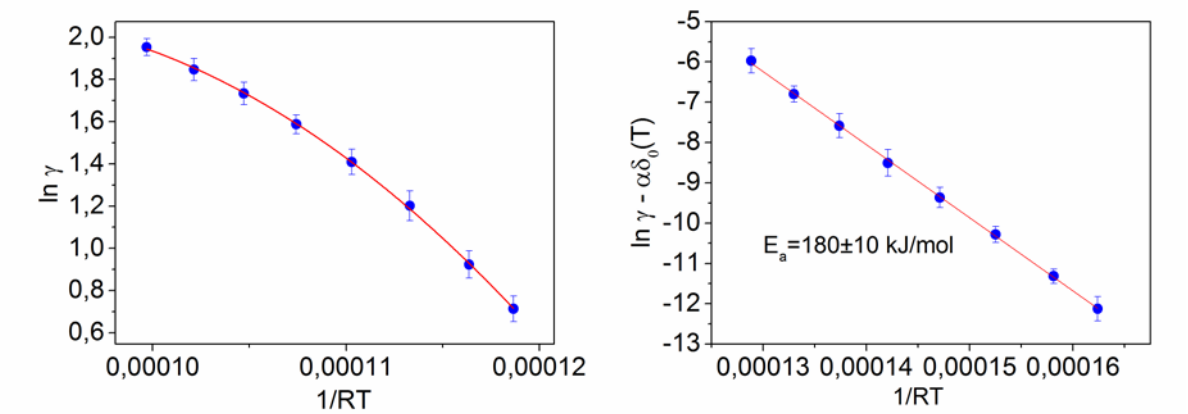

Fig. 2. Arrhenius dependence of oxygen transport for the SCF membrane: (left) – excluding the influence of oxygen nonstoichiometry; (right) – taking into account oxygen nonstoichiometry

The pO_2 relaxation study of oxygen exchange of the MIEC oxide in isostoichiometric mode.

Sergey F. Bychkov, Ilya A. Starkov, Stanislav A. Chizhik, Alexandr P. Nemudry

Institute of Solid State Chemistry and Mechanochemistry, SB RAS; 630128 Kutateladze 18, Novosibirsk, Russia;
bychkov@solid.nsc.ru

In the study of oxygen exchange of the nonstoichiometric oxides, methods based on the measurement of the relaxation rate of the electrical conductivity of oxide at a fixed change in the oxygen partial pressure pO_2 are generally applied. These methods are indirect and based on an assumed linearity between the change in the stoichiometry of the oxide and its conductivity. In processing the experimental data mathematical models which based on assumption that the gas composition changes very quickly and remains constant during the measurement of the conductivity relaxation are commonly used.

In our measurements new relaxation method based on the measurement of the relaxation rate of the oxygen partial pressure in a flow reactor is applied. pO_2 in the gas was measured by the zirconium oxide oxygen sensor. Measurements were carried out by changing the gas composition (oxygen, helium) at the reactor inlet. As shown in [1], the equilibration time of the porous oxide samples with the gas phase is determined by surface exchange rate which is in the case of $SrCo_{0.8}Fe_{0.2}O_{3-x}$ dependent on the initial and final stoichiometry of the oxide, wherein the oxygen partial pressure in the reactor is changing throughout the relaxation experiment. In interpreting the data in such circumstances, we have proposed a simple mathematical model based on the assumption of small deviations from equilibrium.

Feature of our measurements is to use fixed values of the initial and final stoichiometry (isostoichiometric approach) that have been set on the basis of the phase P-δ-T diagram (Fig.1), obtained earlier [2]. Isostoichiometric measurements provide a more reliable parameters for oxygen exchange between the oxide and the gas phase [3] (Fig.2, 3).

The work was supported by RFBR project (N 13-03-00737), Integration project of SB RAS (N 104), by grants of the President of the Russian Federation for support of leading scientific schools (project NS-2938.2014.3).

References:

[1] Ganeshananthan R.,Virkar, A.V., *J. Electrochem. Soc.*, **152** (2005) 1620–1628.
[2] Ilya Starkov, Sergey Bychkov, Alexander Matvienko and Alexander Nemudry, *Phys. Chem. Chem. Phys*, DOI: 10.1039/c3cp52143e.
[3] Ilya A. Starkov, Sergey F. Bychkov, Stanislav A. Chizhik, Alexandr P. Nemudry, *J. Chem. Mater.*, in press.

Figures:

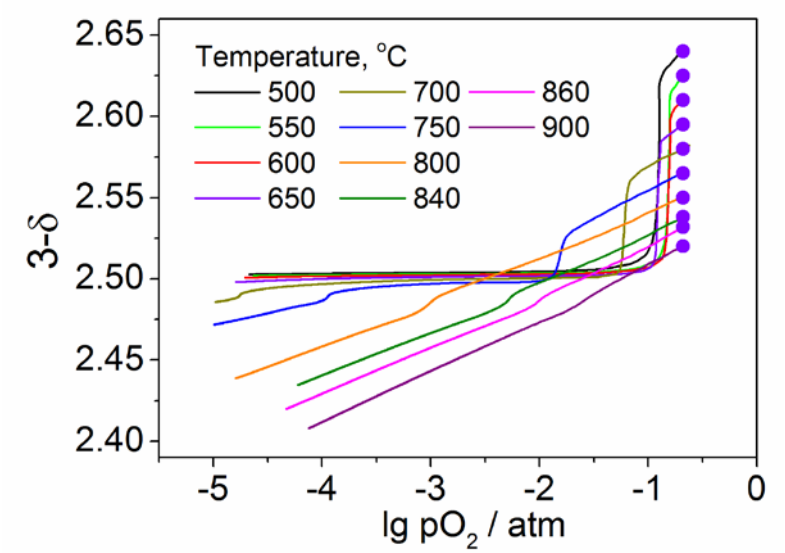

Fig.1. $SrCo_{0.8}Fe_{0.2}O_{3-x}$ sample. The equilibrium diagram "3-δ vs. lg pO_2"

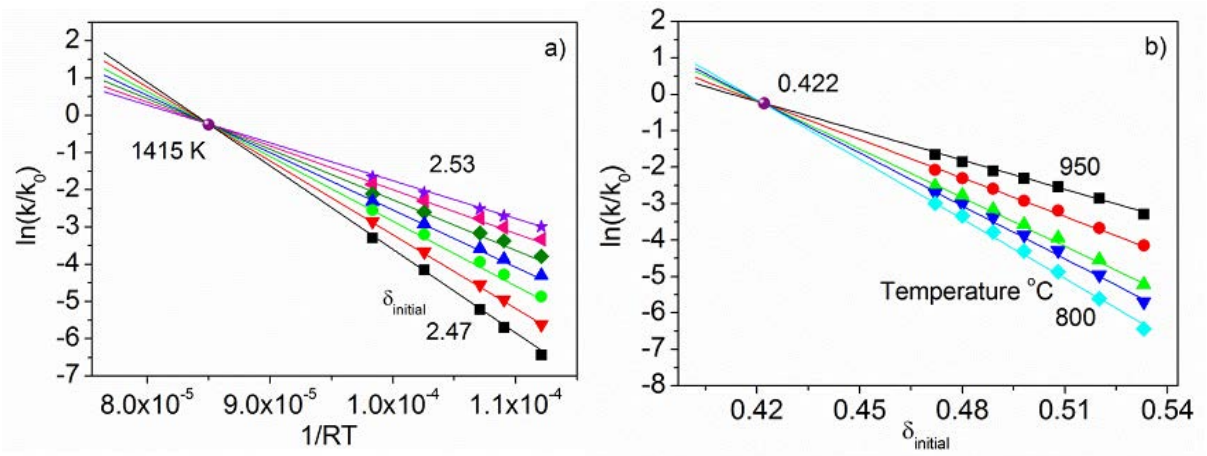

Fig.2. Experimental (symbols) and calculated (lines) values of the relaxation rate constant logarithm depending on the reciprocal temperature (a) and oxide stoichiometry (b).

Effect of B-site molybdenum doping on the transport properties of $SrCo_{0.8}Fe_{0.2}O_{3-\delta}$ oxides

Olga Savinskaya, Alexandr Nemudry

Institute of Solid State Chemistry and Mechanochemistry,
Siberian Branch of Russian Academy of Science, Novosibirsk
nemudry@solid.nsc.ru

Mixed ionic/electronic conducting perovskite oxides have several applications as materials for oxygen-permeable membranes. It is known that high mixed elec-tron/oxygen conductivity among the oxides is exhibited by $SrCo_{0.8}Fe_{0.2}O_{3-\delta}$. Substantial disadvantages of this compound are the phase transition brownmillerite-perovskite with changes in the oxygen content and its chemical instability in the reducing atmosphere which causes destruction of the membrane [1]. The standard way to modify the properties of solids is doping - isomorphic substitution of A and B cations in ABO_3 structure. As a rule, the best transport properties in doped derivatives are achieved with minimal concentrations of the cation substitution, providing stabilization of the cubic phase. It can be expected that the partial isomorphic substitution of B-cations by highly charged Mo^{6+} ions the stabilization of the cubic phase is achived at lower concentrations than in the case of substitution of 3+/4+ charged cations, so a negative effect of substitution on the transport properties can be reduced. Doping of highly charged cations increases the chemical stability of the materials at low pO_2 due to the stable oxidation state (VI) of dopants; reduces the degradation of membrane materials in the atmosphere of CO_2 due to the acidic properties of highly charged cations [2].

The aim of the present work was a detailed study of the effect of B-site molybdenum doping on the transport properties and stability of $SrCo_{0.8-x}Fe_{0.2}Mo_xO_{3-\delta}$ (SCFM) materials in the operating conditions of the catalytic membrane reactor.

Fig. 1 a shows the oxygen fluxes through SCFM membranes versus reciprocal temperature at a fixed partial pressure of oxygen at the feed side of the membrane (p_1 = 0.2 atm). According to the obtained data, an introduction to the SCF structure of highly charged Mo^{6+} cations leads to lower oxygen permeability. Note the increase in the mechanical stability of SCFM membranes at T<700 ^oC and low oxygen partial pressures pO_2 <0.01 atm. The operating conditions of SCF membrane are limited (T<700 ^oC, pO_2 <0.01 atm) as the decrease in temperature and pO_2 is accompanied by a phase transition "perovskite-brownmillerite» [3] and the destruction of the membrane. An interesting feature is also a nonlinear relationship of the oxygen flux on the reciprocal temperature. According to the literature data, nonlinear relationship can be related to the oxygen vacancy order–disorder transition or to the mixed surface exchange and bulk diffusion control. In order to determine the rate-limiting step of oxygen transport through SCFM membranes the dependencies of oxygen fluxes от oxygen partial pressure and membrane thickness were studied. Assuming the ideal mixing of J(He) and $J(O_2)$ fluxes in the reactor, pO_2 values at the permeate side of membranes were determined and the data were successfully linearized in the coordinates $J(O_2) - (p_1^n - p_2^n)$ with 0.2<n<0.5, where p_1, p_2 are oxygen partial pressures at the feed and permeate sides, respectively. According to the literature data, the variable power index n>0 can be related to a mixed surface exchange and bulk diffusion control or a sole surface exchange control [4].

Temperature dependence of the oxygen fluxes across SCFM (x=0.05) membranes with different membrane thickness L (1.35<L<3.20 mm) demonstrates thickness dependence of oxygen fluxes at T>750 ^{o}C (fig. 1 b). Such behavior indicates a mixed surface exchange and bulk diffusion control. Note the contribution of the surface exchange reactions to the overall oxygen permeation was observed to increase with decreasing temperature. The measurements of oxygen permeability through SCFM membranes in CO_2 atmosphere showed that introduction to the SCF structure of Mo^{6+} cations reduces degradation of materials in the CO_2 atmosphere due to the acidic properties of Mo^{6+} cations.

Acknowledgements:

The work was supported by RFBR project (N 14-03-31240), by grants of the President of the Russian Federation for support of leading scientific schools (project NS-2938.2014.3).

References:

[1] J. Sunarso, S. Baumann, J.M. Serra, W.A. Meulenberg, S. Liu, Y.S. Lin, J.C. Diniz da Costa, *J. Membr. Sci.*, **320** (2008) 13.
[2] O.A. Savinskaya, A.P. Nemudry, *J. Membr. Sci.*, (2014) http://dx.doi.org/10.1016/j.memsci.2014.01.074.
[3] I.A. Starkov, S. F. Bychkov, S. A. Matvienko, A. P. Nemudry, *PCCP*, DOI: 10.1039/C3CP52143E (2013).
[4] K. Huang, J. B. Goodenough, J. Electrochem. Soc., **148 (5)** (2001) 203.

Figures:

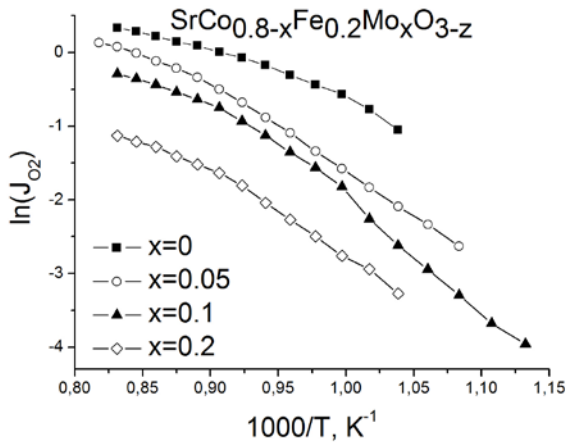

Fig. 1 a. Oxygen permeability of SCFM ceramic membranes versus reciprocal temperature at p_1 = 0.2 atm.

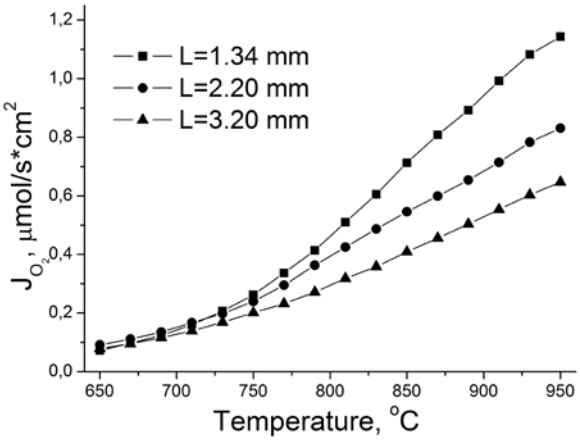

Fig. 1 b. Temperature dependence of the oxygen fluxes across SCFM (x=0.05) membranes with different membrane thickness (p_1 = 0.2 atm).

Thermal recrystallization of natural Th-bearing metamict Lovchorrite

Qiuxiang Cao[a, b], S. V. Krivovichev[a], B. E. Burakov[c], Xiaodong Liu [b]

[a] Saint-Petersburg State University, Universitetskaya emb. 7/9, 199034, St.-Petersburg, Russia;
[b] East China Institute of Technology, Guanglan Road, 418, 330013, Nanchang, Jiangxi, China;
[c] V.G. Khlopin Radium Institute, 2-nd Murinskiy Ave. 28, 194021, St.-Petersburg, Russia.

Metamict minerals may contain significant quantities of U and Th that lead to the transition from the crystalline to the aperiodic, amorphous state [1]. Amorphization occurs mainly due to the effects of heavy-particle irradiation and their crystalline structures can be reconstituted by heating [2]. The metamict state raised important fundamental questions concerning the stability of different structure types in a radiation field [3,4]. The study of metamict minerals is very important to understand the behavior of Th-admixtures (as analogues of artificial actinides such as Pu, Np, Am) during self-irradiation of host-phases and possible recovery of crystalline lattices under heating or other impacts. Initially Th form solid solutions in the crystalline structures of "fresh" host-phases but further metamictization and (or) recovery of damaged structure can be accompanied by destruction of solid solutions and formation of separate phases of radionuclides. This process should be studied in detail because it may essentially increase the migration of radionuclides.

We have studied a large (1-3cm in size) and relatively homogeneous sample of natural metamict lovchorrite (figure 1a). Untreated and annealed in air at different temperatures in order to initiate recrystallization were analyzed in comprison by precise X-ray powder diffraction (XRD), electron microprobe (EMPA) and scanning electron spectroscopy (SEM). The diffraction data for lovchorrite indicated the mineral not to be completely metamict (figure 2). The recrystallization of Rinkite structure (ICDD (PDF-2/Release 2011 RDB):01-071-0440) was continuously monitored with temperature increase starting at 500 ^{o}C in air. The Rinkite phase was stable up to 1000 ^{o}C. However, several other phase (fluobritholite (ICDD (PDF-2/Release 2011 RDB):01-057-0908) - light color and cuspidine (ICDD (PDF-2/Release 2011 RDB):01-013-0410) - black color) started to crystallize at 1100 ^{o}C (figure 1b).

The results obtained demonstrate very complex behavior of single-phase Th-bearing solid solution based on lovchorrite under self-irradiation and recrystallization. Long-term radiation damage may cause metamictization of single-phase minerals without destruction of the solid solution. However, recrystallization caused by heating of the metamict mineral may cause formation of new separate crystalline phases resulting in destruction of the initially homogeneous solid solution. This process is a subject of potential serious concern because it may be accompanied by segregation of Th (and other actinides for artificial minerals) into separate phases. This phenomenon should be taken into account in order to develop optimal ceramic waste-forms for actinide immobilization.

References:

[1] R.C. Ewing, B.C. Chakoumakos, G.R. Lumpkin, T. Murakami. *Mater. Res. Soc. Bull.*, **12(4)** (1987) 58.
[2] D. Malczewski, J.E. Frackowiak, E.V. Galuskin. *Hyperfine Interact.*, **166** (2005) 529.
[3] W.J. Weber, R.C. Ewing, C.R.A. Catlow, T. Diaz de la Rubia, L.W. Hobbs, C. Kinoshita, Hj. Matzke, A.T. Motta, M. Nastasi, E.H.K. Salje, E.R. Vance and S.J. Zinkle. *J. Mat. Res.* **13** (1998) 1434.
[4] B.E. Burakov, M.I. Ojovan, W.E. Lee Crystalline materials fo actinide immobilization. Imperial College Press, Materials for Engineering, Vol.1. (2010)

Figures:

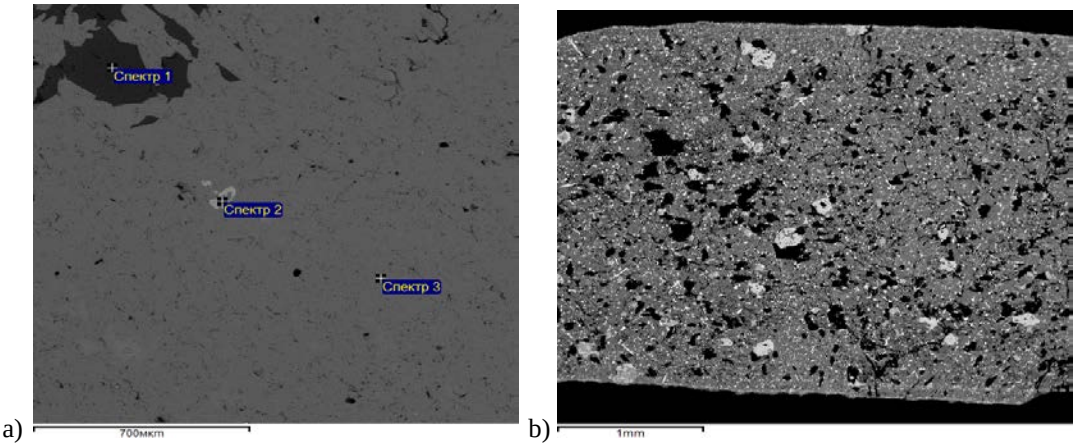

Figure 1. SEM BSE images of natural lovchorrite: a) initial metamict sample; b) fully recrystallized sample after annealing in air at 1100 °C for 1 hour.

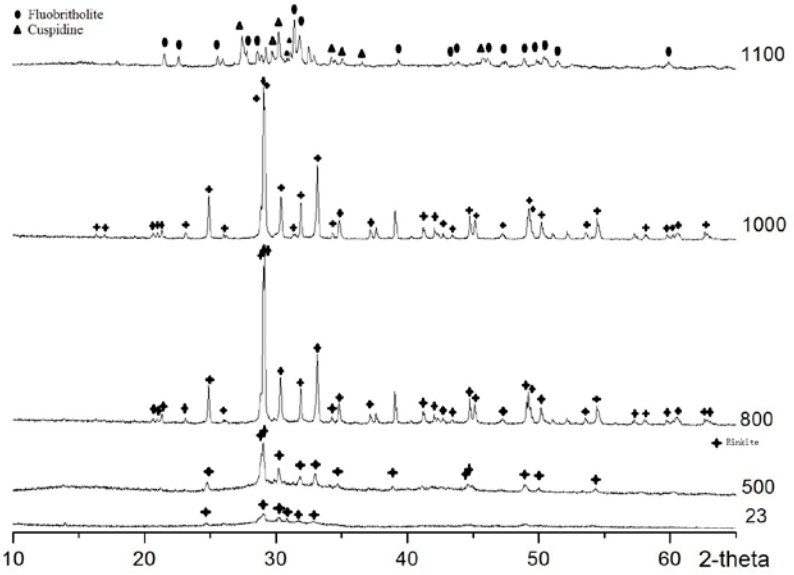

Figure 2. Diffraction patterns of the samples of metamict lovchorrite untreated (room temperature - 23 °C) and annealed (500, 800, 1000 and 1100 °C). The dots denote peak positions of the corresponding phases.

Thermal recrystallization of natural Th-U-bearing fully metamict Y-Fe-niobate

Qiuxiang Cao[a,c], A.I. Isakov[a,b], S.V. Krivovichev[a], B.E. Burakov[b], Xiaodong Liu[c]

[a] Saint-Petersburg State University, Universitetskaya emb. 7/9, 199034, St.-Petersburg,Russia
[b]V.G. Khlopin Radium Institute, 2-nd Murinskiy Ave. 28, 194021, St.-Petersburg, Russia
[c]East China Institute of Technology, Guanglan Road, 418, 330013, Nanchang, Jiangxi, China

Natural minerals may contain significant quantities of U and Th that lead to the transition from the crystalline to the so called "metamict" or aperiodic, amorphous state [1]. Amorphization occurs mainly as a result of heavy-particle irradiation. Damaged crystalline structures can be reconstituted by heating [2]. Metamict minerals are considered as natural analogues of aged ceramic nuclear waste-forms [2-4]. The study of metamict minerals is very important to understand the behavior of Th-U-admixtures (as analogues of artificial actinides such as Pu, Np, Am) during self-irradiation of host-phases and possible recovery of crystalline lattices under heating or other impacts. Initially Th and U form solid solutions in the crystalline structures of "fresh" host-phases but further metamictization and (or) recovery of damaged structure can be accompanied by destruction of solid solutions and formation of separate phases of radionuclides. This process should be studied in detail because it may essentially increase the migration of radionuclides.

A large grain (2 x 3 x 2 cm in size) of fully metamict Y-Fe-niobate from granite pegmatites (Karelia, Russia) was selected for this study. The sample was dense, homogeneous (Figure 1a), conchoidal-fractured and it had no faces. It was observed that mineral was fully X-ray amorphous (Figure 2). The average chemical composition obtained by EMPA during our previous research was (wt. %): Nb_2O_5 – 42.6; Ta_2O_5 – 4.4; TiO_2 – 9.2; UO_3 – 4.4; ThO_2 – 1.0; MnO – 1.3; FeO – 19.4; Y_2O_3 – 16.6 [5]. The pieces of the sample were annealed in air and vacuum at 400 ^oC, 700 ^oC, 1000 ^oC, 1100 ^oC and 1200 ^oC. Then all materials obtained were studied by XRD, SEM, EMPA and other methods. XRD results showed that recrystallization in vacuum and air started at 400 ^oC and 700 ^oC, respectively. Further annealing at 1100-1200 ^oC in all atmospheres caused the change of phase composition (Tab. 1).

The results obtained demonstrate very complex behavior of single-phase Th-U-bearing solid solution based on Y-Fe-niobate under self-irradiation and recrystallization. Long-term radiation damage may cause metamictization of single-phase minerals without destruction of the solid solution. However, recrystallization caused by heating of the metamict mineral may cause formation of new separate crystalline phases resulting in destruction of the initially homogeneous solid solution. This process is a subject of potential serious concern because it may be accompanied by segregation of U, Th (and other actinides for artificial minerals) into separate phases. This phenomenon should be taken into account in order to develop optimal ceramic waste-forms for actinide immobilization.

Table 1.

T, °C	atmosphere			
	air	**air-HT**	**vacuum**	**argon**
25	amorphous	amorphous	amorphous	amorphous
400	amorphous	amorphous	$FeNb_2O_6$ mon	Not studied
700 (750 for Ar)	$FeNb_2O_6$	$FeNb_2O_6$	$FeNb_2O_6$ mon $YNbO_4$	$FeNb_2O_6$ $YNbO_4$
1000	$FeNbO_4$ orth $YNbO_4$ $YTaO_4$ Ta_2O_5	$YTaO_4$ $FeNbO_4$ orth $FeNbO_4$ tetrag Ta_2O_5	$FeNbO_4$ tetrag $YNbO_4$ $FeNbO_4$ orth $FeNb_2O_6$ $YTaO_4$	$FeNbO_4$ orth $YNbO_4$ $YTaO_4$ $FeNbO_4$ tetrag $FeNb_2O_6$ Ta_2O_5
1200	FeNbO4 tetrag $YNbO_4$ $FeNbO_4$ orth Ta_2O_5	Not studied	FeNbO4 tetrag $YNbO_4$ and traces of $YTaO_4$ $FeNb_2O_6$ $FeNbO_4$ orth	$FeNbO_4$ tetrag $YNbO_4$ and traces of $YTaO_4$ $FeNb_2O_6$

References:

[1] R.C. Ewing et al. *Mater. Res. Soc. Bull.*, **12(4)** (1987) 58.
[2] R.C. Ewing et al. *Nucl. Instrum. Methods Phys. Res.*, **B32** (1988) 487.
[3] G.R. Lumpkin, R.C. Ewing. *Phys Chem Minerals.* **16**, 2–20 (1988).
[4] B.E. Burakov, M.I. Ojovan, W.E. Lee Crystalline materials fo actinide immobilization. Imperial College Press, Materials for Engineering, **1** (2010)
[5] Qiuxiang Cao, A.I. Isakov, Xiaodong Liu, S.V. Krivovichev, B.E. Burakov. *Proceedings Mat. Res. Symp. XXXVII Scientific Basis for Nuclear Waste Mana*gement (2014) (*in press*).

Figures:

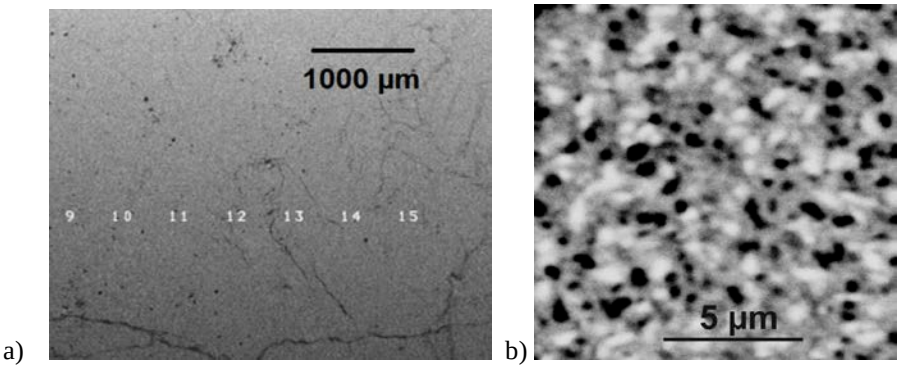

Figure 1. SEM BSE images of natural Y-Fe-niobate mineral: a) initial fully metamict sample; b) fully recrystallized sample after annealing in air at 1100 ^oC for 1 hour. Black dots are pores.

Crystal structure and luminescent properties of $R_{2-x}Eu_x(MoO_4)_3$ (R=Gd, Sm) Red Phosphors

Maria V. Raskina,[a] Anastasiya Pavlenko,[a] Vladimir A. Morozov,[a,b] Artem M. Abakumov,[a,b] Joke Hadermann[b]

[a] Chemistry Department, Moscow State University, 119991, Moscow, Russia;
[b] EMAT, University of Antwerp, Groenenborgerlaan 171, Belgium B-2020.

A large number of luminescent materials such as silicates, vanadates, phosphates, molybdates and tungstates with different crystal structures were investigated as potential host lattices being doped with Eu^{3+} as an activator for red luminescence [1,2]. The Eu^{3+}-doped molybdate and tungstate phosphors demonstrate broad and intense charge-transfer (C-T) absorption bands in the near-UV region and intense red emission with good color purity [3-4]. These make such $R_2(MoO_4)_3$ (R = rare earth elements) materials the promising candidates for red emitting phosphors for the pc-WLEDs (phosphor-converted white-light-emitting-diode).

The purpose of the present study was to obtain $R_{2-x}Eu_x(MoO_4)_3$ (R=Gd, Sm; $0 \le x \le 2$) solid solutions and investigate their structure and luminescent properties as a function of chemical composition and preparation conditions.

$R_{2-x}Eu_x(MoO_4)_3$ (R=Gd, Sm; $0 \le x \le 2$) solid solutions have been prepared by solid-state reaction; two types of host structure (monoclinic (α-) and orthorhombic (β'-)) have been obtained. The transformation from the α-phase to the β'-phase results in notable increase (~24%) in the unit cell volume for all $R_{2-x}Eu_x(MoO_4)_3$ (R = Sm, Gd) solid solutions. Transmission electron microscopy study and Rietveld refinements using the synchrotron X-ray powder diffraction data confirm that α-$Gd_2(MoO_4)_3$ and β'- $Eu_2(MoO_4)_3$ have structures similar to other monoclinic α-$R_2(MoO_4)_3$ and orthorhombic β'–phases, respectively.

The study of luminescent properties demonstrates that all $R_{2-x}Eu_x(MoO_4)_3$ (R=Gd, Sm; $0 \le x \le 2$) phosphors emit intense red light dominated by the $^5D_0 - {}^7F_2$ transition at ~616 nm. The Gd-based $R_{2-x}Eu_x(MoO_4)_3$ solid solutions are the most efficient emitters, having noticeably higher intensity in the range $0 < x < 1.75$ under the same conditions after excitation at 395 nm than Sm-based solid solutions (Fig.1). The $^5D_0 \rightarrow {}^7F_2$ emission intensity of α-$Gd_{2-x}Eu_x(MoO_4)_3$ is significantly higher under 395 nm excitation than that for β'-$Gd_{2-x}Eu_x(MoO_4)_3$ in the range of $0.25 < x \le 1.5$. Switching from monoclinic to orthorhombic structure for $Sm_{2-x}Eu_x(MoO_4)_3$ phases practically does not affect the $^5D_0 \rightarrow {}^7F_2$ emission intensity.

Acknowledgement. This research was supported by FWO (project G039211N, Flanders Research Foundation) and Russian Foundation for Basic Research (Grants 11-03-01164, and 12-03-00124).

References:

[1] B. Yan, J.-H. Wu, *Mater. Chem. Phys*., **116** (2009), 67–71.
[2] M. Md. Haque, H.-I. Lee, D.-K. Kim, *J. Alloys Compd*., **481** (2009), 792–796.
[3] S. Neeraj, N. Kijima, A.K. Cheetham, *Chem. Phys. Lett.*, **387** (2004), 2-6.

[4] Y. S. Hu, W. D. Zhuang, H. Q. Ye, D. H. Wang, S. S. Zhang, X.W. Huang, *J. Alloys. Compd.*, **390** (2005), 226-229.

Figures:

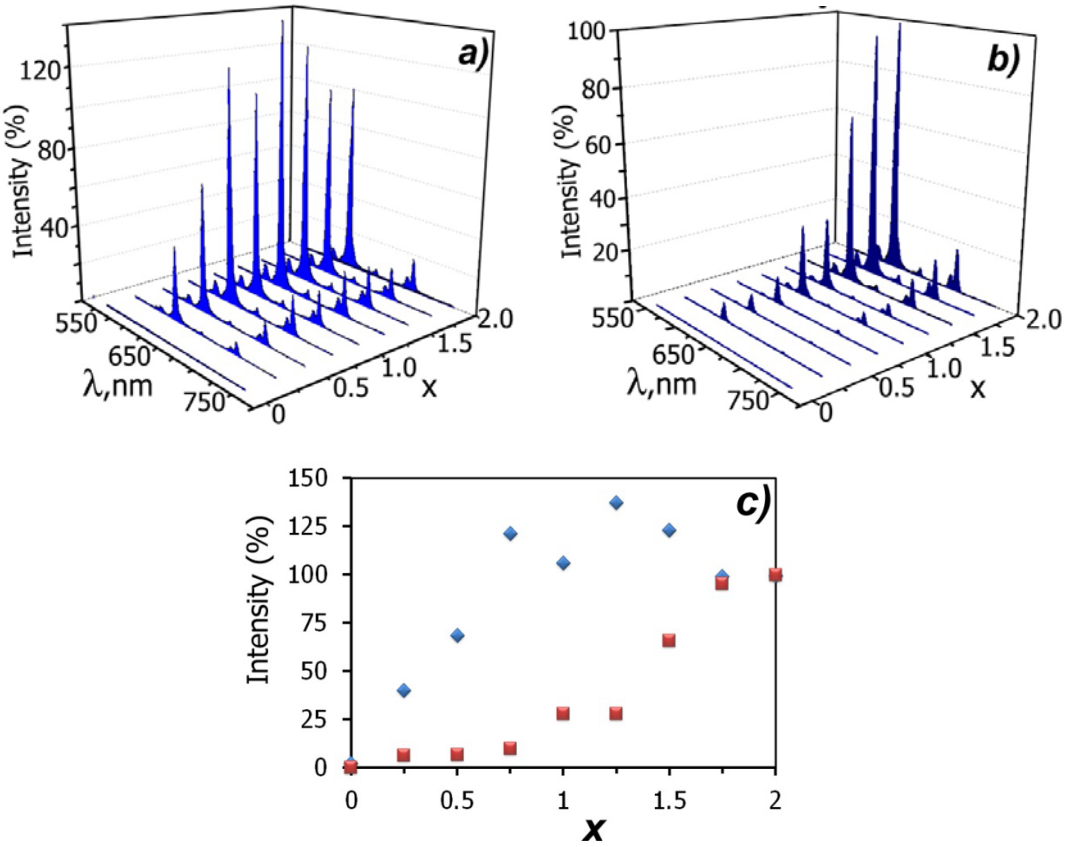

Fig.1. The photo-luminescent emission (λ_{ex} = 395 nm) spectra of α-$R_{2-x}Eu_x(MoO_4)_3$ (R=Gd (a), Sm(b)) and the dependence of the $^5D_0 \rightarrow {}^7F_2$ emission intensity for λ_{max}~616 nm band from Eu^{3+} concentration for R = Gd (blue rhombs) and Sm (red squares) (c).

Defect Chemistry of Lithium and Sodium Peroxide

O. Gerbig, R. Merkle, J. Maier

MPI for Solid State Research, Stuttgart, Germany

In search of new electrochemical storage devices with high specific energy densities, alkali-oxygen batteries have become a field of increasing research activity. In contrast to conventional lithium ion batteries, the alkali metal is not intercalated into a host material at the cathode side, but reacts with oxygen to form either alkali peroxide [1,2] or superoxide [3, 4]. The absence of intercalation hosts typically consisting of transition metal oxides and phosphates gives rise to an increased theoretical specific energy density.

The electrical transport properties and reaction kinetics of lithium and sodium peroxide were studied employing electrochemical techniques such as electrochemical impedance spectroscopy, dc polarization measurements and conductivity relaxation on cells with selectively blocking electrodes. The electrical conductivity was separated into electronic and ionic contributions, and the oxygen partial pressure was used as a control parameter to probe the type of main electronic charge carrier. The ion transport mechanism (alkali vacancies or interstitials) was determined from donor doping experiments. From conductivity relaxation measurements, chemical diffusivity and surface reaction rate constants were obtained.

According to the results, these alkali peroxides are mixed conductors with alkali defects as main ionic charge carrier and p-type electronic conductivity with holes localized on a peroxide site yielding superoxide defects. The transport mechanism of alkali ions differs among the materials. For Li_2O_2, the ionic transport occurs via alkali vacancies, while an interstitial mechanism is observed for Na_2O_2.

A defect model is proposed for Li_2O_2 taking into account the strong association of oppositely charged defects the low measurement temperatures, which are limited by the materials stability [5]. These findings are considered crucial for understanding and addressing limitations and problems in the cathodic reaction in alkali oxygen batteries. The presence of superoxide ions is ambivalent: on one hand they lead to degradation of the common electrolytes, but one the other hand they ase necessary for the electronic transport.

References:

[1] Z. Peng, S. A. Freunberger, Y. Chen, P. G. Bruce, Science 2012, 337, 563.

[2] Q. Sun, Y. Yang, Z.-W. Fu, Electrochem. Comm. 2012, 16, 22.

[3] P. Hartmann, C. L. Bender, M. Vračar, A. K. Dürr, A. Garsuch, J. Janek, P. Adelhelm, Nat. Mater. 2013, 12, 228.

[4] X. Ren, Y. Wu, J. Am. Chem. Soc. 2013, 135, 2923.

[5] O. Gerbig, R. Merkle, J. Maier, Adv. Mater. 2013, 25, 3129.

Reactive synthesis of aluminium matrix composites reinforced by nanoparticles of TiC

Nassim Samer,[a] Jérôme Andrieux,[a] Bruno Gardiola, [a], Laurent Chaffron[b], Sophie Gourdet[c], Olivier Martin[d], Olivier Dezellus[a]

[a] Université Lyon 1, Laboratoire des Multimatériaux et Interfaces, Villeurbanne, France
[b] CEA Saclay, Gif sur Yvette, France
[c] EADS France, Innovation Work, Suresnes, France
[d] MECACHROME, Amboise, France

Context

Thanks to their high specific modulus (E/ρ) and yield stress (σ_e/ρ), metal matrix composites (MMCs) have attracted research and industrial attentions as unique materials for high technological applications such as in the aerospace and automotive sectors. Compared to light weight alloys (Al, Mg, Ti), the mechanical properties of MMCs, such as strength and stiffness, are improved by the use of ceramic reinforcement [1]. Among the common used reinforcement (C, BN, SiC, TiC, Al2O3), TiC has been recognized as one of the most important reinforcing phase for metal matrix composite materials.
The two most common processes to synthesize Al-based MMCs are powder metallurgy and casting techniques. However, these two routes are associated with major drawbacks such as clustering of the reinforcement that leads to the decrease of ductility and toughness. Novel routes of synthesis as "reactive synthesis" could be explored in order to produce composite materials combining high strength properties without any dramatic increase of brittleness.

Experimental

According to the Al-Ti-C ternary system (Fig. 1) [2], a mixture of C and Al_3Ti was used as precursor. In this case, the reactive synthesis of the Al/TiC follows the reaction: $Al_3Ti + C \rightarrow TiC + 3\ Al$ [2-4]. This in-situ reaction occurs for a temperature higher than 812±15 °C meaning that above this temperature aluminium and TiC are in thermodynamic equilibrium. A short time heat treatment was selected in order to favour nucleation and to limit the growth of the reinforcement particles [5]. The MMC was prepared by ball milling under Argon of the starting powders followed by a cold isostatic compaction. Next the reactive synthesis was realized by a flash heat treatment of 1 minute at 1000°C. Finally extrusion of the composite was performed at 500°C.

Tensile testing was performed on metal matrix composite specimens machined from the composite. The Young's modulus, as well as the proof stress ($\sigma_{e0.2\%}$), the ultimate tensile strength (UTS) and the maximum elongation were deduced from the mechanical tests. Al/TiC composite presents a Young's modulus of 106 GPa and an uncommon maximum elongation of 6.0 %. This elongation value is also associated to a high toughness of about 28 $J.cm^{-3}$ (Fig. 2), a value that is similar to the ones reported for pure Al (25-30 $J.cm^{-3}$). To the author knowledge, regarding the high content of reinforcement particles (22 vol.%), this compromise between strength and toughness appears to be uncommon and interesting.

Characterization of the composite microstructure has been performed by several classical techniques such as Scanning Electron Microscopy (SEM), Transmission Electron Microscopy (TEM) and X-ray Diffraction (XRD).

Discussion

This original set of properties is explained by the microstructure resulting from the novel reactive synthesis route: despite the high content of reinforcement particles, no clustering of the particles is observed. Most of the particles remains in the nanometer range (with a mean diameter of about 80nm) and surrounded with percolating veins of Al matrix. Moreover, reactive synthesis led to in-situ formation of the metal/carbide interface avoiding the presence of oxide films and therefore leading more easily to a strong adhesion. As a consequence, no brittle defaults are present in the microstructure and a ductile failure with characteristic dimples is observed, leading to uncommon and promising mechanical properties (Fig. 2).

References:

[1] Miserez, A.G.T. (2003) Fracture and toughening of high volume fraction ceramic particle reinforced metals [dissertation]. Ecole Polytechnique Fédérale de Lausanne, Lausanne, Switzerland.
[2] Viala, J.C., Peillon, N., Clochefert, L. and Bouix, J. (1995) Mat. Sci. Eng. A-Struct. 203, 222-237.
[3] Viala, J.C., Vincent, C., Vincent, H. and Bouix, J. (1990) Mater. Res. Bull., 25, 457-464.
[4] Viala, J.C., Peillon, N., Bosselet, F. and Bouix, J. (1997) Mat. Sci. Eng. A-Struct. 229, 95-113.
[5] Tong, X.C., Fang, H.S., (1998) Metall. Mater. Trans. A, 29, 875-891.
[6] Karantzalis, A.E., Wyatt, S. and Kennedy, A.R. (1997) Mat. Sci. Eng. A-Struct. 237, 200-206.
[7] Kennedy, A.R., Weston, D.P., Jones, M.I. and Enel, C (2000) Scripta. Mater. 42, 1187-1192.
[8] Mitra, R., Fine, M. E. and Weertman, J. R. (1993) J. Mater. Res. 8, 2370-2379
[9] Satyaprasad, K., Hehajan, Y.R. and Bhanuprasad, V.U. (1992) Scripta. Metall. Mater. 26, 711-716.
[10] Mazaheri, Y., Meratian, M., Emadi, R. And Najarian, A.R. (2013) Mat. Sci. Eng. A-Struct. 560, 278-287.

Figures:

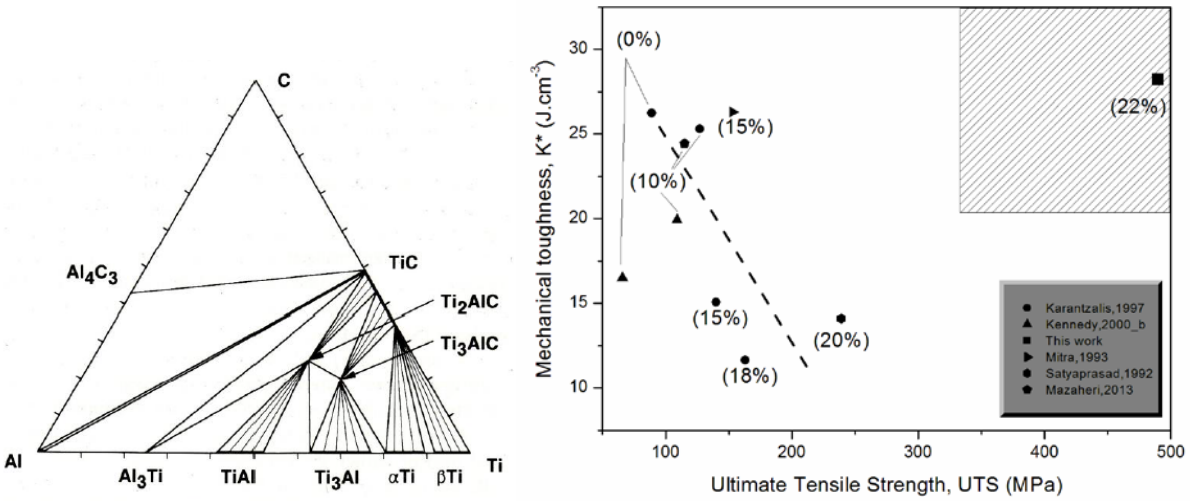

Fig. 1. (Left) Simplified isothermal section at 1000°C of the Al-C-Ti system.
Fig. 2. (Right) Estimated mechanical toughness, K*, as a function of the ultimate tensile strength. The volume fraction of TiC reinforcement in the composites are indicated in brackets [6-11].

Self-organization of the reaction-fracture coupled front on the mesoscopic scale caused by morphological instability of flat reaction front at $CuCl_2 \cdot 2H_2O$ dehydration

S.A. Chizhik, A.A. Matvienko, A.A. Sidelnikov

Institute of Solid State Chemistry and Mechanochemistry, SB RAS; 630128 Kutateladze 18, Novosibirsk, Russia.

The kinetics of heterogeneous solid state reactions like dehydration of crystal hydrates can be described as propagation of the reaction-fracture coupled front appearing as a result of the feedback between the reaction and fracture. The nature of the feedback is that solid state reactions are often accompanied by significant change of volume of the solid reagents. As heterogeneous reactions are characterized by inhomogeneous spatial development the volume change leads to the tension in the reaction zone. The tension results in cracking of the reagent in the reaction zone. The cracks serving as a new reaction surface provide local acceleration of the reaction and advance of the reaction front. Mathematical model of the reaction-fracture front enables one to predict the rate of the reaction front and morphology of the fractured product [1].

Anisotropy of the mechanical properties of reagents results in that the rate of the reaction front depends on its crystallographic orientation. In particular this manifests itself in the dependence of the overall reaction rate on the reagent crystal shape. But in addition a possibility arises for the morphological instability of the reaction-fracture front. If a reaction starts on a crystal face that corresponds to the orientation of the slow front movement then definite local perturbations of the front shape may result in formation of the front regions which move faster and so increasing initial disturbance. Finally the morphological transformation occurs. Initial flat front is partitioned to the pieces in which local crystallographic orientation differs from that of original front. This partitioning takes place on the mesoscopic scale which is intermediate between the macroscopic crystal size and microscopic internal scale of the fractured product. On average the resulting reorganized front retains the initial front orientation but moves faster and produces different fracture morphology and finer cracked reaction product.

This picture was observed experimentally when studying dehydration of $CuCl_2 \cdot 2H_2O$ in vacuum at room temperature (Fig 1). The front starting from faces (110) moves in deep of about 1 mkm, retaining flat shape (Fig 2). Thereafter it partitions to sharp wedged pieces orieted as [010] and positioned in aperiodic manner distanced by 0.5 – 2 mkm from each other (Fig 3). Average rate of the front increases several times. The fracture morphology resulted from the wedges movement resembles a plate-like motif on the mesoscopic scale. These plates internally consist of particles of 50-100 nm which corresponds to the measured specific surface area 15 m^2/g.

With the single-crystal X-ray diffraction it was found out that the product has two main orientation corresponding to the two twins. Deformation tensor was computed from these relations. It turned out that it is characterized by strong anisotropy. In two directions there is shrinkage by 12% and 37% whereas in third an expansion occurs by 6%. We suggest that

during formation of the product in the reaction zone the twins may arise in a ratio providing minimization of elastic strain energy. It is shown that the most significant decrease of the elastic strain energy can be achieved due to twining on the initial (110) crystal face. According to the model of the reaction-fracture front this results in minimal possible rate of the front in this direction. At the same time the twining can not provide a decrease of the stress for the front parallel to the face (100). Consequently such a front could be the fastest one. Thus the most likely perturbations of the initial flat front are the wedge-like formations directed along [010] which provide appearing of local front pieces slightly inclined to the fast direction (100). These theoretical results are fully confirmed by the experiments.

References:

[1] S.A Chizhik, A.A. Sidelnikov, *Solid State Ionics*, 178 (2007), 1487

Figures:

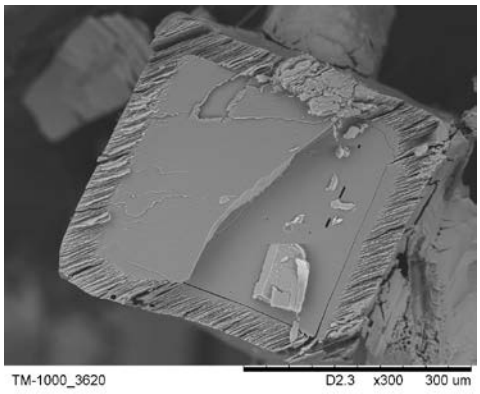

Fig. 1: *The crystal cut demonstrating the reaction-fracture front propagating from the faces (110)*

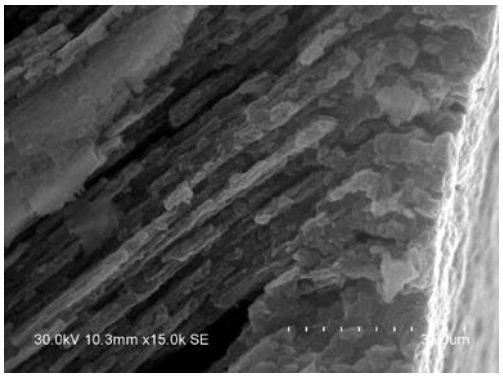

Fig. 2*: Change in the fracture morphology as a result of instability of initial flat front*

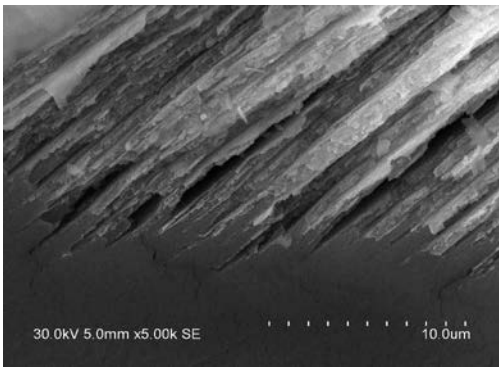

Fig. 3: *Detailed structure of the front reorganized on the mesoscopic scale*

Mechanism of formation, thermal stability and thermodynamic properties of cation-ordered layered perovskite-type titanates

A. Sankovich,[a] I. Zvereva,[a] I. Letyanina,[a] A. Blokhin[b]

[a]Saint Petersburg State University, Universitetskii pr. 26, 198504 Saint Petersburg, Russia;
[b]Belarusian State University, Leningradskaya ul. 14, 220030 Minsk, Belarus.

Layered perovskite-like oxides are objects of close attention as represent one of the most perspective classes of ceramic materials. These compounds exhibit important physical and chemical properties (electric, magnetic, catalytic) owing to the features of their crystal structure and find application in the newest areas of science and technology.

In the report we present results of the study on mechanism of formation, thermal stability and thermodynamic properties of $NaLnTiO_4$ and $Na_2Ln_2Ti_3O_{10}$ (Ln=Nd, Gd) titanates that belong to the Ruddlesden-Popper phases. These compounds are constructed by the intergrowth of alternating perovskite-like blocks (*P*) and rock-salt type slabs (*RS*) with various thickness of perovskite layers.

Mechanism of formation and thermal stability of layered oxides have been investigated by isothermal annealing-quenching method followed by X-ray powder diffraction analysis and synchronous thermal analysis with constant speed of heating coupled with quadrupole mass-spectroscopy. Processes of phase formation in Ln_2O_3–TiO_2–Na_2CO_3 systems have been studied in the temperature range of 500–1100°C, thermal stability of complex oxides has been investigated in the range of 900–1400°C. The structure-chemical mechanisms of oxides formation/decomposition and temperature intervals of phase transformations are defined.

$NaLnTiO_4$ oxides are stable up to 900°C. The decomposition of $NaNdTiO_4$ was found to begin at 950°C, full decay is reached at 1050°C for $NaGdTiO_4$ and 1100°C for $NaNdTiO_4$. $Na_2Ln_2Ti_3O_{10}$ oxides are products of decomposition of $NaLnTiO_4$ together with Ln_2TiO_5 and $Nd_2Ti_3O_9$ or $Gd_2Ti_2O_7$. $Na_2Ln_2Ti_3O_{10}$ oxides are more stable and undergo decomposition on $Nd_{2/3}TiO_3$ and $Nd_2Ti_2O_7$ in the range of 1200–1400°C.

The comparison of oxides stability is performed in terms of crystal chemistry. The essential contribution in the phase transformations is brought by the effect accompanying change of the coordination environment of Ln^{+3} (coordination numbers = 9, 12, 6) and Ti^{+4} (coordination numbers = 6, 5) cations and considerable distortions of their coordination polyhedra. The difference in the length of Na–O bond connecting *P* and *RS* layers also results in the greater stability of $Na_2Ln_2Ti_3O_{10}$ layered structure in comparison with the $NaLnTiO_4$. Less stability of Gd-containing oxides is caused by a mismatch of *P* and *RS* layers to tetragonal symmetry.

Our investigation demonstrates that the single-layer perovskite-type oxides $NaLnTiO_4$ and three-layer oxides $Na_2Ln_2Ti_3O_{10}$ at high temperature tend to be converted into more stable structure, either perovskite or layered structure with a larger number of perovskite layers. This experimental fact proves narrower limits of thermal stability of synthetic cation-ordered layered structures in comparison with structure of natural perovskite. Moreover it points to

the increase of thermal stability in process of increase in number of perovskite layers in layered structure.

The present work combines the results of heat capacity measurements obtained from adiabatic calorimetry and differential scanning calorimetry (DSC). The heat capacities in the low-temperature range (5–340K) are measured in a TAU-10 adiabatic vacuum calorimeter. Standard molar heat capacities, derived enthalpies, entropies, and derived Gibbs energies are calculated. The high-temperature C_p measurements are performed in Netzsch DSC 204 F1 Phoenix calorimeter in the range of 300–920K. An anomaly is observed in the heat capacity curve of $Na_2Nd_2Ti_3O_{10}$ at $T < 7.5$K. It is likely to be a descending branch for a magnetic "disorder-order" phase transition, which lies outside the measuring range of the calorimeter.

A unit cell of the three-layer oxide structure ($Na_2Ln_2Ti_3O_{10}$) can be visually assembled from two fragments of the single-layer oxide structure ($NaLnTiO_4$) by addition of one layer of corner-shared TiO_6 octahedrons. Therefore, the structural fragment of $Na_2Ln_2Ti_3O_{10}$ can be viewed as a combination of $NaLnTiO_4$ and titanium dioxide (TiO_2) structures arranged in a proper way. Good agreement between the experimental and calculated values of thermodynamic properties allows to use the additivity principle for prediction of thermodynamic properties for complex oxides.

This work was supported by Russian Foundation for Basic Research (N 12-03-00761) and St. Petersburg State University research grant (reg. 12.0.105.2010).

Figures:

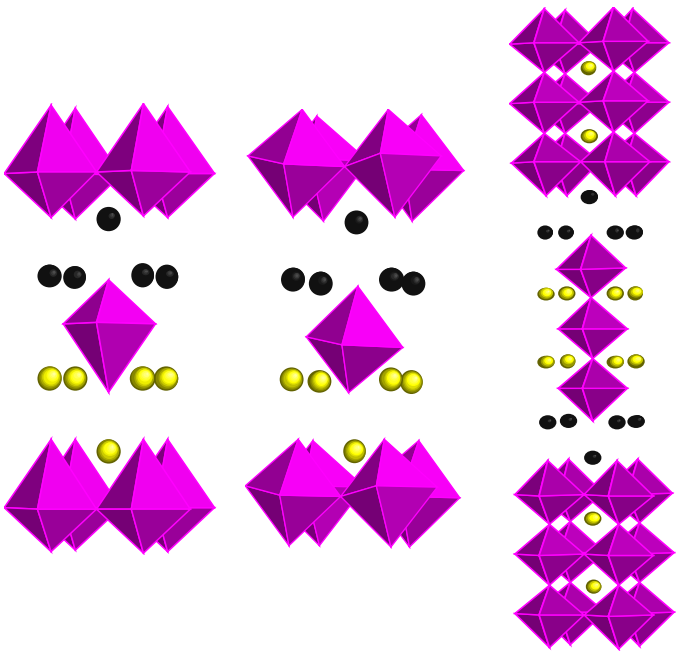

P4/nmm **NaNdTiO$_4$** | **Pbcm** **NaGdTiO$_4$** | **I4/mmm** **Na$_2$Ln$_2$Ti$_3$O$_{10}$**

Synthesis and high-temperature properties of $(Pr,Sr)_2(Mn,Co)O_{4-\delta}$ oxides with K_2NiF_4-type structure.

E.V. Zharikova[a], M.G. Rozova[a], S.M. Kazakov[a], S.Ya. Istomin[a], E.V. Antipov[a]

[a] Department of Chemistry, Moscow State University, Leninskie Gory, Moscow, 119991, Russia

Layered oxides R_2BO_4, R – rare-earth cation, B – late 3*d*-metal cation like Co, Ni and Cu, with K_2NiF_4-type structure are considered as promising cathode materials for intermediate temperature solid oxide fuel cell (IT-SOFC) [1, 2]. In their crystal structures there are perovskite blocks responsible for electronic conductivity and R_2O_2 blocks with rock-salt structure where diffusion of oxide-ions takes place. In the present work we report on the synthesis and study of high-temperature crystal structure, thermal expansion behavior and electrical conductivity properties of novel oxides $Pr_{2-x}Sr_xCo_{1-y}Mn_yO_{4-\delta}$ (x = 1.5,1.0; y = 0.0-0.5).

Ceramic samples of $Pr_{2-x}Sr_xCo_{1-y}Mn_yO_{4-\delta}$, x = 1.0 and 1.5, $0.0 \le y \le 0.5$ were prepared by heating stoichiometric amounts of Pr_6O_{11}, Mn_2O_3, Co_3O_4 and $SrCO_3$ in air at 950°C, 24 h with final annealing at 1250°C, 24 h. Single-phase samples were obtained for $PrSrCo_{1-y}Mn_yO_{4-\delta}$, $0.0 \le y \le 0.5$ and $Pr_{0.5}Sr_{1.5}Co_{1-y}Mn_yO_{4-\delta}$ $0.3 \le y \le 0.5$. Their X-ray powder diffraction patterns were fully indexed in tetragonal unit cells (S.G. I4/mmm). Refinement of the crystal structures of $Pr_{2-x}Sr_xCo_{1-y}Mn_yO_{4-\delta}$ using the Rietveld method confirmed the formation of K_2NiF_4-type structure. The oxygen content of the prepared compounds was determined by iodometric titration. Only slight deviation of the oxygen content from stoichiometric value is observed.

The temperature dependence of the oxygen content in air for the compositions $PrSrCo_{0.5}Mn_{0.5}O_{4-\delta}$ and $Pr_{0.5}Sr_{1.5}Co_{0.5}Mn_{0.5}O_{4-\delta}$ in the temperature range 25 - 900°C showed no significant weight loss. Thermal expansion behavior of the ceramic samples was studied by high-temperature X-ray powder diffraction and dilatometry. Calculated values of the thermal expansion coefficients (TEC) are 15.4 ppm K^{-1} and 17.9 ppm K^{-1} for $PrSrCo_{0.5}Mn_{0.5}O_{4-\delta}$ and $Pr_{0.5}Sr_{1.5}Co_{0.5}Mn_{0.5}O_{4-\delta}$, respectively. High-temperature X-ray diffraction reveals high anisotropy of thermal expansion along *a*- and *c*-axis for $PrSrCo_{0.5}Mn_{0.5}O_{4-\delta}$ with TEC(a)= 11.6 ppm K^{-1} and TEC(c)=22.1 ppm K^{-1} in comparison with TEC(a)= 17.4 ppm K^{-1} and TEC(c)=17.7 ppm K^{-1} for $Pr_{0.5}Sr_{1.5}Co_{0.5}Mn_{0.5}O_{4-\delta}$. Moreover, $PrSrCo_{0.5}Mn_{0.5}O_{4-\delta}$ demonstrates non-linear thermal expansion behavior of along *c*-axis in comparison with $Pr_{0.5}Sr_{1.5}Co_{0.5}Mn_{0.5}O_{4-\delta}$.

Electrical conductivity measurements for $PrSrCo_{0.5}Mn_{0.5}O_{4-\delta}$ and $Pr_{0.5}Sr_{1.5}Co_{0.5}Mn_{0.5}O_{4-\delta}$ ceramic samples were carried out by a standard 4-probe method in air at 25-900°C. Both compounds demonstrate a thermally activated (semiconducting-like) behavior with conductivity values of 7 S/cm and 23 S/cm at 900°C for $PrSrCo_{0.5}Mn_{0.5}O_{4-\delta}$ and $Pr_{0.5}Sr_{1.5}Co_{0.5}Mn_{0.5}O_{4-\delta}$, respectively.

This work was partially supported by RFBR (grant no. 14-03-01083) and MSU-development Program up to 2020.

References:

[1] E. Boehm, J. – M. Bassat, P. Dordor, F. Mauvy, J.-C. Grenier, Ph. Stevens. Solid State Ionics, 176, 2717 (2005)
[2] C. Allanion, P. Odier, J. M. Bassat, J. P.Loup. J. Solid State Chem., 131, 167 (1997)

Study of water intercalation and photocatalytic properties of layered perovskite-type tantalates and niobates

A. A. Burovikhina[a], M. V. Chislov[a], I. A. Rodionov[a], D. A. Porotnikov[a], I. A. Zvereva[a]

[a]Institute of Chemistry, Saint Petersburg State University, 26 Universitetskiy pr., Petrodvorets, Saint Petersburg, 198504, Russia

Perovskite-type oxides of Dion-Jacobson series have attracted attention because of their unique functional properties like superconductivity, ion conductivity, semiconductivity and photocatalytic activity. Some layered oxides are capable of reversible intercalation of water molecules into the interlayer space, which can lead both to increased effective surface area and spatial separation and promotion of the redox centers. Thus, ion exchange and intercalation reactions are possible ways to enhance photocatalytic activity of these compounds.

Therefore the aim of this work was to study the photocatalytic properties of layered oxides $ANdM_2O_7$ (A = H, Li, Na, K, Rb, Cs; M = Nb, Ta) and the factors that may influence it, including water intercalation.

The high-temperature ceramic method allowed to obtain cesium and rubidium-containing compounds from simple oxides and carbonates. Other members of the series can't be synthesized in this way, because they are unstable at high temperature. So they were obtained from stable precursors by ion-exchange method under mild conditions.

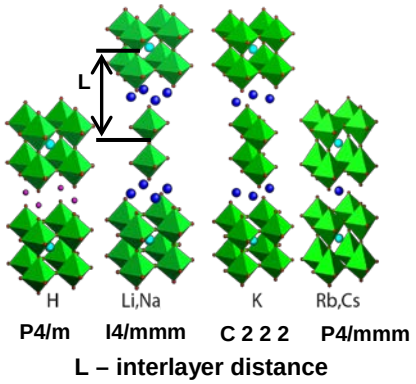

Figure 1. Structure of $ANdM_2O_7$ (A = H, Li, Na, K, Rb, Cs; M = Nb, Ta)

The structure of synthesized compounds is shown at Figure 1. Displacement of perovskite layers depending on the size of the cation in the interlayer space is observed. As a result the oxides crystallize in different structural types.

The possibility of water intercalation into interlayer space was investigated by thermogravimetric method. The weight loss was observed only for the H- and Na-containing compounds, indicating the possibility intercalated water presence.

The method of simultaneous thermal analysis (TGA + DSC) combined with mass-spectrometric analysis of the gas phase and X-ray diffraction served as evidence that the weight loss under heating is caused by intercalated water liberation. The composition and temperature ranges of stable intercalates are presented in Table 1.

Table 1. Intercalated water content in layered oxides

$ANdTa_2O_7$				$ANdNb_2O_7$			
A=H		A=Na		A=H		A=Na	
T, °C	Content of water, mol	T, °C	Content of water, mol	T, °C	Content of water, mol	T, °C	Content of water, mol
<75	0,84	<65	1,35	<60	0,89	<50	1,27
165	0,40	105-125	0,60	160-250	0,44	80-105	0,69
300	0	>165	0	310-360	0	>310	0

Enthalpy of water deintercalation was determined by DSC which showed higher specific endothermic effects for $NaNdTa_2O_7 \cdot 1.35H_2O$ then for $HNdTa_2O_7 \cdot 0.84H_2O$.

The photocatalytic activity was estimated by measuring the hydrogen evolution rate from oxide suspensions in 0.1% isopropyl alcohol aqueous solution irradiated by a mercury lamp. Experiments were carried out in a custom made outer-irradiation photocatalytic reaction cell, attached to a closed gas circulation system. The amount of released hydrogen was determined by gas chromatography (Shimadzu GC-2014). Kinetic curves of hydrogen evolution have a constant slope throughout the experiment. It has been shown that the rate of hydrogen evolution varies among alkali metals non-monotonically, the rubidium-containing oxides being the most active. The values of the band gap energy of $ANdM_2O_7$ were found to be slightly independent on alkali metal A (3.7 for niobates, 4.4 for tantalates). The BET surface area of samples varies from 0.8 to 5.0 m^2/g. In general, for the layered oxides under investigation there was found no correlation between photocatalytic activity, surface area, band gap and capability of water intercalation into the interlayer space. The difference in photocatalytic activity should be attributed to the electronic structure details.

Investigations were performed using a thermal analysis instrument (Netzsch TG 209F1 Iris, Netzsch DSC 204 F1 Phoenix and Netzsch STA 449 F1 + QMS Aeoelos) in the resource center «Center of Thermal Analysis and Calorimetry », SPbSU. Powder X-ray study is carried out in the X-ray Diffraction Centre of Saint Petersburg State University. This work has been supported by the RFBR grant 12-03-00761 and grant SPbSU 12.0.105.2010.

Hydrothermal synthesis of zirconia nanoparticles and their photocatalytic properties

A.N. Bugrov,[a] I.A. Rodionov,[a] O.V. Almjasheva [b], I.A. Zvereva [a]

[a] Institute of Chemistry Saint Petersburg State University;
[b] Ioffe Physical-Technical Institute RAS.

Nowadays more and more attention is paid to the development of photocatalysts based on zirconia nanoparticles which have n-type of conductivity with a band gap energy of 5.0 eV [1]. Conductance and valence band potentials of −1.0 and + 4.0 V allow to use them as photocatalysts for the production of hydrogen through water decomposition. Unfortunately, the wide band gap prevents the absorption of visible light by zirconia nanoparticles, what is a key issue for their use in photocatalysis [2]. Approaches based on the creation of structural defects and change of specific surface area by doping with transition metal ions, deposition of noble metals on the surface and surface modifying functional groups can be used to modify optical properties for effective visible light absorption [3, 4]. In this regard, the aim of this research was the synthesis of ZrO_2 nanoparticles with different phase composition, size, morphology and the study of their photocatalytic activity in the photoinduced hydrogen evolution processes.

Zirconia nanoparticles were synthesized by dehydration of zirconium oxyhydroxide ($ZrO(OH)_2$) or oxychloride ($ZrOCl_2{\times}8H_2O$) under hydrothermal conditions. X-ray diffraction and electron microscopy showed that ZrO_2 samples, obtained from $ZrO(OH)_2$ are spherical shaped nanoparticles predominantly tetragonal (*t*-ZrO_2 ~ 80%) with a narrow size distribution (average diameter of 18÷20 nm, fig. 1*a*). Introduction of 3 mol.% Y_2O_3 into zirconia structure leads to the formation of only *t*-ZrO_2 with an average particle size of 10±2 nm (fig. 1*b*), herewith the specific surface area increased from 87 to 107 m^2/g. Solid solution nanoparticles of lanthanides oxides (1 mol.% Ln_2O_3, Ln = Eu, Tb, Tm, Sm, Er) and zirconia obtained by the hydrothermal synthesis also have a tetragonal polymorph, but their size was 15±3 nm (fig. 1*c*).

Preparation of nanostructures based on ZrO_2 with different morphology was carried out by changing the pH value of the hydrothermal solution. For example, it was found that dehydration of $ZrOCl_2{\times}8H_2O$ in acid-alcohol mixture at pH=3 leads to the formation of hollow spheres with size of 300÷700 nm, and a wall thickness of 50±10 nm (fig. 1*d*). Hydrothermal treatment of $ZrOCl_2{\times}8H_2O$ in the presence of sodium acetate (CH_3COONa) and pH=2, promotes the formation of star-like nanostructures ZrO_2 with size around 80 nm (fig. 1*e*). In the case when NaOH is used as a hydrothermal solution medium (pH=14) ZrO_2 nanorods were obtained with a diameter of 50±5 nm and a length of 200±40 nm, having a monoclinic structure (fig. 1*f*). It was found that mesoporous hollow microspheres, star-like and rice-grain-like zirconia nanostructures are agglomerates composed of m-ZrO_2 crystallites with an average size of 1±5 nm. According to the method of low-temperature nitrogen adsorption (BET), specific surface area of the zirconia nanostructures described above was 140, 91 and 17 m^2/g, respectively. Zeta-potential of dispersions of the ZrO_2 nanostructures in distilled water and greatly dilute solution of NaCl (10^{-3} mol/l) was measured by electrophoretic light scattering method. The optical band gap of obtained crystalline substances were determined based on diffuse reflection spectra with Kubelka-Munk transformation from the onset of fundamental absorption band.

The study of hydrogen evolution kinetics from aqueous suspensions of ZrO_2-based photocatalyst under UV-irradiation was carried out on the specially designed set-up comprising an outer-irradiation reaction cell, equipped with a radiation source, a magnetic stirrer and a closed gas circulation system attached to the gas chromatograph (MolSieve 5A column, TC-detector, Ar carrier).

This work was supported by the Russian Foundation for Basic Research (grant № 14-03-31722) and grant SPbSU 12.0.105.2010

References:

[1] Polisetti S., Deshpande P. A., Madras G., *Ind. Eng. Chem. Res.* **50 (**2011), 12915-12924.
[2] Karunakaran C., Senthilvelan S., *Journal of Molecular Catalysis A: Chem.*, **233** (2005) 1-8.
[3] Du W., Zhu Z., Zhang X., et al., *Materials Research Bulletin*, **48** (2013) 3735–3742.
[4] Du W., Wang X., Li H., et al., *J. Am. Ceram. Soc.*, **96** (2013) 1–8.

Figures:

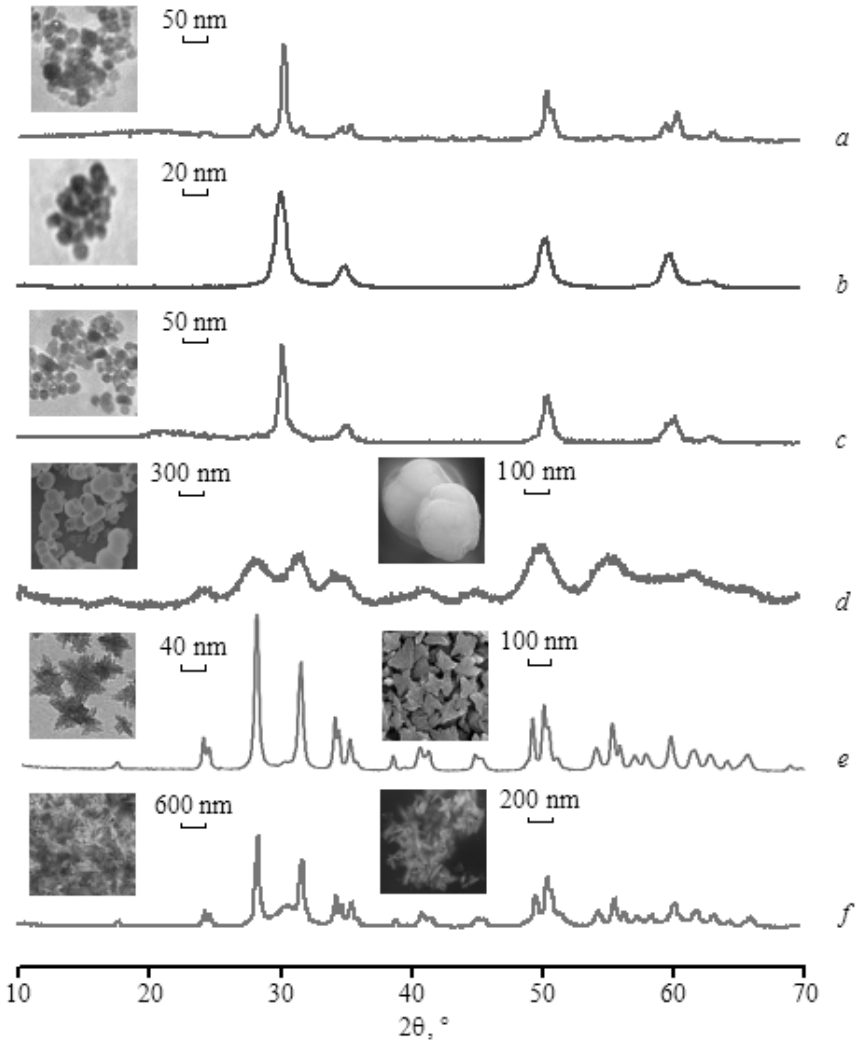

Fig. 1. X-ray diffraction and electron microscopy micrograph of nanoparticles based on ZrO_2, obtained under hydrothermal conditions: *a* - ZrO_2; *b* - ZrO_2-Y_2O_3; *c* - ZrO_2-Eu_2O_3; *d* - hollow spheres ZrO_2; *e* - star-like ZrO_2; *f* - nanorods ZrO_2.

Effect of dopant type (Al, Ga, In) on adhesion of metal/oxide interface

N.S. Nikolaeva [a], A.A. Shubin [a], A.S. Kholtobina [a], A.A. Kuzubov [a], E.N. Fedorova [a]

[a]Siberian Federal University, Krasnoyarsk, 660028, Russian Federation.
E-mail: nsnikolaeva@sfu-kras.ru

The investigation of metal/oxide interfaces is important for many applications such as functional composite materials, oxide-ceramic coatings on metals, electronic materials. In many applications the metal/oxide interfaces in the material have a deep influence on functional properties depending on adhesion.

Among the functional semiconductors, zinc oxide (ZnO) is one of the most significant materials due to its high-electron mobility, high thermal conductivity and wide band gap energy value (3.37 eV). Usually, ZnO is doped by XIIIth group elements (Al, Ga, In) which are the donors of the electrons in purpose to increase a conductivity. M_2O_3 and ZnO form solid solutions with solubility limit. In generally incorporation mechanism of M^{3+} into ZnO lattice is [1]:

$$M_2O_3 \xrightarrow{ZnO} 2M^{\bullet}_{Zn} + 2e' + 2O^{x}_{O} + \frac{1}{2}O_2.$$

But dopants in surface layers reduce the electrostatic interaction energy at interface, meanwhile the oxygen vacancies can decrease adhesion because of the number of M-O bounds decrease [2]. In addition, the adhesion on the M/ZnO boundary will be changed with increasing dopant concentration in the oxide lattice, because the high concentration of the dopants lead to the individual phase formation on the ZnO grain boundaries. Therefore, it is necessary to find the characteristic properties of interfacial interaction in M/ZnO system depending on dopant type and their concentration as a Ag/ZnO system.

In this work, dopant type (Al, Ga, In) influence on microstructure and surface properties ceramics based on ZnO was investigated. Doped ZnO powders were prepared by the aqueous solutions coprecipitation method. Pellets pressed from these powders were sintered at T=1373K in the air. Scanning electron microscopy (SEM) was used to evaluate surface morphology. X-ray fluorescence analysis were performed using a spectrometer ARLQuant`X. X-ray diffraction data were obtained using a X'Pert-Pro (PANalytical) (Cu Kα, λ=0,15406 Å). The work of adhesion (Wa) was determined by measuring the equilibrium contact angle of sessile metal drops on planar oxide substrates at T=1273K. The VASP code [3] was employed to perform electronic structure calculations. The DFT plane wave (PW) basis sets, PAW formalism [3], PBE DFT potential in Periodic Boundary Conditions (PBC) were used.

The surface energy of undoped and doped ZnO (surface (110)) was calculated. The addition of dopants increases the value of surface energy, except for In. The calculation data is correlated with experimental adhesion work-dopant type relation.

It can be stated that interfacial adhesion is improved in the series $Zn_{1-x}In_xO \rightarrow ZnO \rightarrow Zn_{1-x}Ga_xO \rightarrow Zn_{1-x}Al_xO$ (fig. 1). The value of the contact angle is sudden changed with increase of dopant concentration due to $ZnAl_2O_4$, $ZnGa_2O_4$ or $Zn_7In_2O_{10}$ formation on the ZnO grain boundaries.

This work has been supported by National Center for Scientific Research (CNRS, France) through the Projet International de Coopération Scientifique (PICS) Adherons!2 and Russian Foundation for Basic Research (RFBR) Ref n° 13-08-91053-CNRS_a.

References:

[1] F.A. Kroger (1964).The chemistry of imperfect crystals. North-Holland, Amsterdam; Interscience, NY
[2] C. Wöll Prog. Surf. Sci., **82,** (2007)
[3] G. Kresse, and J. Hafner, Phys. Rev. **49**, (1994) 14251.

Figures:

Figure 1. The contact angles and the adhesion work of doped ZnO pellets/Ag

Mechanical Properties of SiO_2 + Si, SiO_2 + TiO_2 + ZrO_2 and Analysis Automated System of Anisotropy

A. P. Onanko, G. T. Prodayvoda, Y. A. Onanko, A. V. Shabatura , A. N. Onischenko[a]

[a]Taras Shevchenko Kyiv national university, Kyiv, Ukraine

onanko@univ.kiev.ua

Introduction

Elastic deformation ε_E takes a place "instantly". Inelastic deformation ε_{IE} is conditioned motion of dislocations [1]. The influencing of ultrasonic deformation ε was researched on elastic and inelastic characteristics of Si + SiO_2.

Experiment

For measuring of elastic module E and internal friction (IF) the impulse method on frequency f ≈ 1,67; 5 MHz was used [2,3]. After irradiation there is diminishing of the velocity value of longitudinal ultrasound elastic waves $V_{\parallel}$, of the velocity value of transversal ultrasound elastic waves $V_{\perp}$, elastic module E and shear module G of specimen. There was a small value of IF background in SiO_2 $Q^{-1}{}_0 \approx 2 \cdot 10^{-6}$ to T ≈ 385 K.

Experimental Results

The free vibrations are under acts of internal forces. The conditions of free vibrations are: 1) one force on specimen are function of coordinates; 2) must be equilibrium position, at withdrawal from which the nonzero resultant of all forces must be direct to equilibrium position; 3) friction forces must be enough small. The Puasson coefficient μ is equal to ratio of relative transversal compression to relative longitudinal lengthening and is equal [1]:

$$\mu = \frac{(\frac{1}{2}V_{\updownarrow}{}^2 - V_{\leftrightarrow}{}^2)}{(V_{\updownarrow}{}^2 - V_{\leftrightarrow}{}^2)}, \qquad (1)$$

where $V_{\updownarrow}$ – longitudinal ultrasound wave velocity, $V_{\leftrightarrow}$ – fast transversal ultrasound wave velocity. Debye model sets the conditions existence stand waves in solid state. The quantum nature of elementary oscillators takes into consideration. The thermal capacity – parameter of the thermodynamic system equilibrial state in Debye model. Therefore waves, that elementary oscillators excite, can't carry the energy. There are stand waves. One oscillator produce 3 waves: 1 longitudinal and 2 transversal. Debye temperature θ_D was determined after the formula [1]:

$$\theta_{\mathrm{D}} = \frac{h}{k_B} \cdot \left(\frac{9\mathrm{N_A}\rho}{4\pi A} \right)^{1/3} \cdot \left(\frac{1}{V_{II}{}^3} + \frac{2}{V_{\perp}{}^3} \right)^{1/3}. \qquad (2)$$

Discussion

The method of atomic-force microscopy is found out the increase of roughness of Si surface as a result of irradiation by the $^{11}B_5{}^+$ ions. It is showed that after irradiation the electrons e^- there is destruction of Si surface layer, predefined the accumulation of vacancy complexes V-V-V. Irradiation of Si surface by $^{11}B_5{}^+$ ions with dose D ≈ $1 \cdot 10^{15}$ ion/sm^2 and with energy W

≈ 130 KeV, when energy output in volume unit considerably anymore at the same run-length particles of these energies in Si L_{11B5+} > 360 000 nm, results to formation of high concentration of defects in Si surface layer, interstitial atoms Si_i.

Conclusions

Thus, the study of influence of structure defects on attenuation of elastic vibrations in Si + SiO_2 wafer-plates allows to estimate the degree of nanostructure. Outcomes of an evaluation of dynamic characteristics interstitial atoms Si_j, vacancy V and O-complexes can be applied for account of a condition of an annealing with the purpose of deriving specific structural defects in Si + SiO_2. The growth of heights IF maximums $Q^{-1}{}_M$ testifies the growth of structural defects concentration in Si + SiO_2 wafer-plate.

References:

[1] L. N. Aleksandrov, M. I. Zotov, Internal friction and defects in semiconductors, Novosibirsk: Nauka, 1979.
[2] A. P. Onanko, O. V. Lyashenko, S. A. Vyzhva et al., *Sensor electronics and microsystem technologies*, **2(8),** № 3 (2011) 14.
[3] A. P. Onanko, *Metalphysics and new technology*, **33**, № 2 (2011) 253.

Figures:

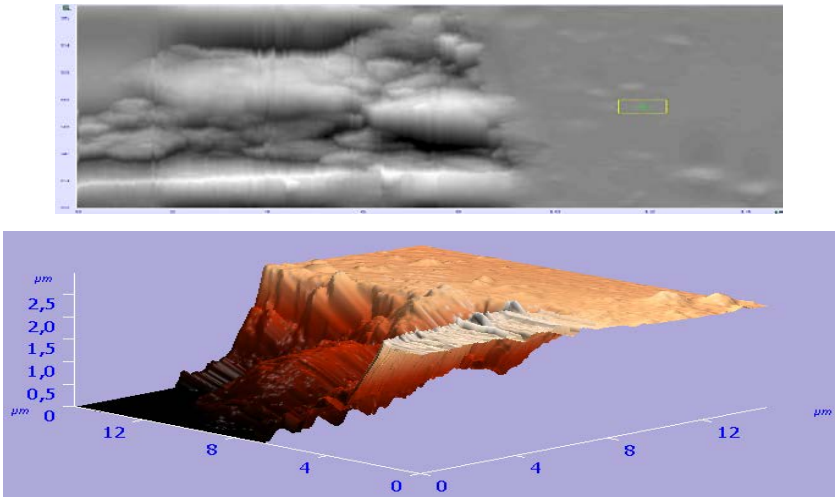

Figure 1. 3D atomic-force microscopy of microstructure image of Si type KEF-7,5 with orientation (100) after irradiation by $^{11}B_5^+$ ions with doze D ≈ $1 \cdot 10^{15}$ ion/sm^2 and energy W ≈ 130 KeV at T = 293 K (15x15 mkm).

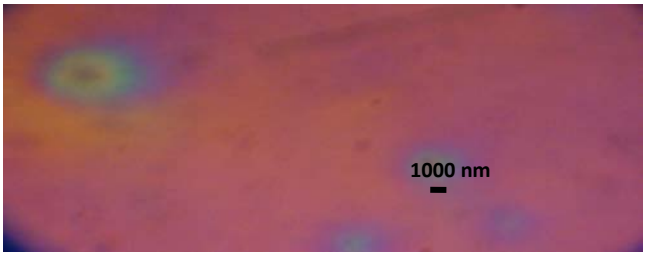

Figure 2. Microstructure of SiO_2 + TiO_2 + ZrO_2 + $Ag_{0.05}$ film with thickness h ≈ 200 nm on Si (100).

Cis-Stereospecific Topochemical Alternating Copolymerizations of 7,7,8,8-Tetrakis(alkoxycarbonyl)quinodimethanes with 7,7,8,8-Tetracyanoquinodimethane

Takahito Itoh[a], Tatsuya Suzuki[a], Takahiro Uno[a], Masataka Kubo[a], Norimitsu Tohnai[b], Mikiji Miyata[b]

[a]Division of Chemistry for Materials, Graduate School of Engineering, Mie University, Japan
[b]Department of Materials and Life Science, Graduate School of Engineering, Osak University, Japan

Solid-state polymerizations of 7,7,8,8-tetrakis(alkoxycarbonyl)quinodimethanes(RCQs) with methoxy(MeCQ,**1**), chloroethoxy(ClEtCQ), and bromoethoxy(BrEtCQ) as alkoxy groups were found to proceed topochemically under UV irradiation and by heating.[1)] Previously, we reported that RCQ with methoxy and ethoxy groups may form charge-transfer complexes with 7,7,8,8-tetracyanoquinodimethane (TCNQ,**2**) in the acetonitrile solution.[2)] We tried to form cocrystals of MeCQ with TCNQ, and then succeeded to obtain the crystalline charge-transfer complex crystals. In this work, cocrystals of RCQs having various alkoxy groups with TCNQ were prepared, and their crystal structures and their polymerization reactivity in the solid state were investigated.

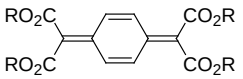

RCQ

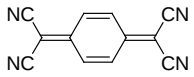

TCNQ

R = -CH_3	(MeCQ)
-CH_2CH_3	(EtCQ)
-$CH_2CH_2CH_3$	(nPrCQ)
-$CH(CH_3)_2$	(iPrCQ)
-$CH_2CH_2CH_2CH_3$	(nBuCQ)
-$CH_2CH(CH_3)_2$	(iBuCQ)
-CH_2CH_2Br	(BrEtCQ)
-CH_2CH_2Cl	(ClEtCQ)

RCQs having methoxy, ethoxy, propoxy, and butoxy groups formed red to orange crystalline charge-transfer complexe crystals with TCNQ, but RCQs with branch-type and halogen-containing alkoxy groups did not. The polymerization of the crystalline charge-transfer complex crystal of MeCQ with TCNQ under UV irradiation and by heating was found to proceed topochemically, as shown by XRD measurement (Fig.1). Cocrystals of RCQs containing ethoxy, propoxy, and butoxy groups with TCNQ showed the polymerization behavior similar to MeCQ/TCNQ cocrystals. X-ray single-crystal structure analysis of the MeCQ/TCNQ cocrystals and the corresponding polymer crystals were performed, and *cis*-stereospecific topochemical alternating copolymerization was confirmed. This is the first example of a *cis*-stereospecific topochemical alternating copolymerization for the substituted quinodimethanes.

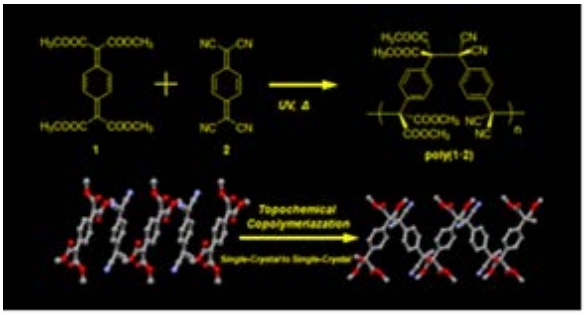

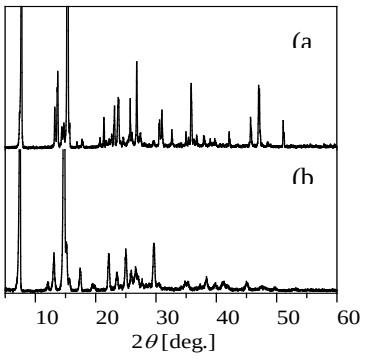

Fig.1. XRD patterns of (a) MeCQ/TCNQ cocrystal and (b) reaction mixture irradiated UV light for 24h.

References:

[1] Nomura, S. et al, (2004) J. Am. Chem. Soc., **126**, 2035.
[2] Iwatsuki, S. and Itoh, T. (1980) Macromolecules, **13**, 983.

Oxygen non-stoichiometry and ion-electron transport in $SrFe_{1-x}Sn_xO_{3-\delta}$

A.A. Markov, M.V. Patrakeev, I.A. Leonidov, V.L. Kozhevnikov

Institute of Solid State Chemistry UB RAS, 91 Pervomaiskaya str.,
620990 Yekaterinburg, Russian Federation

Oxygen ion and electron mixed conductors have numerous important electrochemical applications including ceramic membranes for oxygen separation, solid oxide fuel cell electrodes, etc. The strontium perovskite-like ferrite $SrFeO_{3-\delta}$ is notorious among them for high level of oxygen permeability, which is provided by appreciable contributions to conductivity from both ions and electrons [1, 2]. Also, this ferrite is found to exhibit rather satisfactory stability toward reduction [3]. The most serious material drawback that deleteriously effects transport characteristics is the tendency of oxygen vacancies to ordering in the ferrite [4]. Moreover, the vacancy ordering eventually results in the perovskite to brownmillerite phase transition, and accompanying dimensional changes favor loss of integrity and fracturing of ferrite ceramics and coatings [5]. It is known that partial replacement of iron for other cations having stable oxygen coordination often leads to suppression and complete disappearance of the phase transition [6-8]. The present study is aimed at tracking the influence of tin on structure, non-stoichiometry and transport characteristics in the strontium ferrite.

The ceramic materials $SrFe_{1-x}Sn_xO_{3-\delta}$, where x=0.05-0.5, were prepared via standard ceramic route. The X-ray powder diffraction analysis showed that the as-prepared samples were single cubic perovskite phases. The increase in the concentration of tin is accompanied with the increase of the elementary unit parameters, which reflects replacement of iron for larger tin cations. The oxygen content changes in $SrFe_{1-x}Sn_xO_{3-\delta}$ at 700-950ºC and oxygen partial pressure variations within 10^{-20}-0.7 atm were measured by the using of a coulometric titration technique. The obtained data suggest that tin cations invariably preserve their oxidation state 4+ in the entire range of experimental parameters thus resulting in the decrease of the δ-span in $SrFe_{1-x}Sn_xO_{3-\delta}$. The partial molar thermodynamic functions of labile oxygen in $SrFe_{1-x}Sn_xO_{3-\delta}$ were calculated from the obtained data for equilibrium oxygen content. The analysis of partial molar thermodynamic functions showed that the increase of tin concentration results in the decrease of oxygen binding energy in the crystal lattice of the ferrite while it does not practically influence the enthalpy ~1.3 eV of the reaction $2Fe^{3+} = Fe^{2+} + Fe^{4+}$.

The total conductivity in $SrFe_{1-x}Sn_xO_{3-\delta}$ as a function of oxygen partial pressure and temperature was measured by the four-probe d.c. technique. The analysis of the conductivity isotherms vs. partial pressure of oxygen was used in order to separate contributions from oxygen ions and electrons. It is deduced that replacement of iron for tin leads to a strong disordering of the oxygen sub-lattice and favors suppression of the perovskite to brownmillerite phase transition. X-ray diffraction analysis of the reduced sample x = 0.05 revealed formation of the brownmillerite-like phase at temperatures below 700ºC, while samples with larger tin content retain their cubic structure at reduction. Interestingly, the 5% tin doping leads to increased oxygen ion conductivity in $SrFeO_{3-\delta}$, which is in accord with tin induced oxygen disordering. However, further increase in the doping level results in suppression of the ion conductivity due to excessive oxygen vacancy filling.

The introduction of tin in the crystal lattice does not change the activation energy ~2.2 eV of n-type charge carriers and, hence, the mechanism of electron hopes along Fe-O-Fe transport chains.

This work is supported by the Russian Foundation for Basic Research (grant #13-03-00931). The authors are also grateful to the Ural Branch of RAS for the support of this study through the regional program (grant #12-3-2-002 Arctic).

References:

[1] Y. Teraoka, H.-M. Zhang, S. Furukawa,N. Yamazoe, *Chem. Lett.*, **14** (1985) 1743.
[2] F.W. Poulsen, G. Lauvstad, R. Tunold, *Solid State Ionics*, **72** (1994) 47.
[3] M.V. Patrakeev, I.A.Leonidov, V.L. Kozhevnikov, V.V. Kharton, *Solid State Sci.*, **6** (2004) 907.
[4] J.P. Hodges, S. Short, J.D. Jorgensen, X. Xiong, B.M. Dabrowski, S.M. Mini, C.W. Kimball, *J. Solid State Chem.*, **151** (2000) 190.
[5] T.J. Mazanec, in:H.U. Anderson, A.C.Krandhar, M.Liu (Eds.), Ceramic Membranes I, vol. 5–24,The Electrochemical Society, Pennington, NJ, (1997) 16, PV9.
[6] S. Steinvic, R. Bugge, J. Gjonnes, J. Tafto, T. Norby, *J. Phys. Chem. Solids*, **58** (1997) 969.
[7] M.V. Patrakeev, I.A. Leonidov, V.L. Kozhevnikov, V.V. Kharton, *Mater. Sci. Forum*, **514–516** (2006) 382.
[8] V.V. Kharton, J.C. Waerenborgh, D.P. Rojas, A.A. Yaremchenko, A.A.Valente, A.L. Shaula, M.V. Patrakeev, F.M.B. Marques, J. Rocha, *Catal. Lett.*, **99** (2005) 249.

Ar^+ ions beam irradiation effects on InX semiconductor surfaces .

A.Ouerdane [a,b], M.Bouslama [a], M.Ghaffour [a]; A.Abdellaoui [a] and Souraya Goumri-Said[c]

[a]Université de Khemis Miliana 44225 route de Theniet El Had W.Ain Defla Algeria
[b]*Laboratoire Matériaux LabMAt ENPO Oran Mnaouer 31000.*
[c]Physical Sciences and Engineering Division King Abdullah University of Science and Technology (KAUST) Thuwal 23955-6900, Kingdom of Saudi Arabia
E-mail: ouerdanea@yahoo.fr

Ion beam irradiation is an efficiency technique for phase formation and material modification as a non-equilibrium state. At low energy (300 eV), the Ar^+ ions bombardment lead to the formation of small nanodots on the InX (X=Sb, P, N) surface compounds. We used Auger electron spectroscopy (AES) and electron energy loss spectroscopy (EELS) to detect the presence of these features. The synthesis of nanostructures and their modification by ion beam technique will be illustrated, analyzed and discussed. Annealing processes are required for the complete growth of clusters formed in most of these ion irradiation techniques. Furthermore, reactive sputtering of InX films in oxygen indicated no evidence of direct formation of In_2O_3. It was suggested therefore that oxygen accelerates the formation of an intermediate amorphous indium oxidation process phase inside the InX matrix, which eventually oxidizes InX completely to form In_2O_3. Depending on species (e.g., mass and charge state) and energy range, there are various modes for an energetic ion to dissipate its energy. [1,2]

The advent of nanostructures using ion bombardment on InX semiconductor surfaces has opened a very interesting field of research [3]. By such techniques, it will be possible, under special circumstances, to replace the more expensive technology using lithography and growth process for the development of nanodots and nanowires [1, 4]. These nanostructures increase the surface area and form excellent black-body absorbers which are of great importance for solar cell. Furthermore quantum dots (QDs) of InX (X=P, Sb, In) narrow gap semiconductor, are applied as a potential platform for optoelectronic devices operating in the mid-infrared wavelength region. InP, InSb and InN are the III-V semiconductors with direct band gap. Our purpose is to understand the effect of the argon ion bombardment on these targets at normal incidence, we observe the bombardment effect on the surface and we analyse the variation of their surfaces topographies. Our paper deals first with the careful cleaning of the two surfaces achieved at low energy (300 eV). Afterwards, we study the ionic irradiation of the clean and stoichiometric InP; InSb and InN surfaces. The effect of Ar^+ on these compounds will be shown by using sensitive methods such as AES and EELS to characterize the surfaces. However these techniques alone do not allow us to determine with accuracy their disturbed dimension related to the height and periodicity. For this reason, we combine these spectroscopy methods with the TRIM (transport and range of ions in matter), SRIM (Stopping and Range of Ion in Matter) and Sigmund simulation methods to show the mechanism of interaction between the argon ions and the these InX compounds cited above and determine the dimension of disturbed areas as a function of Ar^+ energy during 30 min.

The Auger electron spectra (AES) and electron energy loss (EELS) spectra are recorded by using a hemispherical spectrometer. For the best compromise between the transmission and the resolution of the apparatus, we use pass energy of 80 eV between the deflectors of the analyzer operating in direct mode N(E) [1,4] The vacuum in the spectrometer chamber was about 10^{-9} Torr.

References:

[1] A. Ouerdane , M. Bouslama, M. Ghaffour, A. Abdellaoui, A. Nouri, K. Hamaida, Y. Monteuil, IOP Conf.Series:Materials Science and Engineering **28** (2012) 012024
[2] A. V. Krasheninnikov and K. Nordlund , Journal of Applied Physics 107, 071301 (2010)
[3] A. Kamarou, W. Wesch, E. Wendler, A. Undisz, and M. Rettenmayr Phys. Rev. B 78, 054111 (2008)
[4] M. Ghaffour, A.Abdellaoui, A. Ouerdane, M. Bouslama,C. Jardin ,Materials Sciences and Applications, 2011, 2, 421-42

Figures:

Fig.1 EELS spectra of InN (left)) ,EELS Spectra following the surface morphology of InSb compounds (middle); AES spectra of InP surface ;(right up) and morphology by AFM (right down)

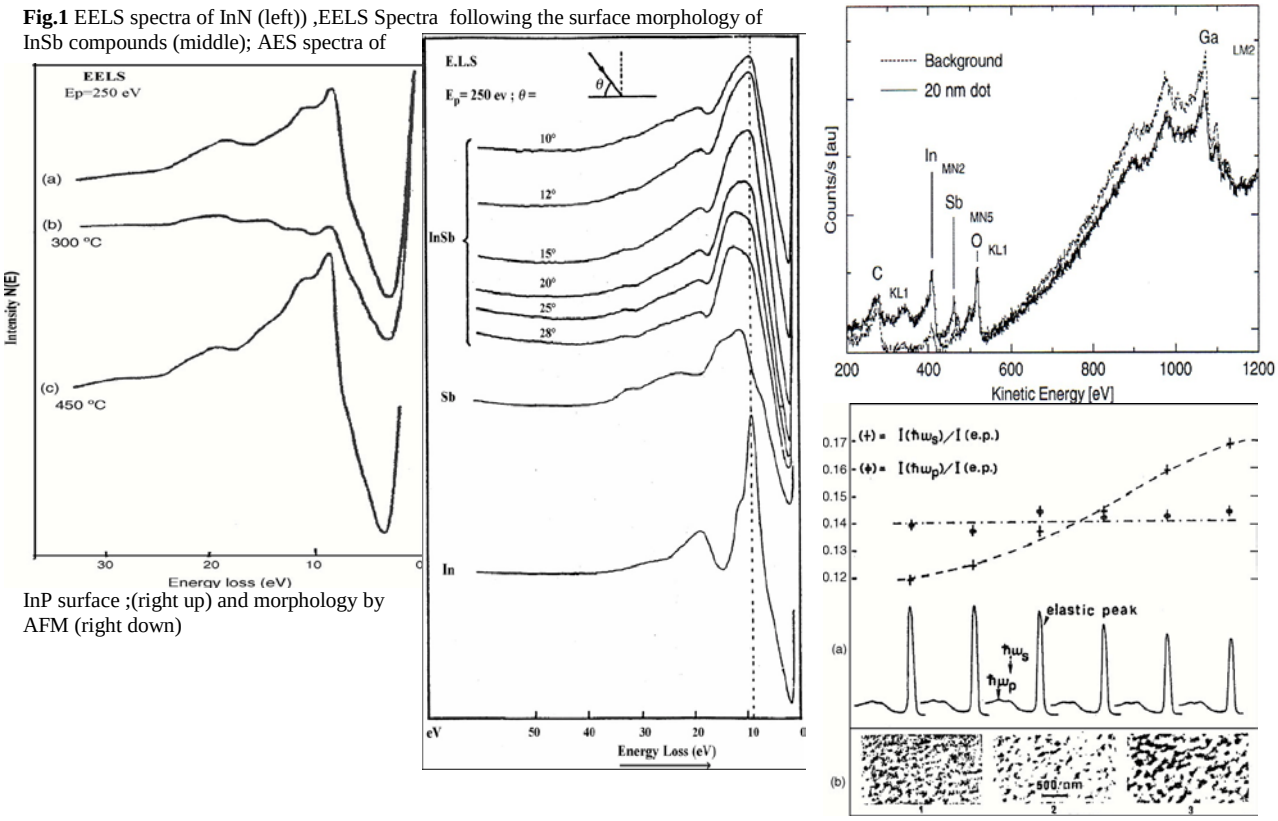

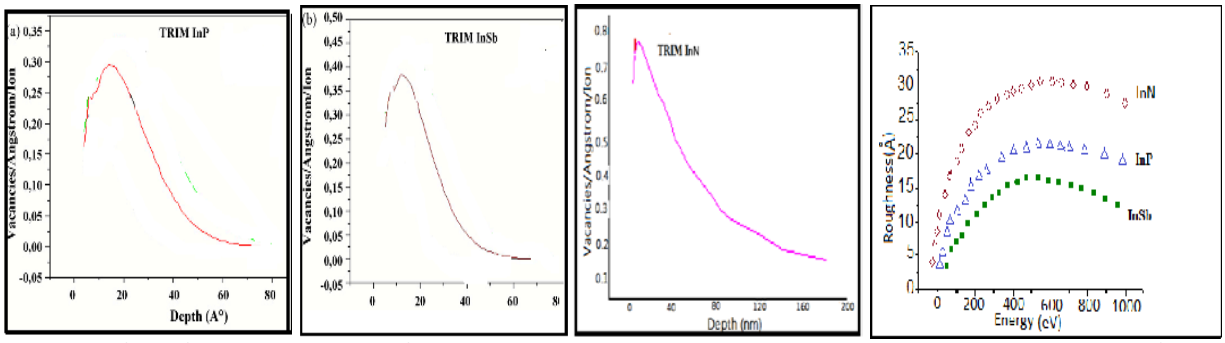

Fig.2 TRIM software for InP InSb and InN (left three curves) ; the roughness using Sigmund theory the periodicity and the high of the nanostructures on the surface compounds InSb ; InP and InN.(right curve)

Magnetic interactions in $ZnFe_2O_4$ nanoparticles

M. Virumbrales[a,*], A. Delgado[a], R. Sáez Puche[a] and M.J. Torralvo[a]

[a]Departamento de Química Inorgánica, Facultad Químicas, Universidad Complutense de Madrid, 28040, Madrid, Spain
**maider.virumbrales@ucm.es*

The unique properties of nanoscaled magnetic particles have generated much interest due to their applications in different areas such as ferrofluid technology, catalysts and medical applications, such as magnetically guided drug delivery, contrast agents in magnetic resonance imaging (MRI) or hyperthermia [1].

On the nanoscale range the properties of the particles depend on finite-size and surface effects that are enhanced as the particle size decreases. In small magnetic particles the size effects are related to the low number of moment carriers inside the magnetic core, and the surface effects are due to the lack of coordination, spin canting and disorder from the surface atoms. Therefore, the magnetic behavior of nanoparticles is the result of the ordered core and the covering shell of disordered spin. Dipolar and canted surface-spin interactions affect the magnetic behavior of nanoparticles because they modify the anisotropy of the system. Moreover, isolated particles can interact with the surrounding media, organic or inorganic shell, polymers or inorganic matrices [2]. These interactions also modify the surface anisotropy and affect magnetic parameters. The contribution and strength of these interactions are different depending on composition, particle size and synthesis conditions and therefore, it can be difficult to separate the size and surface effects on the magnetic properties. In this context, the aim of this work is to study the magnetic behavior of $ZnFe_2O_4$ nanoparticles coated with organic molecules and encased in silica porous matrices in order to investigate the effect of the particle interactions on the magnetic properties.

$ZnFe_2O_4$ nanoparticles were prepared by two different methods. In the first case, zinc ferrite nanoparticles were prepared using thermal decomposition of ferrite precursors in a high boiling point solvent method [3]. $Zn(acac)_2$ and $Fe(acac)_3$ were used as ferrite precursors and phenyleter as solvent. Oleylamine, 1,2-hexadecanediol and oleic acid were used as stabilizing agents in order to protect the surface of the particles (Figure 1a, sample Zn-3.7) and to control the growth. The nanoparticles were also prepared encased in porous matrices. For this purpose, aqueous solution containing stoichiometric amount of Zn nitrate and Fe nitrate was infiltrated in MCM-41 and SBA-15 type materials and the infiltrated materials were kept at room temperature for 24 hours and then, the solids were heated at 600 ºC during 2 hours. After this treatment, ferrite nanoparticles inside the porous networks of the matrices were obtained (Figure 1b-c, samples MH-Zn and SB-Zn respectively).

Representative TEM images corresponding to monodisperse $ZnFe_2O_4$ nanoparticles and nanoparticles embedded in different matrices are collected in Figure 1. The zinc ferrite nanoparticles coated with oleic acid present controlled size and shape and show a narrow particle size distribution with mean size 3.7 nm. In figures 1b and 1c we can see $ZnFe_2O_4$ nanoparticles with size of 2.5 nm and 6-9nm inside the tubular channel of the MCM-41 and SBA-15 matrices respectively.

Figure 1d show the ZFC and FC magnetic susceptibility versus temperature curves of different samples. The high values of susceptibility suggest that, in all cases, the

nanoparticles behave as superparamagnetic above the blocking temperature (T_B) and the values of T_B increase when $ZnFe_2O_4$ nanoparticles size increases. The shape of the FC curve below T_B and the high difference between the ZFC and FC susceptibility values at low temperature suggests that the interparticle interactions are not significant. In the case of zinc ferrite nanoparticles stabilized with oleic acid behave as magnetically independent without interactions. Although the dipolar interactions could exist, they are not intense enough to prevent the increasing in FC magnetization below T_B as it can be observed in figure 1d. In $ZnFe_2O_4$ nanoparticles encased in porous matrices, the nanoparticles are aligned inside the pores of the matrix, therefore must present dipolar interactions due to the geometry of the channels, but these particles can be strongly magnetized. It is noting that the higher values of coercive field at 5K for zinc ferrite nanoparticles encased in MCM-41 and SBA-15 matrices, in comparison to the Zn-ferrite coated with oleic acid, seems to be due to the mechanical stress imposed by the matrix [4].

References:

[1] Y.W. Jun, J.W. Seo , J. Cheon , *Acc. Chem. Res.*, **(2008)** 41 (2) 179-189
[2] V. Blanco-Gutierrez , M. Virumbrales , R. Saez-Puche, and Maria J. Torralvo-Fernandez, *J. Phys. Chem. C*, **(2013)**, 117 (40), pp 20927–20935
[3] S. Sun, H. Zeng, D. B. Robinson, S. Raoux, P. M. Rice, S. X. Wang, and G. Li, *J. Am. Chem. Soc*., **(2004)** 126 (1) 273-279
[4]V. Blanco-Gutiérrez, E. Urones-Garrote, María J. Torralvo-Fernández, and R. Sáez-Puche, *Chem. Mater*., (**2010**) 22 (22) 6130–6137

Figures:

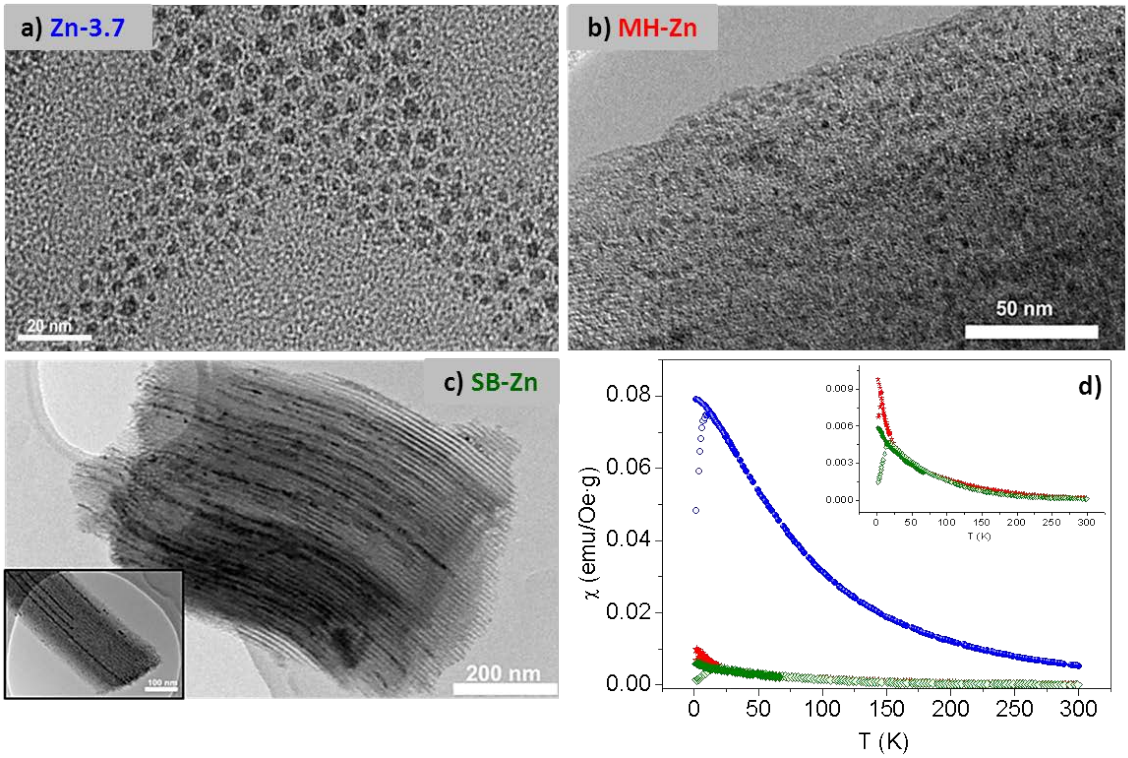

Fig.1. TEM micrographs of: (a) $ZnFe_2O_4$ nanoparticles coated with oleic acid (sample Zn-3.7) and encased in (b) MCM-41 (sample MH-Zn) and (c) SBA-15 (sample SB-Zn) matrices. (d) ZFC and FC magnetic susceptibility curves for the samples.

Technological issues of highly reactive nanopowders synthesis for functional ceramics

G.A. Dosovitskiy,[a] A.L. Mikhlin,[a] K.B. Bogatov,[a] D.E. Kuznetsova,[a] E.V. Grishechkina,[a] A.E. Dosovitskiy [a]

[a] Institute of Chemical Reagents and High Purity Chemical Substances, IREA, Bogorodskiy val str. 3, Moscow, 107076, Russia

Synthesis of high performance dense functional ceramics has two major requirements: 1) high quality of ceramic body, which is default by initial powder microstructure and compaction and sintering procedures; 2) low concentration of certain impurities, which is default by raw material purity control and absence of pollution during synthesis. Most routes of synthesis of transparent and translucent ceramics imply use of nanostructured powders as raw materials (having primary particles smaller than 100 nm), because small primary particle size provides high powder sinterability. This type of ceramics based on rare earth and rare earth containing oxides has existing and promising applications as laser materials, scintillators, LED phosphors, etc. Non-transparent dense functional ceramics, such as SOFC electrolytes or piezoceramics, also require powders with thoroughly controlled microstructure and particle size of near-micrometer scale.

During the development of a given novel material, on initial stage of research the work is mainly focused on obtaining necessary properties of powders and ceramics. Moving forward to technological applications raises a number of additional issues concerning powders production method: cost efficiency and throughput, technological stability, raw materials availability, necessary workers qualification, ecological impact. In order to scale up the process a number of additional studies must be done.

Requirement for minimizing impurity content makes mechanical milling of powders down to nanosize an unfavorable procedure. There are several techniques that are mostly used for synthesis of nanostructured powders by chemical means, such as coprecipitation, sol-gel synthesis, spray pyrolysis, combustion. Among these coprecipitation presents a combination of necessary parameters: allows obtain powders with necessary characteristics [1] and has potential for scaling up. In current work dependence of powder characteristics on synthesis conditions is studied and powder characteristics effect on ceramics sinterability. Technology details, important for scaling the synthesis up, are emphasized.

Binary rare earth oxides and rare earth aluminum garnets were objects of current study. The powders were synthesized in batches 10 g – 1 kg by (co)precipitation from nitrate solutions using ammonium hydrocarbonate, with following calcination above 1000^{o}C. Purity of raw materials was controlled in-house using ICP-MS and ICP-AE techniques. Additional purification of Al nitrate was shown to be necessary and performed. Ceramic samples were compacted using uniaxial press with pressures 10-50 MPa and sintered in air at temperatures up to 1600^{o}C.

Phase composition was controlled using XRD («eMMA» GBC Scientific Equipment). SEM was used to study primary particle size (Hitachi SU 1510). Agglomeration was studied using

SEM, optical microscopy and laser diffraction (Mastersizer 2000, Malvern Instruments). Thermal transformation of powders was studied by DTA (SDT Q600, TA Instruments). Figure depicts a typical set of studies, performed to characterize a powder sample.

Synthesized powders have primary particles with nearly rounded shape and size in the range 50-100 nm, which form agglomerates with size 5-100+ μm. Primary particle size is mostly determined by solutions concentration and precipitant choice, while agglomeration strongly depends on precipitation pH value and precipitate processing (washing, drying). Measurement of technological solutions conductivity has shown to be useful technique to control synthesis process. It was shown, that precipitate ageing could result in drastic microstructure change, as it happens for yttrium oxide: rounded particles transform to plate-like particles during several hours under mother liquor.

It was shown, that powder agglomeration plays crucial role in sintering of ceramics: while differently agglomerated powders demonstrate equal green body density after pressing, powders with high content of hard agglomerates above 80-100 μm form strongly nonuniform ceramics, and uniform and dense ceramics could be formed with weaker agglomerated powders.

References:

[1] Ji-Guang Li, Takayasu Ikegami, Jong-Heun Lee, Toshiyuki Mori, *J. Am. Ceram. Soc.*, **83** (2000) 961

Figures:

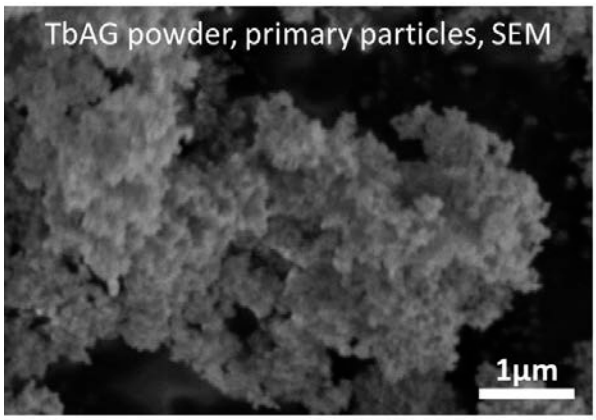

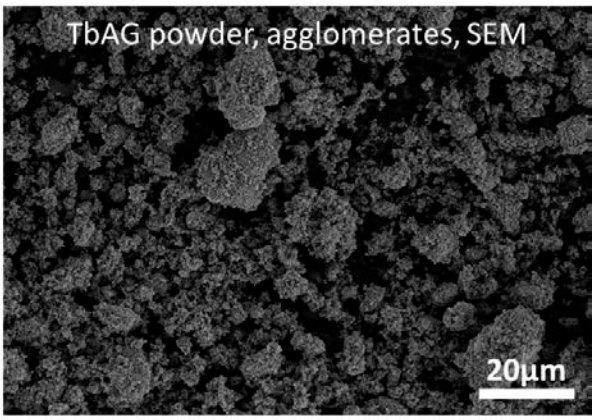

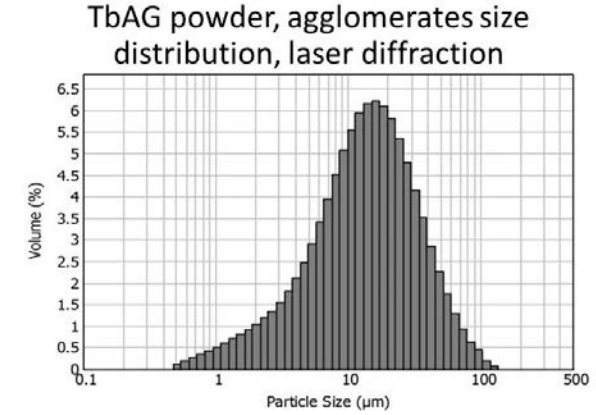

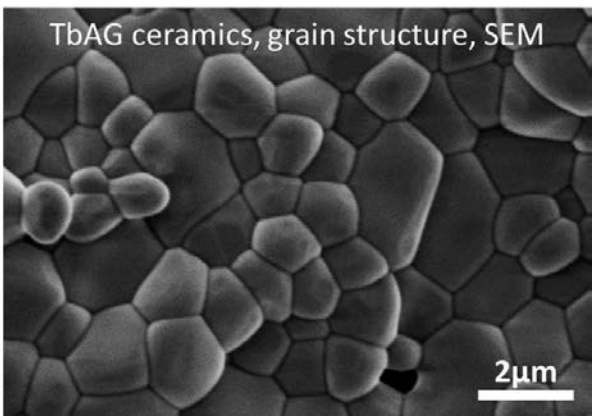

Processing, phase transitions and functional properties of BSPT Ceramics

A.L. Mikhlin[a], A.H. Segalla[b], G.A. Dosovitskiy[a],
A.V. Mosunov[c], A.E. Dosovitskiy[a], E.D. Politova[c]

[a]NeoChem JSC, Profsoyuznaya str. 115-2-331, Moscow, 117647, Russia;
[b]ELPA Company, Panfilovsky pr. 10, Zelenograd, Moscow, 124460, Russia;
[c]Karpov Institute of Physical Chemistry, Obukha s.-st., 3-1/12, Moscow, 105064, Russia

Strong demand for piezoelectric materials, capable of working at high temperatures, drives the development of new piezoelectrics with high Curie temperatures T_C [1]. Ceramics based on solid solutions (1-x)$BiScO_3$ - $xPbTiO_3$ (BSPT) was intensively studied in recent years because its compositions close to the morphotropic phase boundary (MPB) revealed rather high T_C values > 700 K and high piezoelectric activity [2 - 5]. However, functional properties of the BSPT-based compositions are not optimized up to date, and wide variations in ceramics properties may be observed depending on preparation conditions.

In this work, influence of the initial powder preparation conditions on phase content, the unit cell parameters, dielectric and piezoelectric properties of compositions in the BSPT system close to the MPB (with x = 0.635 - 0.65) were studied. Ceramic solid solutions were prepared using the powders obtained from Bi, Sc, Pb and Ti nitrate solutions following the procedure described in [5]. The powders were calcined at 700 - 950^{o}C (2 - 6 h), pressed into pellets and sintered at 1130-1150^{o}C (2 - 4 h) in the PbO-enriched atmosphere, then slowly cooled to the room temperature. Small amounts of Cr_2O_3 were added to some compositions.

Phase composition and crystal structure parameters were determined using the X-ray diffraction (DRON-3M with $Cu_{K\alpha}$-beam). Microstructure of the powders was checked by scanning electron microscopy (SEM) (JEOL JSM-7401F, Analysis Station JED-2300). Dielectric properties were studied by the dielectric spectroscopy method (Agilent 4284 A, 1 V) in the temperature range of 300 – 1000 K at frequencies 100 Hz – 1 MHz. The d_{33} piezoelectric coefficients were measured using YE 2730A d_{33} meter (APC products) with preliminary poling of samples in electric field. The electromechanical coupling coefficient k_t was measured by the standard resonance – antiresonance method.

According to the X-Ray diffraction data, powders obtained at temperatures 750 - 950^{o}C possessed Perovskite-type structure (Figure). The convolutions of the diffraction peaks with $h^2+k^2+l^2=4$ (shown in inserts) demonstrate strong dependence of relative content of tetragonal and rhombohedral phases, typical for the compositions in the vicinity of MPB, on both sintering temperature and composition. Content of tetragonal phase increases with x value. Small displacements of the diffraction peaks indicate small changes in unit cell parameters of the samples caused by changes in composition.

According to the SEM data, average size of synthesized particles varies in a range 0.1 - 1 μm, and grain size in ceramics sintered at 1130 - 1150^{o}C does not exceed 2 - 3 μm. Small grain size may be related to the neighboring of the tetragonal and rhombohedral phases in obtained ceramics, which hinders grain growth by inducing strain during sintering.

Dielectric measurements revealed the 1st order sharp ferroelectric phase transitions marked by peaks in dielectric permittivity $\varepsilon(t)$ and corresponding minima in dielectric loss tg$\delta(t)$ curves at temperatures ~ 700 K. Slight shift of the T_C values determined by both x value and relative content of tetragonal and rhombohedral phases was revealed. It should be noted that strong variations in ε and σ values, more than to 2 times and 1 order, respectively, were observed. High piezoelectric coefficients d_{33} values up to 430 and 340 pC/N were measured in ceramics with compositions, corresponding to x=0.64 and x=0.645, respectively. Additional quenching of poled ceramics [6] allowed us to increase the d_{33} value up to 520 pC/N, which is close to the top values reported for BSPT ceramics [7].

References:

[1] Y. Higuchi, H. Ogawa, D. Kuroda, M. Kimura, H. Takagi, Y. Sakabe, *Key Engineering Materials* **421-422** (2010) 375.
[2] R. E. Eitel, C. A. Randall, T. R. Shrout, P. W. Paul, W. Hackenberger, S. E. Park, *Jpn. J. Appl. Phys.* **40** (2001) 5999.
[3] E.D. Politova, B.V. Egorova, G.M. Kaleva, A.V. Mosunov, S.Yu. Stefanovich, A.H. Segalla, J. Zeng, *Ferroelectrics* **419** (2011) 83.
[4] E.D. Politova, G.M. Kaleva, A.V. Mosunov, A.H. Segalla, J. Zeng, *Key Engineering Materials*, **512-515** (2012) 1363.
[5] E.D. Politova, G.M. Kaleva, A.V. Mosunov, A.H. Segalla, A.E. Dosovitskiy, A.L. Mikhlin, *Journ. Adv. Dielectrics*, **3** (2013) 1350024 (5 pages).
[6]. A.H. Segalla, E.G. Smazhevskaya, N.B. Feldman, E.S. Solov'eva, I.A. Aleksandrova, E.B. Harash, *Izv. Acad. Sci, physics* (in russian) **35** (1971) 1989.
[7] T. Zou, X. Wang, Wei Zhao, and Longtu Li, *J. Am. Ceram. Soc.*, **91** (2008) 121.

Figures:

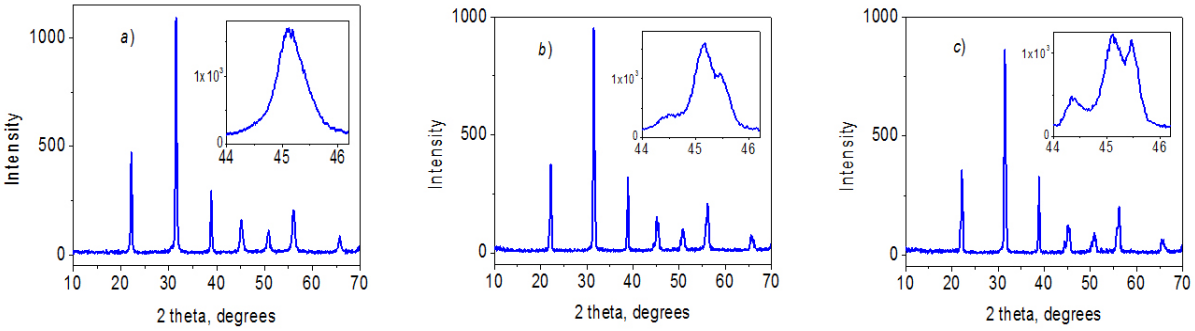

Fig.1. X-Ray diffraction patterns of the samples with x=0.64 annealed at 750°C (*a*), 850°C (*b*), 950°C (*c*). In inserts convolutions of the peaks with $h^2+k^2+l^2=4$ are shown.

Acknowledgments:
The work was partly supported by the Russian Foundation for Basic Research (Project # 12-03-00388).

A_2MPO_4F fluoride-phosphates as high-energy cathode materials for Lithium-ion batteries

Stanislav S. Fedotov,[a] Nellie R. Khasanova,[a] Oleg A. Drozhzhin,[a] Evgeny V. Antipov

[a] Chemistry Department, Lomonosov Moscow State University, Moscow, Russia.
fedotov.msu@gmail.com

The interrelation between structure and property is a crucial principle taken into account when developing new functional materials including electrode materials for Li-ion and Na-ion batteries. Analysis and further tuning of crystal structure and chemical composition pave the way towards the enhancement of various electrochemical properties of such materials, mainly specific capacity, working potential and kinetic characteristics of the ion diffusion in the material.

Considering these ideas, fluoride-phosphates with a general formula of A_2MPO_4F (A – alkali metal, M – 3d transition metal) were proposed and then recognized as a perspective class of cathode materials for Li-ion and Na-ion batteries of various large-scale and grid applications [1,2,3,4]. Indeed, phosphate-groups along with fluorine in the structure give rise to a significant potential increase in comparison to oxide materials; a theoretical possibility to extract more than one alkali ion from the lattice makes us expect a higher specific capacity; moreover, a weaker affinity of lithium towards fluorine than oxygen along with solid-solution intercalation mechanism forecast a faster ion transport in the cell.

Depending on the nature of alkali and transition metal there exist three basic types of frameworks within the class found up to now: stacked Li_2MPO_4F (M = Ni, Co), 3D Na_2MnPO_4F and layered Na_2MPO_4F (M = Fe, Co) [1,2,3]. Among them isostructural Li_2MPO_4F (M = Ni, Co) reveal a remarkable prospective as high-voltage cathodes, operating at potentials up to 5.5V [2,3,4]. However, the absence of a commercial electrolyte, whose range of stability covers these operating voltages, hinders a comprehensive examination of the materials [5]. It is supposed that the solid-solution intercalation mechanism attributed to Li_2MPO_4F enables to linearly shift the potential on substitution of Co and Ni by Fe and Mn, possessing a lower M^{3+}/M^{2+} potential [3,5].

Thus the aim of this work is synthesis and electrochemical investigation of $(Li,Na)_2Co_{1-x}Fe_xPO_4F$ cathode materials.

For the preparation of $(Li,Na)_2Co_{1-x}Fe_xPO_4F$ cathode materials conventional solid-state and freeze-drying methods were utilized. It was shown that the solid-solution range of $Li_2Co_{1-x}Fe_xPO_4F$ was limited to $x \leq 0.3$. A deeper substitution of Co by Fe leads to multi-phase samples. With the increase of x annealing temperature should be elevated up to 750°C. The further rise of temperature results in melting of samples.

Owing to the “elasticity” of Li_2MPO_4F framework [6] it was suggested that the further substitution would be achievable by simultaneous substitution for Na of Li. As a result $Li_{1.6}Na_{0.4}Co_{0.6}Fe_{0.4}PO_4F$ and $LiNaCo_{0.5}Fe_{0.5}PO_4F$ compounds were obtained. The Rietveld refinement of $LiNaCo_{0.5}Fe_{0.5}PO_4F$ structure, based on joint synchrotron and neutron diffraction data (orthorhombic *Pnma*, a = 10.9532(2) Å, b = 6.33704(7) Å, c = 11.3900(2) Å, V = 790.59(2) Å^3), revealed sodium is mainly located in [010]-channels, while other alkali positions are occupied by lithium (figure 1.). Fe oxidation states in the material were determined by Mössbauer spectroscopy, that found only two doublets attributed to Fe^{2+}. The chemical composition of the materials was confirmed by EDS microanalysis.

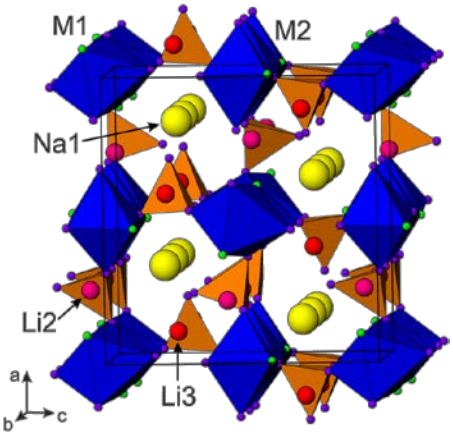

Figure 1. The graphic representation of $LiNaCo_{0.5}Fe_{0.5}PO_4F$ structure.
MO_4F_2 units are depicted as blue octaedra, sodium and lithium are drawn as colored spheres.

Electrochemical behavior of $LiNaCo_{0.5}Fe_{0.5}PO_4F$, prepared by a ceramic route, was examined by means of cycling voltammetry (CV) technique. This material demonstrated a reversible electrochemical activity towards lithium in a potential range of 2.5–4.5 V. The initial discharge capacity was 75% of the theoretical value regarding Fe^{3+}/Fe^{2+} couple. It should be noted that an average Fe^{3+}/Fe^{2+} potential in $LiNaCo_{0.5}Fe_{0.5}PO_4F$ is 0.1V higher comparing to pure $LiNaFePO_4F$, that confirms the idea of fine potential tuning by means of substitution. Going beyond 4.5 V an anodic peak corresponded to an oxidation of Co^{2+} was observed but no cathodic activity was detected, that may be explained by non-optimized particles morphology of the ceramic sample taken for these measurements. $LiNaCo_{0.5}Fe_{0.5}PO_4F$ materials prepared by the freeze-drying technique are now under investigation.

The substitution for all lithium by sodium brings to another structural type with quasi-2D framework [1]. Cathode materials on the basis of $Na_2Co_{0.5}Fe_{0.5}PO_4F$ showed reversible electrochemical activity towards lithium in 2.5–5.4V range. Broad peaks corresponded to Fe^{3+}/Fe^{2+} (2.7–3.5V) and Co^{3+}/Co^{2+} (4.1–4.7V) were identified.

The comparison between synthetic routes and electrochemical properties of two types of fluoride-phosphate materials will be presented.

Acknowledgements:

The work was supported in part by Russian Foundation for Basic Research (RFBR grant 13-03-00495a)

References:

[1] B. L. Ellis, W. R. Michael Makahnouk, W. N. Rowan-Weetaluktuk, D. H. Ryan, L. F. Nazar, *Chem. Mater*., **22** (2010) 1059.
[2] S. Okada, M. Ueno, Y. Uebou, J. Yamaki, *J. Power Sources*, **146** (2005) 565.
[3] N. R. Khasanova, A. N. Gavrilov, E. V. Antipov, K. G. Bramnik, H. Hibst, *J. Power Sources*, **196** (2011) 355.
[4] M. Nagahama, N. Hasegawa, S. Okada, *J. Electrochem. Soc*., **157** (2010) A748.
[5] N. R. Khasanova, O. A. Drozhzhin, S. S. Fedotov, D. A. Storozhilova, R. V. Panin, E. V. Antipov, *Beilstein J. Nanotechnol*., **4** (2013) 860.
[6] N. R. Khasanova, O. A. Drozhzhin, D. A. Storozhilova, C. Delmas, E. V. Antipov, *Chem. Mater*., **24** (2012) 4271.

High Temperature Oxidation of Austenitic Stainless Steels in Relation with the Oxide/Metal Interfacial Behaviour During Tensile Test

E. Fedorova[a,b], M. Braccini[c], D. Monceau[b], D. Oquab[b], V. Parry[c], M. Mantel[c,d], C. Pascal[c], Y. Wouters[c]

[a] Polytechnic Institute of Siberian Federal University, Russia
[b] Université de Toulouse, Institut Carnot CIRIMAT, ENSIACET, France
[c]Université de Grenoble, SIMaP, France
[d]UGITECH SA, Ugine, France

The resistance of high-temperature alloys to combined environmental attack and mechanical stresses is partly governed by their ability to maintain a protective oxide scale, i.e. an oxide layer with low growth kinetics and high adherence to the substrate [1].
The main objective of the present study is to investigate the oxide/metal interfacial behavior during high temperature isothermal oxidation, thermocycling and static mechanical loading. The sulfur content was used as a sensitive parameter influencing the adhesion. The negative effect of sulfur on the adherence of oxide scales grown on alumina or chromia forming alloys after high temperature oxidation have been widely studied and is known to be the major cause of protective layer failure [2, 3].

Two austenitic stainless steels, AISI 304L and AISI 303, provided by Ugitech were chosen as substrates. AISI 304L contains a small amount of sulfur (0.025 wt.%), whereas the other alloy contains 0.249 wt.% S. Isothermal and cyclic thermogravimetric tests were performed using a high precision SETARAM™ TAG 24S thermobalance. To investigate the isothermal oxidation kinetics the samples were oxidized at 1000 °C for 50 hours with a heating rate of 60 °C min^{-1}. Synthetic air flow rate was maintained at 0.6 l/h corresponding to a linear flow of 0.17 cm/s at RT. Tensile specimens were isothermally oxidized in a tubular furnace under the same conditions. During cyclic oxidation, a thermal cycle consisted of a heating period at 50 °C.min^{-1} up to 1000 °C, followed by a dwell of 60 min at 1000 °C and a cooling ramp with an initial rate of 60 °C. min^{-1}. The total duration of one cycle was 180 min.

To study the oxide/metal interface, failure mechanisms and oxide scales morphology after isothermal oxidation and thermal cycling, the oxide scale surfaces and sample cross-sections were analysed by SEM-EDS. The chemical and phase composition of the oxide scales were determined with X-Ray diffraction and Raman spectroscopy.

In situ tensile tests on isothermally oxidized samples of 303 and 304L alloys with different sulfur content were performed using a horizontal tensile machine designed to be placed within the JEOL JSM 6400 SEM chamber [4]. The elongation rate of 100 μm/min was applied. To follow the oxide damages during tensile loading, series of SEM pictures were periodically taken to be treated by image analysis. The data were used to develop a characteristic curve: cracks density vs. applied strain. The dependence was fitted by a semi-empirical relationship [5, 6].

The net mass gain curves obtained during isothermal oxidation at 1000°C for 50 hours showed faster oxidation kinetics for 303 samples. The parabolic rate constant for AISI 304L calculated between 7 h and the end of the experiment was about $3.5 \cdot 10^{-6}$ $mg^2/cm^4/s$ and this parameter was one order of magnitude higher in the case of AISI 303: $2.9 \cdot 10^{-5}$ $mg^2/cm^4/s$.

It was observed that during the tensile test the cracking of the oxide scale on the 303 steel was more intensive: cracking begins earlier, crack density increases faster and the saturation value is higher than for the 304L steel (see Fig.).

The cyclic oxidation behavior of the alloys revealed the expected improvement in scale retention as the sulfur content was decreased. After 85 cycles, the 303 alloy sample underwent significant oxide spallation with an average weight loss of 2.6 mg/cm^2 whereas the weight loss of 0.17 mg/cm2 was observed for the 304L sample after 145 cycles.

All those results are discussed in relation with the sulfur content, oxide scale chemistry and microstructure.

This work is supported by National Center for Scientific Research (CNRS, France) through the Projet International de Coopération Scientifique (PICS) “Adherons!2” and Russian Foundation for Basic Research (RFBR) Ref n° 13-08-91053-CNRS_a.

References:

[1] Neil Birks, Gerald H. Meier, and Frederick S. Petit, *High-Temperature Oxidation of Metals, Second Edition Cambridge University Press*, (2006), 338.
[2] Peggy Y. Hou and John Stringer, *Oxid. Met.*, **38** (1992) 323.
[3] G. Smeggil, A. W. Funkenbush, and N. S. Bornstein, *Metall. Trans.*, **A17** (1986) 923.
[4] A. Galerie, M. Dupeux, Y. Wouters, F. Toscan, *Mater. Sci. Forum* **522-523** (2006) 441.
[5] P. Scafidi and M. Ignat, *J. Adhesion Sci. Technol.* **12** (1998) 1219.
[6] M.S. Hu and A.G. Evans, *Acta metal.* **37** (1989) 917.

Figures:

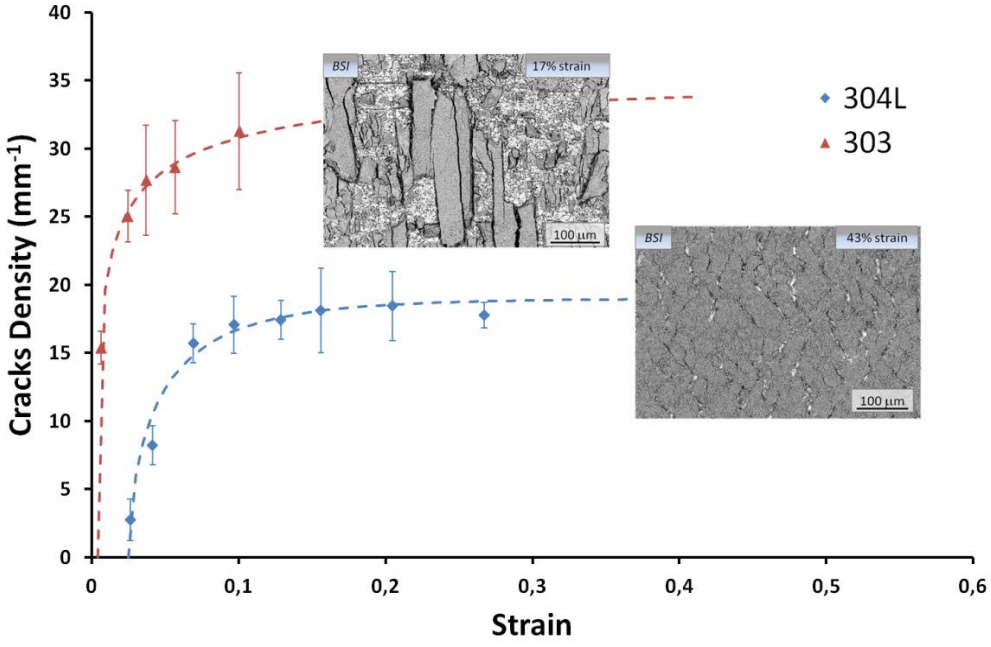

Fig.1. Crack density evolution and oxide scale surface during tensile test

Size effects in monodisperse MFe_2O_4 (M=Fe, Co, and Zn) ferrite nanoparticles

A. Delgado[a], M. Virumbrales [a], R. Sáez Puche [a,*] and M.J. Torralvo [a]

[a]Departamento de Química Inorgánica, Facultad Químicas, Universidad Complutense de Madrid, 28040, Madrid, Spain
**rsp92@ucm.es*

MFe_2O_4 (M = Fe, Co and Zn) oxides crystallize with the spinel-type structure, S.G. Fd-3m, where the M and Fe atomos are occupying 1/8 tetrahedral (Td) and ½ of the octahedral (Oh) sites of the cubic close packing of O^{2-} arrangement. In the case of the $ZnFe_2O_4$ prepared as particle of several microns crystallizes with the so-called normal spinel $(Zn)[Fe_2]O_4$, where () and [] refers to the tetrahedral and octahedral sites of the O^{2-} cubic close packing. As a consequence of this cationic distribution this Zn-spinel is antiferromagnetic with T_N=10K. By contrast the case of the MFe_2O_4 with M= Fe and Co, are inverse spinel $(Fe)[FeM]O_4$ and behave as ferromagnetic with T_C of 848K and 793K respectively. However, when these ferrite spinels are prepared in the nanoscale, a mixed spinel configuration is obtained where the Fe^{3+} and M^{2+} cations are simultaneously occupying both the Td and Oh sites giving as result spinel of general formula $(M_{1-x}Fe_x)[Fe_{2-x}M_x]O_4$ where x is the so-called inversion degree [1]. These materials present superparamagnetic behavior above the blocking temperature (T_B) and their magnetic properties are dependent of the particle size, inversion degree and the interparticle interactions.

Nowadays, many synthetic methods have been developed to prepared nanoparticles with controlled size and shape; however in most of the essays the obtained materials are formed by aggregates that it constitutes a serious problem when these materials are intended to be technologically employed. In order to avoid this problem as well the possible interparticle interactions that will modify their magnetic properties, some alternative synthetic routes have been investigated such as for example encasing the nanoparticles in different organic or inorganic matrices. The present work is focused on the comparative analysis of morphological, structural and magnetic properties of ternary ferrite nanoparticles having iron, cobalt and zinc coated with oleic acid molecules in order to minimize the interparticle interaction and to obtain isolated nanoparticles.

MFe_2O_4 (M=Fe, Co, and Zn) nanoparticles were synthesized following a method of thermal decomposition of ferrite precursors in high-boiling point solvents [2]. Iron (III) and M (II) acetylacetonates were used as inorganic precursors, 1,2-hexadecanediol as a reductant, oleic acid and oleylamine as stabilizing agents and phenyl ether as solvent (BP: 259°C). The reagents were mixed and magnetically stirred under Argon flow. The mixture was heated to 200°C for a certain time and then heated up to the boiling point of the solvent. To obtain nanoparticles with different size the reaction time was changed.

TEM images reveal an homogeneous rounded morphology for all the samples with a particle size of 4.7, 2.6 and 3.7 nm for the ferrites with M=Fe, Co and Zn respectively, as it can be observed in Figure 1. These MFe_2O_4 show a superparamagnetic behavior with a blocking temperatures, estimated from the maxima found in the ZFC susceptibility vs T plots, of 6.35K, 53.6 K and 13.3K for the Fe, Co and Zn ferrite respectively. The higher value of T_B observed in the case of Co spinel, which is due to the intrinsic anisotropy of this ion in comparison with Fe^{2+} and Zn^{2+} cations [3]. Below T_B, FC susceptibility increases that it is

indicative of the absence of interparticle interactions due to the particle coating by the oleic acid.

Magnetization is strongly dependent of the interaction between the surface cations with oleic acid molecules. The nature of bonding of oleic acid with MFe_2O_4 nanoparticles and the amount of oleic acid have been determined from the IR spectroscopy. In the case of magnetite, carboxylate groups are chelating ligands and this fact increases the surface anisotropy that decreases magnetization and it also justify that the smaller T_B value of 6.3K. However, in zinc ferrite the carboxylate groups acting as bridging ligands increases magnetization and the saturation magnetic moment unusually high, takes the value of 80 emu/g which corresponds to an inversion degree of 0.3. By contrast, in the case of the inverse MFe_2O_4 (M=Fe and Co) spinels a remarkable decreasing of the magnetization is observed in comparison with the bulk counterparts as it can be observed in Figure 1c.

References:

[1] V. Blanco-Gutierrez, F. Jimenez-Villacorta, P. Bonville, Maria J. Torralvo- Fernandez, R. Saez-Puche, *J. Phys. Chem. C*, **(2011)** 115 (5) 1627–1634.
[2] Shouheng Sun, Hao Zeng, David B. Robinson, Simone Raoux, Philip M. Rice, Shan X. Wang, and Guanxiong Li, *J. Am. Chem. Soc.*, **(2004)** 126 (1) 273-279
[3] V.Blanco-Gutierrez, J.A. Gallastegui, P. Bonville, M.J. Torralvo-Fernandez, R. Saez-Puche, *J.Phys. Chem. C*, **(2012)** 116 (45) 24331

Figures:

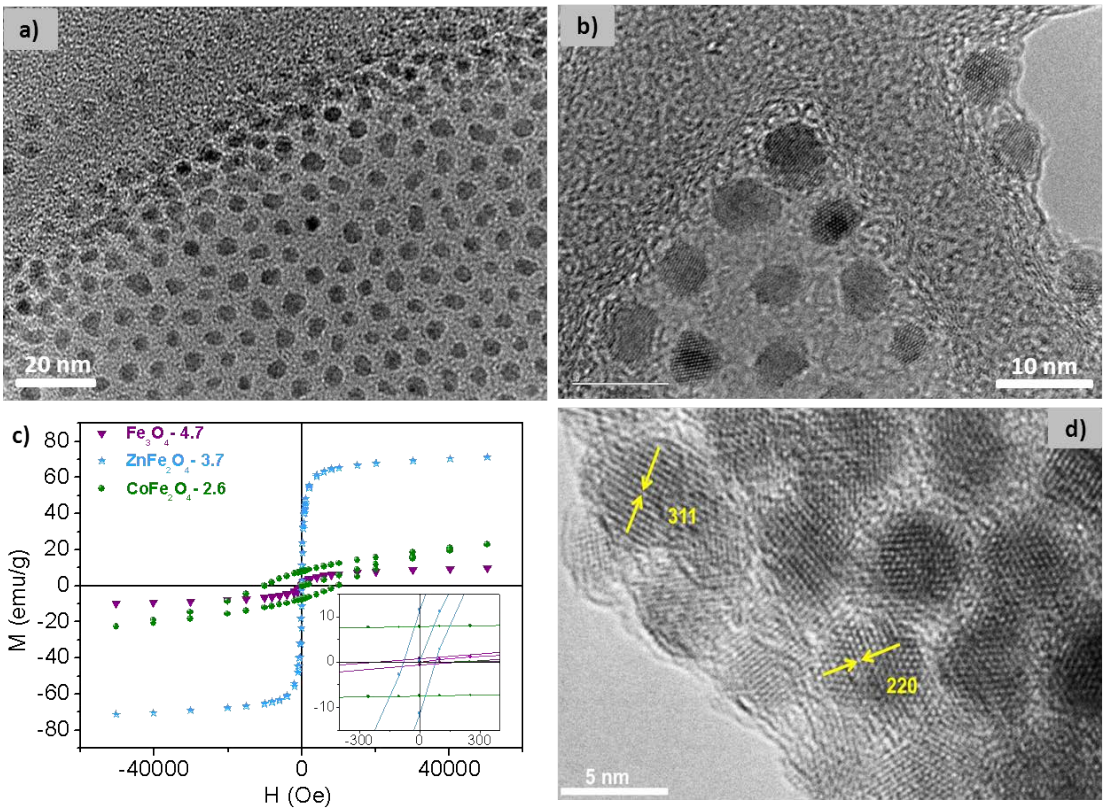

Figure 1. TEM micrographs of the spinel nanoparticles of a) $ZnFe_2O_4$, b) $CoFe_2O_4$ and d) Fe_3O_4; c) Hysteresis M vs. H plots at 5 K for the different MFe_2O_4 spinel ferrites.

Structures and Magnetic Properties of New Quadruple Perovskites $Ba_4LnM_3O_{12}$ (*Ln* = Rare earths; *M* = Ru, Ir)

Yukio Hinatsu,[a] Yoshihiro Doi,[a] Makoto Wakeshima[a]

[a]Department of Chemistry, Hokkaido University, Sapporo 060-0810, Japan

Perovskite-family oxides have attracted much interest due to their exotic electronic, magnetic, and structural properties. It is well known that a perovskite ABO_3 with a tolerance factor less than 1.0 forms a three-dimensional frame network of corner-sharing BO_6 octahedra, which can be described as a stacking sequence *abc*… Perovskites with a tolerance factor (*t*) greater than unity form face-sharing BO_6 octahedra, and the stacking sequence varies with the value of *t*.

If two kinds of cations are present in the B site, the ordering ratio of B and B' cations increases with an increasing difference in charge and size between B and B' cations. Most perovskites $BaLn_{1-x}M_xO_3$ containing both transition metal (*M*) and rare earth (*Ln*) ions exhibit a perfectly ordered B sublattice due to the difference in their ionic radii. The stacking sequence is controlled by changing the ratio of the *Ln* and *M* ions; double perovskites Ba_2LnMO_6 have a 1:1 type B-site cation ordering with the sequence *abc*.., and triple perovskites $Ba_3LnM_2O_9$ crystallize in a 6H-perovskite structure with a 1:2 type B-site cation ordering (the *abacbc*… sequence).

In this study, we report preparation, crystal structures and magnetic properties of quadruple perovskites $Ba_4LnM_3O_{12}$. Polycrystalline samples of $Ba_4LnM_3O_{12}$ (*Ln*= rare earths; *M* = Ru, Ir) were prepared by the standard solid-state reaction. BaO, BaO_2, Ru, RuO_2, $BaIrO_3$, and Ln_2O_3 were used as standard materials. They were well mixed in an agate mortar and pressed into pellets. They were enclosed with platinum tubes and heated at 1250 °C for 12-240 h.

From the powder x-ray and neutron diffraction measurements, it was found that *M* ions are octahedrally coordinated by six oxide ions, and three MO_6 octahedra share faces forming a M_3O_{12} trimer, and that the M_3O_{12} trimers and LnO_6 octahedra are alternately linked by corner-sharing and form the perovskite-type structure with 12 layers (Fig. 1) [1]. The change of lattice parameters (*a*, *b*, *c*, and β) and volume for $Ba_4LnM_3O_{12}$ against the ionic radius of Ln^{3+} show that except for the compounds having *Ln* = Ce, Pr, and Tb, they increase monotonously with the Ln^{3+} ionic radius. However, the values for *Ln* = Ce, Pr, and Tb compounds are considerably smaller than this trend (Fig. 2). For both *M* = Ru and Ir cases, the *Ln* –O bond lengths are close to the Ln^{4+}-O^{2-} lengths calculated from Shannon's ionic radii. These results show that the Ce, Pr, and Tb ions are in the tetravalent state. Therefore, the oxidation states of Ru and Ir are also tetravalent ($Ba_4Ln^{4+}Ru^{4+}{}_3O_{12}$, $Ba_4Ln^{4+}Ir^{4+}{}_3O_{12}$). For other *Ln* ions, the mean oxidation state of Ru and Ir ions is +4.33 ($Ba_4Ln^{3+}Ru^{4.33+}{}_3O_{12}$, $Ba_4Ln^{3+}Ir^{4.33+}{}_3O_{12}$).

Measurements of the magnetic susceptibility for $Ba_4LnM_3O_{12}$ give the contrastive results between the ruthenium-containing compounds $Ba_4LnRu_3O_{12}$ and the iridium-containing compounds $Ba_4LnIr_3O_{12}$. Any of the $Ba_4Ln^{3+}Ru^{4.33+}{}_3O_{12}$ compounds shows similar magnetic transitions at very low temperatures (3~8 K), whereas $Ba_4Ln^{3+}Ir^{4.33+}{}_3O_{12}$ (*Ln* ≠ La, Lu) compounds are paramagnetic down to 1.8 K.

Magnetic properties of $Ba_4Ln^{3+}Ir^{4.33+}{}_3O_{12}$ clearly show that we have to treat the *Ir* ions as the Ir_3O_{12} trimer to understand their magnetic behavior. Both compounds $Ba_4Ln^{3+}Ir^{4.33+}{}_3O_{12}$ (*Ln* = La, Lu) are diamagnetic, indicating that the $Ir^{4.33+}{}_3O_{12}$ trimers are diamagnetic. Other compounds $Ba_4Ln^{3+}Ir^{4.33+}{}_3O_{12}$ (i.e., $Ln \neq$ La, Lu) are paramagnetic down to 1.8 K, and their effective magnetic moments (μ_{eff}) are close to the magnetic moments of Ln^{3+} ions (μ_{Ln}). That is, the contribution of the $Ir^{4.33+}{}_3O_{12}$ trimer to the magnetic properties of $Ba_4LnIr_3O_{12}$ is negligible [2].

$Ba_4Ce^{4+}Ir^{4+}{}_3O_{12}$ orders antiferromagnetically at 10.5 K, while the corresponding ruthenium-containing compound $Ba_4Ce^{4+}Ru^{4+}{}_3O_{12}$ is paramagnetic. These magnetic results were well understood by the magnetic behavior of M_3O_{12} [3]. The effective magnetic moments and the entropy change for the magnetic ordering show that the trimers $Ru^{4.33+}{}_3O_{12}$ and $Ir^{4+}{}_3O_{12}$ have the $S = 1/2$ ground state, and in other cases there is no magnetic contribution from the trimers $Ru^{4+}{}_3O_{12}$ or $Ir^{4.33+}{}_3O_{12}$.

Unique magnetic properties of quadruple perovskites $Ba_4LnM_3O_{12}$ were compared with those of triple perovskites $Ba_3LnM_2O_9$ and double perovskites Ba_2LnMO_6.

Measurements of the electrical resistivity of $Ba_4LnM_3O_{12}$ and its analysis show that these compounds demonstrate two-dimensional Mott-variable range hopping behavior [4].

References:

[1] Y. Shimoda, Y. Doi, Y. Hinatsu and K. Ohoyama, *Chem.Mater.*, **20** (2008) 4512.
[2] Y. Shimoda, Y. Doi, M. Wakeshima, Y. Hinatsu, *J. Solid State Chem.*, **182** (2009) 2873.
[3] Y. Shimoda, Y. Doi, M. Wakeshima, Y. Hinatsu, *J. Solid State Chem.*, **183** (2010) 1962.
[4] Y. Shimoda, Y. Doi, M. Wakeshima, Y. Hinatsu, *Inorg. Chem.*, **48** (2009) 9952.

Figures:

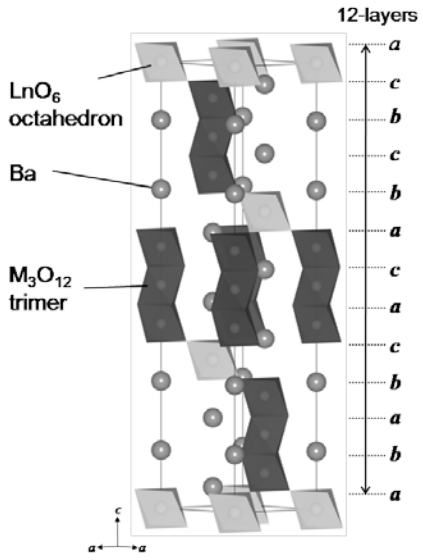

Figure 1: Crystal structure of $Ba_4LnM_3O_{12}$ (M = Ru, Ir)

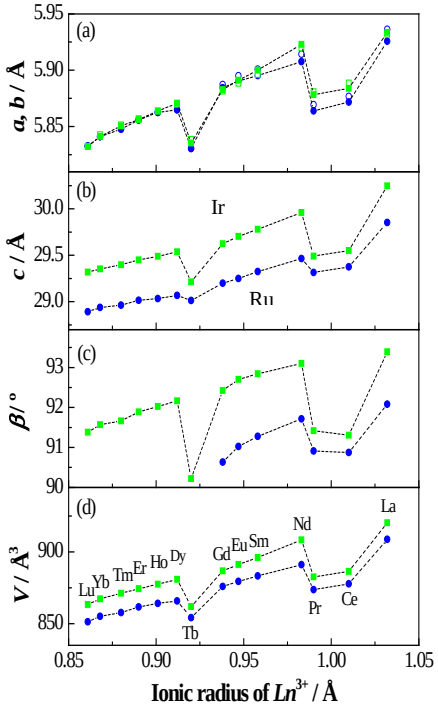

Figure 2: Variation of lattice parameters and volume for $Ba_4LnM_3O_{12}$ (M = Ru, Ir) against the ionic radius of Ln^{3+}.

Evidence of Spontaneous Endotaxial Chemical Nanosegregation in $La_{1/2-x}Li_{1/2-x}Sr_{2x}TiO_3$

E. García-González,[a] E. Urones-Garrote[b], W. Buchelli[c], J. Sanz[c], A. Várez[d]

[a] Departamento Química Inorgánica, Facultad de Ciencias Químicas, Universidad Complutense, 28040 Madrid, Spain esterg@quim.ucm.es
[b] Centro Nacional de Microscopia Electrónica, Universidad Complutense, E-28040, Madrid, Spain
[c]Instituto de Ciencia de Materiales de Madrid, CSIC, 28049 Cantoblanco, Madrid, Spain
[d]Departamento de Ciencia e Ingeniería de Materiales, Universidad Carlos III de Madrid, 28911 Leganés, Madrid, Spain

Over the last two decades, the search for new materials with high lithium ionic conductivity has attracted considerable interest. A wide variety of solid electrolytes with potential applications in all-solid high-energy batteries and other electrochemical devices have been reported [1]. In this respect, the interest in perovskite type oxides of the $La_{(2-y)/3}Li_yTiO_3$ (LLTO) system ($0 < y < 0.5$) has not diminished since the discovery of the excellent electrical properties of these materials [2]. A-sites are partially occupied by La^{3+} ions and small Li cations do not sit on the A sites themselves but in off centered positions or in the O4 windows between two A-sites. Then, low rate A-occupation and adequate A- cation size are crucial factors favoring lithium ions and vacancies to percolate through the crystal.
Powder diffraction studies, either using X-rays (XRD) or neutrons (ND), have shown that LLTO-type materials have a highly defective A-sublattice and High Resolution Electron Microscopy (HREM) has revealed a really complex microstructure. However, in spite of the considerable effort made in this respect the structural factors controlling Li-ion conductivity are still not completely well established.

In this contribution, we present the results obtained in the detailed microstructural investigation performed in the Sr-substituted LLTO compounds $La_{1/2-x}Li_{1/2-x}Sr_{2x}TiO_3$. State-of-the-art scanning transmission electron microscopy (STEM) has been used to explore the solid solution nature from the nanostructure. Powder XRD patterns exhibit cubic symmetry (P*m-3m*) but the microstructure results in a heterogeneous distribution of A-species. From the continuously changing lithium amount, the effective A-vacancy concentration is also continuously changing across the series. A mosaic type structure constituted by small domains is observed in which a double periodicity arises from the partial order of A-species in alternate A-O layers. This is consistent with previous studies. There is a clear dependence of domain size with Sr content and for the highest concentration domains are a few unit cells wide only. Selected Area Electron Diffraction (SAED) showed extra diffraction maxima of the type ½[111] which are not consistent with the average cell symmetry and this diffraction effect become clearer when increasing Sr content. Z-contrast HAADF imaging was used to visualize the chemical distribution in the samples. Local clustering of lithium atoms is observed, in agreement with recently published results [3]. In addition, spatially well distributed crystal regions of a few nanometers size are observed in which contrast in A-O layers correspond to a F-type lattice. The investigations performed led us to propose the local endotaxial segregation of a secondary phase in which La-rich and La-poor positions order in a NaCl-type distribution, thus giving rise to local F symmetry. Across the series, the system retains the perovskite structure by a structural and compositional phase separation, which

occurs solely on the A sites within a single B(Ti)-O matrix. Interestingly, a previous example has been very recently reported in which segregation involves just the B sublattice [4]. Spontaneous Endotaxial Phase Nanosegregation is a concept that applies well to describe this remarkable microstructure and the results we have obtained provide further support.

References:

[1] K. Takada, *Acta Mater.*, **61** (2013) 759.
[2] Y. Inaguma, C. Liquan, M. Itoh, T. Nakamura, T. Uchida, H. Ikuta, M. Wakihara, *Solid State Commun.* **86 (**1993) 689.
[3] X. Gao, C. A. J. Fisher, T. Kimura, Y. H. Ikuhara, H. Moriwake, A. Kuwabara, H. Oki, T. Tojigamori, R. Huang, Y. Ikuhara, *Chem. Mater.* **25 (**2013) 1607.
[4] A. Demont, R. Sayers, Maria A. Tsiamtsouri, S. Romani, P. A. Chater, H. Niu, C. Martí-Gastaldo, Z. Xu, Z. Deng, Y. Bréard, M. F. Thomas, J. B. Claridge, M. J. Rosseinsky *J. Am. Chem. Soc.* **135** (2013) 10114.

In situ surface modification by nickel hydroxide nanoparticles resulting from hydrolysis of polymeric metal complexes for fuel cell applications

Elena Alekseeva[a], Peixia Yang[a,b], Nikita Kuznetsov [a], Valery Malev[a], Oleg Levin[b]

[a] Institute of Chemistry, St. Petersburg State University, Petrodvoretz 198504, Russia
[b] School of Chemical Engineering and Technology, Harbin Institute of Technology, Harbin 150001, China

Fuel cells have been one of the most expected technology to solve many economic and ecologic problems of hydrocarbon economy during last two decades. However, until now, we can speak only about perspectives of such technology due to high cost of energy produced by fuel cells. The catalysts for fuel cells are rapidly poisoned during storage and operation, limiting fuel cell lifetime. Cheaper Ni based catalysts could be used for direct alcohol [1], alkaline [2] or direct borohydride [3] fuel cells. These types of cells are considered as one of prospective types of fuel cells for mass production. To produce fuel cell catalysts many methods exist [1-3], but most of them have some disadvantages – high size of catalyst particles, irregular structure or complicated synthesis route. Here we present a new method for producing fuel cell catalyst *in situ* at functioning the cell, without any previous manipulations for activation of the catalyst. The method works at room temperature, the received catalyst have nano-sizes of metal hydroxyde particles and regular structure with necessary spacing between particles.

In the case *in situ* means that the catalyst could be kept in inactive, stable state for any time as polymer film of metal complexes with Schiff base ligand on substrate layer. Deposition of such complexes is simple and described for variety of substrates [4-6]. Then as the fuel cell work starts, alkaline electrolyte at certain potential destroys the ligand polymer matrix and nanoparticles of metal are kept on the substrate surface and catalyze alcohol oxidation process later. Polymeric structure of the Schiff base complex ensures enough distance between nucleation centers during the hydroxide formation, so no agglomeration of nanoparticles is observed.

Fig 1. demonstrates the scanning electron microscope (SEM) image of the obtained catalyst layer on a polished glassy-carbon surface, where catalyst particles of about 10 nanometers size can be distinguished; fig. 2 proves the catalytic oxidation of ethyl alcohol on the formed catalyst in alkaline electrolyte.

Acknowledgements:
The work has been performed at financial support of Saint-Peterburg State University (grant# 12.38.77.2012) and Russian Found of Basic Research (grant #12-03-00560-a, 13-03-00843-a)
SEM study data presented in this work were obtained using the equipment of Interdisciplinary Resource Center for Nanotechnology of Saint-Peterburg State University.

Figures:

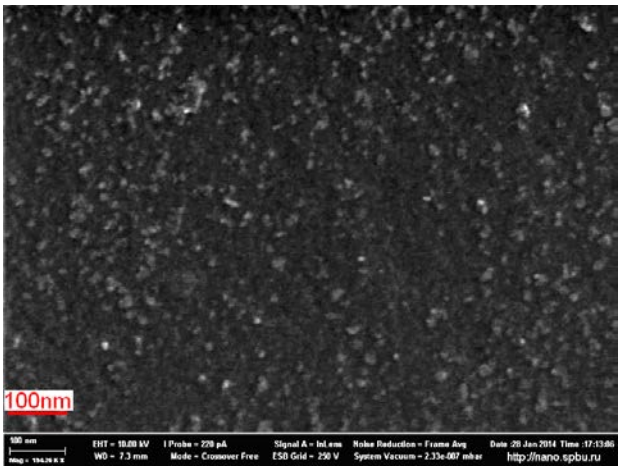

Fig. 1. SEM image of NiOOH catalyst, deposited on a glassy-carbon surface by proposed technique.

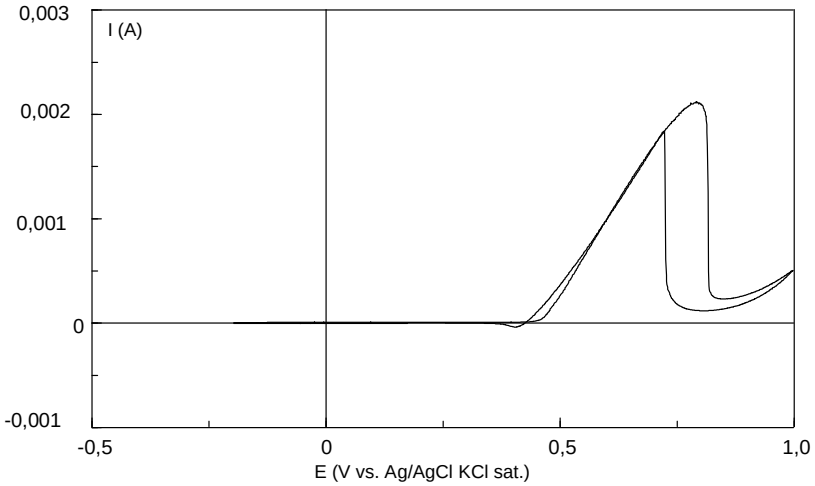

Fig. 2. Electrooxydation of ethyl alcohol on NiOOH catalyst in solution of 0.2 M NaOH and 1 M C_2H_5OH, electrode area is 0.07 cm^2.

References:

[1] Tarasevich M.R., Kuzov A.V., Direct alcohol fuel cells (2010), International Scientific Journal for Alternative Energy and Ecology, 7, pp. 87-108

[2] Guelzow, E., Nor, J.K., Nor, P.K., Schulze, M. A renaissance for alkaline fuel cells (2006) Fuel Cell Review, 3 (1), pp. 19-25

[3] Ma, J., Choudhury, N.A., Sahai, Y. A comprehensive review of direct borohydride fuel cells (2010) Renewable and Sustainable Energy Reviews, 14 (1), pp. 183-199

[4] Delime F., Leger J-M., Lamy C. Enhancement of the electrooxidation of ethanol on a Pt–PEM electrode modified by tin. Part I: Half cell study // J. Appl. Electrochem. 1999. Vol. 29. P. 1249.,

[5] Lamy C.J., Belgsir E.M., Leger J.-M. Electrocatalytic oxidation of aliphatic alcohols: Application to the direct alcohol fuel cell (DAFC) // J. Appl. Electrochem. 2001. Vol. 31. P. 799.

[6] Spinace E.V., Neto A.O., Linardi M. Electrooxidation of ethanol on PtRu/C electrocatalysts prepared from (η-C2H4)(Cl)Pt(μCl)2Ru(Cl)(η3,η3-C10H16) // J. Power Sources. 2004. Vol. 124. P. 426.]

Effect of surface active sites modification on nanocrystalline tin dioxide gas sensor properties

Artem Marikutsa, Marina Rumyantseva, Alexander Gaskov

Moscow State University, Chemistry dept., Moscow, Russia

Nanocrystalline tin dioxide is a perspective material for utilizing in semiconductor metal oxide (SMOX) gas sensors. Its advantages include high sensitivity to low concentrations of toxic and explosive gases in air, stability and low device sizes. The main limitation of semiconductor gas sensors is low selectivity [1]. The gases having similar redox properties interact with the SMOX surface in a similar manner during sensor signal formation. Most toxic gases belong to the group of reducing gases, like CO, NH_3, volatile organic compounds. Interacting non-selectively with oxide surface results in similar sensor properties to each of them and an inability of the sensor to distinguish between the gases. An efficient tool to improve selectivity is sensor surface modification aimed at specific active sites creation [2]. An appropriate choice of the modifiers for selective detection of particular gases discussed in [3,4] is a nontrivial problem because of the fact that the additives influence the active site on SnO_2 surface leading to unpredictable sensor phenomena [5].

In this presentation the results of experimental research of nanocrystalline tin dioxide modification by catalytic noble metal clusters, their influence on the surface active sites and sensor properties to ppm-range concentrations of CO and NH_3 are discussed. They were taken as an example of a pair of chemically different molecules belonging to reductive gases. Bases on literature data, palladium and ruthenium oxides were used as the modifiers aimed at SnO_2 selectivity increase as their specific catalytic activity to CO and NH_3, respectively, is well-known [6,7]. Nanocrystalline SnO_2 was synthesized via aqueous deposition of alpha-stannic acid from $SnCl_4*5H_2O$ solution followed by thermal treatment. Tin dioxide surface modification was performed by $Pd(acac)_2$ and $Ru(acac)_3$ impregnation subsequently annealed at 220-260 ^{0}C. In this way SnO_2, SnO_2/PdO and SnO_2/RuO_2 nanocomposites were obtained with BET surface 90-100 m^2/g and SnO_2 particle sizes 3-10 nm. The modifiers were shown by HRTEM, EXAFS, XANES and XPS to cluster (1-3 nm) on the agglomerates of SnO_2 nanoparticles in the form of amorphous PdO and structured RuO_2.

The following types of active sites on the materials surface were determined: oxidizing sites – chemisorbed oxygen; acid sites – tin cations (Lewis sites) and OH-groups (Broensted sites); spin-centers – O_2^- and OH·; and hydrated species – molecular adsorbed water and its dissociated derivatives. The experimental tools used for their investigation include temperature-programmed methods: reduction by H_2 and desorption of NH_3; electron spin resonance, IR spectroscopy and thermogravimetry. Comparing the results, it was deduced that PdO clusters promote SnO_2 surface hydroxylation leading to the increase of common hydrated species concentration and in particular OH-groups, Broensted acid sites and OH·. This is believed to be due to PdO electron-acceptor properties promoting donor-like H_2O molecules chemisorption. Ruthenium oxide was shown to increase the concentration of oxidizing (chemisorbed oxygen) surface sites. From oxygen isotopic exchange studies [8] this effect is explained by RuO_2-promoted O_2 adsorption and spillover.

The specific modifiers promotion of different active sites on SnO_2 surface results in its gas selectivity increase. Examining the sensor properties by *in situ* DC-conductance measurements to 2-50 ppm of CO and NH_3 in air at various temperature, the increase of CO sensitivity of SnO_2/PdO was observed especially at low (25-50 ^{0}C) temperature. The CO sensitivity increase should be due to PdO catalytic action, while the optimal detection temperature lowering is accounted for by OH-assisted CO oxidation (Fig.1*a*). This suggestion is confirmed by protonic species release during room-temperature SnO_2/PdO interaction with CO deduced from *in situ* impedance measurements [9]. The RuO_2-modified nanocrystalline tin dioxide is highly sensitive to NH_3 at raised temperature (150-200 ^{0}C). The SnO_2/RuO_2 – NH_3 selectivity was observed when testing sensor properties to CO+NH_3 mixtures in air. High ammonia sensitivity and selectivity is accounted for by RuO_2-catalyzed deep NH_3 oxidation to NO_x by chemisorbed oxygen species which are promoted by the modifier (Fig. 1*b*) [10].

References:

[1] *Metal Oxides.* (Ed. J.L.G. Fierro). CRC Press, Boca Raton, 2006.
[2] G. Korotcenkov, *Sens. Actuators B*, **107** (2005) 209.
[3] M.N. Rumyantseva, A.M. Gaskov, Russ. Chem. Bull., Int. Ed., **52(6)** (2008) 1217.
[4] V.V. Krivetskiy, M.N. Rumyantseva, A.M. Gaskov, *Russ. Chem. Rev.*, **82** (2013) 917.
[5] D. Koziej, N. Barsan, K. Shimanoe, N. Yamazoe, J. Szuber, U. Weimar, *Sens. Actuators B*, **118** (2006) 98.
[6] A.K. Santra, D.W. Goodman, *Electrochimica Acta*, **47** (2002) 3595.
[7] X. Cui, J. Zhou, Z. Ye, H. Chen, L. Li, M. Ruan, J. Shi. *J. Catalysis*, **270** (2010) 310.
[8] A. Marikutsa, M. Rumyantseva, D. Frolov, I. Morozov, A. Boltalin, A. Fedorova, I. Petukhov, L. Yashina, E. Konstantinova, E. Sadovskaya, A. Abakumov, Y. Zubavichus, A. Gaskov, *J. Phys. Chem. C*, **117** (2013) 23858.
[9] A.V. Marikutsa, M.N. Rumyantseva, L.V. Yashina, A.M. Gaskov, *J. Solid State Chem.*, **183** (2010) 2389.
[10] A. Marikutsa, V. Krivetskiy, L. Yashina, M. Rumyantseva, E. Konstantinova, A. Ponzoni, E. Comini, A. Abakumov, A. Gaskov, *Sens. Actuators B*, **175** (2012) 186.

Figures:

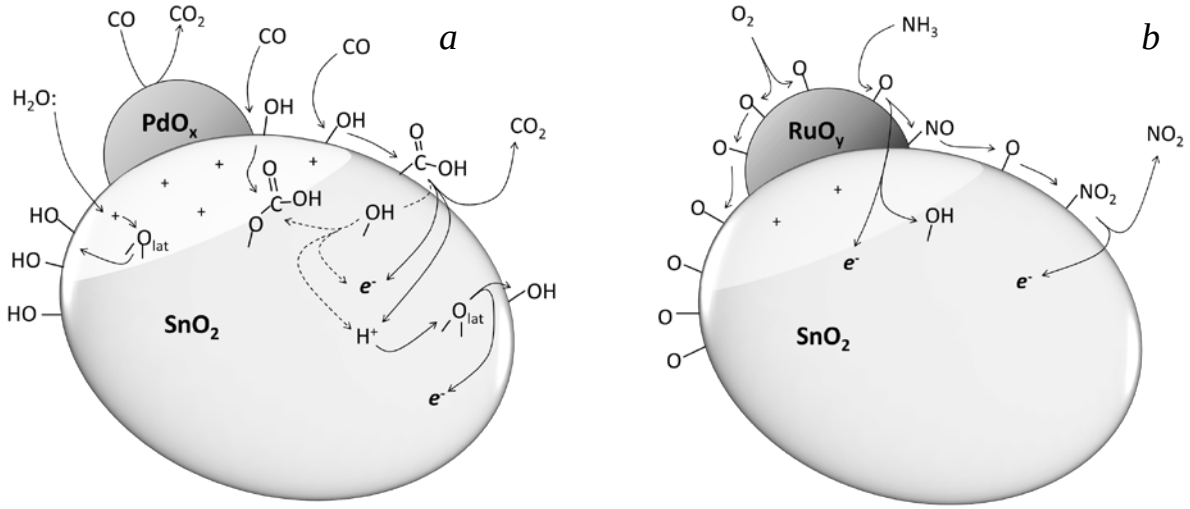

Figure 1. Interaction model of SnO_2/PdO with CO at room temperature (a) and SnO_2/RuO_2 with NH_3 at raised temperature (b) in air.

Manganese Oxides for Thermoelectric Power Conversion

Philipp Thiel[a], Sascha Populoh[a], Gesine Saucke[a], Gion Pirovino[a], James Eilertsen[1], Anke Weidenkaff[b]

[a] Laboratory for Solid State Chemistry and Catalysis, Empa, Überlandstrasse 129, 8600 Dübendorf, Switzerland
[b] Materials Chemistry, Institute for Materials Science, University of Stuttgart, Heisenbergstr. 3, 70569 Stuttgart, Germany

Polycrystalline calcium manganese oxides ($CaMnO_{3-\delta}$) are promising n-type materials for thermoelectric converters sustaining temperatures above 1200 K and oxidizing atmosphere. We are focusing on aliovalent heavy cation substitution on the manganese site, in particular with tungsten ($CaMn_{1-x}W_xO_{3-\delta}$). At high temperatures a partial reduction and a phase transition have a crucial influence on the thermoelectric properties. From about T=1000 K "self-doping" due to the formation of oxygen vacancies dominates the electronic transport, diminishing the effect of the substituent. The analysis of the transport properties yields that in the investigated regime the band filling is sufficiently high to overcome barriers of polaron transport. Therefore the Cutler-Mott approach is considered to describe the transport properties most suitable. The highest figure-of-merit (ZT) of 0.25 is found for x=0.04 at 1225 K [1].

For the fabrication of thermoelectric converters the production of highly dense (~97%) legs without cracks and easy processability are necessary. Therefore, different sintering techniques, including spark plasma sintering, are assessed regarding their practicability and impact on the transport properties. The as produced materials are combined with spark plasma sintered p-type $Ca_3Co_4O_9$ to all-oxide thermoelectric converters. They are characterized in a testing rig up to 1100 K in ambient air yielding high power densities [2].

References:

[1] Thiel et al., *J. Appl. Phys.*, **114** (2013) 243707.
[2] Populoh, Thiel et al., *Funct. Mater. Lett.*, **06** (2013) 1340012.

Substitution with Iron and Nickel for Cobalt in $LaCoO_3$ Perovskite as Efficient Thermoelectric Oxides

Sonya Harizanova,[a] Ekaterina Zhecheva,[a] Vassil Valchev,[b] Mitko Khristov,[a] Radostina Stoyanova [a]

[a] Institute of General and Inorganic Chemistry, Bulgarian Academy of Sciences, 1113 Sofia, Bulgaria
[b] Faculty of Physics, University of Sofia, 1164 Sofia, Bulgaria

The ability of thermoelectric materials to convert heat flux into electricity determines them as a key source of the "clean" energy of the future. Thermoelectric oxides are nowadays considered as more stable and less toxic materials in comparison with the conventionally used metals and semiconductors, but their thermoelectric efficiency is still lower. Therefore, the state-of-the-art research is mainly devoted to identify oxide materials with higher thermoelectric efficiency [1-2].

Lantanum cobaltate, $LaCoO_3$, with a perovskite type structure, is recently considered as a material with potential application in thermoelectricity due to its high Seebeck coefficient ($|S|>500$ μV/K at room temperature) [3]. The transport properties of $LaCoO_3$ are determined (to a great extent) by the ability of Co^{3+} ions to adopt low-spin, intermediate-spin and high-spin configurations in the perovskite structure, leading to an additional spin entropy effect [3]. However, the electrical resistivity is high (about 10 Ωcm at room temperature), which lowers the thermoelectric activity ($ZT<0.01$ at $T=300$ K) [2].

Recently we have demonstrated the improvement of the thermoelectric efficiency of $LaCoO_3$ by double substitution with nickel and iron for cobalt [4]. The improvement is achieved by balancing the opposite effects of nickel and iron ions, as a result of which double substituted $LaCo_{0.9}Ni_{0.1}Fe_{0.1}O_3$ exhibits the best thermoelectric efficiency with ZT=0.16, which is by an order of magnitude higher than that of $LaCoO_3$ at room temperature.

In this contribution we extend our studies on the role of nickel and iron ions for improving the thermoelectric properties of $LaCoO_3$. We examine perovskites with composition $LaCo_{1/2}(Fe_{1/2-y}Ni_y)O_3$, where $0\leq y\leq 0.5$. All perovskites are obtained from freeze-dried citrate precursors at 900 °C. This method is shown to be effective in the preparation of single-substituted perovskites, where Ni and Fe are randomly distributed ($LaCo_{1-x}Ni_xO_3$ and $LaCo_{1-x}Fe_xO_3$) [5]. Structural and morphological characterizations are carried out by powder XRD, SEM and HRTEM analyses. The thermoelectric efficiency of the perovskites is determined by the dimensionless figure of merit, calculated from the independently measured Seebeck coefficient (S), electrical resistivity (ρ) and thermal conductivity (λ).

The formation of $LaCo_{1/2}(Fe_{1/2-y}Ni_y)O_3$ starts at 400 °C by the reaction between $La_2O_2CO_3$ and a spinel phase after the decomposition of the organic components. The solid state reaction proceeds at a nano-scale level, as a result of which well-crystallized $LaCo_{1/2}(Fe_{1/2-y}Ni_y)O_3$ with a rhombohedrally distorted perovskite type structure are formed at 900 °C. The lattice parameters decrease with increasing the Ni-content in $LaCo_{1/2}(Fe_{1/2-y}Ni_y)O_3$, which is consistent with ionic dimensions of cobalt, nickel and iron ions. HRTEM data confirms the

formation of rhombohedrally distorted perovskites with compositions $LaCo_{1/2}(Fe_{1/2-y}Ni_y)O_3$, $0 \leq y \leq 0.5$.

The transport properties of $LaCo_{1/2}(Fe_{1/2-y}Ni_y)O_3$ are effectively modified by double substitution with nickel and iron (Fig. 1). The electrical resistivity (ρ) significantly decreases with increasing the nickel content, while the Seebeck coefficient (S) increases during the progressive increase in the iron content. Contrary to the monotonous changes in the electrical resistivity and the Seebeck coefficient with iron and nickel content, the thermal conductivity displays a non-monotonous change (Fig. 1): double substituted oxides exhibit lower thermal conductivity as compared with single substituted oxides. As a result, the double substituted perovskites display the best thermoelectric efficiency, which is by an order of magnitude higher than that of $LaCoO_3$ at room temperature.

This study demonstrates that by a rational choice of the content of iron and nickel additives it is possible to obtain the $LaCoO_3$-based ceramics with desired thermoelectric efficiency. In addition, the structural approach of selective ion substitution can be extended towards other groups of thermoelectric oxide materials.

References:

[1] Sootsman, JR; Chung, DY; Kanatzidis, MG; *Angew. Chem. Int. Ed.*, **48** (2009) 8616–8639
[2] Maignan, A; Wang, LB; Hébert, S; Pelloquin, D; Raveau, B; *Chem. Mater.*, **14** (2002) 1231-1235.
[3] Terasaki, I; Sasago, Y; Uchinokura, K; *Phys. Rev. B*, **56** (1997) R12685.
[4] V. Vulchev, L. Vassilev, S. Harizanova, M. Khristov, E. Zhecheva and R. Stoyanova, *J. Phys. Chem. C*, **116** (2012) 25, 13507–13515.
[5] S. Ivanova, A. Senyshyn, E. Zhecheva, K. Tenchev, R. Stoyanova and H. Fuess, *J. Solid State Chem.*, **183** (2010) 940-950.

Figures:

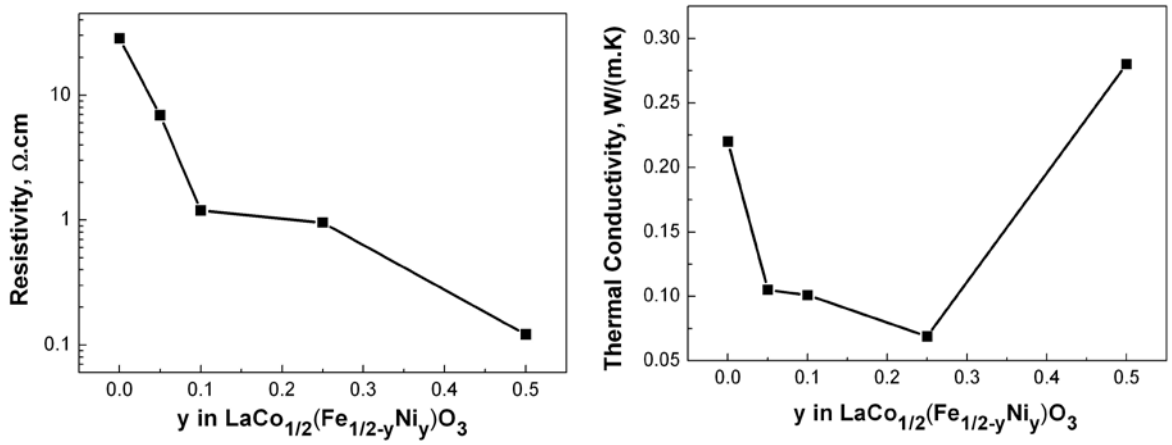

Figure 1. The variation of the electrical resistivity (left) and the thermal conductivity (right at 300 K as a function of the amount of metal additives

Acknowledgments:
Authors are grateful to the financial support from ESF (Grant BG051PO001-3.3.06-0050).

Novel Ga-doped $SrSnO_3$ Electrolytes for High-Temperature SOFCs

G. Skorupsky[a], O. Drozhzhin[b], S. Kazakov[b], A. Tyablikov[b], E. Antipov[b]

[a] 119991 Russia, Moscow, Lomonosov Moscow State University, Department of Materials Sciences
[b] 119991 Russia, Moscow, Lomonosov Moscow State University, Department of Chemistry
gskorupsky@gmail.com

Today, electric energy is one of the most basic, but also the most resource-demanding needs of the modern society. It is from the generation of electric energy that we trace such problems as global warming and greenhouse effect, yet without it, our society would be unable to run. With the ever-increasing population, the needs for electricity continue to rise every day, and the current technologies would soon be unable to support them. For that reason, it is vital to perfect more effective means of electric energy generation, such as the SOFC (solid oxide fuel cell).

The SOFC, like any other electrochemical cell, is composed of a cathode, an anode and an electrolyte. While all the parts of the cell are not yet perfected, in this work, the emphasis is made on the electrolyte materials. Currently, fluorite-structured YSZ (yttria-stabilised zirconia), GDC (gadolinia-doped ceria) and perovskite-structured LSGM (lanthanum strontium gallium magnesium oxide) are considered best suited for this purpose. However, each of them has its own issues, such as their high cost of production and low availability of resources, and it is imperative to research new and better materials to serve as the electrolyte for the SOFC.

In earlier works, Fe-doped $SrSnO_3$ was shown[1-2] to display high conductivity; however, the addition of Fe introduced electronic conductivity, which would hinder its performance as an electrolyte. For that reason, doping of $SrSnO_3$ by Ga was proposed as a potentially effective way of improving the material's conductivity while keeping its electronic component sufficiently low.

$SrSn_{1-x}Ga_xO_{3-\delta}$ powders were prepared from Ga_2O_3, La_2O_3 and $SrCO_3$ powders via solid-state synthesis at temperatures of 1250 to 1350°C. A shift in peaks' positions is visible on the XRD patterns of the powders, with the a parameter of the unit cell ranging from 4.0317(3) Å for $SrSnO_3$ to 4.0234(4) Å for $SrSn_{0.5}Ga_{0.5}O_{3-\delta}$. The oxides' coefficients of thermal expansion were measured via high-temperature X-ray diffraction, the resulting values ranging from $1.09 \cdot 10^{-5}$ for $SrSnO_3$ to $1.28 \cdot 10^{-5}$ for $SrSn_{0.625}Ga_{0.375}O_{3-\delta}$.

Dense $SrSnO_3$ and $SrSn_{0.75}Ga_{0.25}O_{3-\delta}$ membranes were consequently prepared from the resulting mixed oxide powders. The highest densities (95% and 87% correspondingly) were achieved via SPS (Spark Plasma Sintering) of the resulting powders. Other methods of achieving high densities (sintering with the addition of PVA or 5 mol. % $Co(NO_3)_2$ and $Cu(NO_3)_2$) were tried, however those methods yielded considerably lower densities (up to 65%). The materials' conductivities were measured using impedance-spectroscopy. $SrSnO_3$, obtained via SPS sintering, displayed conductivities of $2.68 \cdot 10^{-3}$ $S \cdot cm^{-1}$ at 1073 K and $8.45 \cdot 10^{-5}$ $S \cdot cm^{-1}$ at 873 K, while the one obtained via sintering with addition of 5 mol. % $Co(NO_3)_2$ displayed corresponding values of $5.56 \cdot 10^{-4}$ $S \cdot cm^{-1}$ and $1.39 \cdot 10^{-6}$ $S \cdot cm^{-1}$, which

may be attributed to the higher density of the one synthesised using SPS. $SrSn_{0.75}Ga_{0.25}O_{3-\delta}$, too, displayed lower conductivities of $1.02 \cdot 10^{-4}$ S·cm^{-1} at 1073 K and $1.13 \cdot 10^{-5}$ S·cm^{-1} at 873 K. This can be attributed to the molten admixtures, which, although are invisible on the XRD pattern, can be seen on the SEM image. Currently, we are leading attempts to prepare admixture-pure membranes of $SrSn_{0.75}Ga_{0.25}O_{3-\delta}$ and $SrSn_{0.125}Ga_{0.875}O_{3-\delta}$.

References:

[1] V. Thangadurai, Robert A. Huggins, W. Weppner, *J. Power Sources*, **108** (2002) 64-69.
[2] V. Thangadurai, P. Schmid Beurmann, W. Weppner, *Mater. Sci. Eng. B*, **100** (2003) 18-22.

Figure:

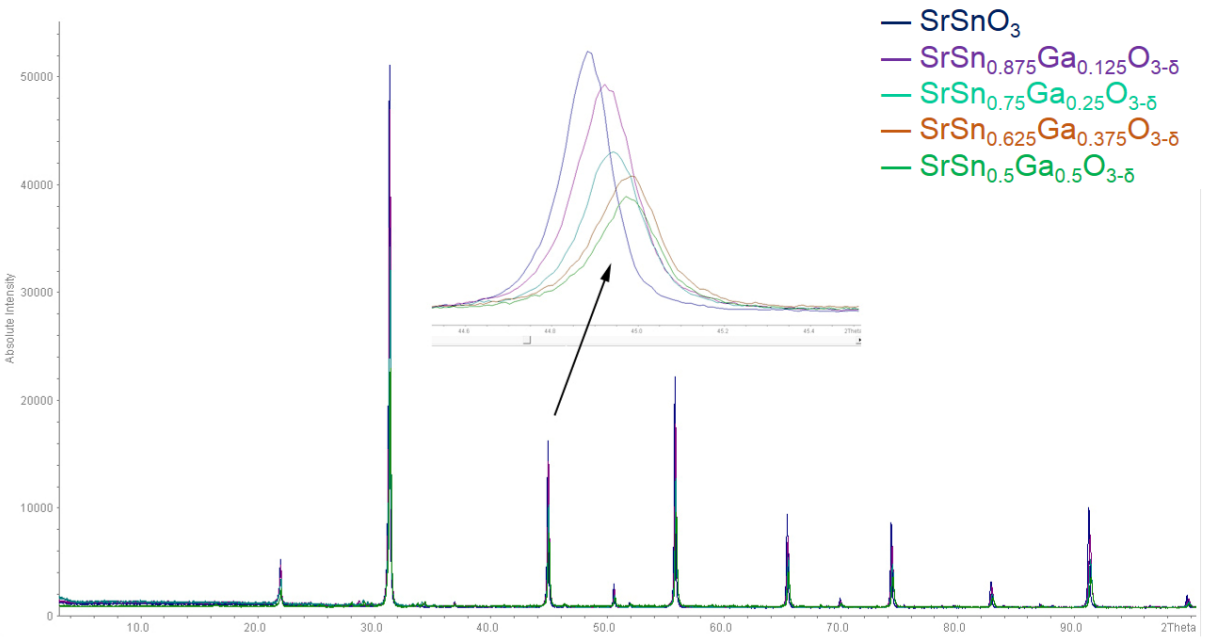

Dittmarite-Type $MMnPO_4.H_2O$ (M = NH_4, K) as Structure-Templates for Low Temperature Synthesis of Olivine-Type $NaMnPO_4$ as Positive Electrode in Alkali Ion Batteries

T. Boyadzhieva, V. Koleva, R. Stoyanova, E. Zhecheva

Institute of General and Inorganic Chemistry, Bulgarian Academy of Sciences, Sofia 1113, Bulgaria

At present, lithium transition metal phosphates, $LiMPO_4$ (M=Fe, Mn, Co and Ni), known as phospho-olivines are attracted great research and technological interest as positive electrode materials for lithium ion batteries with application in the hybrid electric vehicles [1]. The interest is motivated by the numerous advantages of these materials: high theoretical capacity and cyclic stability, excellent safety related to the structure stability, low cost and environmentally benign.

More recently, in response to the current requirements for the development of cheaper "green" batteries the preparation of sodium analogues, $NaMPO_4$ phospho-olivines, becomes very attractive [2]. The synthesis of sodium phospho-olivines is a great challenge and requires original synthesis approaches since the thermodynamically stable $NaMPO_4$ do not form the electrochemically active olivine-type structure. To improve the low rate capability of the phospho-olivine materials there is a need to develop new synthetic methods that enable to control the morphology and the particle size distribution.

The precursor-based methods are a powerful tool for the formation of nanosized and nanostructured electrode materials, where the choice of the proper precursor is a key factor. In respect to the phospho-olivine structure, dittmarite-type compounds having the composition $MM'PO_4.H_2O$ (M^+ = K, NH_4; M'^{2+} = Fe, Mn, Co, Ni) display remarkable structural similarity: the topology of the $M'–PO_4$ layer in the *ac* plane of the dittmarites completely matches the topology of the $M'–PO_4$ layer in the *bc* plane of the phospho-olivines. This makes the dittmarite compounds very suitable as precursors for low-temperature synthesis of lithium and sodium phospho-olivines [3,4].

In this contribution we have extended our studies and report new method on the formation of $NaMnPO_4$ phospho-olivine with controlled particle size distribution and morphology. The method is based on ion exchange reactions with the participation of potassium and ammonium manganese dittmarite precursors as structure and morphology templates.

The ion-exchange of K^+ and NH_4^+ for Na^+ into the dittmarite matrices is carried out using $NaCH_3COO.3H_2O$ taken in excess. The reactions are studied in wide temperature range of 75–250 °C, at various mole ratios from 1:3 to 1:12 between the precursor and the sodium salt and different reaction times from 6 to 24 h. The phase composition in the reaction systems $KMnPO_4.H_2O$–$NaCH_3COO.3H_2O$ and $NH_4MnPO_4.H_2O$– $NaCH_3COO.3H_2O$ is determined by X-ray powder diffraction. It is established that the transformation of the dittmarite precursors into sodium phospho-olivine is a favorable process at temperatures of 200–250 ºC. The structure and morphology of $NaMnPO_4$ prepared from both precursors at 200 °C are characterized by the Rietveld method, IR spectroscopy, SEM and TEM. The thermal stability of the olivine structure is followed by TG-DTA analysis. The Rietveld analysis evidences that

$NaMnPO_4$ derived from both precursors are well crystallized with unit cell parameters a = 10.5275(5) Å, b = 6.3232(3) Å, c= 4.9843(3) Å (space group *Pnma*). A very small antisite mixing (below 1%) between Na^+ and Mn^{2+} on *4a* and *4c* crystallographic sites can be supposed. The SEM images (Fig. 2) show that during the ion-exchange of K^+ and NH_4^+ for Na^+ the plate-like morphology of the precursors is transformed into a rod-like morphology that can be related with the hindered Na^+ diffusion due to its larger ionic radius. The TEM observations confirm the presence of rods (50 nm wide and 250 nm long) and well-crystallized particles with sizes up to 50 nm. The ability of $NaMnPO_4$ to intercalate reversibly lithium is tested in model two-electrode lithium cells of the type Li | $LiPF_6$ EC:DMC) | $NaMnPO_4$.

In conclusion, the ion exchange reactions with the participation of $MMnPO_4.H_2O$ (M^+ = K, NH_4) are effective in the preparation of electrochemically active $NaMnPO_4$ phosho-olivines.

Acknowledgments:
Authors are grateful to the financial support from ESF (Grant BG051PO001-3.3.06-0050).

References:

[1] B. L. Ellis, K. T. Lee and L. F. Nazar, *Chem. Mater.*, **22** (2010) 1059.
[2] B. L. Ellis, L. F. Nazar, *Curr. Opin. Solid State Mater. Sci.*, **16** (2012) 168.
[3] K. T. Lee, T. N. Ramesh, F. Nan, G. Botton, L. F. Nazar, *Chem. Mater.*, **23** (2011) 3593.
[4] V. Koleva, T. Boyadzhieva, E. Zhecheva, D. Nihtianova, S. Simova, G. Tyuliev, R. Stoyanova, *CrystEngComm.*, **15** (2013) 9080.

Figures:

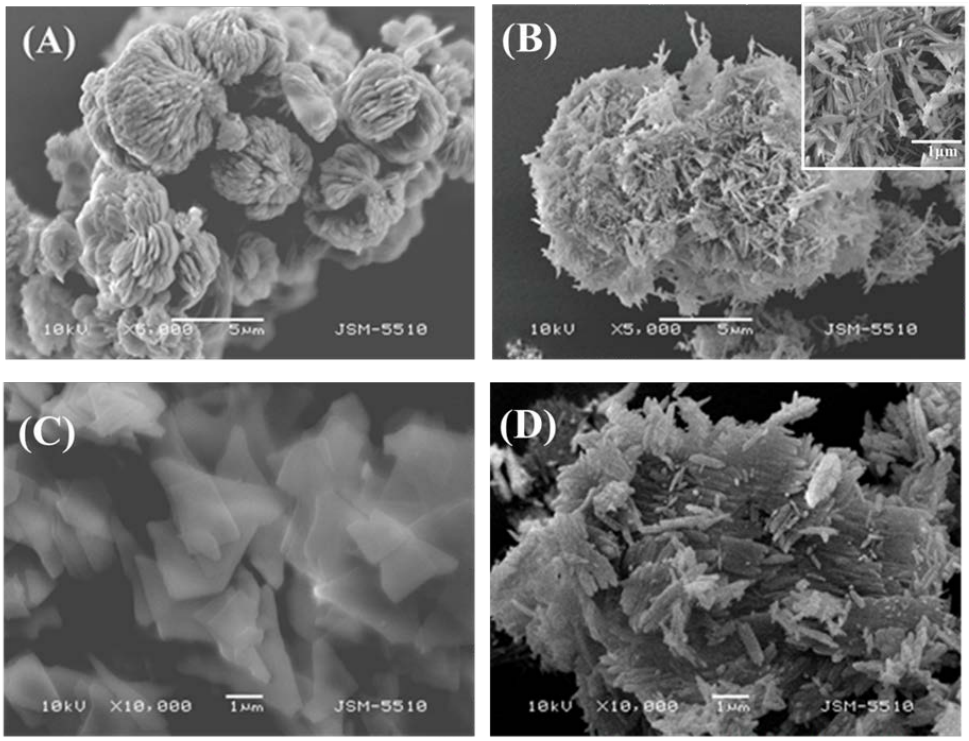

Fig.1. SEM images: $KMnPO_4.H_2O$ (A); K-derived $NaMnPO_4$ (B); $NH_4MnPO_4.H_2O$ (C); NH_4-derived $NaMnPO_4$ (D)

New method of metal fluorides synthesis

Anna Fedorova, Sergey Arkhipenko, Andrey Fedulin, Igor Morozov

Lomonosov Moscow State University, Chemistry Department, Moscow, Russia
E-mail: fedorova@inorg.chem.msu.ru

Metal fluorides have a wide variety of applications. Thus they can be used as ionic conductors, as carriers for catalysts, as laser materials and so on. There are many methods of metal fluorides synthesis. But often they do not permit to obtain metal fluorides with necessary morphology. Besides that the problem of synthesis of complex fluorides is the low degree of homogeneity of the products obtained. Therefore the very important task is the search of new methods of metal fluorides synthesis.

In our work we propose a new method for simple and complex metal fluorides synthesis by decomposing metal trifluoroacetate hydrates in the presence of beta-cyclodextrin. This synthesis method is particularly attractive because it allows obtaining metal complex fluorides at relatively low temperatures. Moreover metal trifluoroacetates using as starting materials are available compounds. An important advantage of this method compared with alternative soft chemistry approaches are its ample opportunities. This method permits to obtain different types of metal fluorides including solid solutions and complex multicomponent fluorides. Also one of the advantages is the lack of need of synthesis of intermediate containing several metals in a definite ratio (single-source precursor), which is often necessary to produce homogeneous products.

This new synthetic method was used for obtaining different types of metal fluorides: a) simple metal fluorides with large surface area (MgF_2, CaF_2), b) solid solutions RF_3-CaF_2 (R = Yb, Nd), c) complex fluorides M_2RF_7, $M_4R_3F_{17}$ (M – Ca, Sr, Ba), d) complex fluoride $NaYF_4$ doped by Yb^{3+} and Er^{3+}.

It was shown that the decomposition of metal trifluoroacetates in the presence of beta-cyclodextrin allows obtaining MgF_2 and CaF_2 with a large surface area (~60-80 m^2g^{-1}). It is interesting to mention that the surface area values depend on the beta-cyclodextrin content in the initial reaction mixture. Thus, the increase of beta-cyclodextrin content in the mixture with magnesium trifluoroacetate from 0 to 50 wt. % leads to a threefold increase in the specific surface of MgF_2. The maximum surface area values were 60 m^2g^{-1} for MgF_2 (beta-cyclodextrin content 66 wt. %) and 80 m^2g^{-1} for CaF_2 (beta-cyclodextrin content 33 wt. %). Increase of the beta-cyclodextrin content lead to decrease of surface area.

Also this synthetic way was successfully used to produce solid solutions of fluorides $Ca_{1-x}R_xF_{2+x}$ (R = Yb, Nd) and complex fluorides M_2RF_7, $M_4R_3F_{17}$, (M = Ca, Sr, Ba; R =Yb, Nd) and $NaYF_4$ doped by Yb^{3+} and Er^{3+}. The formation of solid solutions and complex fluorides with a homogeneous distribution of the elements was confirmed by XRD, X-ray microanalysis and X-ray fluorescence analysis.

It is important to note that the decomposition of the corresponding metal trifluoroacetates without beta-cyclodextrin in case of solid solutions $Ca_{1-x}R_xF_{2+x}$ (R = Yb, Nd) and complex fluorides M_2RF_7, $M_4R_3F_{17}$, (M = Ca, Sr, Ba; R =Yb, Nd) does not lead to the formation of solid solutions and complex fluorides, and the formation of a mixture of simple metal

fluorides was observed. In the case of $NaYF_4$ samples obtained in the presence of beta-cyclodextrin are more homogeneous and have more uniform pore size distribution than those obtained without beta-cyclodextrin. At the same time, the addition of beta-cyclodextrin prevents the pyrohydrolysis process.

In conclusion, we have developed a new soft chemistry synthetic method for preparation of simple and complex metal fluorides and solid solutions of metal fluorides with homogeneous distribution of elements. Advantages of this method are simplicity, availability of precursors and low temperature of the process.

The work was supported by RFBR, grant number 14-03-01032.

Reactivity of peroxide hydrogen on enamel teeth

Isabel Izquierdo-Barba,[a,b,c] Carolina Torres-Rodríguez[d], María Teresa Portolés[c,e], María Concepción Matesanz[e], Javier Linares[e], María José Feito[e], Pedro Esbrit[c,f], Montserrat Colilla [a,b,c] María Vallet-Regí[a,b,c,*]

[a] Dpto. Química Inorgánica y Bioinorgánica. U.C.M., Hospital 12 de Octubre i+12. Madrid, Spain
[b] Centro de Investigación Biomédica en Red de Bioingeniería, Biomateriales y Nanomedicina (CIBER-BBN), Madrid, Spain.
[c] Envejecimiento: red de excelencia española y europea para la prevención y tratamiento local de fracturas osteoporóticas. MINECO. Spain.
[d] Departamento de Salud Oral. F. Odontología, Universidad Nacional de Colombia, Colombia
[e] Departamento de Bioquímica and Biología Molecular I, Facultad de Ciencias Químicas, Universidad Complutense de Madrid, Spain
[f] Laboratorio de Metabolismo Mineral y Óseo, Instituto de Investigación Sanitaria (IIS)-Fundación Jiménez Díaz, Madrid, Spain
*vallet@ucm.es

Introduction

Dental bleaching is commonly carried out to correct discoloration of human teeth. Most bleaching agents are strong oxidizing agents and the most popular is hydrogen peroxide. Although this bleaching agent is highly effective in lightening tooth color, currently some concerns regarding its use have been expressed, due to mainly the associated post-bleaching complications [1]. These include alterations in the morphology of dentine and enamel, change in its chemical composition and increase permeability of the teeth [2,3]. Several studies have shown that the bleaching causes notable changes in the microstructural characteristics in dentine and enamel surface [4]. However, these studies were conducted using the scanning electron microscopy (SEM), which requires a previous specimen preparation, allowing the study on dehydrated teeth and affecting to real microstructural features with respect to fresh teeth. In the present study the environmental scanning electron microscopy (ESEM) has been used to study the real effect of bleaching on structural features of dentin and enamel due to its ability to operate in low temperature and pressure conditions with minimal sample preparation [5]. Moreover, the effects of bleaching on growth, differentiation and activity of osteoclast-like cells on human teeth as well the modulatory action of osteostatin and fibroblast grow factor 2 (FGF2) on osteoclast activity were also evaluated.

Materials and Methods

To preparation of human molar teeth and bleaching, eight third human molars from different patients were extracted, disinfected and stored in deionized water according to Tooth Bank protocol and Local Ethics Committee of the Colombia University. The specimens were treated with 38% H_2O_2 bleaching gel applied for 20 min. Specimens without bleaching were used as controls. ESEM studies were carried out in a FEI QUANTA 200 at an accelerating voltage of 30 kV. For these purposes the specimens were cut longitudinally with a diamond blade after surface bleaching. Previous, to *in vitro* cell evaluation with osteoclast-like cells murine, the molar teeth with and without bleaching were cut transversally with a diamond blade in disks of 2 mm thickness. Osteoclast-like cells were derived from murine RAW macrophages cultured during 7 days on these disks. Different cell parameters were evaluated as osteoclast-like cell proliferation, viability, intracellular content of reactive oxygen species (ROS), pro-inflammatory cytokine (IL-6 and TNF-α) secretion and resorption activity. Moreover, the putative modulatory action of osteostatin and fibroblast grow factor 2 (FGF2) on these osteoclast parameters was also determined.

Results and Discussion

Figure shows ESEM micrographs displaying significant changes concerning the microstructure features of the bleached-enamel surface compared with the unbleached. Typical enamel structure prism is observed in the untreated side **(A)** [6]. However, after bleaching, a total loss of this typical morphology is observed, appearing deep longitudinal cavities through both enamel and dentin **(C)**. This morphological changes increase the porosity owing mainly to the disruption of matrix protein, which causes loss of structural components by free radical oxidation [7]. On the contrary, peritubular dentine structure appeared more resistant to the effects of hydrogen peroxide than enamel, appearing also small cavities in its surface and increasing slightly its porosity (**B and D**, respectively). Concerning the osteoclast activity, the results indicate that bleaching produces increase of osteoclast-like cell proliferation, decrease of cell viability, lower cytokine secretion and higher resorption activity on dentin. The presence of either osteostatin or FGF2 reduces the osteoclast-like cell proliferation induced by bleaching. FGF2 enhances ROS content whereas osteostatin decreases ROS but increases TNF-α secretion. The bleaching effects on resorption activity were increased in the presence of osteostatin, but less evident with FGF2.

Conclusion

The exposure to 38% hydrogen peroxide for 20 min on human molar teeth caused a significant increase in the porosity of the enamel and total loss of its initial enamel structure prism.

References

[1] D. Goo, T. Kwon, S. Nam, H. Kim,K. Kim K, Y. Kim Y. *Dent Mater J* **23**, 522-527 (2004).
[2] B. Fu, W. Hoth-Hannig, M. Hannig. *Am J Dent* **20**, 35-40 (2007).
[3] M. Vallet-Regí M, D. Arcos. Biomimetic Nanoceramics in Clinical Use: From Materials to Applications. Cambridge, UK: RSC Pub (2008).
[4]M. Zalkind, J.R. Arwaz, A. Goldman, I. Rotstein I. *Endodont Dent Traum* **12**, 82–8 (1996)
[5] M. Vallet-Regí, J.M. Gónzalez-Calbet. *Prog.Solid State Chem.* **32**, 1–31 (2004).
[6] J.D. Pasteris, B. Wopenka, and E. Valsami-Jone. *Elements* **4**, 97–104 (2008).
[7] Hanks CT, Fat JC, Wataha JC, Corcoran JF. J Den Res 1993;72:931-8.

Figure:

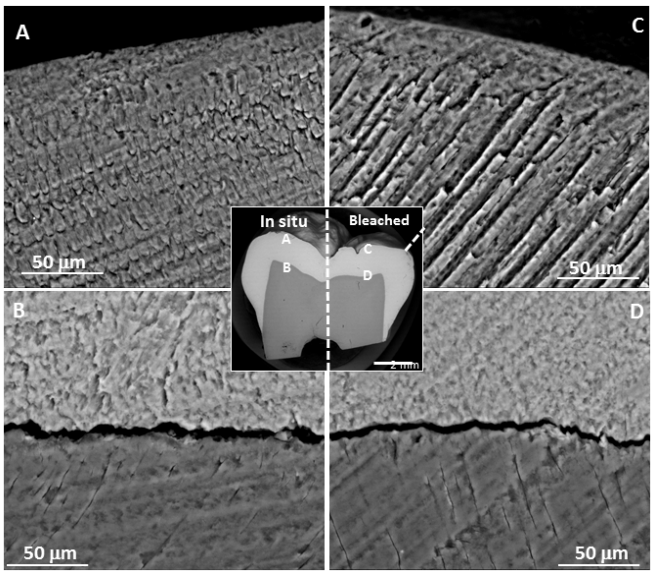

Fig.1. *ESEM micrographs corresponding to a longitudinal section through human molar tooth showing the enamel and dentin before (left) and after bleaching.*

Acknowledgements:
This study was supported by MICINN through the projects MAT2012-35556.

Synthesis of nanocomposites in the system SnO_2-CoO by thermal decomposition of a double hydroxide $CoSn(OH)_6$

A.I. Aparnev [a] , I.A. Kashpur [a] , L.I. Afonina [a,b], A.G. Bannov [a] , N.F. Uvarov [a,b,c], B.B. Bohonov [b]

[a]*Novosibirsk State Technical University, Novosibirsk, Russia*
[b]*Institute of Solid State Chemistry and Mechanochemistry, Novosibirsk, Russia*
[c]*Novosibirsk State University, Novosibirsk, Russia*

Nanocomposites based on tin dioxide with heterogeneous additives of transition metals may be used as anode materials, in chemical sensors or supports for catalysts. As a rule, such materials may be prepared at relatively high temperatures and have relatively large grain size of the components. The aim of this work was to elaborate low-temperature method of synthesis of nanocomposites SnO_2-CoO from a double hydroxide precursor $CoSn(OH)_6$ and study of their physical and chemical properties.

The precursor, $CoSn(OH)_6$, was prepared by sol-gel method from water solutions of $CoCl_2 \cdot 6H_2O$ and $SnCl_4 \cdot 5H_2O$ in 1M hydrochloric acid for the atomic ratio of metals Sn:Co = 1:1. Deposition of sol was carried out by adding of 1M solution of ammonium hydroxide up to pH of 5-6. The obtained amorphous precipitate was filtered, dried at room temperature and annealed at temperatures from 100 to 1000 K. The phase composition and microstructure of the powders was studied using X-ray diffraction technique with a Bruker D8 Advance diffractometer using CuKα-radiation. Average grain size of both components was evaluated from the lines broadening using the Debye-Scherrer formula. Thermal properties of the samples were studied using NETZSCH Jupiter STA 449S synchronous thermo-analyzer coupled with the mass spectrometer QMS 403C Aëolos (TG-QMS) in an argon atmosphere. Surface properties of the powders were studied by low-temperature nitrogen adsorption at 77K using a Quantachrome Nova 1000e specific surface meter.

As a result of the co-precipitation double hydroxide $CoSn(OH)_6$ was obtained in the form of crystals with the average size of nearly 1 micron. On heating its dehydration starts at temperatures higher than 120°C. However, the crystal structure of initial hydroxide remains stable up to temperatures of 250°C when the final decomposition of the hydroxide takes place accompanied by strong endothermic peak. As a result, porous pseudomorph is formed consisting of very fine X-ray amorphous nanoparticles (Fig.1, a). This material has high specific surface area 150 m^2/g and consists of nanoparticles with average size less than 4 nm and very low particle size distribution. Further heating leads to crystallization of SnO_2 and CoO and formation of nanocomposites with particle size of 5 and 8 (± 2) nm, respectively (Fig. 2). Upon further calcination at 800 ° C the grain size of both phases increases, more strongly for CoO (Fig.1, b,c). At 1000 °C the chemical interaction takes place in the systems and all cobalt oxide transforms into new phase $SnCo_2O_4$ with spinel structure [1] (Fig. 2), SnO_2 remaining partially unreacted. In this composite SnO_2-$SnCo_2O_4$ both components have large grain size exceeding 100 nm (Fig.1, d).

In conclusion, we have demonstrated that thermal decomposition of the double hydroxide precursors may be regarded as a reliable low-temperature technique for preparation of well-mixed nanocomposites with very small particles size and narrow particle size distrubution.

Acknowledgement: The work was supported by the Programme of Presidium RAS #27.59.

References:

[1] Zh. Wang, Z. Wang, W. Liu, W. Xiao, X.W. Lou, *Energy Environ. Sci.*, **6** (2013) 87.

Figures:

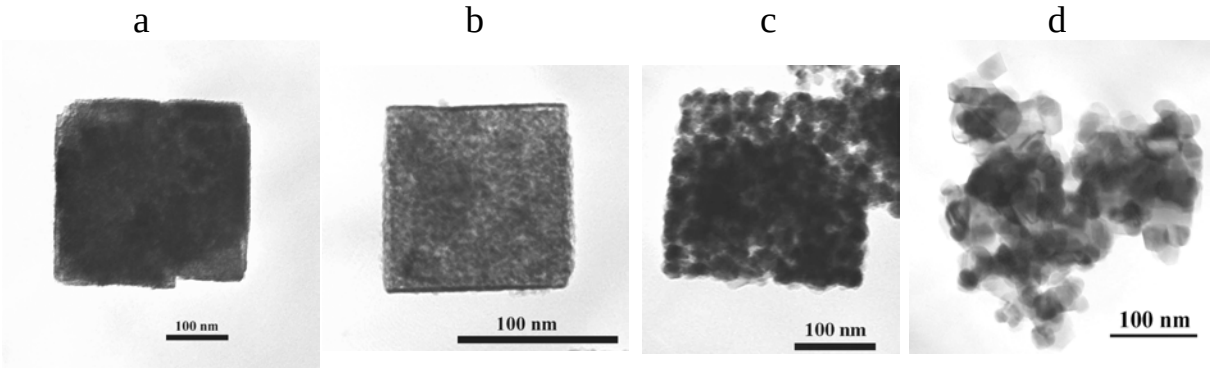

Fig. 1. Electro-microscopy images demonstrating the change in the morphology of a single crystal of the precursor $SnCo(OH)_6$ during its thermal decomposition and further sintering. Heating temperature is 250 (a), 400 (b), 650 (c) и 800 ^oC (d).

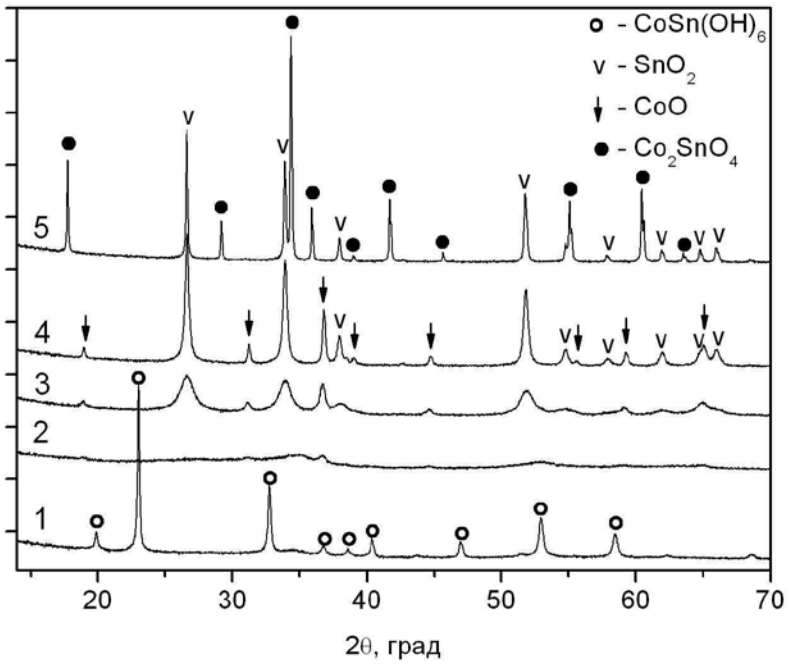

Fig.2. X-ray difractograms of the samples obtained after the heating at 250 (1), 450 (2), 650 (3), 800 (4) и 1000 ^oC (5).

High-throughput materials research under hot isostatic pressing condition

Kenjiro Fujimoto, Hiroki Morita, Yuji Goshima, Yuki Yamaguchi, Shigeru Ito

Department of Pure and Applied Chemistry, Faculty of Pure and Applied Chemistry,
Tokyo University of Science
Yamazaki 2641, Noda, Chiba 278-8510, Japan.
E-mail: fujimoto_kenjiro@rs.tus.ac.jp

Concept of high-throughput materials exploration research in inorganic materials started from the multi-components thin films preparation using sputtering technique by Kennedy et al.[1] and Hanak et al.[2] And, we have also developed the high-throughput materials exploration apparatus "M-ist Combi" based on the electrostatic spray deposition method, which is one of solution processes for obtaining films or fine particles. [3] Including our "M-ist Combi" system, previously reported combinatorial processes have been able to control chemical composition, heat-treatment temperature, atmosphere and pressure under less than atmospheric pressure. Normally, in conventional materials preparation processes, high pressure is important parameter for studying the reactivity of solid. So, we focused on the hot isostatic pressing (HIP) method. The HIP method was invented in 1950s and is used for making sintered bodies, is one of these high-pressure processes.[4] The procedure of the HIP process needs much work time to obtain the product because the process consists of the weighing and mixing of starting materials and heat-treatment under high-pressure. We studied a system for reacting at the same time under high-pressure in a materials array which was obtained by the "M-ist Combi" system. In particular, we designed and fabricated a combinatorial high-pressure vessel for use with HIP apparatus.

In order to develop a high-pressure vessel that can withstand HIP pressures such as 200 MPa, we made a reaction vessel that has high-pressure tightness. We aimed at fabricating a vessel that would fulfill the condition of being able to be put into HIP apparatus and set to the reaction plate (35 mm×35 mm×5 mm^{t}) used in the "M-ist Combi" system. The reaction plate has 36 hollows and a separate function of the HIP capsule for each hollow. Furthermore, we explored candidate metal films for the top of the reaction plate that would allow the vessel to be used for the same function as HIP multiple capsules. In this study, we focused on the commercial flanges (ICF standard flunge, ICF70 (70 mm^{φ})) used in vacuum equipment. Figure 1 shows a schematic diagram of the reaction vessel. The underside of the reaction vessel had a recess for fixing the reaction plate. And, the upper side had through-hole for applying high-pressure to the prepared library. As mentioned above, the most suitable metal cover for achieving the same reaction in the developed vessel as in conventional capsule HIP processing was explored. The metal foils used were SUS304 (0.01 ~ 0.08 mm thickness), Ni (0.01 mm), Mo (0.01 mm) and Cu (0.1 and 0.3 mm). These metal foils were superimposed on the reaction plate, and an overlap was set to the vessel. Then 200 MPa was applied to the vessel using the cold isostatic press (CIP) method under ambient temperature and it was checked whether each metal foil hollowed along the form of the reaction plate without cutting.

Figure 2 shows the actual image of the reaction vessel (75.6 mm^{φ}, 12.7 mm^{t}). Size of the reaction vessel was adjusted for fitting nearly into the inside diameter of HIP apparatus. SUS304 was used as the material of the reaction vessel because, conventionally, we use it in capsule HIP processing. The upside the reaction vessel has edges for imposing on the metal

cover to the reaction plate. And screw holes were used to allow the upper side and underside of the reaction vessel to be fastened with bolts. In addition, the optimum metal foil was SUS304 with a 0.08 mm thickness. Finally, the developed reaction vessel could be used up to 200 MPa and 500˚C. [5]

References:

[1] K. Kennedy, T. Stefansky, G. Davy, V.F. Zackay, E.R. Parker, *J. Appl. Phys.* **36** (1965) 3808-3810.
[2] J.J. Hanak, *J. Mater. Sci.* **5** (1970) 964-971.
[3] K. Fujimoto, T. Kato, S. Ito, S. Inoue, M. Watanabe, *Solid State Ionics* **177** (2006) 2639-2642.
[4] T. Fujikawa, Y. Manabe, *Jpn. Soc. Powder and Powder Metallurgy* **50** (2003) 689-698.
[5] K. Fujimoto, H. Morita, Y. Goshima, S. Ito, *ACS Combinatorial Science* **15**(12) (2013) 622-625.

Figures:

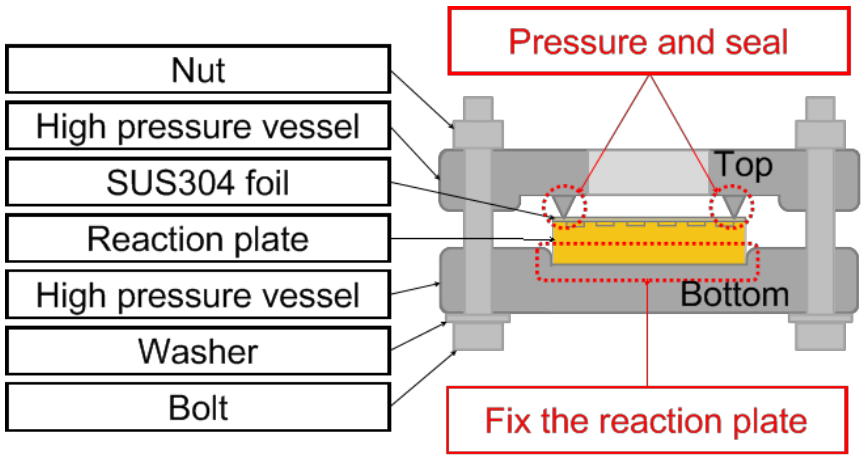

Figure 1. Schematic image of the combinatorial high-pressure reaction vessel

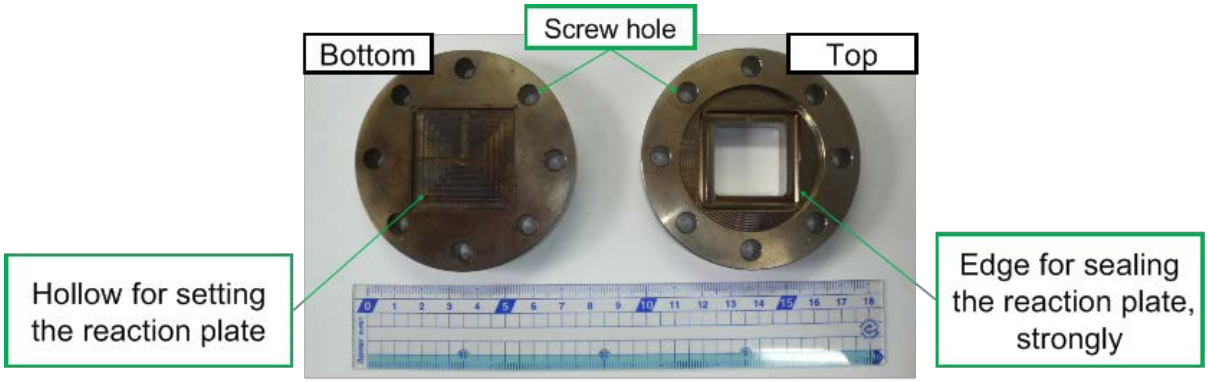

Figure 2. Actual image of the combinatorial high-pressure reaction vessel
(Size of the reaction vessel: 75.6 mm$^{\varphi}$, 12.7 mm^{t})

Oxygen content, thermodynamic stability and electrical properties of $YBaCo_4O_{7\pm\delta}$

D.S. Tsvetkov, N.S. Tsvetkova, A.Yu. Zuev

Institute of Natural Sciences, Ural Federal University, Ekaterinburg, Russia

Complex oxides with chemical formula $LnBaCo_4O_{7+d}$ (Ln=Y and rare-earth ions), a new class of geometrically frustrated magnets, have attracted a lot of attention in the recent years due to their unusual physical properties [1]. The main interesting feature of these compounds is their peculiar crystal structure which leads to the unusual physical properties. These compounds also show a large thermoelectric power factors at high temperature and can be suitable for the thermoelectric power generation. Moreover, these compounds show a high degree of chemical flexibility, having a large capacity for reversible oxygen absorption and desorption in the temperature range 520-720 K, which makes these materials suitable for cathodes of high- and intermediate–temperature solid oxide fuel cells, oxygen membranes, magnetoresistors, emission cathodes for CO_2-lasers, catalysts for oxidation of hydrocarbons and exhaust gases, etc.

However, the main disadvantage of $LnBaCo_4O_7$ materials is instability of their hexagonal crystal structure within the intermediate temperature range 873-1050 K [2]. Therefore knowledge of the thermodynamic stability limits of $YBaCo_4O_7$ type oxides is of key importance. So far there are only data on thermodynamic stability of $YBaCo_4O_7$ in air while there is obvious lack of such data depending on oxygen partial pressure (*pO2*). On the other hand, no reliable data are available in literature on oxygen nonstoichiometry, overall conductivity and thermo-emf of thermodynamically stable $YBaCo_4O_7$ type oxides.

Therefore the priority purposes of the present work were (i) to determine limits of the thermodynamic stability of layered oxide $YBaCo_4O_7$ depending on oxygen partial pressure and, (ii) to measure its oxygen nonstoichiometry, overall conductivity and thermo-emf of thermodynamically stable $YBaCo_4O_7$ as functions of oxygen partial pressure at selected temperature.

Powder sample of the nominal composition $YBaCo_4O_{7\pm\delta}$ was prepared by means of glycerol – nitrate method using Y_2O_3, $BaCO_3$ and Co as starting materials. All materials used had a purity of 99.99%. The powders obtained were finally calcined at 1100 °C for 12 h in air. The phase composition of the powder sample prepared accordingly was studied at room temperature by means of X-ray diffraction (XRD) with Equinox 3000 diffractometer (Inel, France) using Fe K_α radiation. XRD showed no indication for the presence of a second phase for as prepared oxide.

Oxygen nonstoichiometry, δ, of $YBaCo_4O_{7\pm\delta}$ as a function of temperature in air was measured by means of thermogravimetric (TG) technique using STA409PC (Netzsch, Germany) and DynTHERM LP-ST (Rubotherm präzisionsmesstechnik GmbH, Germany) microbalances. The oxygen nonstoichiometry as a function of pO_2 was studied by means of the coulometric titration technique. Absolute value of δ in $YBaCo_4O_{7\pm\delta}$ samples was determined by both direct reduction of the oxide sample by hydrogen flux in the TG setup (TG/H_2) and iodometric titration.

It was found that the onset of low temperature and high temperature oxygen absorption in $YBaCo_4O_{7\pm\delta}$ takes place at about 200 and 675°°C, respectively, during relatively slow heating with rate of 0.5 °C/min in air. Low temperature oxygen uptake at around 350 °C was found to be irreversible in terms of temperature change but does not lead to any phase transition. Therefore, $YBaCo_4O_{7\pm\delta}$ sample slowly cooled from 350 °C to room temperature retains its crystal structure with cell parameters which are slightly different from those of as air prepared sample. On the contrary, enormous oxygen uptake at around 800 °C is accompanied by the $YBaCo_4O_{7\pm\delta}$ decomposition with formation of $YCoO_{3-\delta'}$, $BaCoO_{3-\delta''}$ and Co_3O_4.

It was revealed on the basis of the coulometric titration of $YBaCo_4O_{7\pm\delta}$ that this oxide possesses at 950 °C really narrow range of homogeneity with respect to oxygen, $6.822 \leq 7-\delta \leq 6.765$, which corresponds to a really small change of the average oxidation state of cobalt from 2.133 to 2.161 (See Figure). At high pO_2 stability limit $YBaCo_4O_{7\pm\delta}$ decomposes likewise it happens at 800 °C in air whereas Y_2BaCoO_5, $BaCoO_2$ and CoO were identified as the products of its decomposition at low pO_2 stability limit. Both total conductivity increase with pO_2 and positive sign of thermo-EMF indicate in favor of electron holes as predominant charge carriers in $YBaCo_4O_{7\pm\delta}$.

This work was supported by the Russian Foundation for Basic Research (grant No. 13-03-01031).

References:

[1] M. Valldor, M. Andersson, Solid State Sciences 4 (2002) 923
[2] M. Valldor, Solid State Sciences 6 (2004) 251

Figure:

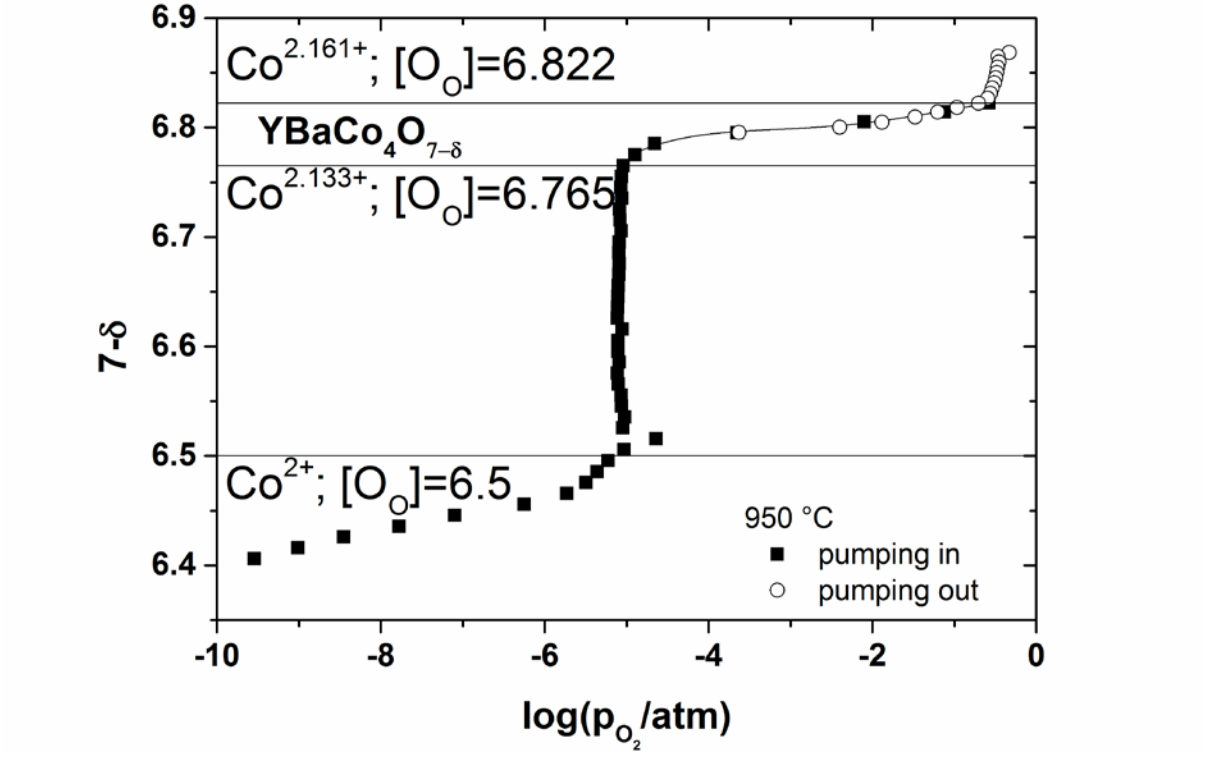

CHEMICAL EXPANSION OF PEROVSKITE-TYPE MIXED IONIC AND ELECTRONIC CONDUCTING MATERIALS

A.Yu. Zuev, V.V. Sereda, D.S. Tsvetkov

Institute of Natural Sciences, Ural Federal University, Ekaterinburg, Russia

Perovskites and double perovskites based upon substituted oxides $LnBO_{3-\delta}$ and $LnBaB_2O_{6-\delta}$, respectively, where Ln=lanthonoid, B=3d-transition metal, are the state-of-the-art materials for a variety of different devices for moderate high temperature applications such as solid oxide fuel cells (SOFCs) and mixed ionic and electronic conducting (MIEC) membranes. The unique feature of the oxides is their ability to undergo both thermal expansion and that induced by the defects of oxygen nonstoichiometry in the oxide lattice. The latter is chemical or defect-induced expansion. The mechanism of this phenomenon is still controversial topic. Recently [1,2] we have evolved the chemical expansion model based on the relative change of the mean ionic radius and showed that the chemical expansion of undoped $LaCoO_{3-\delta}$ and $LaMnO_{3-\delta}$ observed on oxygen deficiency growth is solely caused by this reason. However, the question on the nature of chemical expansion in other MIEC oxides with wider oxygen nonstoichiometry domains still remains open.

It is worth to note that chemical expansion is extremely sensitive to the defect structure of the oxide material. Therefore reliable data on the defect structure of oxide materials is of key importance for understanding the origin of their chemically induced lattice strain. The refinement of defect structure of the selected oxides $La_{1-x}Sr_xFe_{1-y}B_yO_{3-\delta}$ (B=Co or Ni; x= 0.2, 0.3; y=0.1) and $PrBaCo_2O_{6-\delta}$ by means of the quantitative modeling on the basis of the measured oxygen nonstoichiometry was, therefore, the first priority purpose of the present study. The second one was to explain the chemical expansion of MIEC oxides studied on the basis of relative change of the mean ionic radius.

Powder samples of $La_{0.7}Sr_{0.3}Co_{0.9}Fe_{0.1}O_{3-\delta}$, $La_{0.8}Sr_{0.2}Co_{0.9}Ni_{0.1}O_{3-\delta}$ and $PrBaCo_2O_{6-\delta}$ were synthesized by glycerol-nitrate technique described elsewhere [1,2]. The phase composition of the powder samples prepared accordingly was studied by means of X-ray diffraction (XRD) with an Equinox 3000 diffractometer using Cu Kα radiation. XRD showed no indication for the presence of a second phase. Chemical expansion of $La_{0.7}Sr_{0.3}Co_{0.9}Fe_{0.1}O_{3-\delta}$, $La_{0.8}Sr_{0.2}Co_{0.9}Ni_{0.1}O_{3-\delta}$ was measured as a function of pO2 at temperature between 600 and 1050 °C using a home-made dilatometer supplied by pO2 control and adjustment system. Chemical expansion of $PrBaCo_2O_{6-\delta}$ was studied as a function of pO2 in the temperature range 500-1000 °C by x-ray diffraction “in situ” using Equinox 3000 diffractometer equipped with the high temperature camera HTK 16N and pO2 control and adjustment system.

It is generally recognized that the defect structure of the oxygen deficient $LaBO_{3-\delta}$ (B=Mn, Fe, and Co) is based on the simultaneous presence of B–species in different oxidation states such as B^{3+}, B^{4+}, and B^{2+} cations in its structure. The following defect equilibria may, therefore, be written

$$O_O^{\times} + 2Co_{Co}^{\bullet} \Leftrightarrow V_O^{\bullet\bullet} + 1/2O_2 + 2Co_{Co}^{\times}, \; K_1 = \frac{[V_O^{\bullet\bullet}][Co_{Co}^{\times}]^2 \, p_{O_2}^{1/2}}{[O_O^{\times}][Co_{Co}^{\bullet}]^2} \qquad (1)$$

and

$$2Co_{Co}^{\times} \Leftrightarrow Co_{Co}^{\bullet} + Co_{Co}^{/}, \; K_2 = \frac{[Co_{Co}^{\bullet}][Co_{Co}^{/}]}{[Co_{Co}^{\times}]^2}, \qquad (2)$$

where $[Co_{Co}^{\times}], [Co_{Co}^{\bullet}]$, and $[Co_{Co}^{/}]$ correspond to concentration of Co^{3+}, Co^{4+}, and Co^{2+}, respectively. Fe and Ni were assumed to have constant oxidation states +4 and +2, respectively. The defect structure model proposed for $La_{1-x}Sr_xFe_{1-y}B_yO_{3-\delta}$ (B=Co or Ni; x= 0.2, 0.3; y=0.1) was shown to fit the experimental data on oxygen nonstoichiometry really good over the complete pO2 and temperature ranges investigated.

Isothermal defect-induced expansion of $La_{1-x}Sr_xFe_{1-y}B_yO_{3-\delta}$ (B=Co or Ni; x= 0.2, 0.3; y=0.1) was evaluated as normalized change of average ionic radius using concentrations of ionic specie calculated using defect structure model described above. The results of such calculations are shown in Figure (points – experimental data, lines – calculation according to Eq (3)). As seen the model proposed for pseudo-cubic oxides coincides completely with experimental data on chemical expansion for the perovskite $La_{1-x}Sr_xFe_{1-y}B_yO_{3-\delta}$ (B=Co or Ni; x= 0.2, 0.3; y=0.1). On the contrary, chemical expansion of $PrBaCo_2O_{6-\delta}$ along ***a*** axis and contraction along ***c*** axis were found to compensate each other completely in the double perovskite and, therefore, its volume (overall) chemical expansion becomes negligible. As a result the cell volume linearly increases with temperature in air contrary to simple cubic perovskites such as $La_{1-x}Sr_xFe_{1-y}B_yO_{3-\delta}$ (B=Co or Ni; x= 0.2, 0.3; y=0.1).

This work was supported by the Centers of Excellence Program at Ural Federal University, Russia.

References:

[1] A. Yu. Zuev, A.I. Vylkov, A. N. Petrov and D. S. Tsvetkov, Solid State Ionics, V. 179, 2008, 1876.
[2] A. Yu. Zuev, D. S. Tsvetkov, Solid State Ionics, V. 181, 2010, 557.

Figure:

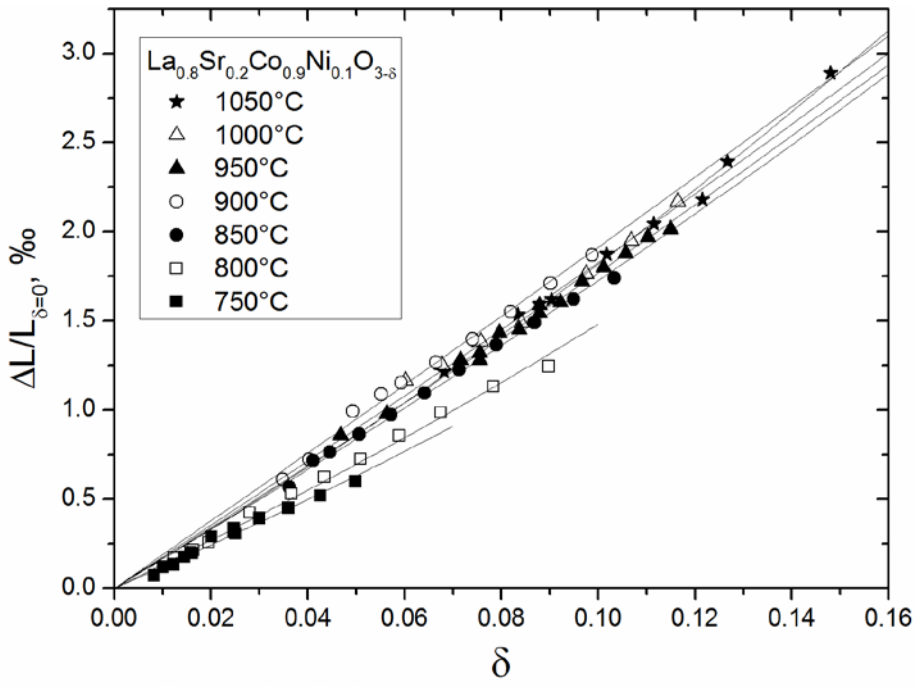

Reversible Lithium Intercalation in Layered $Na_xCo_{1/3}Ni_{1/3}Mn_{1/3}O_2$ (x=1/2, 3/2)

Sv. Ivanova, T. Yordanov, R. Stoyanova, E. Zhecheva

[a]Institute of General and Inorganic Chemistry, Bulgarian Academy of Sciences, 1113 Sofia, Bulgaria

The increasing demand on renewable energy sources requires a relevant increase in energy storage capacity in order to integrate them into a grid. Sodium-ion batteries are considered as a potential alternative of current lithium-ion batteries. In contrast to lithium, sodium is more abundant and economically advantageous. Lithium and sodium ion batteries operate by the same mechanism comprising a reversible electrochemical intercalation of Li^+ and Na^+. The battery performance is closely related with the selection of the electrode materials. Among several groups of electrode materials, lithium-cobalt-nickel-manganese oxide ($LiCo_{1/3}Ni_{1/3}Mn_{1/3}O_2$) and its sodium analogues ($NaCo_{1/3}Ni_{1/3}Mn_{1/3}O_2$) have been considered as promising electrode materials [1,2]. Contrary to the conventional $LiCoO_2$-based electrodes, both $LiCo_{1/3}Ni_{1/3}Mn_{1/3}O_2$ and $NaCo_{1/3}Ni_{1/3}Mn_{1/3}O_2$ display two electron electrochemical reactions during reversible lithium and sodium intercalation, a phenomenon that is generally considered to be rare for layered oxides.

Lithium and sodium analogues have a layered crystal structure composed on discrete transition metal layers [1,2]. The sodium and lithium ions are sandwiched between the $Co_{1/3}Ni_{1/3}Mn_{1/3}O_2$-layers so as to occupy octahedral sites. Based on the number of the $Co_{1/3}Ni_{1/3}Mn_{1/3}O_2$-layers in the unit cell and the symmetry of the sites occupied by Na or Li, the structure of both $LiCo_{1/3}Ni_{1/3}Mn_{1/3}O_2$ and $NaCo_{1/3}Ni_{1/3}Mn_{1/3}O_2$ is classified as *O3*-type according to the notation of Delmas et al. [3]. The deintercalation process from $NaCo_{1/3}Ni_{1/3}Mn_{1/3}O_2$ to $Co_{1/3}Ni_{1/3}Mn_{1/3}O_2$ is accompanied by a reversible structural transformation from the hexagonal *O3* to the monoclinic *P1*-type structure via monoclinic *O1* and hexagonal *P3*-types [2]. In comparison with $NaCo_{1/3}Ni_{1/3}Mn_{1/3}O_2$, the delithiation of $LiCo_{1/3}Ni_{1/3}Mn_{1/3}O_2$ to $Li_{<0.25}Co_{1/3}Ni_{1/3}Mn_{1/3}O_2$ leads to the transformation of the *O3*-type to the *O1*-type structure [4]. Although much research work has been done on $LiCo_{1/3}Ni_{1/3}Mn_{1/3}O_2$, the studies on $NaCo_{1/3}Ni_{1/3}Mn_{1/3}O_2$ remain scarce.

In this contribution, new data on the preparation, structure and lithium intercalation properties of sodium-deficient cobalt-nickel-manganese oxides $Na_xCo_{1/3}Ni_{1/3}Mn_{1/3}O_2$ are provided in order to analyze their potential for direct use as cathodes in lithium ion batteries. This is a novel approach that could open new perspectives in the design of electrode materials. For the preparation of sodium oxides we have used two methods of synthesis: the acetate and the oxalate precursor methods. The acetate precursor method consists in freeze-drying of aqueous solutions of sodium and metal acetates, followed by thermal decomposition at 400 ^oC in air. The oxalate precursors were synthesized using acetate-oxalate precursors, which were obtained mechanochemically at room temperature from metal acetates and oxalic acid. This method has been reported to be suitable for the preparation of nanosized spinels with close particle size distribution [5,6]. Among several sodium-nickel-manganese compositions, the studies are focused on sodium deficient oxides $Na_xCo_{1/3}Ni_{1/3}Mn_{1/3}O_2$ with x=1/2 and 2/3. These compounds are different as electrodes in sodium-ion batteries from the recently proposed stoichiometric $NaCo_{1/3}Ni_{1/3}Mn_{1/3}O_2$ composition [2]. Powder XRD, SEM and

TEM analysis were carried out for structural and morphological characterization of the sodium-deficient oxides. The reversible lithium intercalation in $Na_xCo_{1/3}Ni_{1/3}Mn_{1/3}O_2$ is evaluated in model lithium cells using a galvanostatic mode with lithium as an anode and the examined layered oxides as cathodes. The electrolyte includes the 1M $LiPF_6$ solution in EC:DMC (1:1 by volume). Both acetate and oxalate precursor methods yield well-crystallized $Na_xCo_{1/3}Ni_{1/3}Mn_{1/3}O_2$ with *P3*-type structure. The precursor type affects the particle size distribution: oxides derived from oxalate precursors display nanometric particles with close particle size distribution, while a broad particle size distribution becomes visible for oxides obtained from frieze-dried acetate precursors.

Layered oxides $Na_xCo_{1/3}Ni_{1/3}Mn_{1/3}O_2$ display a reversible lithium intercalation between 1.5 and 4.4 V (Fig. 1). During the first discharge of the electrochemical cell up to 1.5 V, Li^+ ions are inserted in the empty sodium positions, leading to the formation of a mixed Li^+, Na^+ oxide $Li_{1/2}Na_{1/2}Co_{1/3}Ni_{1/3}Mn_{1/3}O_2$ with a structure that deviates from the pristine layered structure. The electrochemical reaction takes place *via* a structural transformation that depends on the rate of the cell discharge and charge (Fig. 1a). A partial exchange of Na^+ with Li^+ occurs during the first few cycles, followed by a steady state performance.

In conclusion, the capability of $Na_xCo_{1/3}Ni_{1/3}Mn_{1/3}O_2$ to intercalate reversibly lithium determines their potential for applications in both lithium and sodium rechargeable batteries.

Acknowledgment:
Authors are grateful to the financial support from ESF (Grant BG051PO001-3.3.06-0050).

References:

[1] X. R. Ye, D. Z. Jia, J. Q. Yu, X. Q. Xin, Z. Xue, *Adv. Mater.*, **11**, 941 (1999).
[2] M. Sathiya, K. Hemalatha, K. Ramesha, J.-M. Tarascon, A. S. Prakash, *Chem. Mater.*, **24**, 1846−1853 (2012).
[3] C. Delmas , C. Fouassier, P. Hagenmuller, *Physica B+C*, **91**, 81-85, (1980).
[4] S.- C. Yin, Y.- H. Rho, I. Swainson, L. F. Nazar, *Chem Mater.*, **18,** 1901 (2006).
[5] Sv. Ivanova, E. Zhecheva, D. Nihtianova, R. Stoyanova, *J. Mater. Sci.*, **46**, 7098 (2011).
[6] Sv. Ivanova, E. Zhecheva, R. Stoyanova, D. Nihtianova, S. Wegner, P. Tzvetkova, Sv. Simova, *J. Phys. Chem. C*, **115**, 25170-25182, (2011).

Figures:

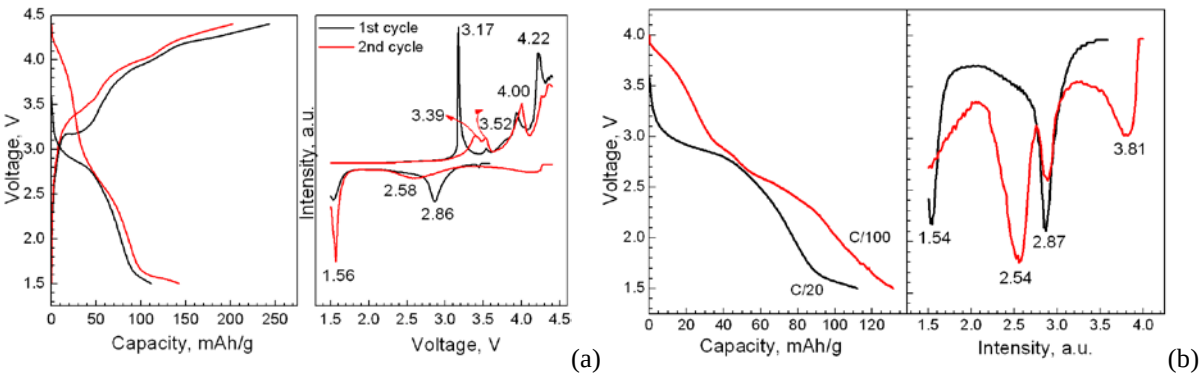

Fig.1: The first and second discharge/charge curves and their first derivatives for $Na_{0.5}Co_{1/3}Ni_{1/3}Mn_{1/3}O_2$ at rate of C/20 (a). The first discharge curves and their first derivatives for $Na_{0.5}Co_{1/3}Ni_{1/3}Mn_{1/3}O_2$ at rate of C/20 and C/100 (b).

Thermal stability of cerium tetrafluoride

Z. Mazej,[a] N.S. Chilingarov,[b] A.V. Knot'ko,[b] I.M. Shlyapnikov,[a] M. Kristl[c]

[a] Department of Inorganic Chemistry and Technology, Jožef Stefan Institute, Jamova cesta 39, 1000 Ljubljana, Slovenia
[b] Department of Chemistry, M. V. Lomonosov Moscow State University, Leninskije Gory 1-3, 119992 Moscow, Russia
[c] Laboratory of Inorganic Chemistry, University of Maribor, Faculty of Chemistry and Chemical Engineering, Smetanova ulica 17, 2000 Maribor, Slovenia

Cerium tetrafluoride is used for selective solid-phase fluorination of C_{60}(s) which yields mainly $C_{60}F_{36}$ [1]. Because of that, it would be beneficial that its thermodinamic data are more precisely determined. In the Ref. [2] it was firstly established that among the known tetrafluorides of rare earth metals (CeF_4, PrF_4, TbF_4), only the cerium tetrafluoride turns into a gas phase upon heating. Later, this conclusion was confirmed by mass spectrometric studies of the vapor composition [3-5]. Up to now reliable thermodynamic parameters of the CeF_4(s) sublimation have not been obtained. The vapor pressure hasn't been determined. Sublimation enthalpies were obtained [4,5], but reported values have a significant discrepancy. In addition, the question about partial pressure of fluorine, which is achieved during CeF_4(s) thermolysis, remains open. This value has never been measured experimentally, although its estimations were made.

The purpose of this study was to examine the following aspects: (1) the possibility to describe the CeF_4(s) thermolysis by means of equilibrium thermodynamics, (2) the influence of the thermolysis on the equilibrium of CeF_4(s) sublimation, and (3) the processes which are responsible for the initiation and course of CeF_4(s) thermolysis in a standard effusion experiment.

In the course of research of CeF_4(s) evaporation by high-temperature mass spectrometry method, the values of the saturated vapor pressure $P°(CeF_4) = 0.28 \pm 0.05$ Pa, at $T = 873$ K, and enthalpy of sublimation $\Delta_{sub}H°(CeF_4) = 257 \pm 6$ kJ/mol, at $T = 840$ K, were obtained. It was found that during isothermal CeF_4(s) evaporation about 50% of substance decomposes into trifluoride. Evaporations were carried out from platinum effusion cell, but fluorine and gaseous platinum fluorides were not detected in the mass spectra. The estimation of the equilibrium pressure of fluorine from the known enthalpies of formation of cerium tetra- and trifluoride is: $P_{eq}(F) = 10^{-5}$ Pa and it doesn't exceed the threshold of sensitivity of our equipment, $P \approx 10^{-3}$ Pa. If a fluorine flow from the effusion cell would be only in agreement with calculated equilibrium pressure $P_{eq}(F)$, the amount of the formed phase CeF_3(s) should be 10^4 times less than observed in the experiment. The amount of fluorine, corresponding to the amount of formed cerium trifluoride was not recorded experimentally due to its loss. However, the total quantity of formed fluorine should be well-measurable, as long as all fluorine leaves the effusion cell through effusion orifice as molecular beam! For that reason, it is necessary to reduce the accumulation of fluorine or fluorination products in the effusion cell as much as possible.

In all experiments, after the isothermal evaporation, the bulk of the resulting cerium trifluoride was accumulated on the inner surface of body and lid of the effusion cell and its quantities were defined by weighing. This implies that almost all original sample of CeF_4(s) turns into vapor.

During the evaporation of CeF_4(s), sorption and desorption of CeF_4 molecules occur, that leads to sample redistribution inside the effusion cell. On the inner surface of the effusion cell the layer of cerium tetrafluoride is formed. This layer is a source of CeF_4 molecules, entering the gas phase. Sublimation of CeF_4(s) is accompanied by thermolysis leading to cerium trifluoride, CeF_3(s), and fluorine atoms (F_S) bonded to the surface of the effusion cell and CeF_3. Since the amount of cerium trifluoride clearly exceeds the equilibrium one, we can assume that the thermolysis is controlled by the flow of fluorine atoms $Q(F_S)$ - the diffusion transfer of F_S atoms from reaction zones of thermolysis to the zones of irreversible drain from the system. Those zones are most likely areas where the integrity of metallic shell of the effusion cell is disrupted (i.e. effusion hole, body-lid connection).

To confirm the assumption of the presence of atomic fluorine drain zones of the effusion cell and to get arguments in favor of the existence of F_S atoms diffusion fluxes, different experiments were carried out. Predetermined amounts of CeF_4(s) were evaporated isothermally (T = 873 K) in the presence of various special designed parts made from platinum or nickel. Those parts were different in size, shape and/or material (triangular plate, tube). Triangular plates made from platinum or nickel were mounted inside the effusion cell so that they were in contact with the inner surface of the effusion cell only by their vertexes. Contrary to triangular plates, the nickel tube was designed on the way to have the maximal contact area between it and inner surface of cell, i.e. outer diameter of the tube was equal to the inner diameter of the effusion cell. In all experiments a direct contact between special Pt (Ni) parts and CeF_4(s) sample was excluded. During evaporation mass spectrometric control of CeF_4 pressure was carried out. At the end of the experiments, the changes of masses of all participants of evaporation process were estimated. Additionally, the surfaces of triangles, tube, lid and body of the effusion cell were analyzed by scanning electron microscope.

It was found that piles of CeF_3(s) particles, formed during thermolysis, are located around assumed drain zones of F_S atoms (i.e. effusion hole, body-lid connection, contacts between triangle plates and body of the effusion cell). Thermolysis of CeF_4(s) is initiated and controlled by the diffusion fluxes of F_S atoms which are directed to drain zones and to reductant (e.g. Ni special parts). In the case of large contact area between the effusion cell and reductant (Ni tube), the equilibrium is perturbed due to large fluxes of F_S atoms, directed from the sample to reductant. Without any special parts or with triangular plates (minimum contact between the effusion cell and plates) low fluxes occur and the equilibrium is retained, i.e. thermolysis does not perturb thermodynamic equilibrium during the process of sublimation.

It can be stated that in the absence of reductants and "leakages" of fluorine from the system, the decomposition of cerium tetrafluoride would be governed only by the thermodynamic equilibrium.

References:

[1] O.V. Boltalina, A.Yu. Lukonin, A.A. Goryunkov, V.K. Pavlovich, A.N. Rykov, V.M. Seniavin, L.N. Sidorov, *Recent Advances in the Chemistry and Physics of Fullerenes and Related Materials. Proceedings of the Symposium. Eds. M. Kadish, R.S. Ruoff. The Electrochemical Society, Inc., Pennington, NJ, USA*, **PV 97-14** (1997) 257.
[2] W.J. Asker, A.W. Wylie, *Aust. J. Chem.*, **18** (1965) 959.
[3] E.W. Kaiser, W.A. Sunder, W.E. Falconer**,** *J. Less-Comm. Met.*, **27** (1972) 383.
[4] E.B. Badtiev, N.S. Chilingarov, M.V. Korobov, L.N. Sidorov, I.D. Sorokin, *High Temp. Science*, **15** (1982) 93.
[5] J.K. Gibson, R.G. Haire**,** *J. Less-Comm. Met.*, **144** (1988) 123.

Superoctahedral F-centered clusters in the crystal structure of natrophosphate

Avdontceva M.S., Zolotarev A.A. ,Krivovichev S.V.

Saint-Petersburg State University.

Natrophoshate is a natural mineral first described by Kapustin, Bykova & Bukin (1972) from pegmatites of Yukspor Mt. (Khibina massif). Its synthetic analogue, the double salt of sodium fluoride and trisodium phoshate was first obtained by Briegled (1856). Neuman (1933) carried out X-ray investigation of this compound and determined its crystal system and probable space group [1].

In our study, the sample of synthetic natrophosphate was prepared by evaporation of an aqueous solution of sodium phosphate and sodium fluoride at 25°C. Single crystal suitable for an X-ray diffraction experiment was fixed on a micro mount and placed on an Agilent Technologies Supernova Atlas diffractometer equipped with CCD detector using micro focused monochromated Cu$K\alpha$ radiation. The unit cell parameters were refined by the least square techniques using 5164 reflections in the 2θ range of 8.94–152.56°. The structure had been solved by the direct methods and refined to R_1 = 0.042 (wR_2 = 0.109) for 812 unique reflections with $|F_o| \geq 4\sigma_F$ by means of the SHELXL–97 program [2]. Empirical absorption correction was applied by means of the CrysAlisPro [3] program using spherical harmonics, as implemented in the SCALE3 ABSPACK scaling algorithm.

The compound has a cubic symmetry, *Fd-3c*, a = 27.978(7) Å. The structure is based upon polycationic complexes consisting of six corner-sharing $NaF(OH_2)_5$ octahedra with one common fluorine vertex. The complexes form hydrogen bonds to PO_4 tetrahedra and are linked to the A site occupied by 25 % of Na, 25 % of H_3O^+ and 50 % of H_2O.

We have been able to locate seven hydrogen-atom positions. The $O_w(4)$ site is splitted into three sites with the site occupancy factors of 0.75, 0.65, and 0.70.

The crystal chemical formula of the compound can be written as $[Na_6F(H_2O)_{18}]_2Na(H_3O)(PO_4)_4(H_2O)$.

References:

[1] H.Baur, Tillmans, Acta Cryst,. 1974, **B30**, 2218.
[2] G. M. Sheldrick, *Acta Cryst.*, 2008, A**64**, 112.
[3]CrysAlisPro, Agilent Technologies, Version 1.171.36.20 (release 27-06-2012).

Preparation and characterization of $Fe^{II}_{1-x}Ni^{II}_{x}Fe^{III}_{2}O_4$ superparamagnetic nanoparticles. Their magnetic and spectroscopic properties

I. Gil de Muro [a], X. Lasheras [b], O. Arriortua [a], M. Insausti [a,b], L. Lezama [a,b], J.M. de la Fuente [c]

[a] Inorganic Chemistry, Zientzia eta Teknologia Fakultatea, UPV/EHU, 48940 Leioa, Spain;
[b] BCMaterials, Parque Tecnológico de Zamudio, 48160 Derio, Spain;
[c] INA, University of Zaragoza, Campus Rio Ebro, 50018 Zaragoza, Spain

Nanomaterials are of great scientific interest because they can exhibit some different properties from the bulk material, special properties that usually depend on the size and shape. Nanoparticles of metals, semiconductors or oxides are of particular interest because of their mechanical, electrical, magnetic, optical and chemical properties. Surface plasmon resonance found in noble metals and superparamagnetism in ferro and ferrimagnetic nanomaterials are two well-known examples of size-dependent properties in nanomaterials unknown in bulk materials until now. In the last few years, nanomaterials and their properties are being exhaustively investigated with the aim of searching for potential new applications beyond the great variety they are already known to exhibit. In this way, the superparamagnetic character of some magnetic nanoparticles is being studied to be used in many different biomedical applications as non-invasive cancer treatment by drug delivery or magnetic hyperthermia, as their magnetic properties allow them to be carried to a defined location or be heated in the presence of an external AC magnetic field [1-2]. In this way, homogeneous SPIO (Superparamagnetic Iron Oxide) nanoparticles, composed by magnetite (Fe_3O_4) and/or maghemite (γ-Fe_2O_3), are the most used due to their high magnetization values and their low toxicity [3].

One of the challenges in this area is to be able to grow oxide nanoparticles while controlling their composition, morphology and size. SPIO nanoparticles have been conventionally prepared by different methods but thermal decomposition of metal-organic precursors in organic solvents with high boiling points has been demonstrated to perform dispersions of nanoparticles with controlled size and shape and narrow size-distributions [4]. In other hand, taking into account that the magnetic properties of the spinel ferrites mainly depend on the occupancy of cations at the tetrahedral (A) and octahedral (B) sites, the already high magnetization values found in the magnetite nanoparticles could even be improved by doping the magnetite material with paramagnetic ions similar in size to Fe^{2+} ions. In that respect, it is known that the Ni^{2+} ions have a strong preference for the octahedral (B) sites in the inverse spinel structure. So, the magnetic moment in the new $Fe_{1-x}Ni_xFe_2O_4$ ferrimagnetic structure would became more unbalanced and the net magnetic moment would be increased [5].

Therefore, in this work we present $Fe_{3-x}Ni_xO_4$ nickel-doped magnetite nanoparticles in the 11-14 nm range, synthesized by the thermal decomposition method using a mixture of $Fe(acac)_2$ and $Ni(acac)_2$ metal acetylacetonates as metal-organic precursors, 1,2-hexadecanediol as dispersant, benzyl ether as solvent and oleic acid and oleylamine as coating. Moreover, some of them have been used as seeds to grow bigger (19 nm) nanoparticles. The structural characterization of the nanoparticles has been carried out by

using X-Ray Diffracttion (XRD) and Inductively Coupled Plasma Spectroscopy (ICPS). The morphology and size dispersion of the samples have been studied by Transmission Electronic Microscopy (TEM) and Dynamic Light Scattering (DLS). The analysis of the magnetic properties of the nanoparticles has been carried out by measuring the magnetization at different magnetic fields and Electronic Magnetic Resonance (EMR) at atmospheric temperature. The EMR results have been fitted to a model of non-interactive particles in order to calculate their ferromagnetic component and the evolution of the signal with the Ni content and the particle size has been analyzed, appearing that a special correlation between the signal-width and the particle-size could exist [6].

References:

[1] S. Mornet, S.Vasseur, F. Grasset, E. Duguet, *J. Mater. Chem.*, **14** (2004) 2161.
[2] E. Kim, K. Lee, Y-M. Hung, S. Haam, *J. Mater. Chem. B*, **1** (2013) 729.
[3] S. Laurent, D. Forge, M. Port, A. Roch, C. Robic, L.V. Elst, R.N. Muller, *Chem. Rev.*, **108** (2008) 2064.
[4] P. Tartaj, M.P. Morales, S. Veintemillas-verdaguer, T. González-Carreño, C.J. Serna, *J. Phys. D:Appl. Phys.*, **36** (2003) R182.
[5] I. Sharifi, H. Shokrollahi, S. Amiri, *J. Mag. Magn.*, **324** (2012) 903.
[6] J. Salado, M. Insausti, L.Lezama, I. Gil de Muro, E. Goikolea, T. Rojo, *Chem Mater.*, **23** (2011), 279.

Figure:

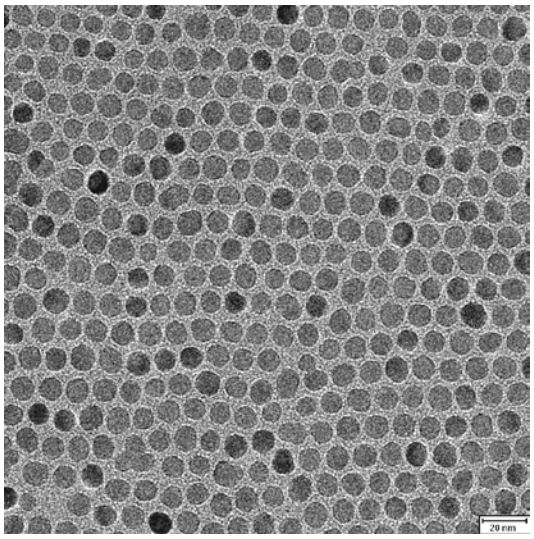

Figure 1. TEM image of $Ni_{0.86}$ $Fe_{2.14}O_4$ sample (average diameter of 11.4 nm)

Preparation and characterization of monodispersed Fe_3O_4 nanoparticles for magnetic hyperthermia

M. Insausti [a,c], O.K. Arriortua [a], X. Las Heras [a], M. Orueta [a], I. Gil de Muro [a], E. Garaio [b], F. Plazaola [b,c] and L. Lezama [a, c]

[a] Dept. Química Inorgánica, [b] Dpto. Electricidad y Electrónica, Facultad de Ciencia y Tecnología, UPV/EHU, Bº Sarriena, 48940 Leioa, Spain.
[c] BCMaterials, Parque Científico y Tecnológico de Bizkaia, E-48160, Derio, Spain.

There is a great interest in magnetic nanoparticles as they are very promising materials in the area of medicine because they can provide approaches to novel diagnostic and therapeutic applications by means of magnetic targeting, drug delivery, magnetic resonance imagining or magnetic hyperthermia [1, 2]. The later one is based on the heating ability of magnetic nanoparticles under an alternating magnetic field and represents a therapeutic concept to cancer treatment, as cancer cells are more sensitive than healthy ones to temperatures higher than 41ºC [3]. In this case, nanoparticles must be biocompatible, which requires a proper optimization of the synthesis method and an adequate surface functionalization, which allows a good stability. Among the magnetic materials Fe_3O_4 nanoparticles are the most interesting ones, as they present high magnetic saturation, high remanence and modarate anisotropy constant together with good biocompatibility.

So, we present the preparation and characterization of Fe_3O_4 nanoparticles to study the influence of the size of the nanoparticles in their magnetic properties. Fe_3O_4 nanoparticles have been synthesized by a modified solution-phase thermal decomposition of an iron precursor with 1,2-hexadecanediol as dispersant, benzyl ether as solvent and oleic acid and oleylamine as coating. The innovation is the utilization of the seeded-growth method based on succesive additions of reagents over previously synthesized magnetite nanoparticles.

The chemical, structural, morphological and spectroscopic characterization was performed by thermogravimetric analysis, X-ray diffraction (XRD), Dynamic Light Scattering (DLS) and Transmission Electron Microscopy (TEM). Dynamic Light Scattering (DLS) and Transmission Electron Microscopy (TEM) studies have concluded that the diameter of magnetic nanoparticles varies depending on the synthetic parameters. The optimization of the synthesis method yields particles from 10 to 30 nm with contents of organic matter in the 15 – 35 % range (Fig. 1), which corresponds to the oleic acid surrounding the nanoparticle. All the samples show typical XRD patterns of magnetite (JCPDS no 19-629), the broad diffraction peaks further suggesting the nanocrystalline structure of the particles. It is to note that the seeded-growth method leads size tunable nanoparticles with high cristallinity.

In order to study magnetic properties of the samples, magnetization measurements were carried out in function of magnetic field and temperature, as well as Electron Magnetic Resonance Spectroscopy (EMR) measurements in dispersed particles assuring a lack of interaction. It has been found a superparamagnetic like behavior for most of the samples with low blocking temperatures. The hysteresis loops of the three samples can been observed below T_b temperature (Fig. 1b) but they do not have coercivity (H_c) nor remanence (M_r) at room temperature as expected for a superparamagnetic behavior. The room temperature EMR spectra of the samples in toluene dispersion show an intense and isotropic line in the samples. The position of the effective resonant field (H_{ef}) and correspondingly the derived effective g

value (g_{ef}), as well as the peak to peak line width changes for one sample to another depending of the size and the dispersion of the nanoparticles. When the size of the NPs increases, the applied external field is able to align them to a certain degree, resulting in a positive HK contribution. This effect causes the signal to shift to lower H_{ef} values with the increase of NP size. This is just the contrary of that found for the linewidth (ΔH_{pp}), it becomes wider when the particle size increase.

Hyperthermia measurements have been performed for nanoparticles with the highest magnetization values. The SAR values were measured by using a previously described homemade device. A, B, C samples in toluene dispersion were exposed to an applied magnetic field of 10 kA/m at different frequencies (in the range 100-900 kHz). SAR values at 853 kHz and 10 kA/m changes depending on the size being the largest value, around 700 W/g_{Fe3O4}. The magnetic study has also led us to find a relationship between magnetic behavior, size, geff value and hyperthermia response.

References:

[1] Y.-M. Huh, Y. Jun, H.-T. Song, S. Kim, J. Choi, J.-H. Lee, S. Yoon, K. Kim, J.-S. Shin, J.-S. Suh, J. Cheon, *J. Am. Chem. Soc.* **127,** (2005) 12387.
[2] J. Xie, , G. Liu, H. S. Eden, H. Ai, X. Chen, *Acc. Chem. Res.* **44** (2011) 883.
[3] Wust, P.; Hildebrandt, B.; Sreenivasa, G.; Rau, B.; Gellermann, J.; Riess, H.; Felix, R.; Schlag, P. M. *The Lancet Oncology* **3** (2002) 487.

Figures:

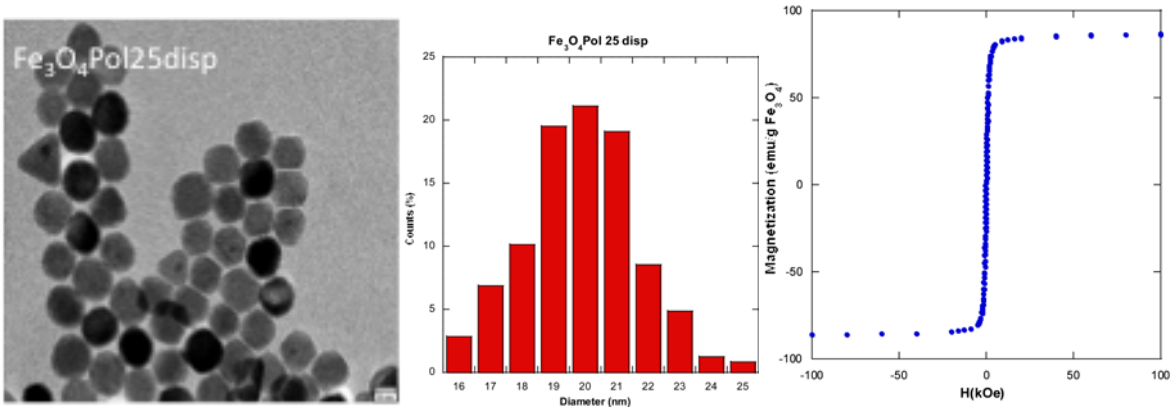

Fig.1. TEM image, histogram of sizes and MvsH measurements for one of the samples.

The effect of chemical activation in $NdCaCoO_{4\pm\delta}$ synthesis by cryochemical processing

Sergey A. Malyshev,[a] Oleg A. Shlyakhtin,[a] Aleksey V. Garshev[b]

[a] Department of Chemistry, Moscow State University, 119991 Moscow, Russia
[b] Department of Materials Sciences, Moscow State University, 119991 Moscow, Russia

Complex oxide materials with controlled microstructure are widely used in catalysis. $NdCaCoO_{4\pm\delta}$, which has teragonal K_2NiF_4 structure, is promising catalytic material due to its high selectivity in partial oxidation of methane to syngas [1]. Conventional way to produce such compounds involves processing at high temperatures that leads to coarse grained body. However, catalytic applications usually demand finely dispersed powders. It is known that chemical synthesis methods provide high homogeneity of the component distribution in precursor. It permits to decrease the temperature and the duration of heat treatment and to obtain materials with smaller grain size and higher specific surface. The common obstacle during application of chemical synthesis methods deals with accelerated formation and stabilization of undesirable intermediate or metastable phases. So, the freeze drying synthesis of $NdCaCoO_{4\pm\delta}$ from nitrates is complicated by the preferential formation of orthorombic $(Nd,Ca)CoO_3$ during thermolysis [2]. Thus the purpose of the present study is developing more effective chemical way to obtain $NdCaCoO_{4\pm\delta}$ fine powder.

In the present study $NdCaCoO_{4\pm\delta}$ is obtained by the *cryogel* technique and by the solid state synthesis method. In the first case the coprecipitation of Nd^{3+}, Ca^{2+} and Co^{2+} by the mixtures of KOH + K_2CO_3 (1) or by NaOH + Na_2CO_3 (2) was used. After washing, the precipitate was frozen by liquid nitrogen and freeze dried. Freeze drying stage allows avoiding considerable agglomeration of coprecipitated particles [3]. Direct solid state reaction between Nd_2O_3, $CaCO_3$ and Co_3O_4 (3) was used as a reference method.

In case of (1) a single-phase $NdCaCoO_{4\pm\delta}$ was obtained by thermal processing of precursor at 1000 °C for 2 hours. However, in case of (2) the temperature of phase formation was reduced to 800 °C. In method (3) single-phase $NdCaCoO_{4\pm\delta}$ was obtained by annealing the initial mixture at 1100 °C for 1 hour.

SEM imaging shows that the grain size of obtained powders correlates well with processing temperature. In (1) and (3) the particle size is 0,8-1.2 μm while in (2) it doesn't exceed 0.2-0.5 μm.

To explain the difference in phase formation temperatures in (1), (2) and (3) synthesis routes, the investigation of $NdCaCoO_{4\pm\delta}$ phase formation was carried out by means of *in-situ* XRD analysis and by EDX mapping. Analysis of the high temperature XRD patterns demonstrates that formation of $(Nd,Ca)CoO_3$ is a necessary step in chemical evolution of both cryogel (1,2) and solid state (3) precursors. In (3), the reaction between crystalline components starts at 800 °C. In methods (1) and (2) reaction mixture remains amorphous up to the 500 °C. However, significant transformation of $(Nd,Ca)CoO_3$ to $NdCaCoO_{4\pm\delta}$ is observed in (1) and (3) at 900-1000 °C only. Hence, the activity of orthorhombic intermediate was found rather limited in both routes.

EDX study reveals the presence of residual Na in samples obtained by method (2). It may be explained by the capture of Na^+ during the coprecipitation due to similarity of ionic radii of Na^+, Nd^{3+} and Ca^{2+}. The X-ray mapping shows the uniform Na distribution in precursor (Fig.1, a,c) and its redistribution during the thermolysis (Fig.1, b,d). This redistribution is confirmed also by the appearance of $Na_{0.6}CoO_2$ peaks in XRD patterns. The $Na_{0.6}CoO_2$ content estimated by the Le Bail decomposition of XRD data is 3 mol. %. So, we suggest that it is activation by side chemical process which provides more intensive formation of $NdCaCoO_{4\pm\delta}$. It results in dramatic decrease of the synthesis temperature from 1100 °C in direct solid state reaction (3) to 800 °C in case of cryogel (2).

It is significant to note also that this kind of activation is not a unique phenomenon. The freeze drying synthesis of $NdCaCoO_{4\pm\delta}$ from nitrates with addition of small amount of $NaNO_3$ results in the formation of target oxide at 800 °C which is similar with (2) reaction route. It implies that activation of intermediate phase by side chemical process is rather general feature of solid state reactions.

References:

[1] A.G. Dedov, A.S. Loktev, G.N. Mazo, at al., *Doklady Phys.Chem*., **441(2)** (2011) 233.
[2] O.A. Shlyakhtin, G.N. Mazo, M.S. Kaluzhskikh et al., *Mater. Let*., **75** (2012) 20.
[3] G.M. Pajonk, M. Repellin-Lacroix, S. Abournadasse et al., *J. Non-Cryst. Solids*, **121** (1990) 66.

Figures:

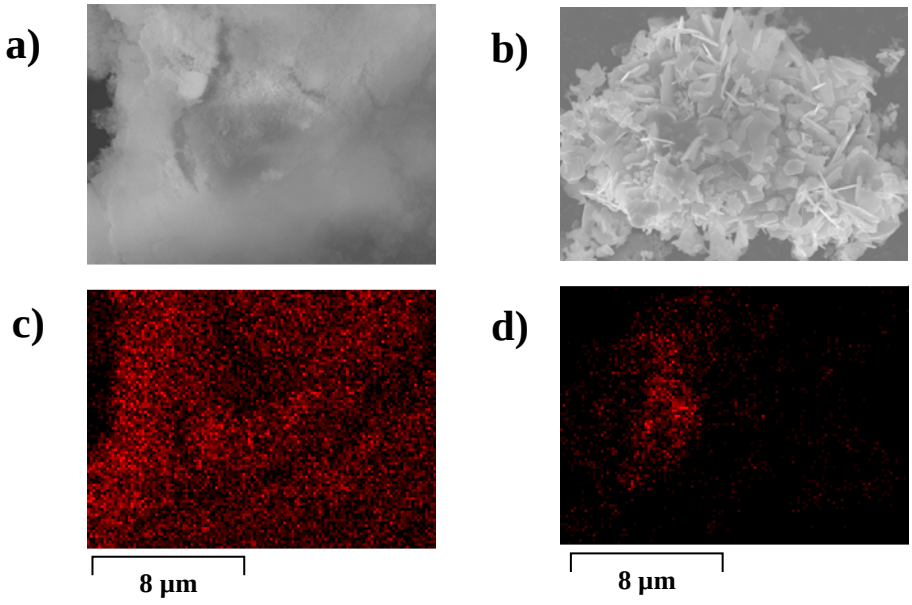

Fig. 1.

Acknowledgements:

The authors acknowledge partial support from the M.V. Lomonosov Moscow State University Program of Development.

Nanocrystalline smooth yttria and alumina thin layers for highly aligned IBAD-MgO templates in HTS heterostructures

I. Martynova,[a,b] D. Tsymbarenko,[a] , V. Amelichev,[b] A. Kamenev, [b] A. Molodyk,[b] S. Samoilenkov, [b] V. Petrykin, [c] S. Lee,[c] N. Kuzmina,[a] A. Kaul [a, b]

[a] Lomonosov Moscow State University, Chemistry Department, 1, Leninskie Gory, Moscow, Russian Federation, 119991;
[b] SuperOx, 20-2, Nauchnyi proezd, Moscow, Russian Federation, 117246;
[c] SuperOx Japan LLC, Sagamihara Incubation Center (SIC-3), 1880-2 Kamimizo, Sagamihara, Kanagawa, Japan 252-0243.

Recently the ion-beam assisted deposition (IBAD) is recognized as effective approach to fabrication of second generation high temperature superconductors (2G HTS). The roughness value of metal tape surface is key factor in this process. The chemical solution deposition of nanocrystalline smooth oxide films of Y_2O_3 and Al_2O_3 is very promising and simple alternative to process of long-length metal tape electro-polishing.

To deposit smooth (roughness < 1 nm) Y_2O_3 and Al_2O_3 films we have suggested new metal organic (MO) precursors based on $M(Carb)_3$ (M = Al, Y; HCarb = aliphatic carboxylic acids) and different N- and/or O-donor ligands (2-ethanolamines, N,N-ethyleneamines, glymes), which can act as hydrolyzing agent and/or solvent. This strategy of precursor design allows to vary concentration, viscosity of the solutions, their surface wettability and thermal stability in required ranges.

The composition of the new precursors and their thermal stability in both solutions and thin films were characterized by 1H NMR and simultaneous thermal analysis with evolved gas mass spectrometry. The most suitable MO precursors were chosen and tested in deposition experiments. We have fabricated long-lengths (50–100m) smooth M_2O_3 films by drawing Hastelloy C276 tapes through precursor solution baths followed by thermal treatment (in up to 10 cycles). Nanocrystalline oxide films were characterized by EDX, XRD, SEM, AFM, TEM, their thicknesses were measured on cross section SEM images.
The smoothing surface effect was achieved. So, the deposition of oxide films with thickness ~ 300 nm on Hastelloy C-276 tape reduced the surface roughness by 11 times (from 9.0 to 0.8 nm on area 5x5 μm^2).

The manyfold repeated deposition and annealing processes resulted in appearance of lamellar structured coats (fig.). According to TEM data that is related with differences in size of M_2O_3 crystallites inside layers (~5 nm) and in interlayer interfaces (~2 nm). Probably, this originates from non-equivalence of annealing conditions (temperature and oxygen potential) in thickness and layers interface. Moreover the annealing temperature sharply influences on crystallinity of films. So, the size of X-ray coherent scattering region grows from ~2 to ~4 nm at temperature increase from 500 up to 550°C.
The suggested approach allowed to obtain the final 2G HTS tapes with the architecture GdBCO/buffer layers/IBAD-MgO/Y_2O_3 with critical superconducting currents > 400 A/cm, which was competitive with up-to-date published results.

Figure:

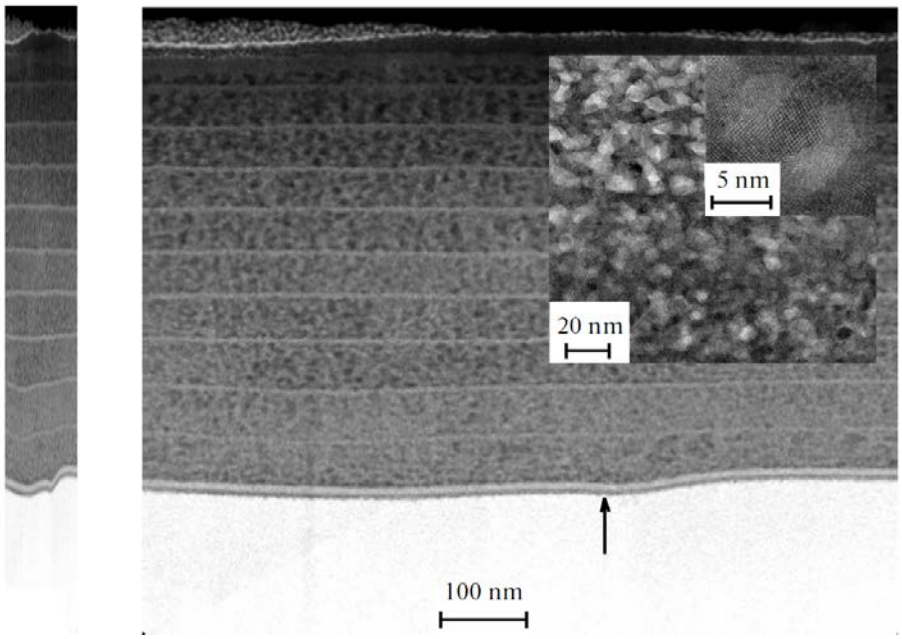

Fig.1. TEM cross-section of Y_2O_3 coat on Hastelloy C276.

Acknowledgments:

The authors thank Dr. Vasiliev A.L. for TEM studies, Dr. Mudretsova S.N. and Dr. Streletsky A.N. for thermal analysis. This work was supported by RFBR (projects No 14-03-00950 and 14-03-31885).

2D LaF_3 nanocrystals synthesized in "soft chemistry" conditions and formation of microtubules from them

Larisa B. Gulina, Valery P. Tolstoy, Igor V. Murin
Institute of Chemistry of St. Petersburg State University
e-mail: vptol@yandex.ru, l.gulina@spbu.ru

Synthesis of 2D-dimensional nanocrystals of inorganic substances is one of the important tasks of modern preparative inorganic chemistry, because it opens the new opportunities to creation of new advanced functional materials. For example, the nano- and microtubules of oxides, sulfides, and other compounds can be prepared from 2D-dimensional crystals. Much attention is being paid lately to synthesis of the nanosized metal fluorides due to the high potential of their practical application. For example, the lanthanum fluoride is used as a superionic conductor, phosphor matrix, solid membranes in to fluoride sensitive ion-selective electrodes, catalyst and for biological fluorescent labeling. Therefore, the development of a facile synthetic method toward highly ordered nanocrystals with uniform size and shape appears to be of key importance for the exploration of new research and application fields.

The new opportunities for such synthesis are opened by the new methods of "soft chemistry". The aim of this work is a presentation of the synthesis results of lanthanum fluoride nanosized particles in "soft chemistry" conditions.

The study of synthesized nanocrystals was done by SEM, XRD, FTIR spectroscopy, and EPMA. It was established that during the synthesis the transparent layers with thickness to 1,5 μm are formed. The layers have crystalline fluocerite (tysonite) - structure. They are formed by arrays of $LaF_3 \cdot nH_2O$ nanosheets approximately 7-15 nm thick and from 0.5 to 2.5 μm^2 in area. As follows from the microscopy results (Fig. 1) these nanosheets are highly ordered and densely packed and are mostly located as perpendicular to the surface of layer.

It was shown also that these layers can be curled up in microtubules of diameter 20 to 80 microns and a length of 2 mm. Examination of the microtubules walls by electron micro probe analysis (EMPA) indicated that the substance of the walls contains La and F atoms. These results were confirmed by the FT-IR spectroscopy data, i.e. by the spectra in which the absorption band at 352 cm^{-1} can be related to La-F stretching vibrations in the LaF_3 crystal tysonite- structure.

In this work we have developed a facile and efficient synthetic method of "soft chemistry" for fabrication of highly ordered 2D nanocrystals of LaF_3 and microtubules from them.
The work was supported by RFBR grant # 12-03-00805-a.

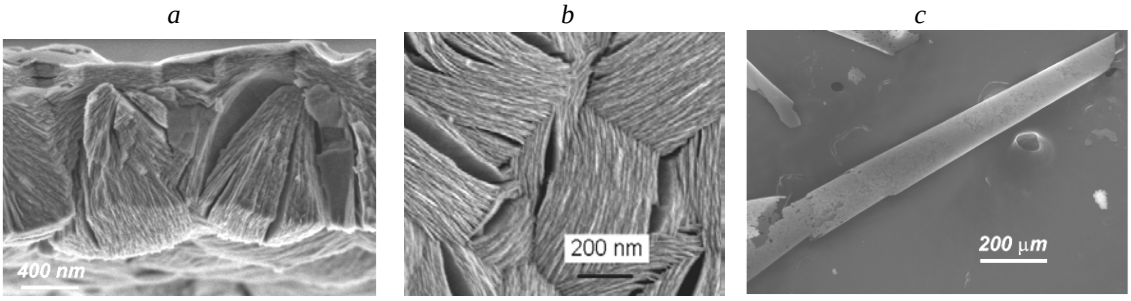

Figure 1. SEM images of LaF_3 layers. *a*- side view, *b*- inside view, *c*- general view of microtubules.

Water assisted room temperature synthesis of YVO_4

T. Kaneko[1], K. Uematsu[2], T. Ishigaki[1], S.W. Kim[1], K. Toda[1], M. Sato[2], J. Koide[3], M. Toda[3], Y. Kudo[3]

[1] Graduate School of Science and Technology, Niigata University, 8050 Ikarashi 2-nocho, Niigata 950-2181, Japan
[2] Department of Chemistry and Chemical Engineering, Niigata University, 8050 Ikarashi 2-nocho, Niigata 950-2181, Japan
[3] N-Luminescence Corporation, 8867-3 Ikarashi 2-nocho, Niigata 950-2102, Japan

Introduction:
Ceramics are generally synthesized at high temperature to increase the reactivity since ion diffusion in a conventional solid-state reaction is very slow at room temperature. In our previous study, it was found that some compounds such as $RbVO_3$ from Rb_2CO_3 and V_2O_5, can be synthesized at room temperature just by mixing the raw materials. In addition, the reaction was accelerated by adding a small amount of water and completed in few minutes.[1, 2)] In this study, we synthesized YVO_4, which has been widely applied as a host material for phosphors and laser materials, using a water assisted room temperature solid state reaction (WASSR) method. We also investigated the reaction mechanism of the room temperature synthesis method.

Experimental:
A stoichiometric ratio mixture of Y_2O_3 (0.2769 g) and V_2O_5 (0.2231 g) was mixed using a mortar for 3 h after addition of different amount of de-ionized water (0, 0.05, 1 g) to synthesize in a single phase. Powder X-ray diffraction (XRD) data were obtained using an X-ray diffractometer.

Result and Discussion:
Figure 1 shows the XRD patterns of the mixture of Y_2O_3 and V_2O_5 mixed for 3 h after the addition of different amount of water. The YVO_4 powder mixed in the presence of the 0.05 g water had a tetragonal rare earth orthovanadate structure as the main phase. In contrast, the sample mixed raw materials without water is observed diffraction peaks of the raw materials, Y_2O_3 and V_2O_5, only in the patterns. The sample mixed raw materials in the presence of the 1 g water is observed the peaks corresponding to YVO_4, however, the peak intensity was extremely smaller than that of the sample mixed in the presence of the 0.05 g water. This is considered to be due to the following reaction mechanism. A schematic of the reaction mechanism is depicted in Figure 2. The reaction mechanism for the WASSR method can be attributed to the conduction of the reaction heat by the covered water. The reaction heat generally generated at the particle-particle contact points cools down rapidly in the absence of water. In contrast, in the WASSR method, the reaction heat produced at the particle-particle contact points is conducted to other particles by the water without heat loss, which enables the reaction to proceed at room temperature. However, excess water leads to a reduction in the number of particle-particle contacts and thus a reduction in reaction heat. Therefore, WASSR method strongly depends on the amount of water added.

References:
1) K. Toda et al., Japanese Unexamined Patent Application Publication No. 2011-16670 (2009).

2) A. Toda et al., in: Abstracts of *216th ECS Meeting*, Vienna, Austria (2009), #3224.

Figures:

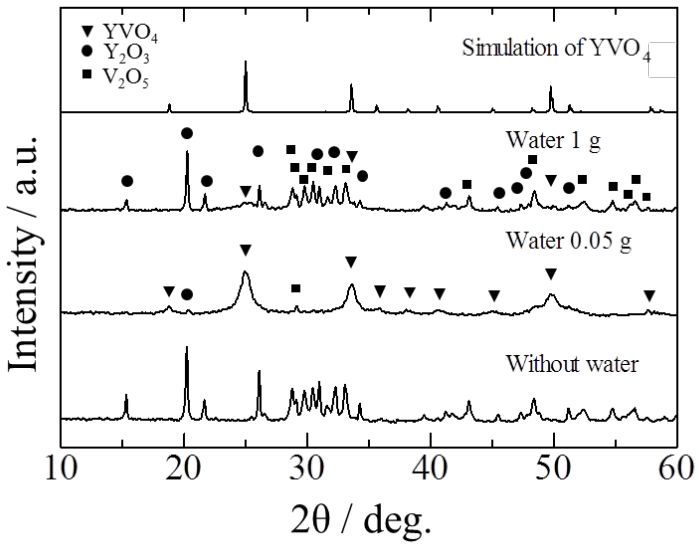

Fig. 1 XRD patterns of the samples mixed Y_2O_3 and V_2O_5 for 3 h after the addition of different amount of water.

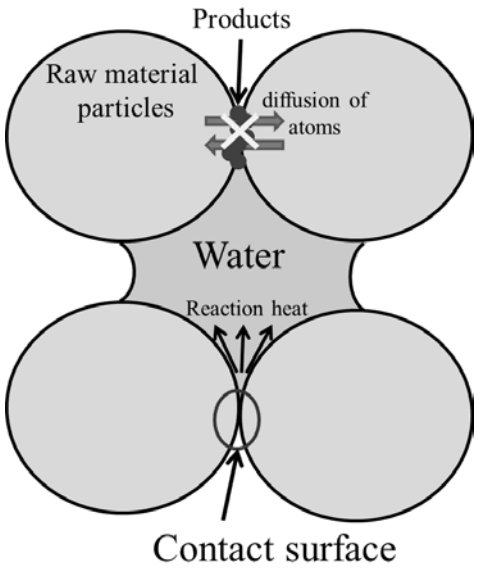

Fig. 2 Schematic of a water assisted room temperature solid state reaction (WASSR) method.

Controlled Topotactic Synthesis of the Layered $[Sr_2O_2]_qCoO_2$

Lassi Karvonen,[a] Bahir Duraki,[a] Songhak Yoon,[a] Simone Pokrant [a] and Anke Weidenkaff [b]

[a] Laboratory for Solid State Chemistry and Catalysis,
EMPA - Swiss Federal Laboratories for Materials Science and Technology,
Überlandstrasse 129, CH-8600 Dübendorf, Switzerland

[b] Materials Chemistry, University of Stuttgart,
Heisenbergstrasse 3, DE-70569 Stuttgart, Germany

Layered cobalt oxides - described with the general formula, $[M_mA_rO_{m+r-\delta}]_qCoO_2$ (M = Co, Bi, Pb, Tl, etc.; A = Ca, Sr, Ba, etc.; m = 0, 1, 2; $q \geq 0.5$; $r \geq 0$; $\delta \geq 0$) - possess a 2-dimensional crystal structure consisting of two types of layer blocks: hexagonal $[CoO_2]$ block and typically rock-salt-structured $[M_mA_rO_{m+r-\delta}]$ block stacked incoherently to each other forming a composite crystal. The high structural anisotropy and weak inter-block interaction result into an easy modifiability of the physical and chemical properties of these compounds making them interesting objects for the research exploring new oxide materials.

In this work we have focused on (r = 2, m = 0, δ = 0)-type phases of the layered cobalt-oxide family featuring an AO bilayer as its rock-salt block. First reported in year 2006, only two compounds have been discovered so far with $[Sr_2O_2]_qCoO_2$ and $[Ca_2O_2]_qCoO_2$ compositions. [1-2] Synthesis of these phases is a sintering procedure taking place under elevated pressures of O_2 (g) and is known to be facilitated by the presence of H_2O (g). [3]

Multi-phase samples with a general composition of $Sr_xCoO_z \cdot rH_2O$ were synthesized using a topotactic synthesis approach, where a (r = 1, m = 0, δ = 1)-type Sr_xCoO_2 layered cobaltite phase with a single non-stoichiometric A-cation layer between the $[CoO_2]$ blocks is promoted to a $[Sr_2O_2]_qCoO_2$ phase through sintering Sr_xCoO_2 + SrO_2 mixtures under elevated H_2O and O_2 partial pressures. To understand the influence of the synthesis pressure and the stabilizing role of the H_2O in the structure, different $p(H_2O) + p(O_2)$, $p(H_2O)/p(O_2)$ values were tested. The phase compositions of selected synthesized samples were evaluated using XRD and thermal analysis.

XRD results indicate, that the $[CoO_2]$ interlayer distance of the $[Sr_2O_2]_qCoO_2$ phase can be controlled through adjusting the $p(H_2O)/p(O_2)$ value. While higher $p(H_2O)/p(O_2)$ increases the $[CoO_2]$ interlayer distance, it also promotes the decomposition of the Sr_xCoO_2 into Co_3O_4 and hydroxidic Sr-salts. Elimination of $p(H_2O)$ on the other hand leads into stabilization of the rhombohedral $Sr_6Co_5O_{15+\delta}$ phase. TGA-MS measurements revealed for the first time, that the phase commonly known as $[Sr_2O_2]_qCoO_2$ contains large amounts of H^+ bound either as H_2O or OH^- species. The almost 1:1 relation of the Sr^{2+} and H^+ in the $[Sr_2O_2]$ block implies that the given block might rather have hydroxide than oxide nature.

References:

[1] H. Yamauchi, K. Sakai, T. Nagai, Y. Matsui, M. Karppinen, *Chem. Mater.* 18 (2006) 155.
[2] M. Shizuya, M. Isobe, Y. Baba, T. Nagai, M. Osada, K. Kosuda, S. Takenouchi, Y. Matsui, E. Takayama-Muromachi, *J. Solid. State Chem.* 180 (2007) 249.
[3] H. Yamauchi, L. Karvonen, T. Egashira, Y. Tanaka, M. Karppinen, *J. Solid State Chem.* 184 (2011) 64.

Synthesis and thermal expansion of Ba-Silicates

L.A. Gorelova [a,b] , M.G. Krzhizhanovskaya [a], R.S. Bubnova [a,b]
[a]Geology Department, Saint Petersburg State University, St. Petersburg, Russia;
[b]Institute of the Silicate Chemistry of Acad. Russ. Sci., St. Petersburg, Russia.
gorelova.ljudmila@gmail.com

The system $BaO–SiO_2$ was first studied in [1], the last study was in [2]. Eight phases is known in this system. There exist homologous series of barium silicates of general formula $Ba_{M+1}[Si_{2M}O_{5M+1}]$ (M = 1, 3, 4, 5, ∞) [3] and silicates with isolated tetrahedra.

This paper present synthesis and thermal expansion of three Ba-silicates Ba_2SiO_4 (with isolated tetrahedra), $BaSiO_3$ (chain silicate, M = 1) and $Ba_2Si_3O_8$ (silicate with triple chains, M = 3). These silicates were obtained by solid-state reactions at temperatures of 1400 ºC for 15-20 hours with intermediate mastication each 5 hours.

Thermal behavior of these silicates was studied using *in situ* high-temperature X-ray diffraction in the range 30–1100 °C with temperature steps of 40 °C in air. The main coefficients of the thermal expansion tensor were determined using second order polynomial approximation of temperature dependencies for the unit-cell parameters by the TTT program [4].

Orthorhombic silicate Ba_2SiO_4 has weak anisotropy of thermal expansion, which decreases with increase of temperature: at 30 ºC $\alpha_a = 20$, $\alpha_b = 12$, $\alpha_c = 10$, $\alpha_V = 42\times10^{-6}$ K^{-1} ($\alpha_{max}/\alpha_{min} = 2$), and at 1100 ºC $\alpha_a = 18$, $\alpha_b = 15$, $\alpha_c = 18$, $\alpha_V = 51\times10^{-6}$ K^{-1} ($\alpha_{max}/\alpha_{min} = 1.2$), that was predictably for silicates with isolated tetrahedra. Orthorhombic chain silicate $BaSiO_3$ (M = 1) has pseudo isotropic thermal expansion at low temperature (at 30 ºC $\alpha_a = 12$, $\alpha_b = 13$, $\alpha_c = 10$, $\alpha_V = 35\times10^{-6}$ K^{-1}), but with increasing of temperature structure of this compound expands intense inside of chain along *a*-axis and normal of chain along *c*-axis, whereas expansion along *b*-axis remains constant (at 1100 ºC $\alpha_a = 28$, $\alpha_b = 11$, $\alpha_c = 24$, $\alpha_V = 63\times10^{-6}$ K^{-1}). The thermal expansion of monoclinic silicate with triple chains $Ba_2Si_3O_8$ (M = 3) is anisotropic: at 30 ºC $\alpha_{11} = 15$, $\alpha_{22} = 11$, $\alpha_{33} = 3\times10^{-6}$ °C^{-1}, μ ($\alpha_{33} \wedge c$) = 10°, $\alpha_V = 29\times10^{-6}$ K^{-1} and at 1100 ºC $\alpha_{11} = 21$, $\alpha_{22} = 23$, $\alpha_{33} = 5\times10^{-6}$ °C^{-1}, μ ($\alpha_{33} \wedge c$) = 38°, $\alpha_V = 48\times10^{-6}$ K^{-1}. Directions of the minimal α_{33} and maximal α_{11} expansion are in the monoclinic plane *ac*, β-angle increases with temperature. The structure expands minimal practically normal to plane of triple chain and maximal in this plane. The character might be caused by shear and hinge deformations inside this triple chain.

The access to the X-ray diffraction equipment was granted through SPbSU X-ray Diffraction Resource Centre.

References:

[1] Eskola P.E., *Am. J. Sci.,* **4** (1922) 331.
[2] Grebenshchikov R.G., Toropov N.A., *Izvestiya akademii nauk USSR*, **4** (1962) (*in russ*).
[3] Liebau F. Structural Chemistry of Silicates: Structure, Bonding and Classification. Springer-Verlag. Berlin/Heidelberg. 1985.
[4] Bubnova R.S., Firsova V.A., Filatov S.K., *Glass Physics and Chemistry*, **39** (2013) 347.

Residual Carbon Influence on Texturing of $La_2Zr_2O_7$ and $La_2Hf_2O_7$ Films Processed by Real-to-Real Chemical Solution Deposition

A. Kharchenko,[a] A. Schukin,[a] V. Chepikov,[a] A. Vasiliev,[b] A. Kaul[a]

[a] Department of Chemistry, Moscow State University, 119991, Moscow, Russia;
[b] National research centre "Kurchatov Institute", 123182, Moscow, Russia.

Oxides with pyrochlore or fluorite structure, $La_2Zr_2O_7$ (LZO) and $La_2Hf_2O_7$ (LHO), due to their low lattice mismatch with the $YBa_2Cu_3O_{7-x}$ (YBCO), can be good buffer layers in the high temperature superconducting tapes [1, 2]. The development of simple buffer layer architectures as well as cheap techniques of the deposition is still important tasks for coated conductor technology. By this the aim of the work was to develop chemical solution deposition (CSD) process to obtain thick <001>(001)-textured $La_2Zr_2O_7$ and $La_2Hf_2O_7$ films on metal substrate.

The coating solutions consisted of a stoichiometric mixture of lanthanum oxide and zirconium or hafnium acetylacetonates dissolved in propionic acid. The advantages of those solutions were their stability at high concentrations and excellent wetting behavior on metal substrate surfaces. The chemistry of the precursor solutions was studied using thermogravimetric analysis and infrared and NMR spectroscopy.
To obtain smooth LZO/Ni-5W coatings with perfect cubic texture and with very small side effect we've developed continuous real-to-real CSD process using carboxilates, followed with continuous texturing thermal treatment. The film texture quality was shown to be drastically dependent on the residual carbon content which is strong function of the film thickness and thermal treatment regime. Thus, the attempt to get sharply textured LZO films with thickness more than 50-nm (this thickness is not enough to stop diffusion of Ni to superconducting layer) using the only thermal treatment in reducing Ar/H_2 atmosphere, recommended in the literature [1, 2], was unsuccessful. For one deposition step obtaining of 200 nm-thick LZO films with sharp biaxial texture we've proposed to combine low-temperature (450^{o}C) oxidative treatment with the following high temperature treatment (1150^{o}C) in H_2 (pH_2= 20-30 mbar). The texture was much improved when the low-temperature oxidation was activated with ozone admixture to the furnace atmosphere. The effective carbon elimination at the low temperature oxidative treatment promotes faster diffusion of oxide components at the high temperature texturing annealing, leading to much higher texture and crystallinity. The possible mechanism of the inhibiting effect of carbon on oxide layer texturing is discussed. The quality of the buffer layers obtained made possible to realize the simplest 2G HTSC tapes YBCO(*MOCVD*)/200 nm LZO(*CSD*)/Ni-5W with J_c = 1.1 MA/cm^2 (77 K, Self Field). The XRD, Auger – spectroscopy, EBSD, SEM, TEM and ED techniques were used to characterize buffer layers.

References:

[1] K. Knoth, R. Huhne, S. Oswald, *Thin. Sol. Films*, **516** (2008) 2099.
[2] L. Molina-Luna, R. Egoavil, S. Turner, *Supercond. Sci. and Tech.*, **26** (2013) 075016.

Quintinite $[Mg_4Al_2(OH)_{12}](CO_3)(H_2O)_3$ distribution in nature

Elena S. Zhitova[a], Victor N. Yakovenchuk[a], Sergey V. Krivovichev[a,b], Grigory Yu. Ivanuck[b], Yakov A. Pakhomovsky[b], Andrey A. Zolotarev[a]

[a] –St. Petersburg, St. Petersburg State University, zhitova_es@mail.ru
[b] –Apatity, Nanomaterials Research Centre, Kola Science Centre, the Russian Academy of Sciences

Quintinite $[Mg_4Al_2(OH)_{12}](CO_3)(H_2O)_3$ is a Layered Double Hydroxide (LDH) and a member of the quintinite group of the hydrotalcite supergroup and also commonly known as «anionic clay». Layered Double Hydroxides are characterized by structures based upon double brucite-like hydroxide layers $[M_n^{2+}M_n^{3+}(OH)_{2(m+n)}]^{m+}$, where M^{2+} = Mg^{2+}, Fe^{2+}, Mn^{2+}, Zn^{2+}, etc.; M^{3+} = Al^{3+}, Fe^{3+}, Cr^{3+}, Mn^{3+}, etc. The positive charge of the layer is balanced by interlayer species that may consist of anions (CO_3^{2-},Cl^-,SO_4^{2-}, etc.) or both anions and cations (Na^+, Ca^{2+}, Sr^{2+}, etc.). Due to their layered character, LDHs display polytypism and layer stacking disorder. Due to their crystal structures and physical properties LDHs have become important to industry and found applications in its different spheres. The main part of research on LDHs was done on synthetic materials, whereas many natural samples, which are prototypes for new materials, require further studying [1-3].

The archetype of LDHs is hydrotalcite $[Mg_6Al_2(OH)_{16}](CO_3)(H_2O)_4$, which was the first phase to be discovered by Hochstetter in Sweden in 1842. X-ray studying of hydrotalcites from four localities revealed presence of two phases rhombohedral one with a = 3.065, c = 23.07 Å and hexagonal phase a = 3.06, c = 15.34 Å. The hexagonal phase was called “manasseite”, which is now hydrotalcite-2*H*. Quintinite was described as a new mineral species by Chao and Gault (1997) on samples from Mont St-Hilaire (Canada) as 3*T* polytype ($P3_112$ or $P3_212$, a = 10.558, c = 22.71 Å) and from Jacuperanga (Brazil) as 2*H* polytype ($P6_322$, a = 10.571, c = 15.139 Å). Distinction of quintinite from hydrotalcite and “manasseite” is by means of the Mg:Al ratio (2:1 vs. 3:1) [4-7].

Within recent years, we have studied dozens of quintinite samples, which have been previously described as ‘hydrotalcites’ and ‘manasseites’. Four quintinite polytypes have been strycturally characterized: 2*H*-3*c* (*R*32, a = 5.2745(6), c = 45.364(10) Å), 2*H*-1*c* (*P*-3*c*1, a = 5.2720(6), c = 15.113(3) Å), 2*H* ($P6_3/mmc$, a = 3.0446(9), c = 15.178(5) Å) and 1*M* (*C*2/*m*, a = 5.266(2), b = 9.114(2), c = 7.766(3) Å, β = 103.17(3)°), from which two have been unknown before our research. Cation ordering and superstructures observed by us in quintinite polytypes are probably common to many natural and synthetic LDHs. At the moment quintinite has been detected by us in four Russian localities: Kovdor alkaline massif (Kola peninsula); Bazhenowo ultrabasic massif (Middle Urals); Rudnogorskoe deposit (Irkutsk region, Ilim river); Malishevskoe (Mariinskoe) deposit (Middle Urals). Our research indicated that quintinite is much more widespread in the nature, than it was though previously [8-11].

It is noteworthy that a review of literature on ‘hydrotalcites’ reveals more cases and localities where ‘hydrotalcite’ or ‘manasseite’ actually appeared to be different polytypes of quintinite. Černý (1963) described a rhombohedral mineral from Věžná (Western Moravia, Czech Republic) with Mg:Al = 2:1 under the name of ‘hydrotalcite’ (Černý, 1963), which is obviously quintinite (Chao and Gault, 1997). The structure determination of this sample showed the space group *R*-3*m* (a = 3.054, c = 22.81 Å) (Allmann and Jepsen, 1969). A

hexagonal sample from evaporate deposits (Pre-Caspian depression, Central Asia) with the composition identical to quintinite was reported as 'manasseite' with the following unit-cell parameters: *a* = 3.042, *c* = 15.12 Å (Drits *et al*., 1987). Recent reinvestigation of 'hydrotalcite' from type locality (Snarum, Norway) found the Mg:Al = 2:1 and 2.3:1 (Stanimirova, 2001), what also corresponds to quintinite [12-15].

This work was supported by the Russian Foundation for Basic Research (project no.14-05-31229).

References:

[1] Evans, D.G., Slade, R. C.T., Structure and bonding, Springer Berlin Heidelberg, **119**, 2006, 1.
[2] Mills, S.J., Christy, A.G., Génin, J-M. R., Kameda, T., Colombo, F. *Mineral. Mag*. **76** (2012) 1289.
[3] Cavani, F., Trifiro, F., Vaccari A. *Catal. Today*, **11** (1991) 173.
[4] Hochstetter, C., *J. Prakt. Chem*, **27** (1842) 375.
[5] Frondel, C., *Am. Mineral*., **26** (1941) 295.
[6] Ingram, L. and Taylor, H.F.W., Mineral. Mag., 36 (1967) 465.
[7] Chao, G.Y., Gault, R.A. *Canad. Mineral*., **35** (1997) 1541.
[8] Krivovichev, S.V., Yakovenchuk, V.N., Zhitova, E.S., Zolotarev, A.A., Pakhomovsky, Ya.A., Ivanyuk, G.Yu., *Mineral. Mag.*, **74(5)** (2010) 821 (a).
[9] Krivovichev, S.V., Yakovenchuk, V.N., Zhitova, E.S., Zolotarev, A.A., Pakhomovsky, Ya.A., Ivanyuk, G.Yu., *Mineral. Mag*., **74(5)** (2010) 833 (b).
[10] Krivovichev, S.V., Yakovenchuk, V.N., Zhitova, E.S., MAAM II (Ed. S.V.Krivovichev) Springer Berlin Heidelberg, (2012) 87.
[11] Zhitova, E.S., Yakovenchuk, V.N., Krivovichev, S.V., Zolotarev, A.A., Pakhomovsky, Ya.A., Ivanyuk, G.Yu. *Mineral. Mag*. **74(5)** (2010) 841.
[12] Černý, P. *Acta Musei Moraviae*, **XLVIII**, 1963, 23.
[13] Allmann, R., Jespen, H.P., *Neues. Jahr. Mineral. Monat*., **1969** (1969) 544.
[14] Drits, V.A., Sokolova T.N., Sokolova G.V., Cherkashin V.I., *Clay Clay Miner*., **35** (1987) 401.
[15] Stanimirova, T., Annual of the University of Sofia,Faculty of Geology, **94** (2001) 73.

OXYGEN NONSTOICHIOMETRY AND DEFECT STRUCTURE OF MAYENITE

D.S. Tsvetkov, A.S. Steparuk, A.Yu. Zuev

Institute of Natural Sciences, Ural Federal University, Ekaterinburg, Russia

Mayenite $Ca_{12}Al_{14}O_{33}$ has recently received great attention as promising mixed protonic, oxygen ionic and electronic conducting material. The unique feature of this material is related to the state of electrons formed during its reduction. They were shown to be localized in the centers of cages in the structure of $Ca_{12}Al_{14}O_{33}$. However defect structure of this compound has not yet been studied although it is well known that defect structure is of key importance for understanding the properties of solid materials.

The priority purpose of the current work was, therefore, the refinement of defect structure of the mayenite $Ca_{12}Al_{14}O_{33}$ by means of the quantitative modeling on the basis of the measured oxygen nonstoichiometry.

Powder samples of $Ca_{12}Al_{14}O_{33}$ was synthesized by glycerol-nitrate technique described elsewhere [1]. The phase composition of the powder samples prepared accordingly was studied by means of X-ray diffraction (XRD) with an Equinox 3000 diffractometer using Cu Kα radiation. XRD showed no indication for the presence of a second phase.

Oxygen nonstoichiometry of $Ca_{12}Al_{14}O_{33}$ as a function of temperature and oxygen partial pressure was measured by thermogravimetric technique using DynTHERM LP-ST (Rubotherm präzisionsmesstechnik GmbH, Germany) microbalances supplied by the pO2 control and adjustment system.

Results obtained are discussed on the basis of the defect structure of the mayenite $Ca_{12}Al_{14}O_{33}$.

This work was supported by the Russian foundation for basic research grant No. 13-03-96118.

References:

[1] A. Yu. Zuev, A.I. Vylkov, A. N. Petrov and D. S. Tsvetkov, Solid State Ionics, V. 179, 2008, 1876.

$Sr_{1-x}Ba_xBi_2B_2O_7$ solid solutions (crystals and glass-ceramics)

A.P. Shablinskii [1], R.S. Bubnova [2], S.N. Volkov [1], S.K. Filatov [1], M.G. Krzhizhanovskaya[1], I.A. Drozdova [2]

[1]*Department of Crystallography, Faculty of Geology, Saint-Petersberg State University, 199034,7/9 University Emb, Russia*
[2]*Institute Silicate Chemistry of RUS, 199034, Makarov Emb. 2, Saint-Petersberg, Russia*

Solid solutions $Sr_{1-x}Ba_xBi_2B_2O_7$ (x = 0.00, 0.25, 0.50, 0.65, 0.75, 0.85, 1.00) have been prepared by glass ceramic crystallization with the starting materials of Bi_2O_3, $BaCO_3$, $SrCO_3$, H_3BO_3 at 600°C for 1 to 30 hours time. These prereacted materials have been grounded and used to press pellets. These pellets have been heat-treated at 600 °C for 2 hours. Then these pellets were placed in platinum crucibles and melted at a temperature range of 900-950°C for 0.5 hour. The melt was poured onto a steel plate at room temperature. The cooled melt was investigated by electron microscopy and DSC and TG methods. Size of crystallites changes from 50 nm to 100 nm in depends of Ba. Glass-ceramics have been investigated by powder X-Ray diffraction. Samples of glass-ceramics are amorphous, but Sr-rich samples (x = 0 and 0.5) have peaks of crystal phase $SrBi_2B_2O_7$ [1].

Single crystal data of solid solutions $Sr_{1-x}Ba_xBi_2B_2O_7$ (x = 0.5, 0.65, 1) were collected by means of a Bruker "Kappa APEX DUO" diffractometer using MoKα radiation. Unit cell parameters of x = 0.5 (SG $P6_3$, Z = 6, a = 9.194(1) Å, c = 13.299(3) Å) have been determined like $SrBi_2B_2O_7$ [2]. Crystal structures of solid solutions (x = 0.65, 1) have been solved by direct methods and refined to R_1 = 0.04, R_2 = 0.023 respectively. Crystal system is hexagonal, space group $P6_3$, Z = 2, a = 5.3378(8) Å, c = 13.583(2) Å, for x = 1 and a = 5.3246(3) Å, c = 13.4013(8) Å, for x = 0.65. On the diffraction pattern of (x = 0.65, 1) solid solutions have been observed very weak and diffuse superstructure reflections. So crystal structures (x = 0.65 and x = 1) refinement has been implemented in reduced cell.

These structures consist of isolated BO_3 triangles, between these triangles three cationic positions are located (*M*1, *M*2 и *M*3). In contrast to $SrBi_2B_2O_7$ [2] where Sr occupied smallest *M*3 position, Ba-rich solid solutions have more complex occupancy of positions (Fig. 1). Each of them is splitted.

The studies have been supported by Russian Fund of Basic Researches project 14-03-32076. The access to the X-Ray Diffraction equipment was granted through SPbSU X-Ray Diffraction Research Centre.

References:

[1] Shablinskii A.P., Drozdova I.A., Volkov S.N., Bubnova R.S., Krzhizhanovskaya M.G. *Glass Phys. and Chem. (in Russ.)*, **38**, 2012, 886.
[2] Barbier J, Cranswick L.M.D., J. *Solid State Chem.*, **179,** 2006, 3958.

Figure:

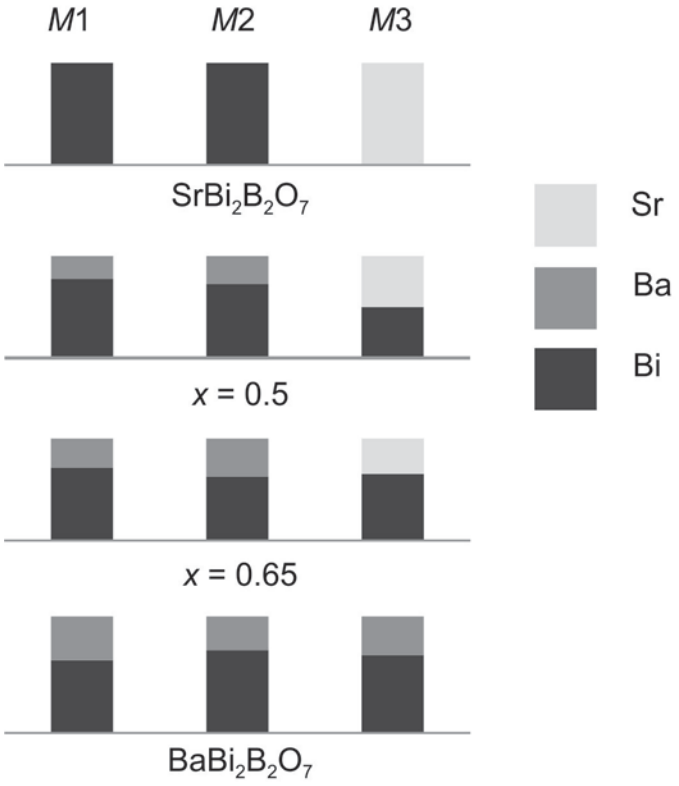

Fig. 1. Occupation of positions these solid solutions.

Transport properties of $LiNO_2$ and $LiNO_2$-SnO_2 composites

Yu.G. Mateyshina [a,b], A.S. Ulihin [a,b], A.V. Ukhina [a], V.S. Minkov [a,b], Matvienko A.A.[a,b], N.F. Uvarov [a,b,c]

[a]Institute of Solid State Chemistry and Mechanochemistry, Kutateladze 18, Novosibirsk, 630128, Russia
[b]Novosibirsk State University, Pirogova 2, Novosibirsk, 630090, Russia
[c]Novosibirsk State Technical University, Prospekt K. Marksa 20, Novosibirsk, 630073, Russia

Solid electrolytes are widely used in various applications, such as power sources, sensors and other electrochemical devices. However for application in lithium batteries they should be chemically stable towards metallic lithium, have wide electrochemical stability window and high lithium ion conductivity. A lot of information about the ionic conductivity of lithium solid ionic conductors has been reported in the literature, including ceramic materials based on Li_2SO_4 [1-2], Li_4SiO_4 [3], Li_3XO_4 (X=P, As, V, Cr) [4-6], Li_4GeO_4 [7], Li_3N [8], lithium phosphates [9], electrolytes of LISICON–type structure [10-11], etc. Due to high volume changes of the electrode materials during charge-discharge cycles it is very difficult to provide reliable contact between and solid electrode and ceramic solid electrolyte. This problem may be, at least partially, solved if solid electrolyte is a plastic salt or when composite solid electrolyte is used instead of the pure salt. Composite solid electrolytes have several advantages compared to pure systems as they usually have enhanced conductivity and their transport and mechanical properties can be easily varied by changing of chemical nature, microstructure and concentration of additives. It has been reported earlier that composite solid electrolytes based on $LiNO_3$ [12] and $LiClO_4$ [13] have high ionic conductivity. Unfortunately, both lithium perchlorate and nitrate are strong oxidizers, especially at elevated temperatures. In this work we present the results of the experimental study of physical and transport properties of pure lithium nitrite $LiNO_2$ and composite solid electrolytes based on $LiNO_2$. Nitrites are known to be moderate oxidants and should be more stable than perchlorate and nitrate analogues at high temperatures in reducing media.

In this work lithium nitrite was synthesized and its structural, thermodynamic and electrical properties were investigated. Lithium nitrite was obtained from aqueous solutions in the form of the monohydrate $LiNO_2 \cdot H_2O$ which has monoclinic crystal structure and dehydrates on heating with formation of pure $LiNO_2$. The change of the crystal structure of $LiNO_2 \cdot H_2O$ was studied by in-situ heating to T = 190°C with the increment of 10°C. Ionic conductivity was studied in vacuum or in humidified atmosphere by means of HP-4284A Meter and NOVOCONTROL Beta Impedance Analyzer on pellets with pressed-in silver electrodes.
It has been shown that the dehydration of $LiNO_2 \cdot H_2O$ proceeds via two stages. On the first stage (at 40-70°C) the sample loses approximately a half of the total water content, however its structure does not change. Complete dehydration takes place at temperatures of 140-180°C and leads to the formation of the anhydrous $LiNO_2$ with the melting temperature of 222°C and the structure not reported in the literature. Pure lithium nitrite $LiNO_2$ has rather low ionic conductivity, near 10^{-5} S/cm at 180°C, which seems to be caused by extrinsic cationic vacancies.

In order to enhance the conductivity of $LiNO_2$ we have prepared $LiNO_2$-based composite solid electrolytes. As a dispersed additive in the composite we have used highly dispersed nanocrystalline tin dioxide SnO_2 prepared by oxidative thermal decomposition of tin oxalate SnC_2O_4 at 220°C [14]. This sample had a specific surface area of 100 m^2/g and the mean

particle size of 9 nm. Solid composite electrolytes LiNO2 – SnO_2 have been synthesized by mixing of preliminary dehydrated components followed by sintering at 200°C and their structural, thermodynamic and electrical properties investigated.

It was shown that the conductivity of composites goes through a maximum. The highest conductivity, $2 \cdot 10^{-3}$ S/cm at 180°C, was observed for composite containing ~ 40 mol% (or 50 vol%) of oxide. Arrhenius plot for this sample is non-linear indicating to formation of amorphous interface phase in the composite. Similar behavior is typical for composite solid electrolytes where the conductivity occurs via ionic salt-oxide interface regions. The conductivity parameters and their variation with the type of oxides is investigated and compared with the relative data obtained earlier for composite solid electrolytes based on lithium perchlorates [13].

Acknowledgements: The work was supported by the Ministry of Education and Science of the Russian Federation and by the Programme of Presidium RAS #27.59.

References:

[1] A.V.N. Tilak, M. Umar, K. Shahi, *Solid State Ionics*, **24,** (1987) 121.
[2] M. Touboul, N. Sephar, M. Quarton, Solid *State Ionics*, **38** (1990) 225.
[3] A.R. West, *J. of App.Electrochem.*, **3** (1973) 327.
[4] Y. A. Dua, N. A. W. Holzwartha, *ECS Transactions*, **13** (2008) 75.
[5] A. K. Ivanov-Shitz, V. V. Kireev, O. K. Mel'nikov, L. N. Demianets, *Crystall. Rep.*, **46,** Iss.5, (2001) 864.
[6] A. Khorassani, A.R. West, *J. of Solid State Chem.*, **15** (1984) 369.
[7] A.R. Rodger, J. Kuwano, A.R. West, *Solid State Ionics*, **15** (1985) 185.
[8] T. Lapp, S. Skaarup, *Solid State Ionics*, **11** (1983) 97.
[9] S.Q. Zhang, S. Xie, C.H. Chen, *Mat. Science and Eng.: B* **121**, (2005) 160.
[10] P. Zhang, M. Matsui, A. Hirano, Y. Takeda, O.Yamamoto, N.Imanishi *Solid State Ionics* **253** (2013)175.
[11] D. Mazumdar, D.N. Bose, *Solid State Ionics* **14**, (1984) 143.
[12] N.F. Uvarov, A.A. Iskakova, A.S. Ulihin, N.N. Medvedev, *Solid state Ionics*, **188** (2011) Iss. 1 78.
[13] A.S. Ulihin, N.F. Uvarov, B.-E. Mellander, *Solid State Ionics*, **179**, Iss. 1-6, (2008) 228.
[14] A. Matvienko, S. Chizhik, A. Sidelnikov *Abstract Booklet of 17th International Symposium on Reactivity of Solids (ISRS), 2011, Bordeaux, France, p. 48*

Figure:

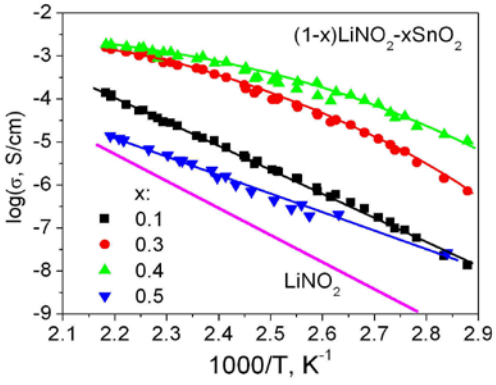

Fig.1. Temperature dependences of conductivity for $LiNO_2$-SnO_2 composites under study.

Ion solvation energy: nonlocal electrostatics calculation. Effects of cut-out ion volume and of charge distribution inside ion

M.A. Vorotyntsev[a,b,c], A.A. Rubashkin[d]

[a] M.V. Lomonosov Moscow State University, Moscow, Russia; mivo2010@yandex.com
[b] Institute for Problems of Chemical Physics, Russian Academy of Sciences, Russia
[c] ICMUB - UMR 6302 CNRS, Universite de Bourgogne, Dijon, France
[d] Institute of Cytology, Russian Academy of Sciences, Saint-Petersburg, Russia

Existence of an internal structure inside a solid or liquid polar medium means a nonlocal relation between the static distributions of the electric displacement, $\mathbf{D}(\mathbf{r})$, and the electric field, $\mathbf{E}(\mathbf{r}')$: $D_\alpha(\mathbf{r}) = \int \varepsilon_{\alpha\beta}(\mathbf{r},\mathbf{r}')\, E_\beta(\mathbf{r}')\, d\mathbf{r}'$ [1]. If the medium occupies the whole space and it is isotropic and uniform, then one can derive analytical expression for the electric potential distribution, $\varphi(\mathbf{r})$ ($\mathbf{E} = -\nabla\varphi(\mathbf{r})$), via longitudinal dielectric function of the medium, $\varepsilon(k)$, and the distribution of immersed charges, $\rho(\mathbf{r})$ [2]. This formula has been used to calculate the solvation energy of a spherical ion for several models of the dielectric function and for various distributions of the electronic density of the ion: uniform charge on the external spherical surface of the ion, $|\mathbf{r}| = r_i$ (Born model for the ion charge) [2-4] or inside this surface [4].

The above approach ignores formation of a spherical cavity inside the medium, $|\mathbf{r}| < r_i$, by the ion. In the absence of correlations of polarization fluctuations between the outer and inner volumes the above nonlocal relation is only valid for points, $\mathbf{r}$, inside the medium, $|\mathbf{r}| > r_i$, while the integration is carried out only outside the sphere, $|\mathbf{r}'| > r_i$. Then, the medium in the outer space is only polarized by the electric displacement *outside the sphere* which is equal to Q/r^2 (Q, total ionic charge). Within the linear response of the medium to the electronic charges of the ion the dielectric response of the medium outside the sphere, $\varepsilon_{\alpha\beta}(\mathbf{r},\mathbf{r}')$, should not depend on the distribution of these charges inside the ion. Thus, the potential profile outside the ion and consequently the ion solvation energy should be identical if the same total charge, Q, is located at the outer sphere or inside it. This conclusion is at variance with the marked dependence of the ion solvation energy on the electronic charge distribution inside the ion found in the model disregarding the absence of the medium inside the ion [4].

The goal of our study was to analyze the origin of this disparity, by considering the ion charge redistribution in combination with the theories which take or do not take into account the cut-out space inside the medium occupied by the ion. To clarify this key question we used the simplest approximations for calculations. The electronic charge was assumed to be located at a sphere, $|\mathbf{r}| = r_e$, with the density, $Q/4\pi r_e^2$, where the radius of the sphere, r_e, is either on the surface of the ion, $r_e = r_i$ (Born model), or inside the ion, $r_e < r_i$. The single-mode formula was used for the dielectric function: $1/\varepsilon(k) = 1/\varepsilon_\infty - (1/\varepsilon_\infty - 1/\varepsilon_S)/[1 + \Lambda^2 k^2]$, where $\varepsilon_S = \varepsilon(0)$ is the macroscopic dielectric constant, $\varepsilon_\infty = \varepsilon(\infty)$ is the dielectric constant at short wavelengths, Λ is the correlation length of the medium.

The ion solvation energy for such system in the approximation of the continuous medium without a cut-out space [2,3] for the spherical distribution of the electronic charge, $|\mathbf{r}| = r_e$, is given by the formula:

$$W_K = (Q^2/2r_e)\{1 - 1/\varepsilon_S - (1/\varepsilon_\infty - 1/\varepsilon_S)[1 - \exp(-2r_e/\Lambda)]\,\Lambda/(2r_e)\} \qquad (1)$$

Since the medium occupies in this approximation the whole space the energy only depends of the charged-sphere radius, r_e, but not on the external ion radius, r_i.

Calculation of the potential distribution inside the medium and the ion solvation energy requires an extra assumption on the relation between the nonlocal dielectric function inside this medium with the cut-out sphere, $\varepsilon_{\alpha\beta}(\mathbf{r},\mathbf{r}')$, and the bulk-volume dielectric function of the medium, $\varepsilon_{\alpha\beta}(\mathbf{r}-\mathbf{r}') = \delta_{\alpha\beta}\ \varepsilon(|\mathbf{r}-\mathbf{r}'|)$ which is Fourier transform of the single-mode dielectric function, $\varepsilon(k)$. The so called dielectric approximation identifies $\varepsilon_{\alpha\beta}(\mathbf{r},\mathbf{r}')$ for any pair of points **r**, **r'** *inside the medium* with $\varepsilon_{\alpha\beta}(\mathbf{r}-\mathbf{r}')$ while there are no spatial correlations if at least one of these points is located outside the medium [5]. Then, one may use a formula for the potential distribution outside the ion derived in [5]. As a result one can obtain an expression for the ion solvation energy:

$$W_V = (Q^2/2r_i)\{1-1/\varepsilon_S-(1/\varepsilon_\infty-1/\varepsilon_S)/\{1+r_i/\Lambda+(\varepsilon_S/\varepsilon_\infty)[(\beta r_i/\Lambda)\coth(\beta r_i/\Lambda)-1]\}\} \quad (2)$$

where $\beta = (\varepsilon_\infty/\varepsilon_S)^{0.5}$. In accordance with the general reasoning above the energy, W_V, is determined by the *external ionic radius*, r_i, while it is *independent of the electronic charge location*, r_e. This result confirms once again that the dependence of the energy, W_K, on the charge distribution inside the ion, r_e in Eq (1) originates fully from the neglect of the cut-out space inside the medium.

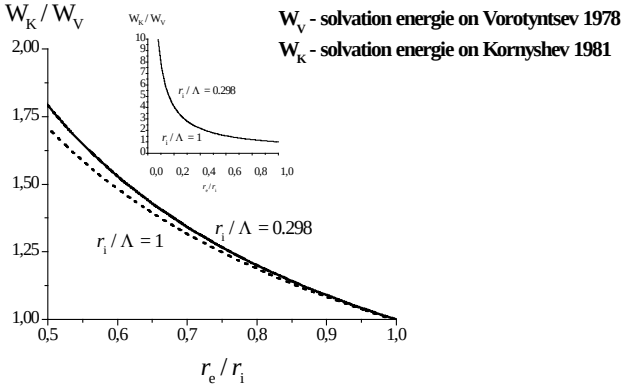

Fig.1 Ratio of the ion solvation energy in two approximations, W_K/W_V, depending on the location of electronic charges inside the ion with respect to the external ion radius, r_e/r_i. ε_S=78.5, ε_∞=1.8, values of r_i/Λ are equal to 0.298 and 1.

Fig.1 demonstrates that for the Born model for the ion ($r_e = r_i$) both approximations gives practically identical values for the solvation energy. On the contrary, the location of the charge density inside the ion results immediately in a significant error in predictions by W_K.

References:

[1] M.A.Vorotyntsev, A.A.Kornyshev, Monograph: Electrostatics of Media with the Spatial Dispersion (in Russian), Nauka, Moscow, 1993.
[2] R. R. Dogonadze, A. A. Kornyshev, *J. Chem. Soc. Faraday Trans.2*, **70** (1974) 1121.
[3] A. A. Kornyshev, *Electrochim. Acta*, **26** (1981) 1.
[4] A. A. Kornyshev, G. Sutmann, *J. Chem. Phys.*, **104** (1996) 1524.
[5] M. A. Vorotyntsev, *J. Phys.C: Solid State Phys.*, **11** (1978) 3323.

Furosemide solvates: can they serve as precursors to different polymorphs?

V.S. Minkov,[a,b] A.A. Beloborodova,[a] E.V. Boldyreva[a,b]

[a]Novosibirsk State University, Novosibirsk, Russia;
[b] Institute of Solid State Chemistry and Mechanochemistry SB RAS, Novosibirsk, Russia.

The importance of polymorphism of molecular crystals is hard to overestimate, especially when dealing with compounds used as materials or drugs. Different polymorphs of a drug substance may have different properties related to their manufacturing, therapeutic usage, or storage (density, hygroscopicity, melting points, thermal stability, solubility, rate of dissolution, surface free energy, toxicity, bioavailability, tabletting, etc.). Different polymorphs, solvates, and co-crystals can be patented, and this opens the way for a competition with brand drugs.

Since the energies of different polymorphs are sometimes very close, producing desirable crystalline forms is quite a challenge and can also be complicated by the phenomena of concomitant polymorphism (when several polymorphs crystallize simultaneously from the same batch), or erratic and poorly reproducible (when crystallization gives different polymorphs even at seemingly identical experimental conditions).

The aim of the present study was to crystallize various solvates of furosemide, to check whether these solvates can be used as precursors for producing different polymorphs of pure furosemide on their subsequent decomposition upon heating, and to search any correlation between the crystal structures of the solvates and on the furosemide polymorphs produced by desolvation. Four solvates of furosemide with tetrahydrofuran, dioxane, dimethylformamide, and dimethylsulfoxide were crystallized. The detailed structural analysis of furosemide-containing crystal structures showed that the molecule of furosemide has a high conformational lability because of the rotations of the sulfamoyl and furanylmethylamino fragments. Some of the furosemide conformations were shown to be stabilized by the intramolecular N−H···Cl H-bond. Desolvation of the four solvates was studied by TG and X-ray diffraction and was shown to give different products depending on the precursor and particle size. Desolvation of large crystals of the solvates of furosemide with tetrahydrofuran, dioxane, and dimethylformamide with characteristic dimensions more than $1 \times 1 \times 1$ mm^3 leads to the formation of the furosemide Form-III, while powders of solvates of furosemide with dioxane, dimethylformamide, and dimethylsulfoxide with characteristic diameter of particles ~1−10 μm give the furosemide Form-I instead.

References:

[1] V.S. Minkov, A.A. Beloborodova, V.A. Drebushchak, E.V. Boldyreva, *Crystal Growth & Design*, **14** (2014) 513-522.

Pressure induced phase transitions in glycine derivatives sarcosine and betaine: relative roles of H-bonds, steric repulsion of methyl-groups, and dipole-dipole interactions

V.S. Minkov,[a,b] E.A. Kapustin,[a] E.V. Boldyreva[a,b]

[a]Novosibirsk State University, Novosibirsk, Russia;
[b] Institute of Solid State Chemistry and Mechanochemistry SB RAS, Novosibirsk, Russia.

Infinite head-to-tail chains of zwitterions present in the crystals of all amino acids are known to be preserved even after structural phase transitions. In order to understand the relative roles of the two types of interactions linking zwitter-ions in these chains (charge assisted N-H···O hydrogen bonds and dipole-dipole interactions) in structural rearrangements, the crystal structures of two N-methyl derivatives of glycine (N-methylglycine, or sarcosine, with two donors for hydrogen bonding, and N,N,N-trimethylglycine, or betaine, with no hydrogen bonds and with an even bulkier amino-group) were studied in a wide pressure range. Though increasing pressure lead to phase transitions in both crystal structures, structural changes were more pronounced in sarcosine, than in betaine. Namely, dramatic changes in the conformations of zwitterions, as well as in intermolecular N-H···O hydrogen bonds were observed for sarcosine, whereas only slight changes within the head-to-tail chains and in the reorientation of the -N-$(CH_3)_3$ group occurred in betaine. Both phase transitions were accompanied by fragmentation of crystals, but it was also different for the two systems: the crystals of betaine cracked into several large fragments, whereas those of sarcosine transformed into fine powder. Phase transitions in sarcosine and betaine strongly depended on the rate of pressure variation: the higher the rate of increasing pressure, the lower the pressure at which the phase transition occurred.

One hydrogen bond - two ways to build a structure. The role of N-H...O hydrogen bonds in crystal structures of N,N-dimethylglycine

E.A. Kapustin,[a] V.S. Minkov,[a,b] E.V. Boldyreva[a,b]

[a]Novosibirsk State University, Novosibirsk, Russia;
[b] Institute of Solid State Chemistry and Mechanochemistry SB RAS, Novosibirsk, Russia.

Crystal structures of amino acids are considered to mimic important interactions in peptides; therefore the studies of the structure-forming factors in these systems attract much attention. N,N-Dimethylglycine is an interesting model compound that was used to test the role of the N−H···O hydrogen bonds in forming the head-to-tail chains, the main structural unit in the crystals of amino acids. It was hypothesized previously [B.A. Kolesov, E.V. Boldyreva. J. Raman Spectrosc. 2010, 41, 670−677] that additional side N−H···O hydrogen bonds play an important role in forming the head-to-tail chains of amino acid zwitterions linked via N−H···O hydrogen bonds between the charged $-NH_3^+$ and $-COO^-$ terminal groups. The twice methylated amino group of N,N-dimethylglycine is able to form only one N−H···O hydrogen bond in the crystal structure, so this hypothesis could be tested. In the present article, we describe the crystal structures of two polymorphs of N,N-dimethylglycine, in which the zwitterions are packed in two different ways. In one polymorph (orthorhombic, Pbca), they form finite four-membered ring motifs not linked to each other via any hydrogen bonds but only by weak van der Waals interactions. However, in the second polymorph (monoclinic, $P2_1/n$, which was never described before), the zwitterions do form infinite head-to-tail chains though the N−H···O bond is the only interaction and is not assisted via any additional hydrogen bonds. The effect of cooling on the two crystal structures was followed by single-crystal X-ray diffraction combined with polarized Raman spectroscopy of oriented single crystals, in order to compare the response of the N−H···O bonds to temperature variations. The crystal structure of the monoclinic polymorph with infinite chain motifs compresses anisotropically on cooling, whereas that of the orthorhombic polymorph with finite ring motifs undergoes a reversible single-crystal to single-crystal phase transition at ~200 K accompanied by nonmerohedral twinning, reducing the space symmetry to monoclinic ($P2_1/b$) and doubling the asymmetric unit from two to four molecules. This phase transition could not be detected by Raman spectroscopy and DSC. The temperature dependent structure and relative stability of both polymorphs were studied by periodic DFT calculations. The monoclinic polymorph appears to be more stable (by 0.8−1.2 kcal/mol, depending on the density), but with the increasing density and decreasing temperature, the difference decreases. The phase transition of the orthorhombic polymorph has no detectable impact on its relative stability.

References:

[1] E.A. Kapustin, V.S. Minkov, J. Stare, E.V. Boldyreva, *Crystal Growth & Design*, (2014) DOI: 10.1021/cg5000183.

Preparation and study of iron-containing nanoparticles obtained by interphase synthesis

Alexander Kudlash,[a] Svetlana Vorobyova,[b] Anatoly Lesnikovich[a]

[a] Department of Chemistry, Belarusian State University, Minsk, Belarus, kudlash@bsu.by
[b] Research Institute for Physical Chemical Problems of the Belarusian State University

Nanoparticles of transition metals continue to attract high interest across diverse areas of science due to their unique physicochemical properties which are quite different from those of bulk materials and are attributable to the quantum size effect. Thus, this tendency discovers a wide range of a potential applications such kind of substances in nanodevices. Especially interesting are the superparamagnetic phenomenon and quantum tunneling effect which appears when the particle size decreases toward a critical value and formation of domain walls becomes energetically unfavorable, so nanoparticles consist of single domain [1]. Bimetallic and core/shell nanoparticles are of great significance because of the combination and modification of the observed properties compared with individual particles that results in enhanced mechanical and oxidation strength, catalytic properties. As a result of the kinetically unstable nature of nanoparticles, various techniques with different stabilizers have been developed for particles synthesis with specific sizes and shapes, for example, preparation in homogeneous solutions, reverse micelles, thermal decomposition etc. [2, 3].

Iron magnetic nanoparticles represent an important class of nanostructured materials and have a great potential for applications in magnetic fluids, catalysts, sorbents, nickel-iron batteries, magnetic resonance imaging, and hyperthermia generation. Depending on the application area, different forms of Fe nanoparticles (aggregates or well-dispersed colloids) are needed [4].

In this investigation, iron nanoparticles were fabricated using interphase synthesis technique [2]. We have studied and demonstrated the preparation possibilities of iron(II) oleate and iron(III) oleate for interphase reduction with $NaBH_4$ solution in heterogeneous systems composed of polar and nonpolar solvents (water/hexane and ethanol/hexane). It was analyzed and shown, the products' localization phase and their state (colloids or dispersed sediments) depend both on type of precursors, their concentrations, nature of two-phase systems, and reagents molar ratio. Particles' size, morphology, composition and crystal structure were characterized by TEM, XRD and FT-IR spectroscopy.

It was shown the dispersed phase in colloidal dispersions consists of 4÷15 nm spherical particles and aggregates of 20÷50 nm (see Fig. 1) and represents Fe^0 and FeO. The experiments designated the catalytic amount of Pd nanoclusters (heterogeneous nucleation seeds) should be added to complete the interphase reduction successfully. As it appeared, $Fe(Oleate)_2$ reduction unlike $Fe(Oleate)_3$ one is more favorable since it allows to control the tendency for particles synthesis with required characteristics.

Magnetization versus temperature was measured using a ponderomotive method in the interval from 100 to 800 K. The results showed Fe nanoparticles with a ferromagnetic behavior and saturation magnetization of 35 emu/g (in contrast to 190 emu/g for bulk Fe), that may be related to a partial surface particles oxidation and strong interaction of the surfactant coated on the nanoparticles [5].

According to the results of IR-spectroscopy, the stability of iron colloidal dispersions and the facility of the metal preparation in nanometer size were achieved by the surfactants formed *in situ* during interphase synthesis and determined nucleation conditions for nanoparticles.

References:

[1] R. Nazir et al., *Nanotechnology*, **19** (2008) 185608.
[2] J. Carvell et al., *Mater. Lett.*, **63** (2009) 715.
[3] A.N. Kudlash et al., *J. Phys. Chem. Solids*, **69** (2008).
[4] K-Ch. Huang, S.H. Ehrman, *Langmuir*, **23** (2007) 1419.
[5] Ch.H. Young et al., *J. Phys. Chem. C*, **111** (2007) 6275.

Figures:

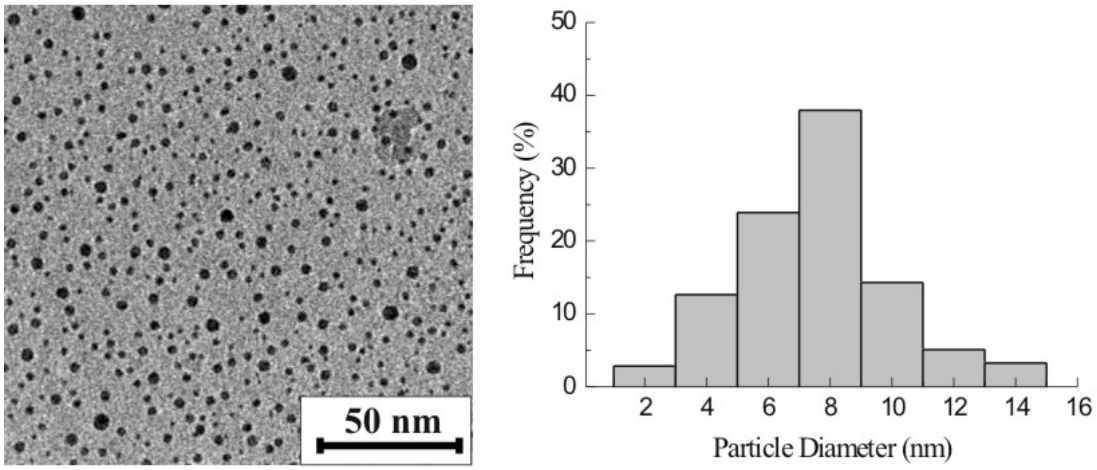

Fig 1. TEM image (left) and histogram of the size distribution (right) of Fe nanoparticles prepared by interphase synthesis of $Fe(Oleate)_2$ [$2 \cdot 10^{-2}$ M] and $NaBH_4$ in hexane–water system

A Single-crystal study of garnet-related type $Li_7La_3Zr_2O_{12}$

Kunimitsu Kataoka,[a] Junji Akimoto,[a]

[a] National Institute of Advanced Industrial Science and Technology;
1-1-1 Higashi, Tsukuba, Ibaraki, 305-8565, Japan

Li-ion rechargeable batteries are most advanced energy storage device, but their application has been presently limited to several portable electronic devices including mobile phones and notebook computers. In the case of applications to large electrical power storage systems such as electrical car and hybrid car, all-solid-state Li-ion rechargeable batteries have attracted attention because of their high energy density and safety desired. Therefore, there has been an extensive effort to develop Li-ion-conducting inorganic materials for the use as solid-state electrolyte which is a key materials of all-solid-state Li-ion rechargeable batteries, including NASICON-type $Li_{1+x}Al_xTi_{2-x}(PO_4)_3$ [1] , perovskite-type $La_{2/3-x}Li_{3x}TiO_3$ [2], and Li_2S sulfide glasses [3]. In recent years, as one of the oxide base Li-ion-conductor, garnet-related type structure have gain solid-state electrolyte. The structure of the garnet-related type structure, two types structures are reported; that is tetragonal-type and cubic-type. $Li_5La_3Nb_2O_{12}$, $Li_5La_3Ta_2O_{12}$, $Li_5La_3Sb_2O_{12}$, $Li_5La_3Bi_2O_{12}$, $Li_6CaLa_2Ta_2O_{12}$, $Li_6BaLa_2Ta_2O_{12}$ and $Li_7La_3Zr_2O_{12}$ show the cubic-type structure, and $Li_7La_3Zr_2O_{12}$, $Li_7La_3Hf_2O_{12}$ and $Li_7La_3Sn_2O_{12}$ show the tetragonal-type structure. Among the garnet-related type materials, cubic-type $Li_7La_3Zr_2O_2$ is reported as the best Li-ion conductivity [4]. The crystal structure of cubic-type $Li_7La_3Zr_2O_{12}$ was determined by the powder X-ray diffraction method [4]. Moreover, the detailed structural parameters have been recently refined using the single-crystal X-ray diffraction data [5]. In the present study, we revealed the crystal structure cubic-type of $Li_7La_3Zr_2O_{12}$ by single-crystal X-ray and neutron structure analysis. Especially, structure analysis with single-crystal neutron diffraction is for the first time. We also demonstrated the characteristic Li site population and occupancy of impurities in the garnet framework structure.

Single crystals of cubic-type $Li_7La_3Zr_2O_{12}$ were synthesized by high-temperature heating at 1100 °C in air. The starting materials used in this study were $LiNO_3$, La_2O_3, and ZrO_2. The mixture was filled in alumina crucible, heated in air, and then cooled naturally. Next, obtained single-crystals was annealed at 300°C in air. The chemical formula, analyzed by electron probe micro analyzer (EPMA) using a single crystal. X-ray intensity data were collected by a single-crystal X-ray diffractometer with an imaging plate (Rigaku R-AXIS RAPID-II) using graphite-monochromatized Mo Kα radiation at room temperature. Neutron intensity data were collected by a single-crystal neutron diffractometer with CCD detector (J-Parc, BL18, SENJU) at room temperature.

The obtained crystals were colorless and transparent, and approximately sphere-shaped with a typical diameter of 0.2 mm. The quality of crystals with diameters less than 0.1 mm was very high. The EPMA analysis revealed that the crystals were contaminated by Al from the crucible and Hf from the ZrO_2 impurity. The results have also been reported previously, the contamination of a small amount of Al is as useful to the stability of the crystal structure. The cubic lattice parameters, determined by a least-squares refinement was a = 13.0064(3) Å by single-crystal X-ray diffraction. This value was in good agreement with the reported values [5]: a = 12.9827(4) Å. A small transparent and sphere-shaped crystal, diameter of 0.1

mm was used for the structure analysis by single-crystal X-ray and neutron diffraction. The single crystal is too small to obtain the neutron diffraction data, but we have succeeded in this measurement. The structure refinement was initiated with the garnet framework structure finding that the La, Zr, and O atoms located at 24*c*, 16*a*, and 96*h* sites, respectively. All calculations were carried out using a computer program Jana2006. Subsequently, two Li, Al and Hf sites were determined by the difference-Fourier map using X-ray and neutron diffraction data. The results, site of Li and Al were occupied 96*g* and 24*d*. Site of Hf was occupied 16*a*. Figure 1 shows the refined crystal structure of cubic-type $Li_7La_3Zr_2O_{12}$ by single-crystal X-ray and neutron diffraction data.

In summary, single crystal of garnet-related type $Li_7La_3Zr_2O_{12}$ with cubic-type was successfully synthesized by a solid-state reaction. A valid crystal structure of cubic-type $Li_7La_3Zr_2O_{12}$ was determined by single-crystal X-ray and neutron diffraction data for the first time. We demonstrated crystal structure including the impurities incorporated into the crystal using X-ray and neutron diffraction data.

References:

[1] H. Aono, E. Sugimoto, Y. Sadaoka, N. Imanaka, G. Adachi, *J. Electrochem. Soc.*, **136** (1989) 590.
[2] Y. Inaguma, C. Liquan, M. Itoh, T. Nakamura, T. Uchida, H. Ikuta, M. Wakihara, *Solid State Commun.*, **86** (1993) 689.
[3] M. Tatsumisago, A. Hayashi, *J. Non-Cryst. Solids*, **354** (2008) 1411.
[4] R. Murugan, V. Thangadurai, W. Weppner, Angew. *Chem., Int. Ed.* **46** (2007) 7778.
[5] J. Awaka, A. Takashima, K. Kataoka, N. Kijima, Y. Idemoto and J. Akimoto, *Chem. Lett.*, **40** (2011) 60.

Figure:

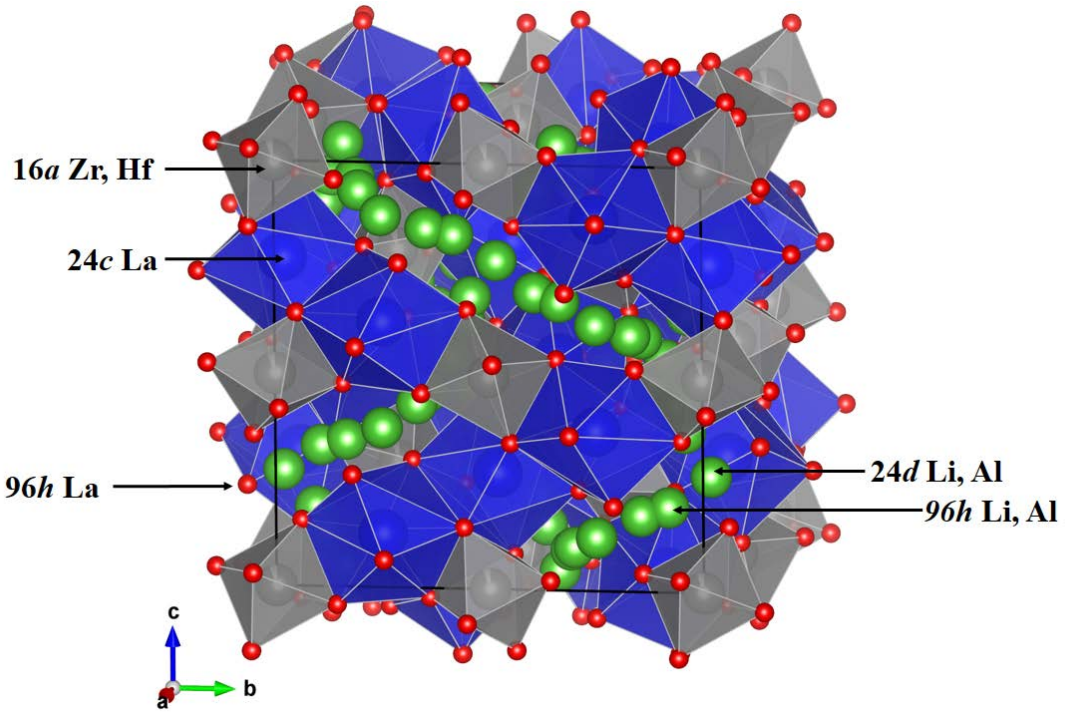

Figure 1. Crystal structure of $Li_7La_3Zr_2O_{12}$

Sol-gel synthesis of complex oxides $GdFeO_3$, $GdSrFeO_4$, $Gd_2SrFe_2O_7$ and their catalytic activity

I. Chislova[a], I. Zvereva[a], V. Panchuk[a], T. Kryuchkova [b], T. Sheshko [b]
[a]Saint-Petersburg State University, Petrodvorets, Universitetsky pr. 26, Saint-Petersburg, 198504 Russia;
[b] Peoples Friendship University of Russia,, Miklukho-Maklaya str. 6 , Moscow, 117198, Russia.
i.v.chislova@gmail.com

There are not so many sufficient examples of the synthesis by low temperature "soft chemistry" methods of highly dispersed powders, fibers, thin films of compounds with complex cationic composition.

In this report we present the results for nanodispersed perovskite-like ferrites $GdFeO_3$, $GdSrFeO_4$, $Gd_2SrFe_2O_7$ synthesized by sol-gel technology. These compounds belong to Ruddlesden-Popper phases and exemplify the 1/1 and 2/1 intergrowths of ABO_3 Perovskite (P) and AO Rock-Salt (RS) type slabs.

At the present time there is no information of the synthesis conditions and physicochemical properties for nanodispersed layered oxides $GdSrFeO_4$ and $Gd_2SrFe_2O_7$. As for the complex oxide $GdFeO_3$- it was recently reported that this compound, obtained by ceramic technology, shows multiferroic properties at 2.5 K [1]. The magnetic properties of these oxides in nanocrystalline state and their dependence on the size of particles have not been investigated yet. The size of particles is also very important for increasing the catalytic activity. Thus it is very necessary to obtain nanopowders of $GdSrFeO_4$ that was used as a catalyst [2] and more stable oxide $Gd_2SrFe_2O_7$, which has not been studied in detail.

$GdFeO_3$, $GdSrFeO_4$ and $Gd_2SrFe_2O_7$ were synthesized by sol-gel technology and by high temperature solid state reactions. The sol-gel technology was performed by using citrate-nitrate techniques in case of $GdFeO_3$, $GdSrFeO_4$, $Gd_2SrFe_2O_7$ and glycine–nitrate techniques in case of $GdFeO_3$. Determination of the temperature of formation of complex oxides $GdSrFeO_4$ and $Gd_2SrFe_2O_7$ performed simultaneous thermal analysis. Methods of powder X-ray diffraction (XRD) and scanning electron microscopy (SEM) have been used for the determination of the structure and morphology of synthesized samples. The decrease in size of particles from 10 μm, obtained by high temperature ceramic synthesis, to 50–200 nm, obtained by sol–gel technology, was demonstrated. Photon correlation spectroscopy have been used for evaluation average particle size and size distribution. Photon correlation spectroscopy data are consistent with scanning electron microscopy at the maximum amount - the length of the particles.

The valent state of iron atoms in complex perovskite-like ferrites have been investigated using Mössbauer spectroscopy. Heterovalent state of iron atoms (Fe^{+3} and Fe^{+4}) was determined only in layered oxide $GdSrFeO_4$. It was shown that iron atoms of complex ferrites obtained by sol-gel technology were in different oxygen surrounding. It hasn't been detected for the same compounds synthesized by high temperature solid state reactions.The results indicate that complex ferrites obtained by sol-gel method exists not only in

ultradispersed state but also in heterovalent iron state with oxygen vacancies that is necessary for catalysis.

The catalytic activity of complex oxides was tested for the reaction of the conversion of the mixture of methane and carbon dioxide. The conversion of CH_4 and CO_2 at 1223 K in presence of powders of investigated oxides reaches 35 and 55 % correspondingly. In spite of high temperatures the catalysts activity does not decrease during 30 hours. Catalytic activity increases in the row $GdSrFeO_4$, $Gd_2SrFe_2O_7$, $GdFeO_3$. For all oxides the quantity of obtained CO was greater than H_2. Heterovalent iron state and oxygen vacancies are favorable for the surface oxidation-reduction reactions and the process of CO_2 activation.

The reported study was supported by RFBR grant 14-03-00940 and grant SPbSU 12.0.105.2010.

References:

[1] Tokunaga, Y., Furukawa, N., Sakai, H., Taguchi, Y., Arima, T., and Tokura, Y., *Nat. Mater.*, **8** (2009), 558.
[2] Christopher, J. and Swamy, C.S., *J. Mol. Catal.*, **68**(1991),199–213.

Nafion-based composite materials containing aerosil and polyorganosiloxane modified by aromatic sulfogroups and water-soluble fullerene derivates

D.V. Postnov, N.A. Melnikova, V.N. Postnov, O.S. Svistunova, I.V. Murin

Saint-Petersburg State University, Saint-Petersburg, Russia
e-mail: postnovdv@rambler.ru

Proton-conductive polymer electrolytes in spite of their comparatively recent origin have provided a base for new electrochemical devices (low-temperature fuel cells, moisture sensors etc.). Nafion membranes ("Du Pont", USA) as well as their russian analogues MF-4SC based on perfluorinated polymers with chemically bonded sulphacid groups are commonly used. They possess rather high proton conductivity and chemical stability, and are mechanically resistant. Nevertheless, the use on Nafion brings with it several problems such as significant reduction of proton conductivity under low water content condition and increased temperature. A possible way to extend the Nafion membranes application range optimizing their properties is to create nanostructured composites with hydrophilic dopant.

A dopant for the Nafion membranes in this investigation was aerosil with aromatic sulfo groups ($\equiv Si - (CH_2)_2 - C_6H_4 - SO_3H$). It was synthesized by precision method of chemical assembly. On the surface of aerosil the chemosorption of 2-phenylethyl- trichlorosilane, and then the sulphonation of phenylethylsilyl groups were carried out. The content of sulfo groups in the synthesized material determined by acid-base titrating method was equal to (C=0,47 mM/g). Polyorganosiloxane containing sulfo groups was synthesized by hydrolytic polycondensation. The content of sulfo groups was equal to 3,8 mM/g. A method of synthesizing nanocomposites on the basis of Nafion and synthesized dopants on dielectric substrates was developed for investigating the proton conductivity of materials. Prior to introducing into Nafion, aerosol was dispersed on ultrasonic disperser. Then the 15 wt% Nafion solution was mixed with a certain volume of colloidal solution of dopant, and then applied on the substrate with drop-by-drop method and dried. Thus Nafion composite films containing 1, 2; 4 and 8 wt % of dopant were obtained. Nafion composite films containing water-soluble fullerene derivates were obtained in the similar way.

The proton conductivity research was carried using impedance spectroscopy method under relative air humidity (RH) 12-97%. Introduction into Nafion of dopants with aromatic sulfogroups results in the increase of proton conductivity as compared with that of pure Nafion within the range of relative humidity 12-59%. The highest electrical conductivity is shown by the 1,2% sulfonated aerosil containing composite material. The same material showed a 150-fold proton conductivity increase under RH=12%, and a 5-fold increase under RH=59%. The increase of proton conductivity as compared with that of pure Nafion was found out for water-soluble fullerene derivates under low humidity.

The research was carried out with financial support of the RFBR, grant №14-08-00885.

Study on the Mechanism of Reversible Lithium Intercalation in *P3*-$Na_xNi_{1/2}Mn_{1/2}O_2$ (x=1/2, 2/3)

Maria Kalapsazova,[a] R. Stoyanova, [a] G. Tyuliev, [b] E. Zhecheva [a]

[a]Institute of General and Inorganic Chemistry, Bulgarian academy of Sciences, 1113 Sofia, Bulgaria;
[b] Institute of Catalysis, Bulgarian Academy of Sciences, 1113 Sofia, Bulgaria.

The systematic study on the relationships of the intercalation properties of solids with their crystal structure paved the way for rational design of cathode materials for lithium ion batteries [1]. Among several groups of compounds, the layered lithium–nickel–manganese oxide, $LiNi_{1/2}Mn_{1/2}O_2$, is considered as a cheaper and environmentally-compatible electrode material in comparison with the widely used layered $LiCoO_2$ oxide. However, $LiNi_{0.5}Mn_{0.5}O_2$ displays a limited rate capability [2] that retards its application in the market.

Recently, the demand for searching cheap electrode materials has become dominant. Since lithium ion batteries are still expensive, sodium ion batteries have been advanced as an alternative [3]. Both lithium and sodium ion batteries operate with the same mechanism comprising a reversible intercalation of Li^+ or Na^+ between the anode and the cathode. Taking into account the intercalation properties of lithium and sodium transition metal oxides, we have proposed recently sodium deficient nickel manganese oxides $Na_xNi_{1/2}Mn_{1/2}O_2$ ($0.5 \leq x < 0.75$) as positive electrodes in lithium ion batteries [4]. Because of the capability of $Na_xNi_{0.5}Mn_{0.5}O_2$ to intercalate lithium reversibly, the battery delivers a reversible capacity of about 130 mAh/g. The good intercalation properties of $Na_xNi_{1/2}Mn_{1/2}O_2$ are a consequence of their stable structure: $Na_xNi_{1/2}Mn_{1/2}O_2$ adopt a layered crystal structure, which can be classified as a *P3*-type (according to the notation of Delmas et al. [5]). This structure differs from the structure of the well known stoichiometric lithium and sodium nickel manganese oxides (*O3*-type for $Li/NaNi_{0.5}Mn_{0.5}O_2$ [2,6]).

In this contribution we provide new data on the mechanism of reversible lithium intercalation in *P3*-$Na_xNi_{1/2}Mn_{1/2}O_2$ (x=1/2, 2/3). For the preparation of the oxides, we have adopted a simple precursor method that consists in thermal decomposition of mixed sodium-nickel-manganese acetate salts obtained by freeze-drying. The structure and morphology of $Na_xNi_{0.5}Mn_{0.5}O_2$ are determined by powder X-ray diffraction, SEM and TEM analysis. The oxidation state of manganese and nickel ions is identified by XPS. The lithium intercalation in $Na_xNi_{0.5}Mn_{0.5}O_2$ is carried out in model two-electrode lithium cells of the type $Li|LiPF_6(EC:DMC)|Na_xNi_{0.5}Mn_{0.5}O_2$. The mechanism of the electrochemical intercalation is determined by ex-situ XRD experiments, chemical and XPS analysis.

Thermal decomposition of freeze-dried sodium-nickel-manganese-acetate precursors yield at 700 ^oC sodium deficient oxides $Na_xNi_{0.5}Mn_{0.5}O_2$ with a *P3*-type structure. The XPS analysis shows that the oxidation state of Ni ions is intermediate between +2 and +3, while Mn ions are in their usual oxidation state of 4+.

The layered oxides $Na_xNi_{0.5}Mn_{0.5}O_2$ display a reversible lithium intercalation between 2.5 and 4.6 V (Fig. 1). During the first discharge of the electrochemical cell up to 2.5 V, Li^+ ions are inserted in the vacant sodium positions, leading to the formation of a mixed Li^+,Na^+

oxide $Li_{\sim(1-x)}Na_xNi_{0.5}Mn_{0.5}O_2$ with a structure that deviates from that of the the pristine oxide. We demonstrate that the capacity of the first discharge *versus* Li anode can be used to estimate the sodium content in $Na_xNi_{0.5}Mn_{0.5}O_2$. The electrochemical reaction takes place with the participation of the Mn^{4+}/Mn^{3+} ionic couple and is accompanied with a structural transformation. The reversible lithium intercalation is accomplished between the $Na_{\sim0.4}Ni_{0.5}Mn_{0.5}O_2$ and $Li_{\sim0.6}Na_{\sim0.4}Ni_{0.5}Mn_{0.5}O_2$ phases. A partial exchange of Na^+ with Li^+ occurs during the first few cycles, followed by a stable performance. In the same potential range, the surface of $Na_xNi_{0.5}Mn_{0.5}O_2$ is covered with lithium, sodium and nickel fluorides together with P_2O_5 and/or Li_xPF_yO. It is noticeable that the profile of the electrochemical charge/discharge curve depends on the potential limits. Our electrochemical studies show that the most favourable potential limits for stable performance are 2.5-4.5 V (Fig. 1).

This study is the first experimental evidence for the direct use of sodium deficient nickel-manganese oxides as cathodes in lithium ion batteries. The results obtained can also be of interest for the development of the newly proposed mixed sodium/lithium ion batteries [7].

Acknowledgements:
Authors are grateful to the financial support from ESF (Grant BG051PO001-3.3.06-0050).

References:

[1] Alcántara R., Lavela P., Tirado J.L., Zhecheva E., Stoyanova R., *J. Solid State Electrochem.*, **3** (1999) 121.
[2] Ellis B.L., Lee K.T., Nazar L.F., *Chem. Mater.*, **22** (2010) 691.
[3] Carlier D., Cheng J.H., Berthelot R., Guignard M., Yoncheva M., Stoyanova R., Hwang B.J., Delmas C, *Dalton Transactions*, **40** (2011) 9306.
[4] M. Kalapsazova, R.Stoyanova, E.Zhecheva, *J. Solid State Electrochem.*, DOI: 10.1007/s10008-014-2399-x.
[5] Komaba S., Yabuuchi N., Nakayama T., Ogata A., Ishikawa T., Nakai I., *Inorg. Chem.* **51** (2012) 6211.
[7] Liang Chen, Qingwen Gu, Xufeng Zhou, Saixi Lee, Yonggao Xia, Zhaoping Liu, *Scientific Reports*, **3**, Art. Number 1946, doi: 10.1038/srep01946.

Figures: (a) First discharge and charge curves expressed as derivatives for $Na_{1/2}Ni_{1/2}Mn_{1/2}O_2$. **(b)** Second charge/discharge curves of the model cell cycled in the potential range of 2.5-4.4 V (top), 2.5-4.5 V (middle) and 2.5-4.6 V (bottom).

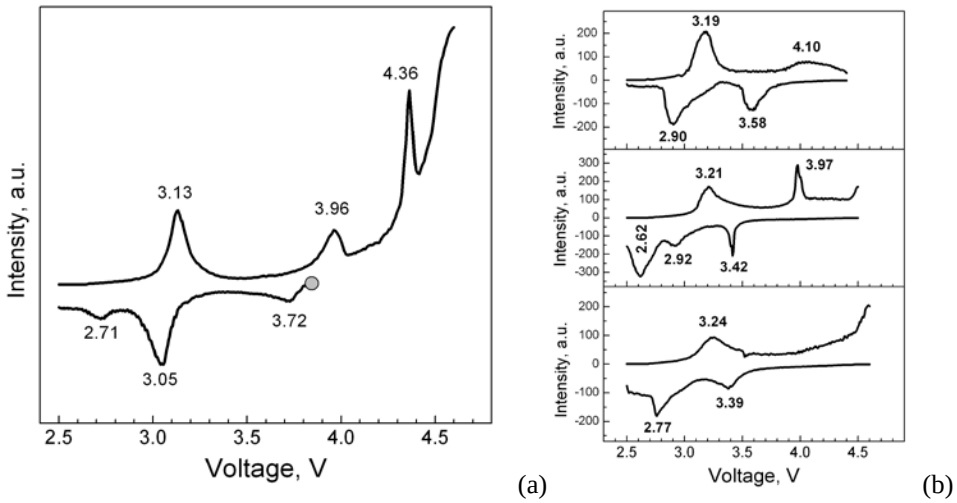

Synthesis and luminescent properties of $NaYF_4$:Yb:Er nanopowders

Kuznetsov S.V.,[a] Yasyrkina D.S.,[a] Fedorov P.P.,[a] Ryabova A.V.,[a] Pominova D.V.,[a] Voronov V.V.,[a] Osiko V.V.[a]

[a]A.M. Prokhorov General Physics Institute, Russian Academy of Sciences

Development of the modern material sciences at the intersection of chemistry, physics and biology results in discovery of the new materials including visible light range fluoride-based up-conversion luminophores for medical applications. One of such materials is sodium-yttrium fluoride $NaYF_4$ (in both hexagonal and cubic forms) studied in the present work [1-4].

We synthesized aforementioned $NaYF_4$ nanopowders via precipitation from vigorously stirred aqueous solutions at room temperature by dropwise addition of aqueous rare earth nitrates to NaF solution (direct synthesis) or by dropwise addition of aqueous NaF to nitrate solution (reversed order synthesis). Obtained precipitates were thoroughly washed with double-distilled water. Some experiments were carried out in the presence of surfactants, e.g., polyethyleneimine (PEI) or citric acid. Concentrations of starting solutions varied from 0.05 to 1.00 M.

X-Ray diffraction and scanning electron microscopy (SEM) data indicate that precipitates, obtained at NaF:Y = 10:1 starting ratio, contained primary 25 nm particles (94 nm area of coherent scattering, $1*10^{-3}$ microdeformations; Fig. 1) that formed 150-300 nm agglomerates.

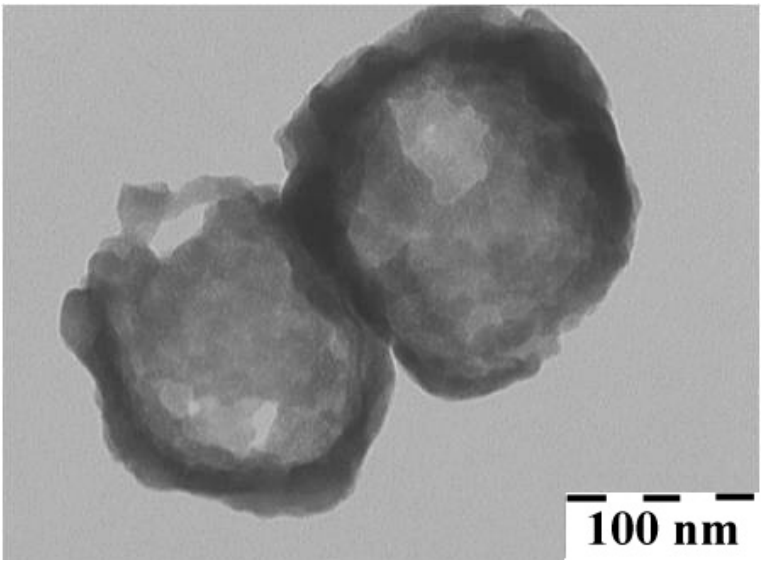

Fig. 1. TEM image of single-phase cubic $NaY_{0.80}Yb_{0.17}Er_{0.03}F_4$ sample (Na:Y=10:1 starting ratio; 0.35 M starting solutions).

We determined the conditions (PEI concentration, reaction mixture pH value, order of reagent mixing, etc.) of the single-phase specimen preparation. Cubic $NaYF_4$ was prepared at pH = 10 when nitrate solution was added dropwise to aqueous NaF, whereas hexagonal $NaYF_4$ was synthesized by addition of NaF nitrate water solutions at pH = 12. PEI concentration was always 9 g/L.

In addition to intrinsic $NaYF_4$, we also prepared Yb/Er-doped nanofluorides $Na_{0.5-x}(Y_{1-y-z}Yb_yEr_z)_{0.5+x}F_{2+2x}$ with 2-90 mol% Yb and 1.5-20 mol% Er and studied their luminescence properties. Luminescence quantum yields of these samples are presented in Fig. 2 and Table 1.

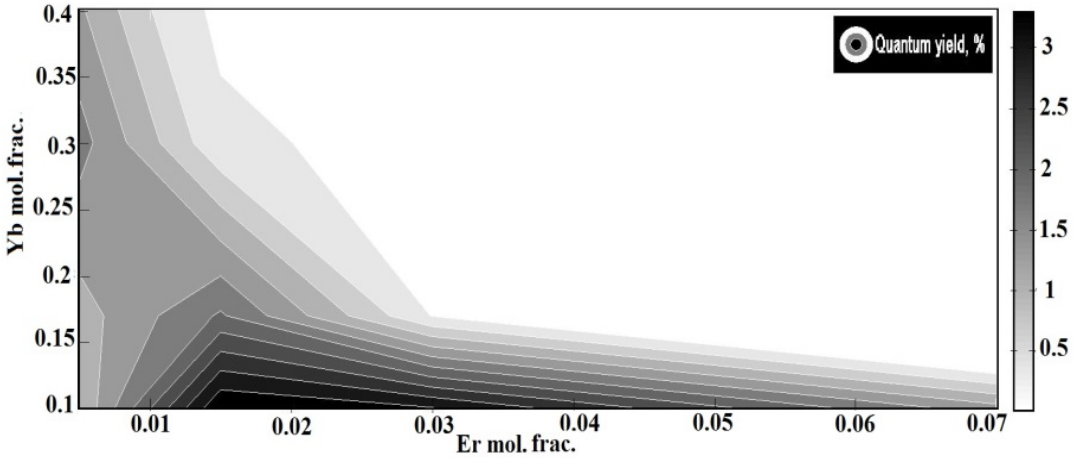

Fig. 2. Luminescence quantum yields of $NaY_{1-x-y}Yb_xEr_yF_4$ samples.

Table 1. Luminescence quantum yields for the doped specimens.*

Sample composition	QY, %	$f_{r/g}$	QY_r, %	QY_g, %
$NaY_{0.87}Yb_{0.10}Er_{0.03}F_4$	3.35	1.12	2.73	0.62
$NaY_{0.885}Yb_{0.10}Er_{0.015}F_4$	3.63	0.55	2.48	1.14
$NaY_{0.815}Yb_{0.17}Er_{0.015}F_4$	2.03	1.01	1.62	0.41

*) $QY = QY_r + QY_g$ – total quantum yield, %; $f_{r/g}$ – red to green peak intensity ratio; QY_r – red peak quantum yield, %; QY_g – green peak quantum yield, %. Pumping power - 1 W/cm^2.

This work was supported grant RFBR 12-02-00851-a and grant Russian President MK-3133.2014.2.

References:

[1] P.P. Fedorov, S.V. Kuznetsov, V.V. Voronov, I.V. Yarotskaya, V.V. Arbenina, *Russian J. Inorg. Chemistry*, **53 (11)** (2008) 1681.
[2] S.V. Kuznetsov, A.V. Ryabova, D.S. Los', P.P. Fedorov, V.V. Voronov, R.P. Ermakov, V.B. Loshchenov, V.V. Volkov, A.E. Baranchikov, V.V. Osiko, *Nanotechnologies in Russia*, **7(11–12)** (2012) 615.
[3] D.S. Yasyrkina, S.V. Kuznetsov, P.P. Fedorov, V.V. Voronov, A.V.Ryabova, D.V. Pominova, A.E. Baranchikov, V.K. Ivanov, V.V. Osiko, *J. Fluor. Chem.*, **158** (2014) 60.
[4] S.V. Kuznetsov, A.A.Ovsyannikova, E.A.Tupitsyna, D.S. Yasyrkina, V.V. Voronov, P.P. Fedorov, N.I. Batyrev, L.D.Iskhakova, V.V.Osiko., *J. Fluorine Chemistry*, (2014) Accepted for publication.

New ferroelectrics based on calcium-bismuth vanadate

D.A. Beskorovaynaya [a], D.V. Deyneko [a], B.I. Lazoryak [a]
[a]Lomonosov Moscow State University, Moscow

At the present time inorganic materials with structure of whitlockite have a wide use due to its fluorescent, nonlinear optical and related properties. Also such compounds have ferroelectric properties. Thus, the effect of second harmonic generation (SHG) is characteristic of whitlokites, what is important, for example to create new sources of laser radiation. Furthermore, the whitlockite type structure is a promising matrix for implementation of valuable luminescent properties of lanthanide-series cations due to optimal distance between the centers of luminescence.

Solid solution with whitlockite structure $Ca_{8-x}Pb_xZnBi(VO_4)_7$, $Ca_{8-x}Pb_xCdBi(VO_4)_7$, $Ca_{8-x}Pb_xMgBi(VO_4)_7$, $Ca_{9-x}Pb_xBi(VO_4)_7$, $0.5<x<1.5$ were obtained by solid phase method in powder and ceramics forms. The synthesis was carried out from stoichiometric mixtures $CaCO_3$, PbO, V_2O_5, ZnO, MgO, CdO, Bi_2O_3 at 900 °C during 150 hours with intermediate triturating. The single-phase of synthesized substances was proved by X-ray phase analysis.

Parameters and volume of unit cell for synthesized compounds growth expectedly according to increase of concentration of lead in the solid solution. Solid solutions crystallize in the polar space group R3c and show ferroelectric and nonlinear optical properties. In this case there is an increase in the SHG effect depending on raising of lead's amount in $Ca_{8-x}Pb_xZnBi(VO_4)_7$, $Ca_{8-x}Pb_xCdBi(VO_4)_7$ systems. The intensity of the second harmonic signal has a maximum in Ca8–xPbxMgBi(VO4)7 systems at x = 1 (Table 1).

Significant increase of nonlinear optical properties in case of introduction of three types of cations and joint settlement of M1 - M3 positions is determined in comparison with previously studied $Ca_{10.5-x}Pb_x(VO_4)_7$ and $Ca_{9-x}Bi_x(VO_4)_7$ [2]. Apparently, introduction of two highly polarized cations Pb^{2+} and Bi^{3+} in vanadate systems increases the crystal-chemical friability of structure and placement of cations Mg, Zn, Cd with r <r (C^{2+}) in the M5 positions provides the additional space for the realization a strongly asymmetric spatial arrangement of electron lone pair, which, as it is well-known, is the main mechanism for the record values of optical nonlinearity.

Table 1. The intensity of SHG signal in $Ca_{8-x}Pb_xM_{1,2,3}Bi(VO_4)_7$ systems of the lead content *x*, $M_{1,2,3}$ - Zn, Cd, Mg

x	M_1	M_2	M_3
0.5	35	140	250
1	70	410	300
1.5	100	450	5

The phase transition temperature is reduced by $Ca^{2+} \rightarrow Pb^{2+}$ substituting. Thus, Curie temperature for $Ca_{6.5}Pb_{1.5}CdBi(VO_4)_7$ vanadate is 600 °C, while Curie temperature for $Ca_8CdBi(VO_4)_7$ is 727 °C [3], and T_c for $Ca_8PbBi(VO_4)_7$ is 635 °C. This corresponds to conservation of mobility tetrahedral VO_4^{3-}, located on the axis c, at the phase transformation to lower temperatures. First obtained vanadates with whitlokite structure exhibit high values of nonlinear optical activity that represents the technical interest for development materials based on them.

Acknowledgement:
This work was supported by the Russian Foundation for Basic Research, project no. 14-03-01100a.

References:
[1] Powder Diffraction File. Cards: 50-340, 45-345, 45-338, 50-1773, 49-503. JCPDS. International Center for Diffraction Data. 1601 Park Lane. Swarthmore. PA 19081.
[2] O.V. Baryshnikova, Diss. New ferroelectrics and ionic conductors in the structural class of whitlokite. 2005. 129.
[3] O.L. Vorontsova, A.P. Malaho, V.A. Morozov and etc, J. Inorg. Chem., **49**, 12 (2004) 1932.

Mechanical properties of chlorpropamide polymorphs determined by instrument nanoindentation

A. Ivanenko,[a,b] B. Janković,[c] J. Stare[d], S. Srcic[c], E. Boldyreva[a,b]

[a] Novosibirsk State University, Novosibirsk, Russia;
[b] Institute of Solid State Chemistry and Mechanochemistry SB RAS, Novosibirsk, Russia;
[c] University of Ljubljana, Ljubljana, Slovenia;
[d] National Institute of Chemistry, Ljubljana, Slovenia.

Evaluation of mechanical properties of solid pharmaceutical materials is an important component of the drug development and formulation. Structural anisotropy, presence of defects and slip planes as well as crystal packing of molecular crystals have significant impact on their behavior during milling and compression (where material is exposed to deformation), as well as affinity towards water which affects in solubility and pharmacokinetics.

Considering organic molecular crystals one should take into account their tendency to form different crystal structures while preserving chemical composition, namely polymorphism. This phenomenon is extremely important on industrial-scale because of noticeably different physicochemical properties of various polymorphs. Apparently, polymorphism plays crucial role in mechanical behavior of pharmaceuticals, for instance due to stress-induced phase transitions which should be taken into account during examination of stability and efficiency of the drug product.

Sulfonyl ureas form a vast class of pharmaceutical compounds which exhibit useful hypoglycemic effect and can be potentially interesting in terms of polymorphic properties. Typical member of the first generation of antidiabetic agents – chlorpropamide ($C_{10}H_{13}ClN_2O_3S$, 4-chloro-*N*-(propylamino-carbonyl)benzenesulfonamide) – exhibit rich conformational polymorphism and can be obtained at ambient conditions as five polymorphs (α, β, γ, δ and ε).

Crystal structures of chlorpropamide polymorphs are stabilized by hydrogen bonded ribbons. Presence of this structural motif in a certain crystallographic plane as well as its direction with respect to the certain crystallographic axis differs from one polymorph to another. Overall organization of hydrogen bonded network is preserved for all polymorphs of chlorpropamide. Significantly different conformations of molecules and their position in relation to each other give rise to different conformational polymorphs of chlorpropamide with various molecular packing.

The key aim of the present work was to study mechanical properties of conformational polymorphs of chlorpropamide in relation to intermolecular interactions, molecular packing and anisotropy of the crystal structure. For the very first time nanoindentation was used for investigation of nanomechanical properties of chlorpropamide polymorphs.
Samples of polymorphs of chlorpropamide (α, β, γ and δ) were obtained from heptane – ethyl acetate mixture by variation of crystallization conditions (solvents ratio, concentration of solution, rate of cooling).

Single crystals with flat clear faces appropriate for indenting were selected from several crystallization batches. Orientation of the crystallographic axes with respect to the external faces and edges of selected crystals was determined on STOE IPDS and Oxford Diffraction diffractometers.

Mechanical characterization of chlorpropamide polymorphs was performed by continuous stiffness measurement (CSM) at nanoindenter. The dominant faces of the thin plates shape single crystals were chosen for the nanoindentation measurements.

Crystal structure characteristics, such as d-spacing, attachment energy and specific interaction energy, of the polymorphs were assessed using quantum mechanical calculations and compared with experimental results.

Nanoindentation results revealed differences in mechanical properties of investigated chlorpropamide polymorphs in respect to molecular packing and orientation of H-bonded ribbons. While indenting the dominant crystal face of α-chlorpropamide, the stress was dissipated along the hydrogen bonded ribbons, which resulted in the slipping effect. This was confirmed with lower indentation hardness (increased plasticity) when compared to β- and γ-polymorphs. Indenting of (001) crystal face of the β-chlorpropamide in normal direction to hydrogen bonded ribbons, the pop-ins (small cracks) occurred at the loading curve. Reduced plasticity and brittle character of β-form can be supported with shorter hydrogen bonds, which are related to stronger interactions between the planes. Nanomechanical properties of γ-polymorph were similar to β-form. Slight increase in Young's modulus of γ-polymorph can be related to monoclinic crystal face and more compacted structure related to short contacts between propyl tails and benzene rings of the neighboring molecules. According to parameters of elasticity and plasticity, the main mechanism of deformation for investigated chlorpropamide polymorphs will be additionally addressed.

The research was supported by a grant for Russia-Slovenia collaboration BI-RU-12-13-038, and the Integration project 108 of the SB RAS.

The effect of Pd loading on the electrocatalytic activity of PEDOT:PSS/Pd composite films towards hydrazine oxidation

Elena G. Tolstopjatova[a], Svetlana N. Eliseeva[a], Veniamin V. Kondratiev[a]
[a]Department of Chemistry, St. Petersburg State University

The aim of the present study was to investigate the appropriate way of the synthesis of aqueous dispersion of PEDOT:PSS/Pd composite and its application for the formation of thin-layered electrode surface. We used a novel method of synthesis of PEDOT:PSS/Pd composite based on commercially available PEDOT:PSS dispersion. Preliminary synthesized PEDOT:PSS/Pd water dispersion was drop cast on glassy carbon electrodes to form thin metal-polymer composite layers. We used this approach in order to develop easy in preparation Pd catalysts with highly dispersed, non-agglomerating nanoparticles. Catalytic properties of PEDOT:PSS/Pd composite films were studied in respect to hydrazine oxidation by cyclic voltammetry and voltammetry on rotating disk electrode.

Previously we have investigated the synthesis of PEDOT/Pd composite by spontaneous electrodeposition of Pd into PEDOT films from $PdCl_2$ /0.1 M H_2SO_4 solutions [1]. The same reaction may proceed in the case of PEDOT:PSS water dispersion at raised temperature. The spontaneous formation of palladium nanoparticles in PEDOT:PSS water dispersion is ascribed to the following spontaneous redox reaction:

$$Pd^{2+} + 2PEDOT:PSS \xrightarrow[t,C^o]{+A^-} Pd^0 \cdot (PEDOT^+:PSS) \cdot A^-$$

where PEDOT:PSS is a redox fragment of a polymer chain, comprising several monomer units.

Composite PEDOT:PSS/Pd films with various Pd loading were obtained. Pd loading was varied by two experimental procedures: 1) number of drop cast layers (from 1 to 8), 2) concentration of Pd^{2+} ions introduced into preliminary formed PEDOT:PSS/Pd water dispersion ($5\cdot10^{-3}$–$5\cdot10^{-2}$ M $PdCl_2$).

A continuous increase of oxidation currents with increase of Pd content was observed, showing that the rate of the process of hydrazine oxidation accelerates with increase of number of accessible metallic Pd particles. Therefore, composite electrodes with higher Pd content show higher sensitivity in respect to hydrazine. It was found that at high level of Pd loadings (corresponding to 4-8 layers) the maximum of limiting current of the N_2H_4 oxidation is observed. Further increase of the number deposited layers does not change the limiting currents. The oxidation wave is shifted to more negative potentials with increase of Pd loading (both for films of different thickness cast from dispersion with constant Pd content and the films of the same thickness cast from dispersions of varied Pd content). The observed dependence of hydrazine oxidation currents on the Pd coverage additionally points to the acceleration of the hydrazine oxidation, which proceeds on the palladium particles.

In general, it can be concluded that the observed phenomenon results from a gradual transition from a small active surface of palladium particles acting as separate microelectrodes at their low contents in PEDOT composite films to the conditions of semi-linear diffusion mass-transfer of reacting particles near electrode surface when increasing the palladium particles coverage.

Amperometric method was also used to examine the sensitivity of PEDOT:PSS/Pd electrodes towards the detection of hydrazine in phosphate buffer solution. A fast, sensitive response to various concentrations of hydrazine was achieved. For a 4-layer composite film the maximum sensitivity of hydrazine determination was calculated from the obtained calibration plot and was $5.7 \cdot 10^{-6}$ A/M cm^2. The limit of detection, LOD= 0.13 μM, was estimated at signal to noise ratio of 3. The obtained value is quite competitive with other data, obtained for hydrazine detection on Pd-containing electrodes.

Acknowledgements:
The authors are thankful to Prof. Oleg Vyvenko and Dr. Yuri Petrov, Dr. Evgeny Ubyivovk from the Interdisciplinary Resource Center for Nanotechnology of St. Petersburg State University for the help we have derived during common SEM and TEM measurements. The work was supported by the Russian Foundation for Basic Research (grant № 13-03-00984) and the research grant of Saint-Petersburg State University (grant № 12.38.15.2011).

References:
[1] V.V. Kondratiev, T.A. Babkova, E.G. Tolstopjatova, *J. Solid State Electrochem*. 17 (2013) P.1621.

Synthesis and Hydration of the Vacancy Ordered Perovskite Type Compound $BaFeO_{2.5}$

Oliver Clemens,[a] Peter R. Slater,[a] Horst Hahn[b]

[a] TU Darmstadt, Joint Research Laboratory Nanomaterials, Jovanka-Bontschits-Straße 2, 64287 Darmstadt, Germany and KIT, Institute of Nanotechnology, Hermann-von-Helmholtz-Platz 1, 76344 Eggenstein Leopoldshafen, Germany.
[b] School of Chemistry, The University of Birmingham, Birmingham B15 2TT, United Kingdom.
oliver.clemens@kit.edu

$BaFeO_{2.5}$ is one of the most (probably the most) complicated vacancy ordered perovskite type compounds (see Figure 1) and its structure was only solved recently using a combination of X-ray and neutron powder diffraction [1]. The structure contains seven crystallographically different iron ions, which show the following coordination scheme:

$$Ba_7(FeO_{4/2})_1(FeO_{3/2}O_{1/1})_3(FeO_{5/2})_2(FeO_{6/2})_1 = Ba_7Fe^{[6]}{}_1Fe^{[5]}{}_2Fe^{[4]}{}_4O_{17.5}$$

Topochemical reactions are known to be viable tools to modify the anion sublattice of perovskite type compounds [2] and have been widely explored for fluorination reactions on the different modifications of $BaFeO_{3-y}$ [3-6]. Usually, F^- and OH^- show a similar coordination chemistry and similar ion sizes, which enforced also to study the hydration chemistry of $BaFeO_{2.5}$.

In recent experiments, we found that $BaFeO_{2.5}$ can incorporate large amounts of water, which then forms hydroxide groups (similar to other oxygen deficient perovskites, e. g. $BaInO_{2.5}$ [7]), which are likely to show proton conductivity. Depending on the hydration temperature, two different water containing, monoclinically distorted perovskites with approximate compositions of $BaFeO_{2.5}(H_2O)_x$ (x = 0.30 and 0.385) could be observed, showing a similarly complex structure than the precursor compound $BaFeO_{2.5}$, which were again investigated by means of X-ray and neutron powder diffraction as well as DSC/TG/MS measurements.

References:

[1] O. Clemens, M. Gröting, R. Witte, J.M. Perez-Mato, C. Loho, F.J. Berry, R. Kruk, K.S. Knight, A.J. Wright, H. Hahn, P.R. Slater, *Inorganic Chemistry* submitted.
[2] K.G. Sanjaya Ranmohotti, E. Josepha, J. Choi, J. Zhang, J.B. Wiley, *Advanced Materials (Weinheim, Germany)* 23 (2011) 442-460.
[3] O. Clemens, A.J. Wright, F.J. Berry, R.I. Smith, P.R. Slater, *Journal of Solid State Chemistry* 198 (2013) 262-269.
[4] O. Clemens, F.J. Berry, J. Bauer, A.J. Wright, K.S. Knight, P.R. Slater, *Journal of Solid State Chemistry* 203 (2013) 218-226.
[5] F.J. Berry, F.C. Coomer, C. Hancock, Ö. Helgason, E.A. Moore, P.R. Slater, A.J. Wright, M.F. Thomas, *Journal of Solid State Chemistry* 184 (2011) 1361-1366.
[6] R. Heap, P.R. Slater, F.J. Berry, O. Helgason, A.J. Wright, *Solid State Commun.* 141

(2007) 467-470.
[7] J. Jankovic, D.P. Wilkinson, R. Hui, *Journal of The Electrochemical Society* 158 (2011) B61.

Figures:

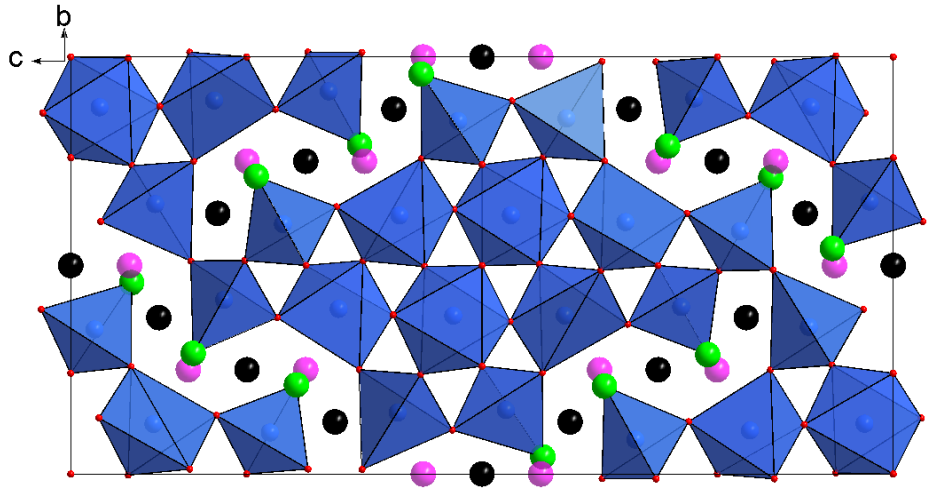

(a)

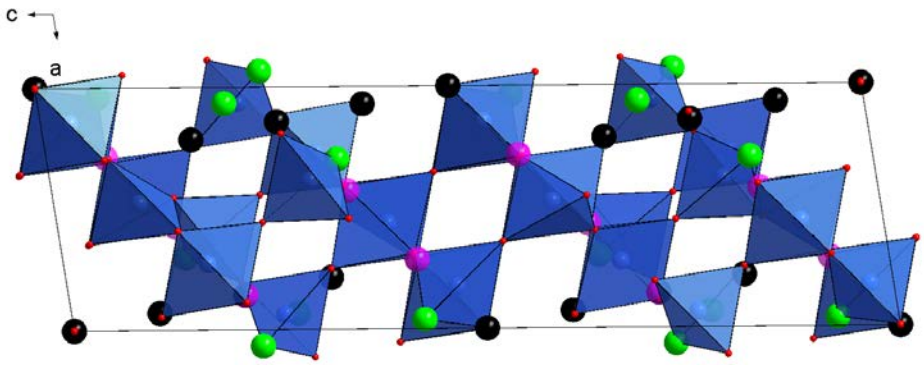

(b)

Fig.1. Schematic representation of the location of the vacancies (black balls) in $BaFeO_{2.5}$ (Ba ions are not shown). Strongly shifted oxygen ions O_2, O_3, and O_4 are shown as green balls, the pseudocubic positions of O_2, O_3, and O_4 are shown as purple balls. Viewing directions were chosen along the a- (a), and the b-axis (b).

Electrochemical fluorination of perovskite-related mixed metal oxides

Andreas Giehr,[a] Horst Hahn,[a] Oliver Clemens,[a]

[a] TU Darmstadt, Joint Research Laboratory Nanomaterials, Jovanka-Bontschits-Straße 2, 64287 Darmstadt, Germany and KIT, Institute of Nanotechnology, Hermann-von-Helmholtz-Platz 1, 76344 Eggenstein Leopoldshafen, Germany.

Mixed metal oxides of the perovskite type with the general composition ABX_3 show a variety of magnetic and electrical properties, thus lending themselves to a number of technical applications. These material properties are often controlled by the detailed oxidation state of the B-site cation, and chemical doping / substitution of the A and X ions is known to have an influence on the average B-site oxidation state.

For modifications of the anion sublattice, chemical doping / substitution with fluoride ions is a viable strategy in the case of oxide materials. However, due to the high thermodynamic stability of the alkaline earth fluorides (and / or lanthanide oxide fluorides), high-temperature synthesis routes are unsuitable and low-temperature topochemical fluorination methods are needed. A number of such synthesis routes have been developed using oxidizing (F_2, XeF_2, CuF_2), non-oxidizing (NH_4F) or reductive (PTFE, PVDF) fluorination agents [1,2].

As a result, the electronic as well as the crystallographic structure of the precursor material can be influenced by changing the oxidation states of the transition metal cations and/or the occupation of anion sites. Three different fluorination mechanisms can be imagined, and all of them have been observed so far: (1) If vacancies are available additional fluoride ions can be added to the structure, increasing the cation oxidation states. (2) One oxide ion may be substituted for two fluoride ions, keeping the metal oxidation states unaffected. (3) Replacing one oxide ion with one fluoride ion leads to a decrease in the cation oxidation states.

The present work explores the possibility of electrochemical (and potentially reversible) fluorination of mixed metal oxides. The experimental setup is based on the report by Reddy et al. [3] who have demonstrated a fluoride ion battery based on conversion type materials. Three-layered pellets are pressed containing powders of a metal fluoride MF_x (e. g. CuF_2 or CeF_3), $Ba_xLa_{1-x}F_{3-x}$ and the respective perovskite type oxide. By application of an external voltage, fluoride ions are released from the metal fluoride MF_x (forming elemental M) and migrate through the solid electrolyte of $Ba_xLa_{1-x}F_{3-x}$ to be incorporated into the perovskite type oxide in an oxidizing manner. In contrast to conventional fluorination agents which act at a given chemical potential against the oxide material, electrochemical methods should allow to specify the potential difference between the two materials via control of the external voltage. The resulting products are characterized by use of diffraction methods, and compared to the corresponding oxyfluorides prepared by conventional chemical fluorination routes.

References:

[1] C. Greaves, M. G. Francesconi, *Curr. Opin. Solid State Mater. Sci.*, **3** (1998) 132–136.
[2] E. E. McCabe, C. Greaves, *J. Fluor. Chem.*, **128** (2007) 448–458.
[3] M. Anji Reddy, M. Fichtner, *J. Mater. Chem.*, **21** (2011) 17059.
[4] O. Clemens, C. Rongeat, M. Anji Reddy, M. Fichtner, H. Hahn, *Dalton Transactions, in preparation.*

Figure:

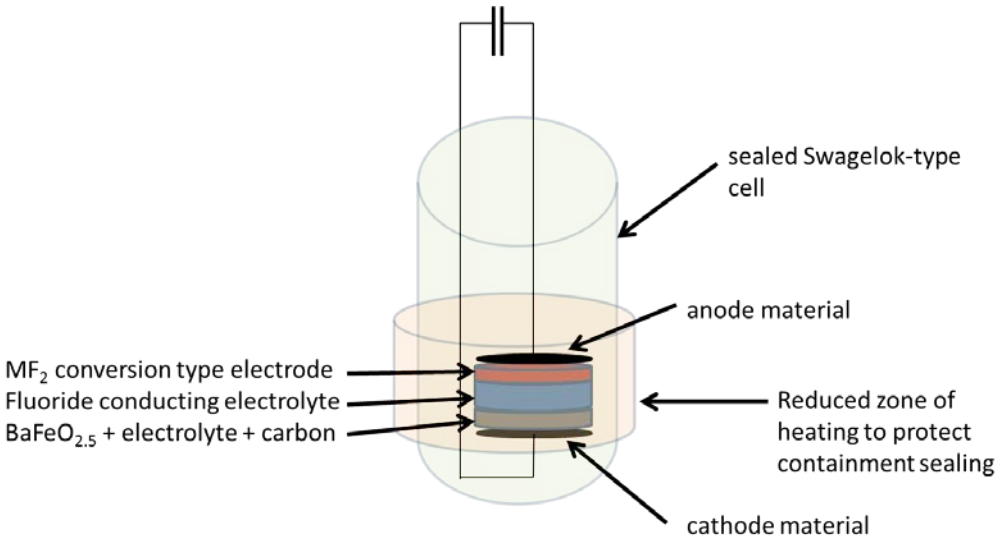

Fig.1. Schematic drawing of the electrochemical fluorination cell and experimental setup; taken from [4]. The terms anode and cathode material are used as it is common in the field of battery research, e. g. based on their respective behavior during discharge of a fluoride ion battery.

Volatile Heterometallic Single-Source Precursors for Prospective Sodium Ion Battery Cathode Materials

Zheng Wei,[a] Alexander S. Filatov,[a] Marina A. Petrukhina,[a] Evgeny V. Dikarev[a]

[a]Department of Chemistry, University at Albany, SUNY, Albany, NY, USA

Lithium ion batteries remain the fastest growing electric power storage systems due to their high energy density, long lifespan, as well as cost-effective and abuse-tolerant properties. At the same time, dramatic developments in the next generation of electrical transportation techniques and utilization of renewable energies will require substantially greater amounts of materials to build large batteries. The low natural abundance of lithium and its non-uniform distribution across the world make large-scale applications of lithium ion batteries problematic. These inherent limitations make the development of secondary batteries based on abundant and cheap alternative elements to become an important new research direction. Similarities between lithium and sodium electrochemistry, coupled with high abundance and low cost of the latter, are major motivations behind the search for experimental sodium ion cells. However, sodium ion intercalation and storage mechanisms are scientifically challenging because Na^+ ion is about 70% larger in radius than Li^+ ion. This makes it difficult to find a suitable host material to accommodate the Na^+ ions and to allow their rapid and reversible insertion/extraction.

Perovskites $NaMF_3$ (M = Mn–Ni) have been identified as prospective oxygen-free cathode materials. High voltage displayed by ternary fluorides can help to overcome intrinsic drawback of sodium ion batteries associated with a lower standard electrode potential compared to that of lithium. Besides that, the strong M–F ionic bonds in this type of materials empower its robust structure of corner-sharing [MF_3] matrix and ensure its stability and safety during the work cycle. Unfortunately, the ionic character of the M–F bonds is the main reason why mixed-metal fluorides exhibit a poor electronic conductivity. Therefore, fine particles and thin films of complex metal fluorides that provide short conductive paths for electrons are required for achieving high Na^+ ion diffusion and improving the capacity of the cathodes. Low temperature methods of the soft chemistry approach are ideal for obtaining particles with narrow submicrometer size distribution as well as compositionally homogeneous thin films. In particular, single-source precursors that offer kinetically attractive decomposition routes at moderate temperatures and permit precise control over the materials stoichiometry can be explored for the preparation of fine particles that exhibit fundamental modification in electrochemical behavior of cathode materials.

We report isolation, characterization, and decomposition study of the volatile heterometallic single-source precursors with a proper sodium:transition metal ratio for non-oxide cathode materials $NaMF_3$. Heterometallic fluorinated β-diketonates $NaM(hfac)_3$ (M = Mn–Ni; hfac = hexafluoroacetylacetonate) [1] were obtained in high yield by simple solid-state reactions that employ commercially available reagents. Substantial scale-up preparation was achieved using a solution approach. The products were crystallized and characterized by single crystal and powder X-ray diffraction. The crystal structure of heterometallic precursors consists of infinite polymeric molecules held together by diketonate ligands acting in a chelating-bridging mode. Importantly, the complexes are stable in open air and highly volatile. Their

mass spectrometric investigation indicates the existence of heterometallic molecules in the gas phase. The presence of heterometallic species in solutions of several solvents was unambiguously confirmed. Heterometallic precursors were shown to exhibit clean, low-temperature decomposition in argon atmosphere that results in phase-pure perovskite fluorides $NaMF_3$, the prospective cathode materials for sodium ion batteries. Single-source precursors were used in the CVD technique for formation of nanocrystals of the target materials.

References:

[1] Zheng Wei, Alexander S. Filatov, Evgeny V. Dikarev *J. Am. Chem. Soc.*, 135, (2013) 12216.

Magnetic properties of nickel manganite synthesized by CPM method

S. M. Savić,[a] M. Tadić,[b] Z. Jagličić[c], L. Mančić[d], K. Vojisavljević[a], G. Branković[a]

[a]Institut for Multidisciplinary research, University of Belgrade, Kneza Viseslava 1, 11000 Belgrade, Serbia
[b]Condensed Matter Physics Laboratory, Vinca Institute, University of Belgrade, POB 522, 11000 Belgrade,Serbia
[c]University of Ljubljana, Faculty of Civil Engineering and Geodesy & Institute of Mathematics, Physics and Mechanics, Jadranska 19, 1000 Ljubljana, Slovenia
[d]Institute of Technical Sciences SASA, Knez Mihailova 35/IV, 11000 Belgrade, Serbia

Spinel materials based on Mn and Ni has been intensively studied over the past years due to their excellent semiconductor properties. Nickel manganite as NTC thermistor is widely used today in different industrial sectors. Here we report the complex polymerization method (CPM) for producing nickel manganite fine particles with a homogeneous distribution of constituent cations in the crystal lattice that ensures formation of dense monophased ceramic with the novel magnetic properties after been sintered in oxygen and air atmosphere.

Phase composition of the synthesized materials was examined by XRPD, while the morphology of the powder and microstructure of ceramic were investigated using FESEM and SEM analyses, respectively. The magnetic properties of the samples have been studied by measuring the temperature and field dependence of magnetization.

Magnetic measurements of M(T) reveal rather complex magnetic properties and multiple magnetic phase transitions. In the case of air atmosphere we found three magnetic phase transitions with transition temperatures at T_{M1}=35 K, T_{M2}=101 K and T_{M3}=120 K. T_{M1} maximum is strongly dependent on the strength of the applied magnetic field (T_{M1} decreases with increasing applied field) whereas the T_{M3} is field independent The values of the coercivity, remanent magnetization and saturation magnetization at 100 K are: H_C = 184 Oe, Mr = 1.92 emu/g and M_S = 7.88 emu/g, respectively. The measured values at 5 K are H_C = 1035 Oe, Mr = 7.70 emu/g and M_S = 14.47 emu/g. These values are comparable with those for nickel manganite systems reported in the literature by authors P.N. Lisboa-Filho et al., 2005. [1]. Moreover, hysteresis properties measured after cooling of the sample in magnetic field show exchange bias effect with an exchange bias field $|H_{EB}|$=196 Oe.

For the sample synthetized in oxygen atmosphere, the magnetization dependence of temperature M(T) and AC susceptibility data obtained from SQUID measurements clearly demonstrates that quadruple magnetic phase transitions can be readily detected at T_{M1}~115 K, T_{M2}~105 K, T_{M3}~38 K and T_{M4}~7 K. These findings suggest the novel magnetic transition for nickel manganite at low temperature T_{M4}. Additionally, temperatures of observed maximums in $\chi'(T)$ and $\chi''(T)$ parts of susceptibility are frequency independent, whereas the height of the peaks decreases with increasing frequency. This behavior is usually observed in ferromagnetic-like and antiferromagnetic-like magnetic transitions. The fact that T_{M4} does not shift with the increase of the frequency leads us to the conclusion that there are no spin-glass/surface effect and/or blocking temperature/finite size effect connected to the $NiMn_2O_4$ ceramic. Therefore, we suggest that the low-temperature peak T_{M4} in AC

susceptibility is associated with ferromagnetic-like and antiferromagnetic-like magnetic transition in the interfacial FM/AFM internal structure. The exchange bias effect was found in a field cooled hysteresis loops at 5 K. The field cooling of the sample was under a magnetic field of 100 Oe and 10 kOe whereas the determined exchange bias fields are $|H_{EB}|$=129 Oe and 182 Oe, respectively.

The analysis of the results and comparison with literature data allowed us to conjecture that the mixed oxidation states of Mn ions and ferromagnetic and antiferromagnetic sublattice orders tailor these interesting magnetic properties.

References:

[1] P.N. Lisboa-Filho, M. Bahout, P. Barahona, C. Moure, O. Pena, J. Phys. Chem. Solids 66 (2005) 1206-1212.

Authors Index

"Pl" = Plenary Lecture
"Inv" = Invited Lecture
"O" = Oral Presenation
"P" = Poster Presenation
Speakers are marked as "sp"
Presenting authors of poster presentations are marked as "m"

Make the SMART move to PDF-4+

ICDD's editorial team works hard to make sure that you get the highest quality data.

Standardized data

More coverage

All data sets are evaluated for quality

Reviewed, edited and corrected prior to publication

Targeted for material identification and characterization

PDF-4+ 2013 features 340,653 entries including 227,102 entries with atomic coordinates.

ICDD®
International Centre for Diffraction Data

ISO 9001:2008 QUALITY ASSURED COMPANY CERT.NR. 11409.1

www.icdd.com | marketing@icdd.com
610.325.9814 | toll-free 866.378.9331
(U.S. & Canada)